In-Situ Microbial Dissolution of Iron Mineral-Bearing Wastes for Metal Recovery

Mark Roberts

This thesis is submitted for the Degree of Doctor of Philosophy

School of Engineering

Cardiff University

June 2018

Abstract

This thesis presents an investigation of whether indigenous iron reducing microbial communities in metalliferous ferric oxide-bearing wastes can be stimulated and exploited for the in-situ recovery of metals within these wastes. A range of ferric oxide-bearing wastes including from mining wastes, water treatment sludges and metallurgical wastes were tested.

When glycerol was introduced to the wastes, only those originating from a former coal mine and those from a former Cu mine displayed stimulation of indigenous iron-reducing communities. A coeval release of Pb and Fe was observed from the latter of these two wastes, during column tests, but direct metal recoveries via effluent extraction was limited. This was attributed largely to the microbial activity causing the pH to increase towards circum-neutral resulting in a decrease in metal solubility. A substantial redistribution of metals of interest between mineral phases of the waste was observed. This resulted in significant increases in the recovery of these metals when the wastes were leached with dilute acid and highlights the potential use of bioreduction as an effective pre-treatment of these wastes.

The stimulated indigenous microbial communities within the wastes were also characterised. It was found that the introduction of glycerol caused a decrease in the community diversity with members of the *Firmicutes* phyla typically dominating the post-experiment waste. The most abundant genus identified was *Desulfosporosinus*, which is known to be capable of adapting to changing conditions by switching between iron and sulphur reduction as necessary and may be doing so within the column tests. *Desulfosporosinus spp.* also proved capable of surviving the autoclaving process. These characteristics demonstrate that this genus is very hardy and potentially exploitable for ex-situ extraction methods.

“Nothing is impossible. Not if you can imagine it. That’s what being a scientist is all about!”

Prof. Hubert J. Farnsworth

Acknowledgements

There are a multitude of people to whom I owe a debt of gratitude for their support during my Ph.D. study. So, to everyone who has helped me in any way, shape or form, I am sincerely thankful and have been humbled by the kindness of strangers in the Cardiff University research community. However, there are a few people who are deserving of specific thanks.

Firstly to my supervisors, Dr Devin Sapsford and Prof Andy Weightman. Thank you very much for all the guidance, support and mostly your seemingly inexhaustible patience with my questions and neuroticism regarding this thesis and for not allowing me to settle for less when I was waning. To Dr Gordon Webster I owe an inordinate level of gratitude, which is unlikely to suitably expressed in this brief paragraph. With your support I have gone from someone who barely got through GSCE biology and was probably a liability to have in a microbiology lab to someone who can now do a vaguely passable impression of a microbiologist.

I would also like to thank Angela Marchbank for guiding me through the murky world of genome sequencing. Also, Jeff Rowlands and Marco Santonastaso, who between them must have analysed well over 1000 samples for me during this work with not even a hint of grumbling when I showed up with even more for analysis after swearing I was finished.

Finally, to my family and friends who have kept me sane (or as close as I'll ever get to it) throughout my work. From chatting nonsense over a few drinks to my parents asking about my work even though it made little sense and probably bored them stiff, it all helped to keep me going. Lastly, but by no means least, to my closest friend and family, my wife Abbie. You have been my driving force throughout all of this. You have put up with me no matter whether I'm stressed and grumpy, acting like a big kid or talking science in my sleep. This is your achievement as much as it is mine because without you I would not have achieved half of what I have done.

List of Contents

List of Figures

List of Tables

List of Acronyms and Terminologies

AMD → Acid mine drainage

DGGE → Denaturing gradient gel electrophoresis

DIRM → Dissimilative iron reducing microbes

DNA → Deoxyribonucleic acid

DO → Dissolved oxygen

EC → Electrical conductivity

FOM → Iron oxidising microbes

ICP-OES → Inductively coupled plasma optical emission spectrometry

ORP/ Eh → Oxidation reduction potential (Eh is corrected to standard hydrogen electrode)

OTU → Operational taxonomic unit

PCR → Polymerase chain reaction

PCoA → Principal coordinate analysis

PSD → Particle size distribution

qPCR → Quantitative polymerase chain reaction

REE → Rare earth elements

rRNA → Ribosomal ribonucleic acid

XRD → X-ray diffraction

There are a number of terminologies used to describe ferric iron minerals, such as goethite, ferrihydrite, in mine wastes. For simplicity, within this thesis the term iron oxyhydroxide will be used as a catchall term to cover terms such as iron oxide, iron hydroxide and iron (hydroxy)oxide amongst others. Similarly, the term iron hydroxysulphate will be used to cover all forms of iron sulphate minerals such as jarosite and schwertmannite.

1. Introduction

1.1. Principles of Resource from Waste

In recent years there has been a significant shift in the way waste is viewed. Along with increasing efforts to reduce the volume of waste produced and sent to landfill, certain wastes are no longer being viewed as waste in the traditional sense and seen as potentially exploitable resources. This is highlighted by the greater preference given to "recovery" of waste compared to disposal of waste within the EU Waste Framework Directive. This has resulted increasing interest in the concept of "technospheric mining", where the technosphere is defined by Johansson *et al.* (2013) as "material stocks established by human agency, and which originates from technological processes, in contrast to stocks in the lithosphere established by slow, primary geological processes". This was then further defined into 3 major stocks, which are potential targets for technospheric mining; tailings ponds (i.e. mine wastes), slag heaps (i.e. industrial metallurgical wastes) and landfills (municipal and industrial). As human activity continually increases these stocks, whilst simultaneously depleting traditional lithospheric stocks, technospheric mining represents a promising future source of metals and other resources.

This changing view is also evident in the growing shift towards establishing a "circular economy". The concept of the circular economy promotes the reduction of primary resource production and waste production. This is achieved by "value optimisation" via the recycling, reuse or repair of a product or material as displayed graphically in Figure 1.1. The application of the circular economy concept has not yet been readily applied to the metal and mineral mining industry, so much so that developed circular economy models have excluded extractive mining (EMF, 2014) and the resultant mine waste (Haas *et al.*, 2015) from the restorative loops of the model. This then suggests that the reprocessing of mine waste to recover residual metal value is a primary extraction method as opposed to an example of recycling as defined by circular economy models (Lèbre *et al.*, 2017). Despite this there is considerable metal value locked within mine wastes and, while their reprocessing with not replace primary resource extraction any time in the foreseeable future (Allwood, 2014), there is likely to be a distinct shift towards their exploitation, for the recovery of metals, as governments and industries

push towards a more circular economy (Sapsford *et al.*, 2016). This will also be driven by the increased need for metals to supply the growing population and the decline in ore grades as a result of increased mine production (Shaw *et al.*, 2013). As the grades of remnant ore bodies decreases and metal value rises the potential value held in waste will also rise.

Particular focus is being given to the recovery of metals to help secure future supplies of elements essential for current and developing technologies such as the "E-elements" (e.g. Co, In, Ga & Te), base metals (e.g. Pb, Zn, Cu & Ni) and precious metals (e.g. Au, Ag and Pd) (Sapsford *et al.*, 2016). Furthermore, there are the European Union's list of 27 supply-threatened critical materials including rear earth elements, platinum group metals (Pt, Rh, Ru, Os & Ir) and metals such as vanadium, magnesium, scandium and tungsten (EC, 2017).

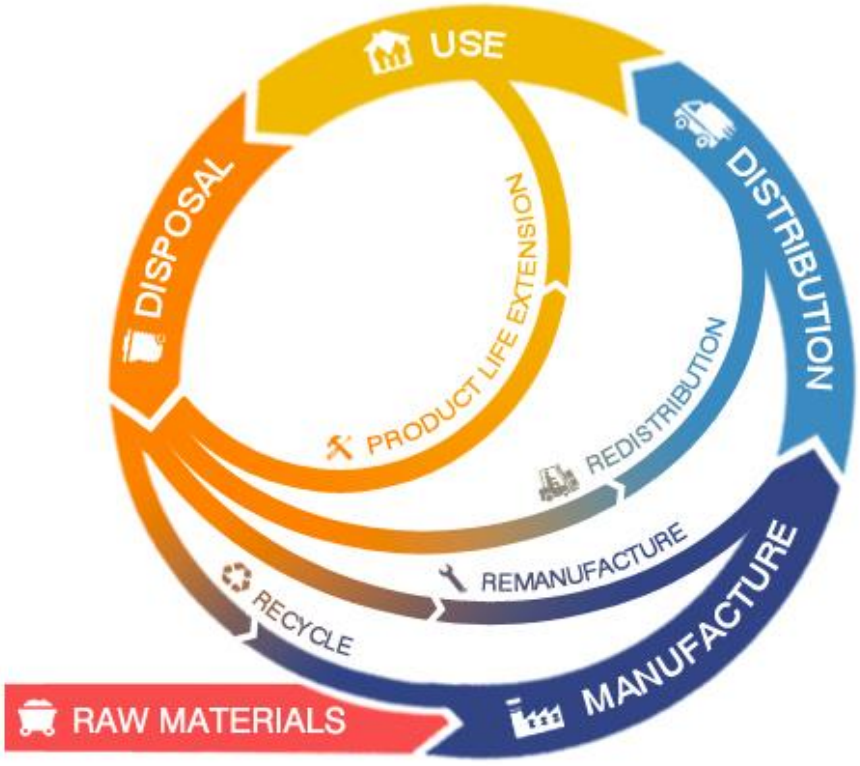

Figure 1.1 Schematic diagram demontrating the concept of the circular economy (Innovate UK, 2017)

The recovery of metals from wastes via leaching has the additional benefit of removing contaminants from the material remaining after leaching i.e. land remediation. This allows for a more complex interpretation of what can be considered a resource to be recovered. Sapsford *et al.* (2016) proposed a new taxonomy for the recovery of resource, subdividing recovery into “direct” and “indirect”. Recovery of metals of interest for economic purposes, or the recovery of methane from municipal solid waste (MSW) landfills, are examples of direct recovery.

Indirect recovery can itself be further subdivided. This may involve the recovery of resource via the removal of contaminants thereby allowing the reuse of that material. Examples include the removal of metals from MSW incineration fly ash to facilitate its reuse (Fedje *et al.*, 2012) or removal of zinc from steelmaking dusts allowing for the dust to be recycled back into the steelmaking process (Calvo *et al.*, 2016). Alternately, recovery may be achieved by alteration of the physiochemical properties of the waste, for example the carbonation of MSW incinerator ash to remove lime and decrease the potential for heavy metal leaching facilitating the reuse of the waste as an aggregate (Van Gerven *et al.*, 2005). Lastly, there is the recovery of the land itself with the removal of contaminants facilitating its use and potential development. Examples for this include any number of land remediation and waste stabilisation studies.

It should be noted that it is possible to achieve both direct and indirect recovery with the same process. Rashid *et al.* (2017) investigated delignification as a precursor for enhanced generation of methane gas. If applied to MSW this would allow for both direct and indirect recovery via increased gas generation and reduced time required before the repurposing of the land respectively. This idea could potentially be extended to metal contaminated wastes and soils. Even if the amount of metal recovered is itself not economically significant, the value accrued may be used to offset the cost of the remediation process. This would result in the direct recovery of metal for sale (and thereby producing reduced costs) and the indirect recovery of the land as a result of its remediation.

1.2. In-situ recovery

As the grade of an ore decreases the exergy and therefore financial cost of removing the metals increases sharply. However, as more energy-efficient extraction methods are applied the exergy cost of mining can be offset, thereby making the resource economically viable (Valero *et al.*, 2011). Calvo *et al.* (2016) noted that copper grades have decreased by ~25% in ten years corresponding with a 30% production increase, while associated energy consumption has increased by 46%. In-situ processes by their nature are far more energy efficient relative to conventional mining methods as the excavation, transportation and physical processing of the waste is not required. This has resulted in the use of in-situ techniques becoming popular for low-grade, large volume ores (Sapsford *et al.*, 2016).

Mining wastes, by their definition, were disposed of because at the time of their production the grade of the target metal was sub-economic for continued processing. Whilst the grade of these materials remains low, shifting commodity values and advances in extraction techniques may result in these wastes becoming economic to process. The other potential path by which these low-grade wastes may be exploited is by overcoming the high exergy cost associated with their processing by applying a low-energy in-situ approach. Pre-existing application of in-situ techniques within both the mining and contaminated land remediation industries present potential templates upon which an in-situ resource recovery from waste technique may be based (Sapsford *et al.*, 2016).

Aside from the financial and environmental benefits of in-situ techniques there are a number of potential ecological and cultural benefits associated with its use for the recovery of resource from mine waste (Crane *et al.*, 2017). Due to the unique physicochemical nature of mine waste sites they are often colonised by rare, specialist, metal tolerant flora such as lichens and liverworts (Welsh Assembly Government, 2002; Rodwell *et al.*, 2017) (Rodwell and Welsh Gov) along with invertebrates, birds and mammals dependant on the habitat (Barnatt & Penny, 2004). This has resulted in a number of former mine sites being designated as Sites of Special Scientific Interest (SSSI) and Special Areas of Conservation (SAC) whilst others are found within local and national nature reserves (Welsh Assembly Government, 2002; Crane *et al.*, 2017). As a much

lower intensity, less intrusive method of resource extraction, in-situ recovery may be more applicable to mine sites with such designations assuming the recovery technique does not remove the conditions which the protected flora/fauna are reliant. I.e. despite not being as physically invasive, an in-situ technique to remove lead may be detrimental to lead tolerant fauna.

Along with ecological value, former mine sites have cultural heritage value. In areas which were historically dependant on the mining industry, local cultural identity is often intrinsically linked to the mining industry e.g. South Wales valleys (Llewellyn *et al.*, 2017). Due to this the waste piles, derelict buildings and processing machinery holds considerable heritage values on both a local and national scale (Howard *et al.*, 2015). This has resulted in sites being designated with official conservation statuses such as Landscape of Historic Interest, Scheduled Monuments and, as in the case of Cornwall and West Devon mining landscape, World Heritage Sites. These designations, and the properties that led to their implementation, also give the sites considerable value to education and research (Crane *et al.*, 2017). Again, the implementation of an in-situ leaching technique for resource recovery would allow the landscapes to remain relatively unaltered (compared with ex-situ technique) and would not require the removal of historical items such as derelict buildings from the site, thereby preserving the sites cultural heritage value.

While these represent potential advantages of the use of an in-situ resource recovery techniques, any implementation would still require either an economic or environmental protection/remediation driver.

1.3. Current uses of Biomining

Biomining is a generic term that describes the processing of metalliferous ores, and mining waste using microbiological techniques to facilitate the extraction of the metals from the ore (Rawlings & Johnson, 2007; Johnson, 2014). In the majority of cases this involves microbially induced dissolution of metal species, and other oxidation related processes, making them available for extraction. Biomining is becoming more widely practiced worldwide as demand for metal commodities increases and high-grade ore deposits are becoming scarcer. It is often applied for the extraction of gold, copper and

other base metals from low-grade ores, concentrates and mine wastes such as spoil and tailings. It is also considered to be a "green" or environmentally benign technology which possesses a low carbon footprint, as many of the microbes utilised in the process are autotrophs and so fix CO_2 (Brierley, 2008; Schippers *et al.*, 2010; Johnson, 2014).

There are 3 main forms of biomining; dump leaching, heap leaching and stirred-tank biooxidation, which are summarised in Table 1.1. The bio-oxidation process is not applicable to oxidised metalliferous wastes, leaving large quantities of potentially valuable metals remaining within these wastes. Whilst not as intensive as conventional chemical leaching of metals, many of these operations are often highly engineered and stringently controlled biomining systems, which utilise physical manipulation and strict management of environmental conditions to achieve metal extraction.

Table 1.1: Brief summary of main variants of oxidative biomining currently practiced

Biomining Type	Brief Description	Typical Target Metals	Example Operation	Refs
Dump Leaching	Large scale "dumps" of low grade ore often >50m in height. Sulphuric acid added to stimulate indigenous acidophilic bacteria to either directly oxidise iron or catalyse iron oxidation causing release of metal	Cu	Escondida, Chile	Brierley (2008); Soto *et al.* (2013)
Heap Leaching	A more refined version of dump leaching. Leach material is ground to fine particle sizes and placed into engineered mounds fitted with irrigation and aeration and dosed with inoculums of cultured iron oxidisers	Cu, Ni, Au	Skouriotissa, Cyprus	Johnson (2014); Brierley & Brierley (1999)
Stirred-Tank Biooxidation	Material is ground to fine size and placed into large tanks where it is constantly agitated, aerated, temperature controlled and supplied with inoculums of cultured iron & sulphur oxidisers. Used in for v. low concentration ores and concentrates due to high recovery rates	Co, Au	Fairview, S. Africa	Morin & D'Huges (2007); Brierley (2008); Batty & Rorke (2006)

1.4. Motivation

Despite in-situ bioleaching being commonplace for sulphidic wastes, and others susceptible to oxidation, it is essentially non-existent at an industrial scale for oxidised wastes. This has resulted in vast quantities of oxidised waste, and the metal value contained within them, being left un-exploited. Ribet *et al.* (1995) highlighted the quantity of metals that could potentially be garnered through re-processing of oxidised waste. Within the oxidised zone of waste repositories, from metal sulphide mines in Sudbury, Canada, it was found that >80% of Fe, Ni, Cu, Cr and Co were "potentially available for release" via the reductive dissolution of iron oxyhydroxides within the waste.

As a result of the large amounts of metal held within these wastes a number of studies have been conducted in an effort to extract these metals, many of these studies have been reviewed in detail within the literature review of this study (Sections 3.2 and 3.3). As will be outlined in the literature review, the majority of these studies have used physical and chemical manipulation of the wastes, specifically selected bacteria and stringent control of the environmental conditions to achieve the highest metal recovery rates possible. However, this level of control generally makes these technologies more expensive and impractical or uneconomic to implement at an industrial scale. They also, generally, require the wastes to be excavated, introducing further cost and potential environmental and human health risks to the operation. To access the metal value of oxidised wastes in an economically viable fashion, whilst the waste remains in-situ, a low-intensity, low-cost method of reductive dissolution is required.

This thesis was the result of two sources of inspiration. Firstly, the observation, by Dr Devin Sapsford, of an olive-green colouration within coal mine drainage ochre suggesting the presence of indigenous iron reducing communities. This led to discussions about the potential to utilise and exploit these communities which in turn made the author aware of the work of Lee *et al.* (2009). Their work demonstrated that, through the addition of glucose as an organic carbon source, indigenous bacteria could be stimulated. Which, in turn, mobilised significantly increased concentrations of arsenic from Au-Ag mine tailings. The work within this thesis focuses on the potential utilisation

of this phenomenon as a mechanism for the in-situ mobilisation and recovery of metals from iron-rich metalliferous wastes.

1.5. Aims of Thesis

The main aim of this thesis is to investigate the potential for resource extraction, primarily metals of economic significance, via the stimulation of indigenous iron-reducing microbial communities. Within this larger aim there are a number of secondary objectives:

- To identify a range of wastes, with significant concentrations of metals of economic interest, which may be targets for bio-reductive dissolution of iron for resource recovery.
- Establish whether microbial communities indigenous to these wastes, can be stimulated whilst in-situ by the application of an organic carbon source to the wastes.
- Determine whether any metals will be released from iron oxyhydroxides, as a result of iron reduction. And whether they will remain in solution and are thereby extractable via the aqueous phase.
- Record any changes in the chemical properties of the waste, beyond metal concentration/ mobility, resultant from the stimulation of indigenous microbial communities.
- Determine the fate of metals not extractable via the aqueous phase. Establish whether these metals may be sequestered into secondary minerals and whether this facilitates alternative extraction methodologies.
- Record any changes into the composition of indigenous microbial communities as a result of bioreduction.

1.6. Organisation of Thesis

Chapter 2: Describes microbial reduction of iron via both direct microbial iron reduction and indirect reduction by the activity of sulphate reducing bacteria. Also discussed are a range of naturally occurring analogues in which iron reduction has resulted in the mobilisation of metals into an aqueous phase.

Chapter 3: Describes the generation and typical physicochemical characteristic of a range of iron oxyhydroxide rich wastes from both mining and metallurgical scenarios. An overview of studies into the recovery of metals from these wastes by both chemical and microbial means is also presented.

Chapter 4: Describes the mechanisms by which ferrous iron is oxidised by either chemical or microbially mediated reactions. The nature and properties of iron oxide minerals formed as a result of ferrous iron oxidation is also described along with the mechanisms by which metals of interest may become associated with them.

Chapter 5: Details the methods used for the characterisation of the solid waste samples, analysis of experimental column effluent samples and microbial community analysis.

Chapter 6: Presents information on the case study sites used within this study including the location, geology and history of the sites. Also detailed are the methods by which each sample was procured

Chapter 7: Presents the results of the physical, geochemical and mineralogical characterisation of the case study waste samples.

Chapter 8: Presents the experimental design and subsequent results of first phase of column testing. This phase of testing investigated and discussed the potential for stimulating indigenous iron reducing communities within a range of waste types.

Chapter 9: Presents the experimental design and subsequent results of second phase of column testing providing a more comprehensive investigation of the waste from the

Parys Mt. 2 case study site. Includes results and discussion of both the geochemical and microbial aspects of experimentation including detailed analysis of the impact of experimentation on the structure of the indigenous microbial community.

Chapter 10: Presents the experimental design and subsequent results of the post-bioreduction leaching of the Parys Mt. 2 wastes with a range of extractants.

Chapter 11: Discusses the efficacy of the work carried out within this study along with considerations into the potential implementation of the research findings at increased scale, and limitations which may inhibit such an implimentation.

Chapter 12: Presents the conclusions and recommendations for future work arising from this study.

2. Microbial Reduction of Fe(III)

2.1. Introduction

This chapter briefly discusses microbial reduction of ferric iron in terms of both direct reduction via dissimilative iron reducing microbes and indirect reduction via the action of sulphate reducing bacteria. Also described are examples of the exploitation of iron-reduction for the purposes of remediation of both organic and metallic contaminants. Particular attention is given to examples of iron reduction in natural environments giving rise to the mobilisation of metals as these are taken as examples of natural analogues relevant to this study

Section 2.2: Dissimilative Iron-Reducing Microbes – Gives a brief description of direct iron reduction by dissimilative iron reducing microbes and the mechanisms by which it is achieved. Also covered are examples of the use of microbially mediated iron reduction for organic and metallic contamination.

Section 2.3: Dissimilative Sulphate-Reducing Microbes – Gives a brief description of indirect iron reduction by the activity of sulphate reducing bacteria. Also covered is the reduction of ferric hydroxysulphates.

Section 2.4: Metal Mobilisation from Iron-Reduction Case Studies – Outlines a number of situations where naturally occurring iron reduction has resulted in the mobilisation of arsenic and mercury.

Section 2.5: Chapter Summary

2.2. Dissimilative Iron-Reducing Microbes

Lovley (2013) defined dissimilatory iron reduction as “the process in which microorganisms transfer electrons to external ferric iron, reducing it to ferrous iron without assimilating the iron”.

A wide range of microorganisms have been shown to be capable of ferric iron reduction enzymatically via fermentation of organics or as indirect result of sulphate reduction Lovley (2013). However, microbes that reduce iron this way do not conserve energy from doing so. A list of organisms known to reduce iron but not conserve energy has been compiled by Lovley (2013). Dissimilative iron reducing microbes (DIRM), by comparison, do garner energy from iron reduction. This is achieved by coupling the oxidation of organic matter to the reduction of ferric iron as shown in Equation 2.1. A model for the oxidation and degradation of organic matter, coupled to dissimilatory iron reduction, in sedimentary environments is displayed in Figure 2.1 (Lovley, 1991; Lovley, 2013).

Equation 2.1

$$(\boldsymbol{Glycerol})\ \boldsymbol{C_3H_8O_3} + \boldsymbol{14Fe^{3+}} + \boldsymbol{6H_2O} \rightarrow \boldsymbol{3HCO_3^-} + \boldsymbol{14Fe^{2+}} + \boldsymbol{17H^+}$$

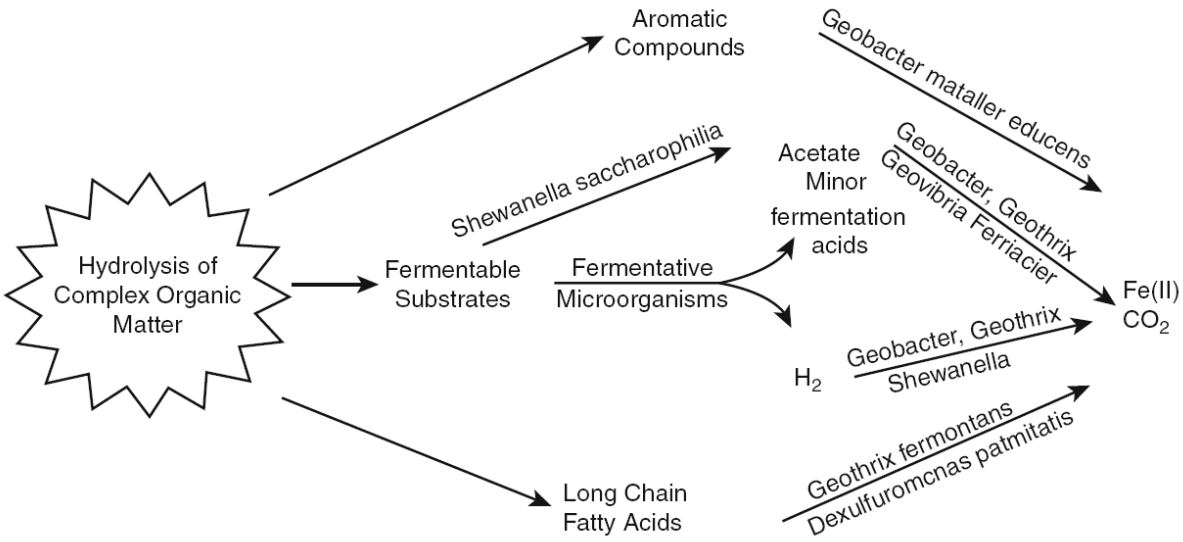

Figure 2.1: Model for the oxidation of complex organic matter coupled with ferric iron reduction (Lovley, 2013)

The dissimilatory reduction of Fe(III) and Mn(IV) (many DIRM can also reduce Mn(IV))) is an important process within sediments for the cycling and distribution of iron in the environment, as well as the degradation of organic matter. This is in part due to DIRM being able to outcompete sulphate reducers and methanogens for organic electron donors (Lovley & Phillips, 1987). Though this has only been proven when poorly crystalline iron oxyhydroxides, i.e. ferrihydrite, are present (Canfield *et al.*, 2005). This

has the added effect that sulphide and methane generation may be suppressed in sediments where DIRM are dominant.

DIRM are phylogenetically diverse (Figure 2.2). Bacterial genera include *Proteobacteria*, *Acidobacteria*, *Deferribacteres* and *Firmicutes*. Achaeal genera are found within the phylum *Crenarchaeota* (Lonergan *et al.*, 1996). Most dissimilative iron reducing bacteria (DIRM) are obligate anaerobes, though some genera such as *Shewanella* are facultive aerobes. DIRM are most commonly found in anoxic freshwater and marine sediments but have been identified in a number of more extreme environments. The bacterium *Geobacter* have been identified in pristine, deep subsurface aquifers. Others have been observed in hydrocarbon contaminated aquifers, utilising the aromatic hydrocarbons as an electron donor. Known DIRMs also include thermophilic, hyperthermophilic and acidophilic strains (Bridge & Johnson, 1998; Madigan *et al.*, 2015).

Scientific interest in DIRM has been increasing since the 1990's. Iron reducers became the focus of much debate when it was theorised that iron reduction represented one of the earliest, if not the first, form of microbial respiration potentially responsible for the formation of Pre-Cambrian banded iron formations (Walker, 1987; Vargas *et al.*, 1998; Weber *et al.*, 2006). Research has also been conducted into the potential utilisation of DIRM for the remediation of both organic and metallic contaminants within soils and aquifers and the mobilisation and ex-situ recovery of metals from metalliferous wastes.

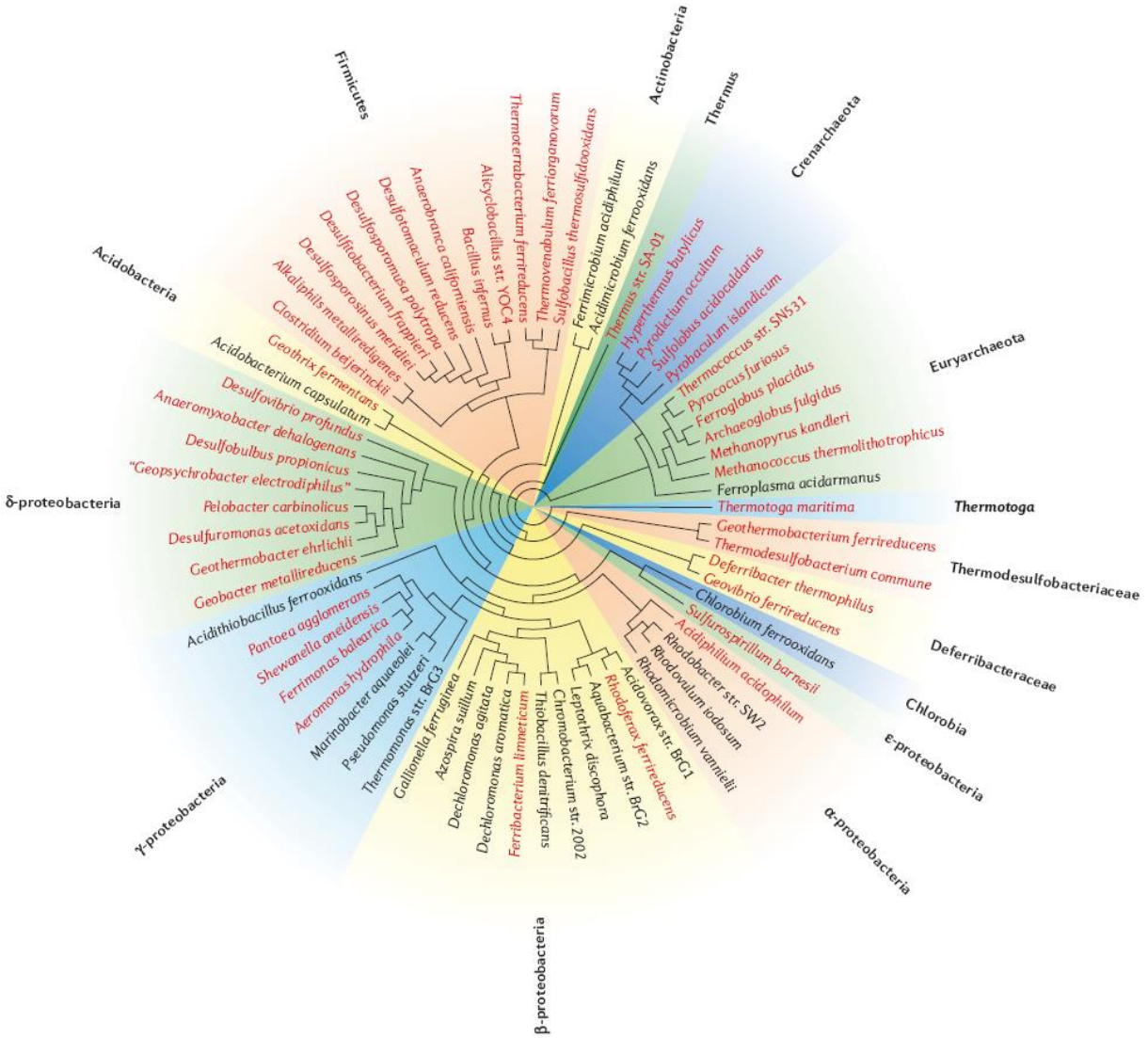

Figure 2.2: Unrooted phylogenetic tree of microorganisms known to contribute to iron redox cycling. Iron reducers are shown in red. Iron oxidisers are shown in black (Weber *et al.*, 2006)

2.2.1. Organics Remediation

When organic contaminants, e.g. petroleum, are released into the environment it typically results in anoxic conditions developing. Within these conditions Fe(III) is usually the most abundant electron accepter to couple with organic matter oxidation, leading to microbial iron reduction as iron reducing bacteria will typically out-compete sulphate-reducers or methanogens for the organic matter (Lovley & Phillips, 1987). A number of studies have observed that certain iron-reducing bacteria are capable of using aromatic hydrocarbons such as phenols, p-cresols (Lovley & Lonergan, 1990), benzene, naphthalene (Anderson & Lovley, 2010) and other BTEX (benzene, toluene, ethylbenzene and xylene) and petroleum compounds (Lovley, 1997) as an electron donor thereby oxidising, and degrading, them whilst reducing ferric iron. There is also evidence that microbial iron reduction can indirectly, and non-enzymatically, reduce poly-nitroaromatic compounds including 4-chloronitrobenzene (Heijman *et al.*, 1993) and 2, 4, 6-trinitrotoluene, better known as the explosive TNT (Hofstetter *et al.*, 1999).

The ability of some DIRM to reduce and dehalogenate chlorinated compounds has recently received increased interest. In some instances this is via direct reduction of the chlorinated compounds, whilst in other cases the reduction is a result of Fe(II) produced by or associated with the DIRM are responsible for the reduction. Compounds susceptible to reduction and dehalogenation by these mechanisms include, amongst others,; 1,1,1-trichloro-2,2-bis(p-chlorophenyl)-ethane (DDT) (Li *et al.*, 2010), tetrachloroethylene (PCE) (Krumholz *et al.*, 1996), trichloroethylene (TCE) (Shin *et al.*, 2007), 2-chlorophenol (He & Sanford, 2003), carbon tetrachloride (Li *et al.*, 2009b), chloroform and pentachlorophenol (PCP) (Li *et al.*, 2009a; Xu *et al.*, 2014).

2.2.2. Metal Remediation

Many DIRM are capable of utilizing metals other than iron as a terminal electron acceptor. The most common metal to be substituted for iron in these reactions is manganese with most DIRM being capable of direct reduction of Mn(IV) to Mn(II). Some DIRM have also developed the ability to reduce other metals. Depending on the oxidation state of the metallic element after bioreduction this can cause the metal to either become more soluble or precipitate out of solution due to a drop in solubility. The

latter case has been investigated as a potential mechanism for the remediation of metal contaminated waters. Bioreduction of the following metals/metalloids by iron reducers has been observed:

- uranium
- technetium
- molybdenum
- cobalt
- silver
- copper
- chromium
- vanadium
- lead
- gold
- mercury

Detailed reviews of the reaction mechanisms controlling the bioreduction of these metals/metalloids, and the resulting impacts on the environment and ecology of the area, can be found within Lovley (1993) and Lovley (1995).

2.3. Dissimilative Sulphate-Reducing Microbes

Like DIRM, dissimilative sulphate reducing microbes (DSRM) are anaerobes that garner energy by coupling the oxidation of organic carbon with the reduction of sulphate to sulphide. The sulphide generated typically takes the form of hydrogen sulphide (H_2S) as shown in Equation 2.2 (Madigan *et al.*, 2015).

Equation 2.2

$$4C_3H_8O_3 + 7SO_4^{2-} + 14H^+ \rightarrow 12CO_2 + 7H_2S + 16H_2O$$

It is often asserted that DIRM will outcompete DSRM for the oxidation of organic carbon in natural anaerobic environments. However, this is an oversimplification. Lovley & Phillips (1987) observed that the introduction of synthetic, amorphous iron oxyhydroxides to a system dominated by sulphate reduction caused a decline in sulphate reduction of between 86 and 100%. This demonstrated the ability of DIRM to outcompete DSRM for access to organic carbon. The balance between iron and sulphate reduction is, however, more complex and is affected by the pH of the system. This is because the reduction potential and hence the energy garnered by microbes of iron oxyhydroxides increase by 59 mV for each pH unit decrease towards acidic conditions.

This results in the reduction of crystalline iron oxyhydroxides being far more energetically favourable in acidic conditions than at neutral conditions. Equally, it results in the reduction of iron oxyhydroxides, including crystalline iron oxyhydroxides, being more energetically favourable then sulphate reduction in acidic environments (Kostka & Nealson, 1995; Postma & Jacobson, 1996; Thamdrup, 2000). At neutral conditions, the energy garnered by the microbial reduction of the crystalline iron oxyhydroxides, as shown in Figure 2.3, is greatly diminished compared with their reduction under acidic conditions (Thamdrup, 2000). This results in only ferrihydrite and other amorphous iron oxyhydroxides such as lepidocrocite (γ-FeOOH) being more energetically favourable to reduce compared with sulphate reduction. This demonstrates that any shift in the pH of an environment, or the form that the iron oxyhydroxides are present in, has a significant bearing on whether iron or sulphate reduction occurs. It is often observed that both processes are occurring concurrently, particularly when iron oxyhydroxides are limited and electron donors are in excess (Bethke *et al.*, 2008). To distinguish which of the two processes is dominant further analysis is often required as described by Chapelle *et al.* (2009).

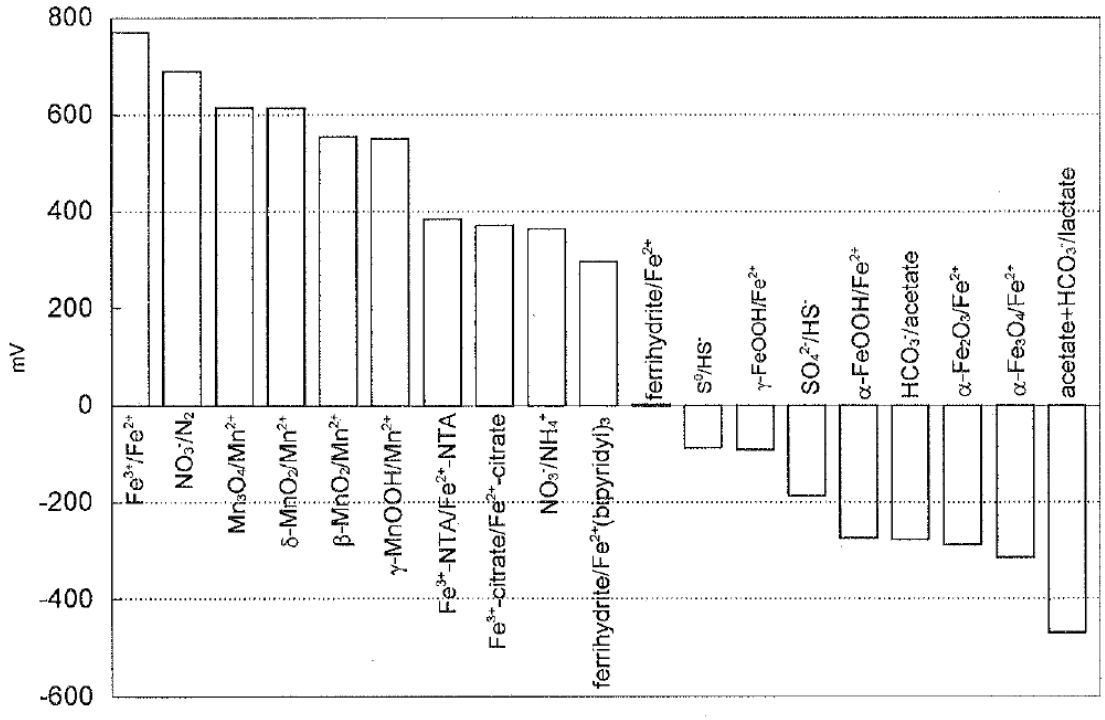

Figure 2.3 Standard redox potential of a range of redox couples typically found in a sedimentary environment. Redox potentials representative of pH =7 and Temperature 25°C. (Thamdrup (2000) and references within)

To take advantage of the greater energy to be gained by reducing ferric iron in acidic conditions some sulphate reducers have evolved the capability to reduce both ferric iron and sulphate. A number of genera capable of this were identified in mine dumps by Schippers *et al.* (2010) including *Desulfobacter*, *Desulfobacterium*, *Desulfobulbus*, *Desulfitomaculum* and *Desulfovibrio*. Other known examples include numerous strains of *Desulfosporosinus* (Spring & Rosenzweig, 2006).

2.3.1. Indirect Reduction of Ferric Iron Oxyhydroxides

Iron oxyhydroxides are effective reagents for the oxidation of H_2S produced by sulphate reduction with a theoretical maximum of 0.6g H_2S/ 1g Fe_2O_3. Furthermore, the iron oxyhydroxides can be regenerated via the introduction of air allowing their repeated use. This has resulted in this system being widely used to remove H_2S from natural gas, industrial processing gases and waste gases (Kohl & Nielsen, 1997; Davydov *et al.*, 1998). The precise stoichiometry of the reaction between H_2S and iron oxyhydroxides is complex though can be summarised by the reaction presented in Equation 2.3. The Fe_2S_3 produced is typically unstable and decomposes to form FeS_2 (pyrite) and Fe_3S_4 (greigite) as shown in Equation 2.4. While these minerals represent the endpoint of the sulphide/ferric iron reaction series, often this point is not reached and iron monosulphides, such as mackinawite or acid-volatile sulphides (AVS) are often formed in anaerobic aqueous environments (Rickard & Morse, 2005).

Equation 2.3

$$2Fe(OH)_3 + 3H_2S \rightarrow Fe_2S_3 + 6H_2O$$

Equation 2.4

$$2Fe_2S_3 \rightarrow FeS_2 + Fe_3S_4$$

These reactions result in the reductive decomposition of the iron oxyhydroxides, potentially releasing any associated metals to the aqueous phase as with biogenic reduction by DIRM. Significantly, biogenic H_2S has been observed to be capable of

reducing the more crystalline iron oxides, such as haematite and magnetite, not readily microbially reduced at circum neutral pH's (Li *et al.*, 2006). However, the chemical reduction of the iron oxyhydroxides can result in the inhibition of DIRM (Koretsky *et al.*, 2003). This coupled with the production of sulphides, which may sequester metals to the solid phase, makes DSRM the less favourable of the two processes with regards to resource recovery.

2.3.2. Reduction of Ferric Hydroxysulphates

The ferric hydroxysulphates jarosite ($KFe^{3+}_3(OH)_6(SO_4)_2$) and schwertmannite ($Fe_{16}O_{16}(OH)_y(SO_4)_z \cdot nH_2O$) are common minerals in environments where iron sulphides are oxidised generating acid rock drainage. At higher pH jarosites and schwertmannite are unstable and will decompose to more stable ferric oxides such as goethite (Bigham *et al.*, 1996; Bigham & Nordstrom, 2000). The presence of both ferric iron and sulphate in the structure of these minerals presents two potential electron acceptors for microbial reduction. The lack of stability of these minerals at circum-neutral conditions, and the higher energy garnered from iron reduction under acidic pH's, results in iron generally being the more favourable target for reduction. This is reflected in the literature. The reductive dissolution of iron hydroxysulphates is not as well studied as the reduction of iron oxyhydroxides. What research there is has generally focused on the reduction of iron within the mineral structure (Jones *et al.*, 2006; Smeaton *et al.*, 2012; Castro *et al.*, 2013; Bingjie *et al.*, 2014).

There is a far smaller pool of research concerning the reduction of structural sulphate within jarosite. Invarson & Hallberg (1976) and Invarson *et al.* (1976) demonstrated the reductive dissolution of jarosite by a sulphate reducing bacteria, *Desulfovibrio desulfifuricans*. Gramp *et al.* (2009) investigated structural sulphate reduction on biogenic jarosite and schwertmannite by utilising the iron oxidiser *Acidithiobacillus ferroxidans* to precipitate these minerals. These were then used as electron accepters, coupled with lactate as an electron donor, for a mixed culture of sulphate reducing bacteria under circumneutral conditions and at a range of temperatures. The mixed cultures of sulphate reducers were enriched from acid mine drainage and a municipal sewage sludge compost pile. At a temperature of 60˚C it was observed that greigite had

formed as a result of the reduction of both schwertmannite and jarosite. It was observed that a greater degree of reduction had occurred in the schwertmannite, indicated by greater abundance of greigite. This was attributed to jarosite being a more crystalline, and therefore more stable, mineral relative to schwertmannite.

As with the indirect reduction of iron oxyhydroxides by H_2S; direct reduction of structural sulphate in ferric hydroxysulphates is less desirable from a metal mobilisation viewpoint than ferric iron reduction. This is again because of the generation of H_2S, the lack of iron release, formation of iron monosulphides and the potential for metals of interest to be held in the solid phase as secondary metal sulphides as opposed to being extractable in the aqueous phase (Jones *et al.*, 2006).

2.4. Metal Mobilisation from Iron Reduction Case Studies

While some metals have been seen to be stabilised via microbial reduction others have been observed to be mobilised, due to their release from iron oxyhydroxides after microbial reduction. Studies documenting naturally occurring instances of metal mobilisation as a result of reductive dissolution of iron oxyhydroxides by DIRM have largely focused on the resultant issues regarding human health and environmental impact. As a result, most documented cases are of the release of highly toxic metals and metalloids such as arsenic and mercury rather than metals targeted for their economic value.

2.4.1. Arsenic Mobilisation

This chapter summarizes a number of instances where the dissimilatory reduction of iron oxyhydroxides is known to be, or believed to be, responsible for the mobilisation of arsenic within natural groundwaters. One of the best documented examples of this is the arsenic contamination of drinking water in Bangladesh and West Bengal. This occurrence has received significant research focus, and wider public attention, due to the devastating impact it has had on the health of the people reliant on the drinking water.

A survey by the British Geological Society and the Bangladeshi Public Health Department showed that 27% of shallow wells (<150m) had arsenic concentrations in excess of 50 µg/l, the upper permissible limit set by the World Health Organisation (BGS & DPHE, 2001). This has resulted in an estimated 30-35 million Bangladeshi's and 6 million people in West Bengal being exposed to >50 µg/l arsenic in their drinking water (Smedley & Kinniburgh, 2002; Joseph *et al.*, 2015). Arsenic is known to be naturally mobilised, from iron oxyhydroxide-bearing sediments, into groundwaters in Bangladesh and West Bengal. The most widely accepted theory is that dissimilatory reduction of iron oxyhydroxides leads to the release of adsorbed and/or coprecipitated arsenic to the groundwater (Nickson *et al.*, 1998; McArthur *et al.*, 2001; Dowling *et al.*, 2002; Harvey *et al.*, 2002; Islam *et al.*, 2004).

Correlations have been observed between ferrous iron and arsenic concentrations in solution in a number of locations in West Bengal (Figure 2.4). A weak correlation between iron and bicarbonate concentrations points towards the presence of iron reducing microbes being active within the subsurface (Nickson *et al.*, 2000). Akai *et al.* (2004) found that little As was associated with carbonates, therefore release of arsenic via the dissolution of carbonates cannot be responsible for this correlation.

Islam *et al.* (2004) observed that when acetate, an electron donating proxy for organic matter, was introduced to samples of sediment from areas of arsenic-rich groundwater a "marked stimulation in the rate of Fe(III) reduction followed by arsenic release" occurred. This demonstrated that arsenic release as a result of iron oxyhydroxide reduction was possible and that the system relied on the presence of an organic carbon electron donor to proceed, strongly suggesting microbial activity. Control experiments with autoclaved samples confirmed the role of micro-organisms in the system as Fe(II), As(V) and As(III)remained constant. The results of DNA extraction and PCR analysis showed that the untreated sediment was microbially diverse. Within the sediment there were a large range of reducing microbes, largely from the *Geobacter* genus in the *Deltaproteobacteria* class, form 11% of DNA clones. 9% of clones were associated with the *Clostridium* species, which are able to reduce some metals/metalloids, including As(V), via the fermentation of organic material. The sediment "stimulated" with acetate showed a significant change in microbial diversity with 70% of clones affiliated with the *Geobacteraceae* family, known to be Fe-reducers. These findings were verified by

performing most probable number (MPN) counts, which also showed a significant increase in Fe-reducing bacteria within the acetate stimulated sediment compared with the untreated sediment (Islam *et al.*, 2004).

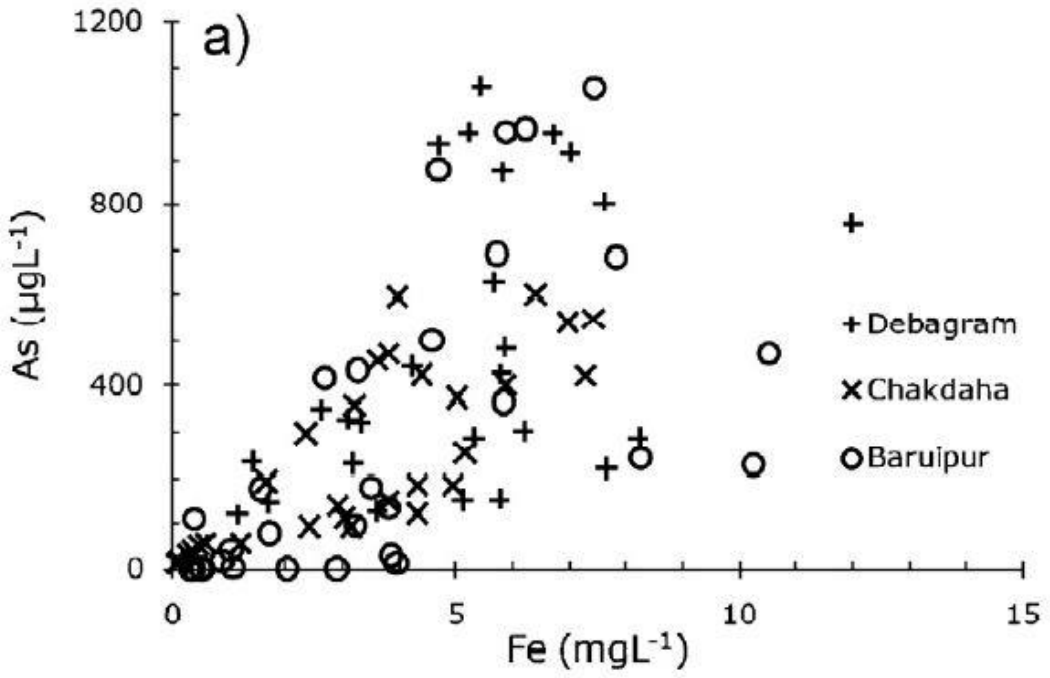

Figure 2.4. Correlation between arsenic and iron in groundwater taken from 3 areas within West Bengal (Bhowmick *et al.*, 2013)

Yadav *et al.* (2015) concluded that microbially mediated reductive dissolution of iron oxyhydroxides was responsible for release of arsenic to groundwater in the Terai region of Nepal. A correlation was observed between Fe(II) and As within groundwater, which along with a high level of HCO_3^- suggests reductive dissolution as the release mechanism. A high concentration of Fe_2O_3 within sediment is also indicative if this process. Pyrite oxidation as a mechanism for release was ruled out as As, Fe and SO_4^{2-} correlate poorly and there is generally a lack of pyrite within sediment samples from the Ganges delta (Das *et al.*, 1996).

Microbial dissolution of iron oxyhydroxides is also responsible for arsenic release to groundwater within the Mekong delta, Vietnam and Cambodia. Polizzotto *et al.* (2008) observed groundwater arsenic concentrations in excess of 1000 μg/L with average concentrations within the aquifer of 500 μg/L. Successive monsoonal events result in

the rapid burial of organic material along with iron oxyhydroxide minerals. This provides a near constant supply of electron accepters and donors for dissimilative iron reducing microbes to utilise (Kocar *et al.*, 2008; Quicksall *et al.*, 2008).

Along with the examples described within South East Asia, a number of arsenic mobilisation case studies are documented within North America. Cummings *et al.* (1999) conducted a study into the effect of dissimilatory iron reduction on the solubility of arsenic sorbed to hydrous ferric oxides (HFO). A known dissimilatory iron-reducing bacteria strain, *Shewanella alga* BrY, was used to reduce HFOs within lake sediments, which have been subject to "extensive contamination" from nearby mining activity in Silver Valley, Idaho, U.S.A. The arsenic sorbed to the HFO, pre-reduction, was found to exist solely as arsenate (As(V)). Arsenate is less toxic and less soluble than arsenite (As(III)). Samples of contaminated lake sediments, inoculated with *Shewanella alga* BrY, showed dissolved As(V) concentrations increased with increasing ferrous iron concentrations. Microbe-free controls showed no increase in the soluble fractions of either of these elements demonstrating unequivocally that the dissimilatory iron-reducing bacteria was responsible for the increased concentrations of soluble arsenic. Arsenite remained undetectable throughout all the experiments ruling out the possibility that the increase in soluble arsenic is attributable to the reduction of arsenate to the more soluble arsenite. This demonstrated that the increase in soluble arsenic can be attributed to desorption of arsenic, as a result of the reduction of HFO, rather than due to changes to the arsenic itself.

Matisoff *et al.* (1982) and Moore *et al.* (1988) observed coeval release of iron and arsenic to groundwaters within Ohio and W. Montana respectively. Both attributed this release to the reductive dissolution of iron oxyhydroxides, however neither paper identified the role of iron-reducing microbes as their significance in nature had yet to be determined.

2.4.2. Mercury Mobilisation

The mobilisation and transport of other toxic and environmentally hazardous metals, such as mercury, have also been subject to recent interest. Bioreduction of iron oxyhydroxides has also been shown to release mercury within tropical oxisols, in French-

Guyana, near the surface as well as subsurface environments (Harris-Hellal *et al.*, 2010). These studies are relatively rare in that indigenous bacteria, cultured from mercury contaminated "site-water" and soils respectively, were utilised rather than introducing non-native inoculated cultures. The methylation and leaching of mercury from iron-rich aquifer sediment has been proven to directly correlate to bacterial iron reduction and Fe(II) release within anoxic column tests. This study also observed sulphate reducing bacteria indirectly reducing iron oxyhydroxides which in turn led to the release of mercury (Hellal *et al.*, 2015).

Lamborg *et al.* (2013) observed a progressive release of mercury to groundwater, in Cape Cod, USA, during dissimilatory iron reduction suggesting release of mercury as a result of iron dissolution. Along with its release, the reduction of Hg(II) to Hg(0) was also noted. The correlation between Hg(0) and Fe(II) in solution is shown in Figure 2.5. Hg(II) complexed in the form of methylmercury (CH_3Hg^+) showed to be particularly susceptible to reduction within the zone of iron reduction. The reduction of methylated mercury suggests that a large number of Fe-reducing *Deltaproteobacteria* strains (e.g. *Geobacter metallireducens* GS-15) could be present in the system as they are known Hg methylators. Non-*Deltaproteobacteria* (e.g. *Shewanella*) are not known to be capable of methylate Hg so may be responsible for the observed iron reduction (Kerin *et al.*, 2006).

Lamborg *et al.* (2013) concluded that a combination abiotic and biotic processes are likely responsible for the mobilisation and reduction of mercury at Cape Cod. As well as mercury being released from iron oxyhydroxides by microbially driven reductive dissolution, it may also be being released from complexed organic matter upon oxidation of the organic carbon. A number of dissimilatory iron-reducing bacteria have been seen to reduce Hg(II) (Wiatrowski *et al.*, 2006), making it possible that rather than being released as a result of iron reduction, the mercury is being mobilised due to direct reduction to Hg(0). Fe(II) is a known reducing agent and is capable of reducing Hg(II) to Hg^0 abiotically, with rates fast enough to account for the Hg(0) concentrations observed in the study (Charlet *et al.*, 2002; Amirbahman *et al.*, 2013). Whilst this mechanism is abiotic it is likely that a significant proportion of Fe(II) was produced as a result of dissimilative iron-reducing microbial action.

Other examples of mercury mobilisation in the USA include studies by Barringer *et al.* (2006) and Johannesson & Neumann (2013) into mercury mobility in the Kirkwood-Cohassey aquifer, New Jersey, and Carrizo Sand aquifer Texas respectively.

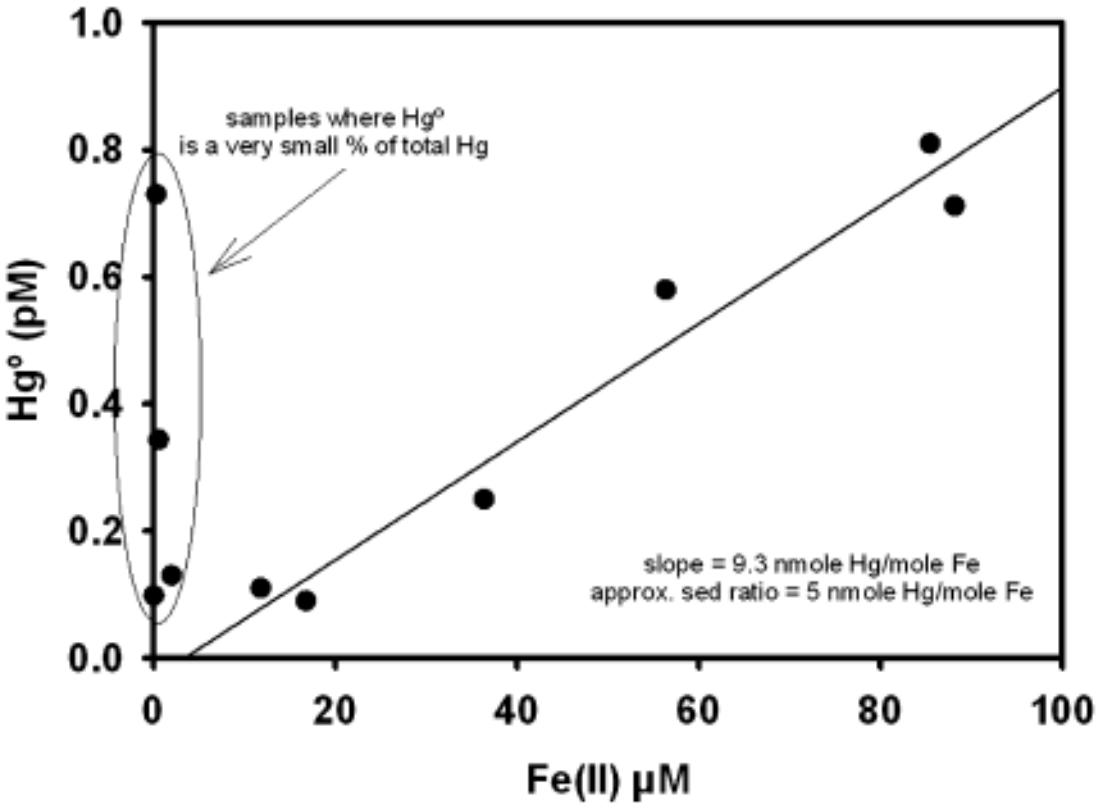

Figure 2.5. Correlation between dissolved Hg^0 and dissolved Fe(II) in a contaminated groundwater plume, Cape Cod, USA (Lamborg *et al.*, 2013)

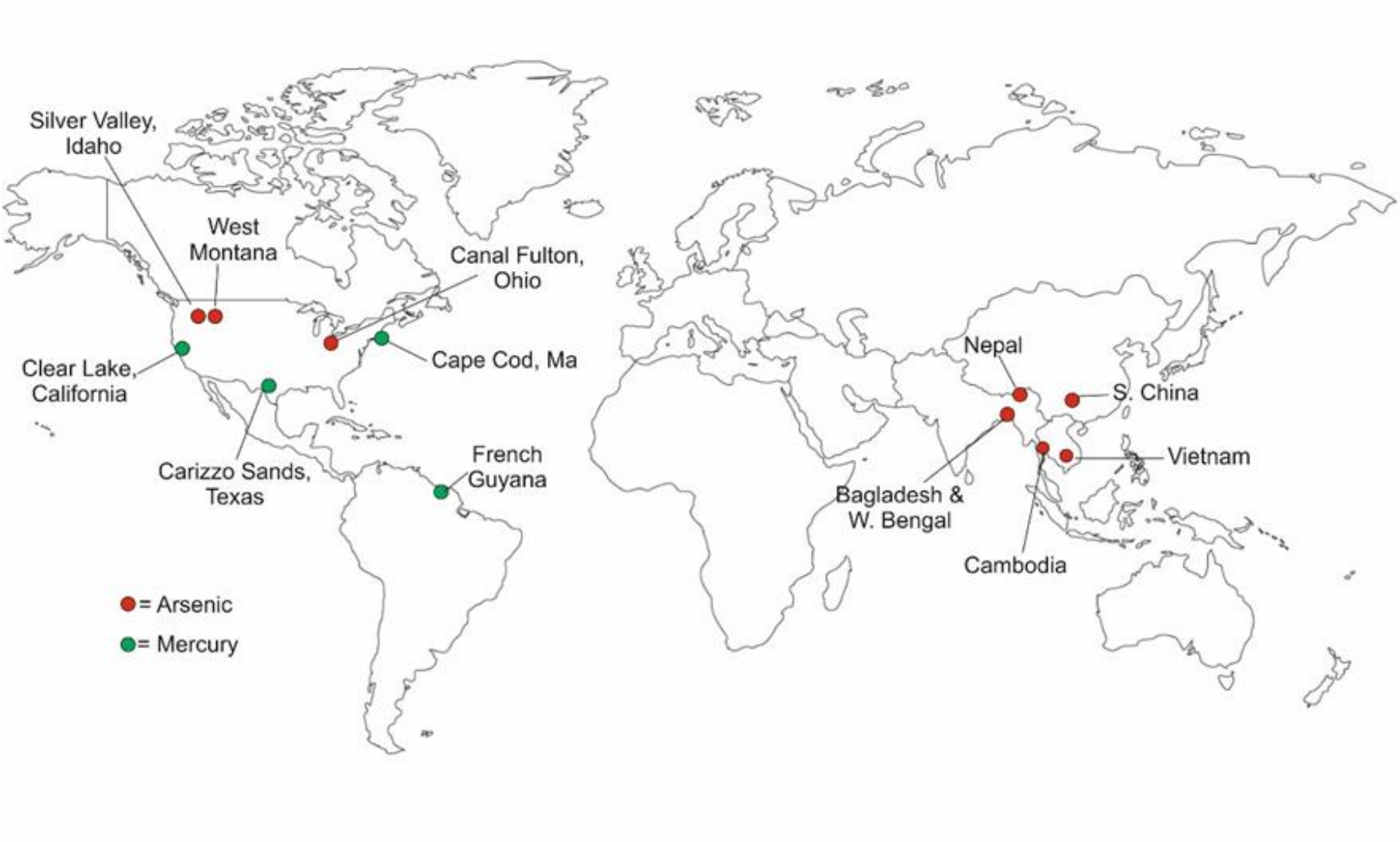

Figure 2.6: Locations of aquifers contaminated with arsenic or mercury as a result of DIRM activity

2.5. Chapter Summary

Chapter 2 has reviewed, and summarised, the literature concerning the microbial reduction of ferric iron. Both direct and indirect reduction were reviewed and a number of naturally occurring analogues of iron-reduction causing the mobilisation of metals were outlined. The key points of the chapter can be summarised as follows:

- Dissimilative iron reduction is the process by which microbes couple the oxidation of organic matter to the reduction of ferric iron, via electron transfer, without assimilating the iron. The transference of electrons to the ferric iron causes its reduction to ferrous iron.

- Dissimilative iron reducing microbes (DIRM) are phylogenetically diverse with examples found within the *Proteobacteria*, *Acidobacteria* and *Firmicute* phyla.

- Where amorphous iron oxyhydroxides are present, DIRM will out compete sulphate reducing microbes for the use of organic carbon electron donors. However, this relationship is pH dependant and under circum-neutral conditions sulphate reduction may be more energetically favourable compared with the reduction of more crystalline iron oxyhydroxides.

- The metabolism of DIRM have been previously exploited for the remediation of soils contaminated with organic contaminants such as BTEX and chlorinated compounds.

- DIRM have also been exploited for metal remediation due to their ability to reduce metals other than iron such as Mn, Cr, V and U. This has allowed the mobilisation and removal of certain contaminants and the precipitation/ stabilisation of others.

- Naturally occurring examples of DIRM activity resulting in the mobilisation and release of metals include arsenic release in Bangladesh and mercury release in French Guyana.

3. Fe-Rich Oxidised Sludges

3.1. Introduction

This chapter gives an overview of the key information regarding a range of oxidised iron-bearing wastes. For each wastes discussed, the mechanisms of waste generation and their typical physicochemical properties are outlined along with a review of literature concerning the recovery of metals of economic interest. Both abiotic and microbially mediated recovery methods are covered but, given the relevance to this study, preference is given to recover methods which have utilised dissimilative iron reducing microbes.

Section 3.2: Tailings and Mine Water Treatment Sludge's – Presents an overview of iron oxide rich wastes produced from the processing of extracted ore material or the treatment of metalliferous mine waters.

Section 3.3: Red Muds – Presents an overview of Red Mud generated during the production of aluminium. Particular focus is given to this waste due to the scale of environmental risk is poses, the potential metal value contained within stored wastes and the extensive research that has been afforded to it.

Section 3.4: Chapter Summary

3.2. Tailings and Mine Water Treatment Sludges

3.2.1. Generation

Mine water discharges occur when groundwater “rebounds” after the active pumping of water from a mine has ceased. Many mines required dewatering as the mineral lode extended below the water table and without pumping the mine shaft would flood. The UK has long history of mining, with evidence for copper mining stretching as far back as the Bronze Age (~4000 years ago) and large-scale mining emerging during the period of Roman occupation of Britain (Johnson *et al.*, 2008). Base metal e.g. lead, copper and zinc and coal mining have been particularly prevalent in the UK and reached a peak during

the UKs industrial revolution. Indeed many of the country's great industrial cities and towns owe their existence either directly to mining or indirectly through exporting or industry associated with the mines.

The extent of historical mining within England and Wales can been seen in Figure 3.1. Given the wide geographical dispersal of mining areas, it is inevitable that mines are located within areas of contrasting geological environments to each other. The relative geological conditions give each mine, or group of mines a set of characteristic traits. The mines in the north of England are largely found in carbonates which results in circum-neutral, or occasionally alkaline, mine drainage being produced from them which are iron-deficient by nature. Conversely the mines within Devon and Cornwall and those in North Wales are primarily sulphidic ore bodies, with no associated carbonates, and as such generate acidic mine drainage (AMD) (Hudson-Edwards *et al.*, 2008). Former coal mines also have the potential to produce metalliferous mine waters due to sulphides within the coal bearing cyclothems. Many of these mine waters have circum-neutral pH due to the acid buffering capacity of carbonate rocks that generally accompany coal deposits.

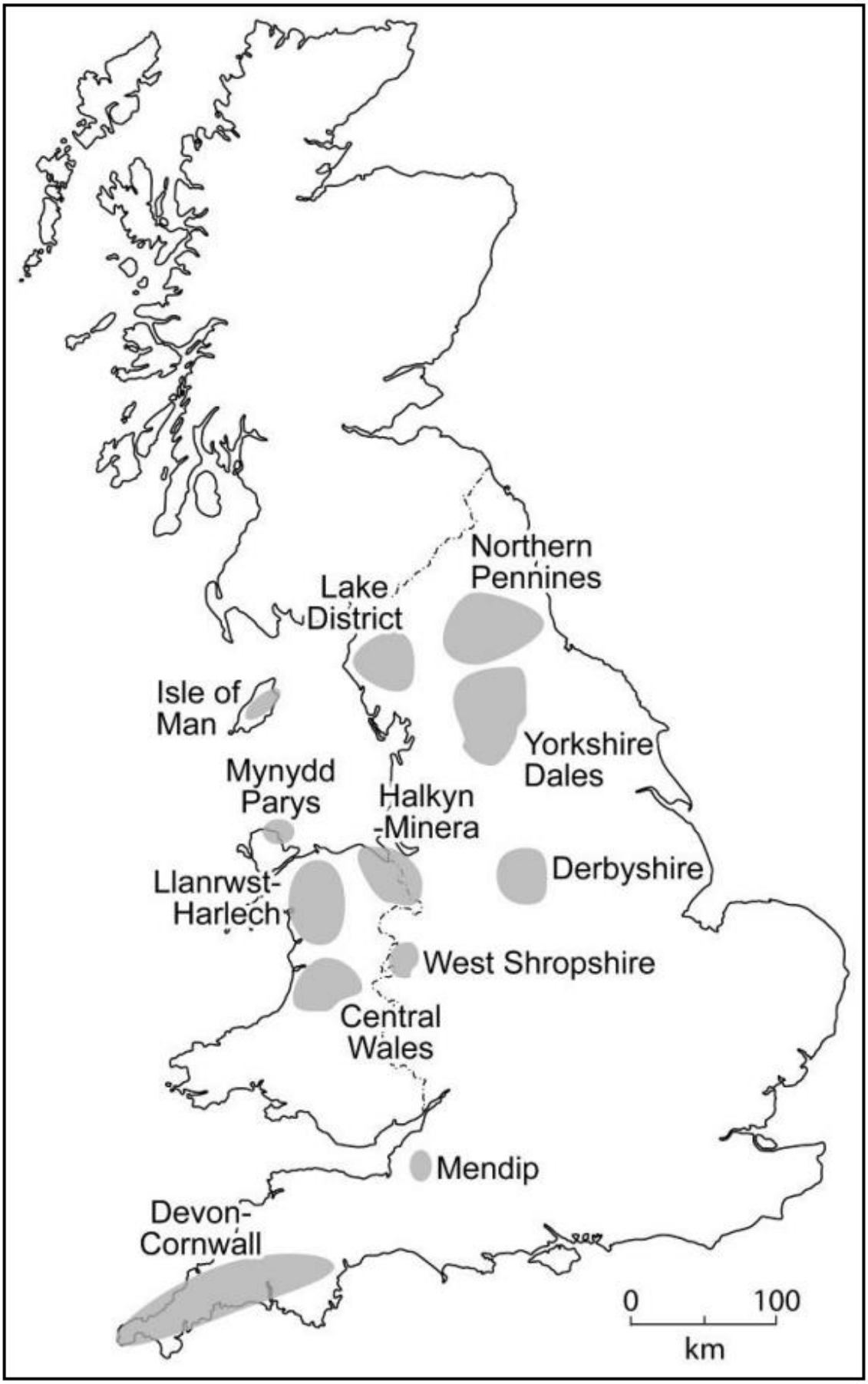

Figure 3.1. Regions of metal mining within England and Wales. (Hudson-Edwards *et al.* (2008) after Dunham *et al*. (1978) and Lewin and Macklin (1987))**.** Regions of metal mining within England and Wales. (Hudson-Edwards *et al.* (2008) after Dunham *et al*. (1978) and Lewin and Macklin (1987))

The acidity, and high iron concentrations, in AMD is derived from the chemical, or biological, oxidation of metal sulphides within the ore body or waste. Pyrite is the most common of these sulphides and is largely responsible for the generation of AMD at the majority of sites. Other metal sulphides that regularly contribute to the generation of AMD, due to oxidation, include marcasite (FeS_2) and pyrrhotite (FeS) (Alpers & Blowes, 1994; Rimstidt *et al.*, 1994). As the most common sulphide, the oxidation of pyrite and its role in generating AMD has been extensively studied. The overall process can be described by the reaction shown in equation 3.1 with the rate of reaction described by (Williamson & Rimstidt, 1994) in Equation 3.2

Equation 3.1

$$4FeS_{2(s)} + 15O_2 + 14H_2O \rightarrow 4Fe(OH)_{3(s)} + 8SO_4^{2-} + 16H^+$$

Equation 3.2

$$r = 10^{-8.19}\, m_{O_2}^{0.5}\, m_{H^+}^{-0.11}\, (mol/m^2/s)$$

The equation demonstrates how the reaction generates large amounts of acidity which, if un-neutralised, result in a decrease in pH. In some areas this effect is intensified to the point where negative pH solutions are generated (Nordstrom *et al.*, 2000). Equation 3.1 is a simplified equation (a combination of 3 separate steps) and doesn't show the oxidation of the disulphide ions and ferrous iron ions. The oxidation of ferrous iron (Fe(II)) to ferric iron (Fe(III)) is critical to the rate of pyrite dissolution. The majority of the ferric iron produced, from the oxidation of ferrous iron, will undergo hydrolysis to produce amorphous iron oxyhydroxides via the reaction shown in Equation 3.4 when pH is > 3 (discussed in greater detail in Section 4.2). This reaction also introduces greater acidity to the system. If the pH is below 3, the precipitation of Fe(III) becomes negligible and dissolved Fe(III) may oxidise further pyrite via the reaction in Equation 3.5.

Equation 3.3

$$4Fe^{2+} + O_2 + 4H^+ \rightarrow 4Fe^{3+} + 2H_2O$$

Equation 3.4

$$Fe^{3+} + 3H_2O \rightarrow Fe(OH)_3 + 3H^+$$

Equation 3.5

$$FeS_2 + 14Fe^{3+} + 8H_2O \rightarrow 15Fe^{2+} + 2SO_4^{2-} + 16H^+$$

The 16 moles of hydrogen ions produced by this reaction contributes heavily to the rapidly decreasing pH. Fe(II) is also produced, which may be oxidised back to Fe(III) by oxygen. When compared to the oxidation of Fe(II) (in the absence of bacteria), which is slow at low pH and faster with increasing pH, the oxidation of pyrite by dissolved ferric iron is a rapid reaction. However, given the low concentration of ferric iron that can remain dissolved higher pH conditions (pH> 3) , oxidation of pyrite by ferric iron is very rarely the dominant reaction in all cases but those with very low pH conditions (Stumm & Morgan, 1996; Appelo & Postma, 2005).

This represents a purely abiotic system. In a natural setting the influence of iron oxidising bacteria can have a significant enhancing effect on the oxidation of pyrite (Kirby & Elder Brady, 1998). Field studies performed on AMD, where the iron oxidising bacteria *Acidithiobacillus ferrooxidans* is present, have reported ferrous iron oxidation rates 5 – 8 orders of magnitude larger than observed in abiotic lab studies (Nioke *et al.*, 1983; Nordstrom, 1985; Williamson *et al.*, 1992). This increase in production of Fe(III) ions can then result in an increase in pyrite oxidation (assuming low pH and Fe(III) in solution) meaning the action of the microbes can have a catalytic effect on pyrite oxidation (Appelo & Postma, 2005). Microbial oxidation of iron is discussed in depth in Section 4.3.

The same process of sulphide oxidation and subsequent oxidation and hydrolysis of ferrous iron to form iron oxyhydroxide sludges occurs within sulphidic mine tails tailings. Due to this many tailings ponds/ piles, once drained, will have an “oxidised” layer on the upper surface.

The “rusty” orange ferric iron oxyhydroxide sludges produced by AMD are not naturally produced from neutral mine drainage, due to their iron-deficiency. Regardless of the potential to form iron oxyhydroxide sludges, all mine drainage have the potential to cause significant environmental damage. As such a number of mine drainage are intercepted and remediated before they enter surface and/or groundwater’s and result in environmental harm.

A number of pilot passive treatment systems have been installed at abandoned UK metal mines including Cwmrheidol, Ceredigion, Parys Mt, Anglesey and South Crofty, Cornwall though none proved to be viable long-term solutions. One of the most intensively studied examples is the Wheal Jane "pilot passive treatment plant" (PPTP). Wheal Jane is a former tin mine located in the Carnon River valley in Cornwall. When the mine was closed in 1991 the dewatering operations were ceased, this led to the build-up and sudden release of contaminated water into the Carnon River, increasing concentrations of, amongst other metals, Al, Cd, Co, Cu, Fe, Pb, Ni, U and Zn (Neal *et al.*, 2005). Emergency pumping and treatment of the contaminated water was carried out to mitigate the contamination of the river.

The PPTP was constructed in 1993-94 to research potential long-term passive treatment options at Wheal Jane and other former metal mines. It consisted of 3 separate treatment components (CL:AIRE, 2004; Whitehead & Prior, 2005);

1. Aerobic cells consisting of reed beds to cause the oxidation and subsequent precipitation of iron as iron oxyhydroxides
2. Anaerobic cells, fed with organic material such as manure, designed to increase the pH via sulphate reduction, leading to precipitation of metal sulphides. Targeting Cu, Pb, Zn, Cd and remnant Fe
3. Aerobic rock filters promoting algal growth to further increase pH and precipitate manganese.

As well as the treatment beds, 3 different "pre-treatment" systems were also tested;

1. Lime dosing (to raise pH)
2. Anoxic limestone drain (ALD) system (to raise pH and remove dissolved oxygen)
3. Lime free system (no pre-treatment)

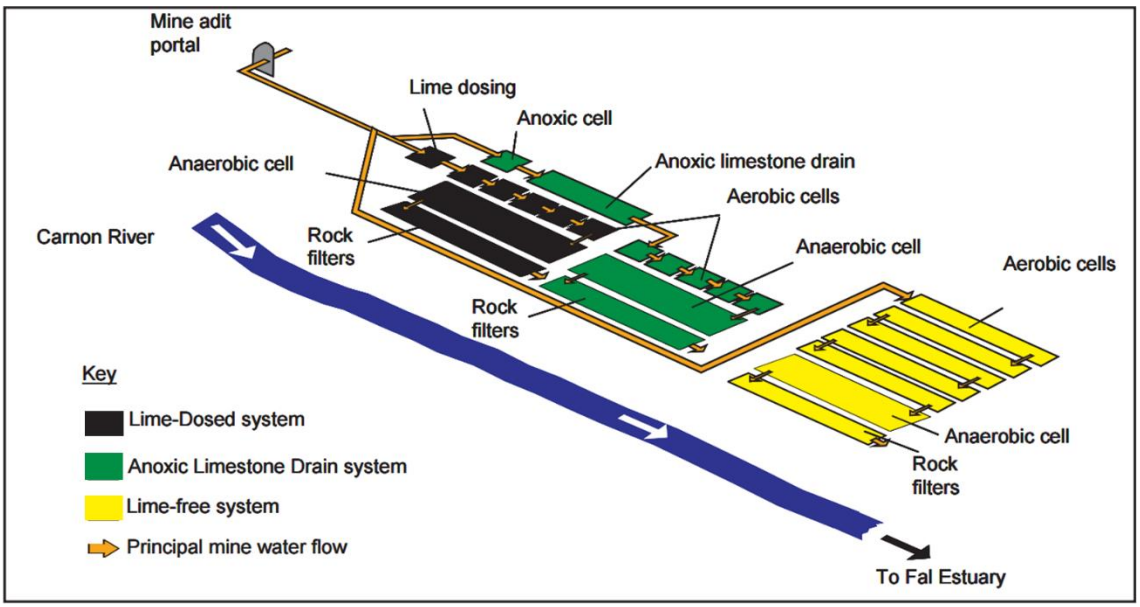

Figure 3.2. Schematic diagram of Wheal Jane PPTP system (CL:AIRE, 2004)

The Wheal Jane PPTP system had mixed success with the anaerobic cells in the lime dosed and ALD in particular failing to function as expected. Whilst the rock filter also failed to perform as well in the lime dosed and ALD system compared to the lime free system. The lime free system appeared to be sustainable, at least over the course of a yearlong study, with evidence suggesting it would be capable of accommodating a flow rate between 10 and 15 times greater (Hall & Puhlmann, 2005; Whitehead *et al.*, 2005).

The only example of a passive treatment system currently being applied to metal mine drainage in the UK (at time of writing) is at Force Crag Mine, Cumbria. Force Crag Mine first opened in 1835 and has, through a number of ownerships, been mined for zinc, lead and barytes throughout its history. The mine was finally closed in 1991 but began producing mine drainage contaminated with zinc, lead and cadmium which entered the local river system including the River Derwent and Bassenthwaite Lake which are designated as a "Special Area of Conservation", and the later a "Site of Special Scientific Interest" (Coal Authority, 2015; DEFRA & Stewart, 2015).

The treatment scheme consists of two geomembrane lined vertical flow ponds filled with a "compost treatment mix". The ponds were constructed using existing bunding from the former mine tailings lagoon. After the water has passed through the ponds it passes into a wetland system which acts as a natural filter for any remnant solids. From

here the water is released to the Coledale Beck (a tributary of the River Derwent). After passing through the treatment system, the water released to the river has had 98% zinc, 94% cadmium and 94% lead removed when compared to mine water at source (Coal Authority, 2015; DEFRA & Stewart, 2015).

Active treatment of mine waters is an option but has inherent high capital and operational costs. After the failure of the passive treatment system at Wheal Jane, Cornwall an active treatment system was installed. This is, at the time of writing, the only large scale active treatment of metal mine drainage in the UK. The active treatment plant is designed to treat all mine water flow from the mine along with supernatant from the toe drain of the Clemows Valley tailings dam and effluent from the PPTP (while it was operational). A total of 330l/sec of mine water is pumped directly from the flooded mineshaft by 6 pumps, though more pumps are planned to accommodate periods of significantly increased rainfall and therefor mine drainage issuing from the mine (Morgan, 2015; Veolia).

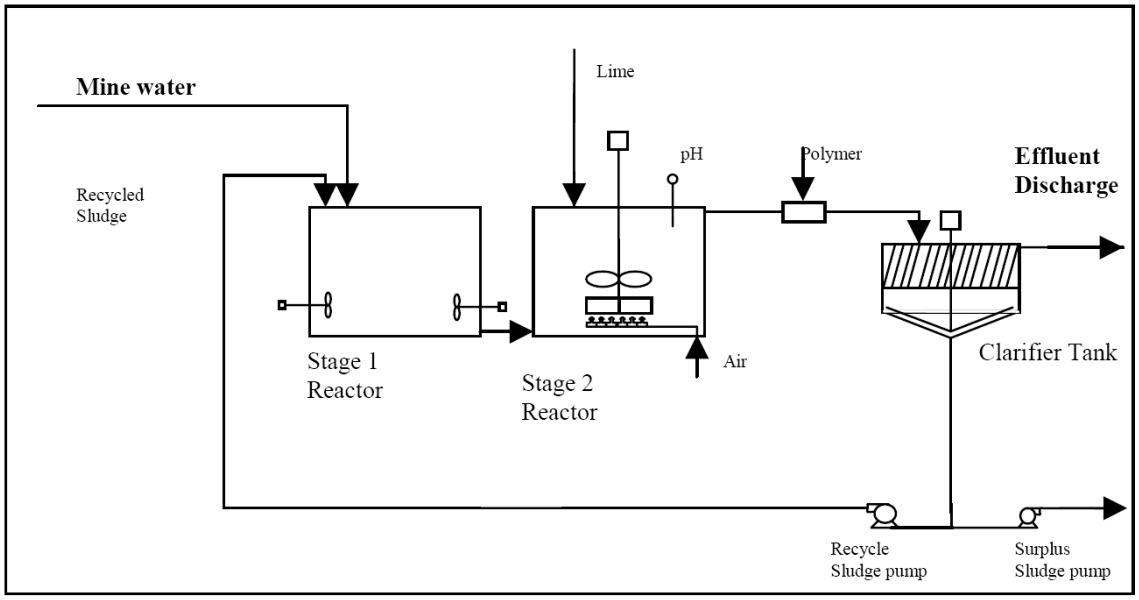

Figure 3.3: Schematic diagram of the Wheal Jane active treatment system (Coulton *et al.*, 2003)

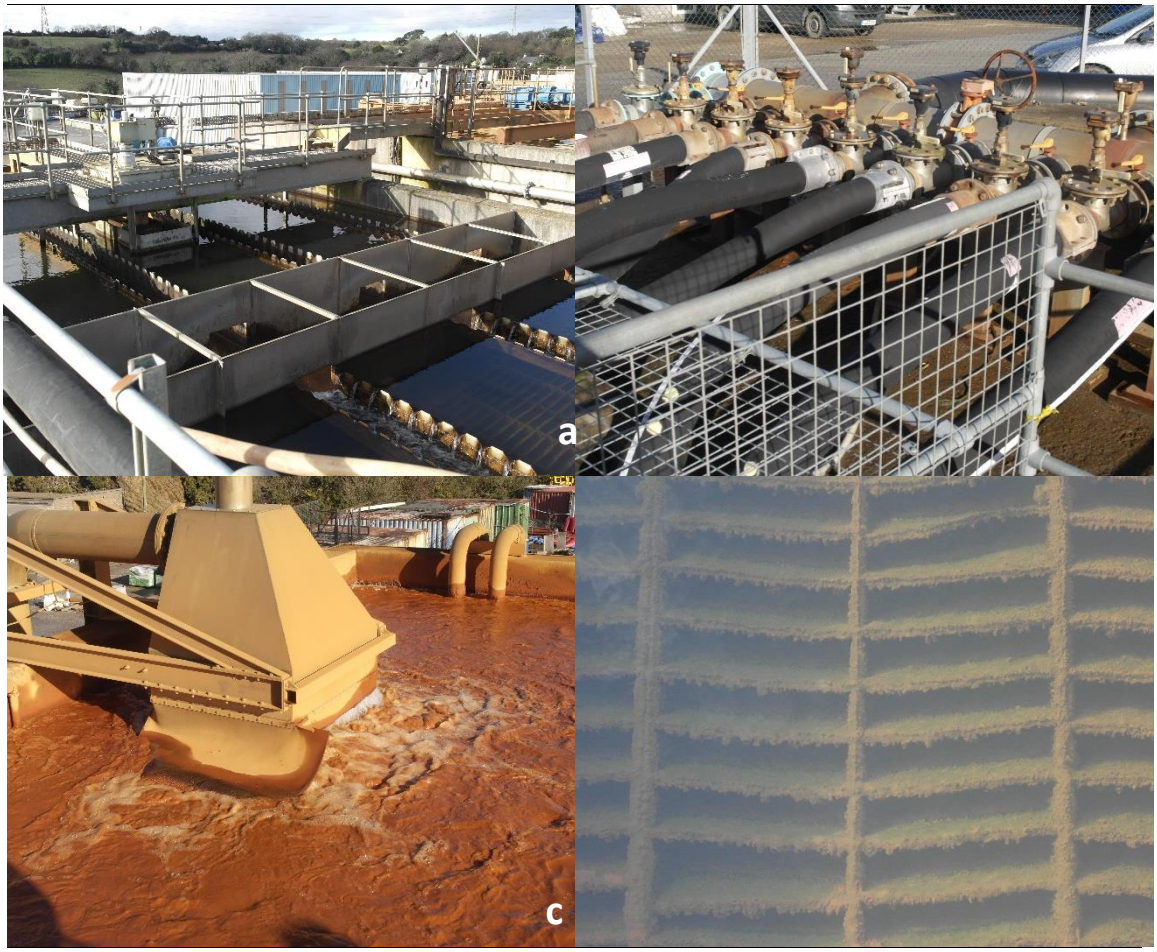

Figure 3.4: a) Wheal Jane active treatment system. b) Pumps extracting mine water from Wheal Jane shaft. c) Mixing of mine water and sludge. d) Lamella clarifier with iron oxyhydroxides on lamellae

Tailings is a widely used term referring to the slurry waste of processing from a number of mining practices. These can be further split into “sands” and “slimes” depending on grain size. Tailings comprise a mixture of pulverised rock e.g. sulphides, oxides, hydroxides, which are no longer workable, and processing fluids from the extraction of metals/minerals from ores or the processing of coal. The ratio between tailings to metal concentrate is typically very high around ~200:1. Though when extracting low-grade ores, such as precious metals, this ratio can be much larger as the majority of the ore is comprised largely of minerals of no interest economically, with >99% of the original mass of the ore producing tailings. As the global trend towards utilising lower grade ores continues greater quantities of tailings will be produced (Lottermoser, 2007; Kossoff *et al.*, 2014).

3.2.2. Physicochemical Properties

Tailings and mine water treatment sludges can be physically and chemically variable, as their composition is dependant of the chemistry of the material from which they originate, while the physical properties are largely controlled by the processing methods used to create them. Within this study iron oxyhydroxide rich sludges are the primary focus and, when observed at a macro scale, visible and physical similarities between iron rich tailings and mine water treatment sludges can be observed. Both often appear as orange-brown, slurries as they are dominated by iron oxyhydroxides or secondary iron oxyhydroxides, carbonates or sulphates. Some generalisations about physical properties of tailings are also possible, with most tailings typically having a high water content, low hydraulic conductivity, low to moderate shear strength, low plasticity, particle sizes <63 µm (Bjelkevik & Knutsson, 2005) and bulk densities generally 1.8 - 1.9 Mg/m^3 for sands and 0.8-2.2 Mg/m^3 for slimes (Sarsby, 2013; Kossoff *et al.*, 2014).

Bjelkevik & Knutsson (2005) observed when investigating the properties of Swedish tailings that ferrous iron tailings tend to be twice as permeable as non-ferrous tailings. Tailings “sands” are, as the name suggests, dominated by sand sized grains, whereas “slimes” are comprised of much finer grained particles and bear more resemblance to sludges from water treatment. Typical grain size distributions of tailing from differing source ores are shown in Figure 3.5. (Note Bauxite tailings are also referred to as “red mud” and are covered within Section 3.3.

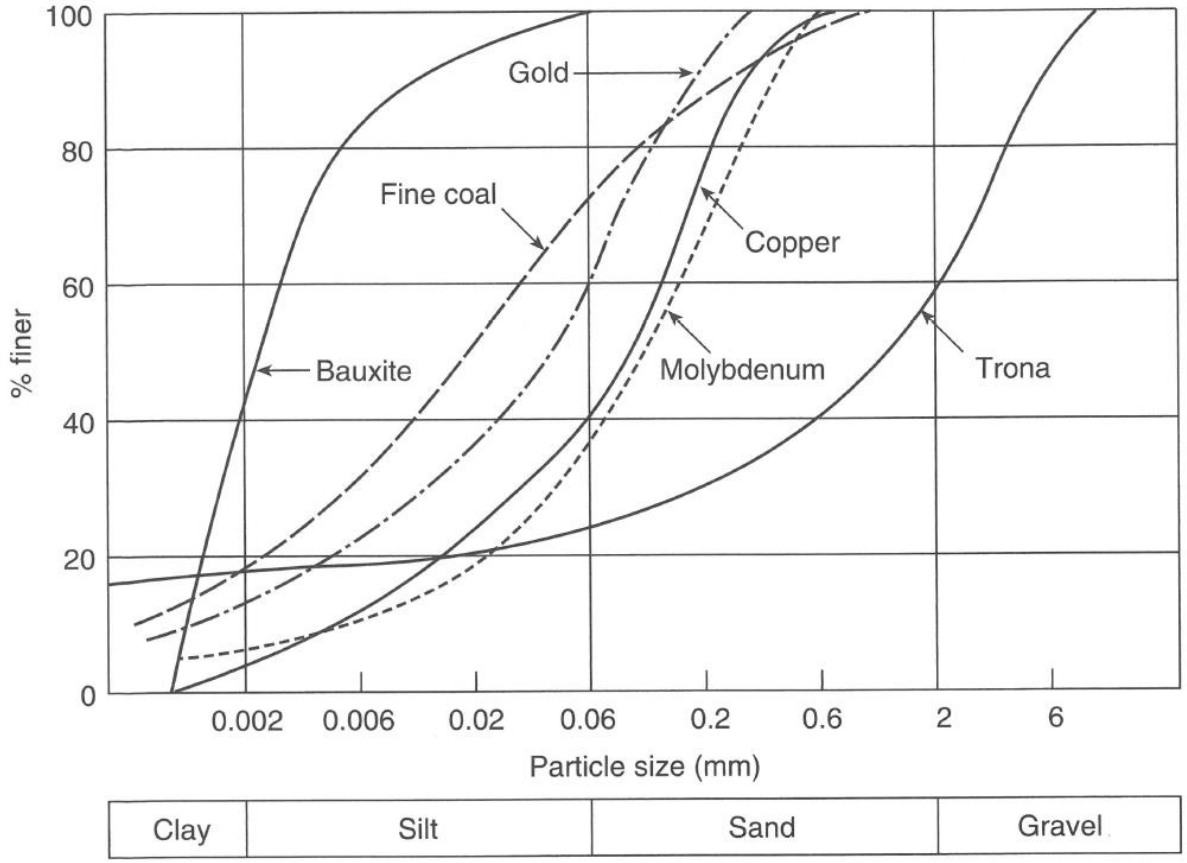

Figure 3.5: Typical grading curves for tailings from a variety of extractive processes (Sarsby, 2013)

Sludges and ochres from the treatment of mine waters are similarly variable as a result of differences in the chemical properties of the AMD source (e.g. mine drainage, tailings). The other significant factor in this variability is the method by which the sludges were formed. As active treatment with lime dosing will invariably lead to higher pH's, which in turn may result in a wider range of minerals forming when compared to passive treatment ochres. Table 3.1 displays some physical properties of a number of mine water treatment sludges, though as the mechanical properties of such wastes are seldom studied, examples in literature are fairly sparse. For comparison, sludges from passive treatment of coal mine drainage by settling ponds and reed bed systems (Taff Merthyr, Wales, Polkemmet & Minto, Scotland) are compared with sludges produced by a vertical flow reactor (VFR) (also situated a Taff Merthyr) and a sludge produced through active lime dosing treatment (Ranger ANSTO, Australia). Dempsey & Jeon (2001) produced an in-depth comparison of the characteristics of sludges generated from the passive treatment of mine waters.

Table 3.1: Comparison of selected physical properties of various mine water treatment sludges. (1): Barnes (2008); (2): Heal *et al.* (2004); (3): Pleysier *et al.* (2009)

	pH	Bulk Density (g/cm^3)	Dry Density (g/cm^3)	Void Ratio	Saturated Hydraulic Ratio [$(m/day)^2$]
Taff Merthyr[(1)]	7.2	1.14	2.34	0.89	-
Taff Merthyr VFR[(1)]	6.8	1.12	3.71	0.95	-
Polkemmet[(2)]	7.2	-	1.8	-	26.0-32.0
Minto[(2)]	6.9	-	0.8	-	0.7-1.7
Ranger ANSTO[(3)]	11.4	1.55	0.55	-	-

Some generalisations regarding the chemical composition of these wastes can also be made. Iron and silica are near ubiquitous in these wastes and, along with oxygen, typically comprise the majority of the mass of the wastes. Within tailings, and sludges derived from metal mines, Al, Ca, K, Mg, Mn, Na, P, Ti and S are usually major component elements. As, Cu, Pb and Zn are also commonly found in high concentrations and have been the received particular focus due to their risk to the environment and/or their economic value (Kossoff *et al.*, 2014).

Coal mine water treatment sludges typically have lower trace metal concentrations than those derived from metal mines but can still exhibit high concentrations of certain elements. Sulphides such as pyrite and, to a lesser extent, chalcopyrite, sphalerite, galena and pyrrhotite can be associated with coal. Therefor chalcophilic elements (e.g. Ag, As, Cd, Cu, Ga, Ge, Hg, In, Pb, Sb & Zn) can be found to be elevated within coal deposits and waste products deriving from them (Gupta, 1999; Dang *et al.*, 2002; Kossoff *et al.*, 2014).

Whilst water treatment sludges are typically dominated by iron oxyhydroxides, as described within Section 4, tailings typically have a more variable mineralogy. Tailings can be broadly separated into 3 components: the gangue minerals, residual sulphide/ oxide fraction and secondary minerals either from weathering or chemical precipitation (Lottermoser, 2007; Kossoff *et al.*, 2014). In the majority of tailings from sulphidic tailings, formed during base or precious metal extraction, the primary gangue mineral is quartz (SiO_2). Other common gangue minerals include feldspars ($(K,Na,Ca)AlSi_3O_8$), chlorite ($(Mg,Fe)_3(Si,Al)_4O_{10}(OH)_2(OH)_6$) and calcite ($CaCO_3$) (Lottermoser, 2007; Kossoff

et al., 2014). The residual sulphide/ oxide fraction is almost always dominated by pyrite (FeS_2) but also commonly contains sulphides or oxides that were the target of extraction but are no longer present in economically viable concentrations. These include sphalerite (ZnS), galena (PbS), chalcopyrite ($CuFeS_2$), magnetite (Fe_3O_4) and arsenopyrite (FeAsS) (Keith & Vaughan, 2000). Beyond the common minerals stated, more exotic minerals are sometimes present but are controlled by, and therefor dependant on, the conditions in which the orebody was formed.

When exposed to the atmosphere, tailings begin to weather and residual sulphide minerals such as pyrite are oxidised resulting in their dissolution. The local conditions (e.g. pH and redox state) then control the precipitation of secondary utilising metals and/or metalloids from the minerals within the tailings. Common secondary minerals to form include ferrihydrite, goethite, jarosite, scorodite and kaolinite (Singer & Stumm, 1970; Kossoff *et al.*, 2014; Zabcic *et al.*, 2014) (many described in detail in Section 4.4). Figure 3.6 displays the mechanisms responsible for the formation of some of these secondary sulphate and oxide minerals from the oxidation of pyritic mine wastes.

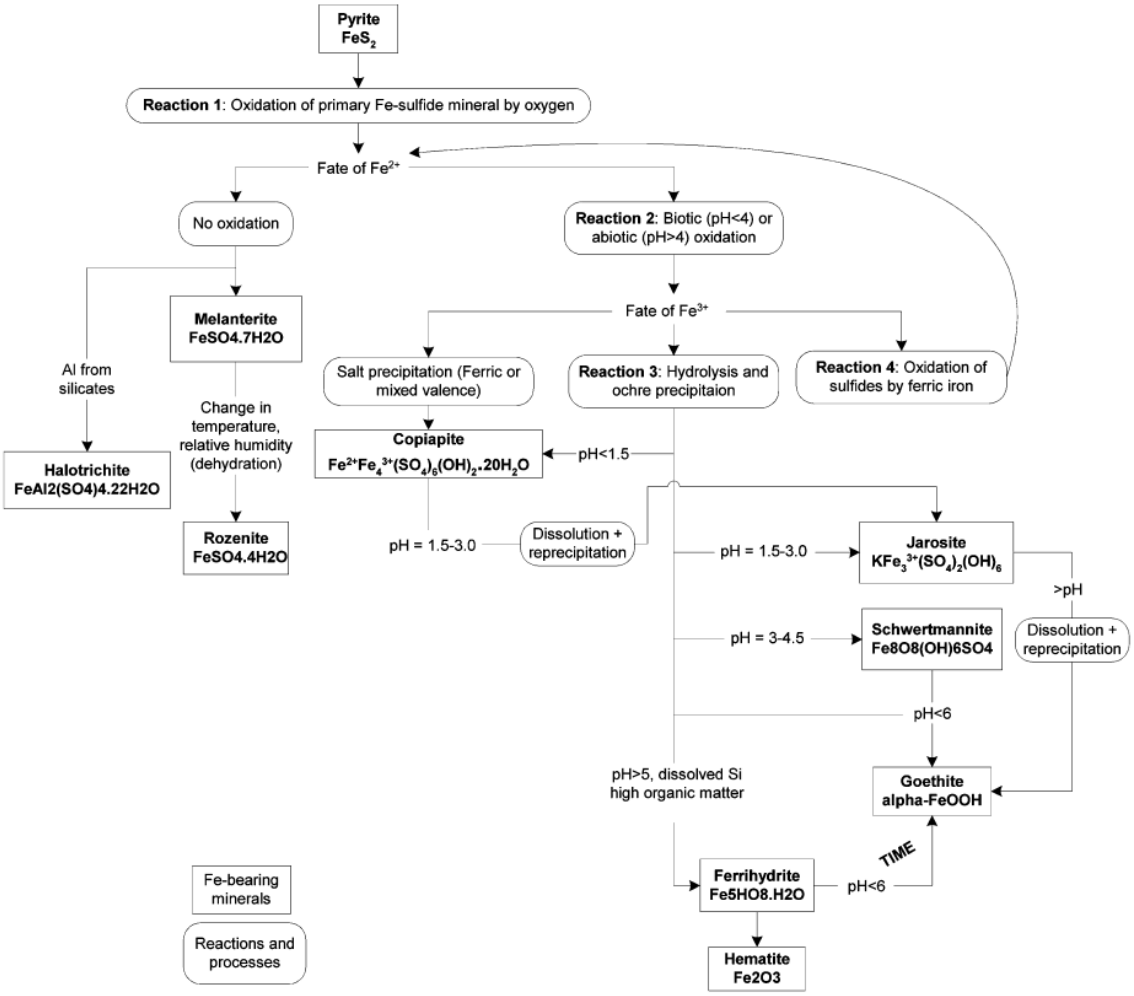

Figure 3.6: Mechanisms of formation of secondary iron oxyhydroxide and sulphate minerals as a result of oxidation of pyrite in mine waste (Zabcic *et al.* (2014) adapted from Hammarstrom *et al.* (2005) and Montero S *et al.* (2005)

3.2.3. Metal Extraction

As a result of the potentially high value metal content within certain metalliferous wastes, there have been an increasing number of studies into the potential extraction of economically significant concentrations of metals from these wastes. The utilisation of chemical extractants is the focus of the greater number of these studies closely followed by bioleaching via bio-oxidation of waste. However, bio-oxidation is not effective for predominantly oxidised wastes such as those within this study. In response to this relatively unexploited waste stream, interest in bioreductive leaching via iron reduction is gradually increasing. As will be summarised in the following chapters, these studies typically use specific microbial species inocula in conjunction with tailored organic carbon sources, elevated temperature and/or other physical manipulation of the wastes to achieve metal extraction. In the subsequent sections a number of abiotic and biological extraction processes are described in detail.

3.2.3.1. Abiotic Leaching

Extensive efforts have been afforded to recovering the metal value held within waste metalliferous wastes. Most published works have utilised physical and chemical manipulation of the wastes and strict controls on the environmental conditions (i.e. pH, temp etc.) to enable the highest recovery efficiencies to be achieved. This section does not represent an exhaustive review of the research material on this topic. Rather it is intended to give an overview of the various methodologies, and their reported effectiveness, when applied to iron oxyhydroxide bearing wastes for resource extraction. Table 3.2 presents a selection of studies into abiotic extraction of metals from a variety of mining and metallurgical wastes including sludges and tailings. A review of various thermal and solvent extractive techniques from sewage sludges, for both metals and energy, and their respective advantages and disadvantages was published by Mulchandani & Westerhoff (2016).

Table 3.2: Brief summary of a selection of extraction techniques for recovery of metals from industrial and mine wastes

Material	Target Metals	Experimental Details	Reference(s)
		Flotation	
Cyanidation Tailings	Zn	Tested the effectiveness of various activators to limit the "depressing effect" of cyanide on metal recovery via flotation. Achieved a maximum recovery of 95% utilising $2X10^{-3}$ mol/L sodium hypochlorite	(Yang *et al.*, 2015)
Cyanidation Tailings	Cu, Zn	Within this study sodium hypochlorite was used as a regulator in the pre-treatment stage of flotation. It was observed to oxidise cyanide to cyanite and increase pH to 10 leading to greater galena and chalcopyrite recovery. This lead to the production of Cu and Zn concentrates with grades of 13.17% and 34.72% and recoveries of 70.0% and 69.58% respectively	(Lv *et al.*, 2015)
Poly-metallic AMD	Cu, Zn, Mn	Selective precipitation from AMD, via oxidation and pH control, was used to form AMD sludges with elevated concentrations of the target metals. The Cu, Zn and Mn sludges were then subjected, separately, to flotation to produce concentrates of 35.72%, 55.13% and up to 45% respectively	(Chen *et al.*, 2014)
Metallic sludge from smelter plants	Zn, Pb, Cu	Hydrothermal sulphidation was performed to reduce the oxide fraction of the waste and increase the sulphide fraction, whilst also causing the target metals to shift into the sulphide mineral fraction. Flotation was then used for recovery of the metals achieving recoveries of 33.3%, 58.9% and 68.8% for Zn, Pb and Cu, respectively, from the sludge.	(Liang *et al.*, 2012)
Metallic sludge from smelter plants	Zn	Performed series of experiments to ascertain optimum conditions for recovery of zinc via hydrothermal sulphidation and flotation. Achieved 92% sulphidation extent and 45.34% zinc recovery when parameters were as follows; L:S ratio 3:1, precursor concentration of 15% and molar ratio of Zn:S of 1:1.2	(Min *et al.*, 2012)
		Magnetic Separation	
Cyanidation tailings	Fe, Au	Experimentation to identify the optimum parameters for the conversion of limonitic iron to magnetite for magnetic extraction. Simultaneously studied the effect of magnetic roasting on the leaching of gold. When roasting is performed at 750°C of 1.25 hours, with reductant at 6%, magnetic susceptibility of iron increases to 86.27%. Gold leaching increases to 46.14% due to increased gold exposure during roasting	(Bailong *et al.*, 2013)
Zinc Calcines	Fe	Decomposed zinc ferrite to zinc oxide and magnetite by roasting, under reducing nitrogen and carbon monoxide-rich atmosphere, at temperatures of up to 900°C. Milling and sonication were found to aid recovery by ~20% giving iron recovery peak of 58.34%	(Peng *et al.*, 2012)

Table 3.2(cont.): Brief summary of a selection of extraction techniques for recovery of metals from industrial and mine wastes

Material	Target Metals	Experimental Details	Reference(s)
		Magnetic Separation (cont.)	
Cyanidation tailings	Fe	Reduction roasting at 50°C for 1h with 100:10:3:10 weight ratios of cyanide tailings/activated carbon/sodium carbonate/sodium sulphate followed by leaching with water at a liquid:solid ratio of 15:1 (ml/g) at 60°C for 5min and stirring at 20rpm. Magnetic separation then achieved a magnetic concentrate of 59.11% and recovery ratio of 75.12%	(Zhang *et al.*, 2012)
Laterite tailings	Ni, Co, Fe	Percolation leaching with oxalic (>99.0%) and tartaric acid (99.7%) followed by precipitation at 80˚C and magnetic separation. Leaching recovered >70% Ni & Co and 30% Fe. Precipitation increased Ni and Co recovery by 10% and Fe 20%. Magnetic separation then produced a product with >50% iron for the steel industry	(Hernandez *et al.*, 2007)
		Roasting & Leaching	
Galvanic sludge	Cu, Zn, Ni	Sulphate roasting for 90min at 550°C with a 1:0.4 ratio of galvanic sludge to pyrite (with pyrite acting as a sulphating agent) followed by a 15min, room temperature, stirred leach with water lead to the recovery of 60% zinc, 43% nickel and 50% copper	(Rossini & Bernardes, 2006)
Galvanic Sludge	Ag, Cu, Zn, Au	Sulphate roasting using same experimental parameters as Rossini & Bernardes (2006) but testing a range of sulphating agents. Maximum recoveries were achieved when sulphur was used as the sulphating agent yielding 80% Ag, 63% Cu and 73% Zn recovery. Sodium thiosulphate was used, in place of water, for the extraction of gold achieving 77% Au recovery	(Amaral *et al.*, 2014)
Vanadium slag	V	Oxidative roasting with calcium oxide at 850°C for 2.5h and a mass ratio of $CaO:V_2O_5$ of 0.42 followed by a stirred sulphuric acid leach at 65°C, pH 2.5 and L:S ratio of 4:1 yielded a vanadium recovery of 93.3%	(Zhang *et al.*, 2015b)
PGM tailings	Al, Fe, Cr, Mg	Ammonium sulphate was mixed with PGM tailings in a solid:solid ratio of 2:6 (m/m) and heated in a furnace at temperatures varying from 350°C to 550°C for 45min. Leaching with 0.6M HNO_3 prevented secondary iron precipitates and achieved leaching rates of ~60% Al, 32% Fe, 27% Cr and 25% Mg as well as ~80% Ca and 32% Si	(Mohamed *et al.*, 2016)
Jarosite residue	Zn, Pb, Cu, Cd, Ag	Roasted at 650˚C for 1 h to sinter jarosite. Followed by leaching with 6 $mol.L^{-1}$ NH_4Cl solution at 105˚C and filtering. 97% Zn, 98& Pb, 87% Cu, 77% Cd and 70% Ag recovered. Later leaching with 30 wt.% NaOH at 160˚C for 1h further removed 94% As and 73% Si from the residue	(Ju *et al.*, 2011)
Zinc leaching residue	Cu, Mn, Zn, Cd	Roasting at 650˚C with Fe(III) sulphate/zinc ferrite at mole ratio of 1:2 for 1h. Followed by water leaching. Recovered 99.3% Cu, 93.3% Mn, 92.4% Zn and 91.4% Cd.	(Jiang *et al.*, 2017)

Table 3.2(cont.): Brief summary of a selection of extraction techniques for recovery of metals from industrial and mine wastes

Material	Target Metals	Experimental Details	Reference(s)
		Electrowinning	
Galvanic Sludge	Cu	Used a combination of chemical leaching and electrowinning to extract copper. Initially the waste was leached with sulphuric acid at 35°C at 3 or 10% weight/volume ratio with semi continuous stirring for 3h. The copper within the leached solution was then recovered by electrowinning with >99% copper in solution being recovered in <2h when a high current (18A) and low flow rate (200l h^{-1}) was applied	(Huyen *et al.*, 2016)
Gold plant waste	Cu	Achieved 99.6% copper recovery using a flow-by-cell system with a reticulated vitreous carbon cathode and cationic membrane. However, to achieve this recovery average current efficiency was low and energy consumption was high.	(Lemos *et al.*, 2006)
		Leaching	
Chromite Overburden	Ni, Co	Pressure acid leaching within autoclaved at 260˚C with H_2SO_4, ammonium sulphate and ammoniojarosite for 3h. Yielded maximum recoveries of 98% Ni and 94% Co	(Das *et al.*, 1997)
Zinc plant residues	Zn, Pb	Utilised a multi-stage leaching process to recover Zn and Pb. Initial leaching with H_2SO_4 at pH 2.5, pulp density of 200 g/L and 80˚C for 1h. A water leach was then performed at 70˚C for 1h. The residue was then crushed (<200 μm) and subjected to a 300 g/L brine leach at 37˚C. A total of 89% of Zn was recovered between the acid and water leach stages. While 89.4% of lead was recovered during the brine leach stage	(Farahmand *et al.*, 2009)

Whilst there is a large quantity of research into metal leaching there has been only limited research into in-situ leaching. This is in part due to the majority of research aiming to remove metals from AMD before it has undergone precipitation to form metalliferous sludges but also due to the economics of metal production being far more favourable to current extractive techniques. Though with decreasing ore reserves and increasing costs associated with obtaining the metals there are signs of renewed interest in to in-situ recovery methods, such as this thesis. One such example of an in-situ recovery process under development is the in-situ leaching and recovery of rare earth elements (REE's) from secondary phosphate streams, such as phosphate tailings and phosphogypsum ponds, with acidic or salt solutions described by Haschke *et al.* (2016).

The authors also detail a number of other in-situ leaching projects under development including the "BioMOre" project for in-situ leaching of Cu from deep copper ore shale deposits and REEs from ion-adsorption clays in Madagascar suggesting potential chemical and oxidative bioleaching recovery methods for each case.

3.2.3.2. Bioreductive Leaching

Whilst the detrimental effects to the environment of toxic metal release due to DIRM activity has been well documented, biological iron reduction clearly has potential for releasing metals for recovery. In an effort to extract either metals of economic interest or to reduce toxic metal concentrations within oxidised wastes, a small number of studies have inoculated wastes with non-indigenous iron-reducers in an effort to establish microbial communities capable of mobilising metals for extraction. To date there are only a few studies focused on wastes, with the majority targeting lateritic ores or overburden for the recovery of nickel and cobalt. As with the abiotic leaching, to achieve the highest metal recovery rates possible, the bacteria introduced to the wastes are often specifically selected and supplied with a carbon source and optimal conditions for microbial growth. A number of these studies have been briefly described within Table 3.4 with a select few being reviewed in greater detail. The use of indigenous, mixed microbial communities has this far not been well studied (Hu *et al.*, 2014).

Utilising the facultative, metal reducing bacteria *Shewanella putrifaciens* Strain CN32, Zachara *et al.* (2001) investigated the solubilisation of coprecipitated Co(III)and Ni(II)

from goethite by dissimilatory iron reduction. The cobalt and nickel appeared to have "no observable influence" on the susceptibility of goethite to reductive dissolution. Release of nickel and cobalt was observed to be at rates and concentrations relative to the generation of Fe(II) and proportional to their mole fraction, thereby increasing the aqueous concentrations of these metal cations. Cobalt was also observed to be reduced by the bacteria into the more soluble Co(II). The fate of the solubilised metals varied on the chemistry of the sample. When carbonate was present, ferrous iron was seen to form siderite ($FeCO_3$) and form vivianite [$(Fe_3(PO_4)_2 \cdot 8H_2O)$] when phosphorus was present. Both of these secondary "biogenic" minerals were observed to incorporate Co(II) within their structural matrix. Other observed sinks for the solubilised metals included re-adsorption as residual goethite or co-precipitation with bio-mineralisation products from the interaction between Fe(II) and residual goethite.

When comparing to previous studies (Zachara *et al.*, 1996; Zachara *et al.*, 1998), it was noted that the synthetically prepared goethite was more resistant to bioreduction, and were adsorbing metal cations with greater strength, compared with natural, crystalline Fe(III) oxides. Zachara *et al.* (2001) therefor concluded that "oxide-entrained trace metals in soil and subsurface environments may be more readily released by dissimilatory iron reduction that observed in this model system study".

Recovery of nickel and cobalt from wastes via bioreduction has received particular focus largely due to the high price of nickel and cobalt's status as an "EU critical raw material". For these reasons nickel laterites have been the subject of a number of studies. Hallberg *et al.* (2011) performed a series of experiments comparing the ability of a number of acidophilic iron reducing bacteria to solubilise nickel from limonitic laterite ore. Each tested bacteria was provided with its ideal electron donor and incubated, at their respective ideal temperatures for promoting growth, for a total of 45 days (Table 3.3).

Of the four bacteria tested only *Acidithiobacillus ferrooxidans* and *Acidicaldus organivorans* were seen to facilitate reductive dissolution of the iron minerals within the nickel laterite. *Acidithiobacillus ferrooxidans* solubilised 8% of available Fe and 17% of Ni compared to <1% and 9% respectively solubilised in the 30°C control. *Acidicaldus organivorans* solubilised 7% Fe and 16% Ni, whilst the 45°C control solubilised 1% Fe and 12% Ni (Hallberg *et al.*, 2011). The failure of *Acidiphilium SJH* to facilitate bioreduction

of the laterite ore was expected as previous research by Bridge & Johnson (2000) had shown its inability to reduce goethite, which is the dominant iron oxyhydroxide in the laterite.

Table 3.3: Summary of bacteria and experimental conditions utilised within Hallberg *et al.* (2011)

Bacteria	Brief Description	Electron Donor	Incubation Temperature
Acidithiobacillus ferrooxidans	Mesophilic sulphur oxidising chemolithotroph, iron oxidising in aerobic environments but facultative iron reducer in anaerobic conditions	Sulphur (5%w/v)	30°C
Sulphobacillus benefaciens	Sulphur oxidising mixotroph, iron oxidising in aerobic environments but facultative iron reducer in anaerobic conditions	Sulphur (5%w/v)	37°C
Acidicaldus organivorans	Moderately thermophilic, sulphur oxidizing heterotroph	Glycerol (10mM)	45°C
Acidiphilium SJH	Mesophillic fermenting heterotroph	Citric acid (10mM)	30°C

Acidithiobacillus ferrooxidans was then chosen for a larger scale experiment. As well as being selected for its performance in the preliminary study, it was selected as its use of sulphur as an electron donor was seen as financially favourable. It was also known from previous studies to outperform the nickel solubilising performance of fungi e.g. *Aspergillus niger* in lateritic tailings (Coto *et al.*, 2008). Within this experiment the *Acidithiobacillus ferrooxidans* was provided with an excess of elemental sulphur (50g) and pH controls to maintain the optimum pH of 1.8. The system was incubated for 30 days at a temperature of 30°C with samples drawn at regular intervals to observe concentration of any solubilised metals. Two grades of ore; crushed (coarser) and milled (finer) were tested.

Somewhat counterintuitively metal solubilisation was more rapid in the crushed ore compared to the milled ore but both achieved >70% Ni release within 20-30 days. Within the milled ore especially, an initial weak correlation (r^2= 0.76) between iron and nickel release rapidly became a very strong correlation (r^2= 0.99) (Figure 3.7) supporting the hypothesis that nickel associated with the iron oxyhydroxides was being release coevally as a result of bioreductive dissolution. Further confirmation of the effect of the *Acidithiobacillus ferrooxidans* was evident when comparing the metal solubilisation figures to the aerobic control. The anaerobic cells solubilised ~70% metals compared

with only ~10% Ni and 1% Fe in the aerobic control. As well as iron and nickel, cobalt and manganese were observed to be released from the ore in significant concentrations. Johnson *et al.* (2013) performed a repetition of this experiment and returned the similar findings as Hallberg *et al.* (2011). However, they also noted the release of chromium from the laterite ore as a result of acid dissolution. The chromium was found to be released as Cr(III), the less toxic oxidative state of chromium.

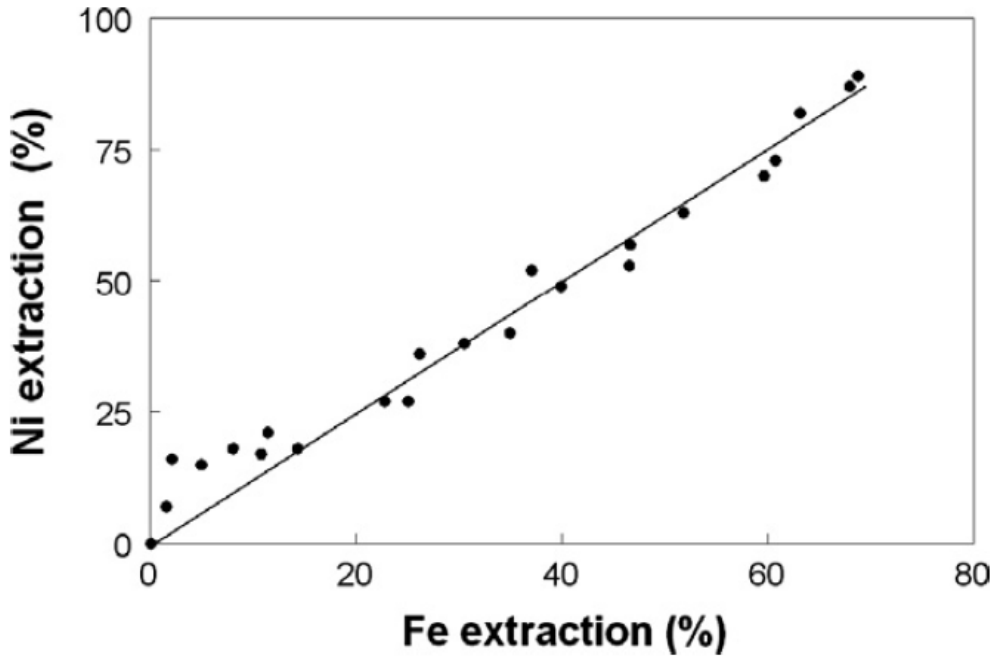

Figure 3.7: Correlation between the extraction of iron and nickel via bioreductive dissolution from the milled laterite ore test (Hallberg *et al.*, 2011).

Whilst many published studies report success, to various degrees, with regards to metal extraction there are impedances to the extraction of metals solubilized as a result of bioreduction. Once such instance is described by Cooper *et al.* (2000) wherein the reductive dissolution of synthetic goethite and lepidocrocite by *Shewanella putrifaciens* 200 causes the transfer of previously surface bound zinc into a secondary mineral phases including magnetite. These secondary mineral phases, and therefor associated zinc, are insoluble in 0.5 M HCl, rendering the zinc immobilised to extraction without the use of a stronger extractant.

Table 3.4: Summary of example bioreduction studies

Waste Material	Target Metal(s)	Microorganisms Utilised	Experimental Details	References
Chromite Over-burden	Ni, Co	Unspecified DIRM "consortium" cultured from soil sample	Bioreduction utilised as part of a multi-step extraction of Ni/Co from waste. Found bioreduced waste subjected to acid leaching yielded greater extraction rates (up to 83.6%) than non-bioreduced waste.	(Esther *et al.*, 2013; Esther *et al.*, 2015)
Copper Laterite	Cu	*Acidithiobacillus ferrooxidans, Acidithiobacillus ferrodurans, Acidithiobacillus caldus & Sulphobacillus thermosulfidooxidans*	Series of experiments where sulphur and/or glycerol provided as electron donor in pH (1.8-2.2) & temperature (30-35°C) controlled stirred bioreactors. Anoxic conditions were maintained by a flow of oxygen free nitrogen. Yielded up to 78% copper recovery	(Nancucheo *et al.*, 2014)
Refractory oxide ores	Ag, Mo, Cu, Mn, Zn	Bacteria from *Bacillius polymyxa* & *Bacillus circulans* groups	Ores were crushed to smaller than 200 mesh particle size and added to 2-litre bioreactors at 15% pulp density. No temperature or pressure controls were used. Unspecified organic additive utilised to enhance bacterial solubilisation of metals. Experiment ran for 12-14 days. 86% Ag, 99.8% Mn, >99% Cu, 91% Zn extracted	(Rusin *et al.*, 1992)
Synthetic Pb-As Jarosites	As	*Shewanella putrifaciens*	Anaerobic cells, circumneutral pH, maintained at 27°C, rotated end over end and supplied with 24 mM Na-lactate as electron donor. Noted that after 336 hours 20.2% and 3% of total arsenic was in solid and aqueous phases, respectively. Arsenic was seen to be reduced from As(V) to As(III) which then moreed to mineral surfaces	(Smeaton *et al.*, 2012)
Cu waste from Ball Milling	Cu	Consortium of dissimilatory metal reducing microbes identified, by comparison to 16S rRNA datanbase, as: *Micrococcus yunnanesis, Staphylococcus arletta, Stenotrophamonas maltophilia, Micrococcus luteus*.	Bioreduction used as pre-treatment to be followed by iron-oxidising bioleaching. Waste ground to <750µm and added at 2% pulp density to mineral salt media. 10% (v/v) of microbial consortia added with 10 mM glucose provided as carbon source. Dark and anaerobic conditions maintained. 29.73% Cu leached by day 35 of bioreduction	(Panda *et al.*, 2015)

3.3. Red Muds

3.3.1. Generation

Red mud is the main waste product generated during the Bayer process which processes bauxite ore to alumina, which in turn is used to produce aluminium. For every tonne of alumina produced approximately 1.5 to 2 tonnes of red mud is produced (Qu *et al.*, 2013; Liu & Naidu, 2014). In 2011 the total amount of red mud worldwide was estimated at 2.7 billion tonnes (Power *et al.*, 2011), though it is predicted to reach approximately 4 billion tonnes in 2015 (Wang *et al.*, 2013). Due to increased demand for aluminium, the rate of red mud production has increased over recent years. Klauber *et al.* (2011) stated that approximately 120 million tonnes of red mud is produced per year, though this number is rapidly increasing.

Red mud has historically been disposed of in a variety of ways including lagooning, "dry" stacking, dry cake disposal and marine disposal. A comprehensive review of these disposal methods and their relative advantage and disadvantages can be found in Power *et al.* (2011). There have been a number of attempts over recent years to reuse red mud, outlined in Figure 3.8, but these utilise only a small fraction the waste produced. The environmental issues associated with the disposal of red mud were brought into public focus in 2010 when a storage lagoon in Ajka, Hungary suffered a structural failure releasing ~700,000m^3 of red mud over ~40km^3 of the surrounding area. This resulted in substantial environmental damage to large areas of agricultural land and 3 villages causing the deaths of 10 people (Gelencser *et al.*, 2011; Renforth *et al.*, 2012).

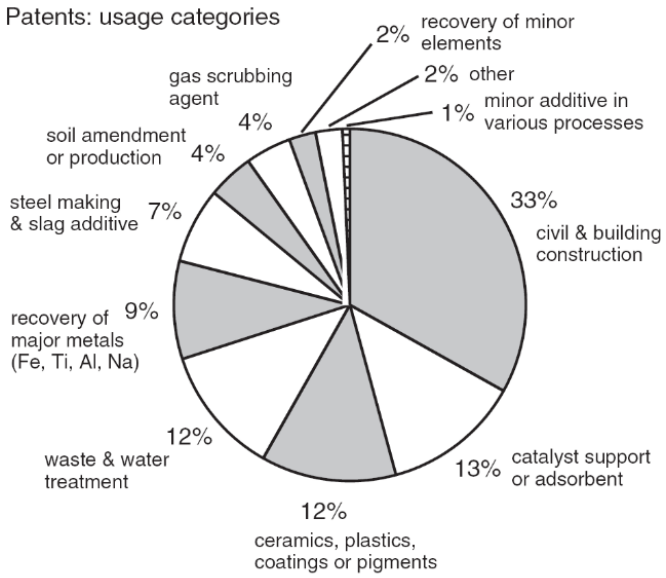

Figure 3.8 Percentage patents (734 patents total) for each reuse process patented between 1964 to 2008 (Klauber *et al.*, 2011). Percentage patents (734 patents total) for each reuse process patented between 1964 to 2008 (Klauber *et al.*, 2011).

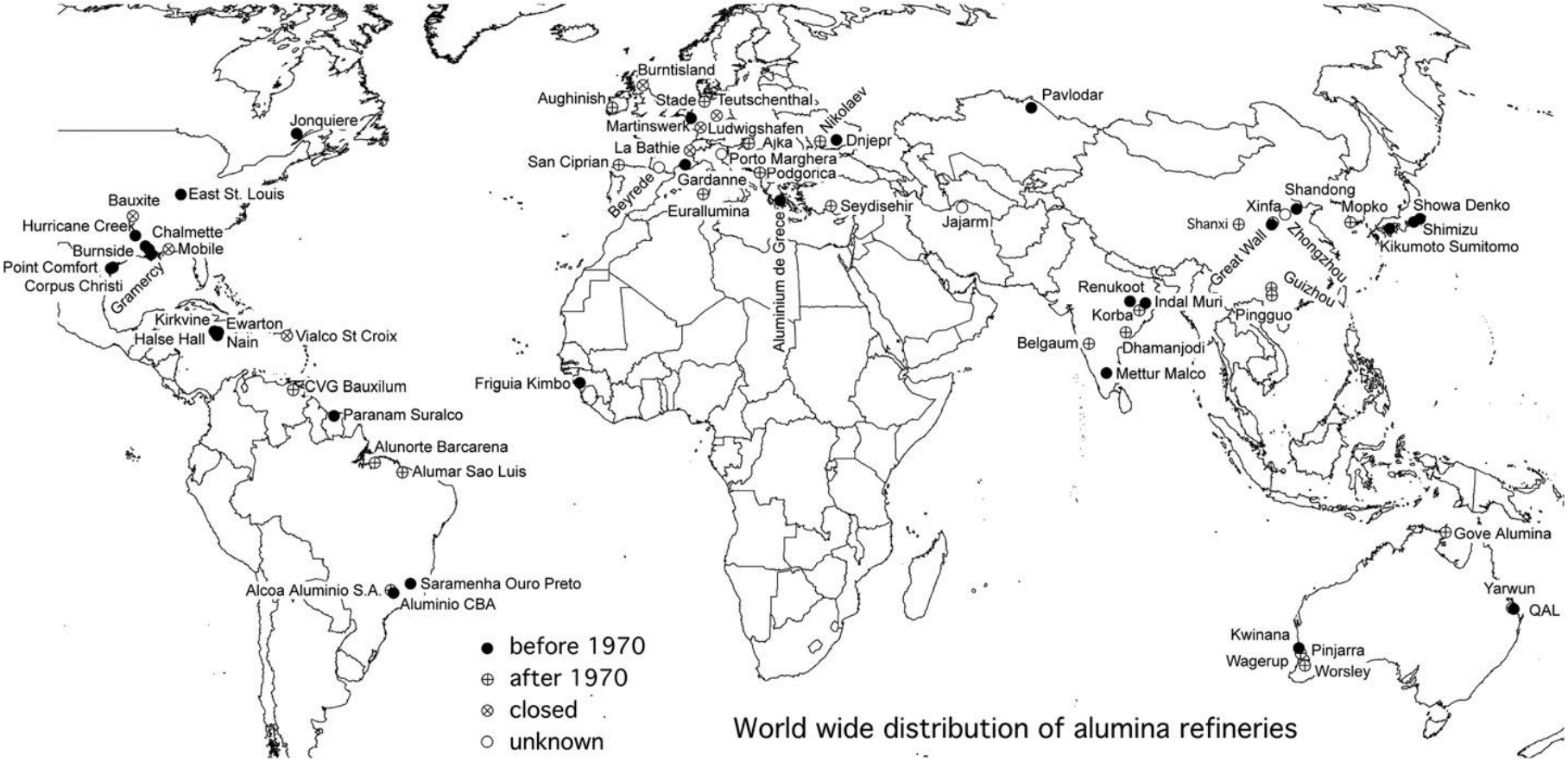

Figure 3.9 Map showing the worldwide distribution of alumina producing refineries by establishment dates (Power *et al.*, 2011)

3.3.2. Physicochemical Properties

Due to the treatment processes employed during the Bayer Process, red mud is highly alkaline with pH values of untreated residues typically between 9.2 and 12.8 (Gräfe *et al.* (2011) and references within). The alkalinity is derived from anions such as OH^-, CO_3^{2-} /HCO_3^-, $Al(OH)_4^-$/$Al(OH)_{3(aq)}$ and $H_2SiO_4^{2-}$/$H_3SiO_4^-$. The particles within red mud are highly compacted, typically resulting in relatively high bulk densities of approximately 2.5 g/cm^3 (Gräfe & Klauber, 2011). High salt contents, especially Na^+, typically give red mud high electrical conductivity. Gräfe & Klauber (2011) reported values ranging from 1.4 mS/cm to 28.4 mS/cm with an average of 7.4±6.0 mS/cm.

Snars & Gilkes (2009) analysed grain size distributions of 14 samples from 11 different refineries. They reported that on average 31% of particles were less than 2µm in size, 46% were between 2-20µm in size and the remaining 23% of particles were greater than 20 µm in size. Snars & Gilkes (2009) also reported the BET specific surface area of each of the samples, with average surface area of 24.8m^2/g and a range of 15-30 m^2/g. Depending on the disposal method, solid contents range from 20-80 wt%. On average, 70% of mineral phases are crystalline and 30% are amorphous. The main components of red mud are iron and aluminium oxides, along with smaller quantities of sodium, titanium, calcium and silicon oxides. Mineralogically the major components are the iron oxyhydroxides; hematite, goethite and magnetite, (though this is excluding any amorphous phase minerals such as ferrihydrite). Sodalite, cancrinite, calcites, aragonites and sodium-carbonates are formed during the Bayer process from the breakdown and solubilisation of phyllosilicate clay minerals (e.g. Kaolinite) and tectosilicate minerals (e.g. quartz & feldspars). The typical metallurgical and mineral compositions of red mud are displayed in Figure 3.10 (Gräfe & Klauber, 2011).

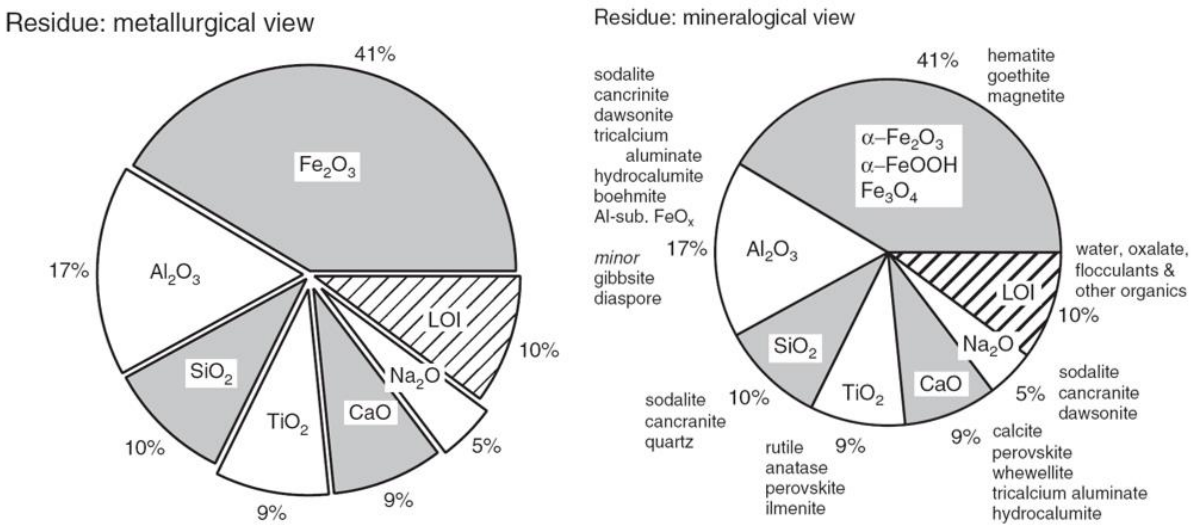

Figure 3.10 Typical metallurgical and mineralogical composition of red mud Klauber *et al.* (2011) with data from (Gräfe *et al.*, 2011)

3.3.3. Typical Metal Contents

As suggested by the mineralogy of red mud, the most abundant metallic element within red muds is typically iron with contents ranging from 4.5-50.6% dependant on refining process (Liu & Naidu, 2014). There are also an abundance of minor elements of interest often contained within red mud including aluminium, sodium, titanium, vanadium, gallium, zirconium, chromium, nickel and zinc (Wang *et al.*, 2013; Liu & Naidu, 2014). Certain red muds also contain a significant proportion of radioactive elements, primarily uranium and thorium making them unsuitable for reuse in construction materials (Smirnov & Molchanova, 1997). Table 3.5 shows the average composition of the Ajka red mud, giving an indication of typical elemental concentrations within red mud.

Table 3.5: Example red mud composition from Ajka red mud spill, Hungary. Left hand column denotes element, right hand column denotes concentration in ppm. Adapted from (Renforth *et al.*, 2012)

Ca	53500	**S**	2692	**Cu**	60.3	**Sr**	290.2
Mg	2982	**As**	78.5	**Ga**	79.3	**Ti**	24800
K	737	**Ba**	59.8	**Li**	57.5	**V**	891.2
Na	39920	**Cd**	4.0	**Mn**	2565.8	**Zn**	179.2
Fe	210300	**Ce**	473.2	**Mo**	14.4	**Zr**	628.9
Al	75200	**Co**	97.1	**Ni**	291.7		
Si	27900	**Ce**	810.7	**Pb**	79.8		

Whilst the valuable constituent of red mud has generally been considered to be aluminium, in recent year's rare earth elements (REEs) have been the subject of increased interest due, in part, to their growing use in industry and the near monopoly China has on their production. Most REEs present within red mud are within the lanthanide group and are contained within minerals such as monazite and xenotime (Samal *et al.*, 2013). Whilst not a rare earth element, scandium is often grouped with the REEs. Due to its high value and higher concentrations within red mud scandium accounts for greater than 90% of the trace metal value within many red muds (Binnemans *et al.*, 2013). This has resulted in the majority of literature focussing on the extraction of scandium rather than other minor elements.

3.3.4. Metal Extraction

As a result of the, potentially, high value metal content within red muds, there have been a large number of studies into the leaching and recovery of the metals contained within them, a selection of which are summarised in subsequent chapters. Most studies have utilized chemical lixiviants to extract target metals though recently more authors have investigated the utilization of microbial processes for metal extraction. The increased focus on bioleaching is due in large parts to the perception of bioleaching as a low-cost and green technology. In the subsequent sections a number of chemical and biological extraction processes are described in detail.

Liu & Li (2015) produced a thorough review of research into metal extraction from red muds categorising the work by the element targeted for extraction. It outlines published work into the extraction of aluminium, sodium, iron, titanium, scandium, gallium and "minor elements" such as REEs and radioactive elements. Liu & Naidu (2014) have also compiled a review of published work on metal extraction from red mud. They have complied work on the extraction of aluminium, titanium, REEs and "minor elements". They have also given greater focus to the extraction of iron, detailing methods including direct magnetic separation, pyrometallurgical processes and hydrometallurgical processes.

3.3.4.1. Chemical Leaching

Ochsenkuhn-Petropulu *et al.* (1996) utilised chemical extraction in an effort to recover lanthanide elements and scandium. They were able to extract up to 90% Y, 80% Sc, 70% of Dy, Er and Yb, 50% of Nd, Sm, Eu, and Gd and 30% of La, Ce and Pr by leaching with 0.5N HNO_3 for 24 hours at 25°C and at a liquid to solid ratio of 50:1. This leaching process was then taken to pilot scale and configured to enable maximum scandium extraction (Ochsenkuhn *et al.*, 2002).

Xue *et al.* (2010) utilized H_2SO_4 as their extractant for scandium from red mud, specifically red mud particles between 65-80μm in diameter. They observed that when the reaction has a liquid to solid ratio of 3:1, and is heated to 90°C, over 80% of scandium within the red mud was leached.

Borra *et al.* (2015) experimented with a range of organic and inorganic acids (hydrochloric, nitric, sulphuric, acetic, methanesulphonic and citric) for major element and REE extraction from red mud. They observed improved extractions with higher acid concentrations, increased reaction times and higher liquid to solid ratios. The highest REE recovery was obtained by using HCl, though this also resulted in very high iron leaching (~60%). Reacting at 25°C for 24 hours with 6N HCl yielded between 70-80% REE recovery. Increasing temperatures weren't observed to have any significant effect on leaching when inorganic acids were used. Temperature did, however, have a marked effect on the performance of citric acid. Percentage REE recovery with citric acid increased with increasing temperature to the point where leaching with citric acid at 90°C is comparable to inorganic acids at 25°C.

Fulford *et al.* (1991) developed, and patented, a procedure for selective extraction of REEs (including scandium and yttrium) from Jamaican bauxite residues whilst leaving iron and titanium largely undissolved. The process involves the use of a dilute acid as a lixiviant, achieved either by SO_2 in water or pumping gaseous SO_2 into a slurry, to reduce the pH to between 1.8-3.0.

3.3.4.2. Bioleaching

Vachon *et al.* (1994) performed a series of experiments, utilizing both chemical and biological extraction processes, to extract aluminium from red muds. The biological leaching portion of the study were carried out using bacteria and fungi. The bacteria were described as "sewage sludge bacteria" which were a range of indigenous bacteria of the genus *Acidithiobacillus*. The fungi investigated were *Aspergillus niger, Penicillium notatum* (now named *Penicillium chrysogenum*), *Penicillium simplicissimum* and *Trichomeda viride*. The highest extraction of Al was produced by bioleaching with *P. simplicissimum* which extracted 75% Al (10550 mg/L). The authors also noted that the acids produced by *P. simplicissimum*, though largely citric acid itself, was able to extract more Al than pure citric acid under the same conditions. Toxicity characteristic leaching procedures were also performed by the authors and showed that leaching toxicity had decreased throughout the leaching process due to the removal of heavy metals.

Qu *et al.* (2013) also utilized *Aspergillus niger* for the bioleaching of heavy metals from red mud. 3 differing processes were tested. One-step, two-step and "spent medium" processes were tested, along with a range of pulp densities. *A. niger* produced citric acid, which acted as the primary lixiviant during the leaching process. The highest leaching ratios observed were 80% of Pb & Zn, 67% Cu, 50% Ni, 44% As, 31% Ba, 26% Cr and 11% Fe & Zr. This was achieved at 1% red mud pulp density using the spent medium process, which involved incubating the fungi within a sucrose medium for 10 days, before the addition of sterilized red mud to the spent medium. This was then incubated at 30°C with continuous agitation at 120rpm.

Qu & Lian (2013) performed research into the extraction of REEs and radioactive elements from red muds. The fungi they used was *Penicillium tricolor* (RM-10), which produced oxalic and citric acids as the main lixiviants. While the maximum leaching ratios of REE and radioactive elements were achieved using a one-step process at 2% pulp density, the highest extraction yields were achieved from a two-step process at 10% (w/v) pulp density.

Following on from their previous studies Qu *et al.* (2015) performed a preliminary study into the extraction of valuable metals from red mud using batch and continuous leaching processes. The valuable metals that were targeted were Ga, Ge, V, Sc, La, Eu and Yb.

Samples of red mud were inoculated with *Aspergillus niger* with sucrose as the organic electron donor. The best leaching ratios achieved during the batch tests were achieved using the spent medium process from the authors' previous study, at 2% pulp density, 30°C and 120rpm agitation. Under these conditions approximately 67% Ge, 59% Yb, 50% Ga, 44% Sc, 40% V and 30% Eu and La were recovered.

The continuous leaching process had, first, a discontinuous stage to allow the fungi time to grow within the reactor. After the discontinuous stage the continuous leaching was started with the same parameters as the batch leaching experiment, with the exception of the residence time being set to 48h. The leaching percentages under these conditions were 60% Ge, 62% Yb, 54% Ga, 45% Sc, 37% V and 30% Eu and 27% La. The continuous leaching process had similar effectiveness to leaching with pure citric acid. As a comparison a brief cost analysis was performed and it was identified that to perform an extraction on 1 ton of red mud the bioleaching would cost approximately half of what it would cost using citric acid.

It was noted that when pulp densities were increased the biomass produced decreased, as did the leaching efficiencies and the production of citric and gluconic acids (oxalic acid production slightly increased). This demonstrated that red mud has an adverse effect on the growth of the non-indigenous *A. niger*. It was also observed, however, that prolonged residence times were beneficial to fungal growth. Though once residence time increased beyond 6 days the effects were marginal.

3.4. Chapter Summary

Chapter 3 has reviewed and summarised the literature concerning the generation and physicochemical characteristics of a range of iron oxide bearing wastes. Particular focus has been given to wastes arising from the treatment of mine drainage and metallurgical process solutions and wastes, such as red mud and tailings, arising from the physical processing of ore material. A summary of a variety of abiotic and microbially mediated metal recovery studies has also been discussed. The chapter can be summarised as follows:

- The oxidation of sulphides within mine wastes or abandoned mine shafts generates metalliferous acidic mine drainages. Oxidation of ferrous iron within these drainages produces iron oxyhydroxide sludges. Given the extensive history of mining there are vast amounts of mine waste and abandoned mines worldwide with the resultant AMD and sludges a significant global issue. Treatment of metalliferous mine waters can be achieved via either passive (e.g. reed bed systems) or active treatment (pH increase via lime dosing) systems.

- Whereas metalliferous sludges are formed from the treatment of mine waters, tailings are formed from the physical processing of ore materials. Tailings are primarily formed of gangue minerals but contain the element of interest albeit at very low grades which are no longer economically viable to process.

- The physicochemical characteristics of both tailings and mine water treatment sludges are highly variable and are generally defined by the source material and the nature of the processing applied to create the wastes. However, there are a small number of characteristics common to wastes of a range of provenances including a high water content, low hydraulic conductivity, particle sizes largely <63 µm and bulk density ~0.8-2.2 Mg/m^3.

- A range of abiotic and biotic extraction techniques have been applied for the recovery of metals from a number of waste streams including cyanidation tailings, smelter plant sludges, zinc leaching residues, laterite tailings and chromite overburden. Treatment methods applied include roasting, leaching, electrowinning, flotation and magnetic separation. Bioreductive leaching studies have primarily focused on the recovery of Co, Ni and Cu from lateritic wastes and chromite overburden.

- Red mud is a waste product produced during the production of alumina. Red mud is highly alkaline, typically dominated by iron and aluminium oxides and often has elevated concentrations of Al, V, Ga, Ni, Zn, Sc and rare earth elements. Approximately 1.5-2 tons is produced per ton of alumina with the waste typically stored in lagoons.

- Due to the vast quantities of red mud and the potential metallic value held within the waste there has been substantial research interest into red muds. Both chemical and biological extraction techniques have been studied with fungi genera such as *Penicillium* and *Aspergillus* utilised for extraction.

- Many of the studies into metal recovery from wastes report high recovery rates. However, these recovery rates are often only achieved when there has been extensive physical manipulation of the waste and stringent controls on the experimental conditions are employed.

4. Iron Oxidation Chemistry and Mineralogy

4.1. Introduction

As the counterbalancing reaction to reduction, and the mechanism by which the majority of the wastes studied in this thesis are produced, it is important to consider the chemistry behind the oxidation of iron. Within this chapter the chemical and microbial oxidation of iron are discussed with particular focus on the impact of microbial iron oxidation. The nature and properties of the iron oxide and hydroxide minerals formed as a result of iron oxidation are discussed at length along with their association with metals of potential economic interest.

Section 4.2: Iron Oxidation Chemistry – Briefly discusses the mechanisms and rates of abiotic oxidation of ferrous iron

Section 4.3: Microbial Oxidation of Ferrous Iron - Discusses the various mechanisms of ferrous iron oxidation by iron oxidising microbes. Including neutrophilic aerobes, neutrophilic anaerobes and acidophilic aerobes.

Section 4.4: Nature and Properties of Iron Precipitates- Describes the formation and properties of a range of iron oxide and hydroxide minerals.

Section 4.5: Coprecipitation of Trace Metals with Iron Oxyhydroxides – Describes the mechanisms by which metals of potential economic interest become associated with iron oxyhydroxides within the waste streams

Section 4.6: Chapter Summary

4.2. Iron Oxidation Chemistry

As the most abundant transition metal within the Earth's crust, iron can be found as silicates, sulphides and oxides. Weathering of these minerals can cause elevated concentrations of dissolved iron within groundwater and mine drainage waters worldwide (Lide, 2004; Nordstrom, 2011). However, in circum-neutral (pH 6.5-7.5)

surface waters the concentrations of iron are lower than would be assumed from the crustal abundance. This is because the products of hydrolysis and oxidation of iron generally have low solubility. Oxidation is recognised as the rate-controlling factor for the precipitation of iron oxyhydroxides at neutral pH (Singer & Stumm, 1970). Stumm & Lee (1961) proposed the reaction shown in Equation 4.1 for the oxidation of Fe(II) by aqueous O_2 to Fe(III).

Equation 4.1

$$4Fe^{2+} + O_2 + 6H_2O \rightarrow 4FeO(OH)_{(S)} + 8H^+$$

There are two potential pathways by which abiotic oxidation of Fe(II), by dissolved O_2, can proceed. Homogeneous oxidation occurs within solutions of circum-neutral pH's and follows Equation 4.2, where pH is the significant rate controlling variable (Sung & Morgan, 1980; Stumm & Morgan, 1996)

Equation 4.2

$$-\frac{d[Fe^{2+}]}{dt} = k_1[Fe^{2+}][OH^-]^2 P_{O_2}$$

Heterogeneous oxidation occurs in association with the surfaces of minerals within the solution. Within this process dissolved Fe(II) sorbs to Fe(III) oxyhydroxides and reacts with dissolved oxygen to form a new iron oxyhydroxide mineral (Tüfekci & Sarikaya, 1996, 1998; Tüfekci *et al.*, 2000; Dempsey *et al.*, 2002; Park & Dempsey, 2004). Experimental modelling has suggested that two surface Fe(ll) species, FeOFe+ & FeOFeOH°, are required for the adsorption of Fe(ll) onto goethite (Coughlin & Stone, 1995), lepidocrocite (Zhang *et al.*, 1992), hematite, and ferrihydrite (Liger *et al.*, 1999). Dietz & Dempsey (2001) observed an increase in the rate of Fe(II) oxidation in AMD sludges when ferric oxides were present due to the autocatalytic effect of the ferric oxides.

4.3. Microbial Oxidation of Ferrous Iron

Iron oxidising microorganisms (FOM) can be subdivided into three groups; 1) neutrophilic, aerobic iron oxidisers, 2) neutrophilic, anaerobic iron oxidisers and 3)

acidophilic, aerobic iron oxidisers. Each will be briefly summarised in the following sections. A phylogenetic tree displaying the diversity of FOM is presented in Figure 2.2 within Section 2.2.

4.3.1. Neutrophilic, Aerobic Iron Oxidisers

Due to the rapid rate of abiotic oxidation of ferrous iron, microbial oxidation of ferrous iron within circum-neutral pH and oxygen-rich conditions is generally considered to be a minor factor in comparison to abiotic oxidation. This often means that aerobic FOM are found to colonise the interface between aerobic and anaerobic zones. This is also due, in part, to many of these aerobic FOM actually being microaerophilic (Hedrich *et al.*, 2011; Ionescu *et al.*, 2015). Continuously-stirred tank reactor field tests with circum-neutral (pH 6-7), oxygenated (4.0-4.5 mg/L) mine drainage, performed Kirby & Elder Brady (1998), displayed Fe(II) oxidation rates within as little as "one-half order of magnitude" from those predicted by the Stumm & Lee (1961) abiotic rate law. This was achieved without considering the impact of neutrophilic FOM given its negligible effect in oxygen-rich environments, highlighting their limited significance in aerobic environments.

Due to their perceived limited impact at circum-neutral pH and oxic conditions, research into aerobic FOM has been limited. All cultivated FOM, which use oxygen as an electron acceptor, belong to the *proteobacteria* with freshwater species generally found within *Betaproteobacteria* (Emerson *et al.*, 2010). Only three genera of aerobic, neutrophilic FOM having been described; *Gallionella, Leptothrix* and *Marinobacter* (Weber *et al.*, 2006).

4.3.2. Neutrophilic, Anaerobic Iron Oxidisers

Neutrophilic, anaerobic FOM can be further divided into two groups; nitrate-respiring FOM and photosynthetic FOM. Nitrate-respiring FOM are more phylogenetically diverse than other FOM and aren't associated with one particular class of *Proteobacteria*, instead being spread fairly randomly throughout the alpha-, beta-, gamma- and *Deltaproteobacteria* classes. This is reflected in the wide range of environments and

temperatures in which these FOM have been found. Nitrate-respiring FOM have been observed in freshwater, marine, hydrothermal and deep sea sediments and found to grow optimally within a range of temperatures, with psychrophilic, mesophilic and hyperthermophilic FOM identified (Weber *et al.*, 2006; Hedrich *et al.*, 2011).

Nitrate-respiring FOM were first identified by Straub *et al.* (1996) within active enrichment cultures containing ferrous iron and nitrate. They isolated and observed 3 Gram-negative bacteria which, whilst capable of oxidising ferrous iron in anaerobic, nitrate-containing media, displayed slow rates of iron oxidation when no organic acid was provided. The end products of the oxidation in all 3 cases were nitrogen gas, small amounts of nitrous oxide (N_2O) and ferrihydrite with an overall reaction equation as shown in Equation 4.3.

Equation 4.3

$$10FeCO_3 + 2NO_3^- + 10H_2O \rightarrow Fe_{10}O_{14}(OH)_2 + 10HCO_3^- + N_2 + 8H^+$$

Further research has shown that the respiration of nitrate coupled to the oxidation of ferrous iron will not occur, or at least will not facilitate growth in circum-neutral conditions without an additional electron donor or organic carbon present (Straub *et al.*, 1996; Chaudhuri *et al.*, 2001; Shelobolina *et al.*, 2003; Weber *et al.*, 2006). Despite this it is believed that the activity of nitrate-respiring anaerobic FOM is more important of iron cycling on a global scale than that of phototrophic FOM as they are not constrained to areas of sunlight (Straub *et al.*, 2001; Weber *et al.*, 2006; Hedrich *et al.*, 2011).

Anaerobic, phototrophic FOM were the first microorganisms identified capable of ferrous iron oxidation in anaerobic environments (Ehrenreich & Widdel, 1994). Phototrophic FOM have been isolated from freshwater and marine sediments with the majority belonging to the *alpha-proteobacteria* class. Most phototrophic FOM utilize light to facilitate the fixation of CO_2 into the biomass, while the ferrous iron acts as a reductant for the reaction (Equation 4.4) (Weber *et al.*, 2006; Hedrich *et al.*, 2011)

Equation 4.4

$$HCO_3^- + 4H^+ + 10H_2O \rightarrow CH_2O + 4Fe(OH)_3 + H^+$$

The impact phototrophic FOM have on iron cycling on a global scale is limited predominantly by 2 factors. Phototrophic FOM have been seen to readily oxidise dissolved Fe(II), but are unable to utilise ferrous iron held within less soluble Fe(II) minerals such as pyrite or magnetite (Kappler & Straub, 2005). Secondly, phototrophic FOM can only metabolise within areas of sufficient light penetration. Ciani *et al.* (2005) state that the maximum penetration of light into soils/sediments is ~200µm, without considering any water cover. These restrictions limit the extent of viable sites for significant phototrophic FOM activity on a global scale.

4.3.3. Acidophilic, Aerobic Iron Oxidisers

Acidophilic, aerobic FOM are the most widely studied of all FOM. This is because of their importance in the generation of acidic mine drainage (see Section 3.2.1) and their extensive use in biomining (see Section 1.3).

Acidophilic FOM are physiologically and phylogenetically diverse with multiple *bacteria* and *archaea* known. A thorough review of the diversity of acidophilic FOM was carried out by Hallberg & Johnson (2001). The environments in which acidophilic FOM have been found is also very diverse. Along with those that are metabolically active in acidic environments (pH < 3), examples of moderate acidophiles have been found which are active at pH of 3-5. Due to wide range of environments and conditions these microbes have been found in, it is common for them to be categorized based on their defining characteristics (e.g. thermophiles, autotrophs, mixotrophs etc.). Due to its importance to industry, one of the more common categorisations is whether the FOM is capable of solubilizing minerals to facilitate biomining. The bacteria, both FOM and sulphur-oxidisers, capable of solubilising minerals typically associated with metallic deposits (e.g. pyrite) are the most widely studied. *Acidithiobacillus ferrooxidans*, the first acidophilic FOM identified, is by far the most studied iron-oxidiser of any kind (Hedrich *et al.*, 2011), though is closely followed by other acidophilic FOM such as *Leptospirillum ferrooxidans and Acidiphillium ssp.* (Johnson & Hallberg, 2003).

4.4. Nature and Properties of Iron Precipitates

At circum-neutral pH the concentration of dissolved Fe is determined by the solubility of the Fe oxyhydroxides. Figure 4.1 shows the Eh-pH stability zones for various iron oxyhydroxides, as found in an aqueous environment. It shows that with an increase in redox potential (Eh) the Fe transitions from soluble Fe(II) into Fe(III) in the form of largely insoluble oxyhydroxides. Fe(III) oxyhydroxide solubility is also a function of the concentration of Fe(III) ions in solution as displayed in Figure 4.2.

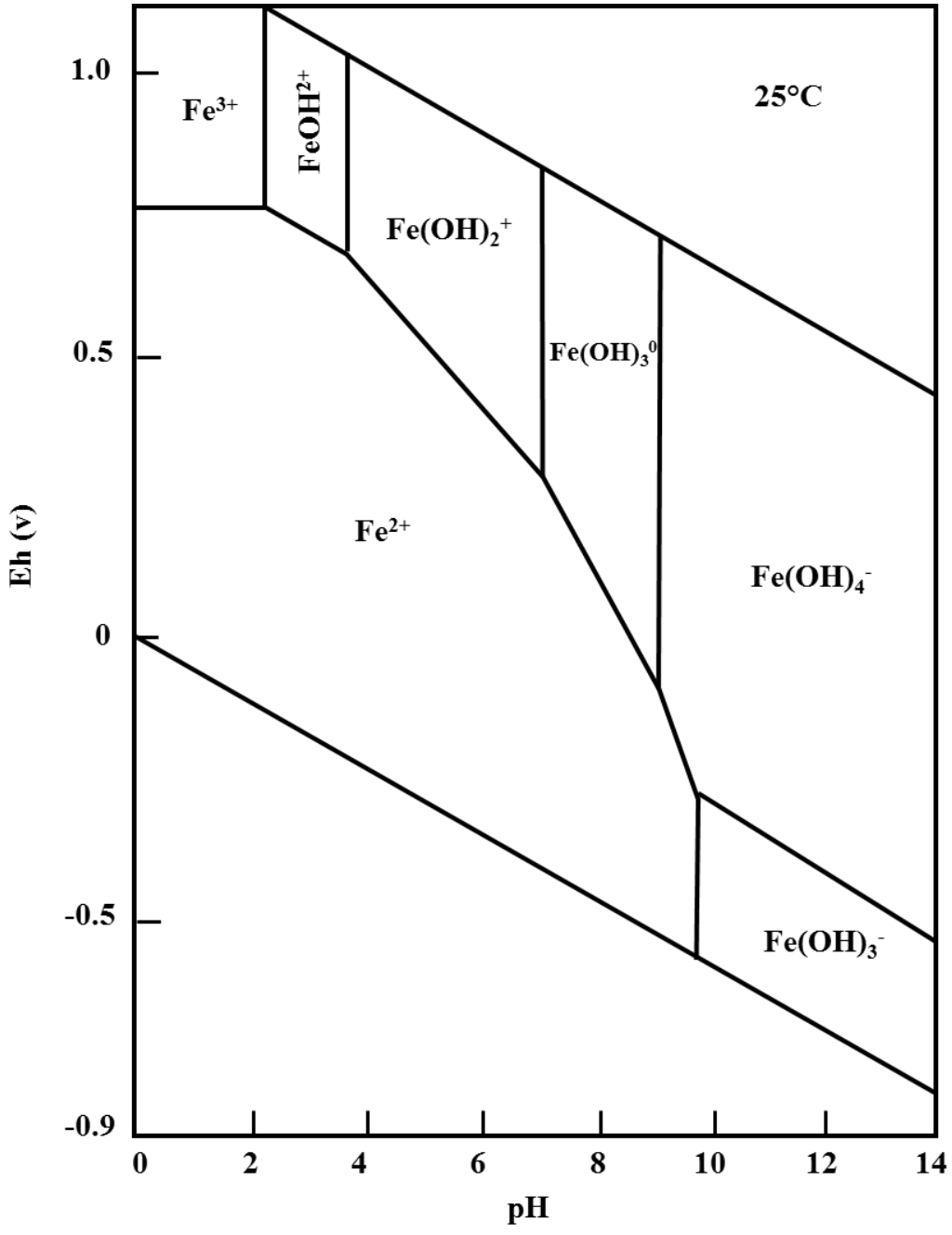

Figure 4.1: Eh-pH Stability diagram for aqueous species of iron oxyhydroxides in the system Fe-O_2-H_2O. Adapted from {Langmuir, 1997 #106}

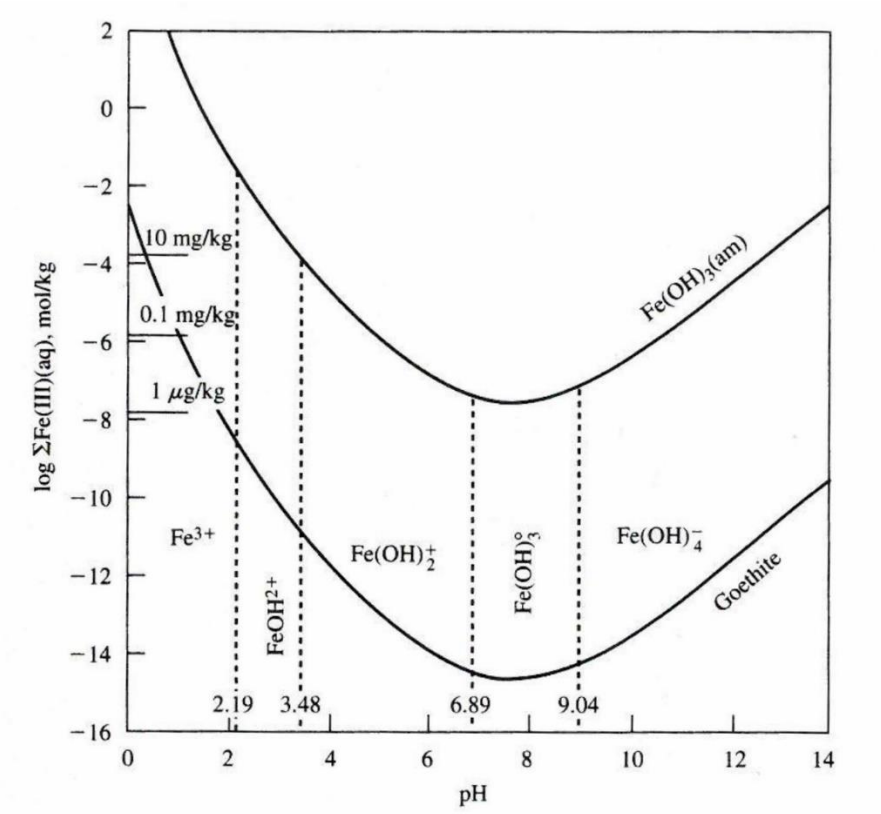

Figure 4.2: Solubility of iron oxyhydroxides as a function of Fe(III) concentration and pH. Upper curve represents pK_{sp} = 37.1 and lower curve represents pK_{sp} = 44.2 (Langmuir, 1997)

4.4.1. Ferrihydrite

The predominant form of iron oxyhydroxides within oxidised mine wastes is ferrihydrite, also sometimes referred to as hydrous ferric oxides (HFO) (Langmuir, 1997). Ferrihydrite is formed due to the rapid oxidation of Fe(II) and hydrolysis of Fe(III). Dousma & DeBruyn (1976) identified 4 steps in this process which are outlined in Figure 4.3. Whilst no one formula is universally accepted, ferrihydrite is believed to have the chemical formula $Fe_5HO_8{\cdot}4H_2O$ (Jambor & Dutrizac, 1998). The rapid formation results in the ferrihydrite being amorphous and generally forms very small particles (1-10nm) as the process is too rapid for crystalline iron oxyhydroxides to form (Crosby, 1983; van Der Woude & De Bruyn, 1983; Dzombek & Morel, 1990). The presence of crystallisation inhibitors, such as organics, phosphate and silicate species, also results in ferrihydrite being amorphous. This amorphous nature coupled with the small particle size of ferrihydrite results in a large surface area often greater than 200 m^2/g (Schwertmann & Cornell, 2000; Cornell & Schwertmann, 2003); though Anderson & Malotky (1979) reported a surface area of 720 m^2/g (Dzombek & Morel, 1990).

Step	Process
1	Rapid formation of iron hydroxomonomers and dimers
2	Rapid combination of hydroxomonomers to small polymers
3	Slower formation of larger polymers via oxolation of hydroxy complexes
4	Formation and precipitation of solid phase ferrihydrite

Figure 4.3: Brief breakdown processes in the formation and precipitation of ferrihydrite

There is often goethite, a more crystalline iron oxyhydroxide, associated with the ferrihydrite though the presence of crystallisation inhibitors, such as co-precipitated sulphate (Brady *et al.*, 1986), silicate (Karim, 1984; Cornell *et al.*, 1987) or phosphates and organic acids (Cornell & Schneider, 1989), act to stabilise ferrihydrite and retard its transformation to more stable minerals like goethite. The exception to this is the organic ligand cysteine which Cornell & Schneider (1989) observed would directly promote transformation of ferrihydrite to goethite. In circum-neutral environments the transformation of ferrihydrite to goethite is a slow process taking months to years. Transformation to goethite (Schwertmann & Cornell, 2000) and haematite (Schwertmann *et al.*, 1999) has even been observed after several years in air-dry samples.

Ferrihydrite can exist as two forms, “6-line-” and “2-line-” named for the number of peaks each returns on a XRD analysis. 6-line-ferrihydrite, while still amorphous, shows more crystal structure than 2-line-ferrihydrite. This is a result of the mechanism by which it forms. 6-line-ferrihydrite forms as a result of rapid hydrolysis of ferric salt solutions at low pH and high temperatures (e.g. 80 ˚C). Whereas 2-line-ferrihydrite is produced as a result of rapid hydrolysis at circum-neutral pH and more moderate temperatures (e.g. 20 ˚C) (Schwertmann & Fischer, 1973).

A comprehensive review of ferrihydrite and its properties was published by Jambor & Dutrizac (1998).

4.4.2. Green Rust

Green rust is a generic term for a group of mixed valence iron (Fe(II)/Fe(III)) (hydroxy)oxide salts represented by the overall chemical formula $[Fe^{II}_{(6-x)}Fe^{III}_{(x)}(OH)_{12}]^{x+}[(A^{2-})_{x/2}\cdot yH_2O]^{x-}$. When found in nature they are sometimes referred to as the mineral fougrite. These minerals can be further divided into two "types". Type one green rusts are characterised by their rhombohedral crystal structure whilst type two green rusts are hexagonal. Green rusts can be further defined by the anions within their structure. The most common varieties are carbonate, chloride and sulphate green rust with the former two belonging to type one and the latter type two (McGill *et al.*, 1976). A defining characteristic of all types of green rust is that they are metastable and even slight changes in environmental conditions can cause them to decompose.

Green rusts are known to be formed both abiotically and biotically. The formation of green rusts by bacteria is known to be an important factor in the biogeochemical cycling of iron in the environment. A range of dissimilatory iron reducing bacteria have been observed to produce green rusts during the reductive dissolution of iron oxyhydroxides, members of the species *Shewanella* being the most intensely studied (O'Loughlin *et al.*, 2007), particularly *Shewanella Putrifaciens* (Fredrickson *et al.*, 1998; Ona-Nguema *et al.*, 2002; Zachara *et al.*, 2002).

Green rusts are known to be precursors to magnetite and siderite formation after the bio-reduction of ferrihydrite within the pH range 6.5-7.5. (Fredrickson *et al.*, 1998; Genin *et al.*, 1998; Zachara *et al.*, 2002). The oxidation of green rusts can also result in the formation of a range of other iron oxyhydroxides such as ferrihydrite, goethite, akageneite, lepidocrocite, hematite or maghemite. The form of iron oxyhydroxide that is formed depends on a range of factors such as pH, the form of the oxidant, rate of oxidation and the degree and rate of dehydration (Loyaux-Lawniczak *et al.*, 2000) Glasauer *et al.* (2003) observed that HFO would be transformed to green rusts when Fe(II) is present and the faster Fe(II) was produced the faster green rust was formed. A general scheme for the formation and potential transformation mechanisms for green rusts is shown in Figure 4.4

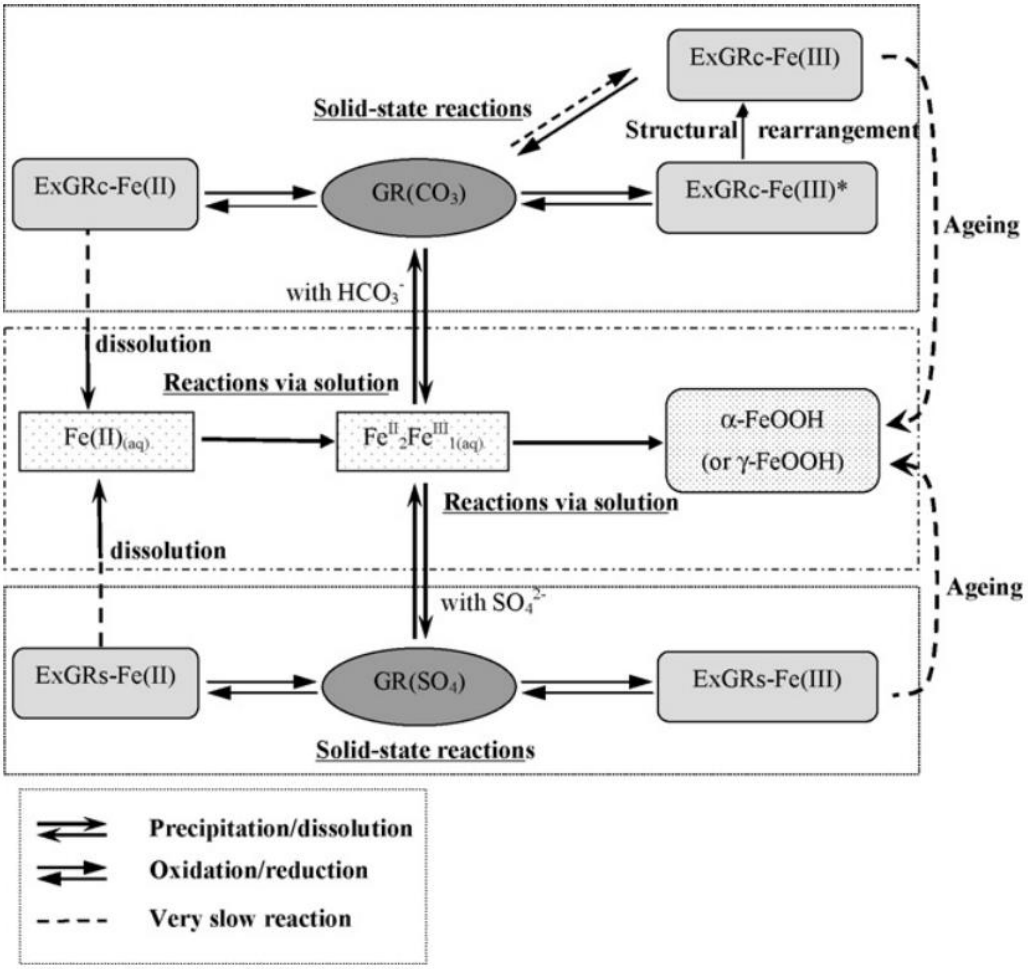

Figure 4.4 Diagram of formation and potential transformation mechanisms for carbonate and sulphate green rusts. ExGrs denotes the products of green rust oxidation or reduction (Antony *et al.*, 2008)

4.4.3. General properties of common iron oxyhydroxides

Table 4.1: Physical and chemical properties of selected iron oxyhydroxide minerals (Cornell & Schwertmann (2003) and references within)

Mineral	Chemical Formulae	Structure	Colour	Density (g/cm^3)	Hardness	Surface Area (m^2/g)	Magnetic Properties	Substituting Cations
Ferrihydrite	$Fe_5HO_8 \cdot 4H_2O$	Hexagonal	Red-brown	3.96	-	200-400	Speromagnetic	Al^{3+}, Cd^{2+}, Mn^{2+}, Ni^{2+}, Pb^{2+}
Goethite	α-FeOOH	Orthorhombic	Yellow-brown	4.26	5-5.5	8-200 (typically 80-150)	Antiferromagnetic	Ni^{2+}, Zn^{2+}, Cd^{2+}, Al^{3+}, Cr^{3+}, Ga^{3+}, V^{3+}, Mn^{3+}, Co^{3+}, Sc^{3+}, Pb^{4+}, Ge^{4+}
Haematite	Fe_2O_3	Rhombohedral Hexagonal	Red	5.26	6.5	2.8-27.4	Weakly ferromagnetic or antiferromagnetic	Al^{3+}, Cr^{3+}, Mn^{3+}, Rh^{3+}, Ga^{3+}, In^{3+}, Nd^{3+}, Ni^{3+}, Cu^{2+}, Ge^{4+}, Sn^{4+}, Si^{4+}, Ti^{4+}
Magnetite	Fe_3O_4	Cubic	Black	5.18	5.5	4-100	Ferrimagnetic	Al^{3+}, Mn^{2+}, Ni^{2+}, Cu^{2+}, Co^{2+}, Zn^{2+}, Ca^{2+}, Ge^{4+}
Maghemite	ɣ-Fe_2O_3	Cubic or tetragonal	Reddish brown	4.87	5	8-130	Ferrimagnetic	Al^{3+}, Ti^{3+}, Sn^{4+}
Lepidocrocite	ɣ-FeOOH	Orthorhombic	Orange	4.09	5	15-260	Antiferromagnetic	Al^{3+}
Schwertmannite	$Fe_{16}O_{16}(OH)_y(SO_4)_z \cdot nH_2O$	Tetragonal	Orange-brown	~3.80	-	125-225	Antiferromagnetic	-

4.5. Coprecipitation of Trace Metals with Iron Oxyhydroxides

Coprecipitation is the process by which a solute, that would be expected to remain in solution, is removed due to interacting with a precipitating mineral. There are 3 mechanisms by which coprecipitation can occur; adsorption, inclusion and occlusion (Harvey, 2000).

Stumm & Morgan (1996) defined adsorption as "the accumulation of matter at the solid-water interface". Sorption of metal ions to iron oxyhydroxides is achieved my means of two processes; surface precipitation and surface complexation. Farley *et al.* (1985) suggested the "two-layer model" for the surface precipitation of divalent cations, such as Fe(II), to a HFO mineral which "allowed for a continuum between surface reactions and precipitation". Within this model low cation concentrations near the mineral surface leads to surface complexation and the formation of a new hydroxide surface. As the concentration of the cation, increases, the surface complex concentration of surface precipitates also increases to the point where the surface sorption site becomes saturated. At this point surface precipitation becomes the dominant sorption mechanism. Once a cation is adsorbed to the mineral surface, it is then treated as the surface of that mineral.

Surface complexation is the multi-component reaction by which cations adsorb to a mineral surface via the formation of bonds with surface oxygen atom. Dzombek & Morel (1990) identified that iron oxyhydroxides have two types of sites to which cations can adsorb, rather than the one type of site described by Farley *et al.* (1985). This allowed the model to fit with sorption data taken from moderate to high sorbate/sorbent ratio systems. "Type 1" or "high-affinity" sites have, as their name suggests, a high affinity for the adsorption of cations and as such will not adsorb anions. "Type 2" or "low affinity" sites by contrast will adsorb both cations and anions by virtue of their lower affinity. "Type 2" sites are present in much greater concentrations than "type 1" sites. This work updated the surface precipitation model for higher high sorbate/sorbent ratios which has allowed the surface precipitation model to be applied successfully to model sorption of metals such as Zn(II) (Dzombek & Morel, 1990), Pb(II), Hg(II) (Zhu, 2002), Cd(II) (Dzombek & Morel, 1986), Cr(III) (Charlet & Manceau, 1991) and Cu(II) (Karthikeyan & Elliott, 1999) onto iron oxyhydroxides.

The sites identified by Dzombek & Morel (1990) are hydroxyl groups on the mineral surface. These groups can coordinate and dissociate protons making the system highly pH dependant. With Dzombek & Morel (1990) suggesting that cation sorption onto hydrous oxides “can increase from 0 to 100 percent over a narrow pH range, typically one or two pH units”. This is because within the “electric double layer theory” protons can determine the charge on the surface of the mineral. Appelo & Vet (2003) noted that when in distilled water at a pH of 8.1 ferrihydrite is chargeless but when in pH 7 conditions, ferrihydrite has a positive surface charge. This limits adsorption of cations to only those which have a chemical affinity to the sorption site greater than the repulsive electrostatic force arising from the protons.

Adsorption of cations is known to be time-dependant and can be broadly defined by two stages. The initial stage is characterised by rapid sorption, while the second is characterised by much slower sorption which persists for considerably longer, potentially up to months (Strawn *et al.*, 1998; Scheinost *et al.*, 2001; Trivedi & Axe, 2001; van Beinum *et al.*, 2005). The amount of a cation that will adsorb is also related to the pH of the system. As displayed in Figure 4.5, as a system decreases in acidity and tends towards neutral the mole percentage adsorbed increases rapidly. This suggests that at circum-neutral pH, assuming other conditions are conducive, a cation will be readily sorbed to a ferrihydrite particle.

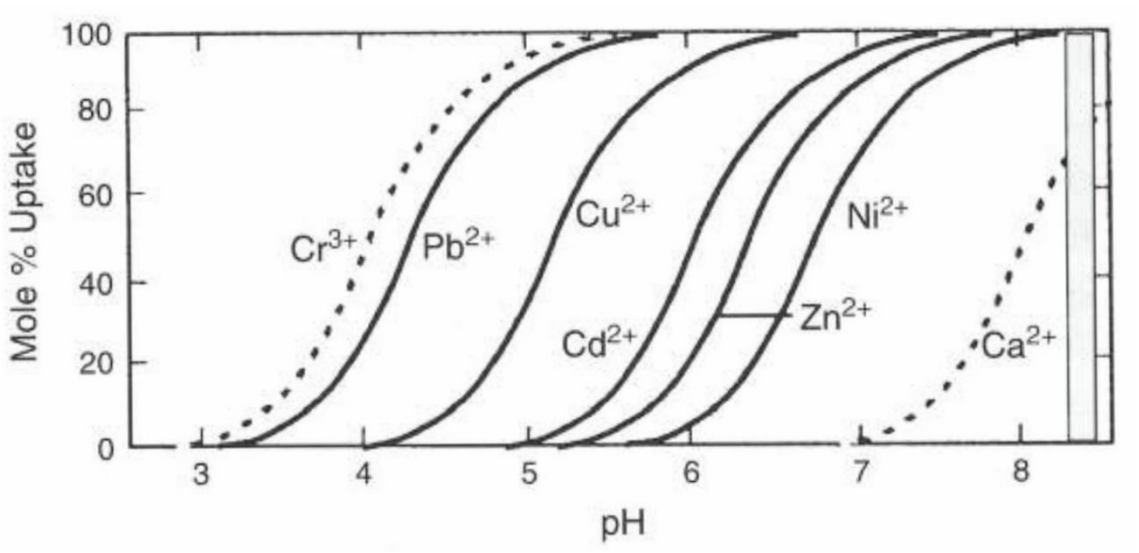

Figure 4.5 Mole % uptake of cations to HFO as a function of pH. Vertical bar situated at pH =8.5 represents pH at which HFO has zero surface charge (Brown Jr. *et al.*, 2008).

Adsorption affinity must also be considered when predicting the adsorption of cations to a ferrihydrite particle. For group 1 and group 2 metal cations, those with larger ionic radii have a greater adsorption affinity (Stumm, 1992) (Figure 4.6) For “d”-block metals the adsorption affinity is related to the configuration of electrons in the cation, described in the “Irving-Williams series which is also displayed in Figure 4.6 (Irving & Williams, 1953; Stumm, 1992).

$$Group\ 1: \quad Cs^{+} > Rb^{+} > K^{+} > Na^{+} > Li^{+}$$

$$Group\ 2: \quad Ba^{2+} > Sr^{2+} > Ca^{2+} > Mg^{2+}$$

$$\text{d-}Block: \quad Zn^{2+} < Cu^{2+} > Ni^{2+} > Co^{2+} > Fe^{2+} > Mn^{2+}$$

Figure 4.6 Relative adsorption affinities of group 1, 2 and d-block cations to hydrous ferric oxides (HFOs) (Irving & Williams, 1953; Stumm, 1992)

While adsorption is the main mechanism by which trace metals become bound to ferrihydrite, the other mechanisms of coprecipitation must also be considered when trying to understand the relationship between metal cations and iron oxyhydroxides. These mechanisms are inclusion and occlusion.

There are two forms of inclusion (sometimes termed substitution) that can potentially cause the removal of cations from solution; isomorphic inclusion and non-isomorphic inclusion. Isomorphic inclusion is the process by which a coprecipitated ion occupies the place of another ion within the crystal lattice structure of the precipitate. For this to occur the coprecipitated ion must have the same charge and similar dimensions to the lattice ion it replaces. Substitution of a contaminant ion into a iron oxyhydroxide may cause changes to the volume and morphology of the crystal lattice (Schulze & Schwertmann, 1987), solubility (Schwertmann, 1991), magnetic properties and the rates of acid and reductive dissolution (Cornell & Schwertmann, 2003).

Figure 4.7 displays the cations that are known to be capable of substituting into a range of iron oxyhydroxides. Aluminium is the metal cation most readily substituted into

goethite and haematite, these substituted minerals are found in natural environments. Further work with laboratory synthesized goethite has shown that Cr(III), V(III), Mn(III), Ni(II), Cu(II), Zn(II) and Cd(II) can all substitute into goethite to levels up to 10% (Cornell & Schwertmann, 2003). Non-isomorphic inclusion occurs when the contaminant ion has difference dimensions to the lattice forming ions. In this situation the inclusion forms a solid solution where impurities within the crystal lattice are uniformly distributed (Murthy, 2008; Dash, 2011).

Oxide	*Substituting cation*
Goethite	Ni^{II}, Zn^{II}, Cd^{II} Al^{III}, Cr^{III}, Ga^{III}, V^{III}, Mn^{III}, Co^{III}, Sc^{III} Pb^{IV}, Ge^{IV}
Lepidocrocite	Al^{III}
Akaganéite	Cu^{II}, Si^{IV}, Mn^{III}, Ni^{II}
δ-FeOOH	Mn^{III}, Ni^{II}, Co^{II}, Zn^{II}, Cd^{II}, Mg^{II}, Ca^{II}
Hematite	Al^{III}, Cr^{III}, Mn^{III}, Rh^{III}, Ga^{III}, In^{III}, Nd^{III}, Ni^{II} Cu^{II}, Ge^{IV}, Sn^{IV}, Si^{IV}, Ti^{IV}
Magnetite	Al^{III}, Mn^{II}, Ni^{II}, Cu^{II}, Co^{II}, Zn^{II}, Ca^{II}, Ge^{IV}
Maghemite	Al^{III}, Ti^{IV}, Sn^{IV}

Figure 4.7. Summary of cations known to substitute for Fe(III) within various iron oxyhydroxides (Cornell & Schwertmann, 2003)

Occlusion is the process by which a solute, in this circumstance a trace metal cation, is physically trapped by another precipitating mineral and is therefore coprecipitated out of solution (Harvey, 2000). The Paneth-Fajans-Hahn rule of adsorption states that “the less soluble the salt the more it will occlude” (Murthy, 2008). This mechanism has not been greatly studied in the context of trace metals being occluded by ferrihydrite. This is largely due to the high adsorption capacity of ferrihydrite causing trace metal cations to preferentially adsorb. Arsenic and nickel are exceptions to this rule as there have been a small number of studies into the occlusion of both the elements to ferrihydrite in under various conditions. For example, Eickhoff *et al.* (2014) observed that nickel readily sorbs to surface of ferrihydrite or becomes occluded while not undergoing inclusion (isomorphic or non-isomorphic) into the crystal lattice.

4.6. Chapter Summary

Chapter 4 has reviewed the literature concerning the oxidation of ferrous via both abiotic and biotic pathways. Also discussed were the nature and properties of iron oxyhydroxides typically formed as a result of ferrous iron oxidation and the mechanisms by which other metals may become associated with these minerals. The key points of the chapter can be summarised as follows:

- There are two potential pathways for abiotic oxidation of ferrous iron; homogenous and heterogenous oxidation.
- Homogenous oxidation occurs in solution and is highly pH dependent under circum-neutral conditions. Under more acidic conditions, the influence of pH decreases.
- Heterogenous oxidation occurs on mineral surfaces. When ferrous iron sorbs to ferric oxyhydroxide surfaces it reacts with dissolved oxygen to form more ferric oxyhydroxide, which in turn reacts with more ferrous iron. This results in an autocatalytic effect on ferrous iron oxidation.
- Iron oxidising microbes can be grouped into 3 distinct types; neutrophilic, aerobic oxidisers, neutrophilic, anaerobic oxidisers and acidophilic aerobic oxidisers. Of the 3 the latter has the most significance with regards to the generation of AMD.
- Solubility of iron within mine drainages or metallurgical processing solutions is a function of pH, redox potential and concentration of iron ions in solution.
- One of the most commonly formed iron oxyhydroxides is ferrihydrite which typically forms amorphous, fine (1-10nm) particles. This will often transform over time to the more crystalline goethite.
- Due to the high surface area of ferrihydrite it has a high sorption capacity for cations including metals of potential economic value. While sorption of cations to iron oxyhydroxides increases substantially under circum-neutral conditions, sorption can decrease substantially at higher pH due to the loss of charge on the mineral surface.

- Green rusts are a group of metastable, mixed valance iron hydroxides often formed by the microbial reduction of iron oxyhydroxides. Magnetite and siderite are end products of such reduction under ideal conditions, while the oxidation of green rusts results in goethite formation.

- As well as adsorption other mechanisms by which metals can become associated with iron oxyhydroxides are occlusion and inclusion within the mineral structure. Ni, Zn, Al and Pb are amongst the metals capable of being substituted into the structure of goethite.

5. Methods and Materials

5.1. Introduction

This chapter presents details of the analytical methods used in the physical and chemical characterisation of the wastes along with those methods applied for measuring key experimental parameters of the effluents generated during experimentation. Also presented are details on the methods utilised for microbial community analysis of the wastes.

Section 5.2: Solid Waste Analytical Methods – Details the methods applied to characterise the physicochemical properties of the solid waste samples both pre- and post-experimentation.

Section 5.3: Analysis of Experimental Effluents – Details methods applied to the effluents generated during experimentation to measure key experimental parameters.

Section 5.4: Microbial Analysis – Details methods used to extract DNA from the wastes and analyse the indigenous microbial communities within the wastes via 16S rRNA gene sequencing.

Section 5.5: Column Experiment Overview – Details the reasoning and benefits behind the use of flow-through columns for experimentation.

5.2. Solid Waste Analytical Methods

5.2.1. Solid Waste Sample Preparation and Drying

All solid waste samples were homogenised before use by stirring/folding. Where samples were stored within multiple buckets, each bucket was thoroughly mixed before a sub-sample (between 1-2.5kg dependent on number of samples) from each bucket was placed into a new 20l polypropylene bucket and all homogenised together to create a singular sample of at least 5kg, indented to be more representative of the total waste mass. Otherwise the samples were kept in the original container and mixed with a

handheld cement paddle mixer, for a minimum of 10 minutes, until satisfactory homogenisation was achieved.

Any samples which were required to be dried for analysis were spread thinly on drying trays (covered with brown paper to prevent cross-contamination) and dried within the oven at 40°C for a minimum 48h as suggested by Schwertmann & Cornell (2000). This temperature was chosen to minimise the recrystallisation of amorphous minerals, like ferrihydrite, to more crystalline forms thereby invalidating and later analysis. After drying the samples were ground using an agate mortar to break up any aggregates from the drying.

During experimentation it became apparent that meta-stable minerals, that are highly susceptible to alteration when conditions (such as exposure to oxygen) change, were present in the wastes. A number of techniques were implemented to minimise the contact between the sample and the atmosphere and to reduce the extent of decomposition of these meta-stable minerals. These included sample preparation under nitrogen within a glovebox and using the freeze drying methodology described by Lewis (1997) to retain these meta-stable minerals. An Edwards Freeze Dryer Modulyo (Thermo Fisher) was used to freeze-dry post experimentation waste samples. While freeze-drying is preferable for retaining meta-stable minerals it is still limited in its efficacy when very fine grained material (e.g. ferrihydrite) is present (Schwertmann & Cornell, 2000).

5.2.2. Laboratory Glassware and Equipment Cleaning

When accurate volumes were essential, i.e. in preparation of chemicals or reagents, grade A glassware was used exclusively. Grade B glassware was used for experiments or situations where the level of accuracy of the measurement was not so paramount, i.e. flasks for effluent collection.

5.2.3. Chemicals and Deionised Water

All chemicals used within this study were laboratory grade and obtained from either Fisher Scientific or Sigma Aldrich. All chemicals were used and stored in accordance with

the material safety data sheets provided. High purity, sterile, 18 MΩ deionised water was used within all laboratory experiments and analysis.

5.2.4. Total Digest

An aqua regia microwave digest was used for the total digestion of the waste samples. The digest medium consisted of 70% (w/w) nitric acid and 37% (w/w) hydrochloric acid in a 50:50 ratio, totalling 6 ml (aqua regia), with 0.15 mg of sample being digested. The acid digest was performed within a 100 ml PTFE lined ceramic vessel with a vented PTFE cap using a Multiwave 3000 microwave under a program where wattage ramped up gradually to 900W over 12 min then held at this wattage for 30 min, reaching a maximum temperature of 200 °C. The sample was then left to cool for 25 min. A blank test using only the acid was performed to measure the temperature and pressure achieved.

The resultant solution was then analysed with Inductively Coupled Plasma Optical Emission Spectrometry (ICP-OES; See Section 5.3.3) for the suite of elements displayed in Table 5.1. This allowed calculation of the concentration of elements within the wastes expressed as parts per million (ppm) using Equation 5.1, where A is the analytical value, V is the volume of the aqua regia solution used to digest the sample and W is the mass of digested sample in grams.

Equation 5.1

$$\boldsymbol{Element\ Conc.} = \frac{\boldsymbol{A} \times \boldsymbol{V}}{\boldsymbol{W}}$$

Table 5.1 Elements analysed for during total digest characterisation

Aluminium	Cadmium	Lithium	Silver	Titanium
Antimony	Calcium	Magnesium	Silicon	Tungsten
Arsenic	Cobalt	Manganese	Sodium	Vanadium
Barium	Copper	Molybdenum	Strontium	Zinc
Beryllium	Chromium	Nickel	Sulphur	
Bismuth	Iron	Potassium	Thallium	
Boron	Lead	Selenium	Tin	

5.2.5. Physical Properties

Measurements of the dry solids content (as a weight percentage), bulk density, dry density, void ratio and specific gravity were performed in accordance, where appropriate, with BS 1377-2:1990. All tests were repeated a minimum of 3 times and an average taken to provide accurate measurements. Equations used to calculate the properties are as follows:

The dry solids content was determined via the oven drying method, described within BS 1377-2:1990, and the formula displayed in Equation 5.2.

Equation 5.2

$$\%(\boldsymbol{w/w}) = \frac{\boldsymbol{100}}{\boldsymbol{W_w}}\ \boldsymbol{W_d}$$

Where $\%(w/w)$ is the dry solids content as a weight percentage, W_w is the wet mass of the waste in g and W_d is the dry mass of the waste in g

Bulk density was determined as follows:

Equation 5.3

$$\boldsymbol{\rho_b} = \frac{\boldsymbol{W_w}}{\boldsymbol{V_w}}$$

Where ρ_b is the bulk density in g/cm^3 is, W_w is the wet mass of the waste in g and V_v is the volume of wet waste in cm^3. This value of bulk density along with the water content can then be used to determine the dry density (ρ_d) of the sample using Equation 5.4:

Equation 5.4

$$\boldsymbol{\rho_d} = \frac{\boldsymbol{\rho_b}}{\boldsymbol{1 + (w/100)}}$$

Where ρ_d is the dry density in g/cm^3, ρ_b is the bulk density in g/cm^3 and w is the moisture content of the waste as a percentage, derived from results of solids content/oven drying method.

Void ratio can be determined by using Equation 5.5 and converting the mass of water measured into a volume, given 1cm^3 = 1g as follows:

Equation 5.5

$$\boldsymbol{e = \frac{V_w}{V_{H2O}}}$$

Where e is the void ratio, V_w is the volume of the waste and V_{H2O} is the volume of water within the wet waste in cm^3.

Specific gravity was determined by following the "small pycnometer" methodology outlined within BS 1377-2:1990 and using Equation 5.6:

Equation 5.6

$$\boldsymbol{G_s = \frac{m_2 - m_1}{(m_4 - m_1) - (m_3 - m_2)}}$$

Where G_s is the specific gravity, m_1 is the mass of the empty, dry pycnometer, m_2 mass of dry waste and pycnometer, m_3 is the mass of waste, distilled water and pycnometer and m_4 mass of pycnometer and distilled water

5.2.6. Paste pH

The pH of the wastes were measured using the paste pH methodology outlined in BS ISO 10390:2005. 5ml of dried, homogenised waste was mixed with 25ml of deionised water. This mix was mixed using a magnetic stirrer for 1 hour and then left, without stirring, for a further hour before measurement of the pH.

pH measurement was performed with a Mettler Toledo InLab™ Expert Pro pH probe calibrated at pH 4, 7 and 10.01 with the manufacturer recommended calibrating fluids.

5.2.7. Particle Size Distribution

Particle size distribution (PSD) of the wastes was performed using the dry sieving methodology described within BS 1377-2:1990. Ideally wet sieving would have been

performed, however access to the necessary equipment was not possible. After homogenisation of the wastes, 1kg of each dried waste was sieved by placing the sieve set on a mechanical shaker for 15minutes. The range of sieve apertures used were; 10mm, 5mm, 3.35mm, 2mm, 1.18mm, 600µm, 425µm, 300µm 212µm, 150µm and 63µm. All sieves used conformed to BS 410-1:2000. Before and after use the sieves were flushed with compressed air to ensure no cross contamination of samples and accurate masses of sample retained in each sieve were achieved. Masses of samples retained were measured using a calibrated mass balance accurate to 0.01g.

Where a significant proportion, or in some cases all, of the waste passed through the finest sieves (150 and 63µm) this proportion was subjected to further testing. This testing was performed using a Malvern Mastersizer 3000 and Hydro EV sample dispersion unit. Along with the requisite software, this enables particle size to be measured via laser diffraction.

Particle density and an estimated refractive index of the samples were inputted into the analysis program along with the refractive index of the dispersing media, in this case distilled water. The estimated refractive index chosen for experimentation was 2.4 based on the recommendation of the refractive index of goethite suggested within the manufacturers guide (Malvern Instruments Ltd., 2007) Deionised water was also used for flushing and calibrating the apparatus for each sample tested. A small sample of waste was added to the dispersion unit and cycled through the apparatus for analysis. If necessary, the sample was sonicated while in solution to prevent flocculation. Five separate measurements were taken and averaged for final result.

5.2.8. X-ray Diffraction

Mineral characterisation was undertaken using fine powder X-ray diffraction (XRD). Dried samples of the wastes were ground, within an agate mortar and pestle, to a fine powder. XRD diffractograms were obtained using a Philips PW3830 X-ray generator, PW1710 diffractometer controller and a cobalt radiation source (Co Kα). For a brief periods copper was utilised as a radiation source (Cu Kα) due to circumstances out of the authors control. The use of either a copper or cobalt radiation source is noted on all

diffractograms. The power settings of the generator were 35kV and 40mA, while the diffractometer was set to a scan angle range of 2θ from 5° to 90°, a step size of 0.02° and scan step time of 0.5s. The traces were analysed using the mineral database software, X-pert Hi Score plus analysis.

5.2.9. Sequential Extraction

A sequential extraction procedure adapted from (Poulton & Canfield, 2005), designed for iron rich sediments, was performed on the samples. A summary of this procedure is presented in Table 5.2. The procedure used deviated from the published method by replacing the final two extractions, targeting poorly reactive sheet silicates and residual minerals, with a single extraction for residual minerals constituting an aqua regia microwave digest. The microwave programme ramped wattage gradually to 900W over 12 minutes then held at this wattage for 30min. The sample was then left to cool for 25min.

The extraction procedure allows the differentiation of various phases ascribed as carbonate associated iron (Fe_{Carb}); easily reducible oxides (Fe_{ox1}) e.g. ferrihydrite; reducible oxides (Fe_{ox2}) e.g. goethite and haematite; magnetite (Fe_{mag}); and residual fractions (Fe_{res}). Metal concentrations within each extraction stage were then analysed by ICP-OES. After the first use of this methodology an initial extraction with deionised water was added to account for any metals within a water-soluble phase (Fe_{wat}). Each sample was analysed in duplicate.

Table 5.2 Summary of sequential extraction phases. Adapted from Poulton & Canfield (2005)

Target Phase	Extractant Used	Extraction Conditions
Water soluble (Fe_{wat})	Deionised water	1h, room temperature
Carbonate phases (Fe_{Carb})	1 M sodium acetate solution acidified to pH 4.5 with 99% acetic acid	24h, room temperature
Easily reducible oxides (Fe_{Ox1})	1 M hydroxylamine hydrochloride with 25% (v/v) acetic acid	48h, room temperature
Reducible oxides (Fe_{Ox2})	50 g/l sodium dithionate solution buffered to pH 4.8 with 0.35M acetic acid/0.2M sodium citrate	2h, room temperature
Magnetite phase (Fe_{Mag})	0.2M ammonium oxalate/0.17M oxalic acid solution	6h, room temperature in darkness
Residual fractions (Fe_{Res})	Aqua regia. 50/50 solution of 65% nitric acid and 37% hydrochloric acid	42m in microwave & 25min cooling

5.2.10. Carbon and Sulphur Analysis

Total carbon and sulphur analysis of the solid waste samples was performed using a Leco SC-144DR furnace. Results of sulphur analysis from this instrument have a precision of ±1% relative standard deviation (RSD) or 2.5ppm, whichever is greater. Total carbon analysis has a precision of ±1% RSD or 25ppm, whichever is greater.

Inorganic carbon was analysed using a Shimadzu SSM-5000A. Analysis with this instrument yields repeatability of ±1%. Measurements of total carbon are performed via combustion. While inorganic carbon is assessed via combustion after and initial treatment with phosphoric acid has removed the organic carbon fraction. The difference between readings of total carbon and inorganic carbon was taken as the organic carbon content of the sample.

5.3. Analysis of Experimental Effluents

5.3.1. Effluent Sample Collection and Storage

Before sampling, the vessel collecting effluent was gently shaken to agitate the effluent and entrain any solids that had precipitated out of solution. Aliquots of effluent were then decanted into 40 ml sample containers and labelled accordingly. These samples

were then acidified with 0.1 ml 20% (v/v) HNO_3. Samples were stored in a refrigerator at 4°C until required for analysis.

5.3.2. pH, Conductivity, Redox Potential, Dissolved Oxygen

For all laboratory experiments, pH was measured using a Mettler Toledo InLab™ Expert Pro pH probe with an integrated temperature compensation function. This was calibrated before using a 3 point calibration (pH 4, 7, 10.01) with manufacturers recommended calibration solutions. Analysis with this instrument has an accuracy of ±0.002 pH units. Conductivity (EC) was measured using a Mettler Toledo LE703 conductivity probe. This instrument was calibrated before use using the manufacturer recommended 1413 µS/cm calibration solution. Analysis with this instrument has an accuracy of ±0.5% of the measured value. Redox Potential (ORP) was measured using a Mettler Toledo InLab™ Redox ORP-probe. This probe was standardized using a reference solution of known redox potential (220 mV). The offset in the reading from the standard was then used, in conjunction with the standard +207 mV value to correct measured ORP to a "standard hydrogen electrode" Eh using a Ag/AgCI electrode. Analysis with this instrument has an accuracy of ±0.1 mV. Dissolved oxygen (DO) was measured using a Mettler Toledo 605-ISM DO probe calibrated with a 2 point calibration of zero oxygen followed by ambient air. The zero oxygen solution was created using Mettler Toledo zero oxygen tablets. Analysis with this instrument has an accuracy of ±0.1 mg/l when readings are between 0 and 8 mg/l, ±0.2 mg/l when between 8 and 20 mg/l and ±10% when between 20 and 50 mg/l. All probes were used in conjunction with a Mettler Toledo SevenExcellence™ Multiparameter system.

5.3.3. Elemental Analyses

Inductively Coupled Plasma Optical Emission Spectrometry (ICP-OES) is used to detect and quantify cationic metal concentrations. The instrument used was a Perkin Elmer Optima 2100 DV in conjunction with an AS90 plus autosampler and WinLab 32 software.

Effluent samples from experimentation were analysed for iron, copper, lead, arsenic, zinc, aluminium, nickel and sulphur. In each case the analysis was calibrated against a set of three commercial standards used to construct a calibration curve covering the

detection range for the expected concentration of each required element. These standards, and an analytical control of deionised water acidified with 2% (v/v) HNO_3, were analysed after every ten samples to identify any analytical drift. If there was ≥10% error in the analysis of the standards the tests of that element were rejected, and the analysis redone. Each sample run also included a duplicate sample. As with the standards, if the duplicate sample returned measurements in excess of 10% error the sample run was rerun.

5.3.4. Ferrous Iron

Given ICP-OES is not capable of discerning ferrous iron concentrations within the effluent, colourimetry was utilised instead. A Hach DR900 colourimeter and Hach ferrous iron, phenanthroline powder, pillows for 25 ml samples were used for ferrous iron determination. The procedure outlined within the DR900 water analysis handbook were followed. This methodology has a maximum detection limit of 3 mg/L when performed under ideal laboratory conditions and an estimated lower detection limit of 0.03 mg/L. Where the maximum detection limit was exceeded, the effluent was diluted with deionised water and the appropriate dilution correction factor was applied to the analytical concentration to give an accurate reading. Precision and accuracy were not determined for this method

5.3.5. Sulphate

Sulphate concentrations were also determined with the Hach DR900 colourimeter using SulfaVer reagent pillows for 10 ml samples. The SulfaVer method as outlined within the DR900 water analysis handbook was followed. This methodology has a maximum detection limit of 70 mg/l and lower detection limit of 2 mg/l under ideal laboratory conditions. As with the iron colourimetry measurements, when this maximum detection limit was exceeded, deionised water was used to dilute the effluent sample and a subsequent correction factor was applied to the analytical concentration. Precision and accuracy were not determined for this method

5.3.6. Alkalinity

The alkalinity of the effluent samples was measured using a Hach 16900 digital titrator. Dependant on the predicted alkalinity of the sample, a 100 ml sample was either taken or an aliquot of the sample was diluted up to 100 ml as per the manufacturer's instructions. Bromocresol green- methyl red indicator was titrated with either a 1.6N or 0.16N H_2SO_4, again dependant on predicted alkalinity, to increase the acidity of the sample. The end point of the titration was determined by the sharp colour change from a blue-green to vibrant pink. At this point the unit reading on the titrator were taken and converted into an equivalent concentration of calcium carbonate in mg/L using the Hach digital titrator guide. Titrations were carried out in duplicate and in triplicate where the first two readings differed by more than 5 mg/L CaCO3 equivalent. Precision of this technique is controlled by the accuracy of the plunger thread within the digital titrator but has been presumed to be within ± 10 % of the displayed value.

5.3.7. Glycerol Analysis

The concentration of glycerol within both the column influents and effluents was measured to allow the mass of glycerol introduced to the columns to be calculated. Glycerol concentrations were measured with a fluorometric free glycerol assay kit (Sigma Aldrich, Gillingham, UK). Fluorometric analysis of the assayed samples was performed with an Infinite® F50 fluorometer and associated "Magellan for F50" software. Where concentrations of glycerol were anticipated to be beyond the detection range of the assay kit they were sufficiently diluted with deionised water. All samples and glycerol standards were tested in triplicate. The Infinite® F50 fluorometer has an accuracy and precision of <1%.

5.4. Microbial Analysis

5.4.1. Autoclaving

Autoclaving of wastes and implements used in microbial analysis were sterilised using a Prestige Medical 2100 Series Autoclave (Prestige Medical, Blackburn, UK). Separate autoclaved were used for waste and lab utensils. Waste samples for sterilisation were loaded into a 2l Pyrex glass beaker and covered with foil before autoclaving. Approximately 250g of waste was autoclaved at a time. Autoclaving consisted of a 15-minute cycle at 121˚C. Autoclave indicator tape was utilised each time material was autoclaved to ensure the requisite temperature was achieved.

5.4.2. DNA Extraction

The extraction of genomic DNA was performed using the "Fast DNA® SPIN Kit for Soil" (MP Biomedicals, Solon, OH, USA). The protocol provided with the DNA extraction kit was followed, with modifications as described by Webster et al. (2003), for extractions from all experiments. 0.50 (±0.05) mg of waste was loaded into the lysing tubes for DNA extraction. Successful DNA extraction was verified via electrophoresis with a 1.2% agarose Tris-acetate-EDTA (TAE) gel. This also facilitated a basic size determination of the DNA with a Bioline Hyperladder™ 1kb for base pair size comparison.

Further verification was achieved by using a "Qubit™ fluorometer 3.0" and either the broad range or high sensitivity "Invitrogen™ Quant-iT™, Qubit™ dsDNA assay kit" (Invitrogen, Carlsbad, CA, USA) as required. This methodology quantified the mass of DNA extracted and reported as ng/µl.

DNA extraction was performed under aseptic conditions to minimise contamination of the samples. All plasticware and pipettes were autoclaved and/or UV-treated while the spatulas used to load waste into the lysing tubes were initially autoclaved and then washed and flame sterilised with ethanol after each use.

5.4.3. PCR Amplification

To minimise contamination the polymerase chain reaction (PCR) preparation was carried out under aseptic conditions, all plasticware and pipettes were autoclaved and/or UV-treated and sterile nuclease free molecular grade water (Severn Biotech Ltd., Kidderminster, UK) was used. Positive (DNA known to successfully amplify with given primer pairs) and negative (molecular grade water in place of DNA) controls were used in all PCR amplifications. All PCR amplifications were performed with PCRBIO Taq DNA Polymerase (PCR Biosystems, London, UK) and a DNA Engine Dyad Thermal Cycler gradient block (MJ Research, Boston, MA). Primers used within this study are described within Table 5.3, all primers were synthesised by Eurofins Genomics (Ebersberg, Germany).

The 16S rRNA gene PCR mastermix, for a final 50 µl reaction, was as follows; 10µl PCRBIO reaction buffer, 0.5µl bovine serum albumin (Promega Corporation, Madison, WI), 0.5µl each of forward and reverse primers (0.2 µmol), 0.25µl Taq DNA polymerase, 1µl template DNA and the requisite volume of water to make up 50µl total volume per sample. The thermocycling conditions varied depending on the primer pair used, these conditions are summarised in Table 5.4.

Table 5.3 Oligonucleotide primers used for PCR in this study

Primer	Target gene	Sequence[#] (5'-3')	Reference
357F$_{gc}$*	*Bacteria* 16S rRNA	CGCCCGCCGCGCGCGGCGGGCGGGGCGGGGGCACGGGGGG CCT ACG GGA GGC AGC AG	(Muyzer *et al.*, 1993)
518R	Universal 16S rRNA	ATT ACC GCG GCT GCT GG	(Muyzer *et al.*, 1993)
109F	*Archaea* 16S rRNA	ACK GCT CAG TAA CAC GT	(Grobkopf *et al.*, 1998)
958R	*Archaea* 16S rRNA	YCC GGC GTT GAM TCC AAT T	(DeLong, 1992)

***= GC-clamp at 5' end for DGGE, GCCCGCCGCGCGCGGCGGGCGGGGCGGGGGCACGGGGGG

Table 5.4 16S rRNA gene PCR thermocycling conditions

Primer pair	PCR Program
357F$_{gc}$ & 518R	95°C for 5min, followed by 94°C for 30sec, 55°C for 30sec, 72°C for 1 Min, cycle to step 2 for 9 more cycles, followed by 92°C for 30sec, 52°C for 30sec, 72°C for 1 Min, cycle to step 6 for 24 more cycles, followed by 72°C for 10 min
109F & 958R	98°C for 1 Min; followed by 35 cycles of 92°C for 45sec, 45°C for 45sec, and 72°C for 45sec, with a final extension at 72°C for 5 min

5.4.4. Quantitative Real-Time Polymerase Chain Reaction Analysis

Quantification of microbial communities (bacterial and archaeal 16S rRNA genes) within the wastes, both pre and post experimentation, was performed with the Agilent Mx3000P quantitative real-time polymerase chain reaction (qPCR) system (Agilent Technologies UK Ltd., Stockport, UK) using SYBRGreen chemistry as described in (Webster *et al.*, 2015). *Anaerolinea thermophila* DSM 14523 and *Methanococcoides methylutens* DSM 2657 were used to produce standard curves and calibration, serial dilutions of full length 16S rRNA gene PCR products. 16S rRNA gene primers 519F/907R (Muyzer *et al.*, 1993) and S-D-Arch-0025-a-S 17F/ S-D-Arch-0344-a-S-20R (Vetriani *et al.*, 1999) were utilised for targeting *Bacteria* and *Archaea* respectively. Target gene sequences for these primers are given in Table 5.5. The thermocycler protocol used consisted of an initial increase in temperature to 95°C for 7 min to dissociate the DNA, followed by 40 cycles of 95°C for 30 s, 55°C for 30 s and 72°C for 30 s. Each cycle was followed by data acquisition at the elongation step (55°C for 30s). The 40 cycles were then followed by a 65°C step for 30 s and a melting curve from 55°C to 95°C to verify amplicon length. This methodology was applied for all qPCR analysis throughout all experiments.

Table 5.5 Oligionucleotide primers used for qPCR analysis

Primer	Target gene	Sequence (5'-3')
519F	*Bacteria* 16S rRNA	GCC AGC AGC CGC GGT AAT
907R	*Bacteria* 16S rRNA	CCG TCA ATT CCT TTG AGT TT
S-D-Arch-0025-a-S 17F	*Archaea* 16S rRNA	CTG GTT GAT CCT GCC AG
S-D-Arch-0344-a-S-20R	*Archaea* 16S rRNA	TC GCG CCT GCT GCG CCC CGT

5.4.5. 16S rRNA PCR-Denaturing Gradient Gel Electrophoresis

Denaturing gradient gel electrophoresis (DGGE) of PCR products was used to identify diversity changes between samples before and after bioreduction. DGGE analysis was performed using the method described by Muyzer *et al.* (1995) with some modifications. Products from the PCR amplification using primer pair $357F_{gc}$ and 518R were used for DGGE analysis. The 16S rRNA gene PCR products were separated using a DCode™ Universal Mutation Detection System (Bio-Rad Laboratories, Hercules, CA) and 1 mm thick (16 X 16cm glass plates), 8% (w/v) polyacrylamide gels (Acrylamide: Bis-acrylamide 37.5:1; Fisher Scientific, Loughborough, UK) with a denaturant gradient between 30 and 60% of urea and tetramethylethylenediamine (TEMED). Gels were poured with a 50 mL Gradient Mixer (Fisher Scientific, Loughborough, UK).

Electrophoresis was performed at 200V for 5 hours (initial 10min was run at 80V) at 60°C within 1 X TAE buffer (pH 8; 40 mM Tris base, 20 mM acetic acid, 1 mM EDTA). Polyacrylamide gels were stained with SYBRGold nucleic acid gel stain (Molecular Probes) for 30min and viewed under UV. Gel images were captured with a Bio-Rad VersaDoc 4000MP imaging system in conjunction with Bio-Rad Quantity One 1-D analysis software. DGGE images were then analysed using GelCompar ii software (Applied Maths, Austin, TX) to identify, define and compare band positions and intensities in the gels. Dendrograms, from cluster analysis of the gels, were constructed using “Dice” similarity coefficient (1% band matching tolerance & optimisation) and the UPGMA method (unweighted pair group method with the arithmetic mean) for cluster analysis.

When necessary, individual, distinct DGGE bands were excised using a sterile scalpel, washed with sterile molecular grade water (Severn Biotech Ltd. Kidderminster), crushed into new sterile molecular grade water and left to incubate overnight at 4°C to allow the liberation of the DNA into the water. This supernatant was used as template DNA for subsequent re-amplification PCR reactions. For re-amplification of DNA from excised DGGE bands a modified bacterial primer pair ($357F_{gc}$ and 518R-AT-M13F) was used, based on O'Sullivan *et al.* (2008). As with other primers the 518R-AT-M13F primer was synthesised by Eurofins Genomics and has the 5’-3’ sequence: GTAAAACGACGGCCAGTAAATAAAATAAAAATGTAAAAAAATTACCGCGGCTGCTGG.

Beyond the alteration to the reverse primer all PCR parameters & conditions we kept constant with the original PCR amplification. Re-amplified samples were then stored at -80°C before sequencing.

5.4.6. Sequencing of excised DGGE Bands

Sequencing of re-amplified excised DGGE bands was performed by Eurofins Genomics (Ebersberg, Germany) using the Sanger sequencing methodology. Returned sequence chromatographs were analysed using the CHROMAS software package version 2.62 (http://www. technelysium.com.au/wp/chromas/). Nucleotide assignment was manually verified by observation of sequence chromatograms, any ambiguous peaks or regions were replaced with N. Any samples with poor quality reads or short reads, with significant portions of the sequence missing, were discarded. The forward and reverse primer regions were then removed the leave only target sequence remaining in the chromatograms. At this point any sequences shorter than 100bp were removed and classified as ambiguous reads. The closest relatives of sequence chromatograms were identified using the National Centre for Biotechnology Information (NCBI) BLASTN suite (https://blast.ncbi.nlm.nih.gov/Blast.cgi) to compare chromatograms against the NCBI sequence database. All nucleotide sequences were then aligned using ClustalW (Thompson *et al.*, 2003) with sequences retrieved from the database. Phylogenetic trees were constructed using neighbour-joining with the Jukes and Cantor correction algorithm in MEGA version 7.0.21 (Kumar *et al.*, 2016). Data was bootstrapped 1000 times to evaluate the support for the nodes generated.

5.4.7. Next Generation Sequencing of Bacterial and Archaeal 16S rRNA Genes

Microbial community analysis by next generation sequencing of 16S rRNA gene amplicons was performed, at the culmination of the column experimentation. This timepoint was chosen for sample convenience and integrity, and due to time and financial restrictions limiting the number of sequencing runs possible. Initial PCR amplification of the DNA at a range of dilutions between neat (undiluted DNA) and 1/200

dilutions were tested to find the dilution state that generated the cleanest PCR product. Dilution was utilised as a method to limit the impact on amplification inhibitors such as humic acids and metals. Alternatiely the extracted DNA could have been put through a clean-up kit(s) designed to remove these inhibitory substances. However, these kits often result in a loss of yield and may introduce a bias to the testing if certain DNA sizes are lost as a result. Therefor dilution was chosen as the preferred method to reduce PCR inhibitor impact.

Utilising 1/100 dilutions of the unaltered DNA extractions previously prepared, a single step PCR amplification, in a 96-well PCR plate, was performed to create the bacterial 16S rRNA gene library for sequencing. Primers targeting the V4 variable region of the 16S rRNA gene were utilised. The forward and reverse primers were constructed following Kozich *et al.* (2013), and consisted of the Illumina adapter sequence (F: 5'-AATGATACGGCGACCACCGAGATCTACAC-3'; R: 5'- CAAGCAGAAGACGGCATACGAGAT-3'), 8-bp i5 and i7 index or "barcode" sequences, a pad sequence to boost the sequencing primer melting temperatures ((F: 5'- TATGGTAATT-3'; R: 5'-AGTCAGTCAG-3'), and a 2-bp link sequence that is anti-complementary to the known sequences (F: 5'-GT-3'; R: 5'-CC-3'). Finally, the 16S rRNA gene V4 specific sequences (F: 5'-GTGCCAGCMGCCGCGGTAA-3'; R: 5'- GGACTACHVGGGTWTCTAAT-3') were attached at the 3' end, giving an overall generic PCR primer sequence as follows:

Forward: AATGATACGGCGACCACCGAGATCTACAC <i5><pad><link><16SF>

Reverse: CAAGCAGAAGACGGCATACGAGAT <i7><pad><link><16SR>

Each well contained 17µl of Accuprime PFX Supermix, 1µl of template DNA, and 2µl of each paired set of index primers. A negative control, consisting of 1µl of nuclease free PCR grade water (Severn Biotech Ltd. Kidderminster) was also performed, while the positive control utilised 1µl of Mock Community (BEI Resources, Virginia, USA). The thermocycler programme used was as follows: 2 mins at 95°C; 30 cycles of 95°C for 20 sec, 55°C for 15 sec and 72°C for 5 mins; followed by a final step of 72°C for 10 mins before maintaining a constant 4°C until removed from the thermocycler. Three separate

amplifications were performed to provide triplicates of each sample to be tested, whilst mitigating against any amplification failures of single samples.

Following PCR amplification each sample was examined for mass and sequence length using a Qubit™ fluorometric assay and Agilent Tape Station™ Genomic DNA ScreenTape –HSD-1000 and Genomic DNA Reagents, Agilent, Santa Clara CA, USA) respectively. Following this quantification, the 3 replicates of each sample were pooled into a singular representative sample. These samples were then simultaneously cleaned and normalised using a SequalPrep™ 96 well normalisation plate (Invitrogen, Carlsbad, CA, USA) (Kozich *et al.*, 2013). Samples were then subjected again to Qubit and Tape Station analysis for mass and amplicon length. Manual normalisation was then performed by calculating and adding the requisite volume of each sample (based on Qubit measurement and calculated concentration) to the pooled library to give each sample a concentration of 0.5nM within the pool. A Qubit measurement showed an average concentration of 0.53nM of this pooled library.

At this point a Tape Station analysis revealed that adapter dimers were still present. For this reason, a SPRIselect magnetic bead clean-up (Beckman Coulter, Brea, CA, USA) was performed using 0.8 volume of SPRIselect beads, chosen using the left hand selection method described by the manufacturer. At this stage the opportunity was also taken to further concentrate the pooled library by reducing the volume of elution buffer used within the clean-up. A final check with the Qubit and Tape Station confirmed the removal of the adapter dimers and a final average pooled library concentration of 2.2nM, which was deemed high enough to facilitate the generation of reliable data.

In total, 84 samples were subjected to next generation sequencing analysis using an Illumina MiSeq™ sequencer (Illumina, San Diego, CA, USA). Sequencing was performed 2bp × 250bp paired-end flow cells and reagent cartridges. Sequencing was carried at the Institute of Medical Genetics based at the Cardiff University Heath Campus.

5.4.7.1. Data Processing and Statistical Analysis

The data generated from the Illumina sequencing was analysed using Qiime v.1.8 (Caporaso *et al.*, 2010). In brief, the analysis consisted of contigs formation via merging

of the forward and reverse paired end reads. Sequences that would not align or contained errors were removed. This was followed by filtering the resultant sequences to remove reads shorter than 200 bp and longer than 300 bp along with QC analysis to remove and low-quality sequences. The remnant sequences were then assigned sample IDs via linking to a prepared mapping file before being grouped into OTU's using UCLUST (Edgar, 2010) with a 97% sequence similarity threshold. The sequences within these OTUs were then reduced so that a unique sequence remained to represent each OTU. Chimeras and singletons were then removed from the dataset. Taxonomy was then assigned using BLAST (Altschul *et al.*, 1990) and the SILVA 128 database with a threshold of 97% similarity.

Statistical analysis of the samples was performed to gain a more detailed understanding of the microbial community and the differences between pre- and post-experiment samples and experimental variants. Statistical parameters including Shannon's and Simpson's indices of diversity, Chao1 (species richness), Good's coverage (library coverage) and an abundance-based coverage estimator (*S*ACE) values were calculated. Weighted UniFrac analysis was performed to calculate the differences between microbial communities within each sample based on phylogenetic information. The resultant distance matrix was used to perform Principal coordinates analysis (PCoA) which was used to visualise the similarities and/or differences in the microbial community relationships.

5.5. Column Experiment Overview

The specifics of the design and construction of column experiments are detailed within the relevant experimental chapters (Sections 8.3.2 & 9.3.2). Leaching of the wastes within an up-flow column system was chosen as the primary method of experimentation. Leaching was chosen as the method for extracting the effluents primarily due to the focus of the project being on the in-situ recovery of resource from wastes. With the wastes having to remain in-situ as a prerequisite for the study, it dictated that any metal resource to be recovered from the waste would have to be partitioned to a liquid phase to facilitate its removal whilst the bulk of the waste remains

in-situ. Furthermore, leaching as a method for recovering low concentrations of resource via bio-oxidation is well established (Brierley, 2008; Johnson, 2014), while it has also seen use in bio-reduction studies, both as the primary treatment (Farahmand *et al.*, 2009) and often in conjunction with other pre-treatments such as roasting (Jiang *et al.*, 2017) and magnetic separation (Hernandez *et al.*, 2007). Leaching also carries the benefit that by leaving the waste in-situ, and removing contaminating substances, the resource being recovered can be the land itself as opposed to the extracted substance.

Vertical columns with an upwards flow of extractant were chosen for a number of reasons. Primarily the design was chosen due to the previous use of upwards flow columns in iron bioreduction studies (Roden *et al.*, 2000; Benner *et al.*, 2002; Hansel *et al.*, 2003). By using an upflow system it is possible to control the flow rate of extractant through the wastes, thereby maximising the residence time of extractant and organic carbon within the columns. Roden & Urrutia (1999) observed that the advective removal of ferrous iron increases both the extent and rate of ferric iron oxide reduction. By having a continuous flow of extractant through the columns biogenic ferrous iron is removed thereby facilitating the greatest possible rate and extent to which the ferric oxyhydroxides within the wastes.

6. Sampling Locations and Collection

6.1. Introduction

This chapter presents information on the case study sites used within this study including the location, geology and history of the sites. Also detailed are the methods by which each sample was procured.

Section 6.2: Lindsay – Details of the waste obtained from the former coal mine, Lindsay.

Section 6.3: Red Mud – Details of the provenance of the red mud/ alumina production waste

Section 6.4: Details of the mine water treatment sludge from Wheal Jane, Cornwall, UK.

Section 6.5: Details of the two sampling locations within Parys Mt., N. Wales a former Cu-Zn-Pb mine.

Section 6.6: Chapter Summary

6.2. Lindsay

6.2.1. Location and Brief Site History

Lindsay is the site of a former drift coal mine located in Capel Hendre, Carmarthenshire, S. Wales (51°46'42 N, 4°02'37 W). The Lindsay drift mine was initially developed in 1960 and later linked with the nearby Cwmgwilli drift mine. These mines were abandoned in November 1996, with the entry shafts being sealed in 1998. The discharge of water from the former Lindsay workings was first noted in December 1999.

In 2002 the Coal Authority commissioned a pumped, aerobic wetland remediation system to deal with the discharge from the mine. Within the system, mine water is collected in a sump and then pumped to a series of aeration cascades which lead to two parallel settling ponds which in turn lead to a series of three reed beds. Once through these reed beds the water is then discharged into Fferrws Brook, a tributary of the

Loughor River. An aerial view of this treatment scheme is shown in Figure 6.1. Waste from this site was chosen for this study, despite its lack of elements of economic interest, due to the known presence of iron-reducing communities. This allowed for the investigation into whether stimulation of indigenous iron communities was possible without the potential for other metals causing inhibitory or toxic effects.

6.2.2. Sampling Methodology

Waste samples were obtained from the cascades leading into the settling ponds Figure 6.2. The upper layer of oxidised ochre was removed to expose the olive-green coloured subsurface ochre waste Figure 6.3. This was then sampled using a garden spade, thoroughly cleaned with deionised water and ethanol to ensure no chemical or biological contamination of the sample. The waste sample was transported to the university in a cool box.

Once returned to the university, sub-samples of the waste were taken for microbial analysis. This sub-sampling was performed in aseptic conditions and the sub-samples were stored in a -80°C freezer to prevent degradation of DNA. The remaining waste sample was stored in a refrigerator at 4°C. This sub-sampling methodology was used for all samples used in this study.

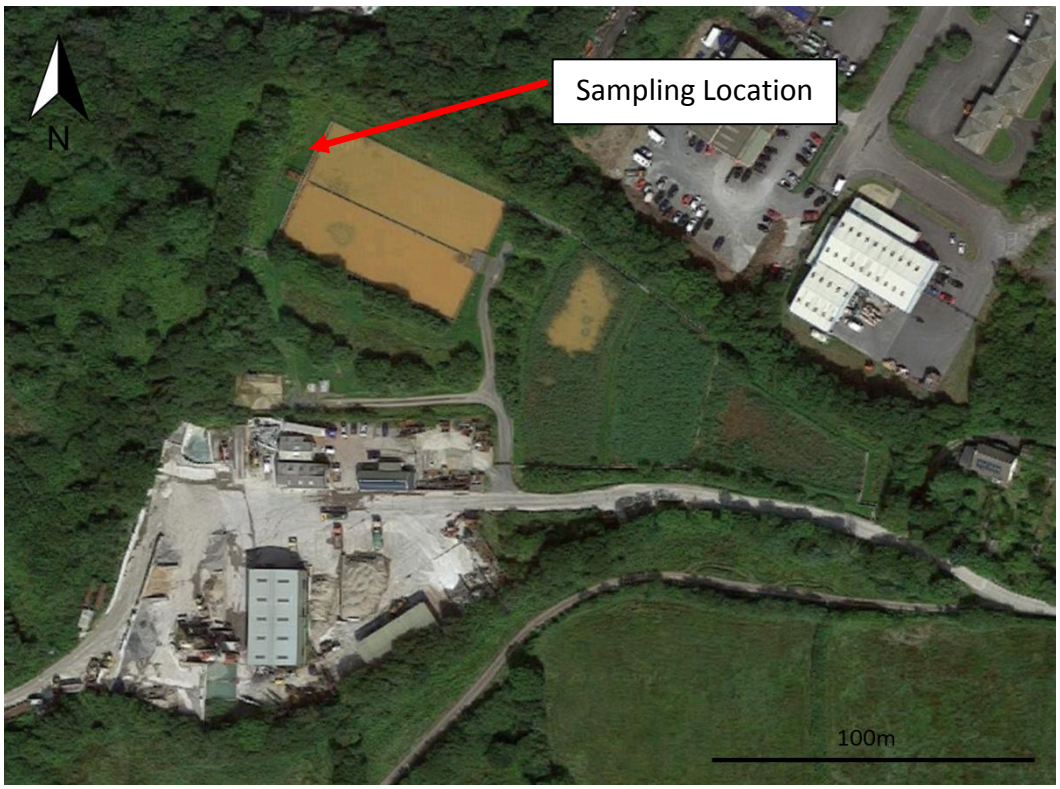

Figure 6.1 Aerial view of Lindsay mine water treatment scheme.

(Image Copyright Google Earth™ 2016)

Figure 6.2 Cascade and settling ponds at Lindsay Mine Water Treatment Scheme.

Figure 6.3 Ochre sludge within cascades at Lindsay Mine Water Treatment Scheme. Note olive-green colouration in recently uncovered ochre.

6.3. Red Mud

6.3.1. Location, Brief History and Sampling Methodology

The precise provenance of the red mud sample used within this study is not known as it was supplied anonymously. Characterisation of the waste was undertaken though due to the limited knowledge regarding its provenance the research focused on this waste has been minimal.

6.4. Wheal Jane

6.4.1. Location and Brief History

Wheal Jane is a former tin mine located in the Carnon River Valley in Cornwall, England (50°14’14 N, 5°07’23 W). When the mine was closed in 1991 the dewatering operations were ceased, this led to the build-up and sudden release of contaminated water into the Carnon River in 1992, increasing concentrations of, amongst other metals, Al, Cd, Co,

Cu, Fe, Pb, Ni, U and Zn (Neal *et al.*, 2005). After an initial attempt to mitigate the environmental impact of the metal-rich mine drainage, using a passive treatment system, the UKs first, and only, active treatment system for a former metal mine was implemented. The scheme is a high density sludge treatment system that can be summarised in three stages; mixing of mine water and sludge, aeration and lime dosing and clarifying, as summarised in Figure 3.3. Mine water is first mixed with re-circulated sludge, this raises the pH of the fluid to ~8.5 resulting in oxidation and subsequent precipitation of ferrous iron as iron oxyhydroxides. This also takes advantage of the autocatalytic effect of iron oxyhydroxides to induce oxidation of ferrous iron within the mine water. The mine water is then passed into a reactor where it is dosed with a lime slurry to raise the pH to 9.25, while being agitated and aerated to aid precipitation of metals. Lime dosed mine water is then dosed with 2.5-3 mg/L polyelectrolyte flocculant (Goldcrest polygold A298B) to aid flocculation and settlement of precipitated oxides. This dosed water is then passed into lamella clarifiers. Effluent water is discharged to the Carnon River, while collected sludge is either re-circulated (to ensure efficient use of lime) or sent to the Clemows Valley tailings dam for storage (Coulton *et al.*, 2003; CL:AIRE, 2004; Whitehead *et al.*, 2005; Veolia, 2016)

6.4.2. Sampling Methodology

Due to restrictions on access to the site this location could not be sampled in person. Instead sampling of the waste was performed by Richard Morgan, deputy regional manager for Veolia, the operating company for the treatment plant. The waste sample was taken from the tailings lagoon where the generated mine water treatment waste is stored long term. The sample was specifically taken from the “oldest, exposed area of waste in the lagoon” (Morgan, 2015) in an effort to obtain waste with the highest chance of having established microbial communities. An aerial view of the tailings facility is shown in Figure 6.4, with an example of the type of material collected shown in Figure 6.5.

As with all waste samples in this study, sub-samples were taken under aseptic conditions and frozen at -80°C as soon as the waste was received at Cardiff University.

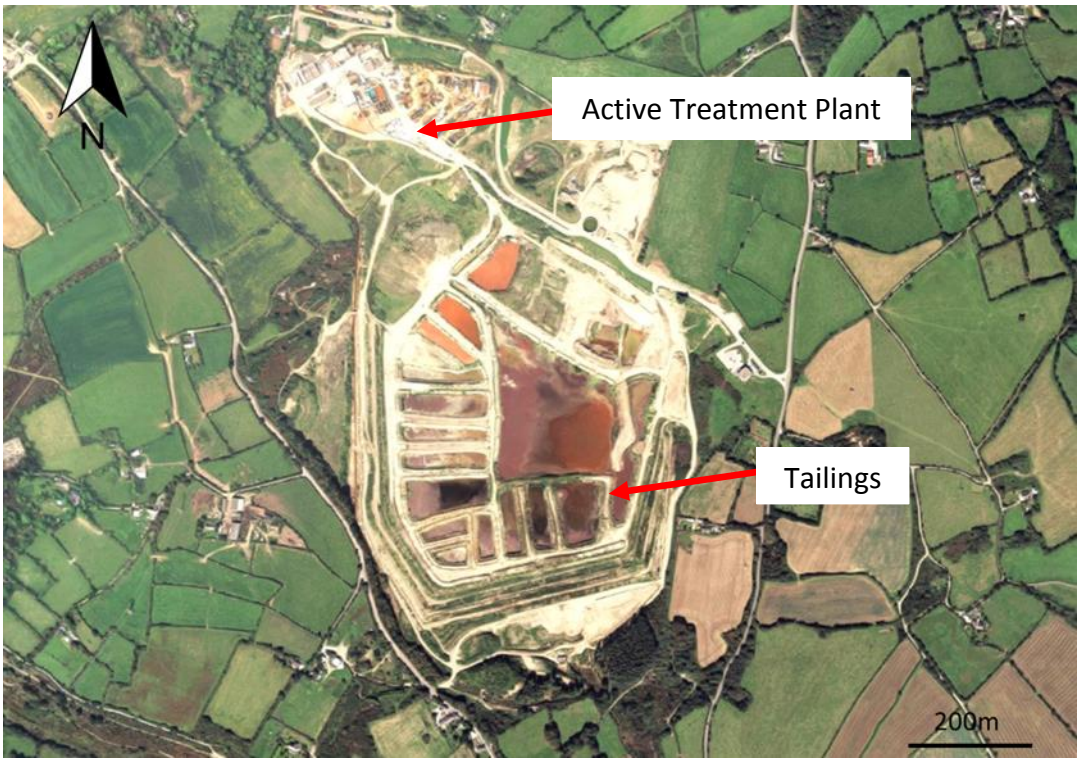

Figure 6.4 Arial view of Wheal Jane Mine Treatment Scheme and Tailings Lagoons

(Image Copyright Google Earth™ 2016)

Figure 6.5 Example of Wheal Jane mine water treatment waste (Note: not from actual sample location)

6.5. Parys Mountain

6.5.1. Location and Brief History

Parys Mountain is a former copper, zinc and lead mine located ~2.5km south of the town on Amlwch in Anglesey, North Wales (53°23'13 N, 4°20'37 W). The site is actually two ancient mines; the Parys Mine and the Mona Mine, which through later opencast mining became one. The site is registered as a Site of Special Scientific Interest (SSSI) and is a scheduled ancient monument due to its scientific and cultural heritage value.

Throughout the mines history the main target was copper, though it has also been worked for zinc and lead when copper prices were low, or when zinc/lead prices were high enough to make it economically viable. By-products such as sulphur, ochre pigments and alum have also been sold (Anglesey Mining Plc, 2016). Parys Mt. has been worked for copper since the Bronze Age and, given the proximity of Roman copper workings at the Great Orme N. Wales along with the finding of "copper cakes", it is generally accepted that Roman mining operations probably also occurred (Ixer & Budd, 1998). The main period of mining started until the 1760's and was coeval with the burgeoning industrial revolution within Great Britain. During this time opencast mining was gradually replaced by underground mining via adits up to 300m deep (Anglesey Mining Plc, 2016). Peak production was reached in the late 18th to early 19th century at which time approximately 3000 tonnes of copper was being produced annually, allowing Great Britain to dominate the global copper market (Pearce, 1994). Conventional mining, both underground and opencast had ceased by 1920 but copper was still produced by precipitation from the AMD generated from the mine. Brick lined precipitation ponds were used to capture the AMD and were then filled with scrap iron which caused the precipitation of copper onto the surface of the iron. This method could yield up to 50% copper recovery (after smelting) from the AMD but was time consuming and labour intensive and so rapidly became uneconomic and ceased in the 1950's (Fuge *et al.*, 1991; Rios *et al.*, 2008). The mine site is currently owned by Anglesey Mining plc. who are exploring the potential for a future resumption of mining for zinc.

Beyond the ongoing work to re-open the mine there has been investment in protecting the mining heritage of the site. However, the majority of work on the site has been involved in remediation and mitigation of the impact of AMD on surrounding land and

watercourses such as the Afon Goch Amlwch and Afon Goch Dulas. Afon Goch translates from Welsh to Red River, a reference to the iron within the river.

In the late 1990's concern was raised, by a group of mining enthusiasts (Parys Underground Group), about the state of a concrete dam which was suffering corrosion and dissolution of the concrete as a result of the acidic mine water it was retaining. The water level of the subterranean reservoir was estimated to be ~31 M above the dam floor. This meant that any failure in the dam could be catastrophic, resulting in a serious flooding and pollution incident in the Afon Goch and the town of Amlwch. In 2003 the reservoir of AMD was drained to allow the controlled removal of the suspect dam. This allowed AMD to now flow through the Dyffryn Adda adit and into the Afon Goch without a large build-up of AMD within the mine workings (Coupland *et al.*, 2004). This redirection of water effectively stopped AMD flowing through the Dyffryn Coch adit to the south. This in turn meant that the settlement and precipitation ponds to the south and east of the site were left with only rainwater to feed them. In dry periods this resulted in dust, with unacceptably high concentrations of arsenic and lead being produced and impacting on residents of nearby homes. The Henwaith settlement ponds, to the east of the main mine site (53°23'23 N, 4°19'52 W), were classified as contaminated land in accordance with Part 2A of the Environmental Protection Act 1990, resulting in remediation works being required. This work consisted on installing capping systems on 14 of the ponds, membrane liners at the base of two ponds and a gravity-fed hydraulic system to maintain water in a further 4 ponds. This prevented dust formation thereby cutting the pollutant linkages (Rowe, 2011).

Samples were taken from the settlement/ precipitation ponds to the south and east of the site, formerly fed by the Dyffryn Coch adit. Specifically one sample, referred to henceforth as Parys Mt. 1, was obtained from the Henwaith settlement ponds. The second sample, termed Parys Mt. 2, was obtained from a settlement pond to the south of the site. Whilst precise evidence is difficult to source, it is likely that this settlement pond had been used for copper precipitation at some point during its existence (Gwynedd Archaeological Trust, 1995). Scrap metal found at the location is provides further suggesting for copper precipitation operations. The locations of these sampling sites are shown on Figure 6.6, with photographs of the sampling locations shown in Figure 6.7 and Figure 6.8.

Samples were taken as close as possible to the centre of the respective ponds, to minimise the influence of any decaying vegetation or contamination from material from the walls of the ponds. When sampling was performed during warmer periods, algal mats were present on the ponds. Where possible sampling was performed to avoid these, including scraping algal mats off the ochre surface. Samples were taken using a garden spade, thoroughly washed with deionised water and ethanol to prevent chemical or biological contamination of the sample. Separate implements were used for the 2 samples to further ensure minimal cross contamination between samples. Samples were returned to Cardiff University on the same day as sampling occurred. Once at the university, sub samples were taken and stored at -80°C for microbial analysis, whilst the remainder was stored at 4°C until required.

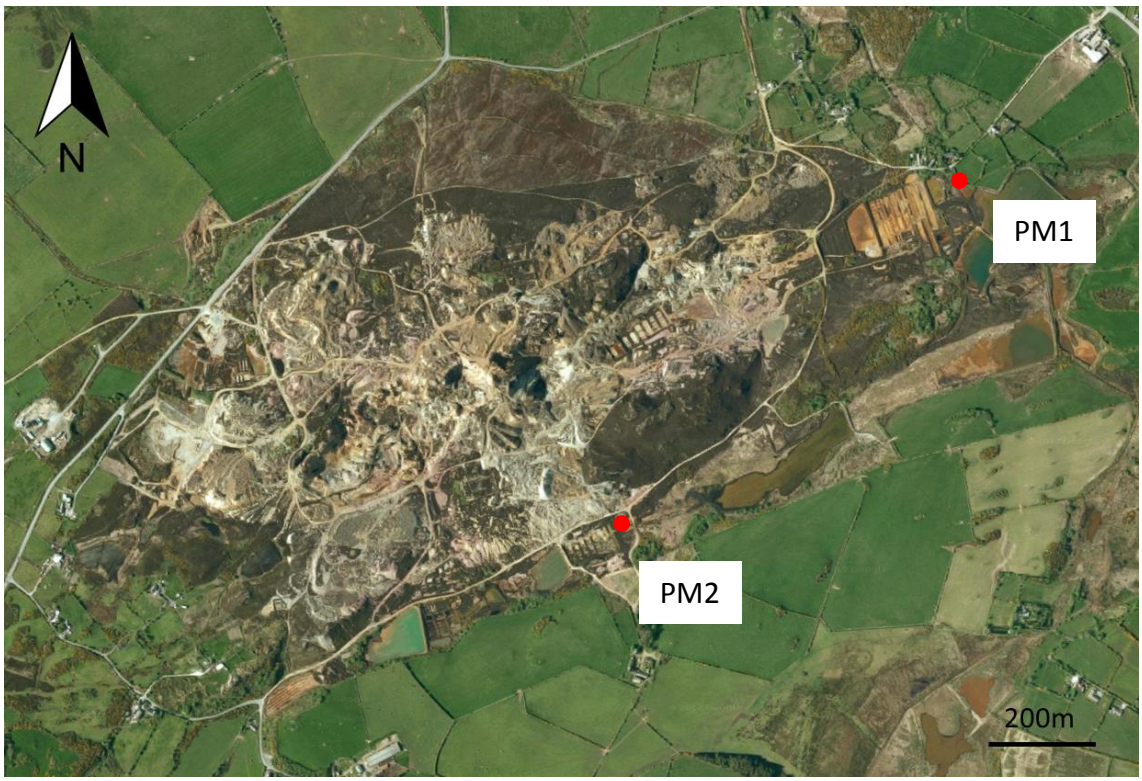

Figure 6.6 Aerial view of Parys Mt. mine, N. Wales. Red dots represent sampling locations (Image Copyright Google Earth™ 2016)

Figure 6.7 Sampling location for Parys Mt.1 sample

Figure 6.8 Sampling location for Parys Mt.2 sample (Note: algal mats on waste surface)

6.6. Chapter Summary

A range of iron-bearing oxidised wastes have identified representing a range of environments and generation pathways. These wastes can be summarised as follows:

- Lindsay: A mine water treatment sludge from a passive treatment system for circum-neutral mine drainage from a former coal mine in South Wales.
- Wheal Jane: A mine water treatment sludge from an active treatment system for a former tin mine in Cornwall, UK. Treatment with lime produces an alkaline metalliferous sludge.
- Red Mud: A waste product of the aluminium production industry. Supplied anonymously.
- Parys Mountain: A pair of acidic mine wastes taken from separate settlement/precipitation ponds located at the former Cu-Zn-Pb mine Parys Mt. located in North Wales.

7. Sample Characterisation

7.1. Introduction

This section presents the results of the waste characterisation work conducted on the range of wastes utilised within this study. Physical, chemical and mineralogical testing was conducted and where possible comparisons have been made to the properties of similar wastes described within literature.

Section 7.2: Lindsay – This section presents and discusses the physicochemical characterisation of the Lindsay mine water treatment sludge

Section 7.3: Red Mud – This section presents and discusses the physicochemical characterisation of the red mud from alumina production

Section 7.4: Wheal Jane – This section presents and discusses the physicochemical characterisation of the Wheal Jane mine water treatment sludge

Section 7.5: Parys Mountain – This section presents and discusses the physicochemical characterisation of the two samples taken from Parys Mt.

Section 7.6: Comparison of Waste Metal Content to Typical Ore Grades – This section discusses the target metals for each waste and their economic viability relative to traditional ores.

Section 7.7: Material Characterisation Summary.

Aside from gaining a more detailed understanding of the properties of the wastes utilised within this study; the more specific objectives of this characterisation work were to:

- To identify wastes dominated by ferric iron oxyhydroxides which may potentially be able to sustain iron-reducing communities, whether indigenous or not.

- Assess the concentrations of metals of economic interest within these wastes and their distribution between mineral phases within the wastes
- Attempt to assess of the efficacy of microbially mediated reductive dissolution of iron oxyhydroxides for these metals and the proportion of these metals that could be feasibly targeted for extraction.

7.2. Lindsay

Samples were characterised using the methods outlined in Section 5.2. Table 7.1 presents a selection of physicochemical properties of the Lindsay mine waste. Where multiple tests or resultant calculations were performed, the standard deviation of the data is given. The dry density of 2.87 g/cm^3 is much lower than the idealised value of 3.96 g/cm^3 for ferrihydrite stated by Cornell & Schwertmann (2003). This suggests that, rather than being heavily dominated by ferrihydrite, the waste is more mineralogically complex potentially containing minerals such as clay fines. These properties are similar to the results characterisation work on a similar ochre from Taff Merthyr mine, S. Wales conducted by Barnes (2008).

Table 7.1 Physicochemical properties of Lindsay mine waste

Determinant	Units	Value	St. Dev
Solids Content	wt. %	32.27	±0.22
Bulk Density	g/cm^3	1.54	±0.06
Dry Density	g/cm^3	2.87	±0.04
Specific Gravity		2.29	±0.06
Void Ratio		1.20	±0.05
Paste pH		7.42	±0.02
Sulphur	wt.%	0.11	
Total Carbon	wt.%	1.21	
Inorganic Carbon	wt.%	0.80	

Total digest and ICP-OES analysis of the waste shows that, of the elements analysed, iron comprised the majority of the waste at 36.5% dry weight (DW) (Figure 7.1). Calcium is the next most abundant element analysed, comprising 1.8% DW of the waste. This demonstrates the dominance of iron minerals within waste. Metals typically targeted for economic purposes such as zinc are only found in low concentrations within the

waste. Zinc, aluminium and lead are present at 0.05%, 0.04% and 0.03% DW respectively. These concentrations are lower than found in the other wastes utilised in this study making the Lindsay waste relatively clean, with regards to these associated metals (dominated by iron oxyhydroxides), compared to the other experimental wastes.

Sequential extraction testing displays that the majority of the iron, which dominates the sample, is contained within the "easily reducible oxide" and "reducible oxide" phases with 23.2% and 38.5% of iron within these phases respectively (Figure 7.2). This suggests that the majority of the iron is present in minerals such as ferrihydrite, lepidocrocite and goethite. A further 29.3% of iron is present within the "magnetite targeted" phase, 8.0% within the "residual" phase and 1.1% within the "carbonate associated" phase.

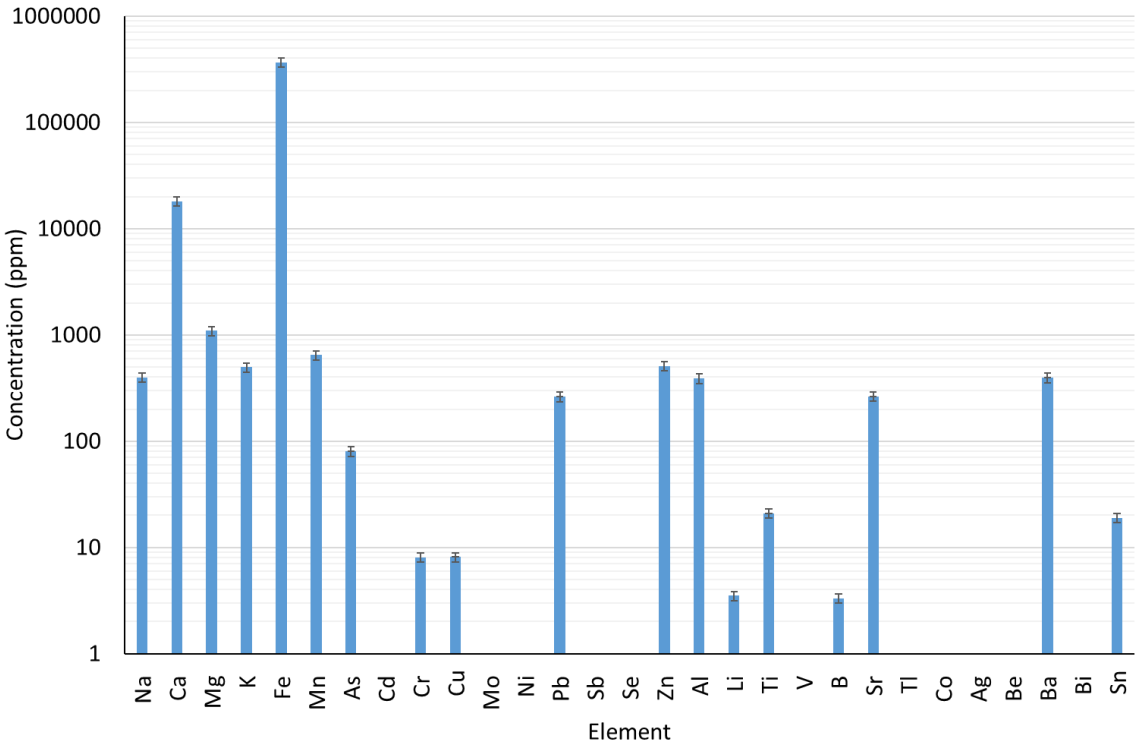

Figure 7.1 Results of ICP-OES analysis of Lindsay waste total digest. (No bar = below quantitation limit)

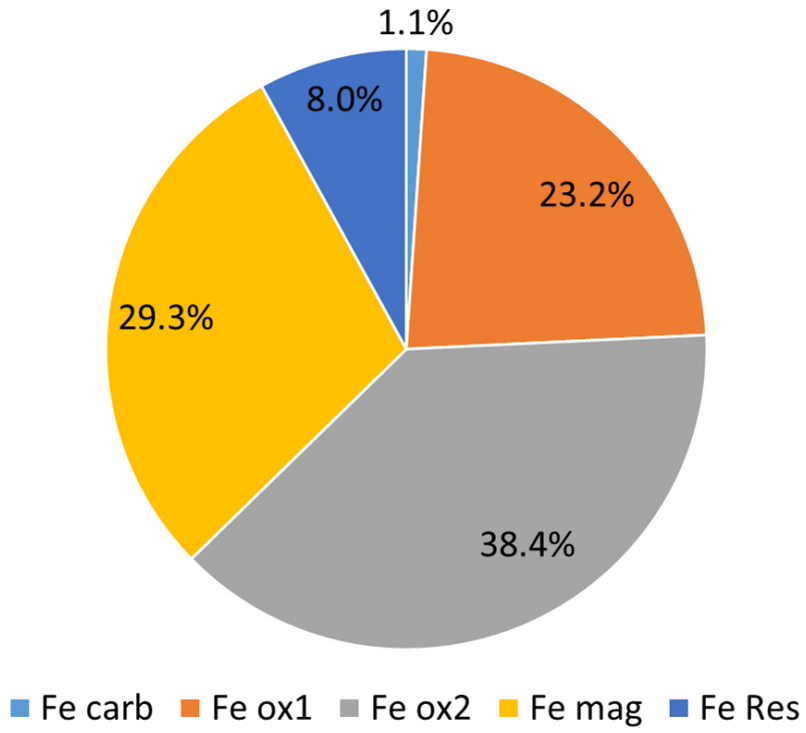

Figure 7.2 Result of sequential extraction displaying the distribution of iron within the Lindsay waste

The dominance of iron oxyhydroxide minerals is also apparent from the XRD diffractogram (Figure 7.3). The background trace shows an undulating peak at 35 °2Theta (Θ) which is characteristic of amorphous ferrihydrite. There is a small undulation at 62.5 °2Θ also indicative of 2-line ferrihydrite (Cornell & Schwertmann, 2003). In addition, a number of low intensity peaks are visible on the trace, all of which are attributable to the presence of goethite. This correlates with the results of the sequential extraction which indicated goethite and 2-line ferrihydrite as the dominant mineral phases in the waste. A single high intensity peak suggests the presence of native iron within the system. However, despite ~30% of total iron being present within the "magnetite targeted" phase, no magnetite was identified by either XRD or when a magnet was introduced to the waste in more simplistic test.

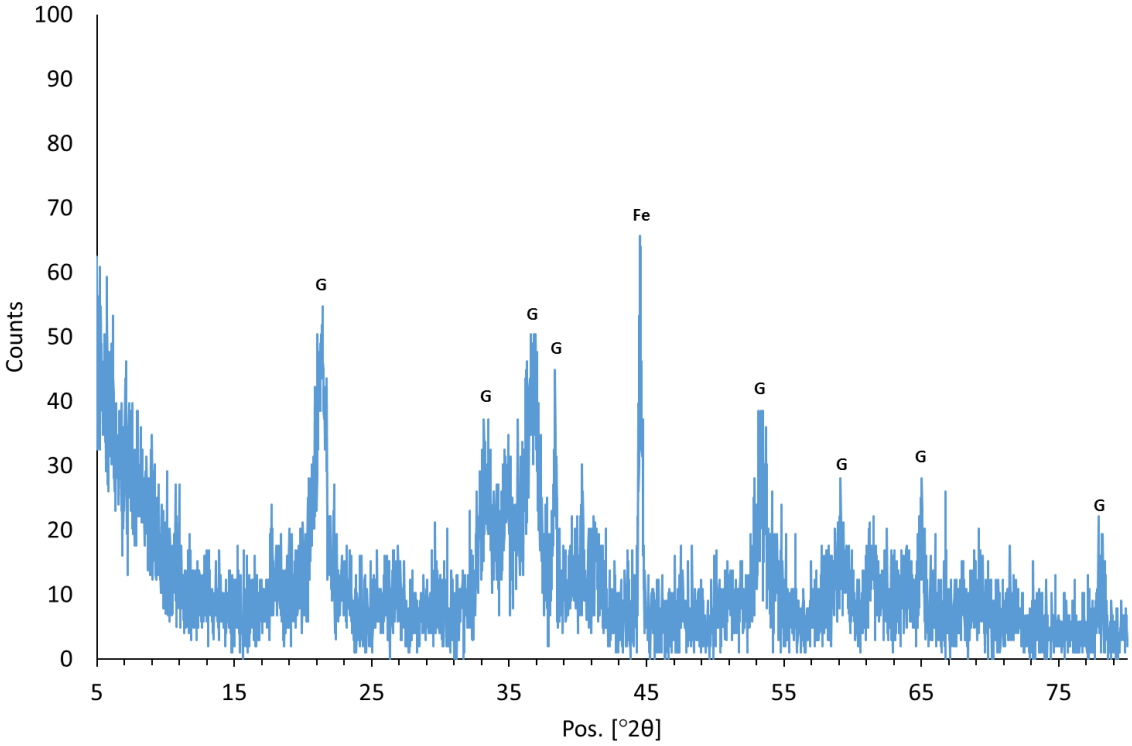

Figure 7.3 XRD diffractogram for Lindsay waste. G = goethite, Fe= Iron. Energy source: Cu Kα

When tested for PSD, the Lindsay waste returned a result where 100% of the sample passed through the 63 µm sieve. A sample of the complete waste (non-sieved) was subsequently tested with the Malvern mastersizer (as described in Section 5.2.7), the results of which are displayed in Figure 7.4. The majority of particles range from 1.79 µm (D_{10}) to 64.3 µm (D_{90}). Two peaks are visible from the profile. The larger of the peaks is located at 4 µm with the smaller peak located at 11µm. The D_{50} value of the waste is 8.16 µm. The observation of particles greater than 63 µm is not consistent with the results of dry sieving. This may be a result of the limited accuracy of dry sieving, measurement of the longest axis of elongate particles, the presence of aggregated dried particles or due to flocculation of smaller particles during the mastersizer process.

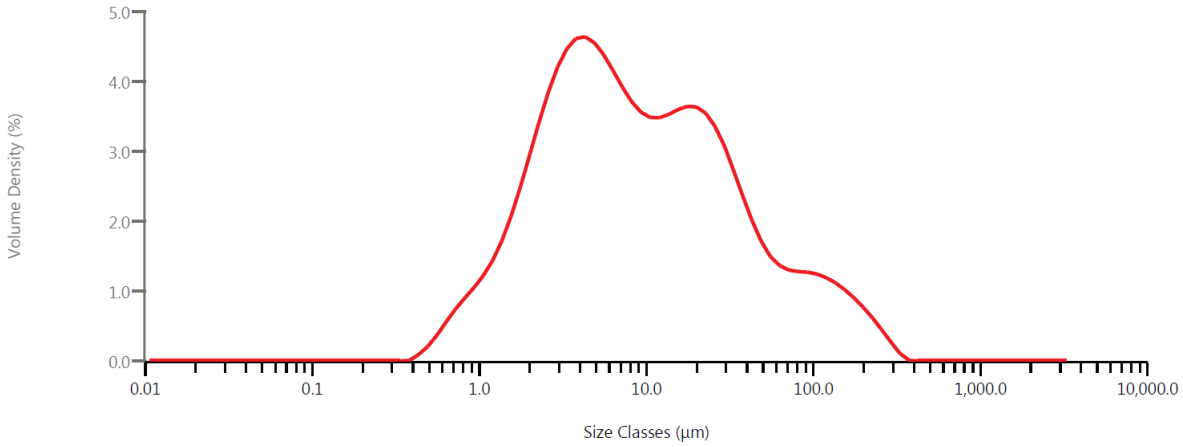

Figure 7.4 Malvern Mastersizer particle size distribution analysis of Lindsay waste

7.3. Red Mud

Table 7.2 presents a selection of physicochemical properties of the Red Mud waste. The sample was relatively dry as received and the difference between bulk and dry density was negligible. A defining characteristic of the waste is the very high pH, with the waste representing the most alkaline of all the wastes tested during this study.

Table 7.2 Physicochemical properties of Red Mud waste

Determinant	Units	Value	St. Dev
Solids Content	wt. %	99.23	±0.04
Bulk Density	g/cm^3	2.68	±0.02
Dry Density	g/cm^3	2.68	±0.02
Specific Gravity		2.55	±0.10
Paste pH		11.72	±0.13
Sulphur	wt.%	0.00	
Total Carbon	wt.%	0.81	
Inorganic Carbon	wt.%	0.64	

The dominant elements within the Red Mud are iron, aluminium, calcium, titanium and silicon comprising 25.7%, 11.1%, 5.6%, 3.3% and 3.0% DW respectively (Figure 7.5). This is typical of Red Mud bauxite residue wastes (Klauber *et al.*, 2011).

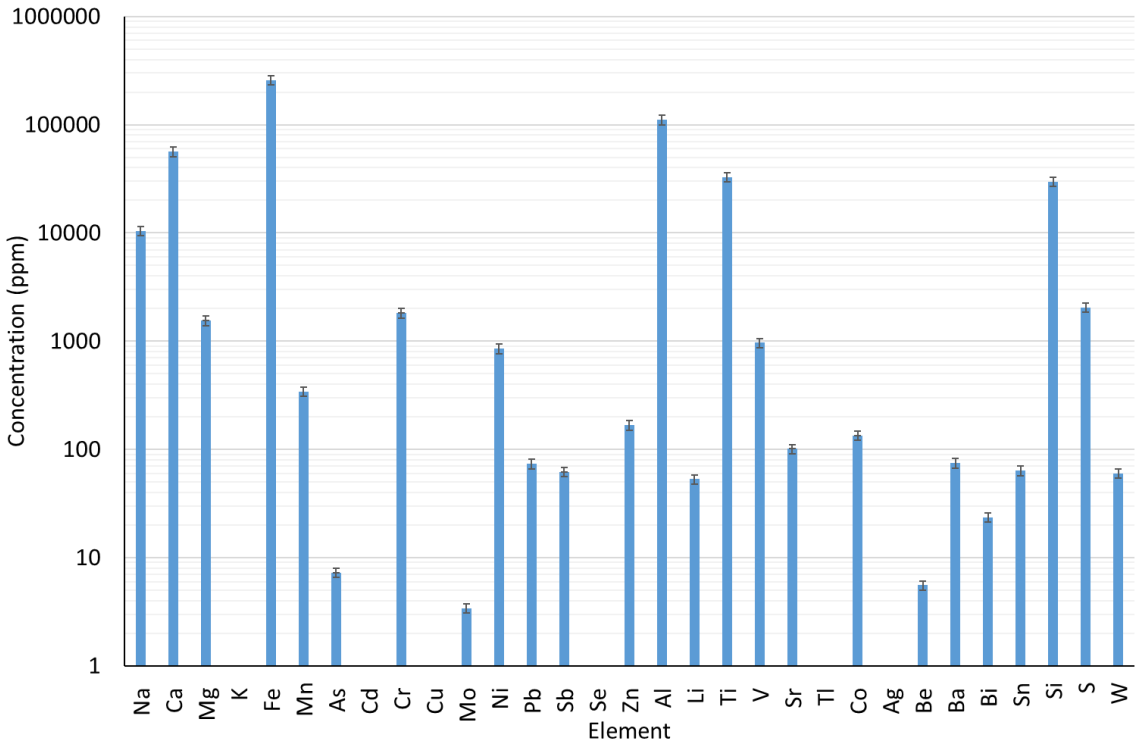

Figure 7.5 Results of ICP-OES analysis of Red Mud waste total digest. (No bar = below quantitation limit)

Sequential analysis suggests that the majority of the iron (65.9%) within the sample is located within the least reactive, "residual" phase, whilst the remainder is broadly held within the "reducible oxide" phase (30.2%). Only minor quantities are located within the "carbonate associated", "easily reducible oxide" and "magnetite targeted" phase (Figure 7.6a). Goethite and haematite are typically found within bauxite residue and are likely represented by the "reducible oxide" phase. The high proportion of iron within the "residual" phase, coupled with the majority of aluminium located within this phase suggests the presence of either aluminium substituted iron oxyhydroxides or other recalcitrant iron bearing minerals such as ilmenite.

Figure 7.6b displays the distribution of aluminium throughout the sequential extraction phases of the waste. The most notable feature is that 25.7% of the aluminium is extracted from the most reactive, "carbonate associated" phase. This may be due to the presence of aluminium carbonate minerals, such as cancrinite and tricalcium aluminate (Klauber *et al.*, 2011). Alternatively, it may be a result of the high mobility of aluminium at high pH enabling extraction within the least reactive phase. The majority of the aluminium is, as with iron, found within the "residual" phase supporting the hypothesis

that aluminium-substituted iron oxyhydroxides are present. A higher aluminium (and iron) content within the “residual” phase may also suggest an abundance of clay minerals. The remaining 14.0% is distributed throughout the other extractive phases.

The distribution of titanium through the extractive phases is more complex (Figure 7.6c). There are only negligible amounts of titanium within the “carbonate associated” phase and minor quantities (4.5%) within the “easily reducible oxide” phase. 19.6% of titanium is contained within the “reducible oxide” phase, suggesting an association with the likely goethite and haematite within this phase. The presence of 29.2% of total titanium within the “magnetite targeted” phase is likely due to the presence of crystalline titanium oxides such as rutile and anatase. The lack of significant iron within this phase suggests iron-titanium oxides, such as ilmenite, are either not abundant or are represented within the “residual” phase instead.

With regards to extracting resource of economic value, the main target metal within the Red Mud is aluminium. A total of 35.7% of total aluminium is contained within the 3 most reactive phases which constitute the “target phases” deemed most susceptible to reductive dissolution by iron reducing communities, though this is predicated on the assumption that the entirety of this aluminium is associated with iron oxyhydroxides susceptible to reductive dissolution.

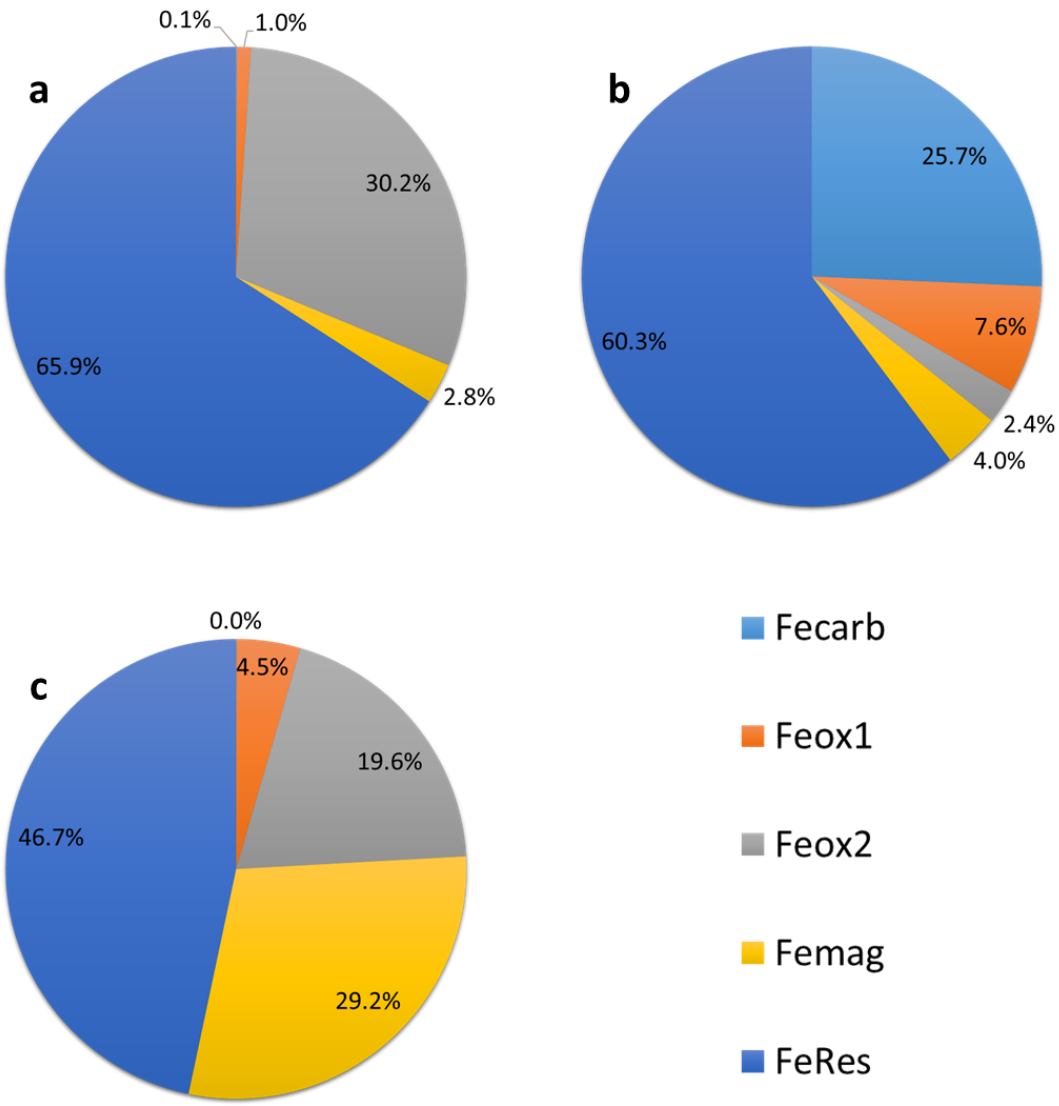

Figure 7.6 Results of sequential extraction analysis showing distribution of metals throughout the Red Mud waste; a) iron, b) aluminium, c) titanium

The dominance of iron and calcium is also reflected by the minerals suggested in the XRD diffractogram (Figure 7.7). The presence of calcite is indicated by the XRD analysis (Figure 7.7). However, notably lacking from the XRD diffractogram are iron oxyhydroxides that would be expected to form a significant proportion of the waste. It is likely that the iron minerals within the waste are largely amorphous and so are not easily detected by the XRD. However, there are no obvious undulations in the trace that would suggest amorphous minerals and the iron oxyhydroxides typically found within red mud are crystalline goethite, hematite and magnetite (Klauber *et al.*, 2011). There minerals may though be present at abundances too low for XRD detection.

The presence of abundant calcite is also suggested by the density of the waste. A dry density of 2.68 g/cm^3 is very similar to the 2.71 g/cm^3 density of calcite. The lower density of calcite is likely compensated for by the higher densities of iron oxyhydroxides that likely comprise the waste (typically 4-5 g/cm^3), despite the lack of identification via XRD (Anthony *et al.*, 2017). This could be resulting in an average density similar to the XRD suggested calcite.

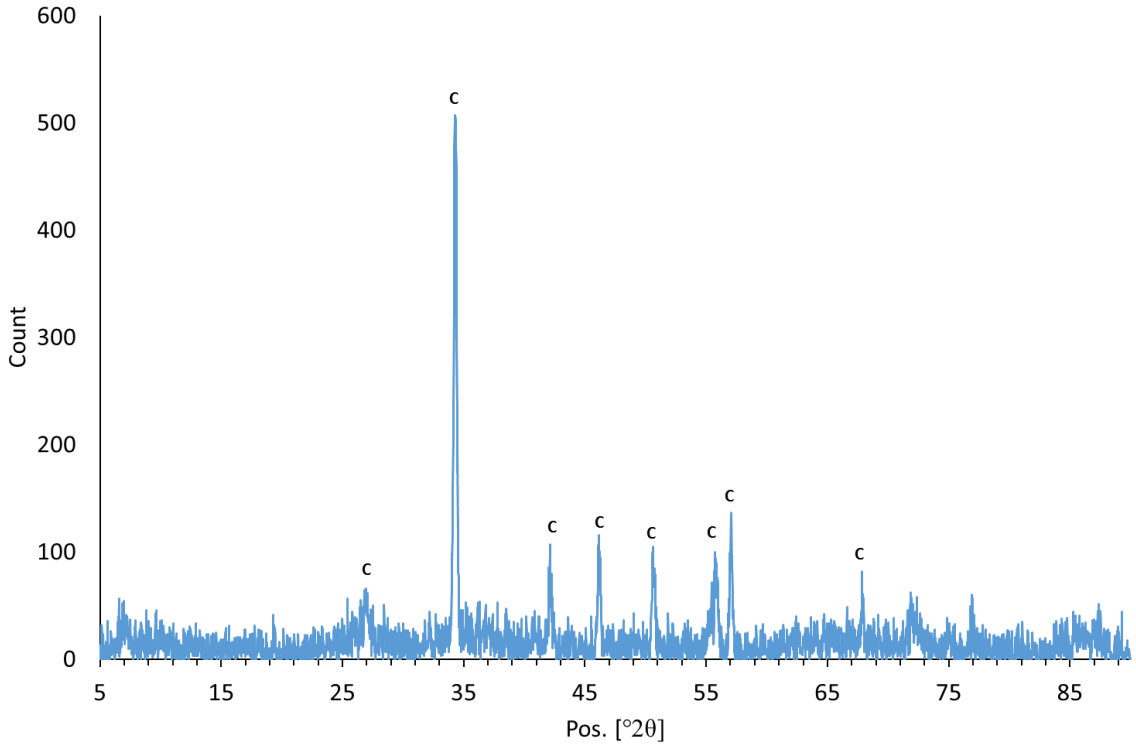

Figure 7.7 XRD diffractogram for Red Mud waste. C = calcite. Energy source: Co Kα

Analysis of the particle size distribution of Red Mud waste shows that the waste is poorly graded with a range of particle sizes present (Figure 7.8). The entirety of the test sample passed through the 212 µm sieve indicating the sample consisted of particles of fine sand or finer sizes. 42.95% of the sample was retained within the 63 µm sieve representing the very fine sand fraction of the waste. In total 60.42% of the waste comprised of fine and very fine sand. The remnant 39.57% of the sample comprised finer silt or clay material. Given the lack of larger particles in the waste, a sample of the total waste was analysed with the mastersizer. The particle size distribution of the sample analysed with the mastersizer displays a significant skew to the right, representing a

dominance of larger particles within the mastersizer range. The majority of particles range from 3.54 µm (D_{10}) to 156 µm (D_{90}), whilst the D_{50} value is 43.7 µm (Figure 7.9). The skew towards the larger particle size may be in part due to the hydrophobic nature of the waste. Some finer particles tended to float on the water surface and required the addition of a surfactant to disperse the particles in the water for analysis. However, the addition of the surfactant also caused increase flocculation. Sonication was used to break up these flocs while recording and averaging multiple reads limited the impact of these limitations.

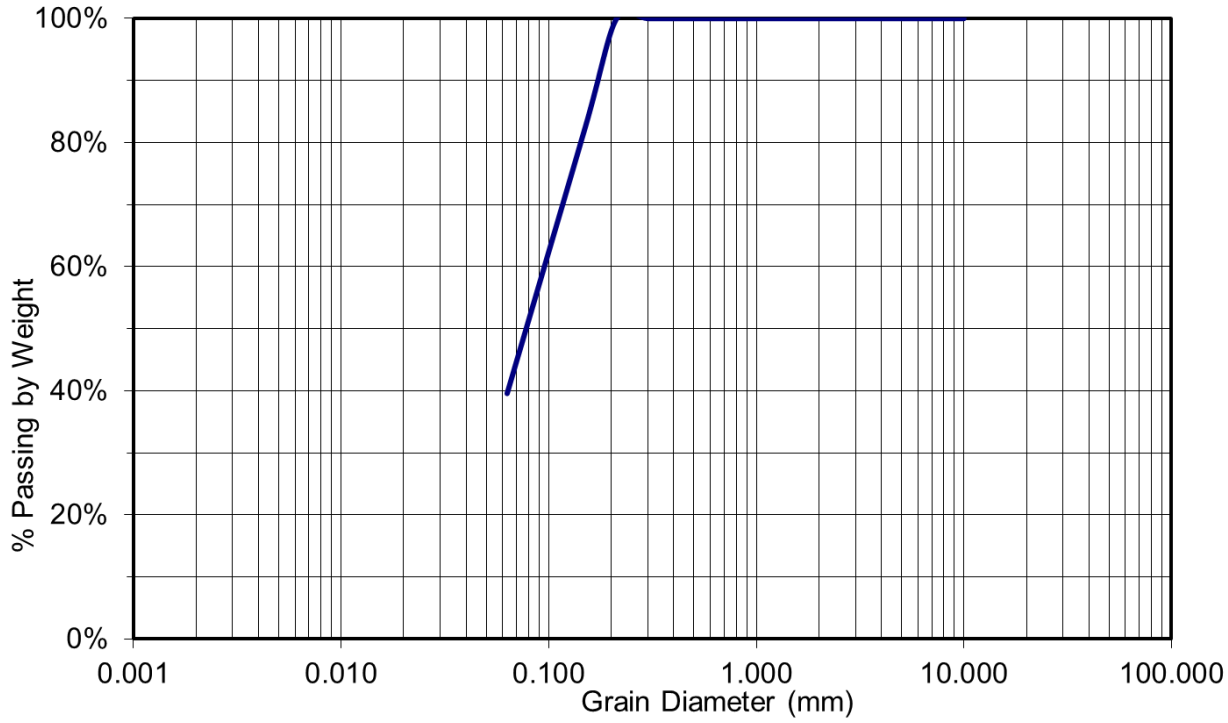

Figure 7.8 Particle size distribution of the Red Mud waste

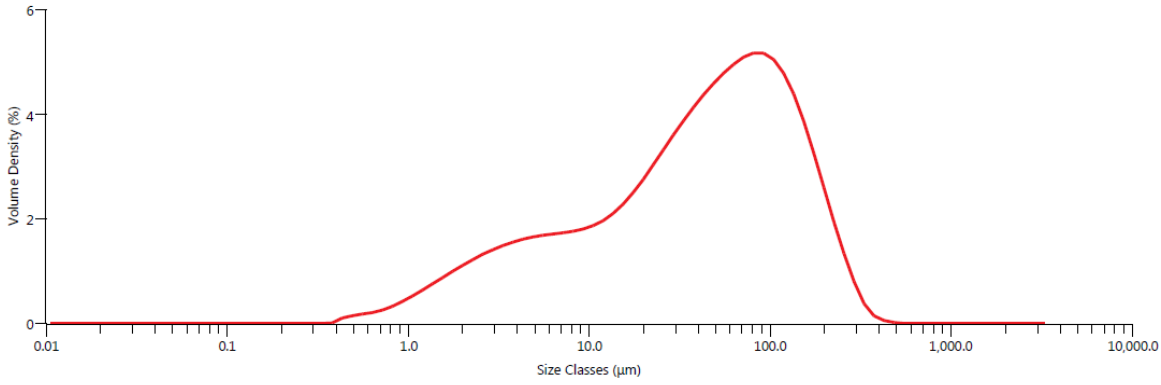

Figure 7.9 Malvern Mastersizer particle size distribution analysis of Red Mud waste

7.4. Wheal Jane

Table 7.3 presents a selection of physicochemical properties of the Wheal Jane mine water treatment waste. The treatment of the mine water with the addition of lime results in the waste having alkaline pH at pH 8.46. It is also indirectly responsible for the high inorganic carbon content of the waste.

Table 7.3 Physicochemical properties of Wheal Jane mine treatment waste

Determinant	Units	Value	St. Dev
Solids Content	wt. %	54.26	±0.73
Bulk Density	g/cm^3	1.65	±0.03
Dry Density	g/cm^3	2.59	±0.14
Specific Gravity		2.28	±0.02
Void Ratio		1.62	±0.11
Paste pH		8.46	±0.18
Sulphur	wt.%	0.01	
Total Carbon	wt.%	5.10	
Inorganic Carbon	wt.%	4.84	

The most abundant elements (of those analysed) in the waste are calcium, iron, zinc and aluminium which constitute 16.3%, 15.1%, 3.97% and 1.82% DW respectively (Figure 7.10). Arsenic concentrations within the waste are also elevated at 0.177% DW (or 1778 mg/kg). This is far higher than the average arsenic concentration within rural UK soils (10.9 mg/kg) (Ross *et al.*, 2007)and also in excess of the high estimate of concentration within mineralised soils in SW England of 424 mg/kg (Alloway, 1995; Vincent & Passant, 2006).

Iron is broadly partitioned into the two most reactive phases of the sequential extraction, with negligible amounts within the remaining phases (Figure 7.11a). Approximately 40% of iron is located within the "carbonate associated" phase, whilst ~60% is located within the "easily reducible oxide" phase. This is reflective of the active remediation system utilising aeration and lime dosing to precipitate iron carbonates, ferrihydrite and other easily reducible amorphous iron oxyhydroxides. Zinc, as the most abundant of the associated metals, is the primary target for recovery from the Wheal Jane waste. The zinc, like iron, is located predominantly within the first two reactive

phases (Figure 7.11b). However, unlike iron, the majority of the zinc (~80%) is located within the "carbonate associated" phase. Whilst a significant proportion of this represents zinc associated with iron carbonates; it is feasible that zinc hydroxides and carbonates are also present as a result of the pH increase during remediation. If present it is likely that these would be removed with the most reactive phases as they are both already slightly soluble at the pH of the waste and the addition of even weak acid would be capable of dissolving and extracting the zinc bound within them (Reichle *et al.*, 1975).

Any zinc present as zinc hydroxides would not be readily recoverable through the action of iron reducing microbes. Given that the extraction does not allow distinction between minerals, or elements previously sorbed to less reactive minerals, within the extractive phases it is not possible to accurately estimate the proportion of zinc within the "carbonate associated" phase that may be feasibly recoverable. However, a conservative recovery target of the ~20% zinc within the "easily reducible oxide" phase can be made with the addendum that more zinc, weakly sorbed to iron oxyhydroxides, is potentially available.

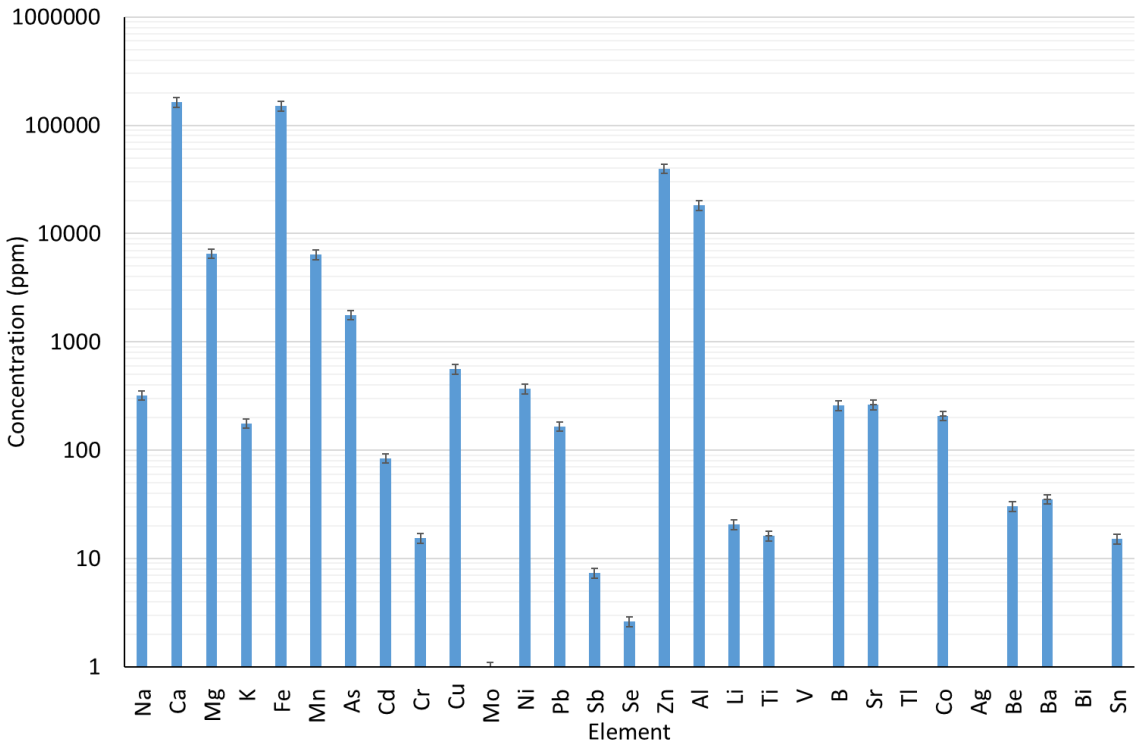

Figure 7.10 Results of ICP-OES analysis of Wheal Jane waste total digest. (No bar = below quantitation limit)

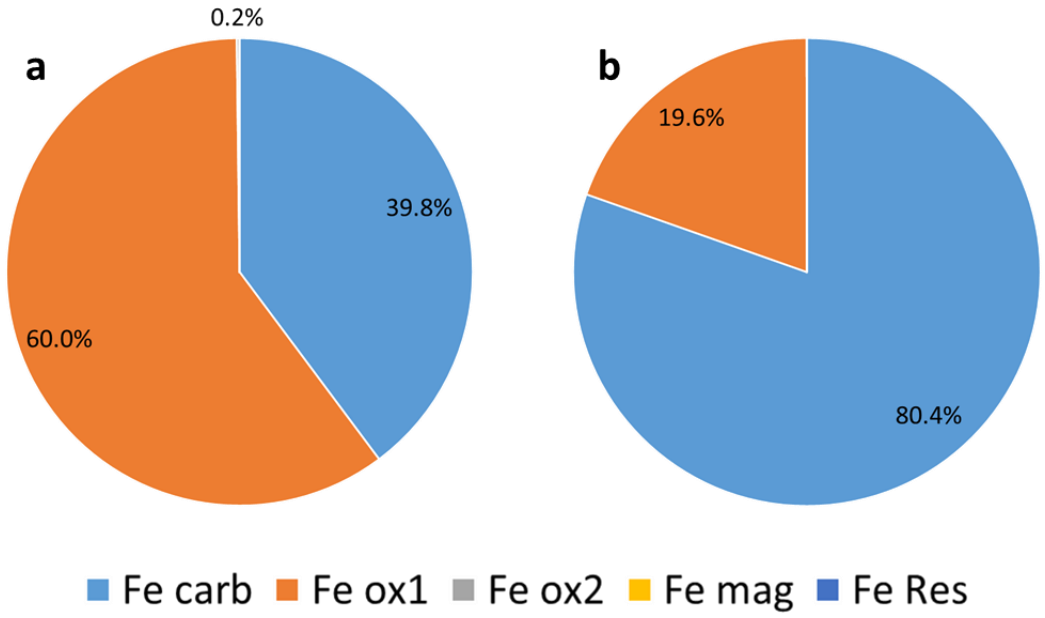

Figure 7.11 Results of sequential extraction analysis showing distribution of metals throughout the Wheal Jane waste; a) iron, b) zinc

The high calcium and inorganic carbon contents are manifested within the XRD diffractogram that suggests an abundance of calcite (Figure 7.12). Somewhat underrepresented in the XRD diffractogram, given the high iron content of the waste, are iron oxyhydroxides. There is a slight undulation at 35 °2Θ which may be an indication of amorphous ferrihydrite, though it is a very minor undulation and not a conclusive indication of ferrihydrite. Amorphous iron oxyhydroxides are to be expected in the waste given the rapid oxidation and precipitation of iron from solution induced by the lime dosing and aeration treatment of the mine water. No peaks relating to zinc hydroxides were identified in the XRD despite the large amount of zinc within the system.

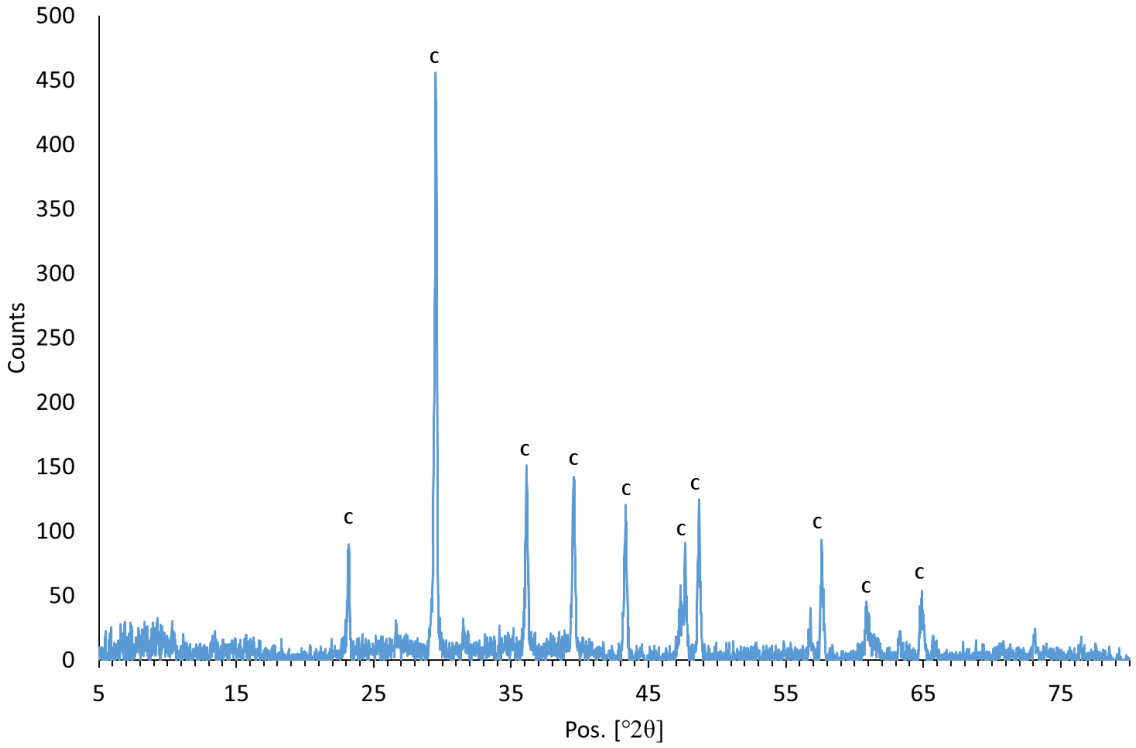

Figure 7.12 XRD diffractogram for Wheal Jane waste. C = calcite. Energy source: Cu Kα

PSD analysis of the Wheal Jane sludge returned a result of 100% passing though the 63µm sieve. Therefore, a sample of non-sieved waste was subsequently used for analysis with the Malvern mastersizer as described in Section 5.2.7 (Figure 7.13). The majority of particles range from 2.78 µm (D_{10}) to 32.5 µm (D_{90}), whilst the D_{50} value is 10.4 µm. A small number of particles have been recorded as having a diameter greater than 63µm. This may be a result of the analytical assumption of spherical particles despite the presence of elongate particles leading to erroneously large particle sizes indicated. Other potential causes are flocculation of particles or aggregation of particles during drying. One of these mechanisms is likely the cause of the minor peak at ~300µm, rather than the existence of a small discrete group of 300µm particles.

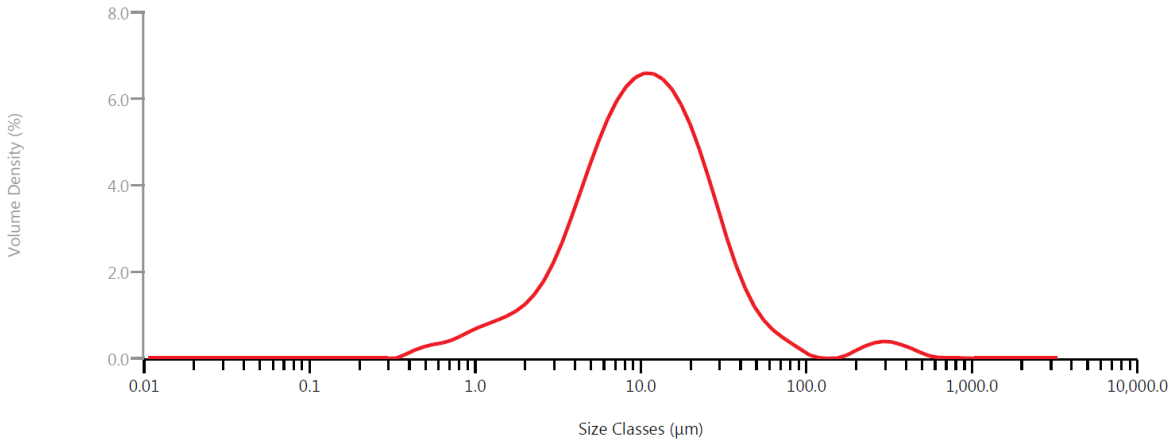

Figure 7.13 Malvern Mastersizer particle size distribution analysis of Wheal Jane waste

7.5. Parys Mountain

7.5.1. Parys Mt. 1

Table 7.4 presents a selection of physicochemical properties of the Parys Mt.1 waste. Parys Mt.1 waste is acidic (pH = 3.37), has a sulphur content of 3.07 wt.% and organic carbon already present within the waste (1.71wt.%). However, this is potentially an underestimation of the waste in-situ as the majority of this organic content is present in the form of grass, leaves and other vegetation. This was evident both during sampling and during the PSD analysis where organic material was separated out along with particle size fractions (Figure 7.14).

Table 7.4 Physicochemical properties of Parys Mt.1 mine waste

Determinant	Units	Value	St. Dev
Solids Content	wt. %	63.84	±1.51
Bulk Density	g/cm^3	1.78	±0.04
Dry Density	g/cm^3	2.09	±0.11
Specific Gravity		2.85	±0.09
Void Ratio		2.05	±0.15
Paste pH		3.37	±0.22
Sulphur	wt.%	3.07	
Total Carbon	wt.%	1.71	
Inorganic Carbon	wt.%	0.00	

Figure 7.14 Elongate organic material in Parys Mt.1 waste. (Image taken from 2 mm sieve during PSD)

As would be expected, given the sites mining history, lead, copper and zinc are the metals of most economic interest within the waste present at 0.15%, 0.12% and 0.10% respectively (Figure 7.15). Aluminium is likely present in the form of aluminium hydroxides, chlorite, alunite or other aluminosilicate clays.

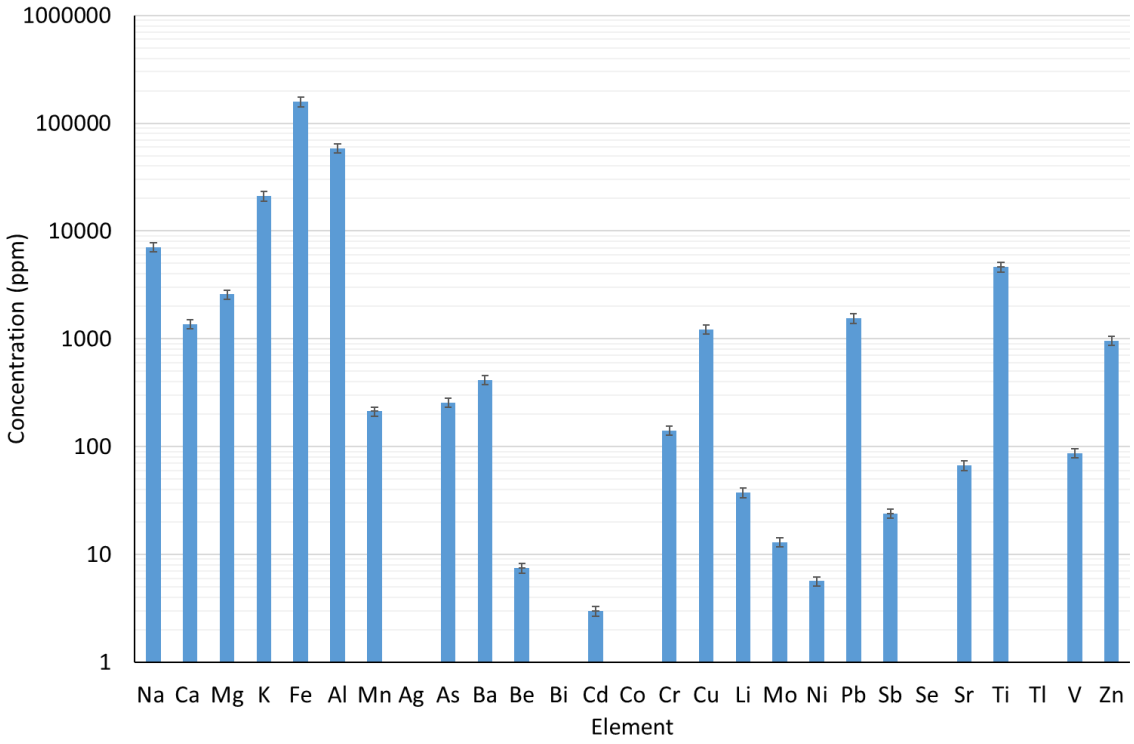

Figure 7.15 Results of ICP-OES analysis of Parys Mt.1 waste total digest. (No bar = below quantitation limit)

Figure 7.16a displays the distribution of iron throughout the sequential extraction phases of the waste. The majority of iron (67.84%) within the sample is located within the “reducible oxide” phase suggesting an abundance of crystalline iron oxyhydroxides. Such minerals would be expected given the geological setting of the waste and the age of the sample which would contribute to transformation of amorphous iron oxyhydroxides (e.g. ferrihydrite) to more crystalline equivalents (e.g. goethite). Approximately 20% of iron is located within the “magnetite targeted” phase suggesting the presence of magnetite or recalcitrant iron oxyhydroxides.

The distribution of zinc and lead (Figure 7.16b&c respectively) bear similarities to each other but little similarity to the iron distribution. Both zinc and lead have large quantities located within the “carbonate associated” phase with ~36% and ~47% respectively within this phase. The lack of iron within this phase suggests that there is very little iron carbonate within the system and the zinc and lead is present as minerals in their own right rather than associated with iron carbonates. In both cases it is likely that these minerals are oxides of the respective metals. Both zinc oxide and lead oxides are typically found in weathered VMS deposits, such as Parys Mt, and residue and are easily dissolved with acid, particularly acetic acid (used in this extraction phase) in the case of lead dioxide. Approximately 19% and 28% of zinc and lead respectively are located within the “easily reducible oxide” phase despite only ~3% of iron being located within this phase again suggesting that a proportion of the metals are not associated with iron oxyhydroxides in the waste. Alternatively, some of the metals within these phases may represent metals sorbed to the surface of iron oxyhydroxides, or other minerals. When compared to the abundance of iron within the “reducible oxide” phase there is relatively little zinc (8.7%) and lead (2.0%) located within this phase. 23.6% and 18.5% of zinc and lead, respectively, are located within the “magnetite targeted” phase.

Copper within the waste shows a significantly different distribution to the other metals analysed (Figure 7.16d). The majority of copper (56.8%) is located within the “residual” phase potentially due to recalcitrant copper sulphides such as chalcopyrite, common in VMS deposits, within the waste. Approximately 10% of copper is located within the “carbonate associated” and “easily reducible oxide” phases respectively, while ~20% is located within the “magnetite targeted” phase. Only 2.4% of copper is located within the “reducible oxide” phase. The extractant used for this phase includes sodium

dithionite which is known to cause copper to precipitate. Therefore, despite the acetic acid and sodium citrate also utilised in the extraction, any copper solubilised will likely be precipitated by the sodium dithionite (Chou *et al.*, 2015). This inability to retain dissolved copper in solution results in the analysis being inherently inaccurate in this circumstance. This may also have a knock-on effect on later extractions. Chou *et al.* (2015) observed that sodium dithionite results in copper precipitating as copper hydroxide. This in turn may result in an over-estimation of the copper content within the "magnetite targeted" phase and/or potentially the "residual" phases.

While the sequential extraction analysis provides an indication of the distribution of the elements of interest throughout the waste the mineralogical complexity limits the accuracy of the results and the ability to estimate the proportion of each metal that can be viewed as feasibly recoverable "target metals". The proportions of the metals within the "easily reducible" and "reducible oxide" phases can be viewed as feasible target metals. However, the proportion of metals held within the "carbonate associated" phase potentially available for recovery via reductive dissolution is more difficult to determine. The contribution of reactive non-ferrous minerals, and metallic cations previously sorbed to more recalcitrant minerals, towards the total extracted metals within this phase cannot be quantified. Therefore determining accurate estimates of the amount of associated metal that can be realistically targeted for recovery is inherently inaccurate and a wide range of target quantities could be assumed. For simplicity it is prudent to only view those metals within phases associated with iron oxyhydroxides susceptible to reductive dissolution as target metals giving conservative estimates of recoverable lead, zinc and copper at ~27%, ~30% and ~14% respectively.

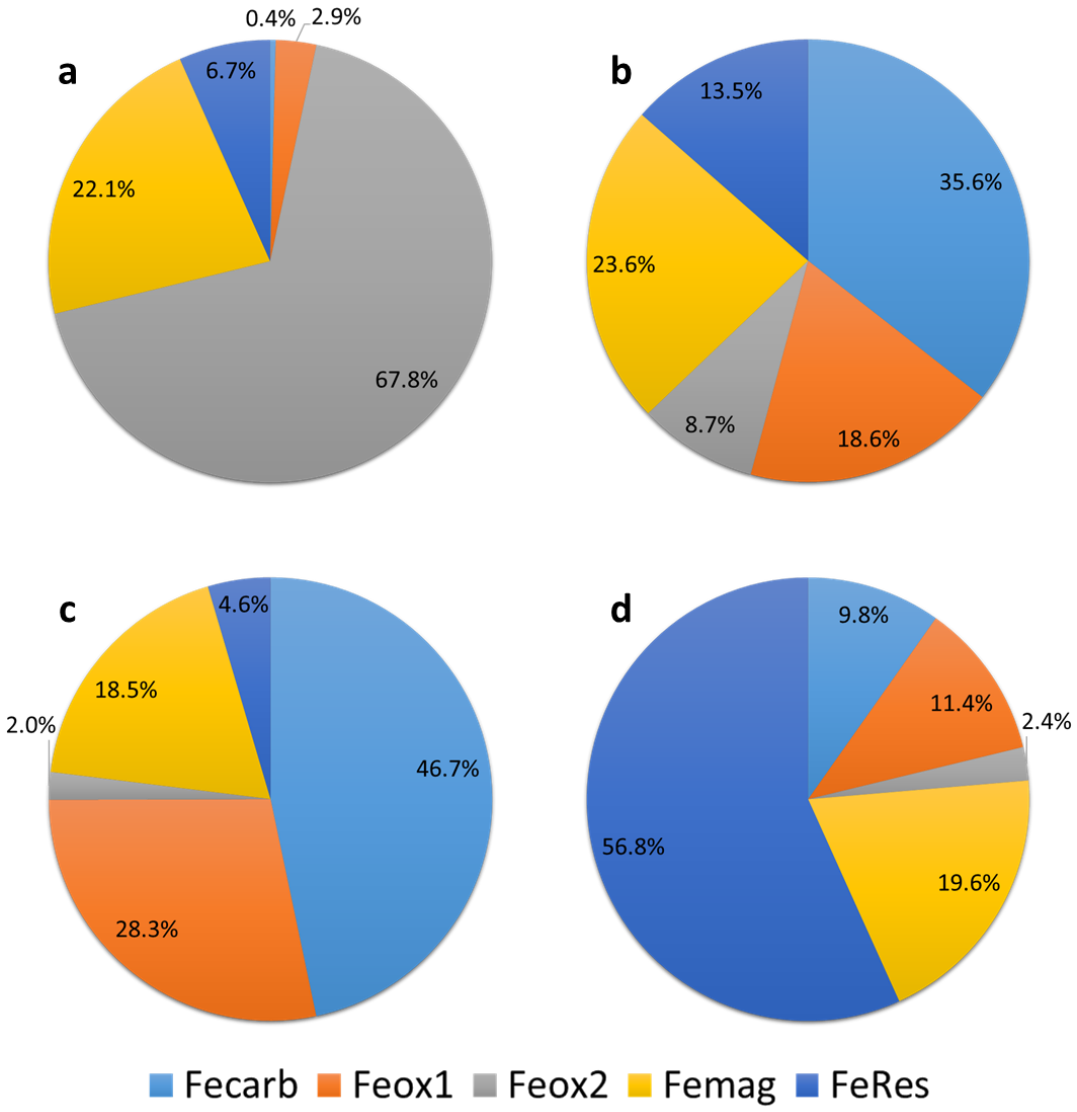

Figure 7.16 Results of sequential extraction analysis showing distribution of metals throughout the Parys Mt.1 waste; a) iron, b) zinc, c) Lead, d) copper

The XRD diffractogram suggests that the major minerals within the waste are quartz, jarosite and goethite (Figure 7.17). This is reflected in the high concentration of iron and potassium within the waste and the majority of iron contained within the "reducible oxide" phase. Given the higher densities of these minerals the low measured dry density of the waste is likely predominantly due to of the high organic carbon content in the waste and the presence of lower density minerals such as quartz.

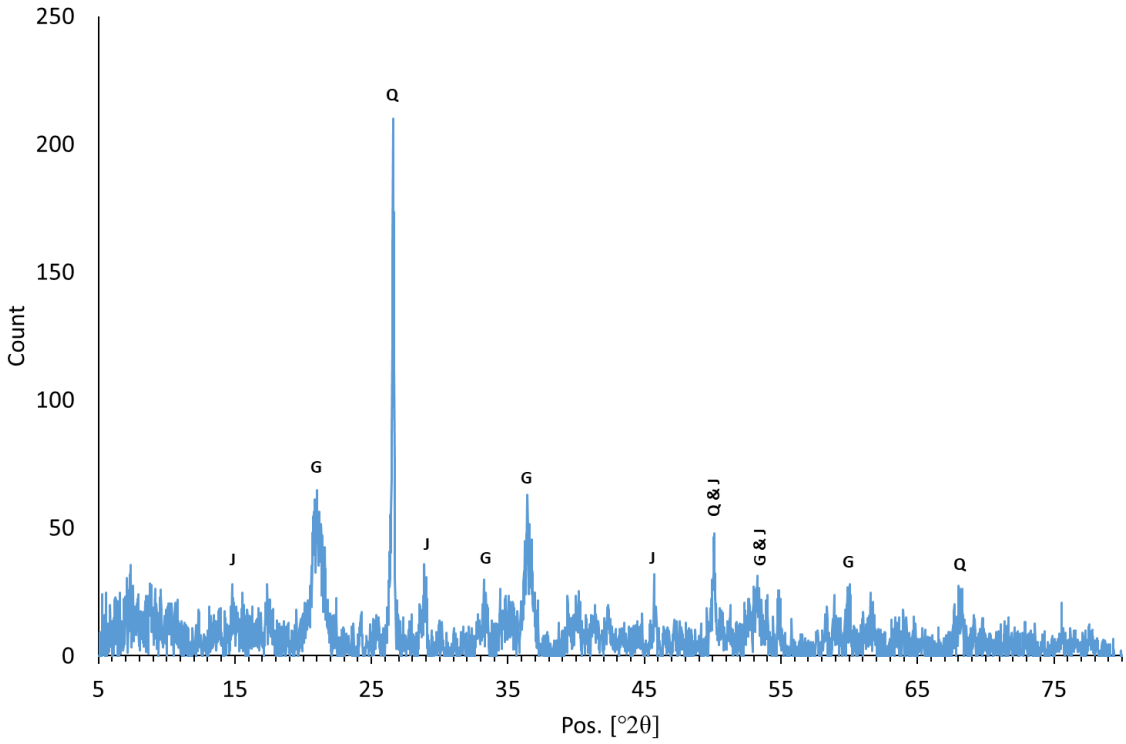

Figure 7.17 XRD diffractogram for Parys Mt.1 mine waste. Q = quartz; J = jarosite; G = goethite. Energy source: Cu Kα

Analysis of the particle size distribution of Parys Mt. 1 waste shows that the waste is well graded with a range of particle sizes present (Figure 7.18). 43.10% of the mass of the waste is comprised of particles of gravel size or greater. Visual inspection of these particles showed that these particles were largely comprised of quartz, organic material or highly weathered iron-rich material likely gossan. 40.61% of the waste is comprised of sand sized particles, whilst the remaining 16.29% of the waste is particles of silt or clay. The fractions of waste passing through the 150 µm sieve were homogenized and analysed with the Malvern mastersizer.

The majority of particles analysed with the mastersizer range from 6.55 µm (D_{10}) to 206 µm (D_{90}), whilst the D_{50} value is 36.6 µm. Along with the major peak there is a smaller peak representing significantly larger particles approximately 1 mm in diameter. Whilst these particles may be aggregation of smaller particles during analysis, though it is more likely that they are elongate particles of organic material similar to those shown in Figure 7.14.

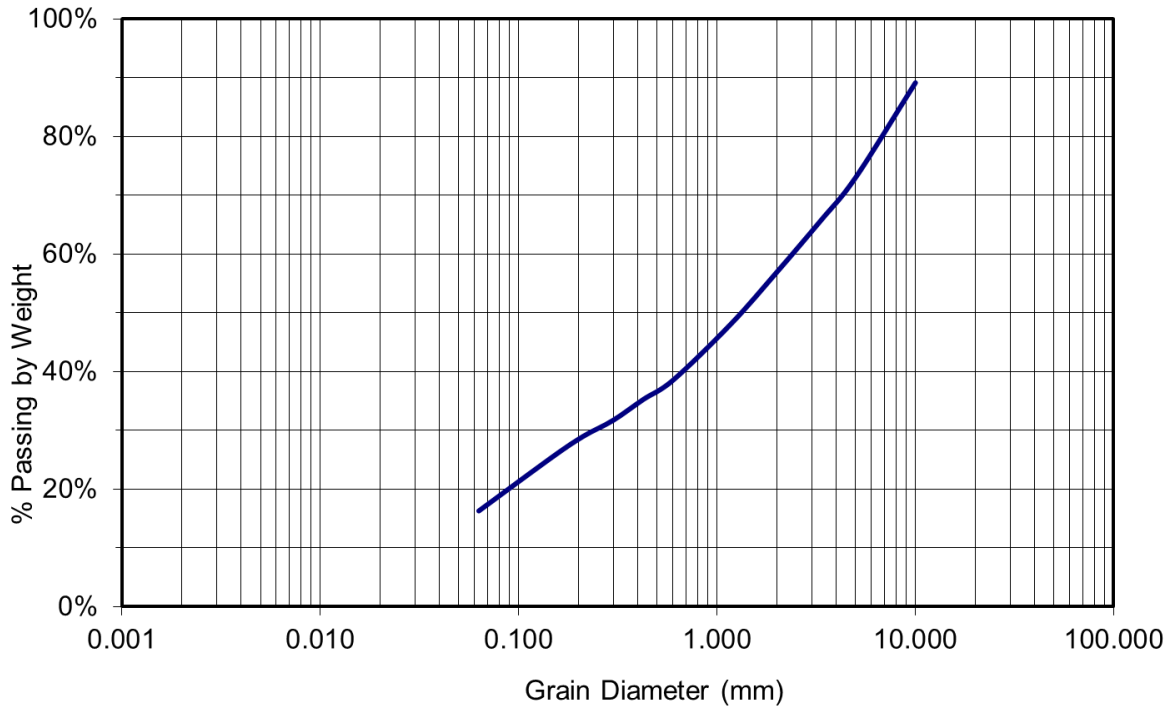

Figure 7.18 Particle size distribution of the Parys Mt.1 waste

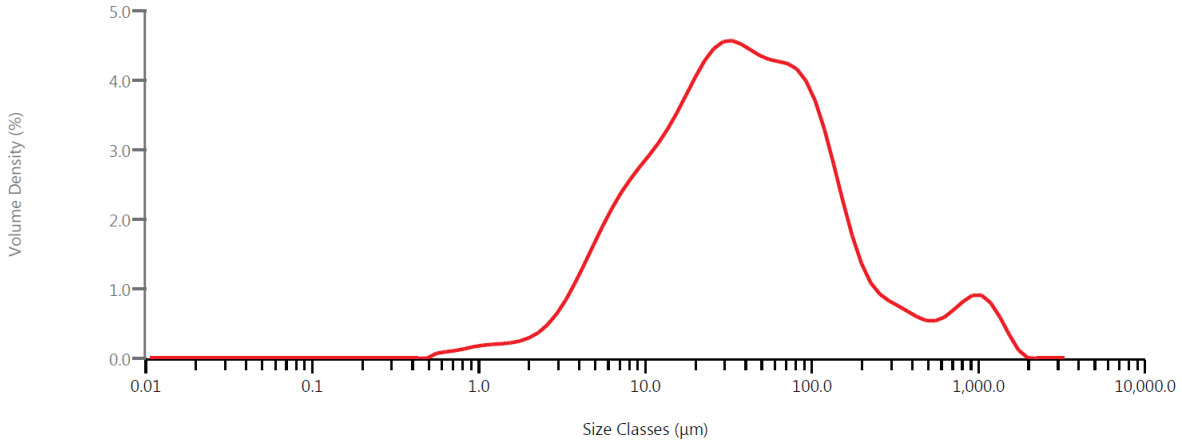

Figure 7.19 Malvern Mastersizer particle size distribution analysis of Parys Mt.1 waste <150µm fraction

7.5.2. Parys Mt. 2

Table 7.5 presents a selection of physicochemical properties of the Parys Mt. 2 waste. The Parys Mt.2 waste has broadly similar properties to the Parys Mt.1 waste. Both have similar bulk densities, sulphur contents and both are acidic. Total carbon content is lower than in the Parys Mt.1 waste at 0.68wt.%. This was also reflected when sampling and characterising the waste as much less organic material, such as foliage, was visible within the waste. The dry density (2.55 g/cm^3) is higher than that of Parys Mt.1, probably due to the lower organic carbon content. The higher dry density also may a result of higher goethite content as suggested by the XRD diffractogram (Figure 7.22).

Table 7.5 Physicochemical properties of Parys Mt.2 mine waste

Determinant	Units	Value	St. Dev
Solids Content	wt. %	73.19	±2.01
Bulk Density	g/cm^3	1.71	±0.15
Dry Density	g/cm^3	2.55	±0.07
Specific Gravity		3.08	±0.15
Void Ratio		1.82	±0.19
Paste pH		2.61	±0.07
Sulphur	wt.%	3.08	
Total Carbon	wt.%	0.68	
Inorganic Carbon	wt.%	0.00	

As with the Parys Mt.1 waste, the metals of economic interest within the Parys Mt.2 waste are lead, zinc and copper. Concentrations of these metals are, however, higher within this waste with zinc and lead present at 0.27% and 0.17% respectively. Increased metal contents at this site may be due to natural variations in the distribution of metals across the site, though the proximity of the sampling location to the, now redundant, Dyffryn Coch adit and the main lode of the mine itself may explain the elevated concentrations when compared to the Parys Mt.1 sample. The concentration of copper within the waste is significantly higher at 0.69%, than in the Parys Mt.1 equivalent waste. The elevated copper content is likely a result of the sampling locations' historical use as a precipitation pond for the recovery of copper. This also raises the possibility of the presence of residual metallic copper. High concentrations of aluminium are likely due to the presence of aluminosilcates and chlorite common in VMS deposits.

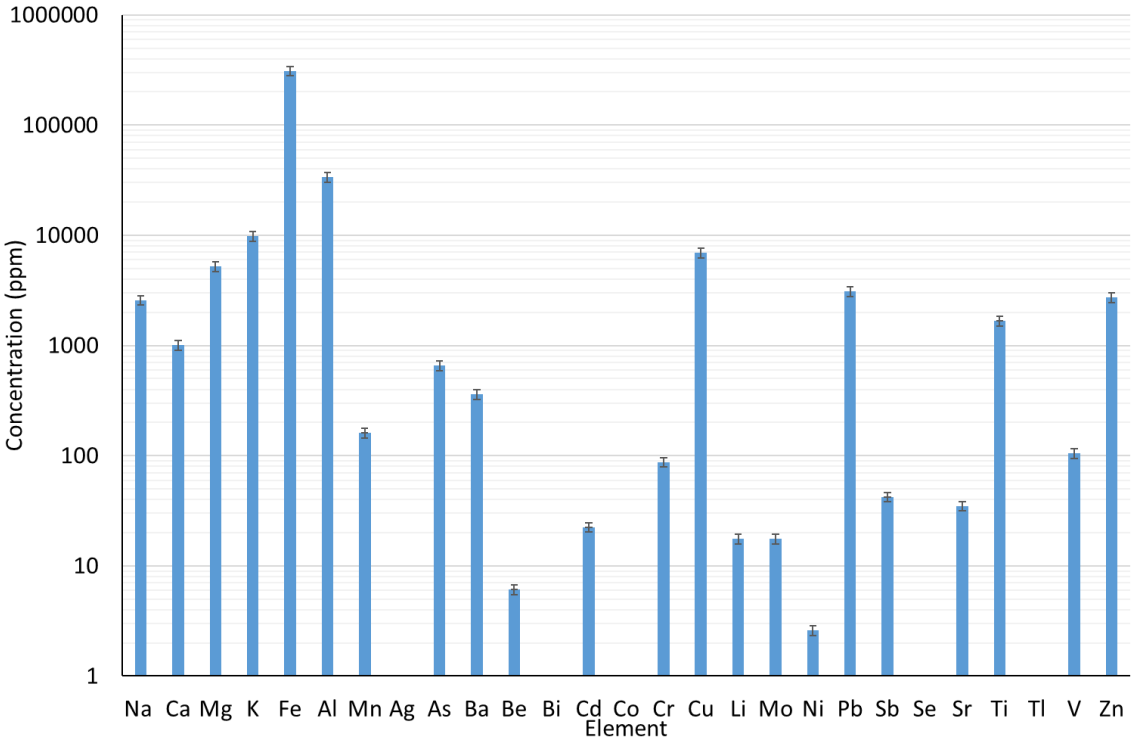

Figure 7.20 Results of ICP-OES analysis of Parys Mt.2 waste total digest. (No bar = below quantitation limit)

Figure 7.21a shows the distribution of iron throughout the sequential extraction phases applied to the waste. As with the Parys Mt. 1 waste, only minor amounts of iron are located within the two most reactive phases, "carbonate associated" and "easily reducible oxide". The "reducible oxide" phase is again prevalent with 40.94% of iron located within this phase. The most significant difference, compared with Parys Mt. 1, is the increased proportion of iron located within the "residual" phase of the waste (40.52%). This may be due to increased iron sulphides, clays and other recalcitrant minerals in the waste relative to the Parys Mt. 1 waste. Alternatively, it may be a result of the historical practice of introducing scrap metal to the mine drainage to induce copper precipitation.

Zinc, like iron, is mostly found within the 3 least reactive phases (Figure 7.21b). The largest of these phases is the "residual" phase with 47.8% total zinc which contrasts with the ~14% within this phase in the Parys Mt. 1 waste. This relative increase in the "residual" phase compared to the Parys Mt. 1 waste is counterbalanced by a relative

decrease in the two most reactive phases. 6.4% and 1.4% of total zinc is located within the “carbonate associated” and “easily reducible oxide” phase respectively both of which are substantially lower than the 25.8% and 19.8% in these phases within the Parys Mt. 1 waste. 23.2% of total zinc is held within the “reducible oxide” phase while the remaining 21.3% is within the “magnetite targeted” phase.

The distribution of lead within the Parys Mt.2 waste is substantially different to that within the Parys Mt. 1 (Figure 7.21c). Over half of the lead is located within the “magnetite targeted” phase (54.1%) while a further 29.5% is located within the “residual” phase. The remaining 16.4% of total lead is spread between the 3 most reactive phases, which represent the target phases for metal recovery via microbial reductive dissolution of iron. The relatively low amount of lead within these target phases suggests that there is significantly less lead associated with iron oxyhydroxides (either co-precipitated or absorbed) or as easily leachable minerals compared with the Parys Mt. 1 waste. Therefor despite the greater amount of lead within the waste it appears that a lower proportion of this waste is available for recovery via reductive dissolution compared with the Parys Mt.1 waste.

The distribution of copper between the sequential extraction phases bears considerable similarities to the distribution of lead (Figure 7.21d). The majority of copper is held within the “magnetite targeted” and “residual” phases with 46.9% and 46.5% of total copper within these phases respectively. The abundance of low reactivity, recalcitrant copper within the waste may be a result of the sites previous function as a precipitation pond. The recovery of copper in this system is predicated on the formation of copper precipitates on scrap iron within low pH waters, indicating low reactivity copper precipitates which correlates with the results of the sequential extraction. Despite the elevated copper within the waste the sequential extraction results suggest that only minor quantities of it are likely accessible for recovery as only 3.1% and 3.5% of total copper is contained within the “carbonate associated” and “easily reducible oxide” phases respectively. It is notable, however, that no copper was extracted in the “reducible oxide” phase representing crystalline ferric oxides such as goethite. This is attributable to the sodium dithionite within this phase’s extractant which causes solubilised copper to precipitate out of solution (Chou *et al.*, 2015). This effect causes copper to be underrepresented in the “reducible oxide” phase and therefore potentially

overrepresented in the subsequent phases. This makes predicting the amount of copper that can be considered feasibly recoverable difficult and inaccurate.

Despite higher concentrations of the primary target metals of zinc, lead and copper within the Parys Mt.2 waste compared with the Parys Mt. 1 equivalent, the sequential extraction data suggests that a smaller proportion of this metal value is potentially recoverable by reductive dissolution of iron. If conservative recovery targets, using only the “easily reducible oxide” and “reducible oxide” phases, are considered then ~24.5% zinc, ~13% lead and ~3.5% copper can be considered feasibly recoverable.

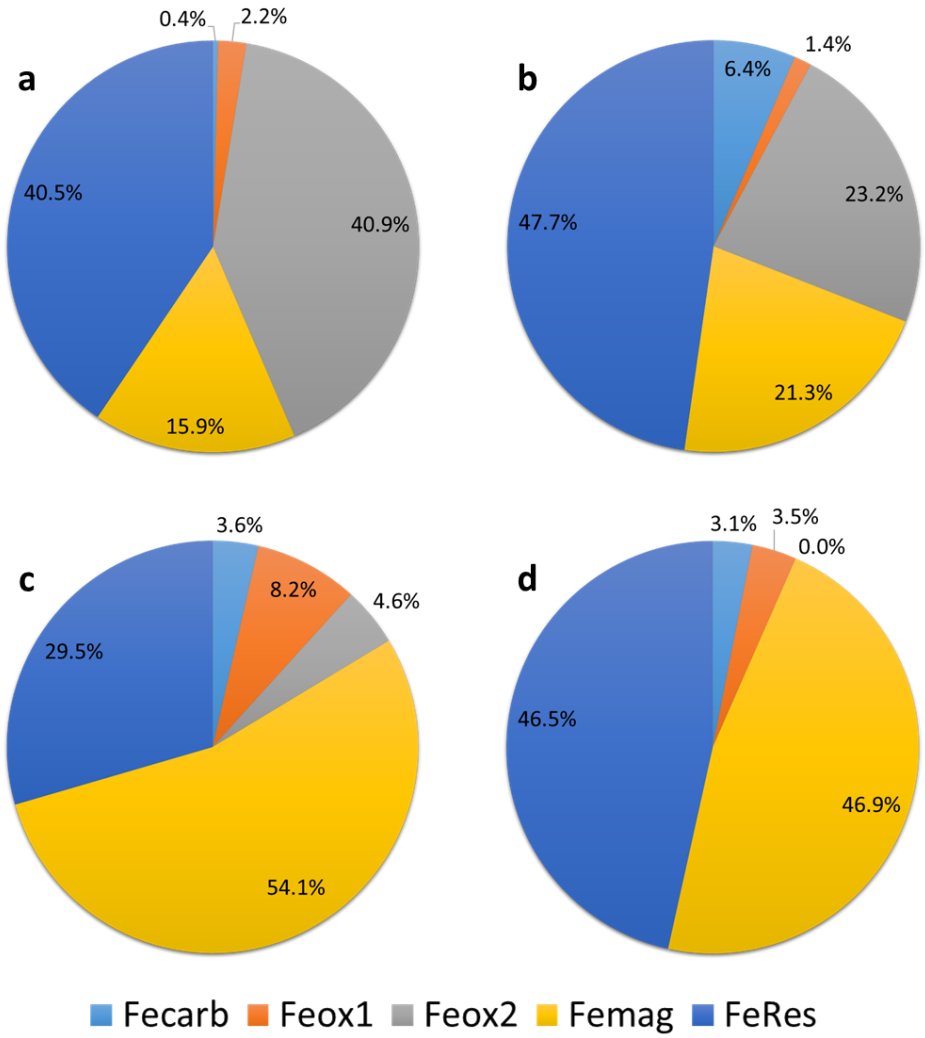

Figure 7.21 Results of sequential extraction analysis showing distribution of metals throughout the Parys Mt.2 waste; a) iron, b) zinc, c) Lead, d) copper

As with Parys Mt. 1, the XRD diffractogram for the Parys Mt. 2 waste suggests a system dominated by quartz, jarosite and goethite. This correlates with the abundance of iron located within the "reducible oxide" phase which targets crystalline iron oxyhydroxides such as goethite. This also correlates with the high iron, sulphur and potassium indicated by the total digest and Leco sulphur analysis. Despite their prevalence in typical VMS deposits, and the abundance of elements such as aluminium, magnesium and potassium, no aluminosilicate clays were identified by the XRD analysis.

Despite the sites former use as a copper precipitation pond, and the high concentration of copper in the total digest, there were no copper minerals identified by the XRD analysis.

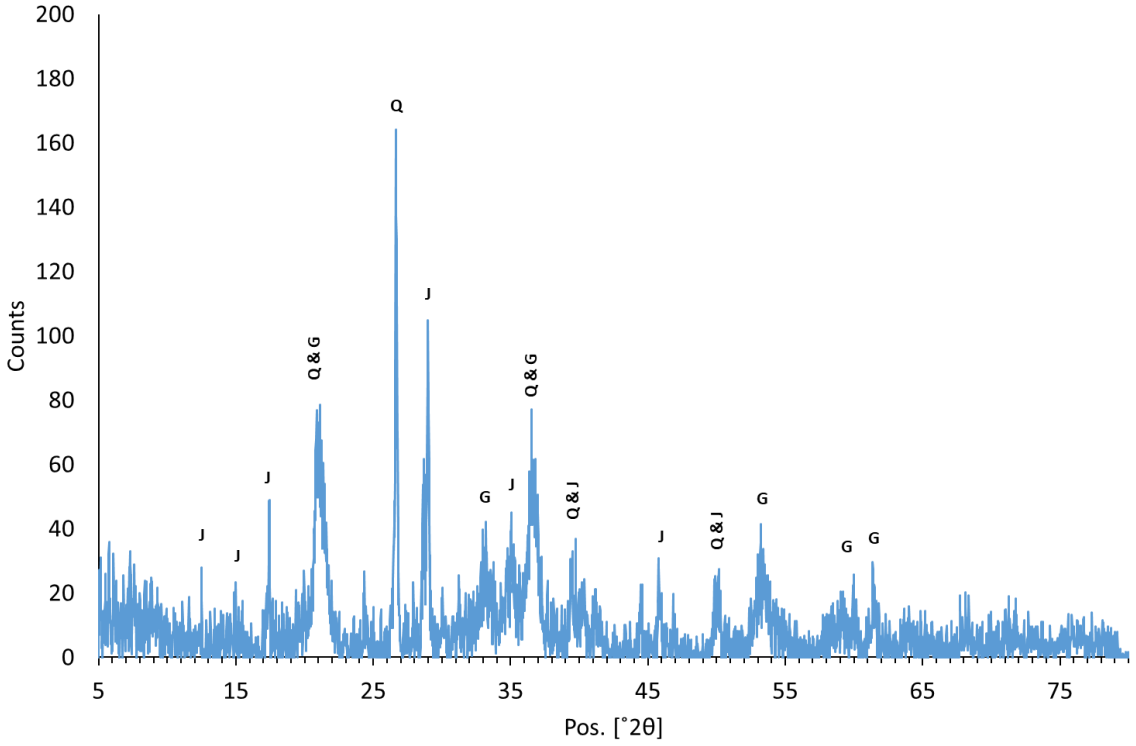

Figure 7.22 XRD diffractogram for Parys Mt.2. Q = quartz; J = jarosite; G = goethite. Energy source: Cu Kα

Analysis of the particle size distribution of Parys Mt.2 waste shows that the waste is well graded with a range of particle sizes present (Figure 7.23). 58.19% of the mass of the waste is comprised of particles of gravel size or greater. The largest proportion of these particles were retained within the 10 mm sieve, though visual inspection of the retained particles failed to find any particles larger than course gravel grade. These larger particles were largely comprised of quartz, silicates highly weathered iron-rich material,

likely gossan. 34.34% of the waste is comprised of sand sized particles, which is fairly evenly distributed though the various grades of sand. The remaining 7.47% of the waste is particles of silt or clay. The fractions of waste passing through the 150 µm sieve were homogenized and analysed with the Malvern mastersizer (Figure 7.24). The majority of particles analysed with the mastersizer range from 2.40µm (D_{10}) to 94.2µm (D_{90}), whilst the D_{50} value is 11.4 µm.

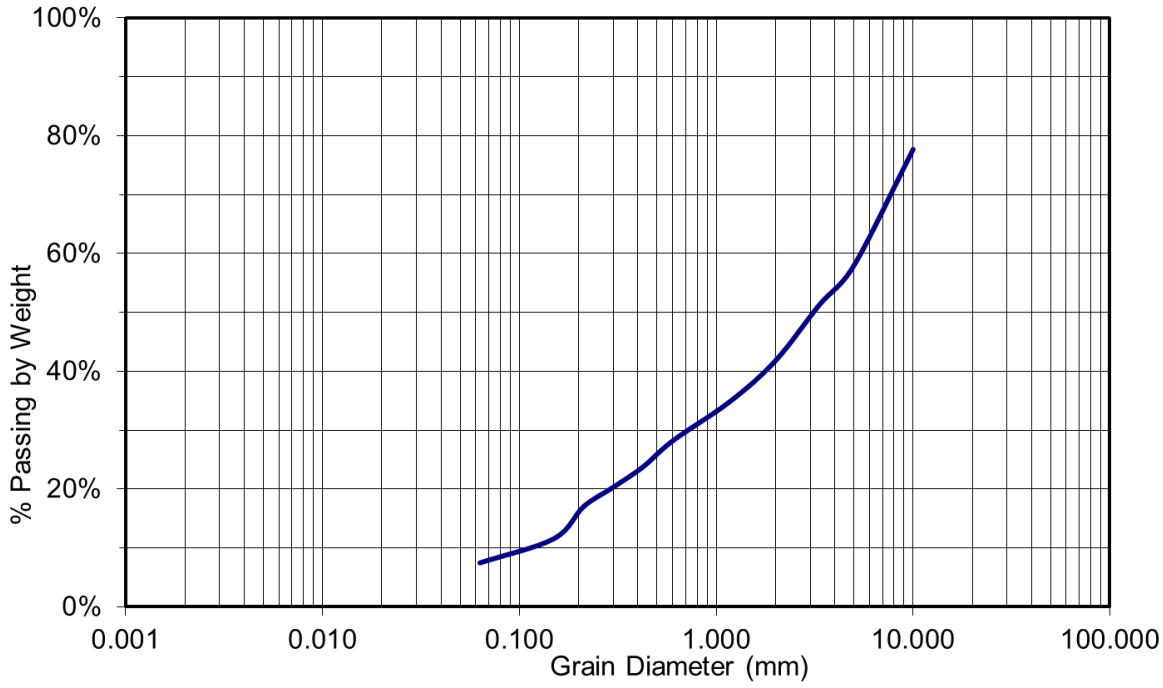

Figure 7.23 Particle size distribution of the Parys Mt.2 waste

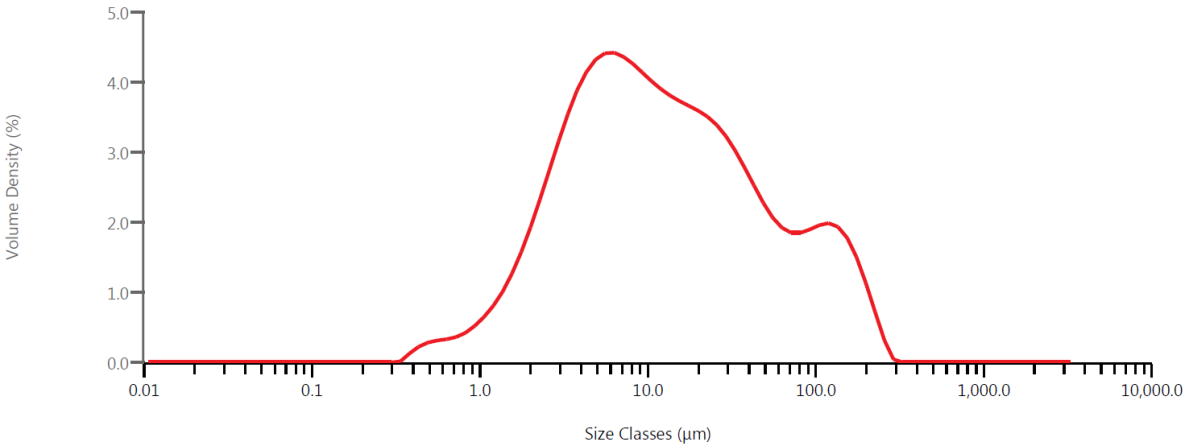

Figure 7.24 Malvern Mastersizer particle size distribution analysis of Parys Mt.2 waste <150µm fraction

7.6. Comparison of Waste Metal Content to Typical Ore Grades

Based on their concentrations within the identified waste streams there are specific metals within each waste which may be considered the target metals for recovery. For the red mud these are aluminium and titanium, for Wheal Jane the target metal is zinc and for the Parys Mt. samples zinc, copper and lead represent the best possible targets for recovery.

Within the red mud waste, aluminium comprises 11.1% of the waste by dry weight; while titanium comprises 3.3% by dry weight. Bauxite is the main ore exploited for aluminium. The lowest grade of bauxite ores commercially mined is 30% Al_2O_3 from mines in the Darling Range in Western Australia. This low grade is only commercially viable due to low silica content (1-2%) allowing for reduced processing costs (Britt *et al.*, 2017). This is approximately three times greater than the concentration of aluminium found within the red mud investigated in this study. The silica content of the red mud (3.0% DW) is higher than that of the bauxite ore suggesting that its value is lessened if processed in a similar method to the bauxite ore. However, as can be seen in Figure 7.25 when the current price of refined aluminium is plotted against the dilution of aluminium within the red mud it plots above the metal specific Sherwood Plot presented (Johnson *et al.*, 2007). The higher above the plot a substance is located the greater the potential for recycling of that substance from the waste. This suggests that the concentration of aluminium within the red mud makes it a viable target for economic recovery.

Titanium within the red mud also falls above the metal specific Sherwood plot suggesting it would also be a feasible target for economic recovery (Figure 7.25). However, the situation with titanium is more complex than other metals. The majority of titanium minerals processed worldwide (92%) originates from the ferro-titanium oxide mineral ilmenite. The other common mineral source of titanium is in the form of the titanium oxide rutile (Woodruff *et al.*, 2017). The majority of titanium (68%) originate from unconsolidated heavy mineral sands rich in ilmenite, rutile and zircon (Woodruff *et al.*, 2017). These sands are grades on their content of heavy minerals rather than a specific metal with grades typically between 0.5% and >20% (Iluka Resources, 2009). The feedstock ores of titanium are typically classified and valued based on their titanium content and the suitability to one of the two predominant processing techniques (known as the chloride and sulphate processes) (Murphy & Frick, 2006). Rutile typically achieves higher prices due to its higher titanium content and it requiring a lesser extent of processing. The high cost of extracting titanium metal from its ore has led to the majority of titanium produced (~93%) being refined into pigment rather than being produced for the metal itself (Murphy & Frick, 2006). This all results in the price of titanium being highly dependent on the form in which the titanium is present and its suitability for further processing. Neither of these details are accurately known about the titanium within the red mud investigated within this study, so an accurate estimation of the metal value held within it cannot be made.

Within the Wheal Jane mine water treatment sludge, zinc is the primary target for recovery. It comprises 3.97% of the waste by dry weight. This is lower than many of the major “SEDEX” zinc deposits which have typical zinc grades of ~10-15% but within the typical range (~2-5%) of the smaller “MVT” deposits (BGS, 2004), suggesting the concentration of zinc with the waste may be economically significant. This is supported by zinc in the Wheal Jane waste plotting above the metals specific Sherwood Plot in Figure 7.25 which indicates there is potential for the zinc within the Wheal Jane sludge to be recycled.

Zinc deposits nearly always have associated lead present at lower concentrations (Calvo *et al.*, 2016). This results in small amounts of lead being produced from deposits in which the lead alone would not be considered economic. Similarly, zinc deposits which are on the borderline of being considered economic can be bolstered by the sale of this

additional lead. Within SEDEX deposits the average lead grade it typically 2-5%, while it is 1-3% within MVT deposits (BGS, 2004). Zinc and lead are present within the Parys Mt.1 waste at grades of 0.10% and 0.15% dry weight respectively. Within the Parys Mt. 2 wastes zinc and lead are found at grades of 0.27% and 0.17% dry weight respectively. For both these sites, zinc and lead are located below the metal specific Sherwood Plot in Figure 7.25, suggesting it is uneconomic to recycle these metals at their current concentrations.

The average grade of currently active copper mines is approximately 0.62% Cu, though this is predicted to decrease as higher grade operations are exhausted (Mudd & Weng, 2012). The copper content of the Parys Mt. 1 waste is considerably lower than this with copper comprising 0.12% of the waste by dry weight, more than 5 times lower than the current average commercially viable grade. Parys Mt. 2 waste, however, has a copper grade of 0.69% by dry weight, commensurate to the average mined grade. This is reflected by copper at Parys Mt. 2 being located on the metal specific Sherwood Plot in Figure 7.25, while Parys Mt.1 plots below it suggesting it is not likely economic to recycle.

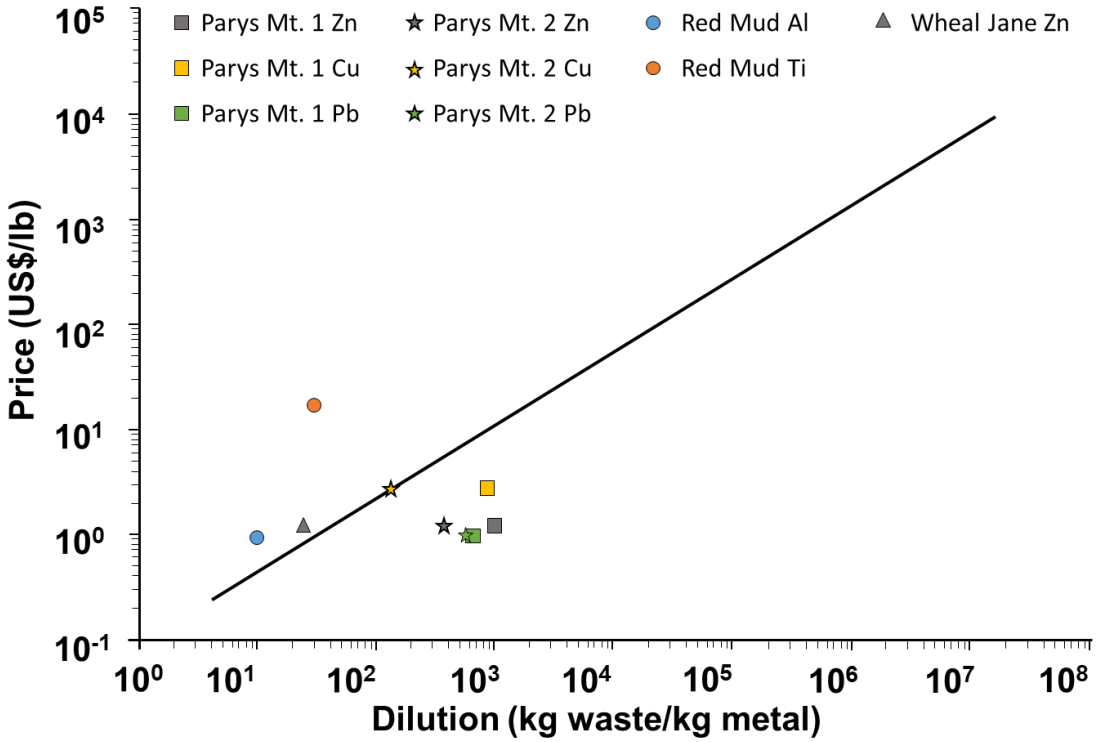

Figure 7.25 Relationship between metal dilution within wastes and the price of the metal. Regression line is the "metals-specific Sherwood Plot" devised by Johnson *et al.* (2007). Adapted from Johnson *et al.* (2007) after (Sherwood, 1959). Aluminium, zinc, copper and lead prices acquired from (Infomine, 2018). Titanium (as titanium sponge) price acquired from U.S. Geological Survey (2018).

While the metal-specific Sherwood Plot is a useful tool in assessing the potential recyclability of metals within waste streams, there are a number of limitations that should be noted.

The factor of scale of the deposit/ waste repository are not considered within a Sherwood Plot. This factors significantly into any economic viability assessment. For example, whilst the grade of copper in the Parys Mt. 2 waste is commensurate to the grade of an average copper mining operation there is far less material and therefore less copper for recovery. This would incur greater costs per unit of copper, limiting the potential viability. Relating to scale are the operating costs of any mining/ metal recovery operation. The metal specific Sherwood Plot is created by comparing the price of metals against grades of ore currently economic to extract. The purpose of this study is to investigate the potential of a cheaper, more energy efficient method of metal recovery. If such a technique became economically viable it would result in a substantial shift towards lower grade materials being exploited and some of the metals/wastes which are located below the metal specific Sherwood Plot may shift to being above it and have greater potential for recyclability.

The Sherwood Plot also only assesses the value of a single metal in isolation, despite it being common for a range of other minor metals to be co-extracted along with the primary target metal (Graedel & Nassar, 2013); as has been outlined briefly with regards zinc-lead deposits. Other examples of metals commonly produced as by-products include indium; which is mostly produced as a by-product of zinc (Schwarz-Schampera & Herzig, 2002), cobalt; produced as a by-product of nickel or copper deposits (BGS, 2009) and silver; 72% of which is produced as a by-product of zinc-lead, copper and gold production (GFMS Ltd, 2018). Therefore, it stands to reason that when exploring the potential recovery of metals from waste streams an economic stance which incorporated all potential valuable metal streams would need to be considered to assess the true value potential held within a waste.

Furthermore, a Sherwood Plot explores economic viability when the metal removed from the waste is being considered the resource. As has been established in Section 1.2, there are multiple interpretation of what can be considered a resource. With regards to those metals which fell below the metal specific Sherwood Plot, and thus were

considered un-economic for recovery, it may be that the value accrued from metals recovered can be used to offset remediation costs and the subsequent decontaminated land is instead considered the resource.

7.7. Material Characterisation Summary

Several wastes have been studied and characterised in terms of their physical, chemical and mineralogical properties. XRD analysis for mineralogy has shown that, of the wastes studied, the Lindsay and Parys Mt wastes are comprised largely of iron oxyhydroxides. Within the Lindsay waste these are predominantly amorphous iron oxyhydroxides, such as ferrihydrite, and goethite. The Parys Mt wastes were largely dominated by quartz though also contained significant amounts of goethite and the iron sulphate jarosite.

Despite small quantities of iron oxyhydroxides detected in the Wheal Jane waste, the XRD analysis suggests both Wheal Jane and Red Mud waste have substantial amounts of calcite. However, due to XRD not picking up amorphous minerals it is likely that this is not a reflection of the true mineralogy and both wastes likely contain abundant amorphous iron oxyhydroxide minerals. The presence of iron oxyhydroxides in these wastes is supported by both their red-brown colouration, typical of iron oxyhydroxides, and the elevated concentration of iron observed in the total digest analysis.

The most interesting result, from an economic standpoint, is the 11.1% of Al within the Red Mud presenting the most concentrated source of a metal of economic interest of the wastes studied. This was a relatively predictable outcome as the aluminium value of Red Mud is well documented and several studies have been conducted into its recovery (Liu & Naidu, 2014; Liu & Li, 2015) as was outlined in Section 3.3.4. Wheal Jane too, has a singular metal of economic interest in the form of zinc, present at a concentration of ~4%. The Parys Mt. wastes by contrast do not have a singular metal with elevated concentration acting as the economic incentive for investigation. Rather, they contain a suite of metals, which, despite lower concentrations compared to the Red Mud and Wheal Jane wastes, are present at high enough concentrations to be potential targets for recovery. Specifically, this study will focus on lead, zinc and copper. Whilst not specifically focused on the wastes utilised here, the potential economic importance of

the Parys Mt site is also evidenced by number of studies into metal recovery from the mine drainage and scoping plans by Anglesey Mining Plc. to restart mining operations at the Parys Mt. site (Anglesey Mining Plc, 2016; Crane *et al.*, 2017). These assessments have been made based on the chemical composition of the wastes solely. No consideration of the quantity of each waste present or available for potential recovery techniques has been made.

Regardless of the metal content of the wastes only the proportion of that metal associated with reducible iron oxyhydroxides such as ferrihydrite and goethite can be considered feasibly recoverable. Despite having elevated concentrations of aluminium, only ~10% of this aluminium is associated with the two "reducible oxide" phases of the sequential extraction form the Red Mud waste. Though 25% is associated with the more reactive "carbonate associated phase. A similar pattern is found with zinc in the Wheal Jane wastes as only ~20% is located within the oxide phases while ~80% is within the "carbonate associated" phase. Of the metals of interest in the Parys Mt. wastes lead and zinc have the highest contents in the target oxide phases in the Parys Mt. 1 and 2 wastes respectively. Despite higher metal contents, the metals within the Parys Mt. 2 waste are seemingly less accessible by reductive dissolution than the Parys Mt.1 equivalent with lower quantities in both the oxide phases and the "carbonate associated" phases.

However, given the often-significant limitations of the sequential extraction technique use to determine metal distribution, these results must be considered with a degree of scepticism and acceptance of the limitations of the data. Alongside the issues of copper precipitation by sodium dithionite and acid-soluble Fe-oxyhydroxide adsorbed cations already addressed; there are issues of non-specificity of extractants and low repeatability (Bacon & Davidson, 2008). Parat *et al.* (2003) tested three sequential extraction techniques (though not the Poulton & Canfield (2005) technique used in this study) and found that repeatability of results were "generally poor for Cu, Pb, and Zn". A significant cause of this poor repeatability is heterogeneity in the samples, as despite extensive homogenisation efforts, test samples of only 200mg will struggle to provide a true representation of the total waste mass. This is exemplified by mass balances for the metals of interest from the extractions. Recoveries of the metals of interest from the Parys Mt. 1 waste ranged from 160% to 406%, whilst in the Parys Mt. 2 waste recoveries were between 10% to 63% of that expected.

Moreover, given the extractions focus on iron minerals, and the non-specificity of extractants towards non-iron bearing minerals, the origin of metals within an extractive phase can be difficult to ascertain. Sodium acetate, used as an extractant for the "carbonate associated" phase is known to also extract exchangeable, acid soluble metals (such as those loosely adsorbed to mineral surfaces) and metals associated with hydroxide minerals (Hanahan, 2004; Bacon & Davidson, 2008). Furthermore, the hydroxylamine hydrochloride used to target crystalline iron oxyhydroxides has been observed to dissolve sulphate and sulphide minerals producing overestimation of the metal content associated with iron oxyhydroxides (Lacal *et al.*, 2003; Peltier *et al.*, 2005). Because of these limitations, the sequential extraction data should be considered as indicative rather than absolute with regard to iron oxyhydroxide associated metals. To summarise

- Iron oxyhydroxides, necessary for DIRM activity have been identified within the wastes.

- The Red Mud, Wheal Jane and Parys Mt. wastes have all been found to contain elevated concentrations of metals of economic interest, such as aluminium, zinc, copper and lead, which warrants further investigation into recovery via microbially mediated reductive dissolution of iron.

- The Lindsay waste has been found to be relatively clean, compared to the other wastes. It is seemingly comprised almost solely of iron oxyhydroxides such as ferrihydrite and goethite and contains no associated metals at significant concentrations.

- Whilst an indication of the distribution of metals of economic interest across mineral phases of the wastes has been obtained. Limitations in the sequential extraction procedure prevents accurate determination of the quantities of metals that could be feasibly targeted by via microbially mediated reductive dissolution of iron.

8. Column Testing – Phase 1

8.1. Introduction

This chapter presents the experimental design and subsequent results of first phase of column testing. This chapter is split into the following sections:

Section 8.2: Introduction and Objectives – Outlines the background to the experiment and the key objectives being investigated.

Section 8.3: Experimental Design, Materials and Methods – Describes in detail the specifics of the experimental design, the materials utilised and the analytical methods employed to measure experimental parameters.

Section 8.4: Results and Discussion – Presents, interprets and discusses the results and of column experimentation on Lindsay, Wheal Jane, red mud and Parys Mt. wastes.

Section 8.5: Conclusions and Key Points for Subsequent Work

8.2. Objectives

As has been established within the literature review (Section 2-4), it was possible to establish iron-reducing communities within metalliferous wastes to facilitate metal recovery. The purpose of this preliminary test was to determine whether indigenous iron-reducing communities can be stimulated to produce extensive reduction of iron with the addition of an abundant source of organic carbon. This phase of experimentation consisted of two sets of column testing. The Lindsay waste was initially subjected to a more rigorous testing regime than the other wastes. The reasons for this are twofold. Firstly, it is the only waste that exhibits any pre-existing visual indications of iron reduction whilst in-situ, in the form of subsurface olive-green discolouration of the waste (Figure 6.3). Secondly, as a more consistently homogenous waste it represents a simpler system with less potential for variation compared with the other more heterogeneous wastes tested, which originate from mine sites and metallurgical operations tested.

Alongside the additional, more rigorous testing of the Lindsay mine waste system, this phase of experimentation also included a number of single column, preliminary tests. These tests aimed to assess whether DIRM communities can be stimulated within a range of other metalliferous wastes, other than the Lindsay waste, by the introduction of organic carbon.

Furthermore this experiment is designed to assess the effectiveness of an aqueous phase organic carbon source rather than the solid phase source of manure employed in the preliminary study (Appendix 1).

To summarise, the primary objectives of this stage of experimentation were:

1. To determine whether glycerol is an effective aqueous phase organic carbon source capable of stimulating DIRM communities
2. Determine whether bio-reduction of iron could be stimulated within a range of iron-rich mine wastes.
3. Determine, whether that indigenous microbial communities are responsible for any iron-reduction induced in the Lindsay waste
4. Describe any significant changes in physicochemical conditions and mineralogy as a result of the introduction of organic carbon to the waste.
5. Determine the fate of any metals mobilised by the action of stimulated microbial activity

8.3. Experimental Design, Materials and Methods

Specific details of the materials, analysis techniques and procedures stated or outlined briefly in this section can be found in Section 5.2.

8.3.1. Materials

Ferric iron oxyhydroxide sludge used within the 1st stage of this study was sourced from a passive mine water treatment scheme at the former Lindsay coal mine treatment scheme in S. Wales (described in Section 6.2). This waste was chosen due in part to the observed colour change from an orange-brown colour to a lighter brown with a grey-

green tint, indicative of ferrous iron minerals and therefore indigenous DIRM activity. It was also chosen for its relative simplicity in chemical composition meaning fewer variables in experimentation. In total 3 columns contained Lindsay ferric iron oxyhydroxide sludge with 2 of the 3 acting as an sterile control wherein the waste had been subjected to autoclaving (as described within Section 5.4.1) and a control where the sludge was provided with only deionised water and starved of any external organic carbon source (cf. Melton *et al.* (2014)). These 3 columns are henceforth termed "Live, Autoclaved and Organic Starved".

Along with the columns containing the Lindsay sludge, a range of other wastes were subjected to preliminary testing within individual columns to ascertain which, if any, were worthy of future research focus. Individual columns were set-up with waste from Wheal Jane mine water treatment scheme (Section 6.4), Parys Mountain eastern and southern settling ponds, termed "Parys Mt. 1" and "Parys Mt. 2" respectively (Section 6.5) and one column containing red mud (Section 6.3). These wastes represented a wide range potential ferric iron –rich waste sources with differing ages, provenance, and physicochemical characteristics. For example, the Parys Mt. wastes were highly acidic with pH values ≈2.5-3, Wheal Jane were mildly alkaline (pH≈8) and red mud highly alkaline (pH≈11). Each of these columns were treated identically to the "Lindsay Live" column with a 5 mM glycerol solution provided as an organic carbon source.

All wastes used within this study were individually homogenised thoroughly, by at least 10min of continuous stirring and "folding" of the wastes within a bucket. After a 1 hour rest period excess surface water was removed, to give a natural, settled water content, followed by performing a 2nd homogenisation of a further 10min of stirring. After a further rest and removal of surface water the wastes were then ready for experimentation. Samples of each wastes were taken at this point, under aseptic conditions, for pre-experiment mineralogical, chemical and microbiological characterisation. These samples also provided a comparative reference for later results.

Glycerol, at a concentration of 5mM, was chosen as the aqueous carbon source as it has been previously utilized in previous DIRM studies at a range of concentrations from 5 mM to 25 mM (Bridge & Johnson, 1998; Bridge & Johnson, 2000; Hallberg *et al.*, 2011; Johnson, 2012; Nancucheo *et al.*, 2014), with 5 mM being the minimum concentration

found by the author within the published literature. Glycerol has also been used as an electron donor in studies of sulphate-reducing bacteria (Bertolino *et al.*, 2014), whilst metabolic products of the anaerobic oxidative degradation of glycerol, such as 1,3-Propandiol (Barbirato *et al.*, 1998), n-propanol, acetate and 3-Hydroxypropionate (Qatibi *et al.*, 1998), have also been identified. Acetate is known to be one of the common breakdown products of glycerol and is itself widely used as an organic carbon electron donor for DIRM (Lovley *et al.*, 1992; Lonergan *et al.*, 1996). Furthermore, glycerol is a relatively cheap and abundant organic carbon source as it is a by-product of the biodiesel industry. With the projected increase in demand for biodiesel there is expected to be an excess of glycerol produced leading to a decrease in price (Bertolino *et al.*, 2014).

8.3.2. Experimental Design

A photograph of the experimental setup is shown in Figure 8.1. Columns were constructed of 1L HDPE bottles fitted with an inlet/outlet valve at either end. Each bottle was washed 3 times with deionised water and autoclaved before use to prevent chemical or biological contamination of the experiment. Columns were filled with the relevant waste with washed and autoclaved instruments to further prevent outside or cross-contamination between columns. Filling of columns with waste was performed with periodic vibration, by a repurposed sieve shaker, to ensure even packing and to minimise the potential for trapped air pockets while making every effort to not cause granular convection (also termed the “Brazil nut effect”), where larger particles will migrate to the surface. Precise masses of wet waste placed within the columns were recorded and samples taken for water content determination, which allowed a calculation of dry mass of sludge within each column. An initial flow rate of approximately 0.4 ml/min was used which with an estimated porosity of 30%, produced a residence time of approximately 12.5 hours. The dry masses of waste in each column are shown in Table 8.1..

Table 8.1 Dry mass of waste within each column at the start of experimentation

Waste	Dry Mass in Column (kg)
Wheal Jane	0.257
Parys Mt.1	0.693
Parys Mt.2	0.932
Lindsay	0.281
Lindsay Autoclaved	0.313
Lindsay Organic Starved	0.257
Red Mud	0.257

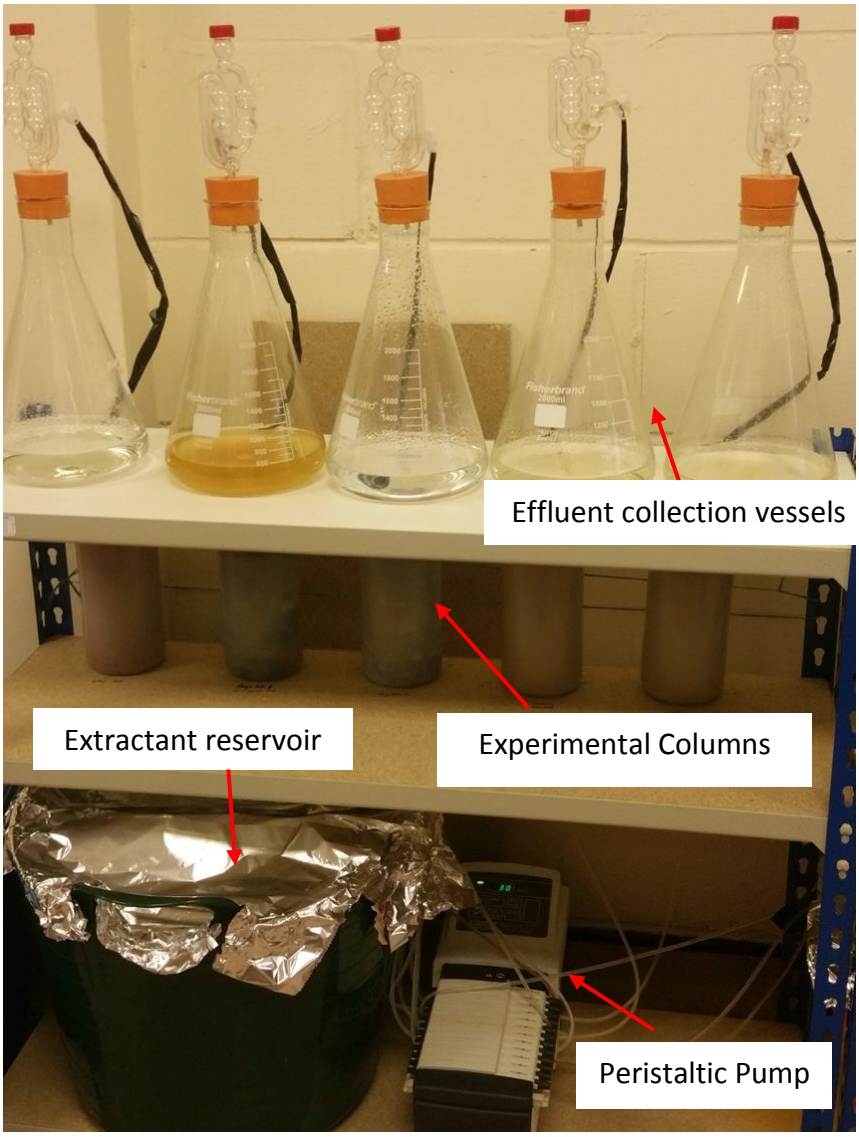

Figure 8.1 Photograph of phase one testing column experiments. Tin foil is placed over extractant reservoir to prevent foreign objects contaminating extractant.

The flow of extractant was generated by using a Watson Marlow 205U peristaltic pump with 12 channel cassette attachment. Flow rate was initially set at approximately 0.4 ml/min, though slight variations in flow rate existed due to varying permeability of the wastes tested. The columns were placed at a greater elevation to the extractant reservoirs and peristaltic pump, and the sample collection vessel was placed at a higher elevation to the columns. The collection vessel consisted of a 2L Erlenmeyer flask fitted with a 2-hole rubber bung. One hole was used for the effluent inflow tube from the column whilst the other was fitted with a brewer's airlock "bubbler" valve. This allowed the release of any pressure, above 1atm, within the flask without allowing external air into the flask (Figure 8.2). Before each use the flask was purged with nitrogen which, in conjunction with the brewer's valve, gave an environment with less oxygen for effluent to collect in, thereby minimising the oxidation of ferrous iron. This allowed more accurate readings to be taken. When observable iron oxyhydroxides precipitated at the base of the vessels, and at the end of experimentation, each flask was washed with 37% hydrochloric acid to recover any precipitated metals from the flasks. The masses of these metals were calculated from subsequent ICP-OES measurements and added to masses recovered via effluent to generate accurate extraction data.

Figure 8.2 Brewers airlock "bubbler" valve setup which facilitated sample collection within an environment with restricted air ingress

8.3.3. Sampling and Analytical Methods

Specific details of the analysis techniques and procedures outlined briefly in this section can be found in Section 5.3.

Columns were operated for 75 days in total. Effluent samples were collected, initially, on a daily basis before reducing to every other day sampling (excluding weekends). Samples were obtained and shaken (without exposure to atmosphere) to re-suspend any precipitated solids before measurements for pH, EC and ORP were recorded. This sampling technique resulted in measurements representing average conditions over the period between a measurement time and the preceding measurement time. Colourimetry analysis was performed daily to measure the concentration of ferrous iron within the sample and total iron separately. Ferrous iron measurements were taken as soon as the effluent was exposed to the atmosphere to mitigate against oxidation of the ferrous iron, due to exposure to the atmosphere, skewing results. Samples were also subjected to ICP-OES analysis to validate the iron concentration data obtained by colourimetry and measure the concentrations of other elements within the sample. The elements analysed for by ICP-OES were; iron, zinc, lead, aluminium, copper, arsenic and nickel. These elements were chosen based on their abundance indicated during earlier geochemical characterisation of the wastes.

Measurements of DO and alkalinity were taken more infrequently. Approximately once every 5 days for a DO measurement and one every 7 days for a measurement of alkalinity. When DO measurements were required, this was performed immediately after the exposure of extractant to the atmosphere to minimise the effect of atmospheric exposure. Effluent samples taken from the “Lindsay live” column, along with samples of input water were analysed for glycerol concentration to ascertain whether all the glycerol was utilized within the system. At the cessation of column experiments, samples were removed for chemical and microbial analysis.

Post-experiment samples were obtained by removing the waste from the column and homogenising before sub-samples were taken, under aseptic conditions. Pre- and post-experiment samples of each waste were subjected to total digest, XRD and sequential extraction analysis. The fractions targeted by the sequential extraction were; carbonate associated iron (Fe_{carb}); easily reducible oxides (Fe_{ox1}) e.g. ferrihydrite; reducible oxides

(Fe_{ox2}) e.g. goethite and haematite; magnetite (Fe_{mag}); and residual fractions (Fe_{res}) following (Poulton & Canfield, 2005). Microbiological analysis was performed, under aseptic conditions, on both pre- and post-experiment samples from the Lindsay columns only. Analysis comprised DNA extraction, quantification of mass with a "Qubit assay kit" and qPCR analysis. A fluorometric glycerol assay was performed on the input extractant and Lindsay "Live" samples only to quantify glycerol uptake rates.

8.4. Results and Discussion

8.4.1. Lindsay Waste Experimentation

8.4.1.1. Physicochemical Parameters of Column Effluents

As displayed in Figure 8.3 the first two weeks of experiment total iron concentrations from all columns was negligible. The negligible concentrations of iron within the samples at this stage, indicates that any subsequent increase in iron concentrations is likely the result of iron reduction, solubilisation and export of iron from the column initially as soluble ferrous iron (Fe(II)), with later oxidation and precipitation to ferric iron minerals. The entrainment of particulate ferric iron in the effluent flow is unlikely given the very low flow rate of the extractant and no visible ferric particles observed in the effluent from the column.

After 14 days the "Live" column (with glycerol) showed increasing concentrations of total iron within the effluents. This increase in iron concentration was rapid with concentrations increasing from 0.31 mg/l to 82.8 mg/l within the space of 10 days. This rapid increase, following an initial period of inactivity, is typical of microbial growth. From this time until the cessation of the experiment, total iron concentrations within the effluent followed a general trend of slowly increasing concentration, though there are periods of short term decrease or stagnation of iron concentration within the overall trend. The peak total iron concentration from ICP analysis was recorded at 206.4 mg/l on day 54 of experimentation. This represents an 8 fold increase in peak iron generation compared to a preliminary study performed with the Lindsay waste, where manure was used as a solid phase organic source (Appendix 1). By the end of the experiment after 75 days 4.8% of iron initially in the column had been extracted from the column. Ferrous

iron concentrations show a similar pattern to the total iron concentrations, with an initial rapid growth followed by a period of gradually increasing concentrations to the cessation of experimentation. Ferrous iron concentrations are, however, noticeably lower than total iron. Peak ferrous iron concentration within the "Live" column effluent was 80.5 mg/L measured on day 61 of experimentation, 7 days after peak total iron was measured (Figure 8.4). Lower ferrous iron concentrations within the effluent are likely a result of oxidation of ferrous iron by residual oxygen within the collection vessel which is also promoted by the autocatalytic effect of iron oxyhydroxides within the vessel (Lottermoser, 2007).

The critical Eh for ferric iron reduction is between 300 mV and 100 mV at pH 6 to 7 (Gotoh & Patrick, 1974), though has been reported as low as -100 and -240 mV at pH of 7-8 (Stumm & Morgan, 1996). As can be seen in Figure 8.5, the initial sharp increase in iron generation coincides with a rapid decrease in the Eh of the system (corrected to standard hydrogen electrode) to within, and even beyond, this window for ferric iron reduction. The rapid decrease in ORP is likely due to the onset of iron reduction (Stumm & Morgan, 1996). From this point the ORP remains relatively constant at approximately -170±20 mV, well within the critical limits suggested by Stumm & Morgan (1996). While a decrease in ORP is expected for microbial reduction of iron, a decreasing pH is not. Reduction of ferric oxides is known to cause a pH increase (Ponnamperuma, 1972). However, pH can be seen to decrease as the concentration of iron within the effluent increases (Figure 8.6). The scale of this pH decrease is minor with a shift from pH≈7.7 to ≈7.0, which may be attributable to equilibration with the extractant and the ochre within the column or to the precipitation of $Fe(OH)_3$ within the effluent collection vessel producing acid and consequently decreasing pH. Alternately, it may be a result of CO_2 production during microbial iron reduction. It should be noted that this decrease in pH was also observed in the preliminary experiment (Appendix 1). This drop in pH is also apparent within the "Autoclaved" column but not from the "Organic Starved" column. This suggest that the drop is pH is a result of either microbial activity, in contradiction to published evidence, or more likely related to the organic carbon source. Aqueous glycerol is weakly acidic and may be responsible for the pH decrease. Conductivity showed an increase coeval with the increase in iron within the effluent, this could be due to the increase in dissolved metal concentrations, as a result of microbial activity or

a combination of this and the weakly acidic glycerol solution (Krishnamurti & Kate, 1951). After 30 days the EC began to decrease steadily, despite increasing iron concentrations, before stabilising at ≈600 µS/cm. This represents a net 200 µS/cm decrease in conductivity over the duration of the experiment. DO within the effluent initially dropped rapidly, likely a result of the expulsion of remnant air pockets within the column, before a slower decrease in DO from ~3 mg/L to 1 mg/L eventually stabilising at <1 mg/L by the end of experimentation (Appendix 2). Given the necessary exposure of effluents to the atmosphere in order to conduct DO analysis, it is likely that the vast majority of the small dissolved oxygen measured is a result of atmospheric contamination, or inefficiencies in the anoxic collection vessel system, skewing results. Alkalinity remained relatively constant throughout the experiment at between 217-294 mg/l $CaCO_3$ equivalent. This was unexpected given that dissimilatory iron reduction is known to be alkalinity producing (Appendix 2).

The “Autoclaved” Lindsay sample showed no significant iron generation for 42 days of experimentation, which contrasts sharply with the “Live” column where iron in the effluent was detected after 14 days. Once iron was detected in the effluent after 36 days concentrations displayed a steady increase from 1.8 mg/L to a peak of 145.7 mg/L after 71 days from the start of experimentation. The onset of iron reduction was again marked by a drop of ORP to within the -100 mV to -240 mV window for reduction. The initial low iron concentrations <0.5 mg/L at the start of the column experiments clearly demonstrates that 5 mM of glycerol does not have a solubilising effect on the ochre sludge without the additional action of DIRM. As in the “Live” column, the ferrous iron concentrations within the “Autoclaved” column effluents displays a similar pattern to the total iron concentrations, albeit with lower concentrations. Ferrous iron concentrations begin to show an increase at approximately day 40 before rapidly increasing for the remainder of the experiment. Peak ferrous iron was recorded on day 75 of experimentation at a concentration of 46.5 mg/l.

The eventual generation of iron from the “Autoclaved” sample can be attributed to residual microbes in the waste eventually proliferating to great enough numbers to cause significant iron release from the column. These microbes may have survived the autoclaving procedure due to their ability to form bacterial spores (Breitenstein *et al.*, 2002; Burkhardt *et al.*, 2011; O'Sullivan *et al.*, 2015). This is discussed in more detail in

Section 9.4.3. Conductivity measurements showed an unexplained rapid increase to a peak of 930.2 µS/cm despite no notable increase in concentration of iron, or any of the other analysed metals, within the effluent. The result of increasing concentrations of ions, not analysed for during this study, potentially released as a result of the autoclaving process. Beyond peak conductivity EC steadily decreased though was highly variable. A slight but constant increase in EC was observed at the late onset of iron bio-reduction within the sample. Again, this is likely due to the microbial activity and/or the increasing metal content of the effluent. As with the "Live" column, the effluent pH decreased even when iron-bioreduction began. DO measurements decreased initially before stabilising at ~1 mg/L dissolved oxygen while alkalinity remained relatively stable ranging between 180-289 mg/l $CaCO_3$ equivalent (Appendix 2).

The "Organic Starved" column effluents yielded no significant iron extraction throughout the experiment. With a peak of 1.67 mg/L total iron, measured on day 61, representing the maximum iron concentration measured and only occurrence of total iron concentration surpassing 1 mg/L. Ferrous iron concentrations were consistently low throughout the experiment with a peak of 0.16 mg/l also recorded on day 61 of experimentation. This demonstrates that indigenous microbes alone are not capable of generating elevated iron concentrations seen in the effluent of the "Live", glycerol-fed sample. While also confirming that the total iron measured within the effluents of the "Live" and "Autoclaved" columns is a result of the oxidation of ferrous iron within the collection vessel. When compared to the "Autoclaved" control, the iron concentrations within the effluent of the "Live" column suggests that indigenous DIRM within the waste are responsible for the Fe(III) reduction but are only capable of doing so when supplied with the glycerol as an organic carbon source.

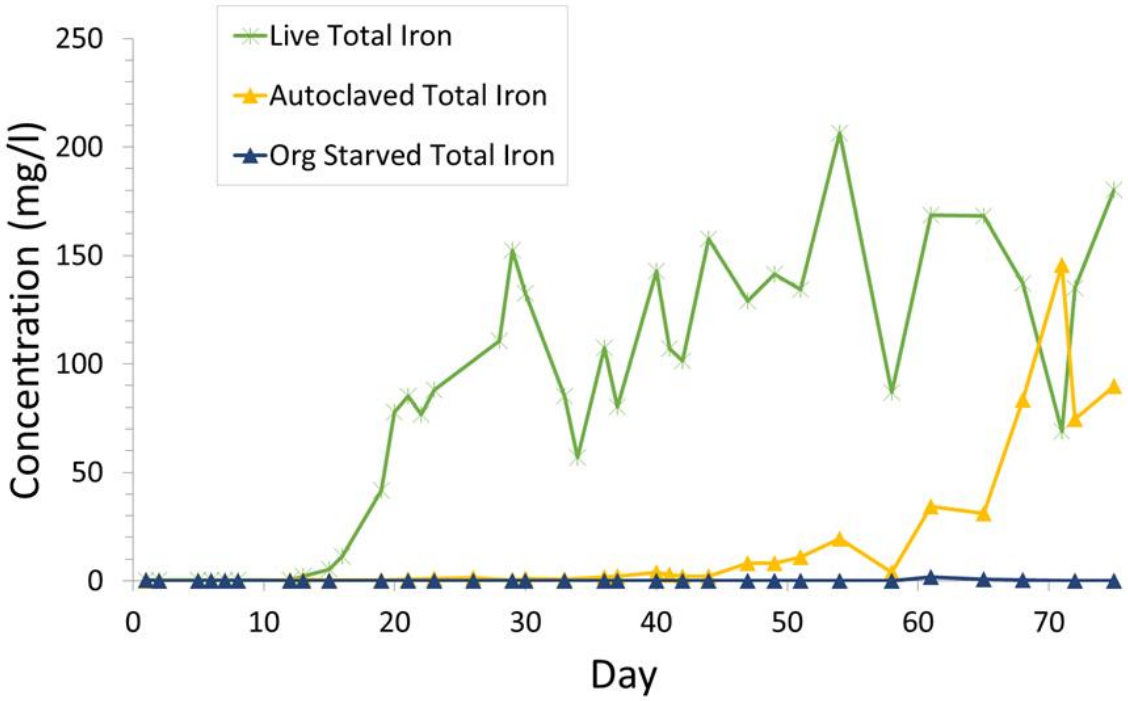

Figure 8.3 Total iron concentrations (measured with ICP-OES) within effluents throughout the duration of experimentation.

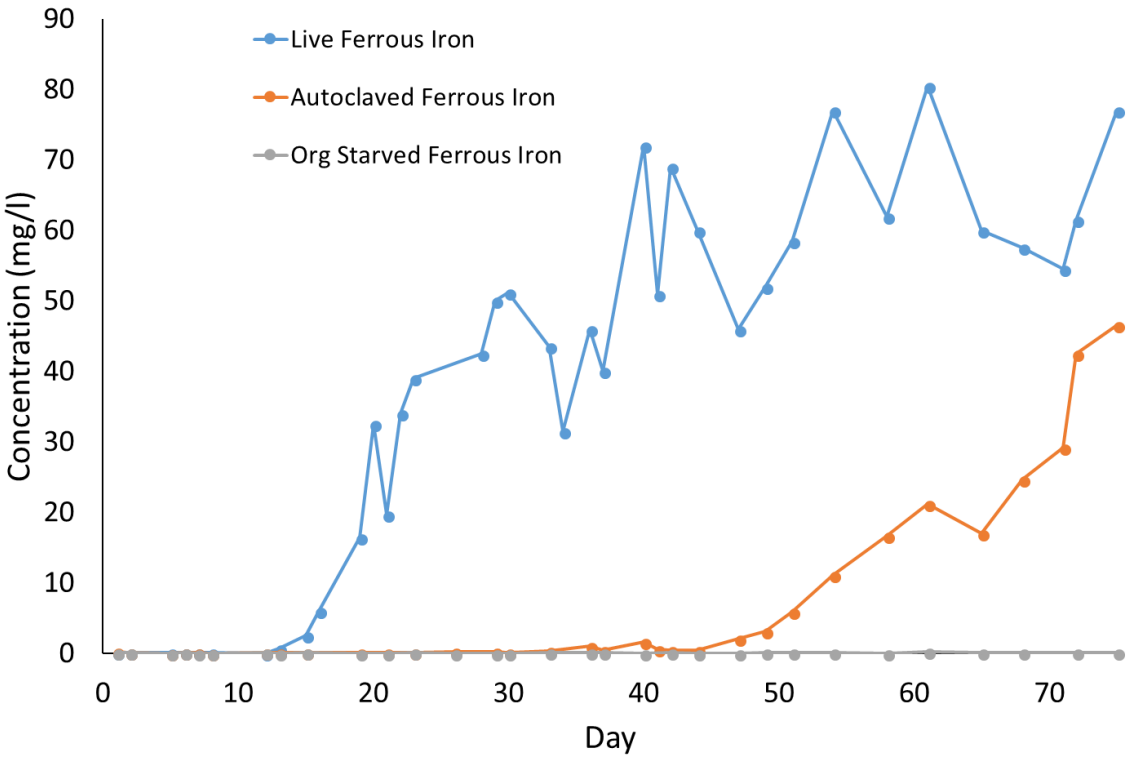

Figure 8.4 Ferrous iron concentrations within effluents throughout the duration of experimentation.

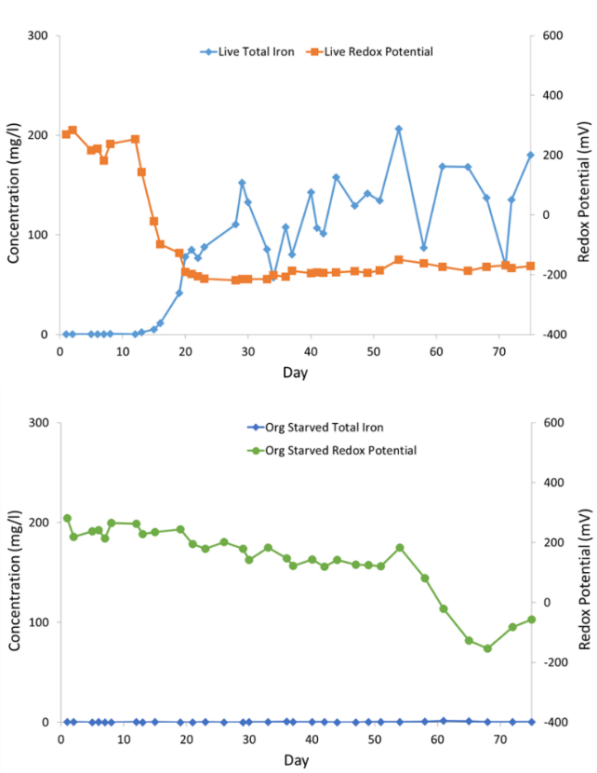

Figure 8.5 Comparisons of redox potential and total iron concentrations within effluents from Lindsay Live, Autoclaved and Organic Starved columns throughout the duration of experimentation

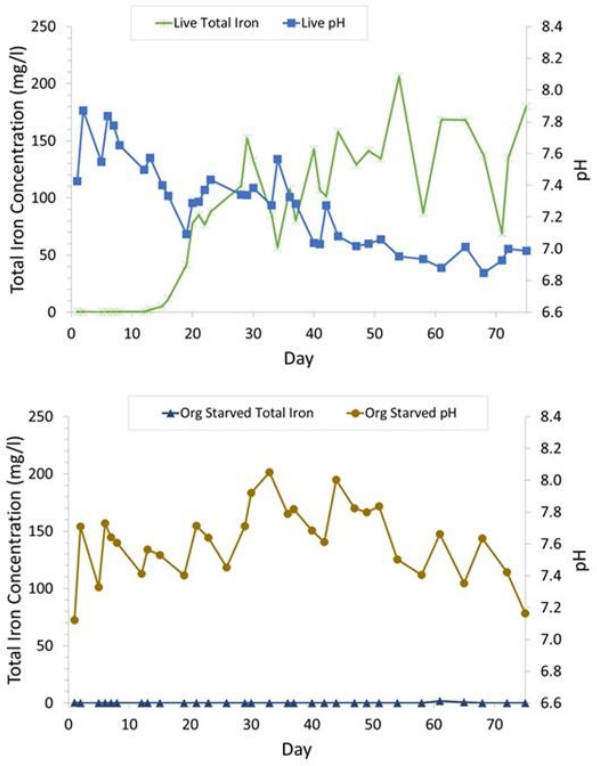

Figure 8.6 Comparisons of pH and total iron concentrations within effluents from Lindsay Live, Autoclaved and Organic Starved columns throughout the duration of experimentation

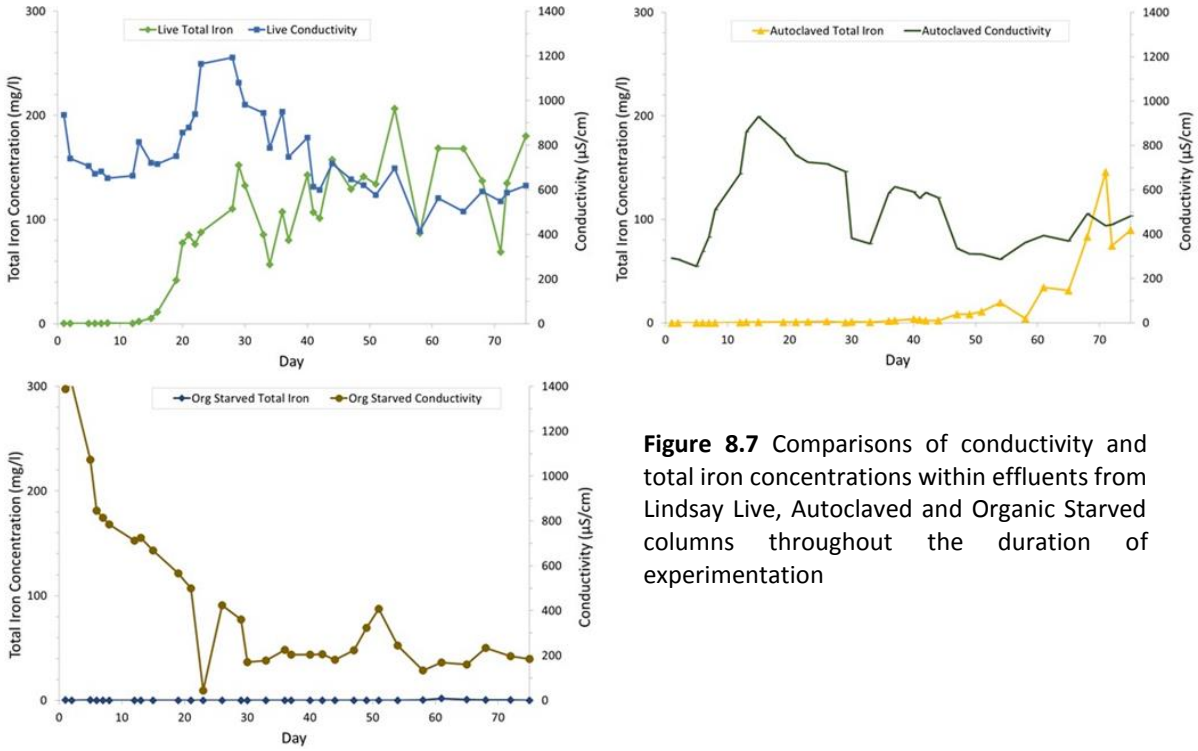

Figure 8.7 Comparisons of conductivity and total iron concentrations within effluents from Lindsay Live, Autoclaved and Organic Starved columns throughout the duration of experimentation

Figure 8.8 displays the theoretical maximum solubility of ferrous iron (present as $Fe(OH)_2$) as a function of pH at each given sampling point. This value was calculated using a solubility product constant (K_{sp}) value of 8 X 10^{-16} as suggested by Stumm & Lee (1961) and Langmuir (1997). When this is compared with the measured concentration of total iron. It is notable that at no point during the experiment do total iron concentrations approach the point at which saturation is reached. The highest recorded pH was 7.87 on day 2 of the experiment. This gives a maximum ferrous iron solubility of ~81 g/l. Peak total iron was recorded at 206.4 mg/l on day 54 of experimentation. This is far lower than peak solubility at the highest pH recorded, despite being recorded while pH was lower thereby increasing solubility. This suggests that chemical equilibrium is not a limiting factor on the concentration of iron within the effluents and the concentration of iron within the effluent is a reflection of the iron mobilised via microbially mediated reductive dissolution of iron.

The maximum solubility of ferric iron as $Fe(OH)_3$ (at the lowest recorded pH), assuming K_{sp} $=1.58 \times 10^{-39}$ suggested by Langmuir (1997), was 3.51×10^{-13} mg/l. This is a near negligible solubility, which, in conjunction with the low effluent iron concentrations at early stages of the experiment precluding the impact of suspended solids, supports the assertion that all iron within the effluent has been mobilised from the column in the form of ferrous iron, most likely produced by microbially mediated reductive dissolution of iron-bearing minerals.

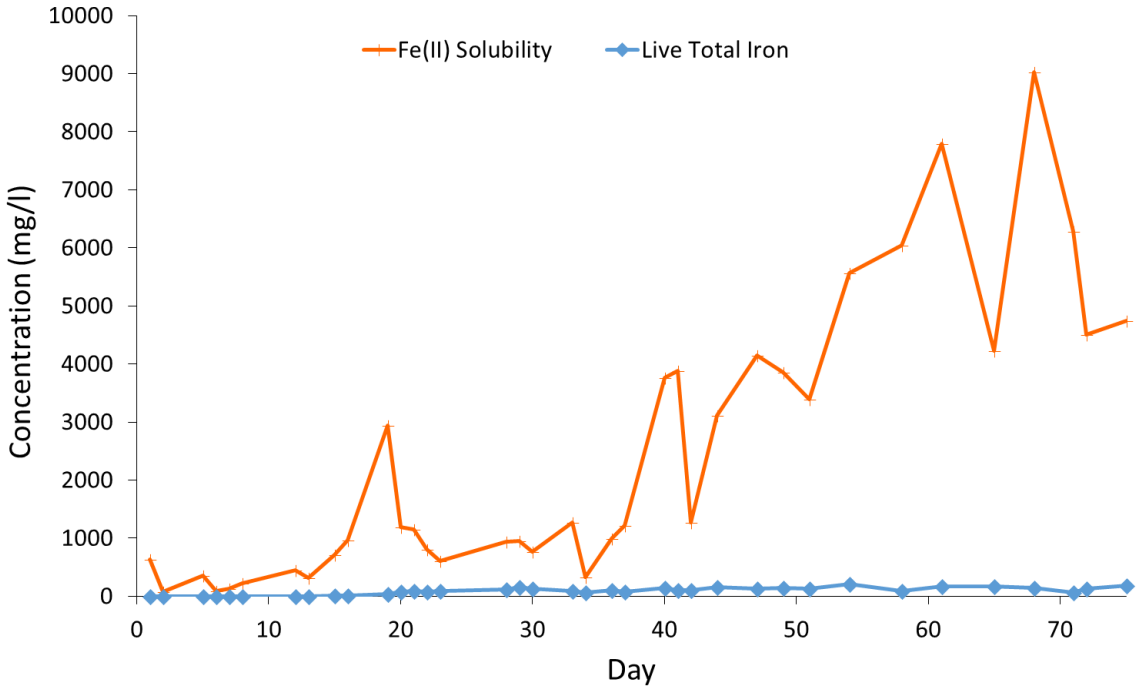

Figure 8.8 Comparison of ferrous iron solubility and effluent total iron concentrations from the Lindsay "Live" column throughout the experiment

Figure 8.9 displays the concentration of glycerol within both the input extractant, fed to the "Live" and "Autoclaved" columns, and the effluent from the "Live" column. Input extractant consistently shows glycerol concentrations of ~4.5mM, though all readings are within 1 standard deviation from the 5 mM target. The slightly lower than expected concentration may be due to variations or error in the assay. Alternatively this could be due to degradation of glycerol in the time between sampling and analysis, though this is unlikely as samples were stored at 4°C for this duration and glycerol is stable in the aqueous phase and does not decompose at room temperature (Pagliaro & Rossi, 2008). The input concentration is relatively consistent throughout, guaranteeing continual and constant supply of glycerol to the columns as opposed to a single large dose.

Concentrations within the "Live" column effluent are initially variable. The first sample analysed, taken from day 1, returned a concentration of 2.14mM. This is substantially lower than the 5 mM input extractant likely due to dilution of the extractant with residual water within the waste at the start of experimentation giving a lower than expected initial concentration. This then spiked to 6.6mM, higher than the input extractant, possibly due to build-up of glycerol within the column. From this point onwards, the glycerol concentrations show an inverse relationship to iron

concentrations within the effluents. Between days 8 and 15, glycerol concentrations drop to 0.57 mM as the rapid growth phase of microbial communities within the columns resulted in a sharp increase in effluent iron concentrations. From this point onwards, glycerol concentrations remained below 1 mM as the iron concentrations remained high, suggesting glycerol is being oxidised by indigenous DIRM via a ferric iron reduction- organic carbon oxidation coupled mechanism.

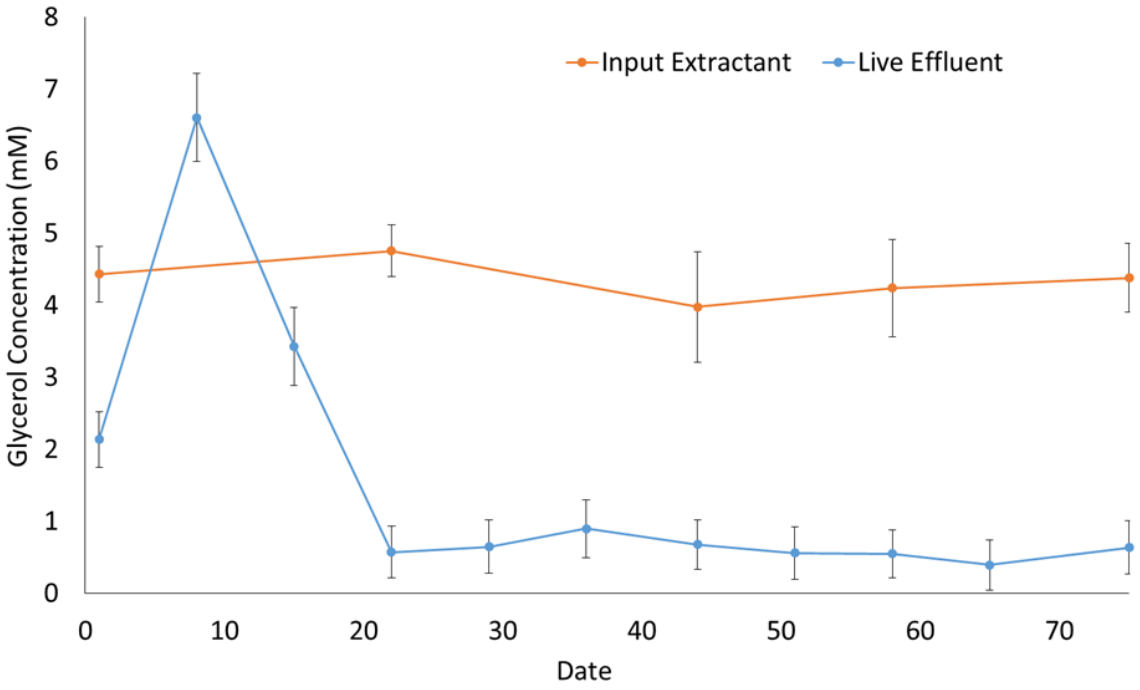

Figure 8.9 Glycerol concentrations within input extractant and effluent from Lindsay "Live" column. Error bars represent 1 standard deviation

In total, 0.017kg of glycerol was introduced to the Lindsay "Live" column over 75 days. This equates to 0.061kg glycerol per kg of dried Lindsay sludge. In December 2017 the price of 80% crude glycerine (a mixture of glycerol and water) destined for disposal was ≈£175 per metric ton. This is predicted to decline as glycerol production increases (Oleoline, 2017). Using these prices as a guide the cost of implementing this system would average less than £0.01 per kg, and therefore <£10 per tonne, of dry Lindsay sludge treated.

The other potential source of glycerol is the waste bio-glycerol generated from the biodiesel industry. Due to the increased demand for biodiesel the quantity of bioglycerol

on the market has increased at a commensurate rate, with >2 million tonnes generated in 2012. This in turn led to a dramatic fall in the price of bioglycerol. By 2010 crude bioglycerol had lost all economic value and was a waste product, while refined glycerol (99.5% kosher grade) had decreased to ~€450 per tonne having cost ~€4000 per tonne in 2000. By utilising waste crude glycerol as the organic carbon source the system negates any initial costs for organic carbon as one waste product is utilised to treat another (Ciriminna *et al.*, 2014).

If the stoichiometry of the reduction of iron with glycerol as an organic carbon source, as presented in Equation 2.1 (Page.12), is considered then an approximate efficiency for the use of glycerol can be calculated. There was 102.7g of iron (in all forms) within the "Live" column before any bioreduction occurred. Sequential extraction analysis showed that of this quantity only 64.4g (62.7%) was found to be associated with mineral phases expected to be susceptible to bioreduction (Figure 8.11). A total of 11.8g (0.12mol) of the glycerol introduced to the column was either retained in the column or utilised for bioreduction. Under an ideal stoichiometry this would enable 99.8g of iron to be reduced, more than is contained within the "target phases". However, a total of 4.9g of iron was recovered from "Live" column as a result of experimentation. This represents only 4.9% of the iron that is theoretically recoverable by the addition of 11.8g of glycerol.

This does, however, represent and idealised scenario with a simplified idealised stoichiometry and assumes that 100% of the glycerol retained in the column has been utilised for iron reduction. This is unlikely to be the case, with some glycerol retained in the column potentially being sorbed to residual iron oxyhydroxides or simply not being utilised for bioreduction. There is also the potential for preferential flow paths in the column preventing glycerol from contacting all areas of the column. Any iron held within these glycerol deprived areas would have far less chance of being bioreduced, thereby lowering the overall efficiency of the column.

8.4.1.2. Visual, Chemical and Mineralogical Analysis

At the end of the experiments the columns were opened to allow the extraction of the waste, and samples taken for both mineralogical and microbiological analyses. It was

immediately apparent that the waste within the “Live” and “Autoclaved” columns had undergone a noticeable alteration as the “rusty” orange brown colour had been replaced by an “olive green” colour. When exposed to the air the green colour rapidly became paler as the iron minerals re-oxidised. No colour change or reaction to air was observed for the “Organic Starved column”. The green colour and the lack of stability when exposed to the atmosphere suggests the presence of Fe(II) minerals such as green rusts within the post-experiment waste. These minerals are metastable and are known to be precursors to magnetite and siderite formation after the bio-reduction of ferrihydrite within the pH range 6.5-7.5 (Fredrickson *et al.*, 1998; Genin *et al.*, 1998; Zachara *et al.*, 2002). The presence of these minerals within the “Live” and “Autoclaved” samples, but lack of change in the “Organic Starved” samples is a further indication of the stimulation of indigenous iron reducers by addition of glycerol.

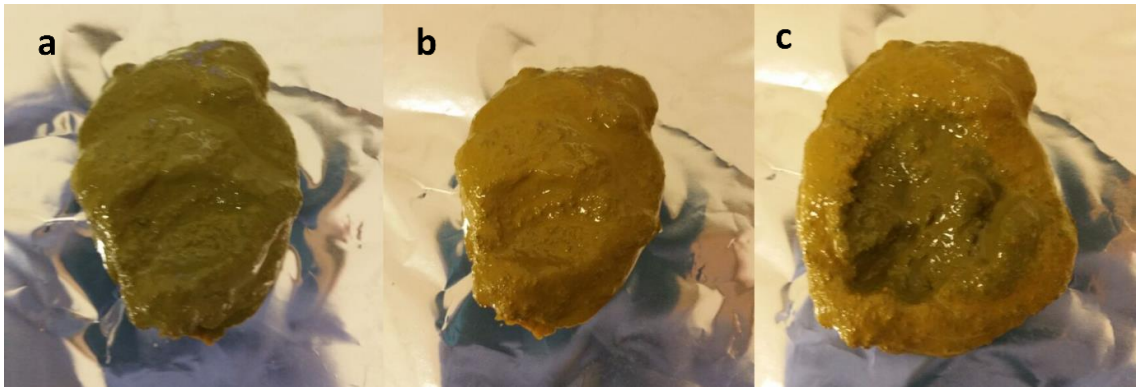

Figure 8.10 Photographs of post-experiment sample from Lindsay “Live” column. a) Waste immediately after extraction, b) Waste 30 seconds after extraction and exposure to atmosphere, c) newly exposed area of waste to demonstrate colour comparison pre- and post-oxidation.

Sequential extraction of the extracted ochres showed that during the experimentation the abundance of iron within the “easily reducible oxide” phase (representing minerals such as ferrihydrite) was diminished and while the proportion of iron within the more crystalline “reducible oxide phase” increased. This is suggestive of the transformation of ferrihydrite, or similar amorphous ferric minerals, to goethite (Figure 8.11). Within the pre-experiment ochre 23.2% of iron was present within the “easily reducible oxide” phase. By comparison only 5.0%, 2.7% and 4.3% of iron was present within this phase within the “Live”, “Autoclaved” and “Organic Starved” columns respectively at the

cessation of experimentation. The proportion of iron retained within the "reducible oxide" phase increased from 38.5% in the pre-experiment ochre to 67.4% within the "Live" column, which experienced the highest rate of ferrous iron release. XRD analysis supported the sequential extraction data with patterns indicative of more crystalline material, with peaks corresponding to goethite displaying increased counts within these post-experiment samples relative to the pre-experiment ochre (Figure 8.12). This goethite likely forms the bulk of the "reducible oxide" phase.

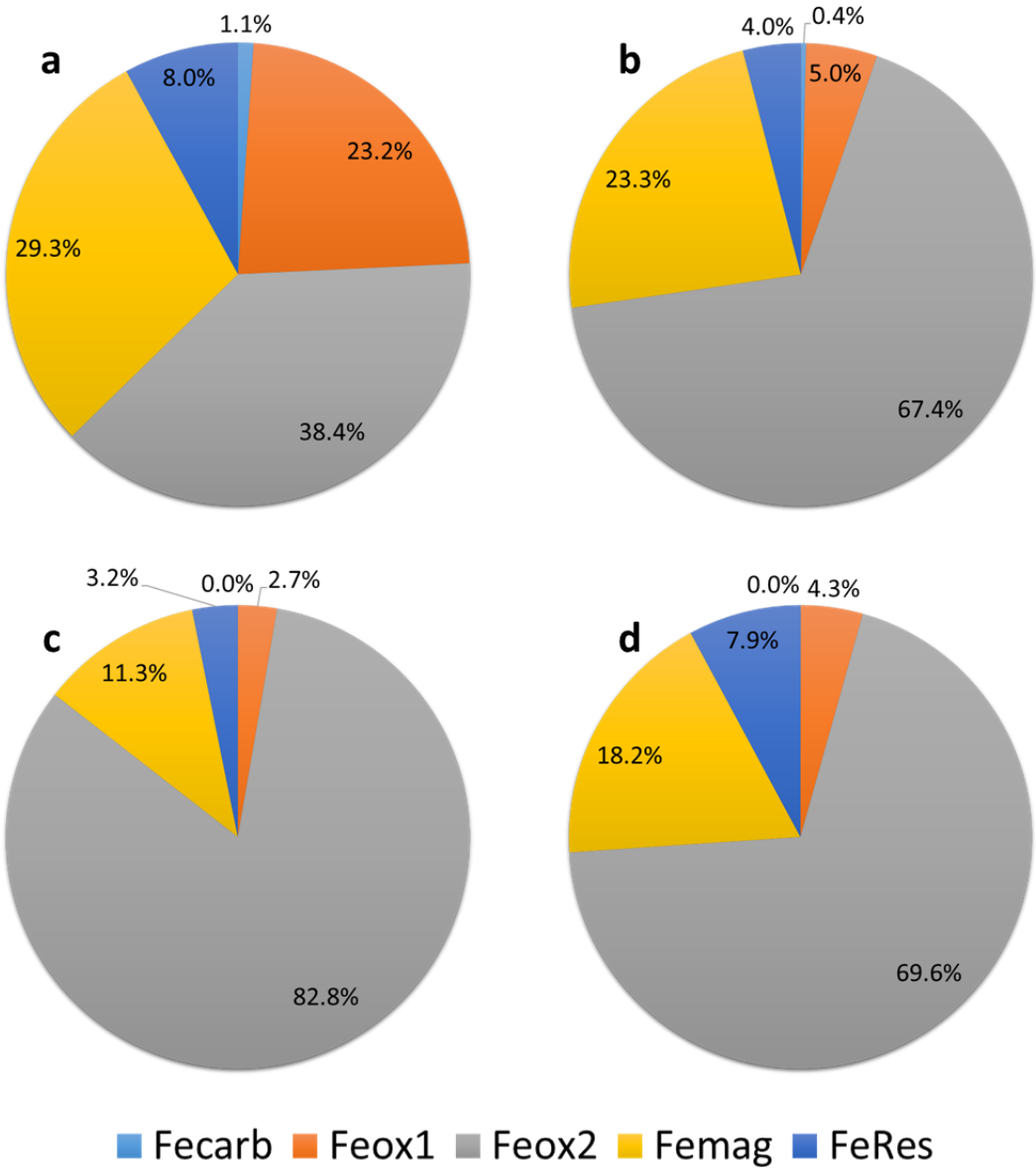

Figure 8.11 Sequential data analysis of iron distribution within Lindsay waste both pre- and post-experiment. a) Pre-experiment waste; b) Lindsay "Live" post-experiment; c) Lindsay "Autoclaved" post-experiment; d) Lindsay "Organic Starved" post-experiment.

Under circumneutral, aerobic, aqueous conditions at room temperature, ferrihydrite will gradually transform to the more crystalline and thermodynamically stable goethite (Das *et al.*, 2011). However, this process is generally a slow one and so can at most account for a small fraction of the goethite formed. The anaerobic conditions within the column further limits the potential impact of this mechanism. The limited significance of this mechanism is reflected in the lower count of goethite within the XRD analysis of the "Organic Starved" column; as despite retaining aerobic conditions in the column less goethite has formed (Appendix 2). The other potential mechanisms by which goethite may have formed from ferrihydrite are reliant on aqueous ferrous iron being present within the system. Liu *et al.* (2007) observed that the transformation of ferrihydrite to goethite (or other iron oxyhydroxides) was accelerated by the presence of Fe(II). The two columns that displayed ferrous iron generation both showed higher goethite counts in their XRD diffractograms compared with the "Organic Starved" column (Figure 8.12 & Appendix 2). An increased concentration of goethite within the samples is indicative of this mechanism and the "Autoclaved" sample has a lower count possibly due to the lower amount of Fe(II) generated for a shorter time period.

The other mechanism by which goethite may have formed is via a green-rust intermediate. Once green rust is formed by the interaction of ferric and ferrous iron it is only meta-stable and susceptible to environmental changes. If the concentration of Fe(II) in the system decreases or the green rust is exposed to aerobic conditions it rapidly decomposes to goethite (Cornell & Schwertmann, 2003), potentially explaining the increased goethite in post-experiment samples. The bioreduction of magnetite to green rust minerals, recently observed by Etique *et al.* (2016), presents another potential mechanism. However, magnetite was not identified by the pre-experiment XRD analysis (Figure 8.12) and the specific bacteria (*Shewanella putrefaciens*) used in their study was not present within this study (Section 8.4.1.3). This makes the presence of this mechanism for goethite formation highly unlikely in the Lindsay wastes.

It is likely that a combination of some these mechanisms is responsible for the increased iron present within the "reducible oxide" phase of within all columns post-experiment. With the iron within this phase probably being present in the form of goethite.

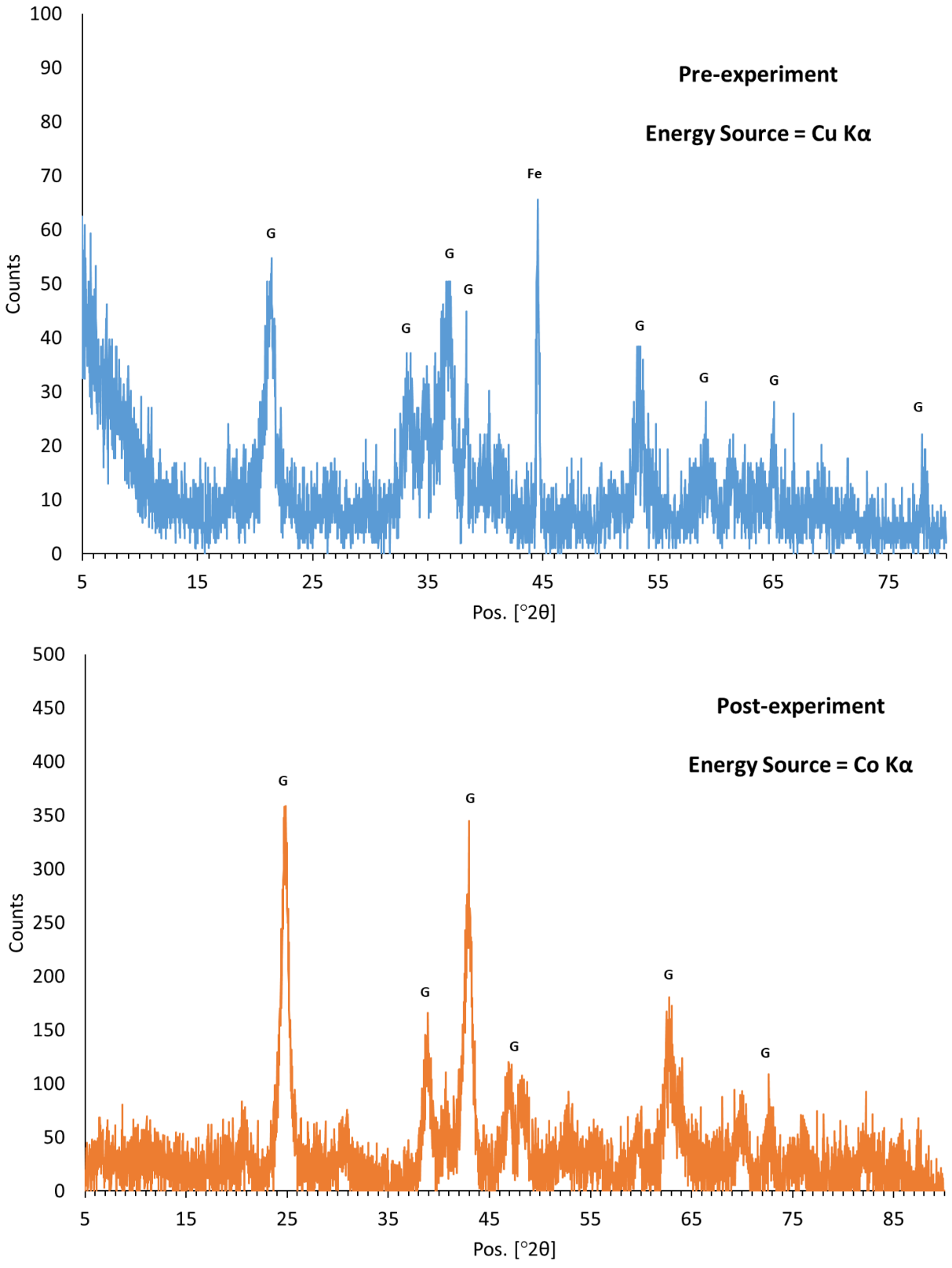

Figure 8.12 XRD diffractograms for the Lindsay ochre samples, both pre- (above) and post-experimentation (below). G = goethite

1.3.1.4. Quantitative (qPCR) analysis of microbial 16S rRNA genes

Quantitative (qPCR) analysis of the microbial population within the ochre samples showed that autoclaving of the ochre caused a reduction in the size of both bacterial and archaeal communities within the ochre (Figure 8.13). For example, bacterial 16S rRNA gene copies per gram dropped from 6.42×10^9 to 5.47×10^8. The post experimentation samples from the "Live" column (fed with glycerol) show the effect the glycerol has had on the size of the microbial communities. The glycerol fed sample showed a substantial increase in bacterial numbers with an average additional 9.71×10^9 gene copies/gram by comparison with pre-experiment ochre. Conversely, the ochre starved of organic carbon showed a distinct decline of 2.82×10^9 gene copies/gram during the same period. These results clearly show that significant Fe(III) reduction was only observed when the indigenous microbial population was present and stimulated to grow by the addition of organic carbon the system. The control (autoclaved) sample showed a recovery from the autoclaving process to 7.05×10^9 gene copies/gram, slightly above the initial concentration within the non-autoclaved sample. This corresponds with the rapid increase in Fe(II) generation late in the experimental run, potentially attributable to the re-activation of bacterial spores that have survived the autoclaving process.

Analysis of archaeal gene copies returned results two orders of magnitude lower than their bacterial equivalents. However, similar patterns to that of the bacterial population between columns were observed. Autoclaving reduced the average gene copies per gram from 4.26×10^7 to 5.77×10^6 within the pre-experiment samples. The "Live" column showed enrichment of archaeal gene copies, though not to the same degree as within the bacterial analysis, with an additional 3.03×10^7 gene copies per gram in the post experimentation sample. This further suggests that the bacteria are dominant within the system and are mainly responsible for metabolising the glycerol, thereby limiting archaeal growth. There was an increase of 2.71×10^7archaeal gene copies per gram within the "Autoclaved" column. Unlike the bacteria, this increase was not enough to return the gene copies per gram to pre-autoclaving levels. Again, this suggests that archaea were being outcompeted by the bacteria for the glycerol electron donor. Within the "Organic Starved" column there was a slight increase in archaeal gene copies per gram to 4.81×10^7.

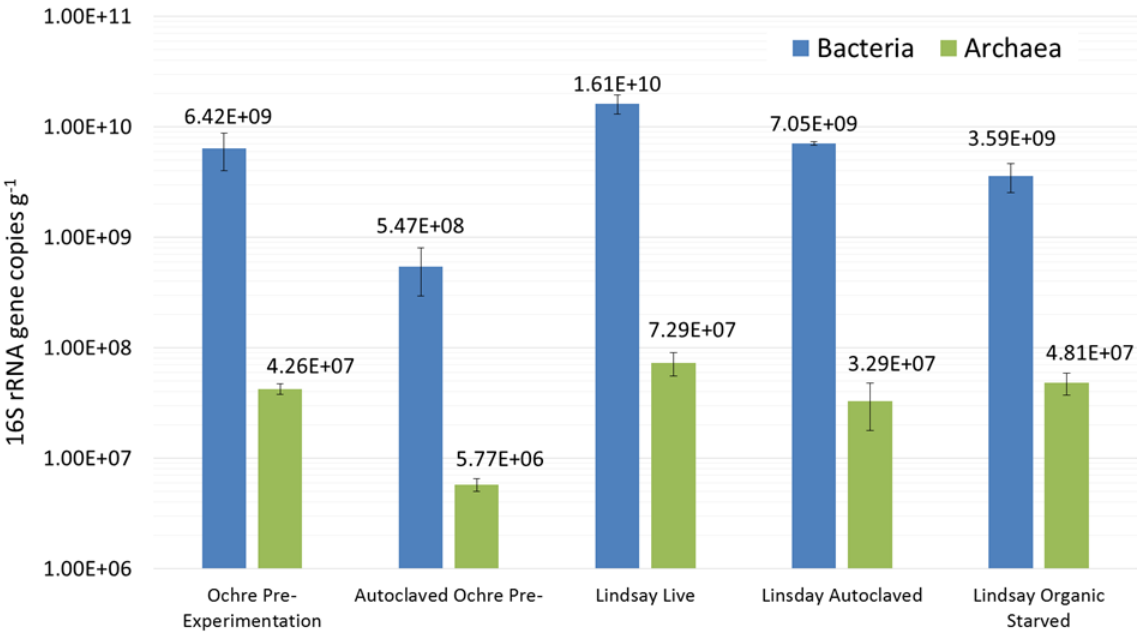

Figure 8.13 qPCR analysis of bacterial and archaeal 16S rRNA gene copies in pre-experiment samples and columns post-experiment.

8.4.1.3. Taxonomic Identification of Microbial Communities

Sequences (16S rRNA gene) generated by next generation Illumina sequencing were used to identify and characterize microbial communities within the Lindsay wastes both pre- and post-experiment. Sequences were classified from phyla to genera level and quantified by relative abundance. The relative abundance of a bacteria group was defined as the number of sequences in a group divided by the total number of sequences within a sample.

Within the pre-experiment sample OTUs were matched closest (with >97% sequence identity) to a total of 40 different phyla, consisting of 35 bacterial phyla and 5 archaeal phyla. Of these 40 only 14 were present at ≥1% relative abundance, none of which were archaea. As shown in Figure 8.14, by far the most often matched phylum within the waste is the *Proteobacteria* which comprise 59.5% of total sequences. Within this phylum the *Betaproteobacteria* are the dominant class representing 26.1% of relative abundance, followed by *Gammaproteobacteria* representing 15.5% while alpha- and *Deltaproteobacteria* comprise 8.2% and 9.3% of relative abundance respectively. Other matched phyla with lower abundances identified included *Bacteriodetes* (7.3%),

Acidobacteria (4.4%), *Spirochaetae* (3.9%), *Hydrogenedentes* (3.8%) and *Firmicutes* (2.5%).

In total 16 genera were found to have relative abundances of ≥1%. As can be seen in Figure 8.15 the genus matched to most OTUs identified in the DNA extracted from the waste is *Gallionella* (20%), reflecting the dominance of *Betaproteobacteria* previously described. *Gallionella* is a known genus containing several neutrophilic, aerobic iron-oxidising species (e.g. *Gallionella ferruginea*) and is often found present within mine drainage environments including coal mine drainage (Bearcock *et al.*, 2006; Schippers *et al.*, 2010; Hedrich *et al.*, 2011). This result is also reflective of the sampling location and conditions, at the base of passive remediation aeration cascades, where there is abundant ferrous iron of *Gallionella spp.* to utilise. The second most abundant genus identified was *Acinetobacter* (11.5%) representing the majority of sequences within the *Gammaproteobacteria* class. Species within this genus are not known to oxidise or reduce iron but have been identified previously in mine wastes (Schippers *et al.*, 2010; Wei *et al.*, 2014; Ma *et al.*, 2015). Other OTU matched genera included *Bacteriovorax* (4.1%), *Shinella* (1.5%) and *Sideroxydans* (1.9%), the latter of which is a known iron-oxidising bacteria (Hedrich *et al.*, 2011). In total 44.6% of all sequences either belonged to genera with less than 1% abundance or were not identifiable at genera level, demonstrating that the waste contains a diverse community despite the dominance of the iron-oxidising *Gallionella*.

OTUs matched closest (with >97% sequence identity) to a total of 32 different phyla in the post-experiment "Live" samples, 28 of which are bacterial phyla and 4 archaeal phyla (Figure 8.14). This represents a decrease in 7 bacterial and 1 archaeal phyla identified compared to the pre-experiment sample. Only 8 bacterial phyla were identified at ≥1% abundance, 6 fewer phyla than identified in the pre-experiment sample. The phyla declining to <1% relative abundance were Armatimonadetes, Hydrogendenetes, Ignavibacteiacae, Nitrospirae, Plantomycetes and Verrumicrobia.

The most often matched phyla identified in the post-experiment "Live" samples were the *Firmicutes* comprising 44.3% of total sequences identified. This represents a significant increase from the pre-experiment sample (2.5%). The majority of these *Firmicutes* are present as the class *Clostridia* (34.4%). The abundance of *Proteobacteria*

has decreased from the initial 59.5% to 38.2% in the post-experiment samples. Though this decline in *Proteobacteria* is more complex than simply a decline in all classes within the phyla. alpha-, beta- and gamma–*Proteobacteria* decreased from 8.2%, 26.1% and 15.5% to 2.0%, 4.2% and 4.4% respectively. Partially offsetting these decreases is an increase in the abundance of *Deltaproteobacteria* from 9.3% to 27.6%.

At genera level there have been extensive changes coinciding with bioreduction. In total OTUs matching with >97% sequence identity to 13 genera have been identified within the post-experiment "Live" samples, three fewer than the pre-experiment sample (Figure 8.15). This is a simplistic view though as 13 of the genera identified in the pre-sample at abundances of ≥1% have decreased to beneath this chosen cut-off value. This includes the genus *Gallionella* which has decreased from 20% to 0.8% relative abundance. This is reflective of the change in conditions in the waste from an aerobic to anaerobic environment, unsuited to the aerobic, iron oxidiser *Gallionella*. Of the 3 genera that were identified in both the pre- and post-experiment samples only *Anearomyxobacter* has been observed to undergo a large increase in abundance from 1.2% to 10.2%, making it the third most abundant genus identified. This is reflective of the increase in relative abundance of *Deltaproteobacteria*. Various *Anearomyxobacter spp.* have been identified that are capable of coupling the dissimilatory reduction of ferric iron to the oxidation of acetate (He & Sanford, 2003; Hori *et al.*, 2010), citrate or glucose (Treude *et al.*, 2003). Interestingly, the most abundant genus identified in the post-reduction "Live" waste is *Acetobacterium* (20.4%). Species within this genus are acetogens, capable of producing acetate via the reduction of carbon dioxide (and potentially glycerol) (Balch *et al.*, 1977), which in turn is likely utilised by the *Anearomyxobacter,* and other bacteria e.g. *Geobacter,* within the community for iron-reduction.

The second most abundant genus identified was *Geobacter* (13.3%), in the class *Deltaproteobacteria*, which was previously present at <1% in the pre-experiment samples. *Geobacter*, along with other genera in the family *Geobacteraceae*, are amongst the most intensively researched. Many species of *Geobacter* are known to be capable of oxidising organic carbon compounds, including acetate, completely to carbon dioxide, while utilising ferric iron as the sole electron acceptor (Lovley, 2013). *Geobacteraceae* are often identified in a range of oxidised mine wastes so their presence in the Lindsay

wastes is not unexpected (Kock & Schippers, 2006; Kock & Schippers, 2008; Schippers *et al.*, 2010). Other genera, known to contain species capable of iron-reduction, increased in relative abundance in the post-experiment "Live" samples. These included *Thermincola* (6.7%) (Sokolova *et al.*, 2005; Zavarzina *et al.*, 2007; Carlson *et al.*, 2012), *Pelosinus* (1.9%) (Brown *et al.*, 2012) *and* an uncultured genus within the *Veillonellaceae* family (7.8%) (Gihring *et al.*, 2011). Aside from those already discussed, a total of 29.3% of sequences belonged to genera present at <1% abundance. This represents a decrease of 15.3% of sequences belonging to these minor genera in the post-experiment sample suggesting a decrease in diversity. The Shannon and Simpson's indices also demonstrate this decrease in diversity decreasing from 7.06 and 0.96 respectively in the pre-sample to an average of 5.78 and 0.92 respectively. Richness of the samples was also observed to decrease with Chao1 values decreasing from 6478 to an average of 5370 (Table 8.2)

PCoA was used to visualise and compare the differences between the pre- and post-experiment "Live" samples. The first two coordination axis explain 81.95% of the variability in the microbial communities, while the third axis increases this to 92.98% of variability explained (Figure 8.16). The post-experiment "Live" samples are seen to cluster separately from the pre-experiment sample, supporting the substantial diversity changes between the pre- and post-experiment samples. The PCoA also shows that there are only minor differences in the communities vertically through the column, with the "upper, middle and lower" samples all being grouped together. However, Shannon, Simpson's and Choa1 indices do suggest the lower diversity and species richness in the lower part of the column compared with the other two column sections (Table 8.2).

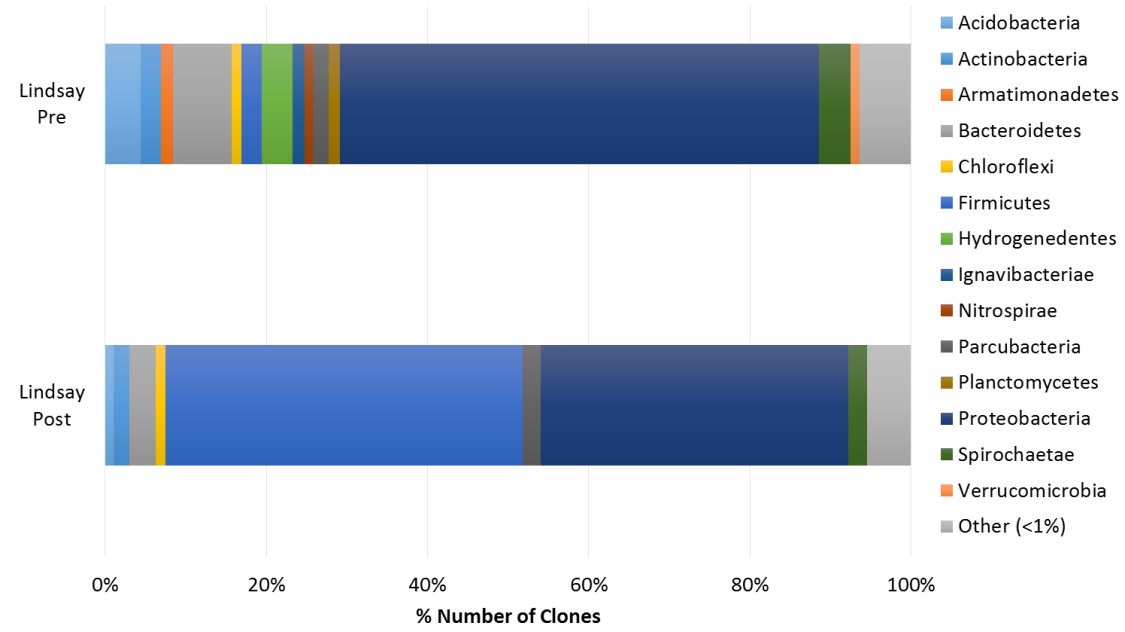

Figure 8.14 Taxonomic classification of 16S rRNA gene reads at phylum level in Lindsay pre- and post-experiment samples

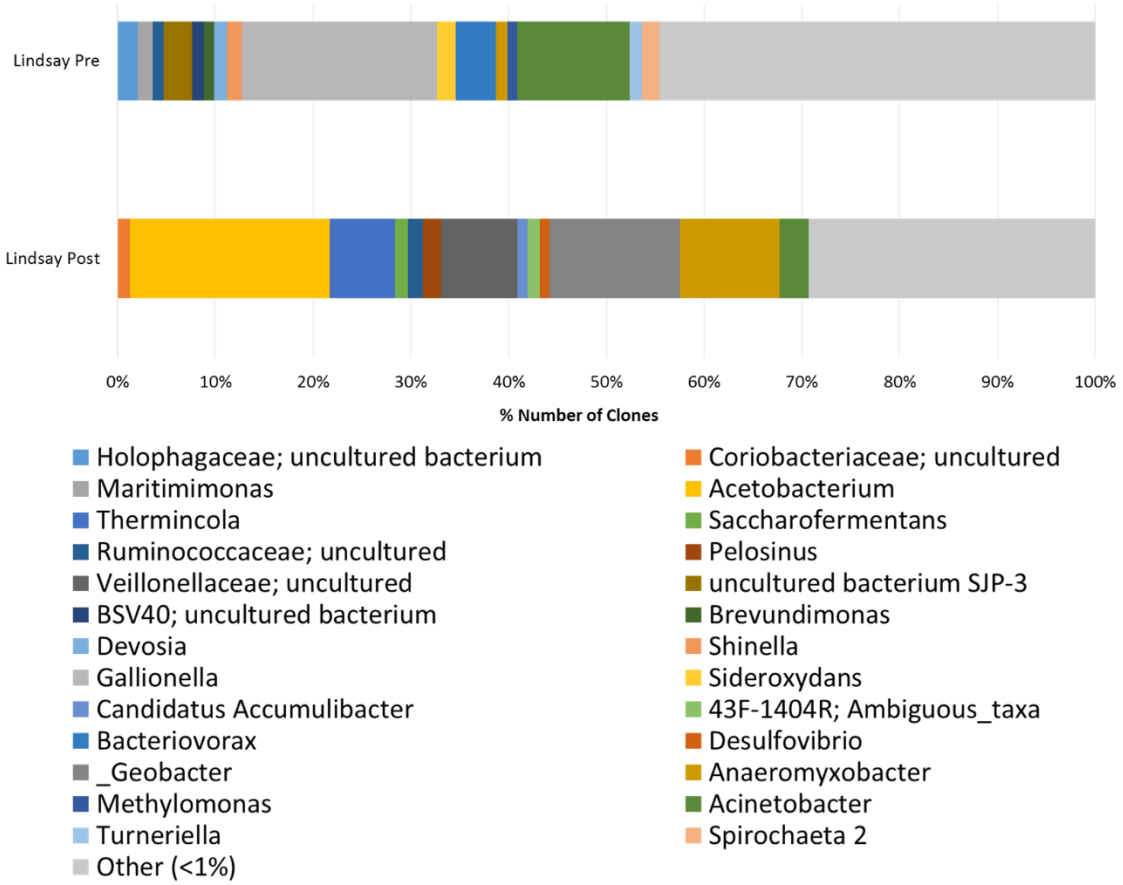

Figure 8.15 Taxonomic classification of 16S rRNA gene reads at genus level in Lindsay pre- and post-experiment samples

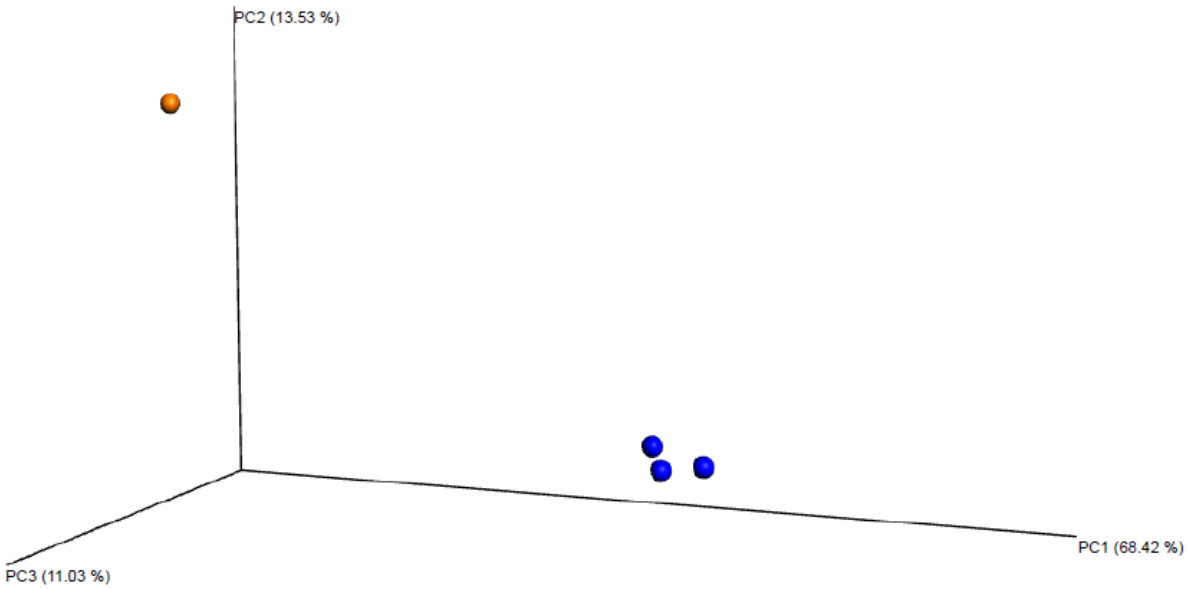

Figure 8.16 3D PCoA plot based on sequence data Lindsay "Live" experimentation. Orange= Lindsay pre-experiment, blue = Lindsay "Live" post-experiment

The post-experiment "Organic Starved" column samples, by contrast, show much less alteration of the microbial communities compared with the pre-experiment sample (Figure 8.17). In total OTUs matched with >97% sequence identity to 48 different phyla, including 8 archaeal phyla, were identified within the post-experiment "Organic Starved" samples. 14 bacterial and 1 archaeal phyla were identified at relative abundances ≥1%. Despite a decreasing abundance *Proteobacteria* (49.5%) remained the most regularly matched phylum within the post-experiment "Organic Starved" samples. Within this phylum the *Beta-* and *Gammaproteobacteria* classes both decreased from 26.1% and 15.5% to 14.7% and 11.4% respectively. *Alpha-* and *Deltaproteobacteria* both exhibited slight increases in abundance from 8.2% and 9.3% to 9.4% and 13.7% respectively. As in the "Live" samples *Gallionella* has declined (from 20.0% to 5.3% abundance) as a result of the establishment of anaerobic conditions.

Slight increases in relative abundance were observed for the bacterial phyla *Acidobacteria, Actinobacterua, Chloroflexi, Nitrospirae* and *Plantomycetes*, though none of these increases represent a significant enrichment of a phyla known to contain iron-reducing bacteria as seen in the "Live" sample, this correlates with the observed lack of iron reduction during the column tests. Sequences matching closest to the archaeal phylum *Euryarchaeotai* have also increased in abundance, an occurrence not observed

in the “Live” samples. The increases in the abundances of these phyla do not translate into increases in individual genera within these phyla. Conversely, it appears that there have been marginal increases in a wide variety of genera rather than a specific enrichment. The alpha-diversity estimates also support this observation. An average of ~5700 OTUs were observed in post-experiment “Organic Starved” samples compared with ~4450 observed in the pre-experiment equivalent. Substantially higher average values of Chao1 (8850), Shannon (8.65) and Simpson’s indices (0.987) also point to greater species richness and diversity within the post-experiment “Organic Starved” samples in contrast to the decreasing richness and diversity observed in the “Live” samples (Table 8.2). PCoA also shows a much closer association between the pre- and post-experiment “Organic Starved” samples than the “Live” equivalents, though there are still discernible differences between the pre- and post- samples (Figure 8.18).

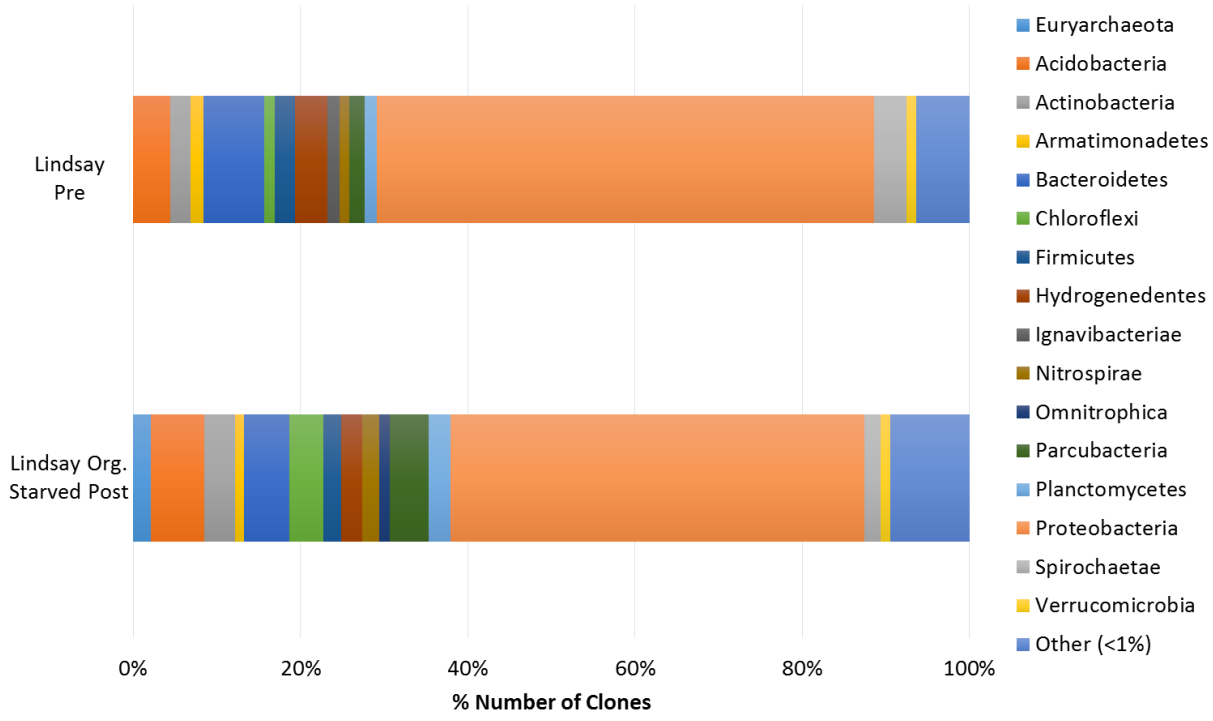

Figure 8.17 Taxonomic classification of 16S rRNA gene reads at phylum level in Lindsay “Organic Starved” pre- and post-experiment samples

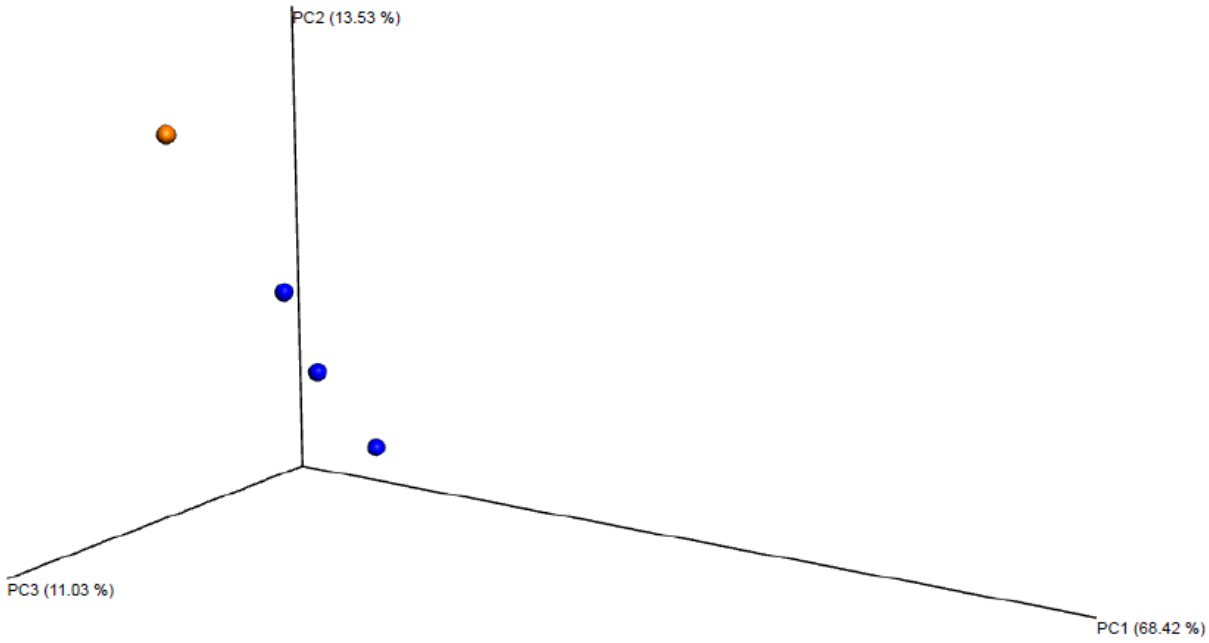

Figure 8.18 3D PCoA plot based on sequence data for Lindsay "Organic Starved" experimentation. Orange= pre-experiment, blue = post-experiment

Identified OTUs within the autoclaved pre-experiment sample matched closest (with >97% sequence identity) to 44 different phyla, 7 of which were archaeal phyla (Figure 8.19). Of the 44 phyla identified only 11 were present at ≥1% relative abundance, fewer than the non-autoclaved equivalent. *Proteobacteria* is again the dominant phylum identified with 53.4% relative abundance. The *alpha-*, *gamma-* and *Deltaproteobacteria* classes are present at 7.0%, 12.2% and 7.8% relative abundances respectively. These are lower than observed in the non-autoclaved equivalent, though *Betaproteobacteria* is present at a similar relative abundance (26.0%). Unlike the non-autoclaved pre-experiment sample, *Bacteroidetes* represents the second most often matched phylum (18.6%). In total 8.9% of sequences were identified as phyla with <1% relative abundance.

At genera level the OTUs matching closest to *Proteobacteria* are again largely matching closest to *Gallionella* (20.0%) and *Acinetobacter* (9.1%). Other *Proteobacteria* genera identified include *Devosia* (1.2%), *Shinella* (1.1%), *Methylophilus* (1.2%), *Sideroxydans* (1.9%) and *Bacteriovorax* (4.3%). The majority of the sequences belonging to the *Bacteroidetes* are present as *Maritimimonas* (13.6%), which have been previously identified in water from coal mines in the USA (Zhang *et al.*, 2015a; Park & Liang, 2016).

A large fraction (42.8%) of sequences identified belonged to genera with <1% relative abundance (Figure 8.20).

As with the "Live" samples there have been substantial changes in the dominant phyla in the post-experiment "Autoclaved" waste (Figure 8.19). Only 4 phyla are identifiable at relative abundances of ≥1%. The abundance *Proteobacteria* is seen to decline drastically from the initial 53.4% to just 15.7%, largely driven by the decrease in *Betaproteobacteria* from 26.0% to 3.0% of total abundance. *Bacteroidetes* is also observed decreasing to just 4.8% of total abundance. Only 2.9% of identified sequences are attributable to phyla present at <1% abundance suggesting a sharp decline in diversity. The decrease in sequences matching this phyla are countered by increases in sequences matching closest to *Firmicutes* and *Acidobacteria* both of which have increased from 3.7% and 2.0% abundances to 53.8% and 22.8% respectively. An increase in the abundance of *Firmucutes* was also observed in the equivalent "Live" samples, though the increase in *Acidobacteria* is the opposite of what was observed in the "Live" samples, where *Acidobacteria* was seen to decrease as a result of the introduction of glycerol.

At genera level the *Firmicute* matched OTUs are present predominantly as 4 genera all known to have species capable of iron-reduction; *Thermincola* (24.1%), *Pelosinus* (10.4%), *Desulfosporosinus* (5.4%) and uncultured genera in the family *Veillonellaceae* (7.7%) (Figure 8.20). *Thermincola* (Lusk et al., 2015), *Desulfosporosinus* (Spring & Rosenzweig, 2006), *Pelosinus* (De Leon et al., 2015) and the *Veillonellaceae* family (Yutin & Galperin, 2013) are known to have species capable of sporulation, explaining their ability to survive autoclaving. Within the *Proteobacteria* phylum, *Gallionella* was seen to decrease from 22.1% to 1.8% as a result of the change from aerobic to anaerobic conditions within the waste. *Geobacter*, an anaerobic iron-reducer, has proliferated and increased its abundance from 0.5% to 7.7%. As with the phyla, a far smaller quantity of sequences (15.9%) are associated with genera present at <1%, again suggesting a decline in species diversity in the waste.

As can be seen in Table 8.2, autoclaving the Lindsay waste has resulted in a substantial decrease in the Chao1 index estimate for species richness; from ~6240 to ~4700 in the non-autoclaved and autoclaved pre-experiment samples respectively. This indicates a

loss of a number of species as a result of the autoclaving which is also reflected in the decrease in number of observed OTU's from ~4450 to ~3650. Shannon and Simpson's indices, 6.87 and 0.94 respectively, have also decreased as result of autoclaving the waste describing a decreasing species diversity. The introduction of glycerol as an organic carbon source has resulted in further decreases in Chao1, Shannon and Simpson's indices to averages of ~3550, 4.73 and 0.89 respectively reflecting the observed decrease in species richness and diversity seen during taxonomic identification. Again, observed OTUs decreased, from an initial ~3650 to an average of ~2140. It is noticeable, though, that the sample taken to represent the middle portion of the column has returned Chao1 and Shannon index values much higher than the upper and lower post-experiment samples. The Chao1 value (~5280) is higher even than the pre-experiment value suggesting an increase in richness and therefore an increase in the number of identified species, though the observed OTUs is lower at ~2975. This result appears to be an outlier, potentially caused by contamination of the sample or simply natural variation of the sample, as it is unlikely that new bacterial species were introduced to the waste during experimentation. Visualisation with PCoA shows the distinct differences between the pre-experiment "Auto" waste and the post-experiment "Auto" samples. Within the PCoA it is again noticeable that, while substantially different from the pre- sample, the post-experiment "middle" sample is plotted apart from the "upper" and "lower" samples. This could be an outlier.

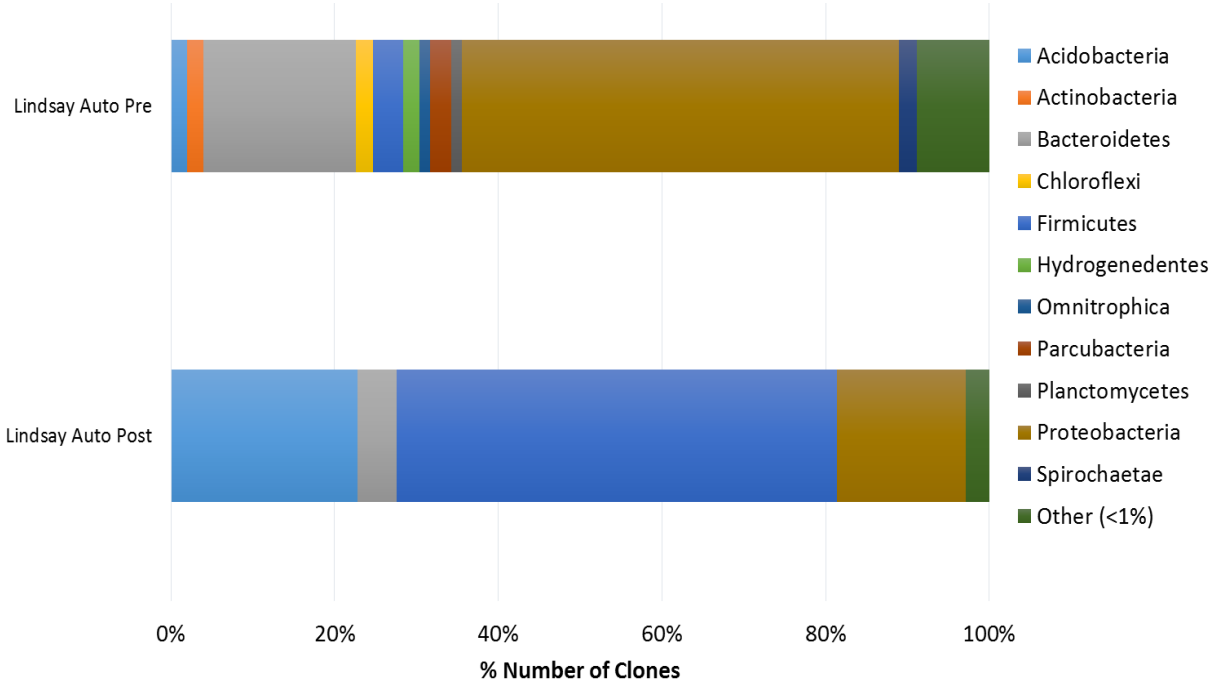

Figure 8.19 Taxonomic classification of 16S rRNA gene reads at phylum level in Lindsay "Auto" pre- and post-experiment samples

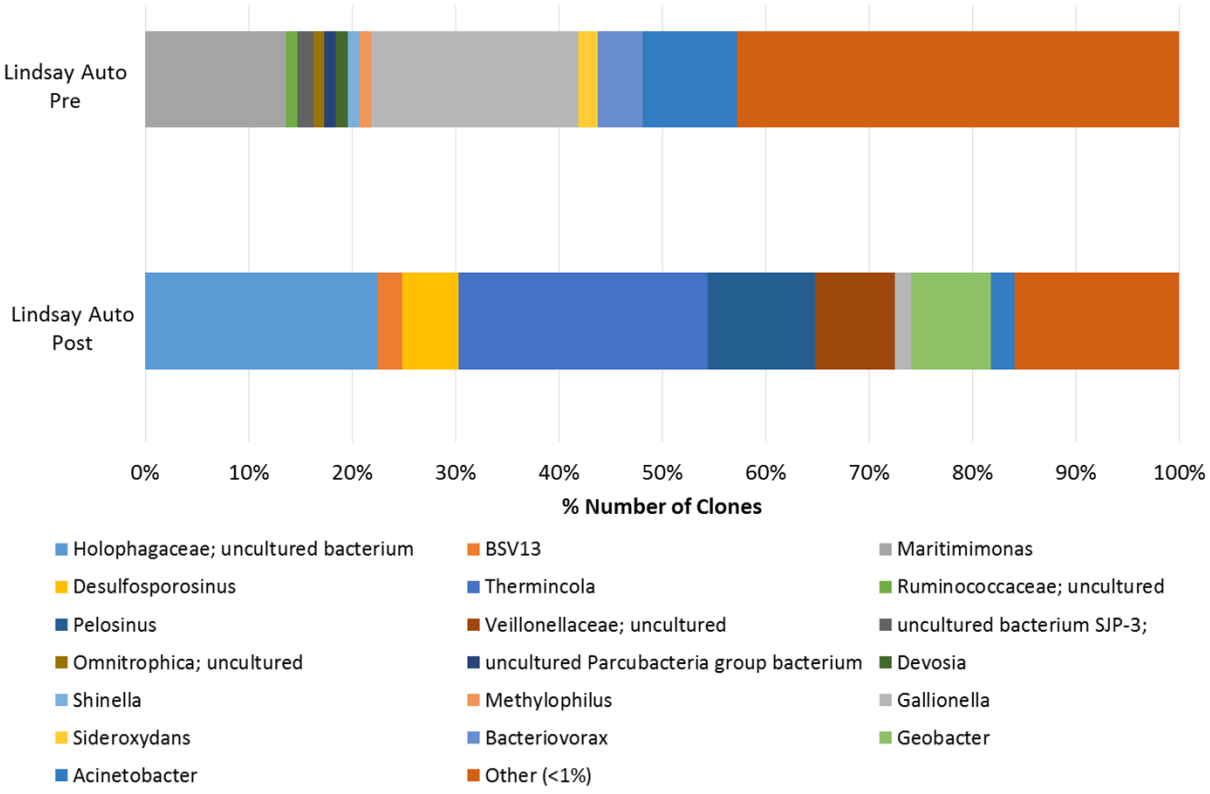

Figure 8.20 Taxonomic classification of 16S rRNA gene reads at genus level in Lindsay "Auto" pre- and post-experiment samples

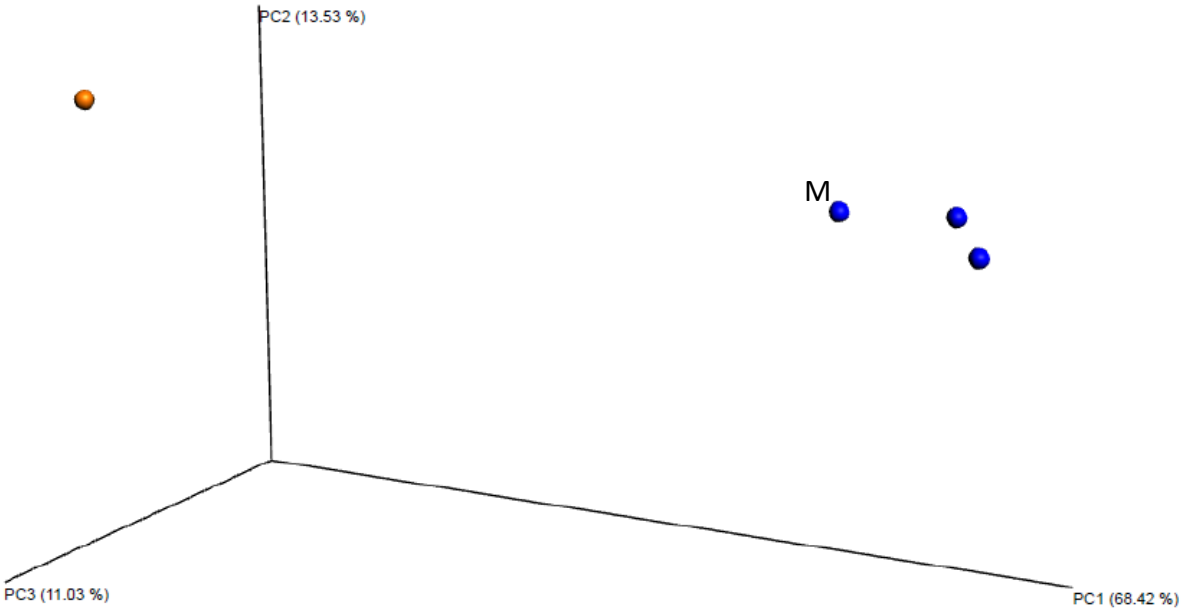

Figure 8.21 3D PCoA plot based on sequence data Lindsay "Auto" experimentation. Orange= Lindsay pre-experiment, blue = Lindsay "Live" post-experiment. M= mid column sample

Table 8.2 Diversity indices for Lindsay bioreduction experimentation samples 16S rRNA sequences. U, M & L refer to "upper", "mid" and "lower" sections of the columns.

Sample ID	No of QC Reads	Unique OTUs	Shannon's Diversity Index (*H'*)	Simpsons's Diversity Index (1-*D*)	Choa1	Goods Coverage (%)	S_{ace}
Lindsay Pre	127534	1745	7.07	0.956	6477.56	0.986	6545.25
Lindsay Auto Pre	91618	1202	6.87	0.942	4878.96	0.987	4840.15
Lindsay Live U	122594	1587	6.02	0.943	5450.59	0.987	5876.76
Lindsay Live M	119683	1644	6.14	0.943	5720.58	0.986	6135.95
Lindsay Live L	136404	1413	5.17	0.865	4939.39	0.990	5209.89
Lindsay Auto U	151397	673	4.59	0.915	2415.91	0.996	2526.60
Lindsay Auto M	106496	1513	5.23	0.901	5284.76	0.986	5506.70
Lindsay Auto L	166674	801	4.35	0.867	2943.92	0.995	2946.84
Lindsay OS U	111013	2445	8.91	0.990	9031.23	0.978	9298.44
Lindsay OS M	70896	2758	8.81	0.989	9800.80	0.961	10373.81
Lindsay OS L	129101	2068	8.24	0.983	7720.59	0.984	7935.40

8.4.2. Wheal Jane

Concentrations of total iron within Wheal Jane effluents were consistently low throughout the experiment. A maximum iron concentration of 0.2 mg/l was recorded on day 72. Iron concentrations were only observed to exceed 0.1 mg/l nine times throughout the experiment (Figure 8.22). Ferrous iron concentrations were even lower with a maximum recorded concentration of 0.07 mg/L observed on day 1 of experimentation (Appendix 2). In total less than 0.01% of iron was removed from the column, emphasising the low iron concentration within the effluent. The consistently low concentrations of both total and ferrous iron suggest that no bio-reduction has occurred within the column. pH data is inconclusive as after ~ day 40 pH shows a steady increase, a characteristic associated with bio-reduction though this is in contradiction to all other data (Figure 8.23). The lowest measured pH was 7.70 recorded on day 12 of the experiment. This equates to a maximum Fe^{2+} solubility of ~176 mg/l (assuming $K_{sp} = 8 \times 10^{-16}$ (Stumm & Lee, 1961; Langmuir, 1997)) which is far higher than the observed total iron concentrations. This suggests that chemical equilibrium is not a limiting factor for effluent iron concentrations for the majority of the experiment. The only exception to this is in the last week of experimentation. At this stage the pH is increasing thereby reducing the maximum solubility of ferrous iron. The maximum pH recorded was 9.09 on day 75 of the experiment. This equates to a maximum ferrous iron solubility of 0.30 mg/l. Measured total iron concentrations at this point were 0.17 mg/l. Whilst this is not in excess of the theoretical maximum solubility and is a measurement of total iron rather than ferrous iron, it still raises the possibility that the increasing pH is due to increasing microbial activity but any iron released to solution as a result is being limited by the chemical equilibrium of the system.

ORP and conductivity data, however, supports the suggestion that negligible microbially mediated iron-reduction took place. No sudden decrease in ORP, characteristic of the onset of bio-reduction, was observed. Conductivity initially increased but then steadily declined before plateauing at approximately 100 µS/cm, indicative of declining metal concentrations within the effluents. The recovery of zinc, as the most abundant metal economic interest, was also poor with less than 0.03% of total zinc recovered from the column via the effluent.

Figure 8.22 Total iron concentrations (measured with ICP-OES) within Wheal Jane effluent throughout the duration of experimentation.

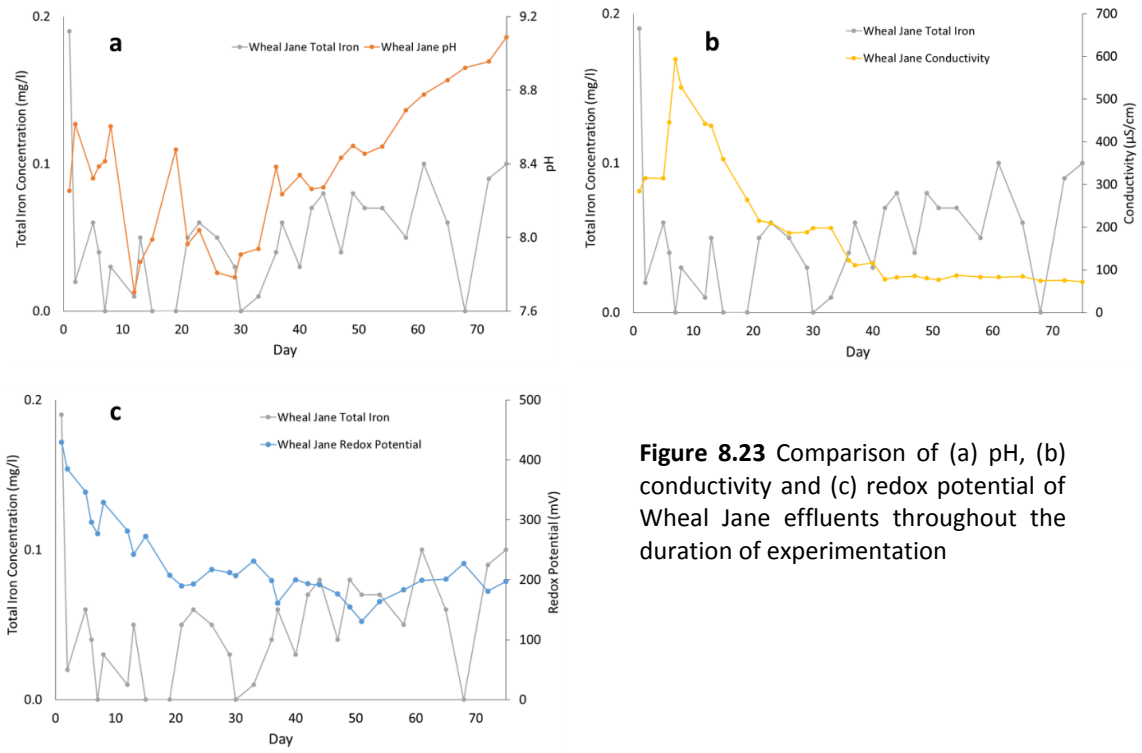

Figure 8.23 Comparison of (a) pH, (b) conductivity and (c) redox potential of Wheal Jane effluents throughout the duration of experimentation

The lack of microbial activity within the waste is again strongly suggested by the inability to extract DNA in detectable concentrations from the waste. Qubit analysis of DNA mass extracted from the waste failed to detect DNA within the extraction fluid in either pre- or post- samples of Wheal Jane waste. The broad range Qubit assay is capable of detecting as low as 100 pg/µl of DNA. While the failure of the DNA extraction kit to successfully extract DNA cannot be ruled out, particularly as the kit is designed for soil and the waste has markedly different physical and chemical properties, it was successfully used on the majority of wastes and so it is likely that the result is a true reflection of the DNA mass within the waste. Therefore, it is almost certain that no significant level of microbial activity has occurred within the waste bio-reductive or otherwise.

Sequential extraction and XRD data displayed no substantial differences between the pre- and post-experiment samples. Calcite and ferric iron oxyhydroxides were the dominant minerals in both pre- and post- samples, reflected by the dominance of the carbonate and easily reducible oxide phases in the sequential extractions (Appendix 2). This further suggests that the waste remained relatively inert within the column for the duration of the experiment, with regards to metal dissolution/ mobilisation.

8.4.3. Red Mud

As with Wheal Jane, the only other alkaline waste tested, total iron concentrations were negligible throughout the experiment. At no point were total iron concentrations detected above 0.005 mg/l. Ferrous iron concentrations measured suggested minor ferrous iron within the effluent contradicting the ICP-OES readings of total iron (Appendix 2). The samples were re-run through ICP-OES for validation and proved consistent with the original analysis; suggesting the error lay in the colorimetric measurement of ferrous iron. In total <0.00% of iron was removed from the column, similarly to the Wheal Jane column. The consistently low concentrations of both total and ferrous iron strongly may suggest that no bio-reduction has occurred within the column. However, this conclusion cannot be drawn using iron concentrations alone. The high pH of the system severely limits the solubility of iron. The lowest recorded pH of 11.26 equates to a maximum ferrous iron solubility of 1.35×10^{-5} mg/l (assuming K_{sp}

= 8×10^{-16} (Stumm & Lee, 1961; Langmuir, 1997)). Therefore, under the conditions present in the waste any ferrous iron formed by microbial iron reduction would not remain within the aqueous phase due to the limited solubility. Only 0.63% of total aluminium (the most abundant metal of economic interest) was recovered from the column. Though this recovery is largely due to an initial flush of aluminium from the column at the start of experimentation (Appendix 2).

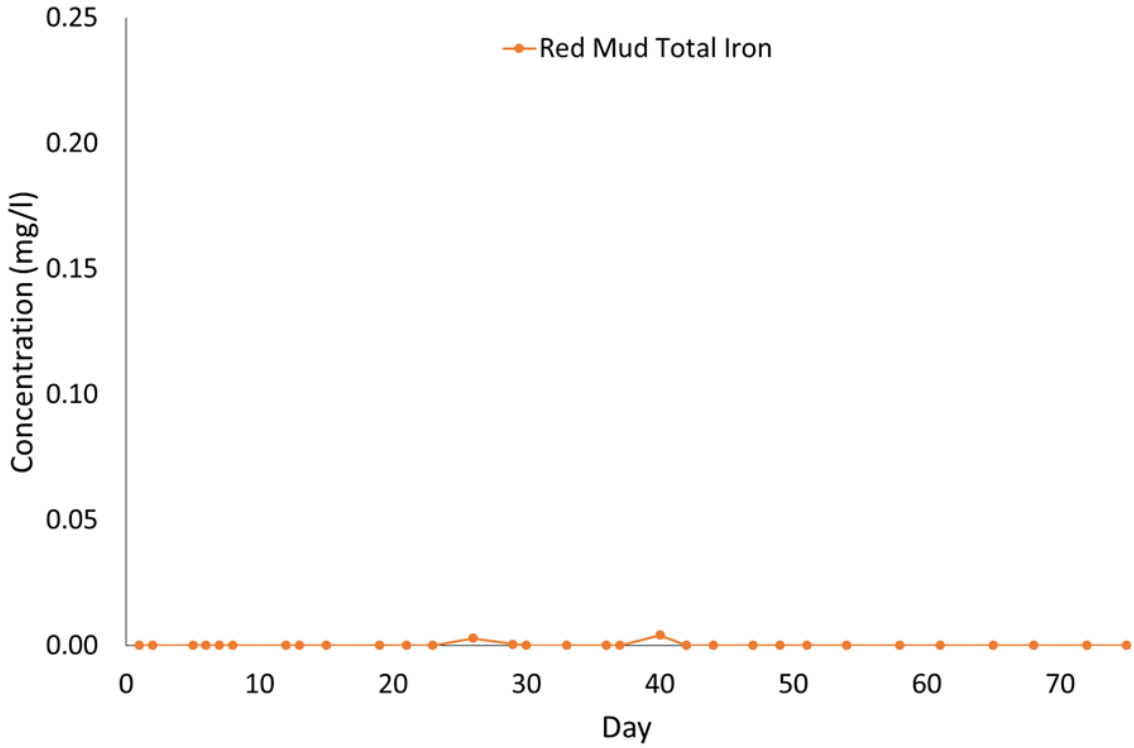

Figure 8.24 Total iron concentrations (measured with ICP-OES) within Red Mud effluent throughout the duration of experimentation.

The consistency of the pH of the effluent suggests a lack of any significant bioreduction. Similarly, the rapid decline in conductivity is indicative of rapidly declining metal and ion concentrations within the effluent and is reflective of the declining aluminium concentration in the effluent. The ORP overall showed a steady decrease from ~0 mV to ~150 mV. Within this overall decrease there is a degree of variability with two distinct rapid decreases to approximately -150 mV clearly visible. Whilst this may be an indication of microbial activity, the exact cause of this short-lived decrease in ORP is unknown.

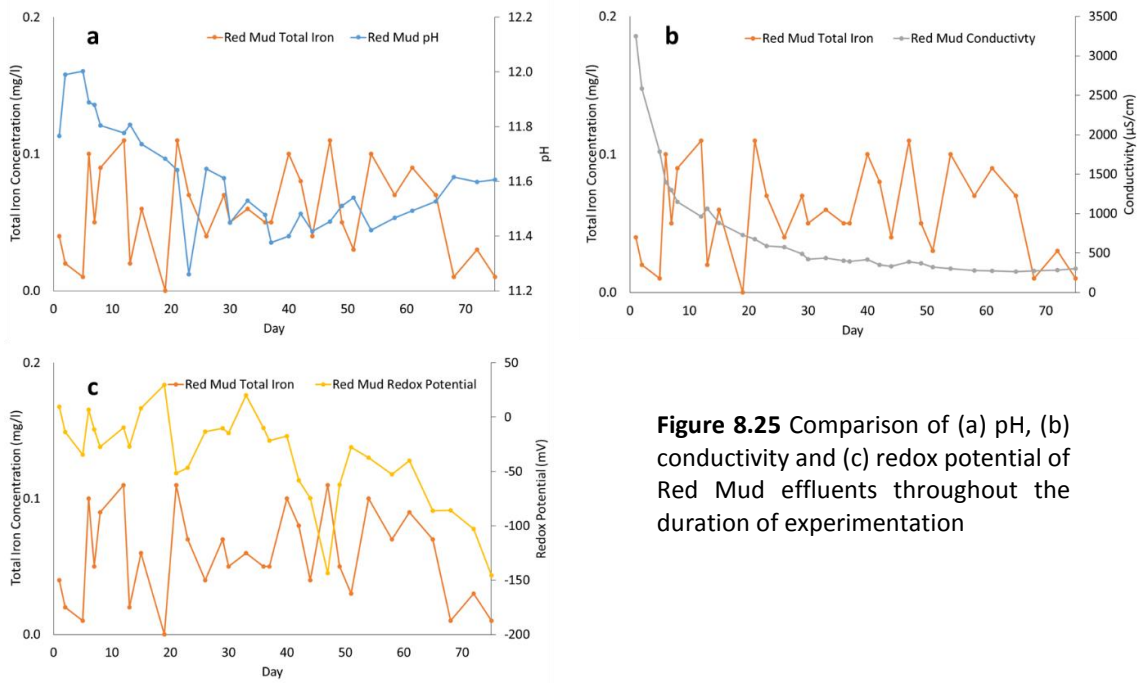

Figure 8.25 Comparison of (a) pH, (b) conductivity and (c) redox potential of Red Mud effluents throughout the duration of experimentation

XRD analysis of the red mud pre- and post-experiment showed no major differences in either trace profile or intensity, with calcite indicated as the dominant mineral in both cases. Similarly the results of sequential extractions showed negligible changes in the distribution of aluminium (the metal of most economic interest) throughout the phases extracted, while the only alteration in iron distribution was a small (8%) increase in iron within the recalcitrant residual iron phase at the expense of iron within the goethite phase (Appendix 2). Qubit analysis of DNA mass extracted from the waste failed to detect DNA within the extraction fluid in the pre-experiment waste. However, within post experimentation samples an average DNA mass of 0.3 ng/µl was measured suggesting that there has been some, albeit minimal, microbial activity within the sludge. This low DNA mass is not unexpected. The red mud was supplied as a dried powder with uncertain provenance, meaning any microbial communities within the waste may have been destroyed or at least significantly impacted by the drying process. Furthermore, it is known that there are relatively fewer alkaliphilic DIRM compared to their acidophilic and neutrophilic counterparts (Ye *et al.*, 2004; Hicks *et al.*, 2010). This is largely due to the difficulty of microbes to maintain the proton-motive force across the cell membrane, necessary for dissimilatory metal reduction, when the external pH is much higher than that of their cytoplasm (Hicks *et al.*, 2010). This only applies to microbes that utilise a respiration metabolism and not those which use fermentative metabolisms or those which utilise sodium transport (in place of protons) for ATP

production. This results in a bias towards fermentative metal reducers and those with Na^+-coupled ATP synthases within alkaline environments (Schmitz *et al.*, 2006; Madigan *et al.*, 2015). The limitations from the alkalinity of the system will also apply to the Wheal Jane column despite the weaker alkalinity within the Wheal Jane column.

Despite the increase in DNA mass and the limits on iron solubility (precluding its use as an indicator), there has been no notable impact on the chemical conditions of the effluent or on the mineralogy of the waste, suggesting that either no microbial reduction of iron has occurred or it has only occurred at a scale which is not significant enough to result in bio-reduction on the scale necessary for large scale metal mobilisation.

8.4.4. Parys Mountain

8.4.4.1. Parys Mt. 1

Both total iron and ferrous iron concentrations within the Parys Mt. 1 effluents were elevated, when compared to the Lindsay columns, from the start of experimentation with initial concentrations of 120.1 mg/L and 45.5 mg/L respectively recorded. Total iron concentrations raised rapidly to approximately 370 mg/L and remained at this level, with a peak of 385.5 mg/L recorded on day 2, before rapidly declining and remaining relatively constant broadly between ~150-200 mg/L for the remainder of experimentation. Ferrous iron concentrations followed a very similar trend to the total iron, albeit at lower concentrations, exhibiting a rapid increase and short period of elevated concentrations before a rapid decrease and steady state conditions for the remainder of the experiment. Peak ferrous iron was recorded on day 8 at 176 mg/L, while the steady state period consisted of concentrations largely between 50 and 100 mg/l (Figure 8.26).

Chemical equilibrium of iron is not believed to have limited the recovery of iron from the waste. The highest recorded pH was 7.20 on day 34 of experimentation. This equates to a ferrous iron solubility of 1793 mg/l (assuming $K_{sp} = 8 \times 10^{-16}$ (Stumm & Lee, 1961; Langmuir, 1997)) which is far larger than any measurement of total iron within the effluents. Given that for large parts of the experiment the pH was substantially lower, thereby facilitating greater iron solubility, the fact that the lowest solubility for ferrous

iron was never exceeded suggests that chemical equilibrium is not limiting the recovery of iron from the column. The maximum solubility of ferric iron within the effluent throughout experimentation was 0.02 mg/l (assuming K_{sp} $=1.58 \times 10^{-39}$ (Langmuir, 1997)), coinciding with the lowest pH of 3.26. This suggests that the majority of ferric iron within the effluent collection vessel is a result of the oxidation of ferrous iron within the vessel, and near negligible concentrations of iron are mobilised from the column in the ferric (Fe^{3+}) oxidation state. It is improbable given the low flow rate of the effluent, that entrainment of iron oxyhydroxides contributed to the overall concentration within effluents

In total 3.52% of iron within the column was mobilised and recovered from the waste via the effluent. High concentrations of ferrous iron suggest that bio-reduction occurred within the waste, though the elevated initial concentrations and early establishment of steady state conditions suggest iron bio-reduction was already occurring with the waste before the addition of glycerol. Given the 1.7wt% of organic carbon within the Parys Mt.1 waste, it is possible that iron-reducing conditions already existed within the waste before experimentation began. However, due to the lack of organic starved controls the pre-existence of iron-reduction cannot be verified.

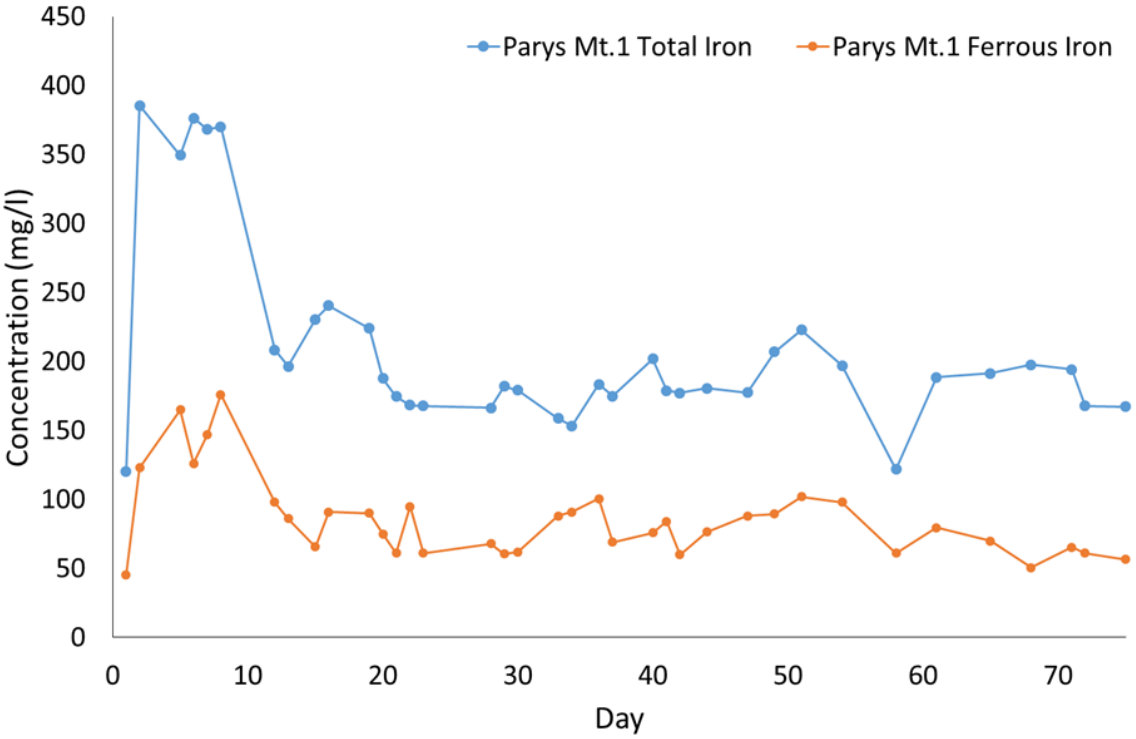

Figure 8.26 Total iron (ICP-OES) and ferrous iron (colourimetry) concentrations within Parys Mt. 1 effluent throughout the duration of experimentation

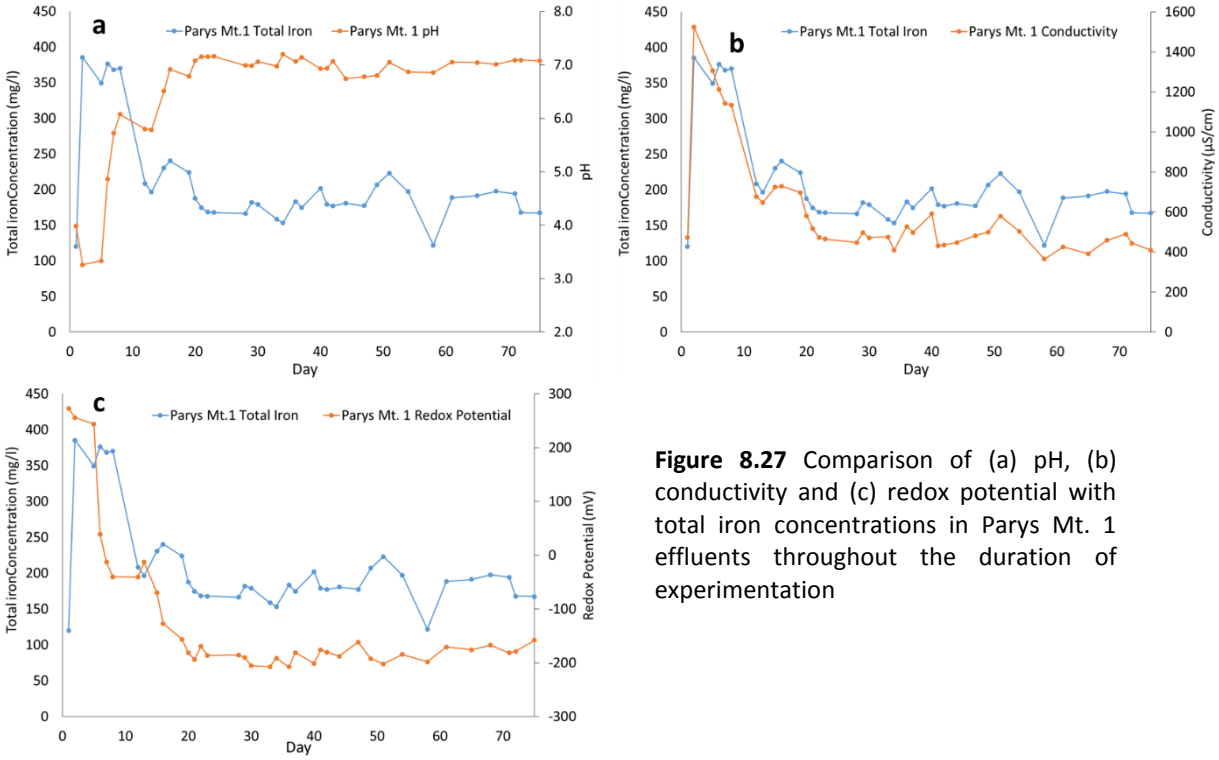

Figure 8.27 Comparison of (a) pH, (b) conductivity and (c) redox potential with total iron concentrations in Parys Mt. 1 effluents throughout the duration of experimentation

Zinc, lead and copper concentrations within the effluent displayed initially high concentrations before rapidly declining and remaining at negligible concentrations (<0.1 mg/L) for the remainder of the experiment (Appendix 2). The initial elevated concentration of metals can be attributed to desorption and "wash off" of water soluble metals already within the waste, rather than as a result of bio-reduction Given the organic carbon already present in the waste it is possible a degree of bioreduction had already been occurring in the waste before the introduction of glycerol. In total 1.89%, 0.79% and 0.12% of zinc, lead and copper were recovered from the column respectively.

The pH of the Parys Mt. 1 effluent was observed to rapidly increase during the short period of elevated total iron concentrations (day 2 – 8), rising from 3.9 on day 1 to 6.0 on day 8 representing an increase of 0.26 pH units per day. At this point the rate of pH increase slowed as iron concentrations decreased, reaching pH 7 on day 20 of the experiment. The pH of the effluent then remained relatively constant for the remainder of the experiment (Figure 8.27a). This may be a result of the buffering capacity of the sludge being overcome by the circum-neutral glycerol solution. However, the increasing alkalinity, and resulting pH increase, along with the increasing iron effluent concentrations is highly indicative of iron bio-reduction (Appendix 2) (Ponnamperuma,

1972; Howell *et al.*, 1998). Similarly the rapid decrease in ORP in the early stages of experimentation are an indicative characteristic of oxygen depletion and the decomposition of organic carbon coupled to iron bio-reduction (Lovley, 1991). As with the pH measurements, ORP remained relatively constant, between approximately -180 mV and -200 mV, during the period where iron concentrations remained constant within the effluent (Figure 8.27c). The effluent conductivity profile is shows substantial similarities in shape to the total iron concentration profile. This is expected as higher dissolved metals and cations within the effluent would give rise to higher conductivity. The significance of the similarity of the trends is that it is indicative that the most abundant metal, and therefore the metal with the greatest influence on conductivity, within the effluent is iron.

When extracted from the experimental column, the waste had broadly changed to an olive-green colour similar to that observed in the Lindsay waste post-experiment (Figure 8.28). When left exposed to the atmosphere the green colouration could be seen to rapidly fade and an increasingly brown colouration could be seen to become more prevailent. This is indicative of metastable minerals succeptable to oxidation, such as green rust being present in the waste. The presence of these minerals is another positive indication that bio-reduction has been occuring with the column as green rusts are known end or intermediate products of the bioreduction process (Fredrickson *et al.*, 1998; Genin *et al.*, 1998; Zachara *et al.*, 2002).

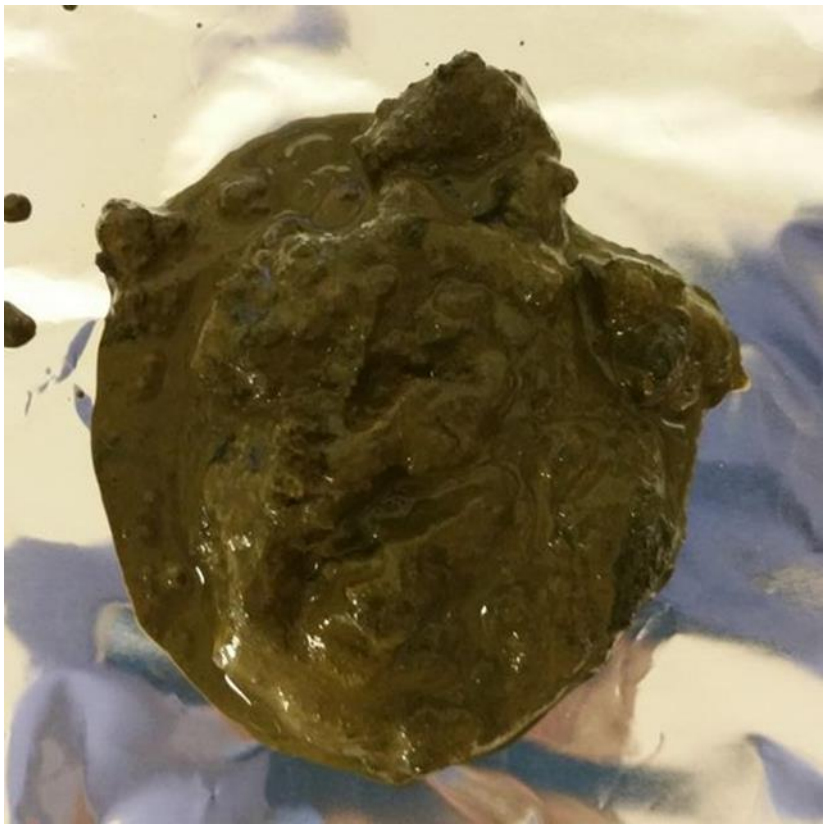

Figure 8.28 Parys Mt. 1 waste extracted from column post-experiment

XRD analysis of Parys Mt.1 waste both pre-and post-experiment shows that extensive alteration of the mineral composition has occurred. Within the pre-experiment sample the iron was found largely between two iron-bearing minerals, jarosite and goethite. However, within the post- sample jarosite was not identified having seemingly been replaced with goethite, which displays higher counts in the post-experiment waste. This suggests that jarosite was the mineral undergoing iron reduction, with goethite a result of the reaction of residual iron oxyhydroxides with dissolved ferrous iron within the effluent. Alternately the goethite may be the result of the oxidative breakdown of metastable iron bearing phases such as green rusts. The generation of goethite is further supported by the results of the sequential extraction testing. Figure 8.30a&b show the percentage of iron reporting to the “reducible oxide” phase (e.g. goethite) has increased by ~14% representing a ~4 mg increase in mass extracted at this stage.

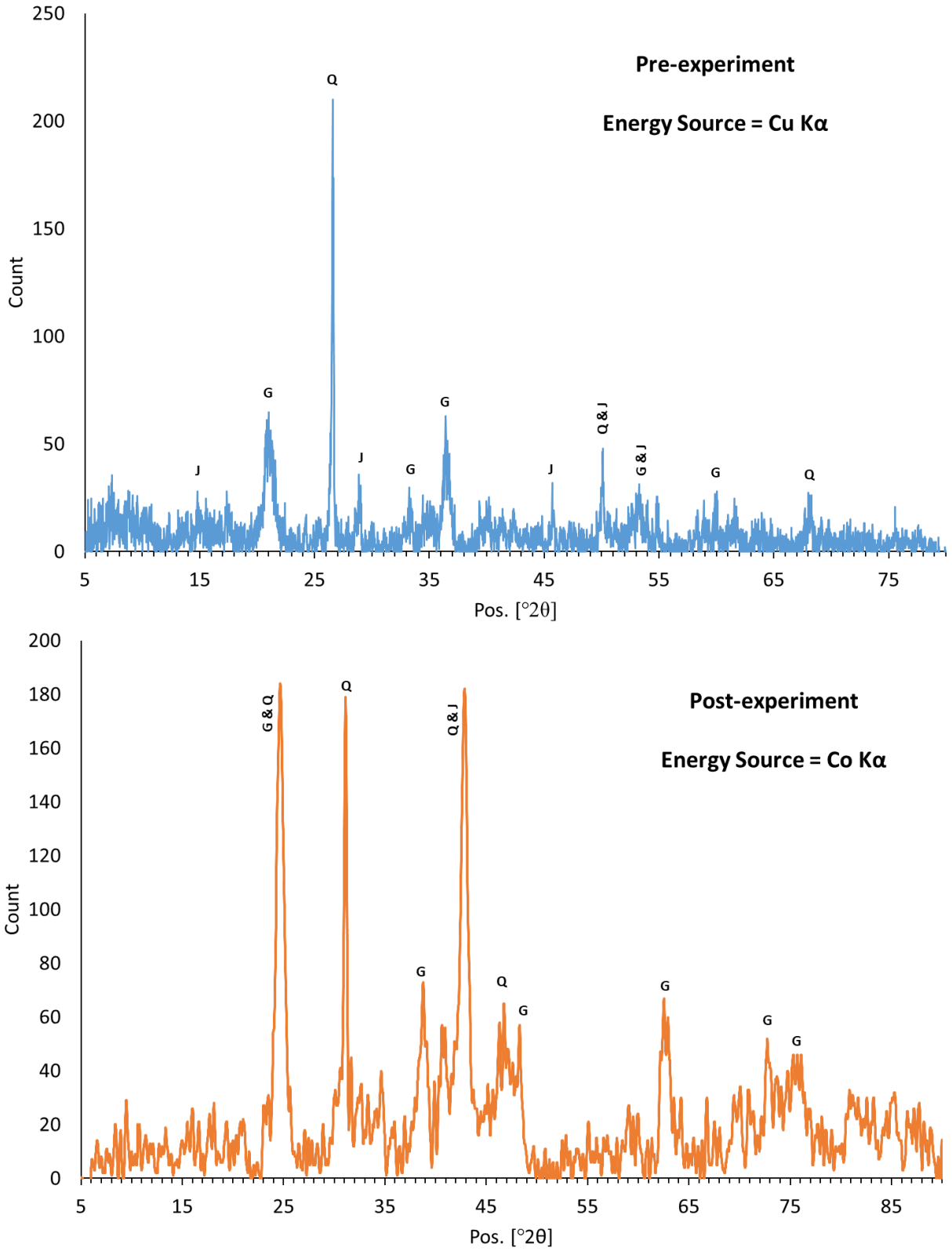

Figure 8.29 XRD diffractograms of Parys Mt. 1 waste both pre- (above) and post-experiment (below) Q=quartz, J= Jarosite & G= goethite

Distribution of lead within the waste underwent only minor change within the more crystalline phases with ~25% of lead located within the “reducible oxide”, “magnetite targeted” and “residual” phases in both pre- and post- samples. Within the more labile phases lead has been redistributed from the “carbonate” phase to the “easily reducible oxide” phase. This would suggest that the lead recovered from the column has originated from the “carbonate associated” phase predominantly, likely as a result of the aforementioned “wash off effect”. The distribution of copper in the system is more difficult to interpret. An initial review of the data presented in Figure 8.30e&f suggests a redistribution of copper to the “reducible oxide” (e.g. goethite) phase largely from the “residual” phase. The mass of copper extracted within the “residual” phase from the pre-experiment sample was 0.56mg while the post-experiment sample had only 0.10mg extracted, potentially representing an erroneous measurement in the pre-experiment sample. This could potentially be explained by the presence of a recalcitrant copper mineral, potentially metallic copper residual from the sites previous use as a copper precipitation pond. Masses of copper extracted from other phases remained largely consistent between pre- and post- experimentation samples resulting in this larger mass within the pre-sample “residual” phase skewing results and suggesting greater copper removal from this phase than possibly is truly representative. Furthermore, the lack of copper within the “reducible oxide” phase is potentially a result of the use of sodium dithionate as part of the extractant, which is known to induce the precipitation of copper from solution (Chou *et al.*, 2015). This would cause the underestimation of copper in this phase and an overestimation of the copper content in the “magnetite-targeted” and “residual” phases. Zinc distribution within the system remained broadly similar after experimentation. The exception being a ~10% reduction within the “carbonate” phase and subsequent increase of ~13% within the “reducible oxide” phase (Figure 8.30g&h). This is likely a result of both the “wash off effect” removing the most mobile zinc from the “carbonate” phase and the re-adsorption or co-precipitation of mobilised zinc onto minerals within the “reducible oxide” phase.

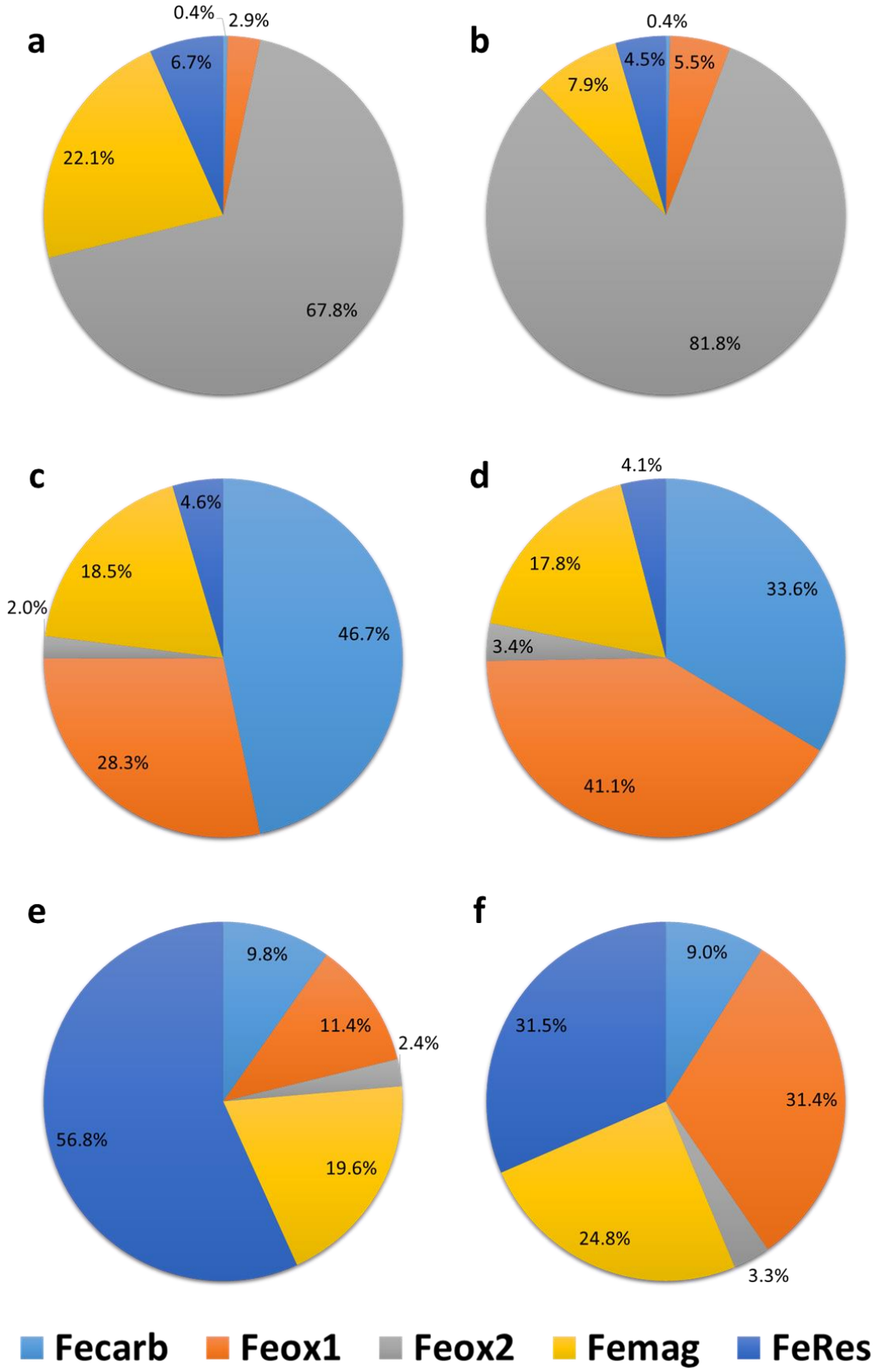

Figure 8.30 Results of sequential extractions showing distribution of metals within Parys Mt. 1 waste pre- and post- experimentation; a) Iron pre-, b) iron post-, c) lead pre-, d) lead post-, e) copper pre-, f) copper post-

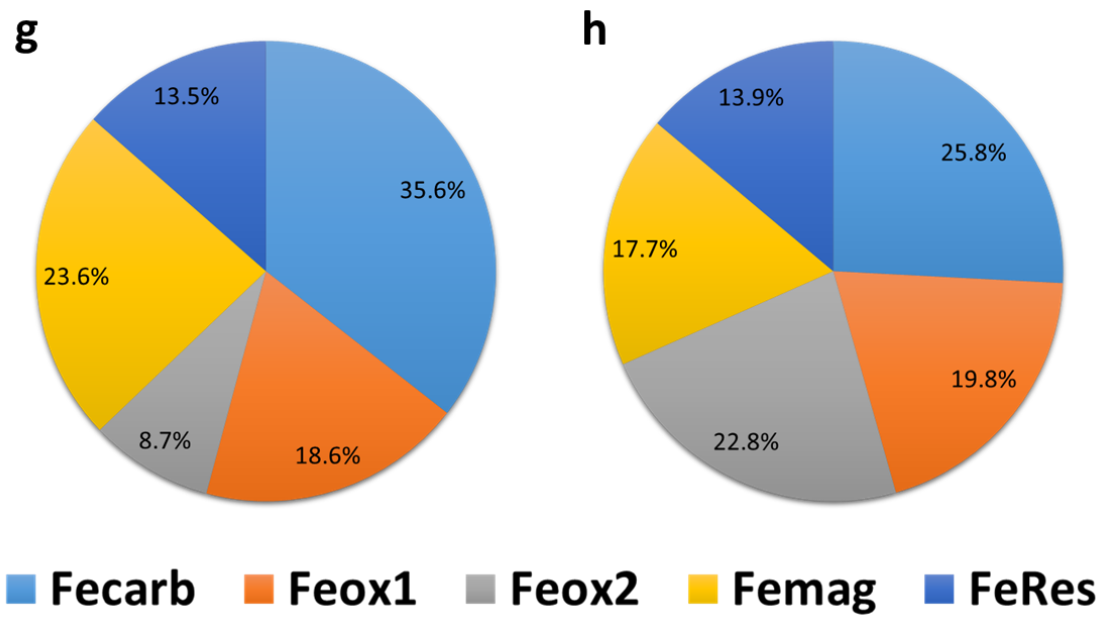

Figure 8.29(cont.) Results of sequential extractions showing distribution of metals within Parys Mt. 1 waste pre- and post- experimentation; g) zinc pre- and h) zinc post-

8.4.4.2. Analysis of DNA Mass

Qubit analysis of mass of DNA extracted from the waste shows an increase in DNA within post-experiment samples. Extractions from pre-experiment samples contained 8.3 ng/µl, whilst the post-experiment extractions contained an average DNA concentration of 66.8 ng/µl representing an eight fold increase in DNA mass within the waste. This confirms that there has been extensive proliferation of microbial communities within the waste, with the physicochemical data highly suggestive of the presence of DIRM communities.

8.4.4.3. Parys Mt. 2

In contrast to the Parts Mt.1 column, iron concentrations within Parys Mt.2 effluents were negligible at the start of experimentation (Figure 8.31). The Parys Mt.2 waste also contains pre-existing organic carbon though seemingly no bioreduction was already occurring before experimentation. The negligible initial iron concentrations demonstrate that any later increase in iron cannot be attributed to the entrainment of colloidal iron particles as these are not seen within the initial “wash-off”, where they are

most likely to be observed. Total iron concentrations began to show considerable increases from day 12 of experimentation, whilst ferrous iron increases from day 15. From this point concentrations of both forms of iron dramatically increased. Total iron reached its peak concentration of 385.5 mg/L on day 23, representing a rate of 33.37 mg/L/day increase from the first observed elevated iron concentration on day 12. Ferrous iron showed a similar pattern of increasing, albeit lower, concentrations. Total iron concentrations then decreased slightly before remaining relatively constant until day 49 of experimentation, at this point total iron concentrations rapidly decrease to 168.6 mg/L before slowing and remaining relatively constant, at ~150 mg/L, through to the cessation of experimentation. This last period of near constant iron concentrations is similar in concentration to the Parys Mt.1 results, suggesting that between 150-180 mg/L of total iron represents steady state conditions for the system within these wastes at the conditions imposed during the experiment.

Again, as in the Parys Mt.1 testing, the pattern of ferrous iron concentrations showed a high degree of similarity with the total iron though at lower concentrations, suggesting reduction of ferric iron from the column. This result, combined with the negligible initial concentrations, demonstrates that the total iron within the effluent is intrinsically linked to the ferrous iron generation and that the ferric iron component is likely a result of oxidation of ferrous iron. This is further indicated by assessing the maximum potential solubility of ferric iron in the system. The lowest pH recorded was 2.66 on day 1 of experimentation which equates to a maximum ferric iron solubility of 0.92 mg/l (assuming K_{sp} =1.58×10^{-39} (Langmuir, 1997)). Given pH only increases from this point, and therefore ferric iron solubility decreases, it can be assumed that near negligible concentrations of iron are mobilised from the column in the ferric (Fe^{3+}) oxidation state. The initial “lag” phase demonstrating that entrainment of suspended solids was not a significant factor. Chemical equilibrium of ferrous iron was not believed to have limited the recovery of iron from the waste. The highest recorded pH was 6.60 on day 75 of experimentation. This equates to a ferrous iron solubility of 28036 mg/l (assuming K_{sp} = 8×10^{-16} (Stumm & Lee, 1961; Langmuir, 1997)) which is far larger than any measurement of total iron within the effluents. Given that for large parts of the experiment the pH was substantially lower, thereby facilitating greater iron solubility,

the fact that the lowest solubility for ferrous iron was never exceeded suggests that chemical equilibrium is not limiting the recovery of iron from the column.

The increase in pH from 2.66 to 6.60 and the decrease in ORP from 561.2 mV to -145.4 mV are also highly suggestive of microbial reduction of iron. Though the expected sharp increase and decrease in pH and ORP, respectively, at the onset of iron bio-reduction is not observed but rather a more gradual and constant change in both parameters is observed (Figure 8.32a&c). The increasing alkalinity is further indication that the pH increase is a result of bioreduction of ferric iron within the column as opposed to a neutralisation effect from the extractant. Conductivity on the effluent can again be seen to closely mirror the pattern of iron concentrations, with the exception of the first 12 days where decreasing conductivity can be attributed to the "wash-off" of water soluble ions from the waste (Figure 8.32b).

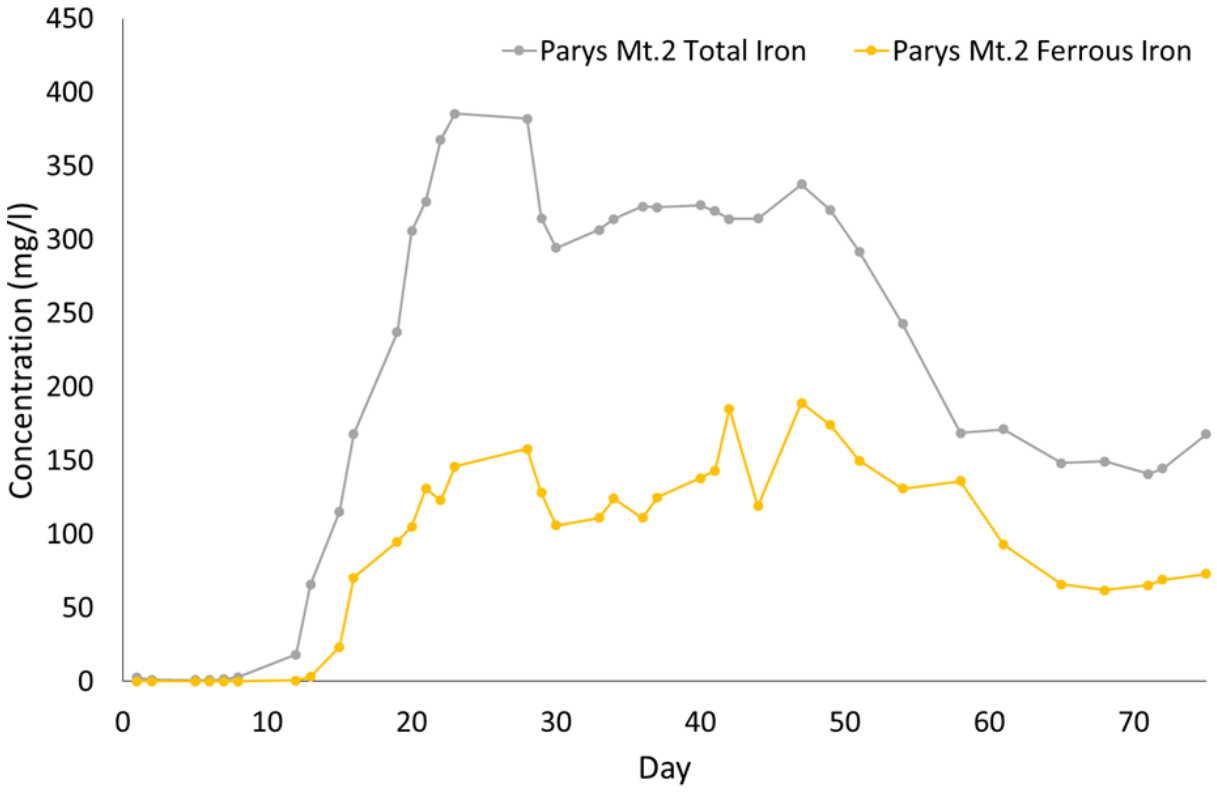

Figure 8.31 Total iron (ICP-OES) and ferrous iron (colourimetry) concentrations within Parys Mt. 2 effluent throughout the duration of experimentation

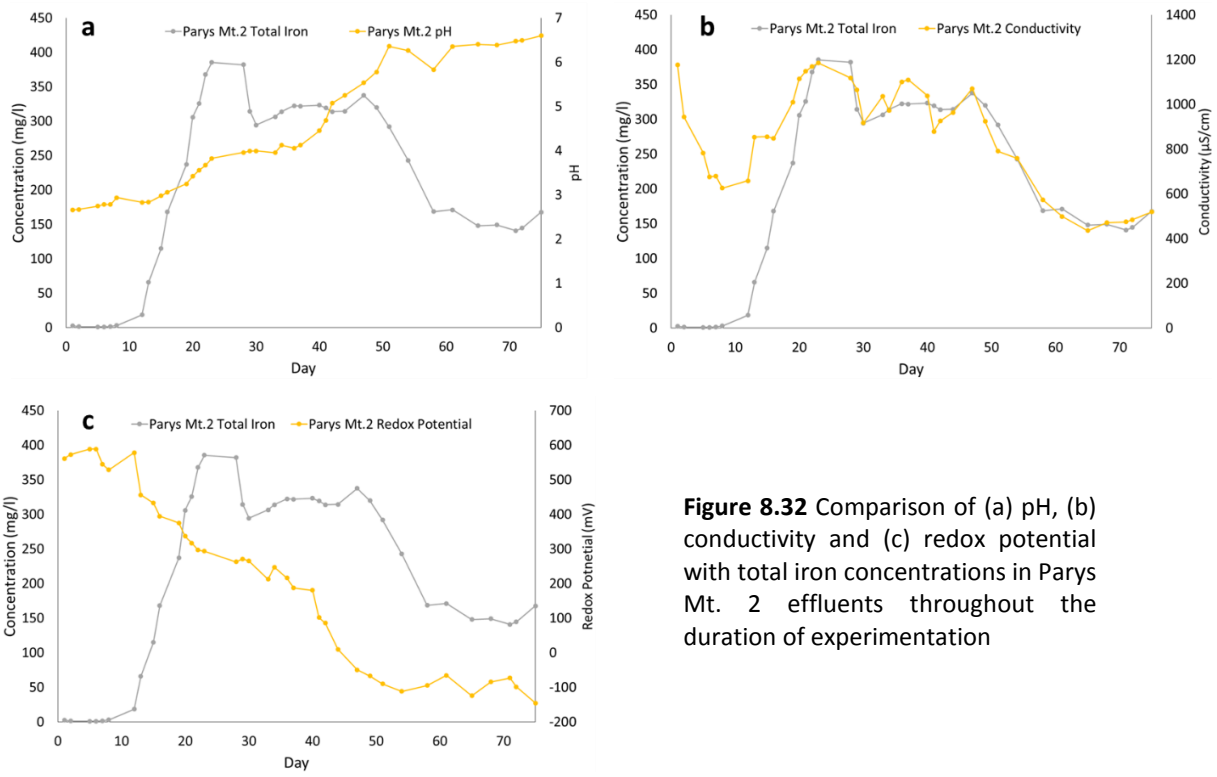

Figure 8.32 Comparison of (a) pH, (b) conductivity and (c) redox potential with total iron concentrations in Parys Mt. 2 effluents throughout the duration of experimentation

In total 3.45% of iron originally within the column was mobilised and recovered from the waste via the effluent. This value is very similar to the iron recovery from the Parys Mt.1 experimental results. Zinc and copper recoveries were 2.22% and 0.32% respectively. However, the largest proportion of these recoveries were achieved due to the initial high concentrations of these associated metals in the first emergent effluents. Therefore, the majority of these metals extracted is as a result of "wash-off" rather than mobilisation as a result of microbial induced iron bio-reduction (Appendix 2).

Lead recovery showed a different relationship however. In total only 0.62% of lead was recovered from the column but unlike zinc and copper this was not as a result of "wash-off" only. As can be seen in Figure 8.33, lead concentrations increase commensurately with total iron before decreasing at a similar rate. This suggests that lead mobilisation is related to the reduction and mobilisation of iron and is potentially released into solution from the reductive dissolution of iron oxyhydroxides and hydroxysulphates. The decrease in lead concentration may be a result of pH increases as much as it is a result of the decrease in iron reduction. The sharp decrease in lead at day 40 is commensurate with the increase in pH to approximately pH 5 at which point ~90% of lead will re-adsorb to iron oxyhydroxides, removing it from solution (Figure 4.5).

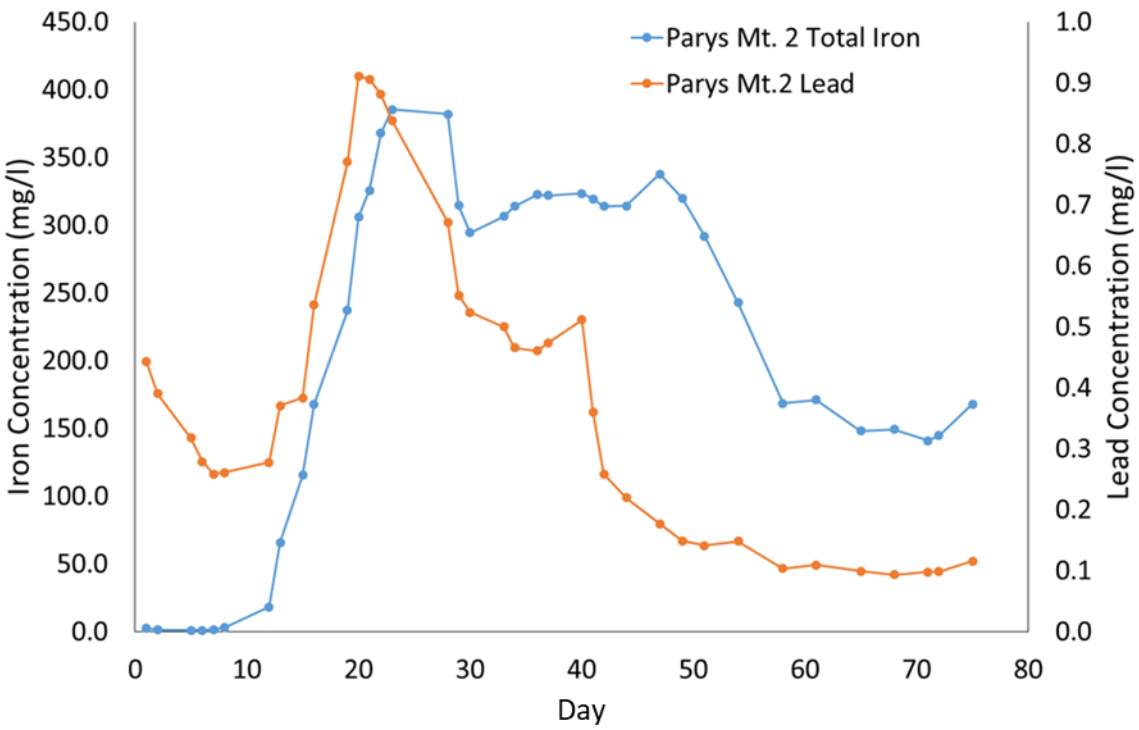

Figure 8.33 Comparison of total iron and lead concentrations within Parys Mt. 2 effluents throughout the duration of experimentation

When extracted from the column the waste had undergone a significant colour change (Figure 8.34). Rather than the largely iron orange-brown observed pre-experiment (a), the waste contained bands of near black colour interspersed with dark green areas and areas which retained the initial orange brown colouration (b) similar to the colour change described by Benner *et al.* (2002). The darker regions were observed to become lighter and browner in colouration with time, suggestive of metastable minerals such as green rust, though did so as a much slower rate and not as extensively as previous wastes. Despite their name, green rusts can often appear black. Though, there are other iron minerals that are typically black in colour such as sulphides or magnetite. However, when a magnet was introduced there was no observable interaction between the black minerals and the magnet suggesting they are not magnetite. This left either metastable iron sulphides or green rusts as the likely cause of the colouration.

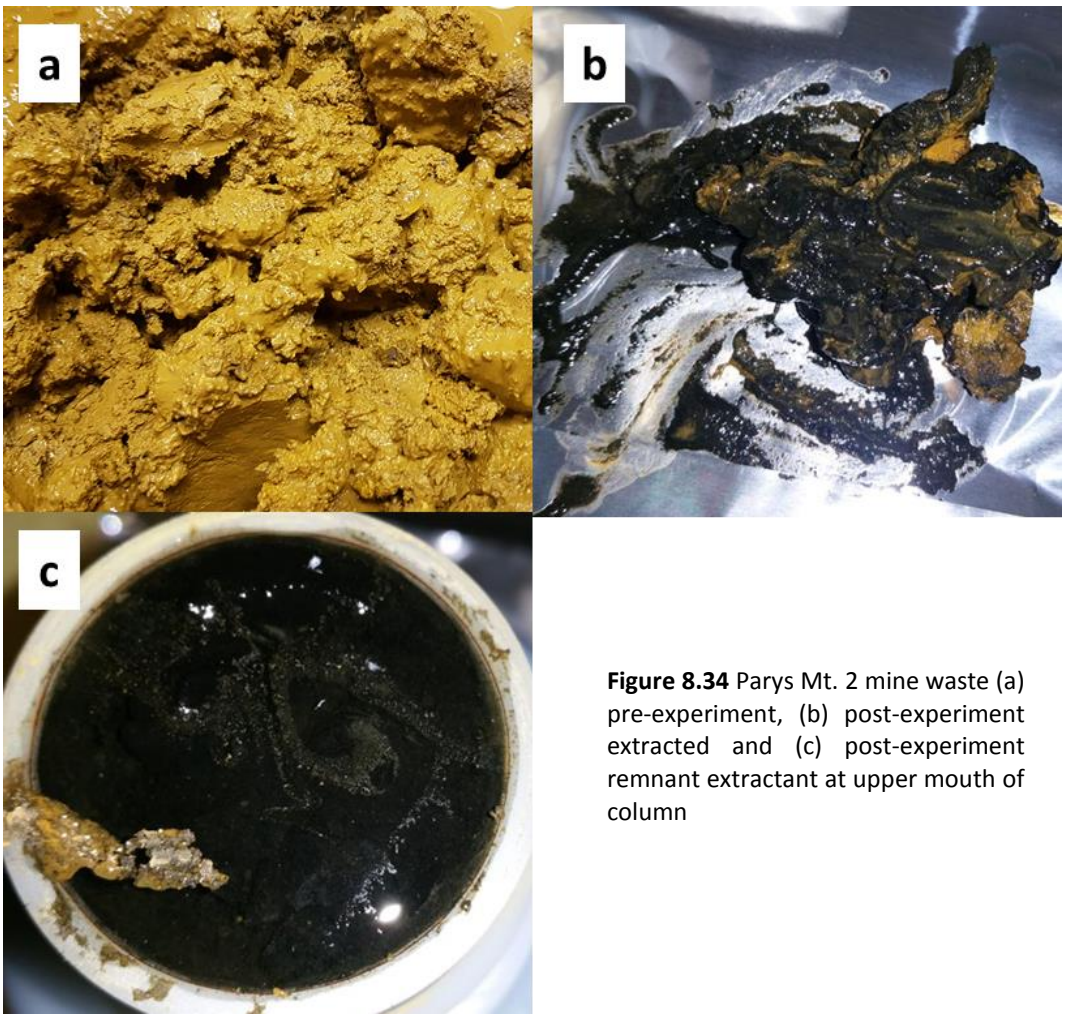

Figure 8.34 Parys Mt. 2 mine waste (a) pre-experiment, (b) post-experiment extracted and (c) post-experiment remnant extractant at upper mouth of column

XRD analysis of Parys Mt.2 waste both pre-and post-experiment suggests that alteration of the mineral composition has occurred. Within the pre-experiment sample the dominant iron-bearing minerals were goethite and jarosite. The high iron and sulphur content identified within the waste correlates with the identification of goethite and jarosite (see Section 7.5.2). Within the post-experiment sample the jarosite are no longer present, though counts for goethite have increased and an unnamed ferric iron oxide peak was identified. There are no indications of the presence of amorphous minerals, though high counts for quartz (despite filtering and correcting trace for outliers) mask the visibility of the characteristic “undulations” that signify the presence of amorphous iron oxyhydroxide. This suggests that jarosite is the iron mineral primarily being reduced within the system. There is potential that goethite is also being reduced but secondary goethite from post-experiment oxidation has resulted in increased counts masking the removal of initial goethite.

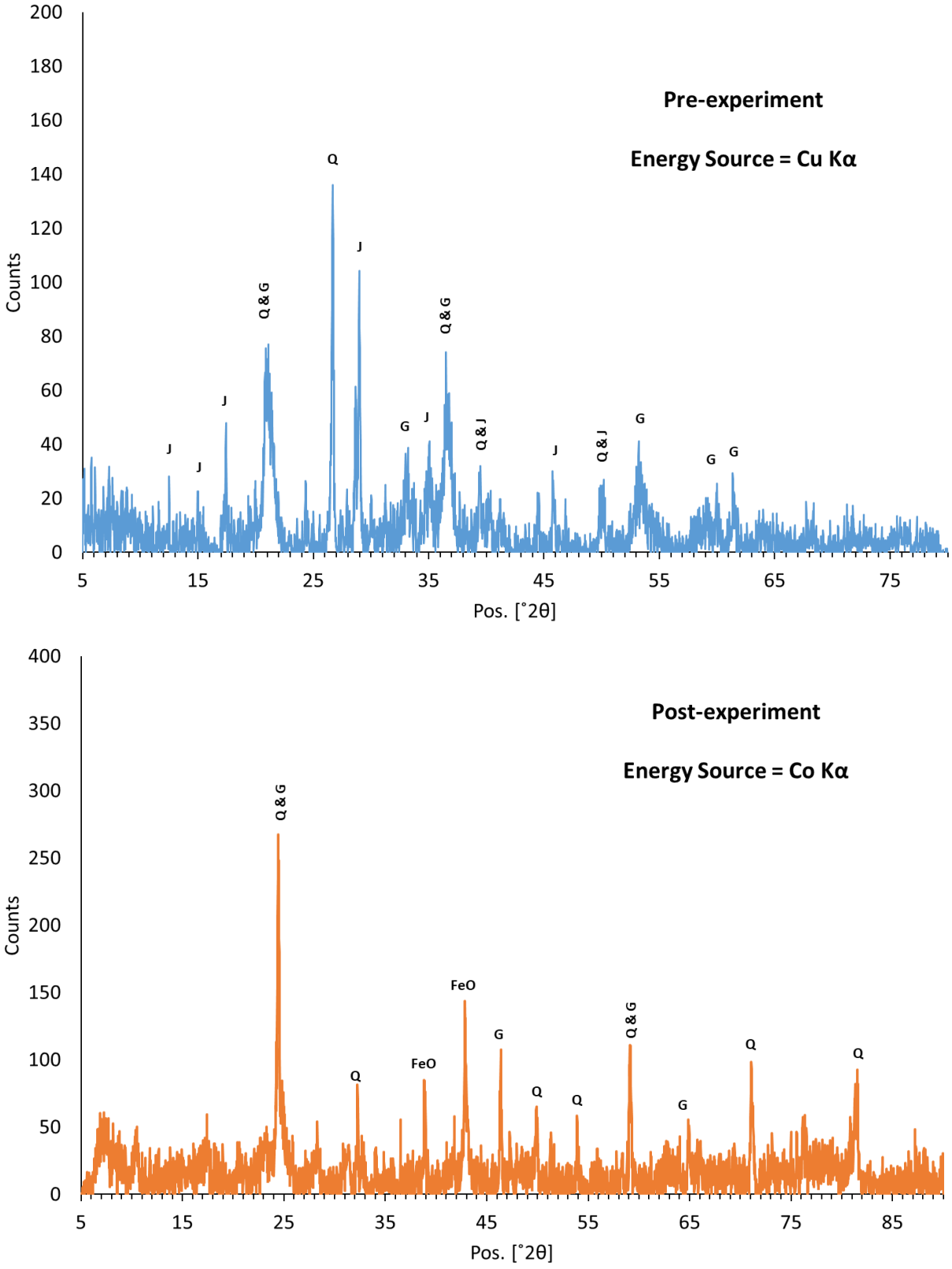

Figure 8.35 XRD diffractograms of Parys Mt. 2 waste both pre- (above) and post-experiment (below) Q=quartz, J= Jarosite, G= goethite & FeO = ferric iron oxide

The distribution of iron within the waste, as indicated by the sequential extractions, suggests that the undefined iron oxide mineral within the XRD diffractogram is likely to be goethite, magnetite or a similar iron oxyhydroxide. The distribution of iron within the "carbonate", "easily reducible oxide" and "reducible oxide" phases has remained relatively similar to the pre-experiment sample. There has been a reduction in the iron situated within the residual phase and an increase in the iron present as magnetite or similar minerals (Figure 8.36a&b). The distribution of copper in the system is again difficult to assess with confidence. The most notable alteration to have occurred is an increase of 14.4% of total copper within the "easily reducible oxide" phase which appears to have originated largely from the "magnetite-targeted" phase. Beyond this the only substantial redistribution of copper is the movement of ~10% of copper, seemingly again from the "magnetite-targeted" phase, into the "residual" phase (Figure 8.36e&f). However, these results again must be viewed with a degree of scepticism as copper is absent from the "reducible oxide" phase due sodium dithionate within the extractant inducing copper precipitation. This prevents a true representation of copper distribution in this and later extraction phases (Chou *et al.*, 2015).

As with the effluent metal recovery, lead provides the most interesting results from the sequential extractions. Before the experimentation the majority of lead was contained within the "magnetite-targeted" and "residual" fractions of the waste. Only 16.4% were initially situated within the first 3 extraction phases, which represents the primary "target lead" for recovery. The post-experiment sample shows an increase in the proportion of lead (52.5%) now contained within the first 3 extraction phases with the majority of this contained within the "carbonate" and "easily reducible oxide" phases. This represents a considerable redistribution of lead from less reactive phases to more microbially-labile phases (Figure 8.36c&d). When considered in combination with the recovery of lead via the effluent it suggests that a greater quantity of lead was mobilised as a result of release from bio-reduced iron oxyhydroxides than suggested by the concentration of lead within the effluent. A large proportion of mobilised lead seemingly is resorbed to residual iron oxyhydroxides (and/or other minerals) within the column. The increasing pH of the system decreases the solubility of lead, and other metals, in the effluent thereby increasing the likelihood of sorption.

Zinc redistribution, between sequential extraction phases, bears a strong similarity to the distribution of iron in the waste (Figure 8.36g&h). The “magnetite-targeted” phase has had an increase of ~20% total zinc compared to the pre-experiment sample broadly at the expense of the “residual” phase, as seen with iron distribution. This increase in zinc within the magnetite phases could potentially be attributable to zinc immobilisation and incorporation into magnetite, though none were detected by XRD analysis (Cooper *et al.*, 2000).

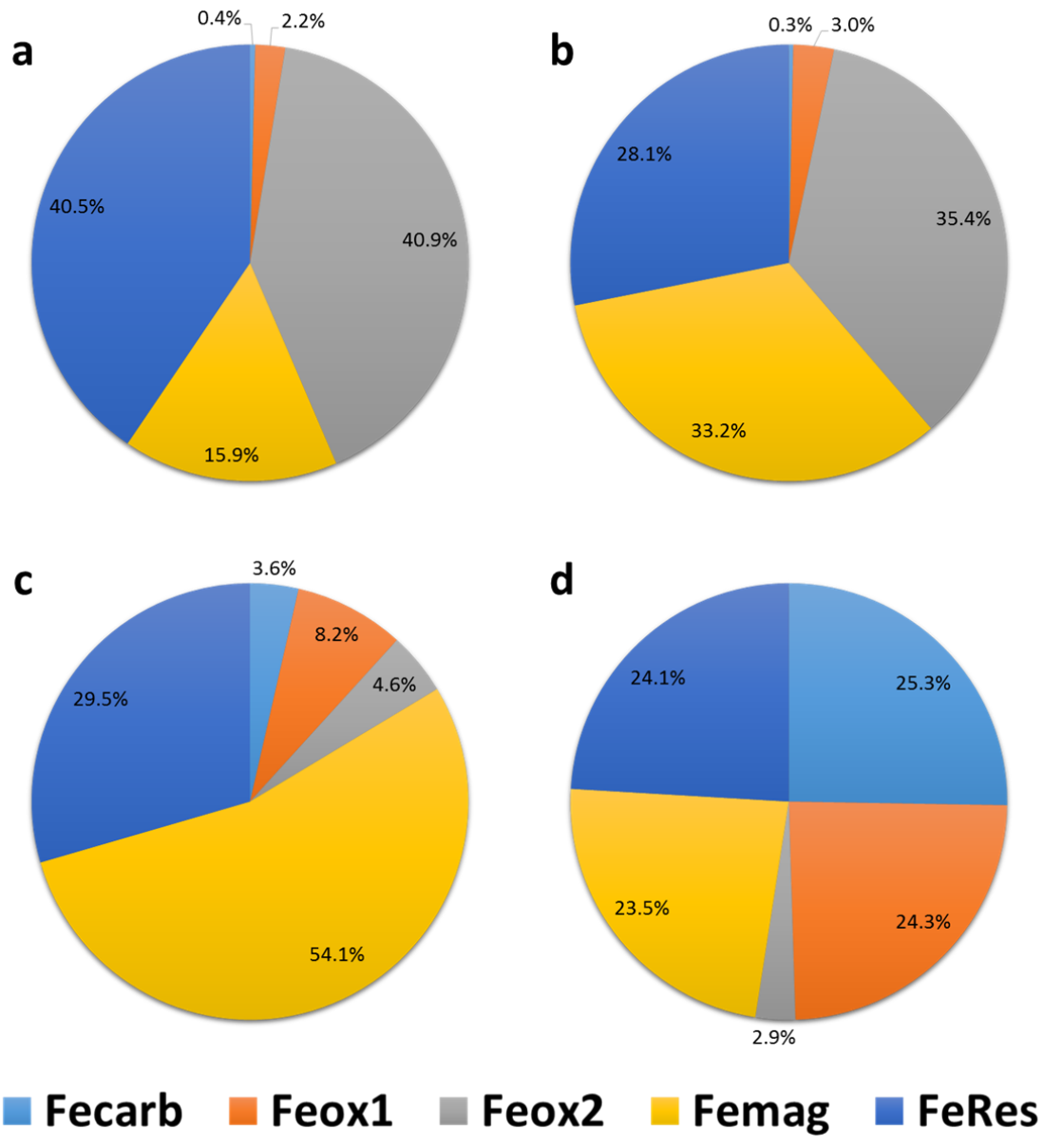

Figure 8.36 Results of sequential extractions showing distribution of metals within Parys Mt. 2 waste pre- and post- experimentation; a) Iron pre-, b) iron post-, c) lead pre-, d) lead post-

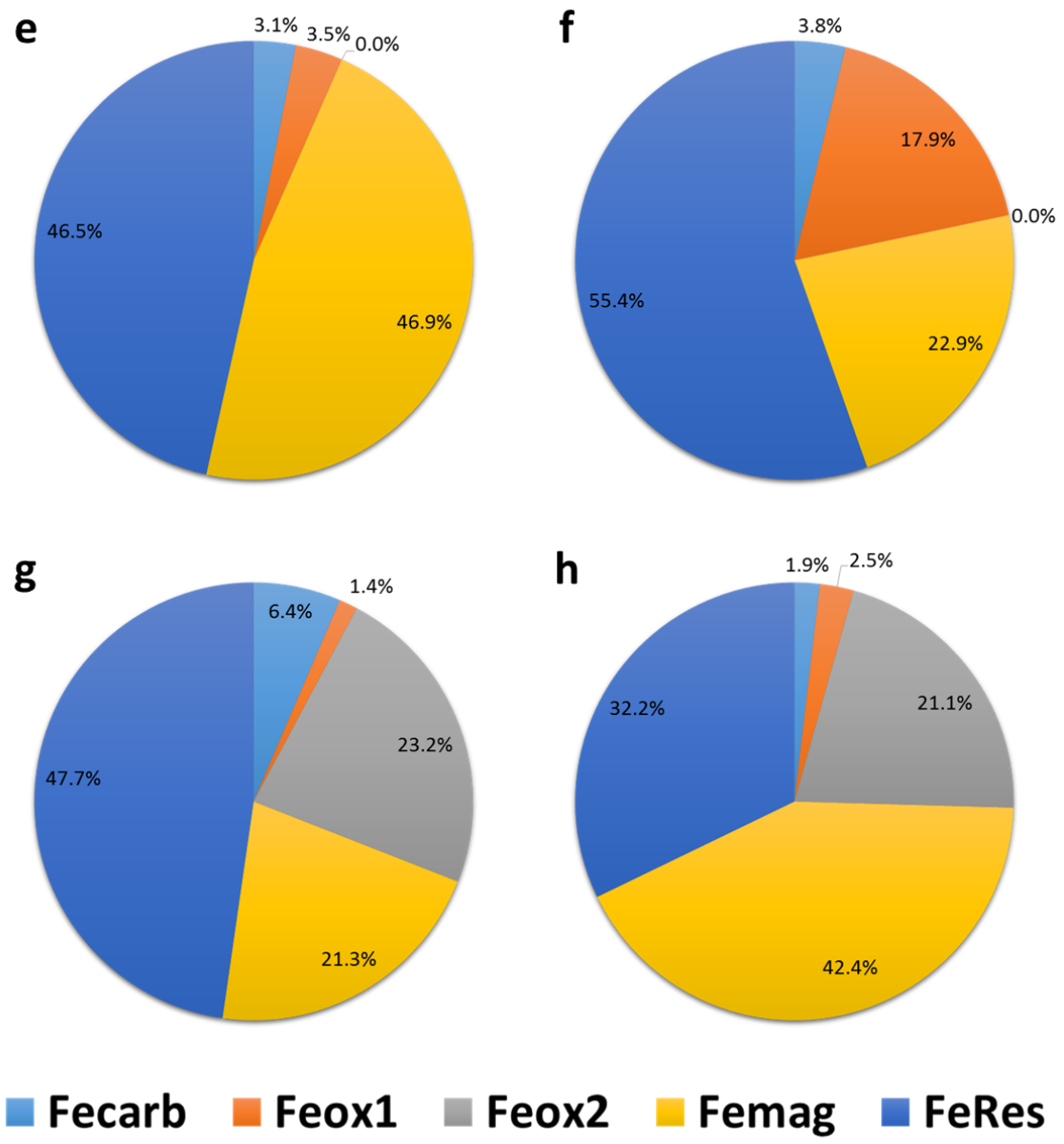

Figure 8.36(cont.) Results of sequential extractions showing distribution of metals within Parys Mt. 2 waste pre- and post- experimentation; e) copper pre- and f) copper post-, g) zinc pre-, h) zinc post-

8.4.4.4. Analysis of DNA Mass

Qubit analysis of mass of DNA extracted from the waste are variable. The pre-experiment waste sample contained 29.4 ng/µl, far greater than the equivalent sample from the Parys Mt.1 waste. Samples of the post-experiment waste all showed large changes in DNA mass from the pre- sample. Two of the samples tested had average DNA masses of 7.54 ng/µl and 10.3 ng/µl, a decrease of ~75% and ~65% from the pre-experimental mass respectively. The third sample contained an average of 46.4 ng/µl of

DNA, a 58% increase in DNA mass compared to the pre- sample. The increased DNA mass correlates with the observations of effluent physicochemical conditions which suggest the proliferation of indigenous microbial communities within the waste. The discrepancy between the samples may be a result of sampling bias or a reflection of the heterogeneous growth of microbial communities within the waste caused by preferential flow paths limiting the pervasiveness of glycerol through the column. Alternatively, the two results showing a depletion in DNA mass may be due to samples being taken from a section of the column where the microbial communities were in decline. There is evidence to suggest this as the total iron concentrations, taken as a proxy for microbial activity, appear to have entered the death phase of microbial growth by the end of experimentation (Figure 8.31).

8.5. Conclusions and Key Points for Subsequent Work

Iron was released from the Lindsay "Live" columns in the effluent at a much greater rate than was observed in its equivalent preliminary test (Appendix 2). Peak total iron was recorded as 206.4 mg/L, a concentration eight times greater than observed within the preliminary study where manure was utilised as the organic carbon source. This suggests that the use of a labile aqueous phase carbon source, such as glycerol, is an effective organic carbon source for stimulating iron reducing microbial communities. Furthermore, it has proven to be more effective at stimulating extensive microbial iron reduction than the use of a solid phase carbon source such as manure. Additionally, this increase in iron-reduction/ mobilisation rate increases the viability of the system for use on a larger scale for potential resource recovery in more metal-rich wastes.

Ferrous and total iron concentrations in effluent from the "Live" column both exhibited patterns typical of microbial growth curves. As well as exhibiting a typical microbial growth curve, the high degree of similarity between the pattern of total iron and ferrous iron effluent concentrations combined with the relative lack of iron within the "Autoclaved" and "Organic Starved" control columns is indicative of the microbially mediated reduction of ferric iron within the columns. Analysis of the microbial communities in the waste and qPCR analysis shows that the addition of glycerol stimulates the proliferation of iron-reducing bacteria such as *Geobacter,*

Anaeromyxobacter, Pelosinus and *Thermincola.* Interestingly it has also resulted in the proliferation of non-iron-reducers such as *Acetobacterium* which produces acetate likely then utilised by DIRM. This hints at the potential for a more complex system where a wider range of DIRM, including those unable to utilise glycerol, are able to respire on the its breakdown products showing an advantage of a more varied indigenous community compared with a low diversity inoculum. A summary of these processes is displayed in Figure 8.37. The "Organic Starved" samples have shown no change in their microbial communities that is of any consequence, while the only iron-reducers identified at relatively high abundances in the "Auto" samples were all sporulators potentially capable of surviving the autoclaving process. When considered together these observations confirm iron-reduction, and the proliferation of DIRM, as the mechanism for the mobilisation of iron observed.

Experimentation with a range of metal-bearing wastes yielded mixed results. The alkaline wastes, Wheal Jane and Red Mud, showed no signs of iron-reduction, associated metal mobilisation or microbial stimulation and proliferation. There is an abundance of published literature regarding bio-reduction and metal extraction from red mud (Vachon *et al.*, 1994; Qu & Lian, 2013; Qu *et al.*, 2013; Qu *et al.*, 2015) and alkaliphilic iron reducers (Fuller *et al.*, 2014; Fuller *et al.*, 2015). However, these studies did not utilize indigenous microbial communities and the failure of the Red Mud, and similarly the Wheal Jane waste, to demonstrate iron reduction may be a reflection of the sterile nature of the waste either naturally or as a result of previous treatment of the wastes.

Due to the lack of positive result of these experiments, with regard to microbial stimulation, further work utilising these wastes would likely yield fewer and less significant results than other potential work and so were not be considered for future work. It was found that both the acidic wastes from Parys Mt. generated effluents with higher iron concentrations than the Lindsay waste when supplied with glycerol. The physicochemical characteristics of the effluents of both wastes also point to extensive bio-reductive dissolution of iron oxyhydroxides & hydroxysulphates within the wastes. However, counterbalancing these positive indications are the lack of microbial growth curve within Parys Mt.1 data, and the reduction of DNA mass post experimentation within the Parys Mt.2 waste. These unexplained results along with the lack of control experiments presented a logical pathway for the next stage of experimentation.

The most compelling reason for the continuation of research into Parys Mt. waste is the mobilisation and redistribution of metals suggested by sequential extraction experimentation and directly observed with regard to lead in Parys Mt.2 effluent.

Despite showing promising signs of potential metal recovery, these results should still be treated with a degree of caution. The data represents only a singular result from preliminary experimentation which is more susceptible to error and sampling bias. To fully understand whether the mobilisation of lead suggested by these results is a reflection of the true situation multiple replications of the experiment and analysis compared against with control samples are needed. To summarise:

- Addition of glycerol to the Lindsay waste sludge has stimulated iron reduction resulting in the mobilisation of iron from the experimental columns and alteration of the mineral composition to metastable iron bearing minerals such as green rusts.

- Microbial community analysis has indicated the proliferation of iron-reducing genera such as *Geobacter*, *Anaeromyxobacter*, *Pelosinus* and *Thermincola*.

- Also having proliferated is the acetogen *Acetobacterium* suggesting a more complex community wherein glycerol breakdown products are further utilised and the resultant acetate is utilised by *Anaeromyxobacter* for iron reduction.

- Red mud and Wheal Jane wastes have not exhibited definitive evidence of microbial iron reduction in response to the addition of glycerol. This limited evidence is insufficient to merit proceeding with experimentation on these wastes.

- Both Parys Mt. waste samples exhibited iron-reduction in response to the introduction of glycerol. In both wastes, effluent iron concentrations were higher than those achieve during the Lindsay waste experimentation.

- Coeval solubilisation of iron and lead was observed in the Parys Mt. 2 waste effluents providing compelling evidence for further investigation into the extraction of metals from this waste.

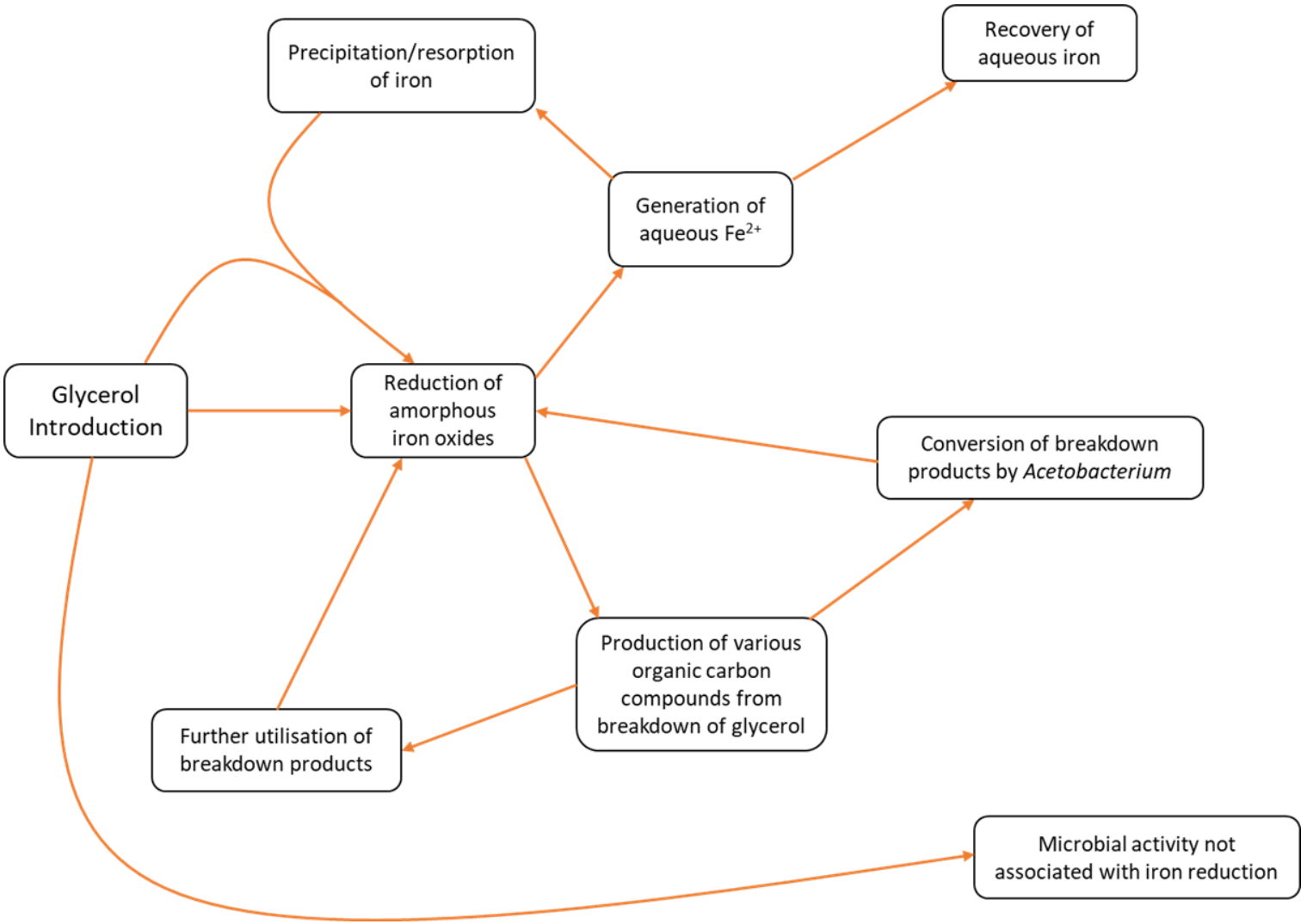

Figure 8.37 Conceptual model of biogeochemical processes occurring within the Lindsay "Live" column as a result of the introduction of glycerol

9. Column Testing – Phase 2

9.1. Introduction

This chapter presents the experimental design and subsequent results of second phase of column testing focusing on the waste from the Parys Mt. 2 case study site. This chapter is split into the following sections:

Section 9.2: Objectives – Outlines the background to the experiment and the key objectives being investigated.

Section 9.3: Experimental Design, Materials and Methods – Describes in detail the specifics of the experimental design, the materials utilised and the analytical methods employed to measure experimental parameters.

Section 9.4: Results and Discussion – Presents, interprets and discusses the results and of column experimentation Parys Mt.2 wastes including in-depth microbial community analysis of pre- and post-experimentation waste.

Section 9.5: Conclusions and Key Points for Subsequent Work

9.2. Objectives

Analysis of results from the first round of column testing demonstrated that the addition of glycerol, as a soluble organic carbon source, to the Lindsay and Parys Mt. mine wastes resulted in the reduction of iron as shown by the elevated ferrous iron within the column effluents. The most significant results from the previous experiment, with respect to metal recovery, were achieved from the preliminary testing with the Parys Mt. 2 waste. Iron concentrations within the effluent were amongst the highest observed throughout all of the experiments and displayed a trend similar to a typical microbial growth curve providing further suggesting of bioreduction (Madigan *et al.*, 2015). Lead concentrations within the effluent increased, and decreased, coevally with iron concentrations demonstrating the correlation between microbial iron-reduction and the release of lead. Also observed was a redistribution of target metals (e.g. lead, copper and zinc) from

more crystalline phases of the waste towards more amorphous, labile iron oxyhydroxide phases suggesting the release of the metals and subsequent sorption to residual minerals.

Due to these results the predominant focus of this subsequent experiment was a continued and more thorough investigation of iron bio-reduction within the Parys Mt. 2 waste. The concentration of organic carbon introduced to the system was increased to determine whether the increase in iron-reduction observed was proportional to the increased concentration of organic carbon. Post-reduction leaching of the wastes was also undertaken to ascertain whether the redistribution of metals occurred.

Extraction of DNA from the waste, both pre- and post-experiment and subsequent genomic sequencing was performed to provide an insight into any changes in the microbial community composition induced by the experimental process.

To summarise, the primary objectives of this stage of experimentation were:

- To study, in greater detail, the effects of glycerol introduction to the Parys Mt. 2 waste and ascertain whether the results of the phase 1 study are an accurate representation of a biogeochemical response.
- Identification of the microbes present within the waste and a qualitative description of changes in the communities as a result of the introduction of glycerol
- Determine changes in the structure of indigenous microbial communities resulting from the experiments. Including whether there were any differences in community structure at differing heights within the experimental columns
- To investigate whether the concentration of glycerol introduced into the system and the rate of iron-reduction are proportional.

9.3. Experimental Design, Materials and Methods

Specific details of the materials, analysis techniques and procedures stated or outlined briefly in this section can be found in Section 5.

9.3.1. Materials

This phase of experimentation represents a refinement of the previous work performed in phase 1. Rather than the multitude of wastes studied previously the only waste utilised within this phase of the experimentation was the Parys Mt. 2 waste. In total, 9 columns containing the Parys Mt. 2 waste only were constructed. As with the Lindsay waste experimentation, "Live", "Autoclaved" and "Organic Starved" columns were constructed. With "Live" denoting columns with unadulterated waste being provided with glycerol, "Autoclaved" denoting columns with waste that was been autoclaved, as described in Section 5.4.1, and provided with glycerol and "Organic Starved" denoting columns containing unadulterated waste with no external source of organic carbon introduced. Each of the experimental columns were performed in triplicate. Before loading into the column, the Parys Mt. 2 waste was homogenised thoroughly, by at least 10min of continuous stirring and "folding" of the wastes as described in Section 5.2.1. After a 1 hour rest period excess surface water was removed before loading into the experimental columns. Samples of each wastes were taken at this point, under aseptic conditions, for mineralogical, chemical and microbiological characterisation of initial conditions.

Glycerol was again used as the aqueous phase organic carbon source though at an increased concentration of 10 mM, equivalent to a loading rate of $\approx 0.45 \times 10^{-3}$ kg/day or 0.05 kg glycerol/kg of dry sludge in total over the 91 days of experimentation. The concentration was increased to study the response to increasing organic carbon concentrations, though the 10 mM concentration was chosen specifically due to its previous use within published DIRM studies (Bridge & Johnson, 1998; Bridge & Johnson, 2000; Li *et al.*, 2009b; Hallberg *et al.*, 2011).

9.3.2. Experimental Design

The physical design of the experiment and methods used to load the waste into the columns remained unchanged from the previous experiments (see Section 8.3.2). The only notable alteration made to the previous experimental setup was the reduction of flow rate from ~0.4 ml/min to ~0.2 ml/min (accurately known) to double the residence

time of the extractant within the column to ~25h, thereby allowing greater time for the utilisation of the glycerol, and its breakdown products, by the microbes within the system. Following the column testing the sludge was extracted from the columns and subsampled for further analysis. Precise masses of wet waste placed within the columns were recorded and samples taken for water content determination, which allowed a calculation of dry mass of sludge within each column. The dry masses of waste in each column are shown in Table 9.1.

Table 9.1 Dry mass of waste within each column at the start of experimentation

Column	Dry Mass (kg)
Live 1	0.685
Live 2	0.725
Live 3	0.679
Autoclaved 1	0.641
Autoclaved 2	0.676
Autoclaved 3	0.635
Org. Starved 1	0.654
Org. Starved 2	0.738
Org. Starved 3	0.684

9.3.3. Sampling and Analytical Methods

Specific details of the analysis techniques and procedures outlined briefly in this section can be found in Section 5.

Columns were operated for a total of 91 days. Effluent samples were collected every other day (other than weekends). As previously, the effluent samples were agitated, whilst still sealed in the collection vessel, to re-suspend any precipitated solids before physicochemical parameters were measured. The pH, EC and Eh were recorded at each sampling point. DO and alkalinity were measured more infrequently, with one measurement of these parameters taken each week. When DO measurements were

required they were given priority to mitigate against equilibration between the effluent and the atmosphere. Colourimetry analysis was used to measure the concentration of ferrous iron within the effluent (see Section 5.3.4). As with DO measurements, ferrous iron measurements were taken as soon as the effluent was exposed to the atmosphere to mitigate against oxidation of the ferrous iron. The concentration of sulphate within the effluent was also measured using colourimetry (see Section 5.3.5). Given the anticipated high concentrations of total iron, suggested by the preliminary experiment, Fe was measured solely by ICP-OES as large dilution was required to allow colorimetric analysis which would impact negatively on precision and accuracy. ICP-OES was also utilized to measure the concentrations of other elements of interest within the effluents. To minimise the impact of precipitated oxides on the walls of the collection vessel drawing metals out of solution, a number of acid washes were undertaken. Approximately every 2 weeks each flask was washed with 10 ml 37% hydrochloric acid to remove precipitated material. The flasks were thoroughly cleaned, washed with deionised water and filled with nitrogen before re-use. The wash acid was diluted and analysed using ICP-OES. The subsequently calculated mass of precipitated metals were added onto the masses extracted via the effluent to give accurate extraction rates. The elements analysed for by ICP-OES were; iron, zinc, lead, aluminium, copper, arsenic, nickel and sulphur

Before post-experiment samples were taken, the columns were sealed and placed within a -80°C freezer for 48h. After this, the columns were cut, using a hand saw, into 3 equal sized cylinders representing the upper, middle and lower portions of the column (Figure 9.1). This procedure was performed under aseptic conditions. Saw blades used to dissect the columns were thoroughly cleaned and autoclaved after each use to minimise the risk of microbial cross-contamination both spatially within columns and between various columns. Once the cylinders were cut they were placed on sterilised aluminium foil and left to thaw slightly within a laminar flow cabinet. Once the samples had partially thawed, sub-samples were taken using modified sterile plastic syringes to remove discrete samples for microbial analysis following the method described by Parkes *et al.* (1995) (Figure 9.2). Three sub-samples were taken from each cylinder, and by using a predetermined reference point on the columns samples from the upper, middle and lower portions of each column could be directly compared to allow vertical

as well as horizontal variations in microbial communities to be analysed. Again, this was performed under aseptic conditions. These sub-samples were returned to the -80°C freezer until required for analysis. The remainder of the waste from the cylinders was then placed in a single container and homogenised before further sub-samples of the waste were taken for mineralogical and chemical analysis. The sub-samples and the remainder of the waste were returned to the freezer until required for analysis.

Pre- and post-experiment samples of each waste were subjected to total digest, XRD and sequential extraction analysis (see Sections 5.2.4, 5.2.8 & 5.2.9 respectively). Post-experiment samples were dried via freeze-drying (Edwards Freeze Dryer Modulyo) as opposed to conventional drying in an oven. This was to minimise the loss of metastable, oxygen sensitive minerals such as green-rusts (Lewis, 1997; Schwertmann & Cornell, 2000) that were observed in the previous experiments. This was critical to return data that was representative of the waste and conditions whilst in-situ within the columns rather than after any secondary reactions as a result of interaction with the atmosphere. The fractions targeted by the sequential extraction were; water soluble phase (Di_{wat}) carbonate associated iron (Fe_{carb}); easily reducible oxides (Fe_{ox1}) e.g. ferrihydrite; reducible oxides (Fe_{ox2}) e.g. goethite and haematite; magnetite (Fe_{mag}); and residual fractions (Fe_{res}). The addition of an initial deionised water extraction, to the procedure used in phase 1, was to distinguish between water soluble cations and the Fe_{carb} phase.

Figure 9.1 Dissection of frozen experimental column into 3 cylinders of waste material before sub sampling for microbiological analysis

Figure 9.2 Sampling of part-frozen waste with modified syringe for microbial analysis

A greater amount of microbiological analysis of the wastes was undertaken than in previous experiments. Alongside the DNA extraction, "Qubit" and qPCR analysis, further analysis comprised PCR amplification and DGGE analysis which was performed to study the relative diversity of the microbial communities within the wastes and qualitatively identify any changes the diversity as a result of experimentation. To identify genera that had been preferentially enriched, selected bands were excised from the DGGE gels, chosen based on their prominence/brightness and location within the gel, and re-amplified and sequenced using the Sanger sequencing technique and analysis described in Sections 5.4.6. Furthermore, DNA extracts were subjected to next generation sequencing by Illumina MiSeq under the protocol described in Section 5.4.7. This was performed to generate a more comprehensive understanding of the diversity of the microbial communities.

9.4. Results and Discussion

9.4.1. Physicochemical Parameters of Effluents

9.4.1.4. "Live" Column Effluents

On the first day of experimentation average total iron concentrations from the Live columns measured ~425 mg/l (Figure 9.3). This is in contrast to the negligible initial concentrations observed in the preliminary Parys Mt.2 experiment, though is similar to what was observed in the Parys Mt. 1 experimentation with high initial concentrations. This average initial concentration is higher than the peak iron concentrations previously observed in either of the preliminary Parys Mt. experiments. Due to the very short amount of time elapsed, it is unlikely the addition of glycerol would have caused this result. This suggests a high degree of variability in the response of the waste to this form of experimentation. This variability is also expressed in the initial concentrations of individual columns. Replicate Live column 2 exhibited negligible initial concentrations, similar to the preliminary study, while replicate Live column 1 produced initial total iron concentrations of 770 mg/L despite thorough homogenisation and validation of this homogenisation via total digest (Appendix 3).

At day 4 of experimentation the average concentration of total iron begins to exhibit the rapid increase in concentration indicative of the rapid proliferation of microbes in response to the addition of an organic carbon source (Figure 9.3). This increase continues until day 21 of experimentation reaching a peak total iron concentration of 1363 mg/L, with an average rate of concentration increase of ~55 mg/L/day. The peak total iron concentration observed within an individual column was also observed on day 21 with 1975 mg/L measured within effluent from replicate column 3. Compared with the peak total iron of 386 mg/L recorded in the preliminary experiment, the average peak total iron concentration observed represents an increase of ~250%. If the individual column peak is considered then this increase is >400%. This suggests that doubling the concentration of glycerol introduced to the system, in conjunction with increased residence time, elicits a large increase in iron concentrations in the column effluents generated. After this peak in total iron concentrations there is a steady decrease in total iron concentration until day 56 of experimentation. During this decrease the average concentration decreases from 1363 mg/L to 367 mg/L representing an average decrease of 28.4 mg/L/day. This may be indicative of declining microbial activity in the wastes. From this point onwards, until day 75, total iron concentrations remained relatively constant at approximately ~350 mg/L, though a period of variability resulting in a further decrease to ~200 mg/L occurred from day 75 through to the end of the experiment. The variability between replicate samples remained high to the point of peak iron concentration. After the peak the variability was seen to decrease as the average iron concentration decreases. In the latter stages of experimentation (day 75 onwards) variability in iron concentrations shows a slight increase.

Whilst the differences in iron generation between the replicate columns may be a reflection of the heterogeneity of the waste, it is likely that differing hydraulics has also had an impact. Preferential flow paths may have reduced the residence time of water in the columns relative to the others, thereby eliciting a lower extraction of iron.

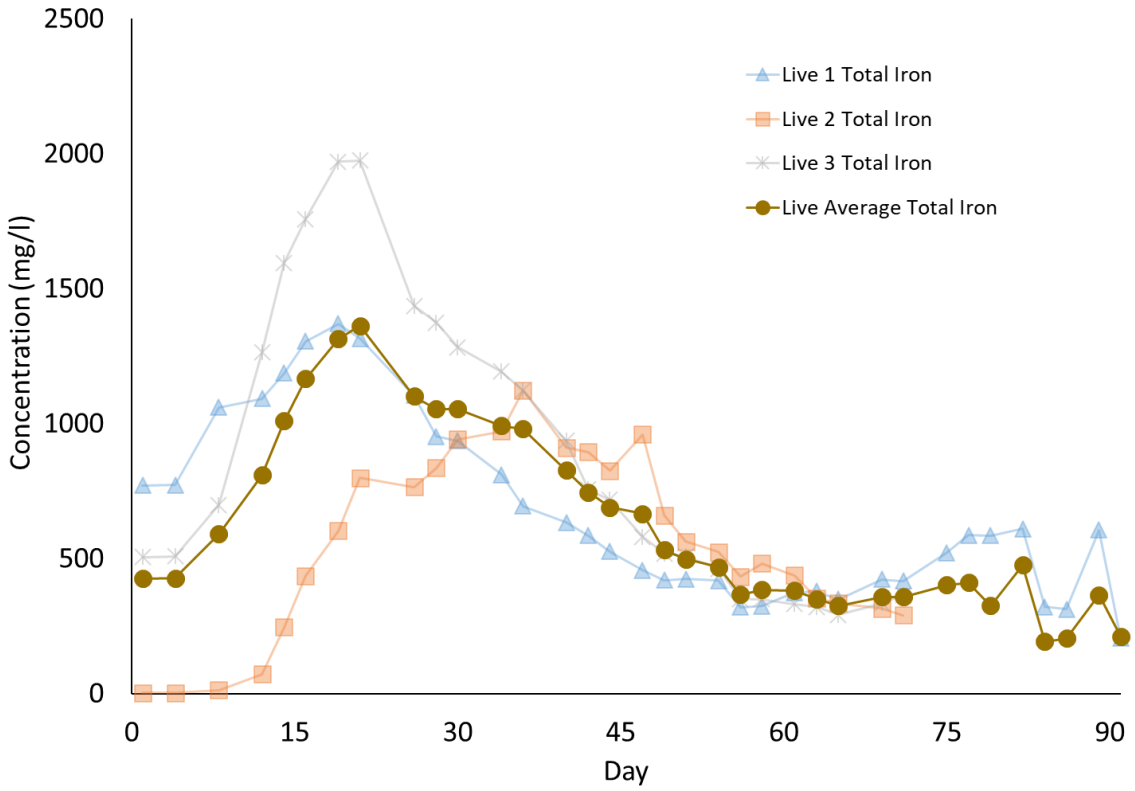

Figure 9.3 Total iron concentrations within "Live" column effluents, and average total iron concentration, throughout the duration of experimentation.

Ferrous iron concentrations within the effluents display a similar pattern to the total iron concentrations, though the timing of significant changes are more varied (Figure 9.4). Initial concentrations of ferrous iron within the effluents were low to negligible, suggesting that the high total iron concentrations observed at the start of experimentation were largely caused by ferric iron entrained in the effluent rather than the generation of ferrous iron. The initial rapid growth phase occurs from day 8 until peaking at 434.7 mg/L on day 40 of experimentation, 19 days later than the total iron peak. This ferrous iron peak is more than double than the peak ferrous iron observed in the preliminary experiment while also greater than the peak total iron recorded in the preliminary experiment.

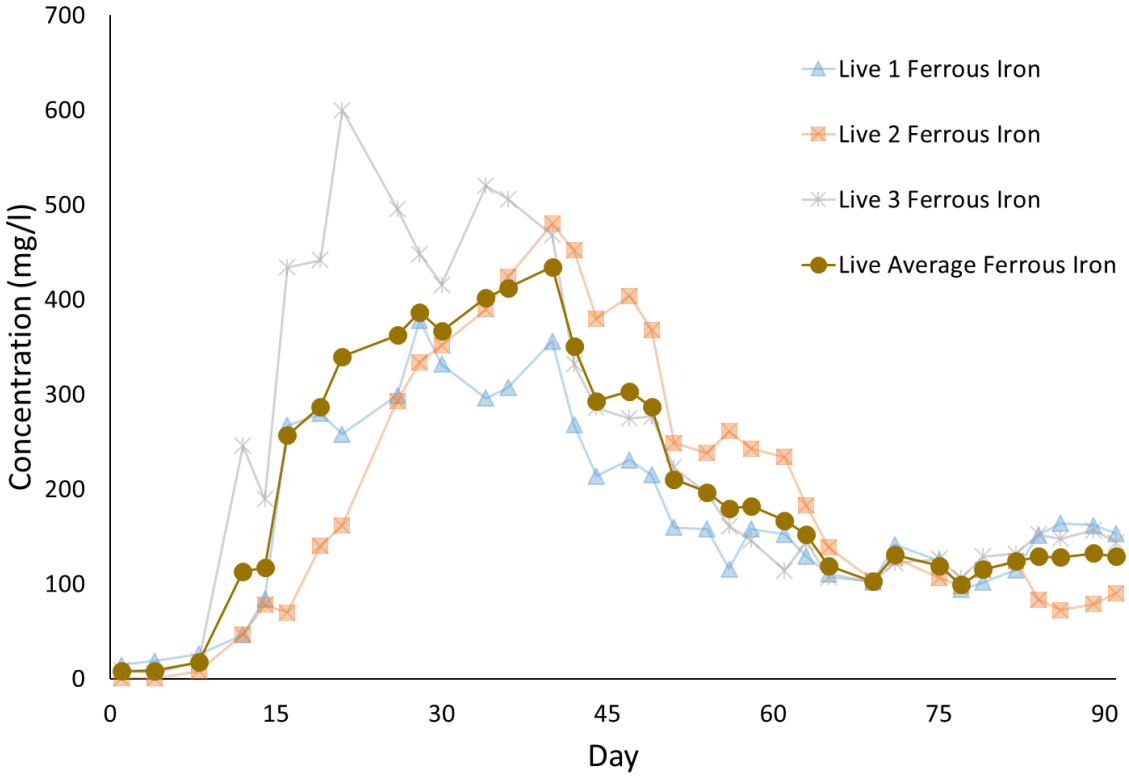

Figure 9.4 Ferrous iron concentrations within "Live" column effluents, and average ferrous iron concentration, throughout the duration of experimentation.

As with the preliminary experiment, chemical equilibrium is not considered to have had a limiting impact on measured concentrations of iron within the effluents. The highest average pH was 6.74 on day 86 of experimentation. This equates to a ferrous iron solubility of 28036 mg/l (assuming $K_{sp} = 8 \times 10^{-16}$ (Stumm & Lee, 1961; Langmuir, 1997)) which is far larger than any measurement of total iron, either averaged or individual column measurements, within the effluents. Given that for large parts of the experiment the pH was substantially lower, thereby facilitating greater iron solubility, the fact that the lowest solubility for ferrous iron was never exceeded suggests that chemical equilibrium is not limiting the recovery of iron from the column.

The lowest average pH was 3.15 on day 1 of experimentation which equates to a maximum ferric iron solubility of 0.03 mg/l (assuming $K_{sp} = 1.58 \times 10^{-39}$ (Langmuir, 1997)). Given pH only increases from this point, and therefore ferric iron solubility decreases, it can be assumed that near negligible concentrations of iron are mobilised from the column in the ferric (Fe^{3+}) oxidation state. The initial "lag" phase demonstrating that entrainment of suspended solids was not a significant factor.

The pH of the effluent changed significantly throughout the experimentation, increasing from an initial pH of 3.15 to a final pH of 6.68 (Figure 9.5). This increase and the pH of the system at the end of experimentation was also seem in the preliminary experiment. However, when the pattern of pH is more closely studied it is evident that there are significant differences between this stage of experimentation and the preliminary. Whereas the pH increase in the preliminary experiment was largely continuous, the changes within this phase of experimentation are more varied. After an initial period of inactivity the pH rapidly increases coevally with the rapid increase in iron concentrations, demonstrating the relationship between these two parameters and suggesting the proliferation of iron-reducing microbes in the system (Ponnamperuma, 1972). This increase results in a minor peak at day 21, as with peak iron, and subsequent decrease before pH increases as a relatively constant rate for the remainder of the experiment. Increasing alkalinity in the effluents is also indicative of the role of microbial activity in causing the increasing pH; as opposed to any dilution/neutralisation effect from the input extractant (Appendix 3). The extent of variability in pH measurements also show similarities to the iron concentration data, with significantly greater variability in the early stages of experimentation compared to the later stages. The increasing pH, as a result of microbial activity, may be partly responsible for the decreasing iron concentrations observed after the initial peak, as iron solubility decreases as the pH tends towards circum-neutral. Though solubility of ferrous iron remains relatively high despite this reduction. Increasingly neutral conditions, and the rapidity of such pH change, are likely to present challenges to the indigenous communities established in the waste, which given the initial low pH of the waste are, logically, likely to be predominantly acidophiles and so potentially may have been adversely impacted by the change to circum-neutral conditions.

The increasing pH also has the effect of limiting the phases of iron oxyhydroxides that are energetically favourable to microbes for reduction. The reduction potentials of iron oxyhydroxides are known to be highly pH dependent with each unit decrease in pH causing a 59 mV increase in the reduction potential. At circum-neutral conditions only the reduction of amorphous iron oxyhydroxides such as ferrihydrite and lepidocrocite are energetically favourable compared to sulphate reduction. However, under acidic conditions the increased reduction potentials result in more crystalline minerals such as

goethite being more energetically favourable to reduce than sulphate reduction (Postma, 1985; Kostka & Nealson, 1995; Thamdrup, 2000). Thus increasing pH removes these crystalline minerals from the reserve of potentially reducible oxides available to the microbes thereby limiting their proliferation, and potentially contributing to the reduction in effluent iron concentrations observed.

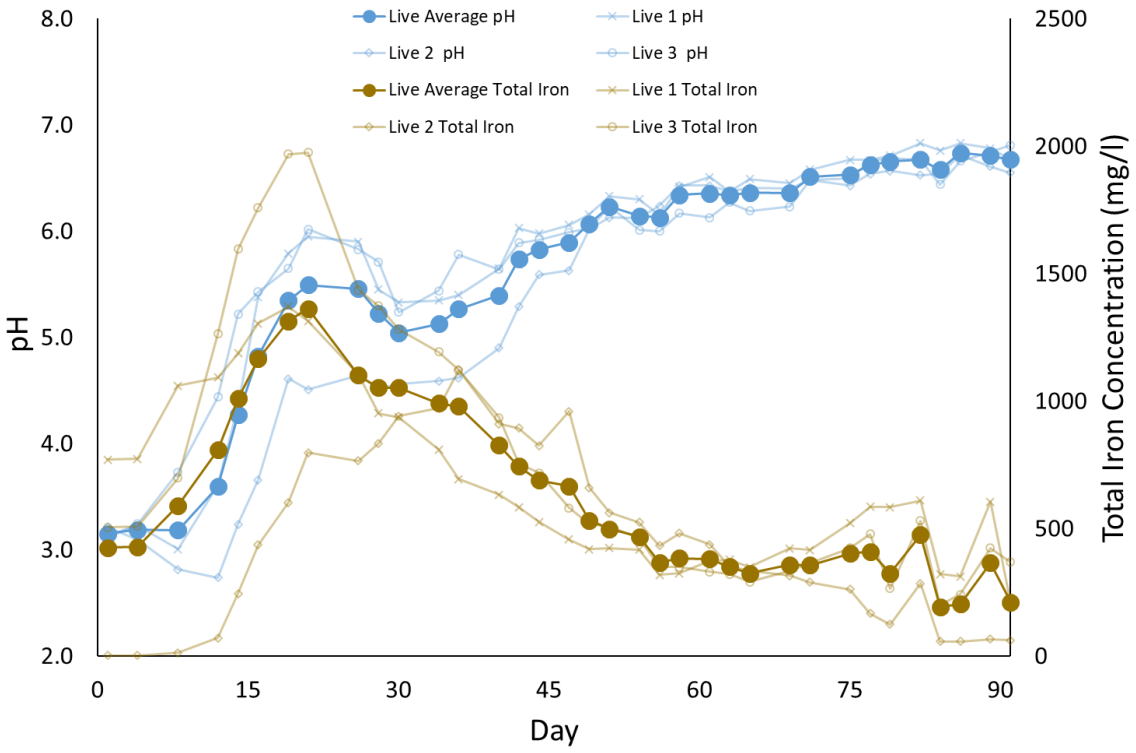

Figure 9.5 Comparison of pH and iron concentrations, including averages, within effluents from Parys Mt. 2 "Live" columns throughout the duration of experimentation

The occurrence of sulphate reduction, and hence the indirect reduction of iron via biogenic hydrogen sulphide (see Section 2.3), within the columns is unclear from the data but other anecdotal evidence of its presence was observed (discussed in Section 9.4.2). Effluent sulphate concentrations show a similar trend to iron concentrations with sulphate appearing to increase, and decrease, in concentration coevally with total iron (Figure 9.6). The lower pH, which favours iron reduction, and high sulphate concentrations in the early stages of the experimentation suggests that microbial sulphate reduction is not the significant driver of iron reduction within the first half of experimentation. In this case the high sulphate concentration and similarity between

the trends is likely the result of the release of sulphate to the aqueous phase during reductive dissolution of iron oxyhydroxides and hydroxysulphates. However, during the 2nd half of experimentation both iron and sulphate concentrations are seen to reduce whilst pH increases to circum-neutral conditions. At this point the balance between iron reduction and sulphate reduction is more ambiguous. It may be the case that iron-reduction is still prevalent and the reduction in sulphate concentrations is a reflection of the slower rate of iron reduction and dissolution. Alternatively, it can be postulated that the decrease in aqueous sulphate concentrations was due to increasing sulphate reduction, given it is more energetically favourable to reduce sulphate (compared with crystalline iron reduction) as a result of the rising pH. Decreasing iron concentrations may potentially be due to either, the slight reduction in ferrous iron solubility at circum-neutral pH, or due to microbial iron reduction being limited to the remnant amorphous iron oxyhydroxides and the reduction of the same iron oxyhydroxides by H_2S produced by sulphate reduction. To gain a more robust understanding of the balance between these two mechanisms further study, with a focus on H_2S generation, would be required (Lovley & Phillips, 1987; Chapelle *et al.*, 2009).

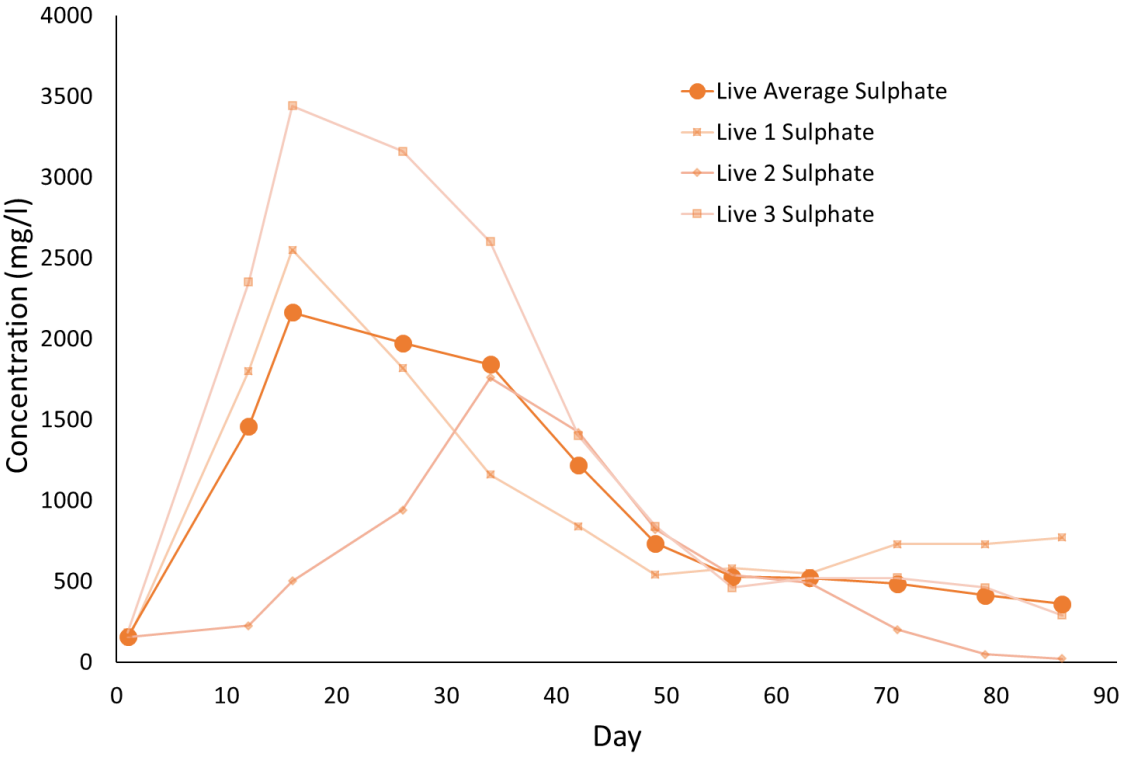

Figure 9.6 Sulphate concentrations within "Live" column effluents, including average sulphate concentration, throughout the duration of experimentation

Eh steadily decreased throughout the experiment, with the rate of decrease slowing towards the later stages of experimentation (Figure 9.7). As with other parameters, the variability in the measured Eh of replicates is far greater in the early stages of the experiment before decreasing with replicates becoming more consistent. By the end of experimentation, where pH was circum-neutral, the Eh has decreased to ~-70 mV, well below the ~100 mV critical Eh suggested by Gotoh & Patrick (1974) for ferric iron reduction at such pH, though is within the -100mV described by (Stumm & Morgan, 1996). Though it is also higher than the critical Eh (-150 mV) for sulphate reduction at circum-neutral conditions (Connell & Patrick, 1968). However, the action of analysing the effluent redox potential exposes the effluent to the atmosphere and as such may increase the redox potential. Therefore, it may be the case that the redox potential within the columns is actually lower than indicated by analysis and potentially within the window for sulphate reduction.

Conductivity of the effluents shows close correlation to the total iron concentration within effluents (Figure 9.8). The conductivity can be seen to initially sharply increase, peaking on day 21, before steadily declining to, and subsequently remaining relatively constant at, ~1200 µS/cm for the remainder of experimentation. The close correlation between the conductivity and the iron concentration within the effluent suggests that iron concentration, along with it counterions e.g. SO_4^{2-}, is the controlling parameter with regards to conductivity and other metals/ions in the effluent impart only minor influence. DO within the effluents was initially high, a reflection of the expulsion of oxygen from the column, but soon dropped below 1 mg/L and remained below this for the remainder of experimentation indicating anaerobic conditions (Appendix 3).

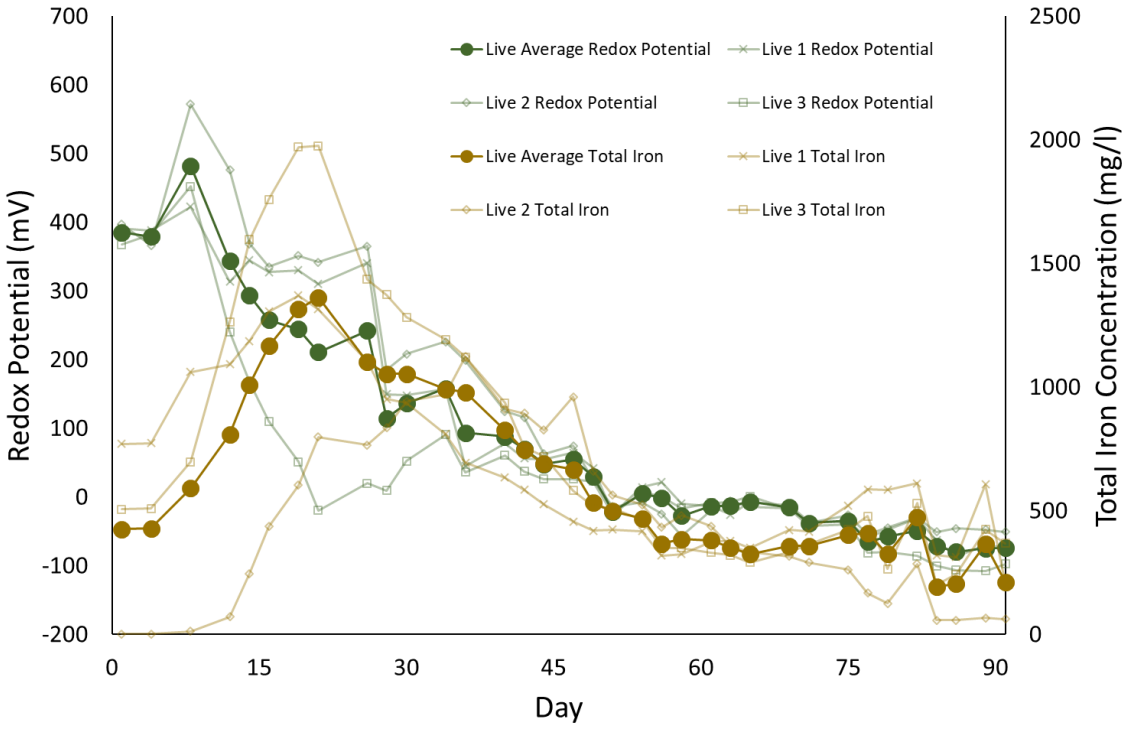

Figure 9.7 Comparison of redox potential and iron concentrations, including averages, within effluents from Parys Mt. 2 "Live" columns throughout the duration of experimentation

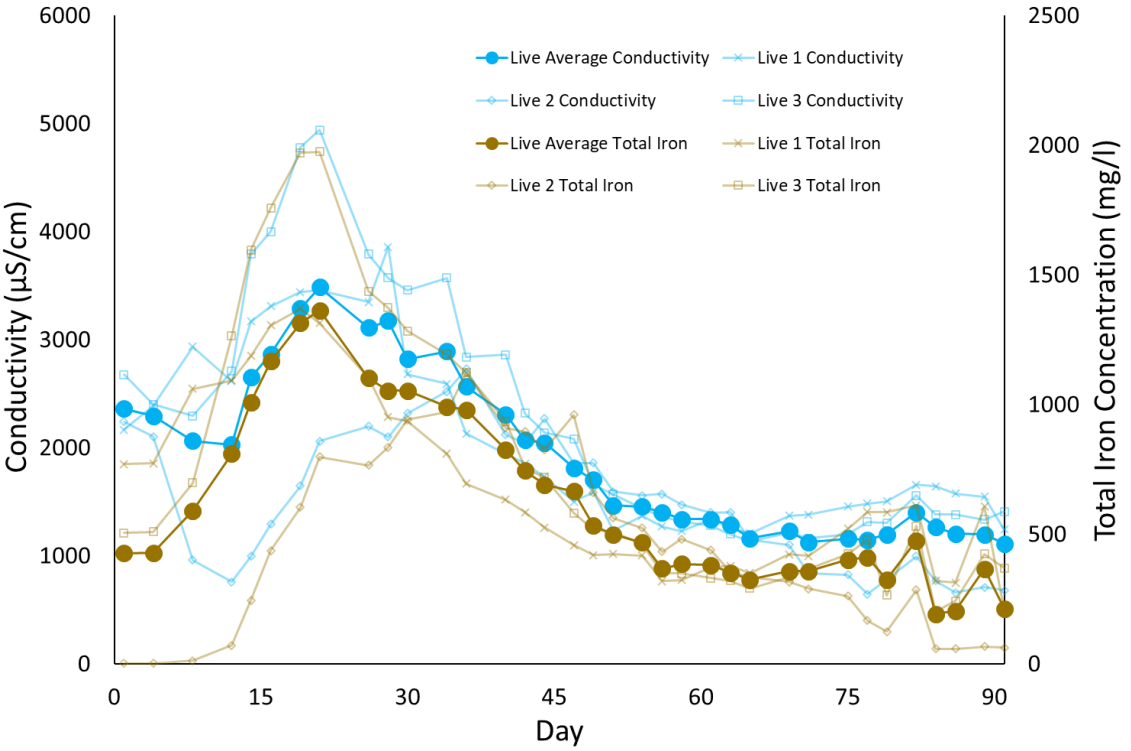

Figure 9.8 Comparison of conductivity and iron concentrations, including averages, within effluents from Parys Mt. 2 "Live" columns throughout the duration of experimentation

At the end of experimentation an average of 6.8% of iron had been removed from the columns. This is 1.96 times greater than the recovery rate of the preliminary experiment, suggesting that doubling of the organic carbon concentration fed into the waste has doubled iron recovery rates. Though this experiment was run for 16 days longer than the previous experiment. At day 75 an average of 5.9% of iron had been recovered representing a recovery 1.73 times greater than the previous experiment with double the glycerol and an increased residency time. It appears likely that, despite significantly higher peak concentrations compared to the preliminary tests, iron recovery was limited by the rapid decline in iron concentrations post-peak iron. An average of 3.1%, 0.3% and 0.1% of total zinc, copper and lead respectively were recovered from the Autoclaved columns. The majority of zinc, and copper especially, was recovered in the first few weeks of experimentation and can be largely attributed to “wash-off” of water soluble or weakly sorbed zinc/copper within the waste. No correlation between the concentration of metal and iron concentrations, expected if iron reduction is causing associated metal release, is suggested from the data, supporting the “wash-off” theory (Figure 9.9b&c). Lead, despite having a very low recovery, shows a degree of correlation with the iron concentrations in the effluent, as in the preliminary study of this waste. Concentrations of lead within the effluents can be seen to rise briefly at approximately day 14-16 before declining at a similar rate to the decline in iron concentrations before maintaining a constant concentration coevally with the steady state phase of iron concentrations, though it should be noted that the only replicate column to display a sharp increase in effluent lead concentration was “Live” replicate column 2 (Figure 9.9a). The similarity between these trends is not as pronounced as in the preliminary study data; with a high degree of variability in the data over the first month.

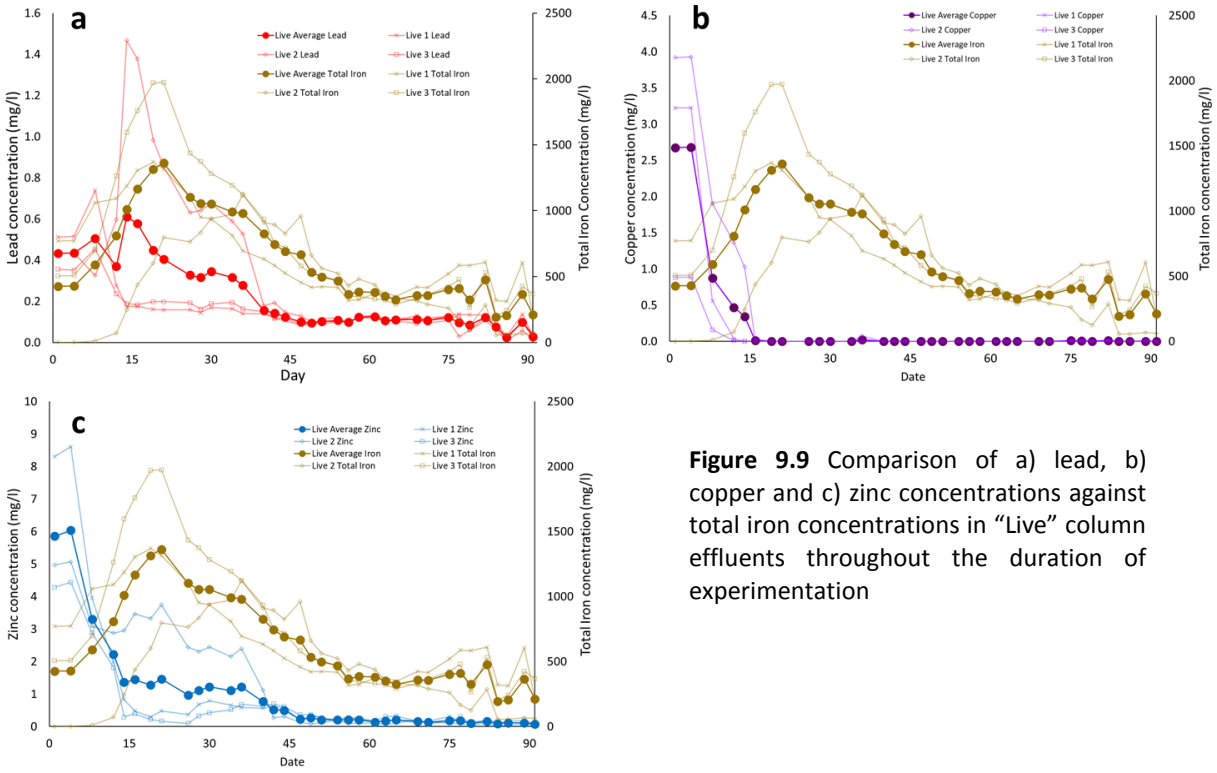

Figure 9.9 Comparison of a) lead, b) copper and c) zinc concentrations against total iron concentrations in "Live" column effluents throughout the duration of experimentation

9.4.1.5. Autoclaved Column Effluents

Autoclaving of the Parys Mt. 2 waste appears to have had limited effect on its indigenous microbial community. As can be seen in (Figure 9.10), total iron concentrations are initially seen to remain constant, at ~340 mg/L, for approximately 14 days before increasing sharply. A similar pattern is seen in the ferrous iron concentrations with low concentrations of ~10-14 mg/L recorded until concentrations begin to sharply increase from day 12 onwards (Figure 9.11). This "lag phase" is substantially longer than the 4 day equivalent observed in the Live columns suggesting autoclaving has had at a negative effect on the activity of the indigenous microbial communities. After this lag phase both total iron and ferrous iron concentrations began to increase. The rate of increase was lower than that observed in the Live columns; with total iron increasing gradually at an average rate of 27.5 mg/L/day to a peak of 791.0 mg/L on day 44 of the experiment. The highest reading taken from an "Autoclaved" column was 985.9 mg/L recorded on day 44 from replicate column "Autoclaved 2" After this point, total iron concentrations steadily decreased to approximately 150 mg/L at the end of the experiment. Unlike the Live columns, the iron concentration against time curve is much broader, lower and more long lived that the equivalent from the Live columns. Ferrous

iron concentrations against time show a similar pattern to the total iron with a broader curve peaking later in the experiment than the Live column equivalent. Unlike the total iron concentrations, the average peak ferrous iron concentration, of 400.0 mg/L, was far closer to the Live column equivalent (Figure 9.11). This may be a result of a limitation of the effluent collection system with ferrous iron being limited to approximately this concentration by oxidation with residual oxygen within the flask. Iron concentrations appear to display trend similar to a typical microbial growth curve with the initial growth phase, followed by a period of relative stability (lacking in the Live column effluent data) and eventual death phase (Madigan *et al.*, 2015). The solubility of ferrous iron, as in the Live columns, has not limited the recovery of iron from the columns. The lowest calculated ferrous iron solubility was ~56198 mg/l (assuming $K_{sp} = 8 \times 10^{-16}$ (Stumm & Lee, 1961; Langmuir, 1997)), relating to the highest average pH of 6.45. This is substantially higher than any of the measured total iron concentrations, the majority of which were taken when the pH was lower and thus the solubility higher.

Within the previous experiments with Lindsay waste (see Section 8.4.1), an autoclaved column was observed to seemingly "revive" late in the experiment giving the ineffectiveness of autoclaving a precedent within this study. While the failure of autoclaving to fully remove sporulating microbes has been documented in published literature (O'Sullivan *et al.*, 2015). The relatively rapid response of the waste (in the form of iron and other iron release) to the introduction of an organic carbon source might be indicative of sporulating microbes. Failure of the autoclave to function properly can be ruled out by the positive indications given by autoclave indictor tape used. Trends within other physicochemical parameters of the effluent are also indicative of microbial iron reduction. The identity of these surviving microbes are discussed in Section 9.4.3.

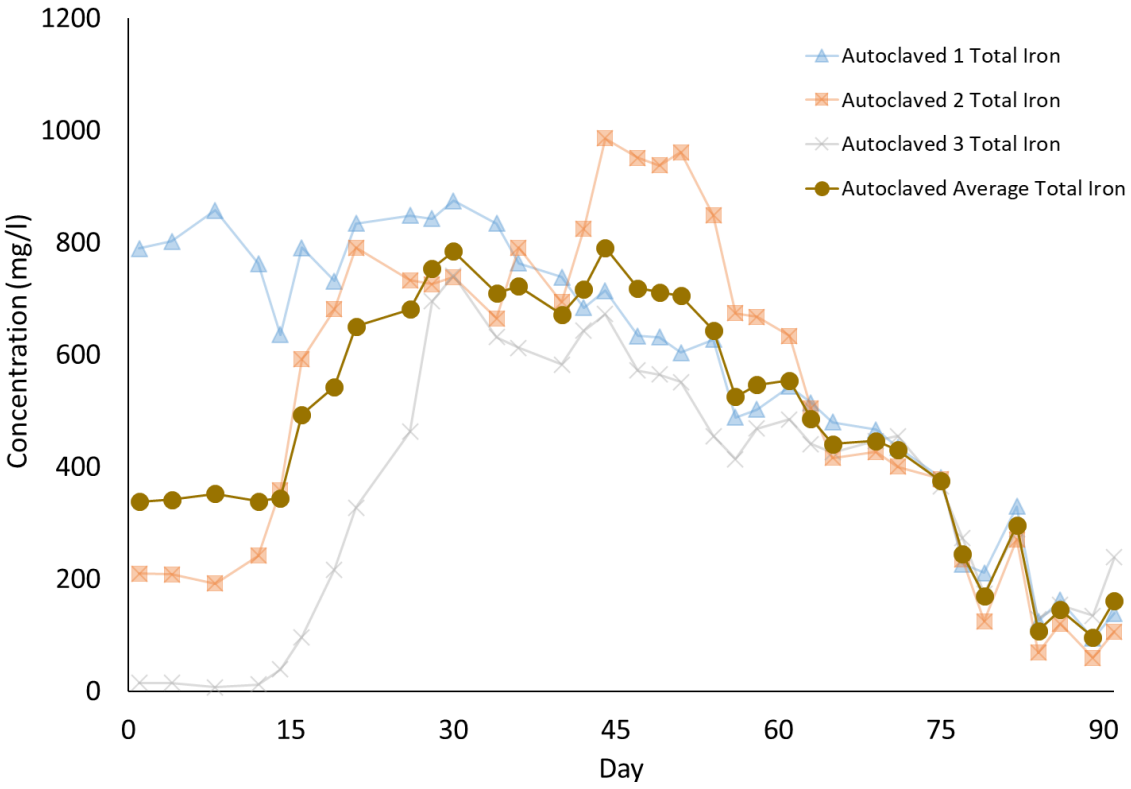

Figure 9.10 Total iron concentrations within "Autoclaved" column effluents, and average total iron concentration, throughout the duration of experimentation.

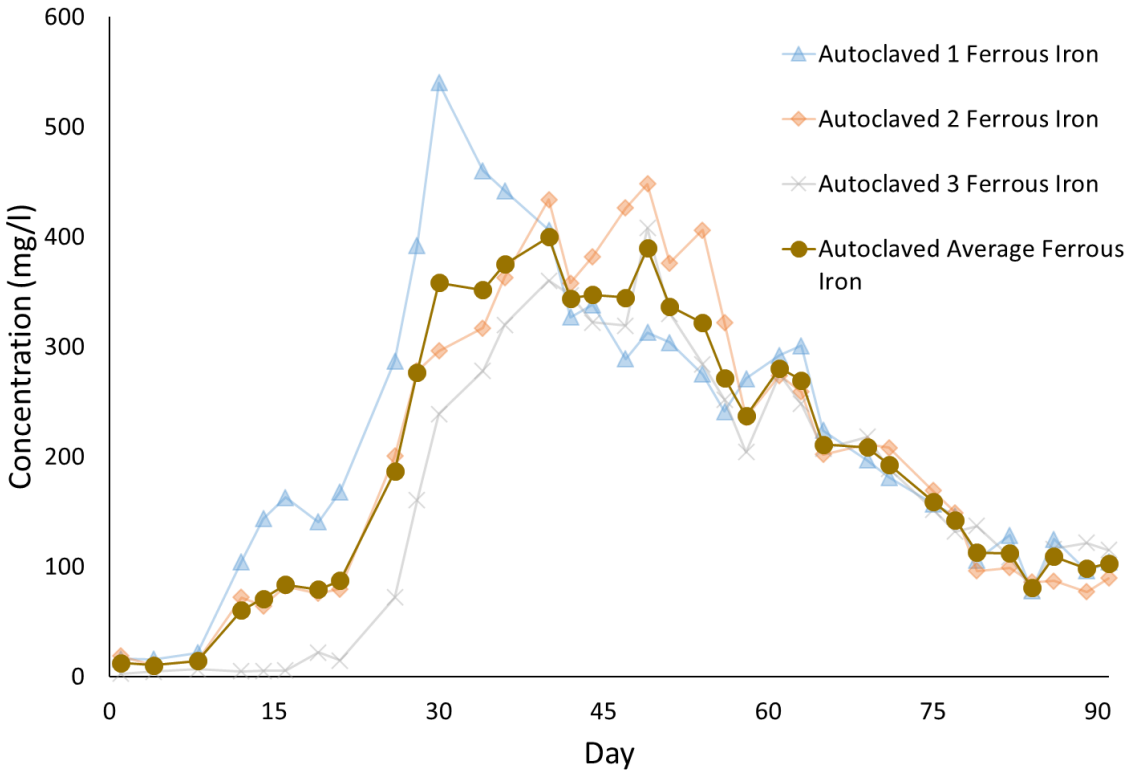

Figure 9.11 Ferrous iron concentrations within "Autoclaved" column effluents, and average ferrous iron concentration, throughout the duration of experimentation.

The pH of the Autoclaved column effluents shows a relatively similar trend to their Live column equivalents (Figure 9.12). The pH is seen to remain relatively unchanged for the first 8 days of the experiment; as with the iron concentrations. From this point onwards pH begins to steadily increase coevally with the increase in iron concentrations in the effluents. Between day 8 and day 44, when effluent iron concentrations peaked, the pH rises 2.95 pH units from 2.88 to 5.83. The rate of pH increase then slows significantly, increasing only 0.62 pH units in the remaining 47 days of the experiment. Throughout the experiment alkalinity was also observed to increase (Appendix 3). These trends are indicative of microbial activity within the wastes. By coupling the reduction of iron to the oxidation of organic material iron reducing microbes produce bicarbonate ions which increase the alkalinity, thereby increasing the pH of the system. The significant decrease in the rate of pH increase post-day 44 is likely a reflection of decreasing microbial activity in the columns as also evidenced by the decreasing iron concentrations.

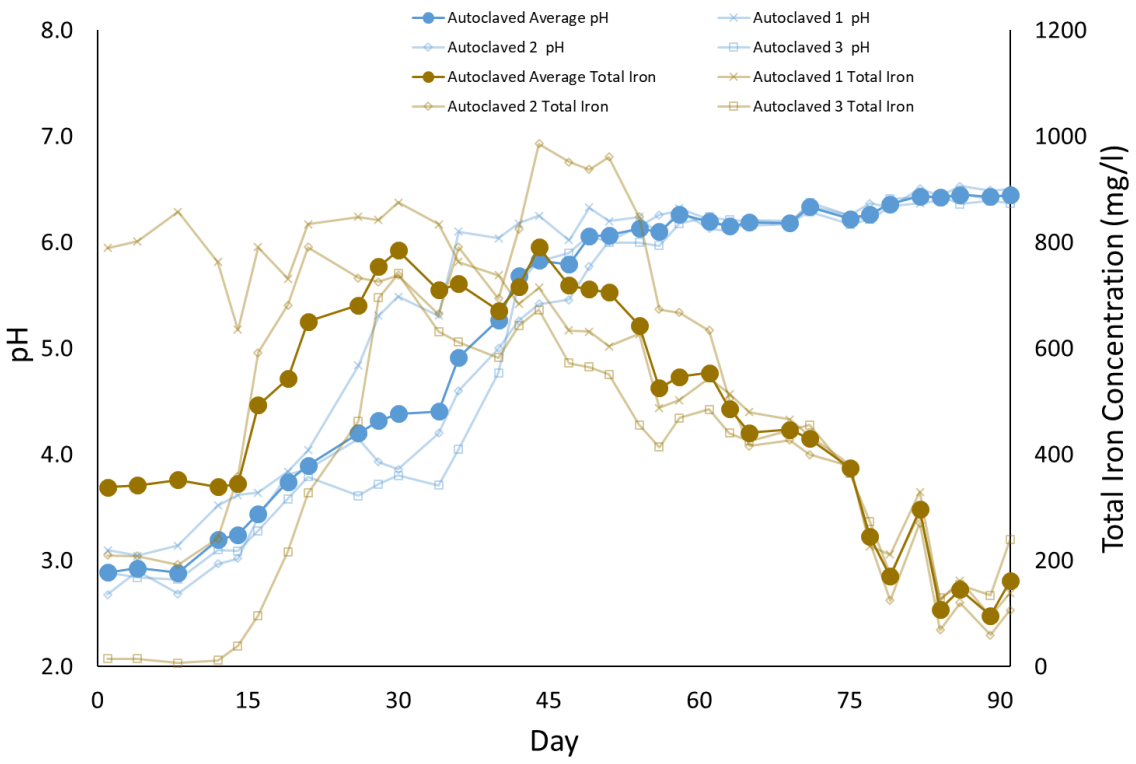

Figure 9.12 Comparison of pH and iron concentrations, including averages, within effluents from Parys Mt. 2 "Autoclaved" columns throughout the duration of experimentation

Aside from the first 12 days of the experiment; where Eh remained constant, Eh steadily decreased throughout the duration of the experiment (Figure 9.13) ending the experiment at ~-70 mV as seen in the Live columns. There are similarities between the Eh of the Live and Autoclaved column effluents, particularly in the later stages of the experimentation. The onset of Eh decrease coincided with the increase in iron concentrations. This is a further indicator of microbial activity and the failure of the autoclaving process to sterilise the waste. DO was observed to rapidly decrease to <1 mg/L and remain there for the duration of experimentation indicating anaerobic conditions, ideal for microbial dissimilative iron reduction (Appendix 3). Conductivity is again seen to closely follow the trend of the total iron concentration, suggesting again that iron is the dominant cation within the effluent (Figure 9.14).

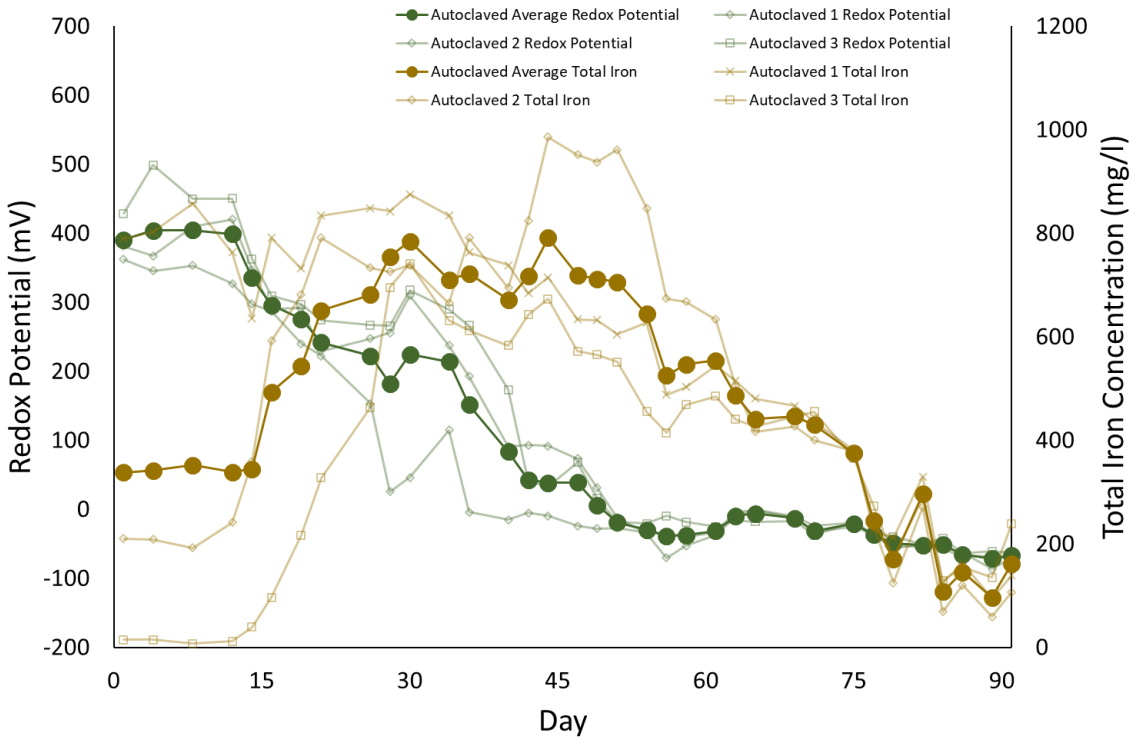

Figure 9.13 Comparison of redox potential and iron concentrations, including averages, within effluents from Parys Mt. 2 "Autoclaved" columns throughout the duration of experimentation

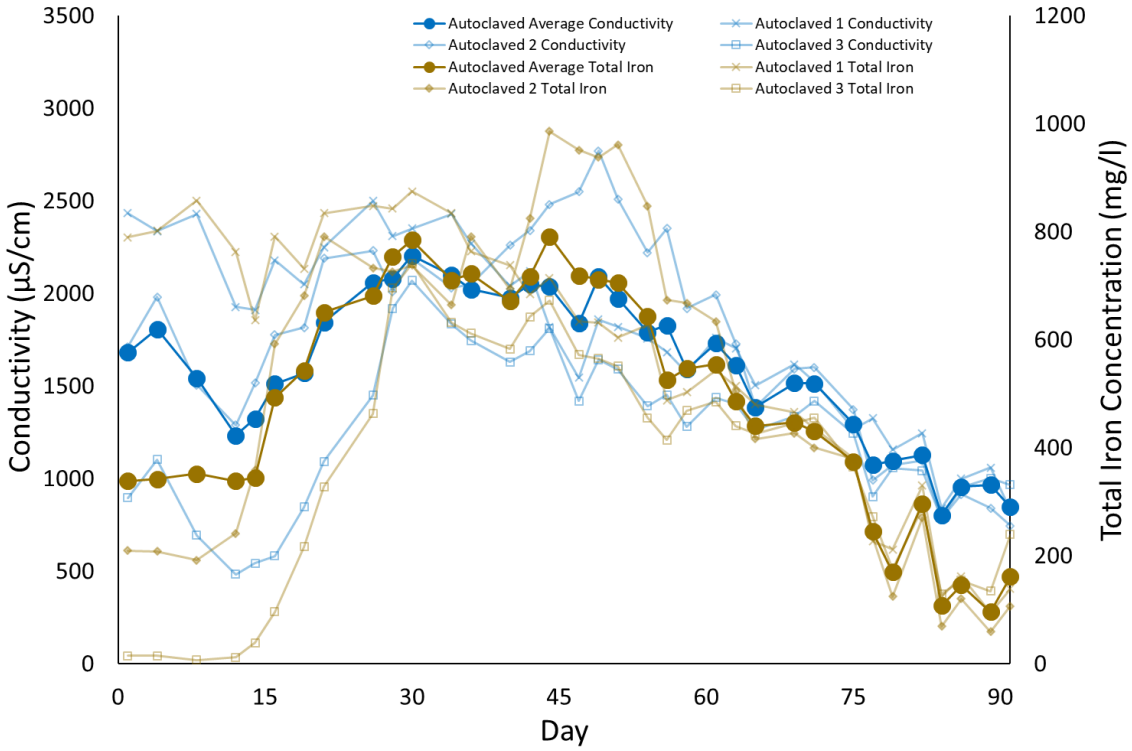

Figure 9.14 Comparison of conductivity and iron concentrations, including averages, within effluents from Parys Mt. 2 "Autoclaved" columns throughout the duration of experimentation

Through the course of the experiment an average of 5.4% of total iron was recovered from the Autoclaved columns. Despite the lower recovery of iron, compared with the Live columns, there were greater recoveries of other metals of interest. 5.1%, 0.8% 0.2% of total zinc, copper and lead, respectively, was recovered through the course of the experiment. As previously the majority of the zinc and copper recovered has been within the early stages of experimentation and rapidly declined to negligible concentrations suggesting "wash-off" (Appendix 3). The consistently elevated "wash-off" concentrations in Autoclaved samples could potentially be an unintentional side-effect of the autoclaving process; as this is the only difference in treatment of the Autoclaved and Live wastes. It is possible that autoclaving has induced the transformation of amorphous ferrihydrite (or similar) to goethite thereby reducing the surface area and its ability to adsorb associated metals (Das *et al.*, 2011).

Effluent lead concentrations display a slight degree of similarity to iron concentrations (Figure 9.15a). After decreasing for 12 days lead concentrations began to increase before peaking at 0.8 mg/L on day 16 before decreasing again and stabilising at

concentrations of approximately 0.1 mg/L for the remainder of the experiment. The peak of lead coincides with the onset of rapidly increasing iron concentrations but fails to increase further as iron concentrations themselves increase. Given that the pH of the effluent was approximately 3.5 at the point of peak lead, it is unlikely that the decrease in lead immediately after is a result of extensive re-sorption to iron oxyhydroxides as at these pH conditions lead cations are typically soluble while the mole % uptake of lead to the surfaces of such minerals is ~10% (Brown Jr. *et al.*, 2008). Despite the high variability in the data in the early stages of the experiment (as is observed with all parameters) it is clear there is a relationship between the iron and lead within the system. Effluent concentrations of zinc and copper again display a "wash-off" trend (Figure 9.15b&c). As with the Live samples, the trend in average effluent sulphate concentrations is similar to the total iron concentration within the Autoclaved effluents with a broad curve peaking at 1200 mg/L at day 42 (Figure 9.16).

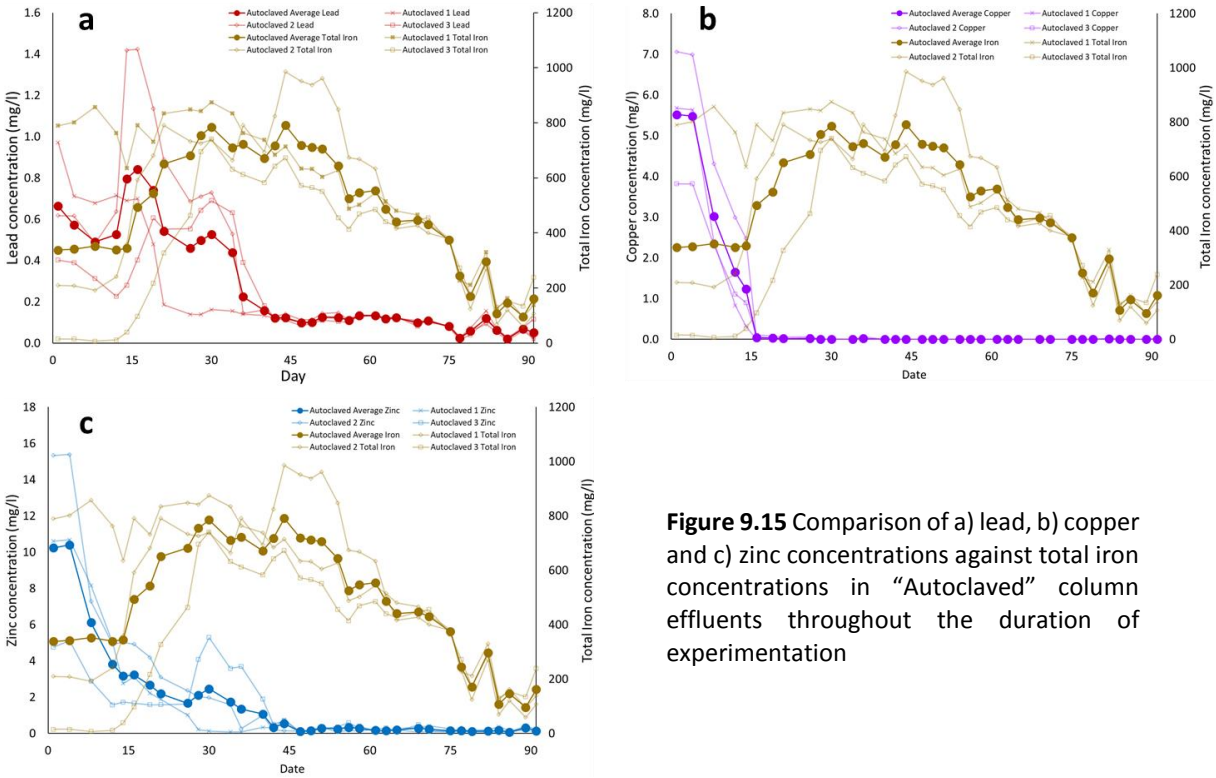

Figure 9.15 Comparison of a) lead, b) copper and c) zinc concentrations against total iron concentrations in "Autoclaved" column effluents throughout the duration of experimentation

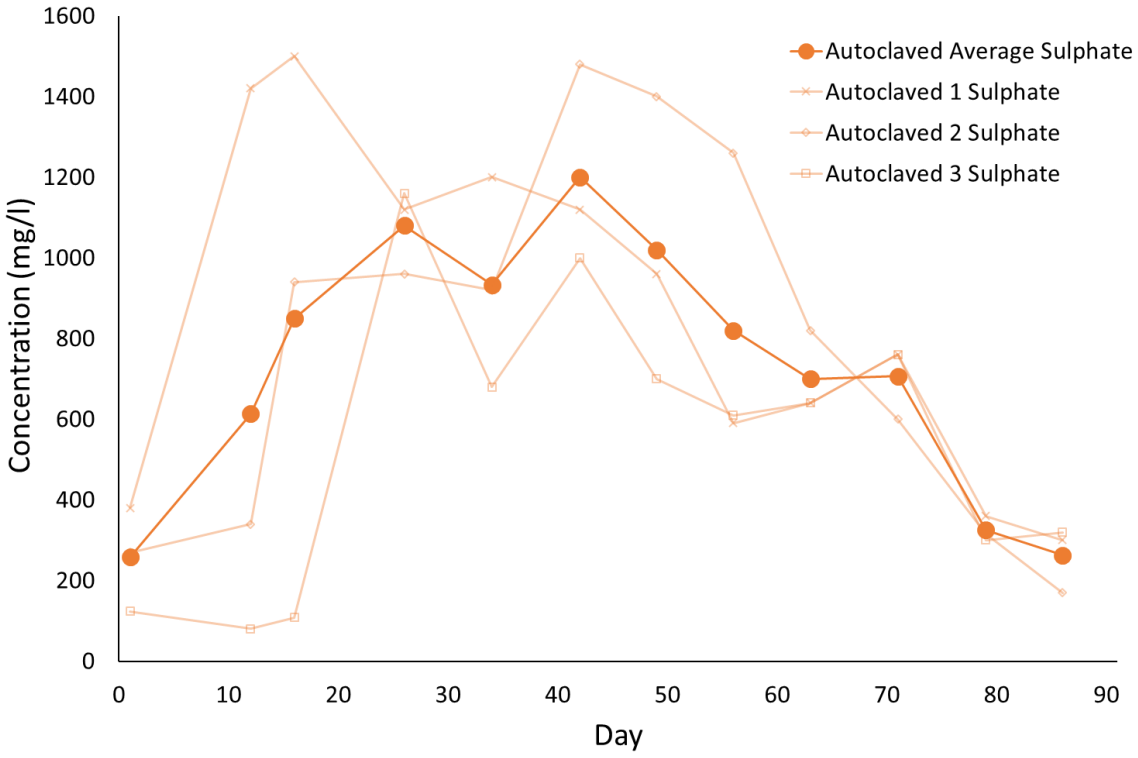

Figure 9.16 Sulphate concentrations within "Autoclaved" column effluents, including average sulphate concentration, throughout the duration of experimentation

9.4.1.6. Organic Starved Column Effluents

The Organic Starved control experiment was, throughout the duration of the experiment, relatively inactive. Concentrations of total and ferrous iron within the effluents decreased as soon as the experimentation began; soon stabilising to approximately 70 mg/L and 30 mg/L respectively for the majority of the experiment (Figure 9.17 & Figure 9.18). As with other experiments and parameters there is a greater variability early in the experiment while there is much greater consistency between the column effluents in the later stages. The lack of any significant increase in iron concentrations again displays the requirement for an externally sourced organic electron donor to stimulate indigenous microbial DIRM communities and thereby the reductive dissolution of iron oxyhydroxides.

pH and Eh remain consistent throughout the experiment averaging approximately 3 pH units and 420 mV ±25 mV respectively (Figure 9.19 & Figure 9.20). Due to the acidic pH, alkalinity remains undetectable throughout the experiment (Appendix 3). Conductivity

follows a similar trend to iron concentrations, as it has in the other experiments (Figure 9.21). Sulphate was lower than observed in the other experimental columns, consistently at concentrations of ~240 mg/L (Figure 9.22). This demonstrates that the sulphate released in the other experimental columns has been released as a result of the dissolution of iron minerals. This would either be as sulphate sorbed to mineral surfaces or the dissolution of iron hydroxysulphates such as jarosites. The lack of any significant change to these parameters is another indication that significant microbially induced iron-reduction, or sulphate-reduction, has not occurred within the columns. DO rapidly dropped to negligible concentrations, reflective of the anaerobic conditions within the columns (Appendix 3).

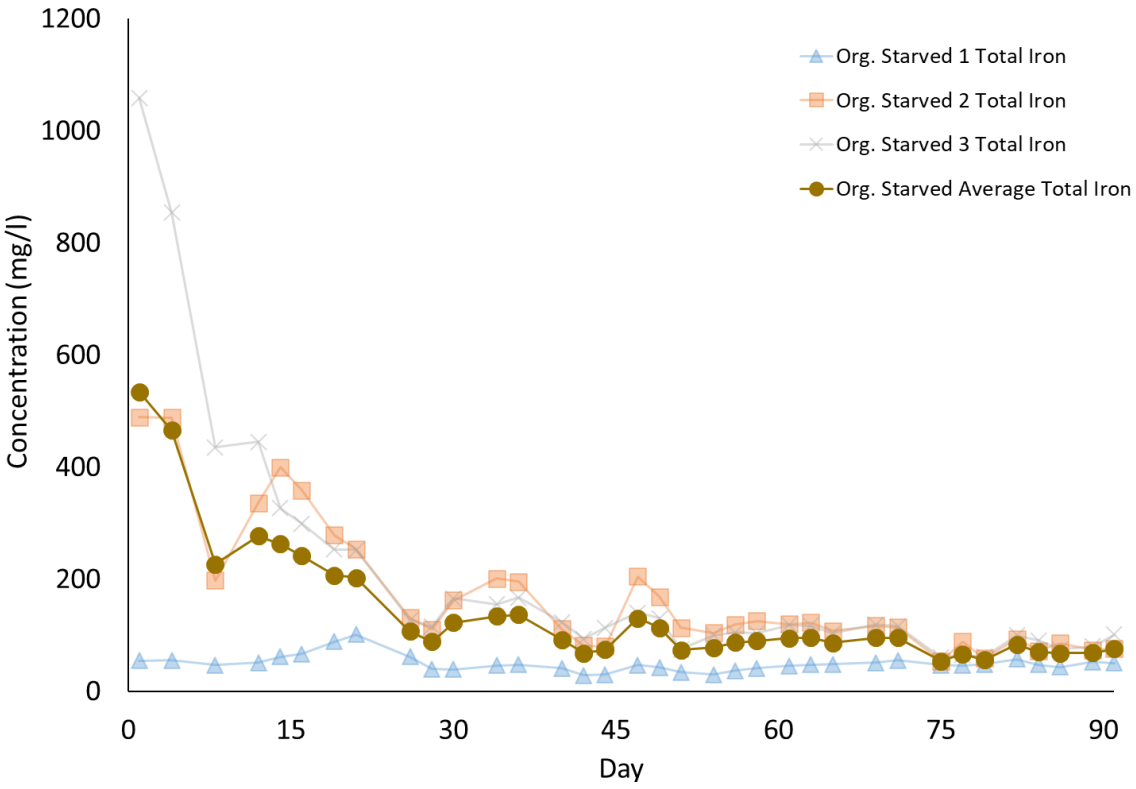

Figure 9.17 Total iron concentrations within "Organic Starved" column effluents, and average total iron concentration, throughout the duration of experimentation.

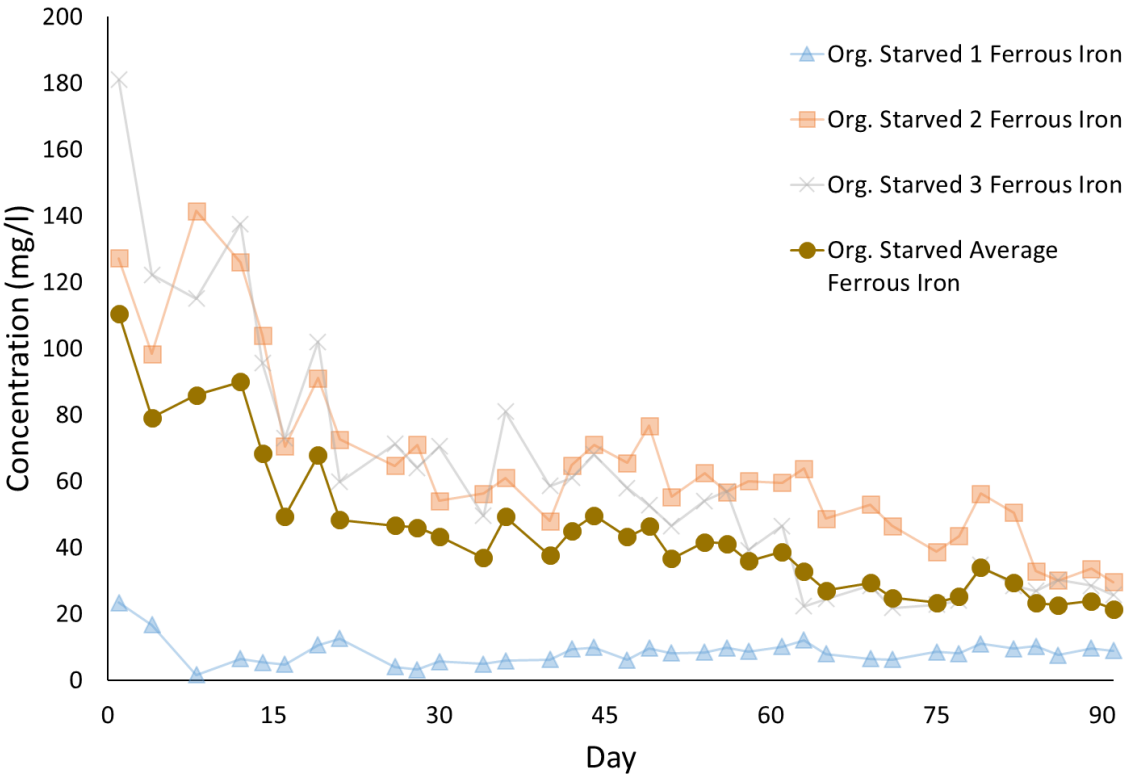

Figure 9.18 Ferrous iron concentrations within "Organic Starved" column effluents, and average ferrous iron concentration, throughout the duration of experimentation.

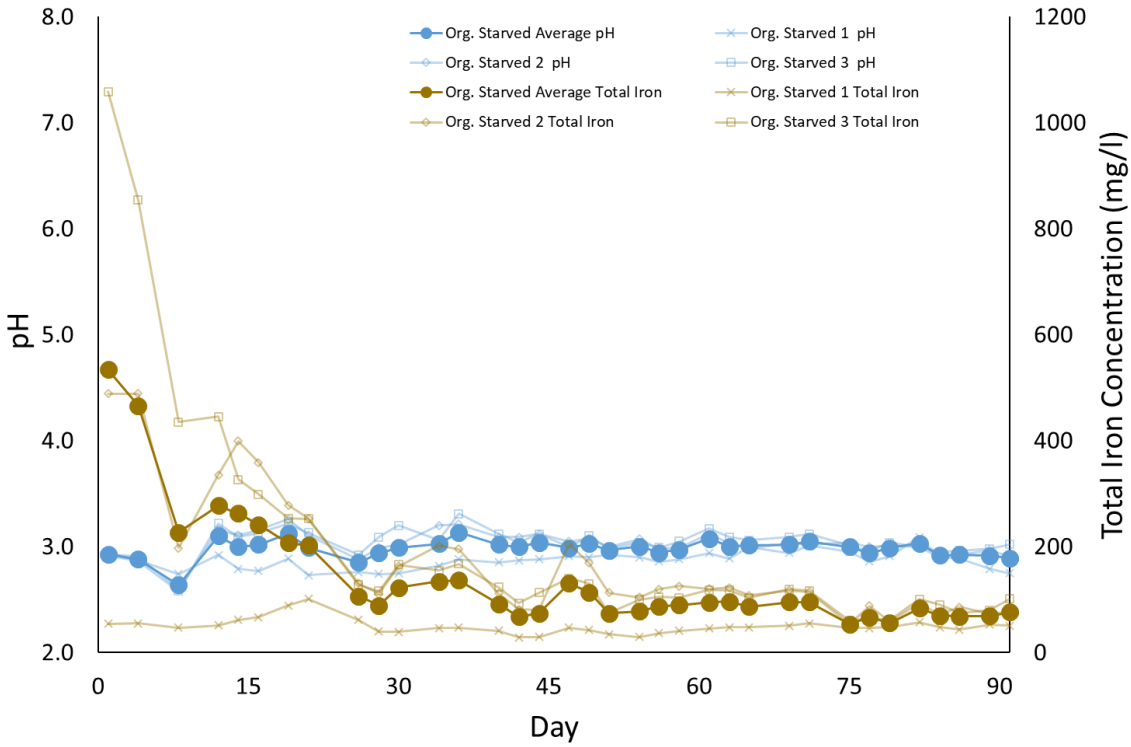

Figure 9.19 Comparison of pH and iron concentrations, including averages, within effluents from Parys Mt. 2 "Organic Starved" columns throughout the duration of experimentation

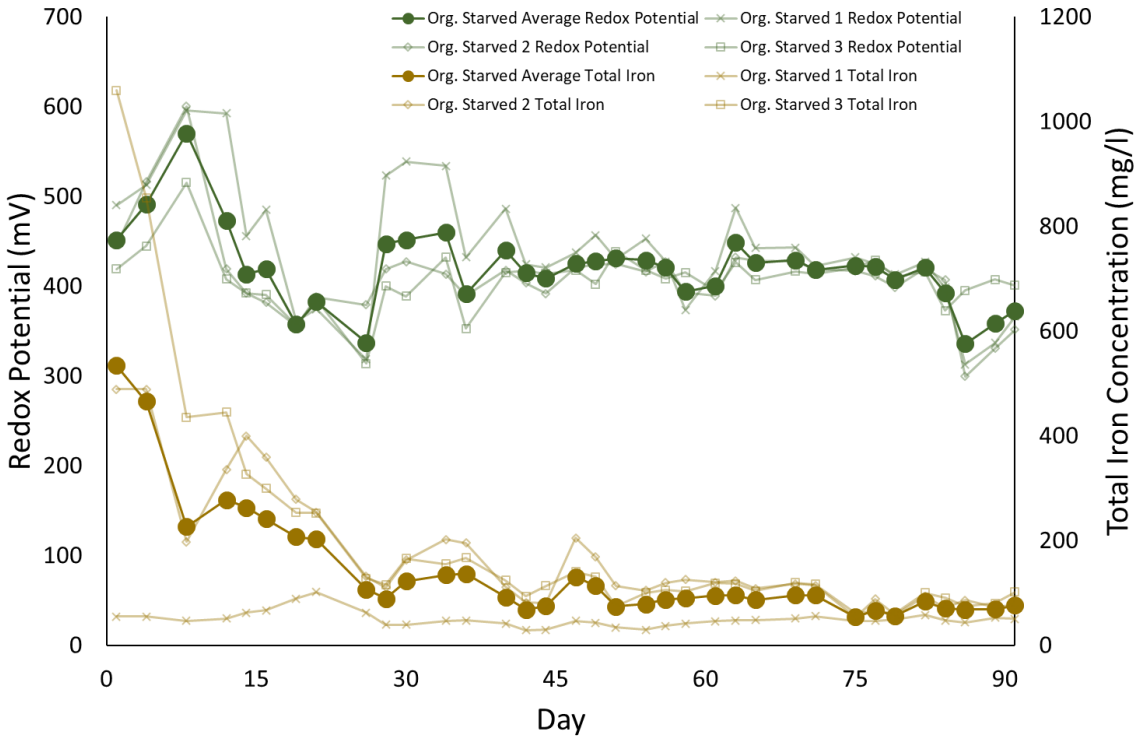

Figure 9.20 Comparison of redox potential and iron concentrations, including averages, within effluents from Parys Mt. 2 "Organic Starved" columns throughout the duration of experimentation

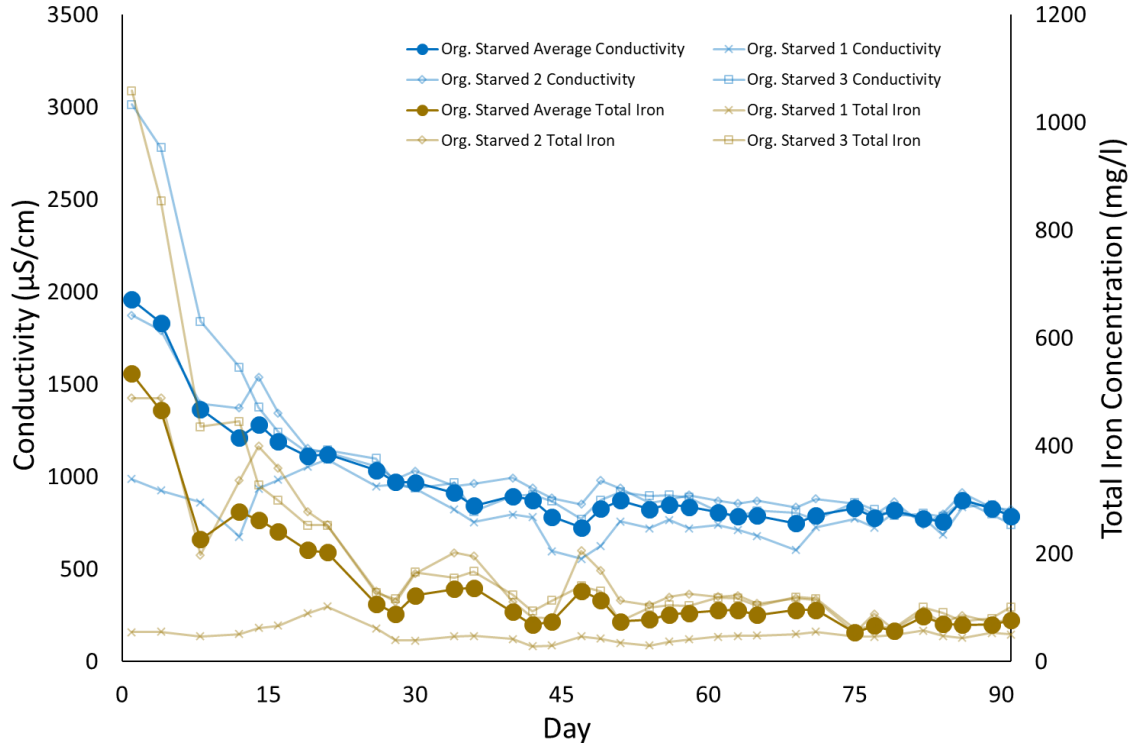

Figure 9.21 Comparison of conductivity and iron concentrations, including averages, within effluents from Parys Mt. 2 "Organic Starved" columns throughout the duration of experimentation

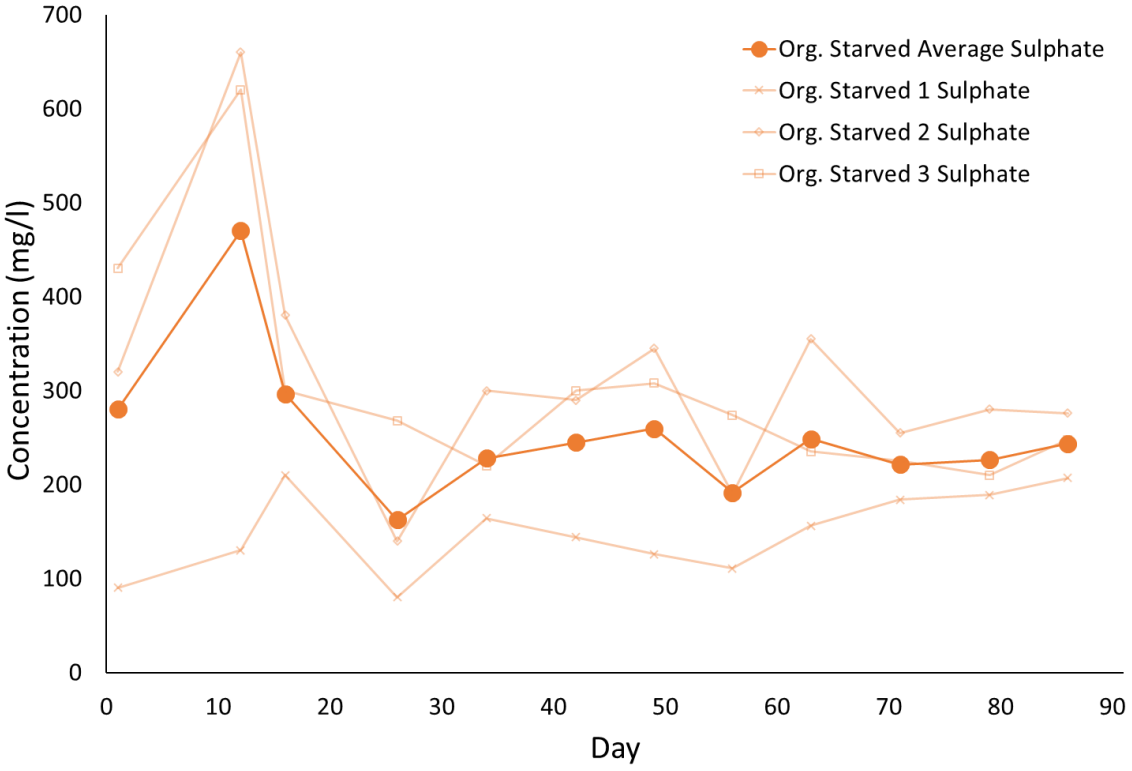

Figure 9.22 Sulphate concentrations within "Organic Starved" column effluents, including average sulphate concentration, throughout the duration of experimentation

An average of 1.6%, 4.7%, 0.7% and 0.1% of iron, zinc, copper and lead were recovered from the columns. With the exception of iron, the recoveries of these metals exceed that achieved from the Live columns. This highlights the failure of the Live columns to extract significant quantities of metals of interest. Zinc and copper concentrations within the column effluents both exhibit the rapidly decreasing concentrations typical of "wash-off" (Figure 9.23). The consistently low zinc and copper recovery from the "Org. Starved" columns demonstrate that the low recoveries of these metals observed in the "Live" and "Autoclaved" columns is not a result of the pH increases observed in the latter two; as pH remained consistently low in the "Org. Starved columns. Lead by contrast remained relatively consistent at ~0.3 mg/L throughout the experiment, though variability increases in the latter half of the experiment; the reverse of the trend observed in all other parameters (Figure 9.23a). The lack of relationship between iron and lead effluent concentrations confirms the assertion that the increased concentrations observed in both the "Live" and "Autoclaved" columns (coeval with increasing iron concentrations) is a consequence of the reductive dissolution of iron hydroxysulphates in the waste. It also supports the theory that the decline in lead within

these effluents is a result of increasing pH; as lead is observed to remain relatively constant in Org. Starved effluents which also exhibit stable pH.

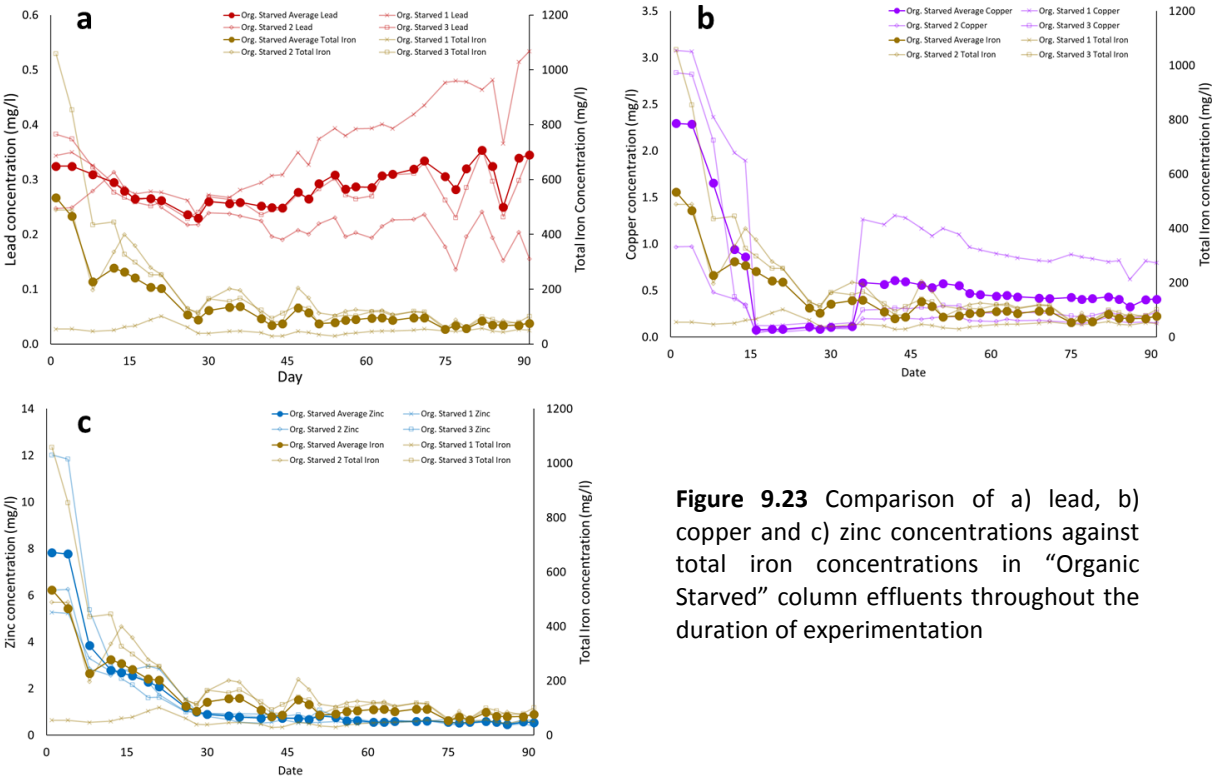

Figure 9.23 Comparison of a) lead, b) copper and c) zinc concentrations against total iron concentrations in "Organic Starved" column effluents throughout the duration of experimentation

The ratios of iron to zinc, copper and lead concentrations in the unadulterated waste are 263:1, 139:1 and 44:1 respectively. Over the course of experimentation, the ratios of these metals recovered via the aqueous phase are substantially smaller than those in the pre-experiment waste. The average Fe:Zn, Fe:Cu and Fe:Pb concentration ratios in the effluents from the "Live" columns are 654:1, 3030:1 and 2857:1 respectively. Similarly, the ratios have decreased to averages of 229:1, 1000:1 and 1786:1, respectively, in the "Autoclaved" effluents. This are slightly higher than those of the "Live" columns but still much lower than observed in the unadulterated waste. The cause of these lower ratios of iron to other metals is not clear. It is possible that the iron hydroxysulphates being targeted for microbial reduction are more deficient in associated metals relative to other non-targeted minerals. Alternately, the associated metals may be being released at a similar ratio to that within the solids but the later loss

of these metals to precipitation/resorption has skewed the ratios to reflect the lower recoveries.

The lower ratios are not necessarily a negative result. Whilst the aim of the study it to extract metals in the aqueous phase, the preferential removal of iron has two potential benefits. Firstly, the generation of a purer form of iron has a potential use as a method of iron pigment production from mine wastes (Ryan *et al.*, 2017). Secondly, by removing iron from the waste there is a concentration effect on the remnant target metals within the residual waste.

9.4.2. Visual, Chemical and Mineralogical Analysis

Whilst the data obtained from the analysis of the effluents was inconclusive with regards to if or when sulphate reduction occurred, anecdotal visual and olfactory evidence of sulphate reduction was noted. The effluents from the Live and Autoclaved columns were initially clear and colourless. Over time these effluents changed to a brown colour before transitioning to a dark black colour causing the effluent to become opaque. Along with the change of colour of the effluent a fine black precipitate also formed, while the rubber bung sealing the vessel was also discoloured (despite no contact with the effluent) suggesting the presence of a reactive substance (Figure 9.24). Along with the colour change, a strong distinct "H_2S" smell was noted within the effluents. The colour change and odour from each column occurred at different stages in the experiment but in all columns they occurred after peak total iron concentrations were observed. Neither the black colouration nor the hydrogen sulphide smell was observed in the Organic Starved effluents. Neither of these observations were made during the preliminary testing of either Parys Mt. waste and is potentially a result of the increased glycerol concentration within the extractant.

These observations confirm that microbial sulphate reduction has occurred within the columns resulting in the production of hydrogen sulphide. It is postulated that a proportion of the hydrogen sulphide has abiotically reacted with iron oxyhydroxides present within the wastes or precipitated within the effluent collection vessel (Santos Afonso & Stumm, 1992; Melton *et al.*, 2014) to form black iron sulphide minerals such

as iron monosulphide (FeS) and mackinawite, also referred to as acid-volatile sulphides (Morse *et al.*, 1987). These minerals are typically metastable and nanoscale and susceptible to rapid oxidation and as such are difficult to identify using XRD (Rickard & Morse, 2005). The presence of magnetite, as a result of sulphate green rust transformation, was ruled out as the black precipitate displayed no attraction to a magnet. Furthermore, Sumoondur *et al.* (2008) suggests that sulphate green rusts are stable at pH7 and will only transform to magnetite at pH values higher than those observed within the effluents.

Figure 9.24 Black colouration of effluent, precipitate in collection vessel and staining on rubber bung

When the frozen columns were cut open at the end of the experiment a significant change in colour of the waste was apparent. The previously orange-light brown waste had largely changed to a more olive-khaki green colour. Figure 9.25 shows this colour change but also highlights the variability in colour throughout the column. The outside of the column which has been heavily disturbed by the action of the saw during column

dissection, appears largely dark green and relatively uniform. However, in areas not affected by the sawing action the colour can be seen to be more variable with regions in the centre of the column exhibiting a lighter brown colouration. This is a clear visual demonstration of the impact of preferential flow paths within the waste with discrete areas undergoing less extensive bio-reduction, which would inherently limit the amount to target metal that could be extracted by the flow of extractant.

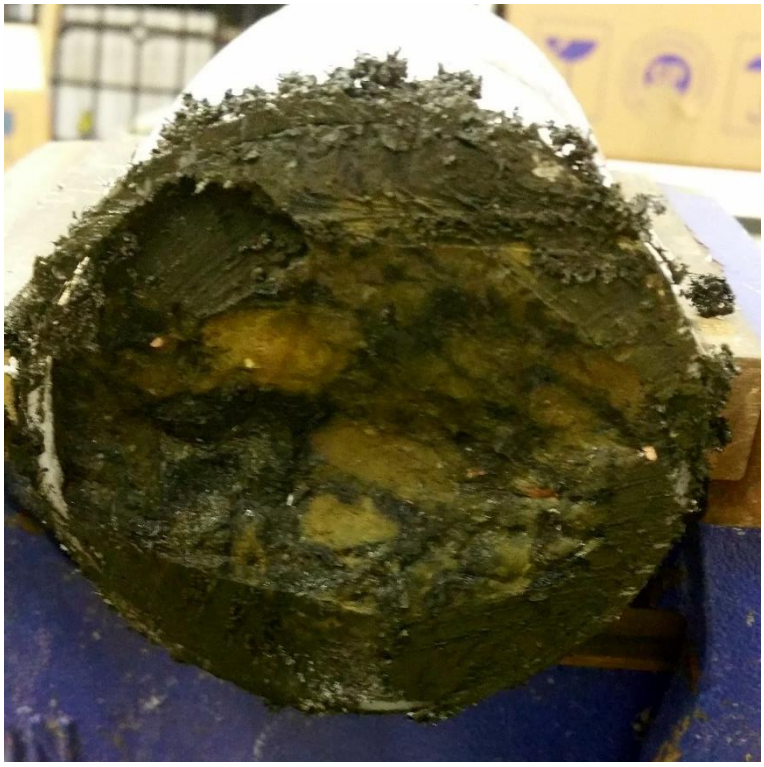

Figure 9.25 Photograph of dissected experimental column showing green colouration of post experimentation waste

XRD analysis shows limited but significant differences between pre- and post-experiment wastes. When comparing the traces shown in Figure 9.26, the only significant difference between these pre-experiment and post-experiment “Live” waste traces is the loss of the peak at ~34 °2θ which is indicative of jarosite in the sample. This suggests that jarosite has been the primary electron accepter for DIRM metabolic activity in the system; as amorphous iron oxyhydroxides are seemingly, given the lack of undulating peaks, not abundant. The counts for jarosite at ~20 °2θ have decreased in the post-experiment sample providing further indications that jarosite has been

preferentially targeted. This correlates with the observations from both the waste characterisation, where amorphous minerals were not observed, and the preliminary study wherein jarosite was identified as one of the likely candidates for reduction.

Given the suspected sulphate reduction in the system, iron sulphides are conspicuous by their absence; as they are known to be formed during the reduction of solid phase iron oxyhydroxides and hydroxysulphates both biotically and abiotically. However, it is possible that treatment of the waste post-experiment has caused the loss of the iron sulphides. As previously discussed the iron sulphides typically formed in these reactions are metastable and susceptible to rapid oxidation (Rickard & Morse, 2005). Despite freeze-drying in an effort to maintain metastable minerals, losses are possible as the waste is exposed to the atmosphere for a considerable period during preparation for XRD analysis.

The diffractogram for the pre-experiment autoclaved sample is broadly similar to the non-autoclaved Live equivalent (Appendix 3). Though analysis did identify lepidocrocite at ~43 °2θ and ~59 °2θ in the autoclaved sample while it was not identified in the Live sample. This suggest that autoclaving has had a limited effect, if any, on the mineralogy of the sample. This contradicts the observations of the column effluents, where increased initial “wash off” of iron was observed from the “Autoclaved” columns. The trace for the post-experiment waste from the Autoclaved columns shown no significant difference to the Live column equivalent (Appendix 3). Again, the jarosite peak at ~34 °2θ is absent suggesting that jarosite is also the primary electron accepter within the autoclaved columns. The Organic Starved column trace has, by contrast, retained the jarosite peak at ~34 °2θ. This correlates with the hypothesis that jarosite is being preferentially reduced by the stimulated microbial communities.

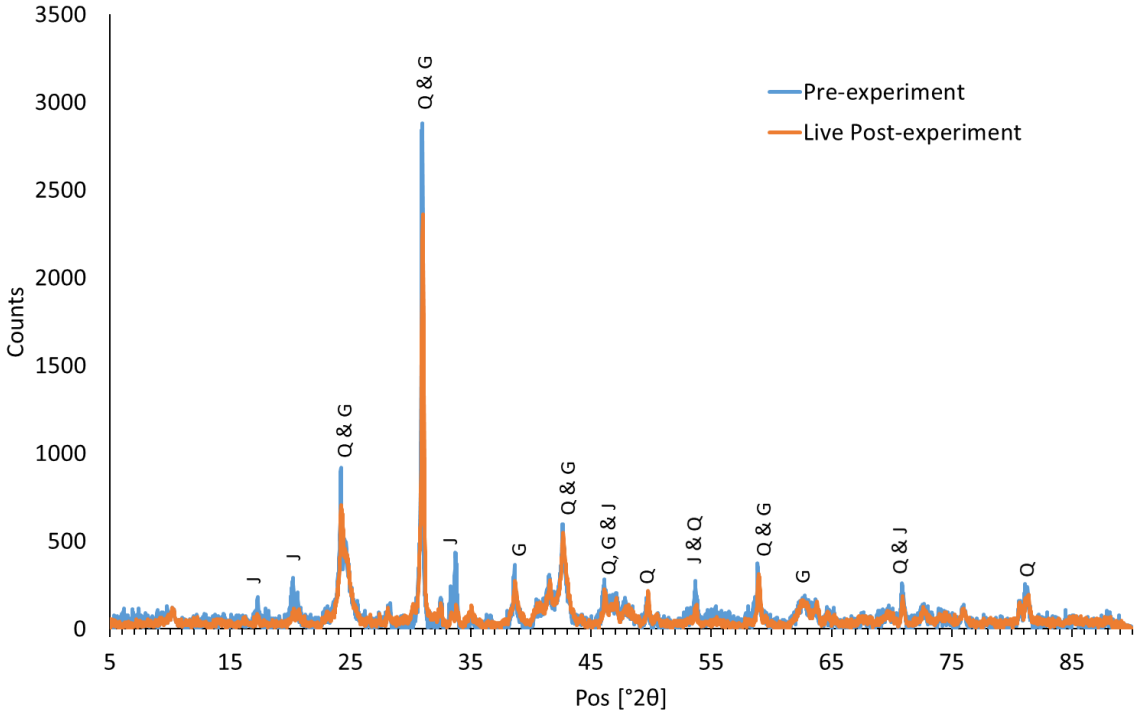

Figure 9.26 XRD diffractogram for Parys Mt. 2 waste pre-experiment compared with the average trace for the post-experiment "Live" waste. Q = quartz; G = goethite; J = jarosite. Energy source = Co Kα

Sequential extractions show that the distribution of iron within the waste in the Live columns has undergone very little alteration, despite the bio-reduction apparent from the effluent analysis Figure 9.27a&b). This contrasts with the observations from the preliminary study; where the proportion of iron within the residual phase was reduced and the proportion of iron within the magnetite-targeted phase increased. The majority of iron is held within the 2 least reactive phases (magnetite-targeted and residual) though this is not reflected by the minerals identified within the XRD diffractogram.

Despite the very limited changes to iron distribution, lead has undergone a more extensive redistribution compared to other metals analysed (Figure 9.27c&d). Total lead located within the 2 least reactive phases has reduced from 45.8% to just 18.1%. This reduction of 27.7% total lead within these 2 phases is similar to what was observed in the preliminary study where a 36.1% reduction in these phases occurred. However, this may, in part, be a result of a much larger proportion of lead initially within the magnetite-targeted phase in the preliminary study. Initially 54.2% of total lead was contained with the first 4 extraction phases (water soluble through to reducible oxides) which also represents the initial "target lead" (lead associated with phases susceptible

to iron bioreduction). This is considerably larger than suggested by the preliminary study of Parys Mt.2 waste. The majority of this lead (42.6%) is located within the “easily reducible oxide” phase. 9.4% of total lead is located within the “carbonate-associated” phase, whilst the other 2 phases in the “target lead” group contain only minor quantities of lead. Negligible amounts of lead were present in the “water soluble” phase post-experiment. The largest increase can be seen within the most reactive “carbonate-associated” phase with an increase of approximately 20% of total lead contained within this phase and a ~10% increase observable in the “easily reducible oxide” phase.

This is interpreted as a consequence of one of two events, either; the resorption of aqueous phase lead to the mineral surfaces of residual iron oxyhydroxides, in response to increasing pH. Leaving it more readily leachable than if previously held in a mineral matrix; or, the increased exposure of lead within the mineral matrices as a result of bio-reductive action on the minerals as described by Esther *et al.* (2013). Given the coeval mobilisation of lead and iron, it seems more likely that the former scenario is responsible for this increase in lead leachability.

Copper also displays a notable shift towards higher concentration of copper within the “easily reducible oxide” phase with an increase from 9.2% to 30.9% of total copper within this phase (Figure 9.27e&f). Initial inspection of the sequential extractions suggests the majority of this redistribution is sourced largely from the “magnetite-targeted” phase. This transition of copper between these phases correlates with the observations from the preliminary testing. However, the inability of the sodium dithionite extractant used for the “reducible oxide” phase to extract copper may result in an overestimation of the proportion in the “magnetite-targeted” phase (Chou *et al.*, 2015). Regardless of whether the copper has originated from the “reducible oxide” or “magnetite-targeted” phase the increase within the more reactive “easily reducible oxide” phase strongly suggests increased surface exposure or a mobilisation/re-adsorption mechanism within the waste as a result of bio-reductive dissolution of iron oxyhydroxides. The negligible amount of copper within the “water soluble” phase reaffirms the lack of mobility of copper when the extractant has a circum-neutral pH.

It is noticeable that the pattern of negligible copper within the “reducible oxide” phase is also seen in the distribution of lead through the phases. Whilst this lack of copper in

the “reducible oxide” phase can be explained by the precipitation of copper by sodium dithionite (Chou *et al.*, 2015) at the time of writing there is no published literature describing whether sodium dithionite has a similar impact on aqueous lead. No other mechanism that may cause this suspect underrepresentation of lead in the “reducible oxide” phase has been identified and more dedicated research would be required to ascertain the precise cause of this feature.

As seen in the preliminary experimentation, the distribution of zinc through the extraction phases bears substantial similarities to that of iron (Figure 9.27g&h). There has been only minimal change in the distribution of zinc as a result of the bio-reduction. An increase of ~2% of total zinc has occurred in the “carbonate-associated” and “easily reducible oxide” phases, which has been offset by a ~4% decrease in zinc within the “residual phase”. As with other metals analysed, negligible amounts of zinc is located within the “water soluble” extraction phase emphasising the low solubility in the later stages of experimentation. The lack of zinc in the “water soluble” phase pre-experiment also highlights one of the limitations of sequential extraction. An average of 3.1% of zinc was recovered from the “Live” columns, predominantly as “wash-off”. However, the sequential extraction suggested that “wash-off” should comprise 1.0% of total zinc. This highlights how the small size of samples used in sequential extractions (~200mg) can result in poor representation of the waste mass at a larger scale.

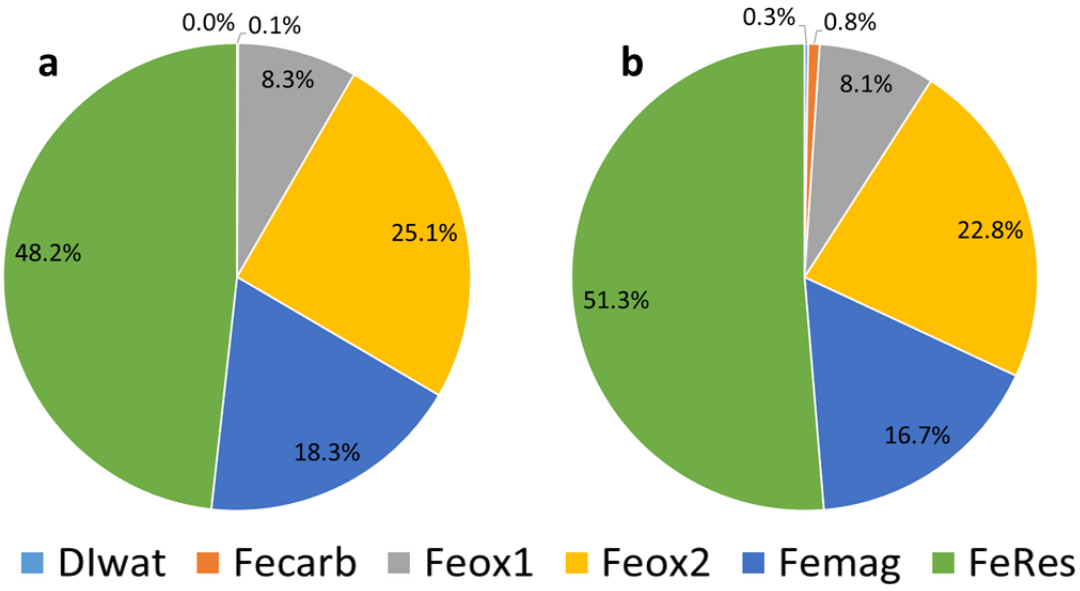

Figure 9.27 Sequential extractions showing distribution of metals within Parys Mt. 2 “Live” waste pre- and post-experiment; a) iron pre-, b) iron post-

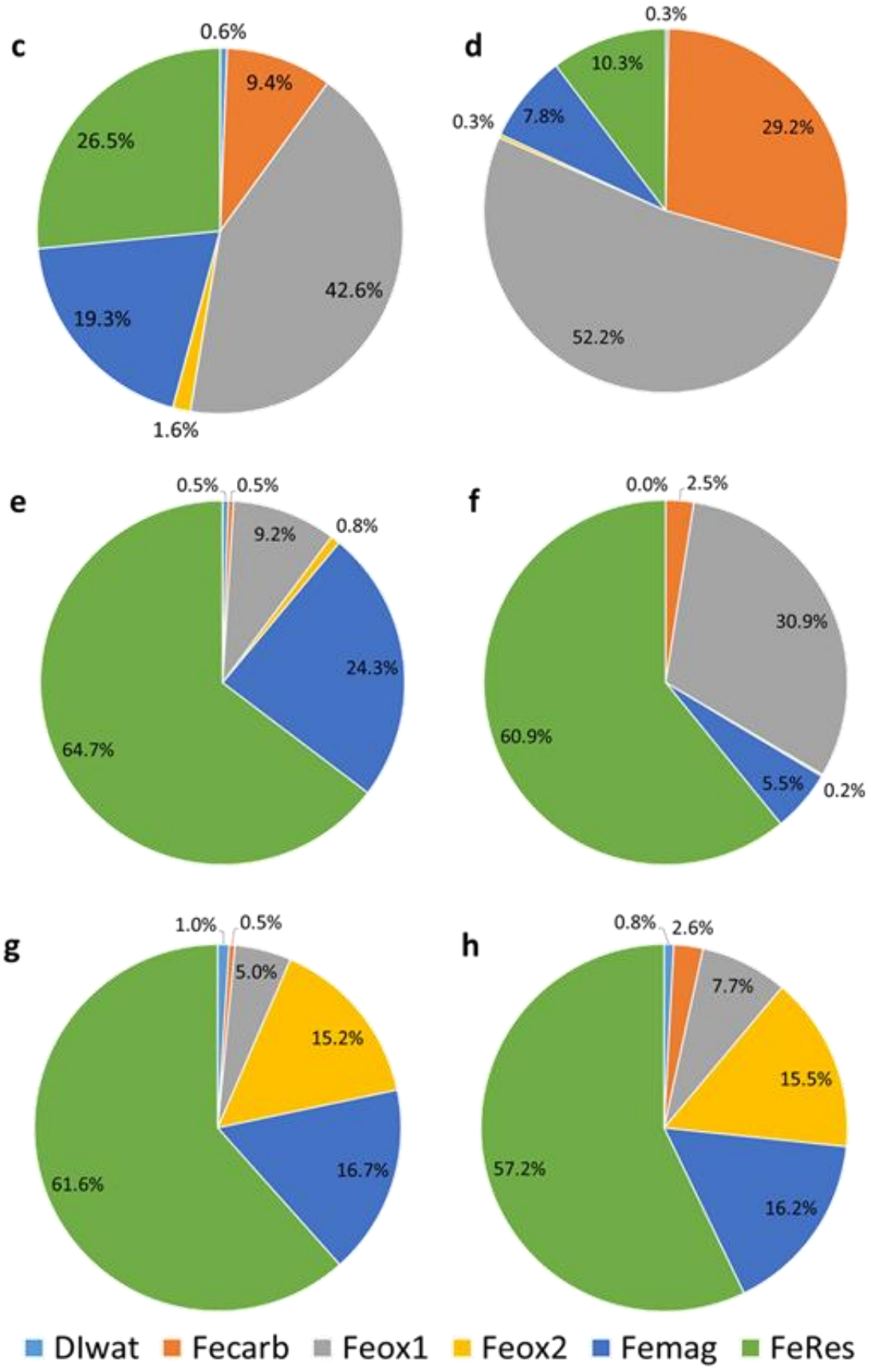

Figure 9.27(cont.) Sequential extractions showing distribution of metals within Parys Mt. 2 "Live" waste pre- and post-experiment; c) lead pre-, d) lead post-, e) copper pre- and f) copper post-, g) zinc pre- and h) zinc post-

The distribution of iron between extraction phases for the pre-experiment, Autoclaved Parys Mt. 2 waste bears strong similarity to the Live column equivalent. With iron being predominantly located within the “residual” phase, followed by the “reducible oxide” and “magnetite targeted” phases (Figure 9.28a). This is an ideal scenario as it suggests that the elevated temperatures and pressures involved in the autoclaving process have had only minimal impact on the mineralogy, which correlates with the observations from the XRD analysis. As with the pre-experiment samples there is a high degree of similarity in iron distribution between Autoclaved and Live post-experiment samples (Figure 9.28b). Negligible quantities of iron are located within the first two extraction phases with 8.1%, 27.4%, 18.5% and 45.3% located within the “easily reducible oxide” “reducible oxide” “magnetite targeted” and “residual” phases respectively. This similarity suggests that, despite much lower iron concentrations in the effluents, the extent to which bio-reduction has impacted the wastes is similar.

Whilst autoclaving appears to have had little impact on iron distribution within the wastes, the opposite is seen regarding lead distribution (Figure 9.28c&d). Whilst most lead in the pre-experiment, non-autoclaved sample was located within the “easily reducible oxide” phase (42.6%), the autoclaved equivalent had a much greater proportion of lead (69.4%) contained within the “residual” phase with the “easily reducible” phase containing only 16.7% of total lead. Distribution of lead within the other extractive phases is also greater in the non-autoclaved sample compared with a relatively more restricted dispersion of lead throughout the phases. Despite the extensive differences between the pre-experiment samples, the post-experiment samples returned remarkably similar results. As with the Live samples, the lead has redistributed into the more reactive “easily reducible oxide” and “carbonate associated” phases increasing from 16.7% to 49.5% and 2.2% to 25.8% respectively. These increases are facilitated by a significant reduction in the “residual” phase from 69.4% to 11.5%. This is again suggestive that a similar level of microbial reduction of iron and mobilisation/redistribution of lead has occurred in the Autoclaved columns as in the Live columns despite the initial autoclaving of the waste.

The distribution of copper through the extraction phases in the pre-experiment autoclaved waste shows only negligible differences when compared to the non-autoclaved equivalent suggesting limited impact from the autoclaving treatment (Figure

9.28e). This correlates with the observations from iron analysis though contradicts those from lead. Only 11.9% of total copper were initially located within the first 4, most reactive extraction phases, representing the "target copper ". Of the 88.1% of remaining copper, 63.5% of it is located within the "residual" phase. The post-experiment analysis also bears strong similarities with the "Live" column equivalent (Figure 9.28f). The "residual" phase remains the dominant repository for copper with 59.8% located within this phase. The most substantial change in copper distribution is the movement of copper to the "easily reducible oxide" phase seemingly from the "magnetite targeted" phase. Though given the previously discussed limitation of copper extraction from the "reducible oxide" phase there is increased uncertainty. "Carbonate associated" copper also increased from 0.4% to 5.9% but most interestingly the proportion of copper located within the "water soluble" phase increased from 0.6% to 5.6%.

Zinc distribution has undergone very little change as a result of autoclaving, with only negligible differences between the autoclaved pre-experiment sample and the non-autoclaved Live equivalent (Figure 9.28g&h). Similarly, there has been only minor changes to the zinc distribution as a result of the bio-reduction experimentation. "Easily reducible oxide" associated zinc increased from 4.4% to 7.3%, "magnetite targeted" phase zinc increased from 14.2% to 16.3% while the "residual" phase zinc decreased from 62.8% to 55.6%. Much like copper there has also been an apparent increase in "water soluble" zinc from 1.0% to 2.4%.

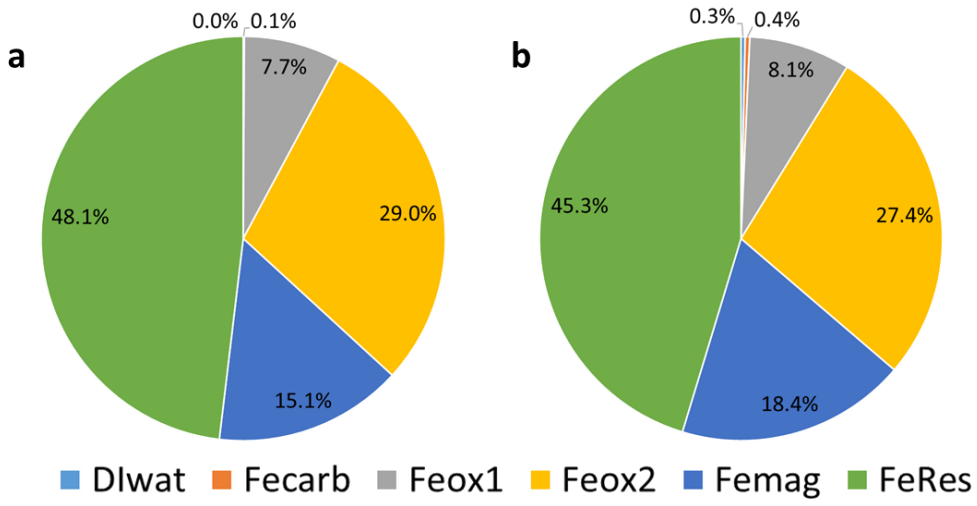

Figure 9.28 Sequential extractions showing distribution of metals within Parys Mt. 2 "Autoclaved" waste pre- and post-experiment; a) iron pre-, b) iron post-,

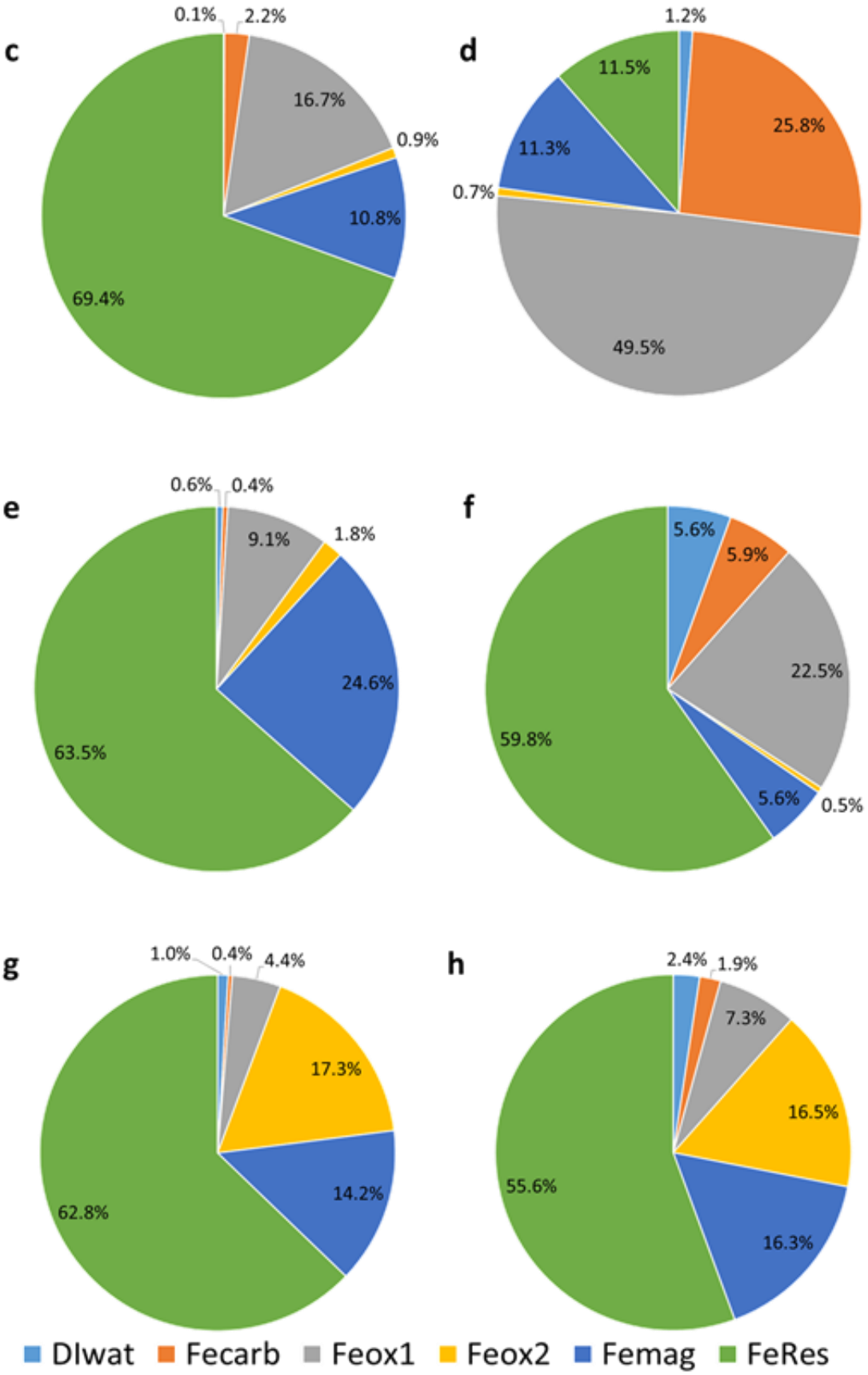

Figure 9.28(cont.) Sequential extractions showing distribution of metals within Parys Mt. 2 "Autoclaved" waste pre- and post-experiment; c) lead pre-, d) lead post-, e) copper pre-, f) copper post-, g) zinc pre- and h) zinc post-

As expected, given the relative lack of activity in the Org. Starved columns suggested by the effluent analysis, there has been only minor alterations in the distribution of the target metals as a result of experimentation. Despite relatively low iron effluent concentrations, suggesting limited bio-reduction, there has been some change in the distribution of iron (Figure 9.29a&b). The proportion of iron within the “reducible oxide” phase has increased from 25.1% and 31.7%. This would typically be interpreted as an increase in goethite within the waste as a result of the transformation of ferrihydrite. However, the increase in the “easily reducible oxide” iron, from 8.3% and 11.1%, would itself suggest there has been no decrease in in ferrihydrite from this transformation mechanism. These minor variations may, instead, be due simply to natural variation in the samples.

Distribution of lead has not undergone the extensive alteration seen in the other experimental columns (Figure 9.29c&d). The most notable change that can be observed is that there has been a substantial reduction in lead within the very reactive “carbonate associated” phase from 9.4% to 2.5%. This may represent the phase from which lead has mobilised into the aqueous phase. However, the 6.9% of total lead lost from this phase is significantly greater than the 0.1% of lead recovery via the effluent, suggesting this lead transitioned into different phases. Beyond this there have been minor increases, or decreases, in the proportion of lead in other phases to accommodate the decrease in the “carbonate associated” phase. There is no evidence of the significant shift in lead towards more reactive phases as observed in the Live and Autoclaved columns.

Copper distribution pre- and post-experiment does show a similar relationship to that observed in the other columns with copper within the “easily reducible” phase increasing from 9.2% to 15.9%. The “magnetite targeted” phase copper meanwhile has reduced from 24.3% to 21.4% (Figure 9.29e&f). These trends replicate what was seen in the other columns, albeit on a smaller scale. This may suggest that a small part of this redistribution is as a result of mechanisms unrelated to the bio-reduction. Though given the relatively small scale of these changes natural variation of the samples cannot be ruled out as the cause. No substantial movement of copper into the “water soluble” and “carbonate associated”, as seen in the autoclaved columns, has occurred.

Zinc as in other columns exhibits negligible changes in distribution through extractive phases as a result of experimentation (Figure 9.29g&h). However, in this instance zinc does not mirror iron distribution as it has in the Live and Autoclaved column extractions.

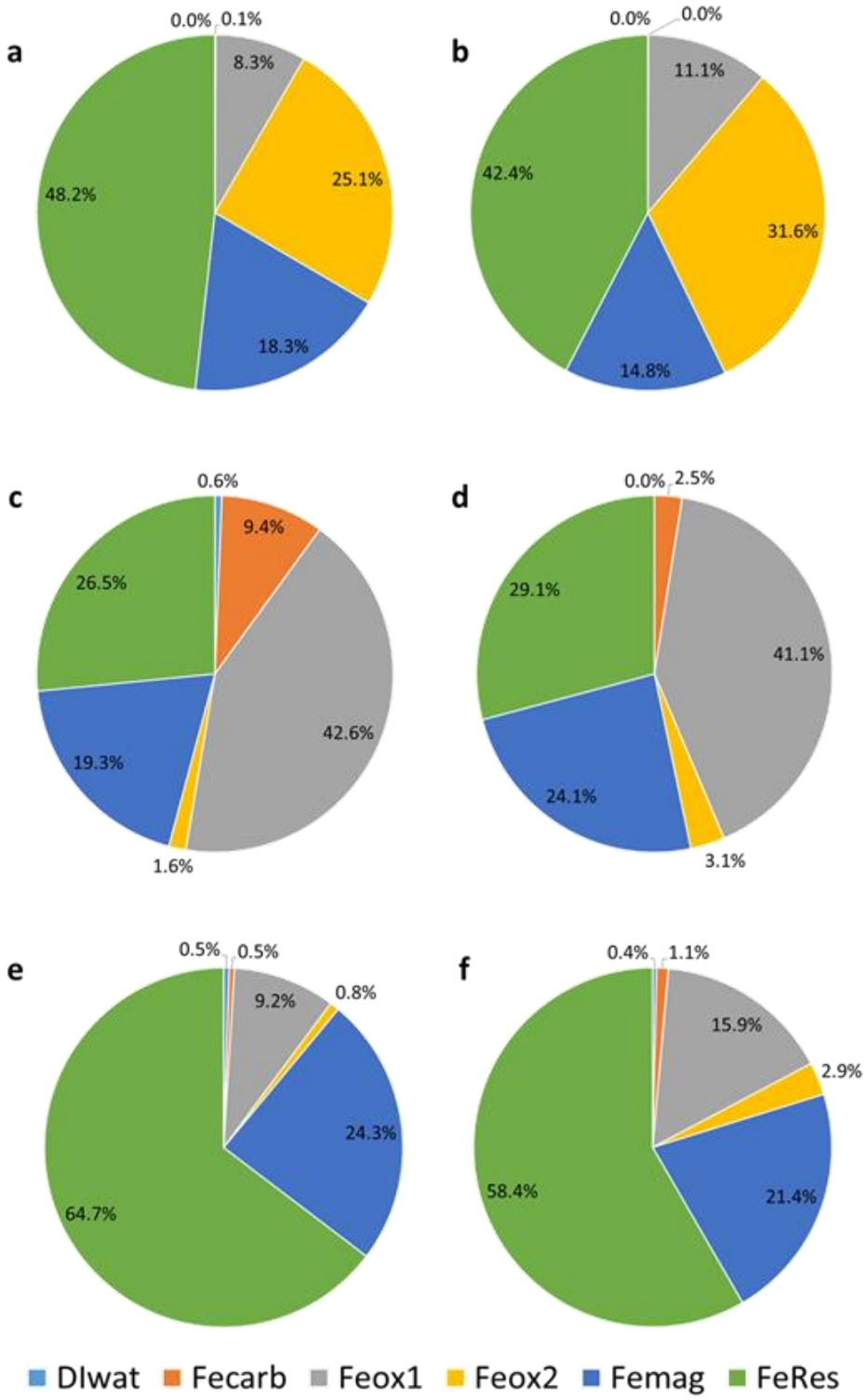

Figure 9.29 Sequential extractions showing distribution of metals within Parys Mt. 2 "Organic Starved" waste pre- and post-experiment; a) iron pre-, b) iron post-, c) lead pre-, d) lead post-, e) copper pre- and f) copper post-

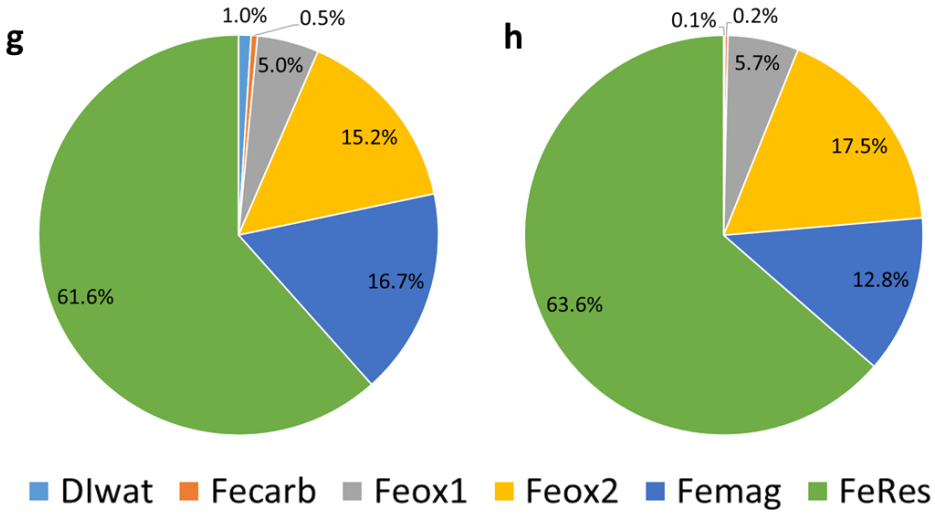

Figure 9.29(cont.) Sequential extractions showing distribution of metals within Parys Mt. 2 "Organic Starved" waste pre- and post-experiment; a) zinc pre-, b) zinc post-,

When the 3 experimental variants are directly compared there is a clear difference in the changes in metal partitioning between the columns dosed with glycerol and the "Organic Starved" columns with metals in the latter experiencing only minimal redistribution through the extraction phases as a result of experimentation. In both the Live and Autoclaved samples iron distribution has undergone only minor changes despite iron reduction occurring. The same can be said of zinc within these samples. This would suggest that despite one of the samples starting with a microbial community that had undergone autoclaving the extent to which bioreduction affected the Live and Autoclaved wastes was similar.

Copper and lead in the wastes displayed a much higher degree of redistribution between the extraction phases. A comparison of lead distribution both pre- and post-experimentation across all three column variants is displayed in Figure 9.30. Again, the Organic Starved columns have undergone substantially less change than the other columns. The Organic Starved columns are the only ones to have shown a reduction in lead within the "carbonate associated" phase while the Live and Autoclaved both show large increases in lead in this phase. In both the Live and Autoclaved columns there has been and increase in lead within the first 4 extractions representing the target phases. Again, despite the differing pre-treatments the distribution of lead at the end of experimentation is broadly similar, suggesting a similar degree of bioreduction has occurred in the experimental columns of these two variants

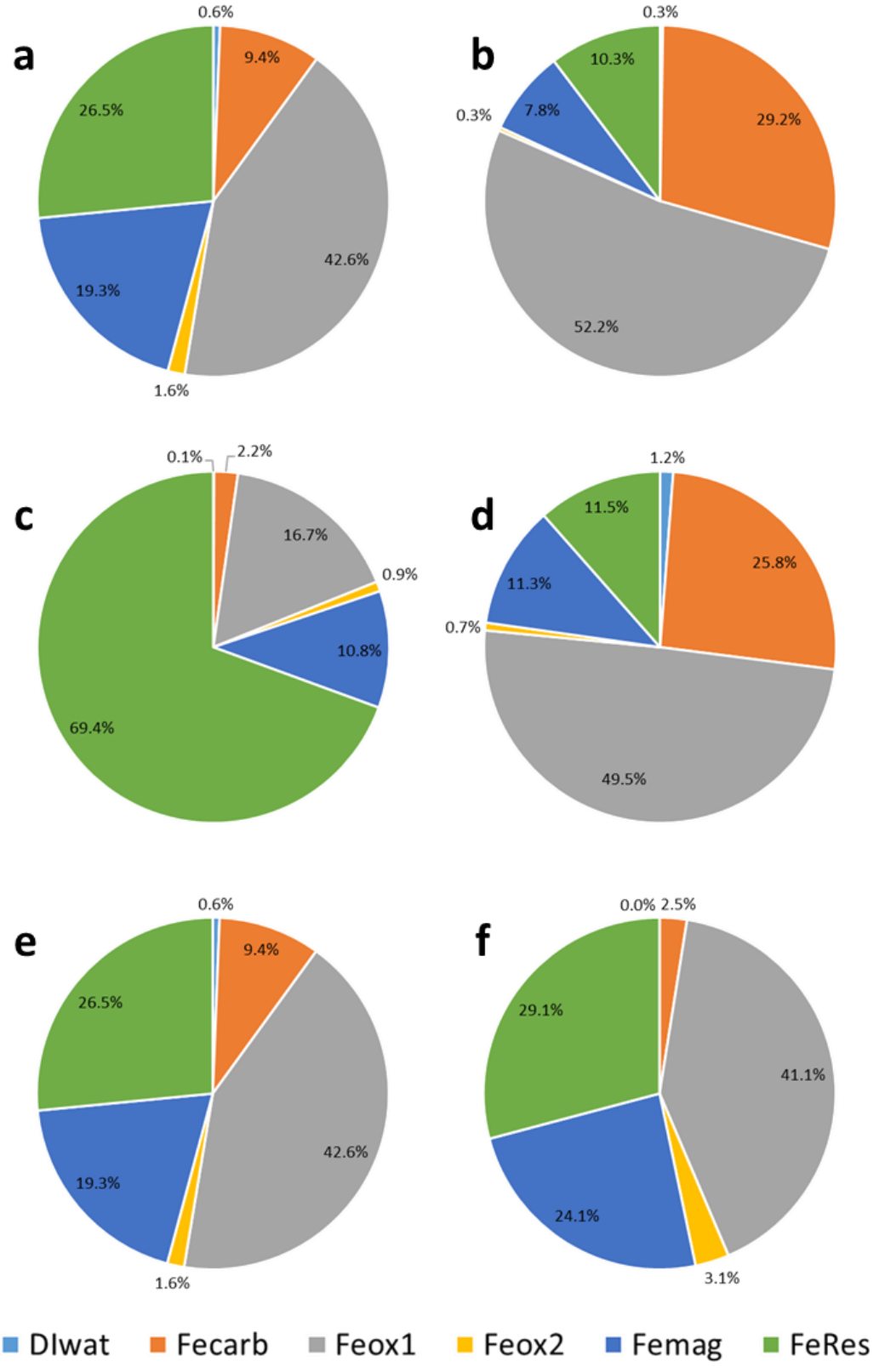

Figure 9.30 Comparison of sequential extractions showing distribution of lead within Parys Mt. 2 experimental columns both pre- and post-experiment; a) Live pre-, b) Live post-, c) Auto pre-, d) Auto post-, e) Org. Starved pre- and f) Org. Starved post-

9.4.2.4. Glycerol Utilisation

Analysis of the glycerol concentrations in both the extractant (at point of input) and the effluent from the "Live" columns is displayed in Figure 9.31. The concentration of glycerol in the input extractant is consistently around the 10 mM target. Any variation in the concentrations, either above or below the intended concentration, are all within 1 standard deviation from the 10 mM target. This variation is likely due to either human error in measurement of the minor quantities of glycerol required or due to variations and/or errors associated with the assay.

Concentrations of glycerol remaining in the "Live" column effluents bear substantial similarity to the analysis of glycerol concentrations in the effluents from the previous experiments with Lindsay waste. Concentrations of glycerol in the column effluents are initially elevated and variable between ~4.5 and 6.5mM. Between day 12 and day 19 of the concentration of glycerol in the effluent decreases sharply to ~1 mM. This correlates with the observations of rapidly increasing iron concentrations in the effluent during this period of the experiment; suggesting the rapid consumption of glycerol by microbial processes. Concentrations of glycerol in the effluent then remain below 1 mM for the majority of the remainder of experimentation. The only exception to this is a brief increase, to approximately 2 mM, around day 61 of experimentation which then quickly returns to <1 mM.

An average of 0.020 kg of glycerol was introduced to each of the Parys Mt. "Live" column. This equates to 0.027 kg glycerol per kg of dried Parys Mt. 2 sludge. In December 2017 the price of 80% crude glycerine (a mixture of glycerol and water) destined for disposal was ≈£175 per metric ton. This is predicted to decline as glycerol production increases (Oleoline, 2017). Using these prices as a guide the cost of implementing this system would average less than 1p per kg of dry Parys Mt. sludge; equating to ~£5.00 per metric ton treated.

As previously discussed, the other potential source of glycerol is the waste bio-glycerol generated from the biodiesel industry which is being produced in large quantities and is viewed as a valueless waste product. By utilising waste crude glycerol as the organic carbon source the system negates any initial costs for organic carbon as one waste product is utilised to treat another (Ciriminna *et al.*, 2014).

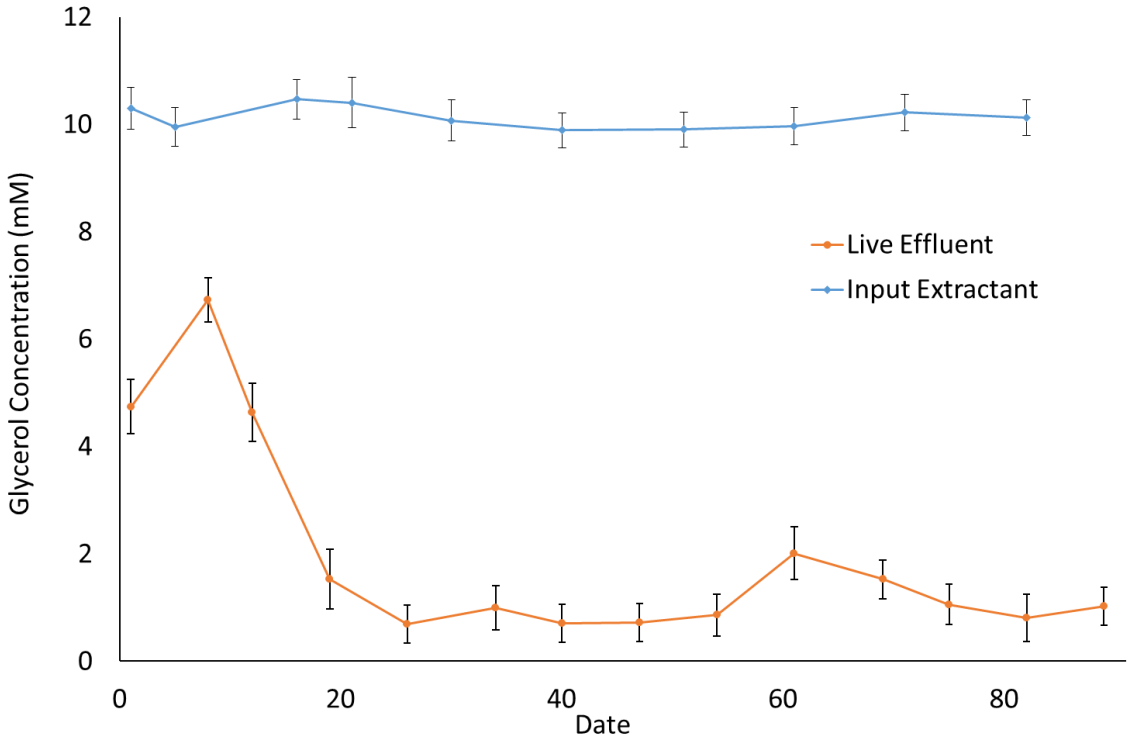

Figure 9.31 Glycerol concentrations within input extractant and effluent from Parys Mt. "Live" column, Error bars represent 1 standard deviation. (PM "Live" replicate column 1 used as representative)

If the stoichiometry of the reduction of iron with glycerol as an organic carbon source, as presented in Equation 2.1 (Page.12), is considered then an approximate efficiency for the use of glycerol can be calculated. Taking "Live" replicate column 1 as a representative for the "Live" columns, there was 212.8g of iron (in all forms) within the experimental column before any bioreduction occurred. Sequential extraction analysis showed that of this quantity only 115.4g (54.2%) was found to be associated with mineral phases expected to be susceptible to bioreduction (Figure 9.27). A total of 14.9g (0.16mol) of the glycerol introduced to the column was either retained in the column or utilised for bioreduction. Under an ideal stoichiometry this would enable 126.8g of iron to be reduced, more than is contained within the "target phases". However, a total of 14.8g of iron was recovered from "Live" replicate column 1 as a result of experimentation. This represents only 11.6% of the iron that is theoretically recoverable by the addition of 14.9g of glycerol.

This does, however, represent and idealised scenario with a simplified idealised stoichiometry and does not consider the effect of physicochemical conditions on the reaction. As has already been discussed, pH has a substantial impact on which phases of

iron oxyhydroxides are energetically favourable for bioreduction. Increasing pH may also have caused the sorption or precipitation of reduced iron limiting the quantity extracted. In this eventuality, it would be likely that the amount of iron reduced would be larger than the amount extracted, therefore making the reaction more efficient even if the recovery system is not.

Given the evidence for preferential flow paths within the columns it is also likely that areas of the waste did not come into contact with sufficient glycerol to reduce the iron within these areas. This would have further limited the amount of iron that could feasibly have been reduced and recovered from the column.

Sulphate reduction has been shown to potentially have occurred within the columns, this will likely have sequestered a portion of the glycerol thereby preventing its use for iron bioreduction. Given the use of an indigenous microbial community it is also likely that there are other metabolic processes occurring within the waste that sequester glycerol but have no positive impact with regards the reductive dissolution of iron and the recovery of associated metals. It should be noted though that the indigenous community may also present opportunities for increased efficiency with a greater range of microbes increasing the chance that the breakdown products from glycerol oxidation will be further utilised for iron reduction.

9.4.3. Microbiological Analysis

9.4.3.1. Quantitative real-time PCR (qPCR) of bacterial and archaeal 16S rRNA genes

qPCR analysis of the waste samples showed that the autoclaving of the Parys Mt. waste caused a significant reduction in the size of the bacterial and archaeal communities within the waste (Figure 9.32 & Figure 9.33). Bacterial numbers (16S rRNA gene copies per gram) dropped from an average of 2.22×10^{10} to an average of 5.93×10^{7} representing a 99.7% decrease in bacterial numbers. The average archaeal gene copies per gram decreased from 1.09×10^{8} to 1.17×10^{6}, a 98.9% decrease in archaeal numbers

Despite increasing iron concentrations, and changes in physicochemical properties of the column effluents, indicating significant iron reduction, and proliferation of iron reducing communities within the "Live" columns, the qPCR analysis does not show evidence for this. Rather than the expected increase in gene copies per gram, the average bacterial numbers of the post-experiment "Live" samples has decreased slightly from an initial 2.22×10^{10} to 1.16×10^{10}. Archaeal 16S rRNA gene copies per gram also decreased from an average of 1.09×10^{8} to 2.69×10^{7} (Figure 9.32 & Figure 9.33). While all 3 "Live" column replicates showed reduced archaeal and bacterial gene copies, the replicate "Live 2" has the lowest average archaeal and bacterial gene copies per gram of 8.51×10^{6} and 3.36×10^{9} respectively.

The "Organic Starved" columns, on average, showed a very slight decline in bacterial numbers from 2.22×10^{10} to 1.67×10^{10} (Figure 9.32). However, this is a simplistic view of the data and more detailed analysis reveals that replicate column "Organic Starved 3" has undergone a slight increase in bacterial gene copies per gram to 2.51×10^{10}, while "Organic Starved 1" bacterial gene copies per gram has decreased to 9.39×10^{9}. These changes are relatively minor, however, and the general trend of the data suggests that very little change in the total number of bacteria has occurred. Conversely, there has been a notable change in amount of archaeal 16S rRNA gene copies per gram in the "Organic Starved" wastes. Archaea increased to an average of 1.39×10^{9} gene copies per gram from an initial 1.09×10^{8}. This is substantially higher than found in the "Live" wastes and highlights the dominance of bacteria in the "Live" system

outcompeting the archaea. It is notable that replicate column “Organic Starved 3”, which exhibited higher numbers, has the smallest increase in archaeal gene copies. The other 2 replicate columns however, which had reduced bacterial gene copies, have undergone more substantial increases in Archaea.

The introduction of glycerol to the “Autoclaved” wastes has caused a notable increase in bacterial gene copies, correlating with the observed increase in iron concentrations within the effluents and the inferred microbial iron reduction. The average bacterial gene copies per gram in the post-experiment “Autoclaved” wastes was 9.29×10^9, representing an increase of 9.23×10^9 gene copies per gram (Figure 9.32). While this does not represent parity with the communities within the non-autoclaved pre-experiment waste or the post-experiment “Live” columns, it does highlight the ability of glycerol to stimulate bacterial communities within the wastes. The survival of bacteria within the “Autoclaved” wastes is attributable to bacteria capable of sporulation when under stress, discussed further in Section 9.4.3.2 and 9.4.3.3. Archaeal gene copies have also increased, though to a much lesser extent than the bacteria, increasing from an average of 1.17×10^6 to 4.78×10^6 gene copies per gram in the post-experiment waste (Figure 9.33). This suggests the majority of microbial community proliferation, and thereby iron reduction, is attributable to bacteria as opposed to archaea.

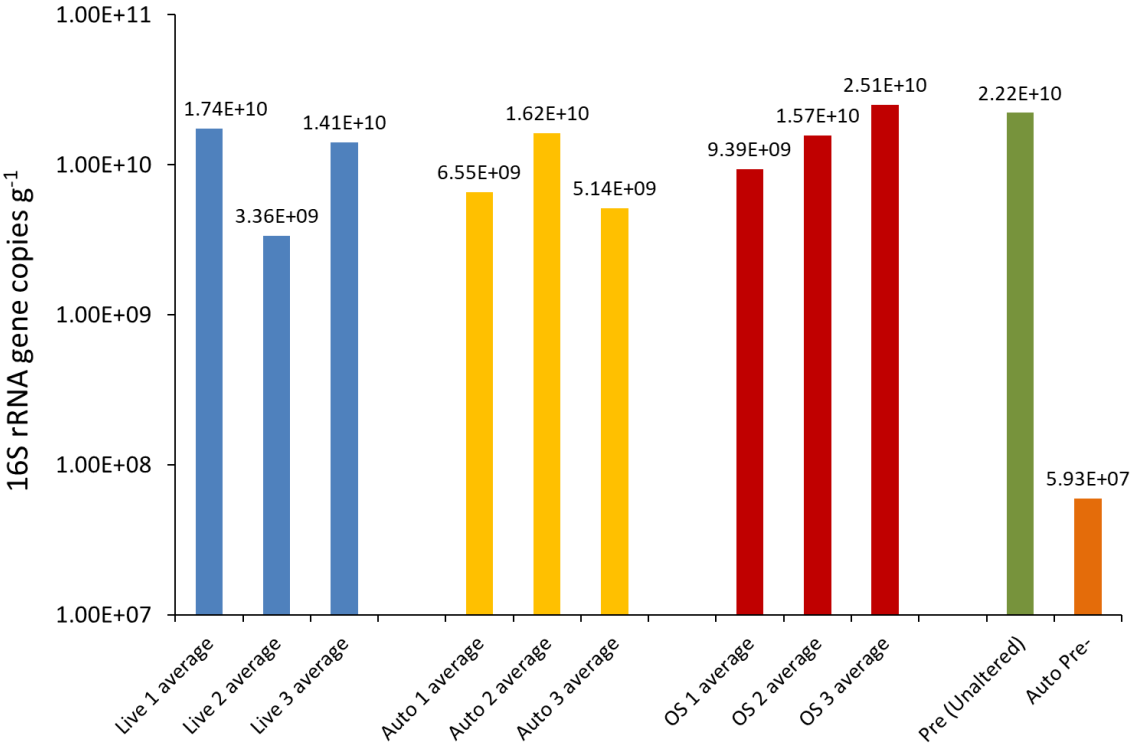

Figure 9.32 qPCR analysis of bacterial 16S rRNA gene copies in pre- and post-experiment Parys Mt. 2 waste samples

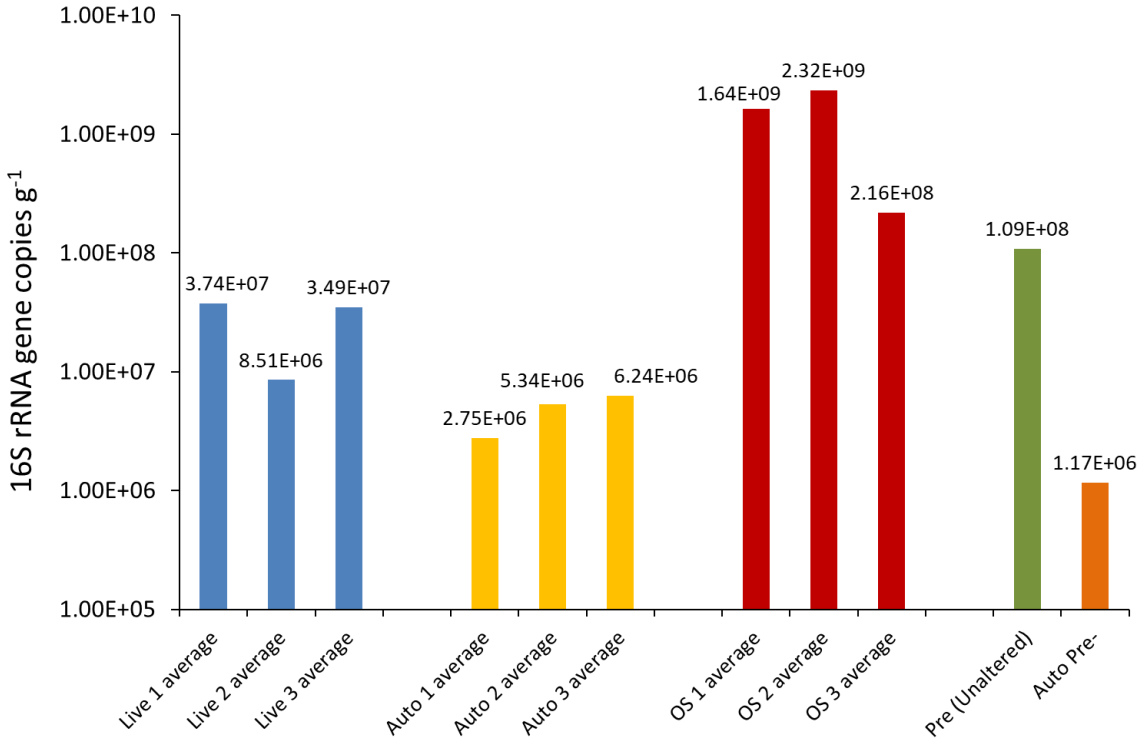

Figure 9.33 qPCR analysis of archaeal 16S rRNA gene copies in pre- and post-experiment Parys Mt. 2 waste samples

As can be seen in Figure 9.34, the average number of bacterial 16S rRNA gene copies per gram decreases as you sample higher up the columns in both the “Live” and “Autoclaved” columns. This is likely a result of the organic carbon source being introduced from the base of the column enabling these communities to metabolise the glycerol first at the bottom of the column, which has allowed increased growth of microbial communities at the base. The smaller communities in the upper portions of the columns is likely a result of a reduction in the availability of glycerol and potential reliance on secondary products from the oxidation of glycerol. It is notable, however, that despite the decreasing trend shown there are significant error margins in the data suggesting the trend may not be significant. The “Organic Starved” columns do not show any clear decrease in bacterial community size as a function of height within the columns, and again any differences can be potentially explained by the error margins of the data. When archaea are considered, a similar trend of decreasing gene copies with height can be seen in the “Live” columns; albeit the scale of this decrease is not as pronounced as in the bacteria and again differences can be accounted for within the error margins of the data (Figure 9.35). Archaea in the “Organic Starved” columns also show a very slight decreasing trend with height despite there being no organic carbon added to the waste. The may be down to natural variation in the wastes as described by the error margins. Alternatively, this may be due to the communities relying on H_2 and CO_2 as the substrates for growth, both of which would diffuse through the column more readily than glycerol. Within the “Autoclaved” wastes there is no obvious trend of decreasing (or increasing) Archaea community size in relation to height within the columns.

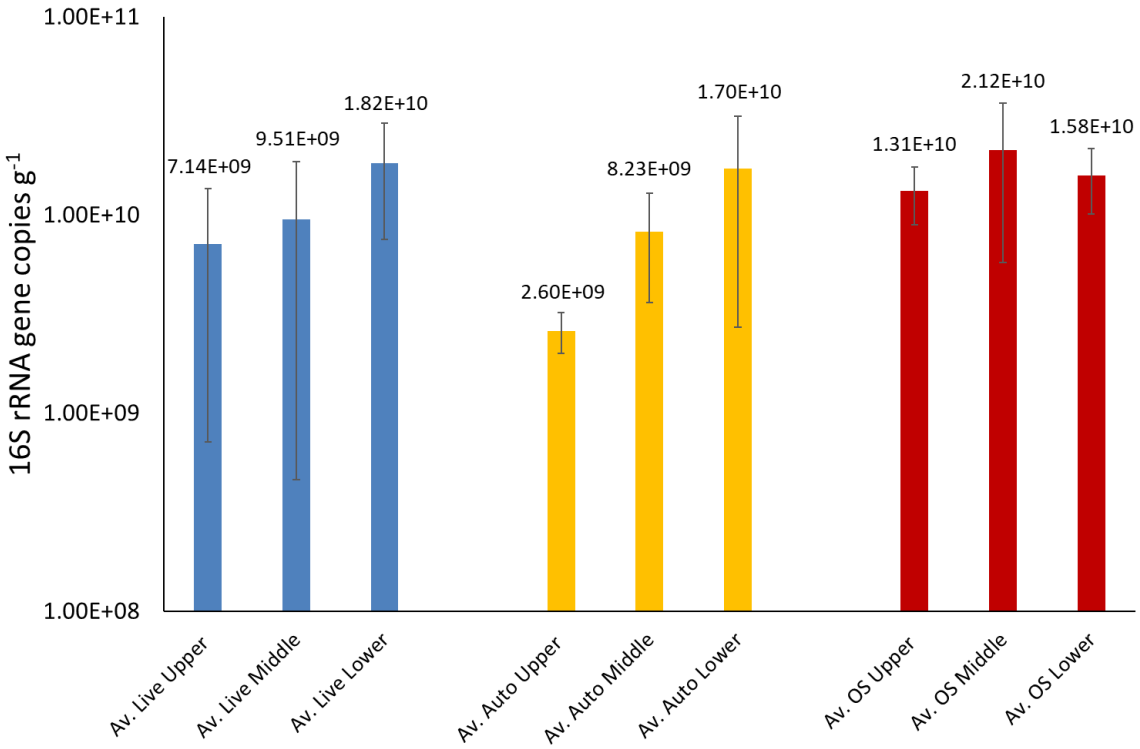

Figure 9.34 qPCR analysis of average bacterial 16S rRNA gene copies in post-experiment Parys Mt. 2 waste samples taken from various heights within columns

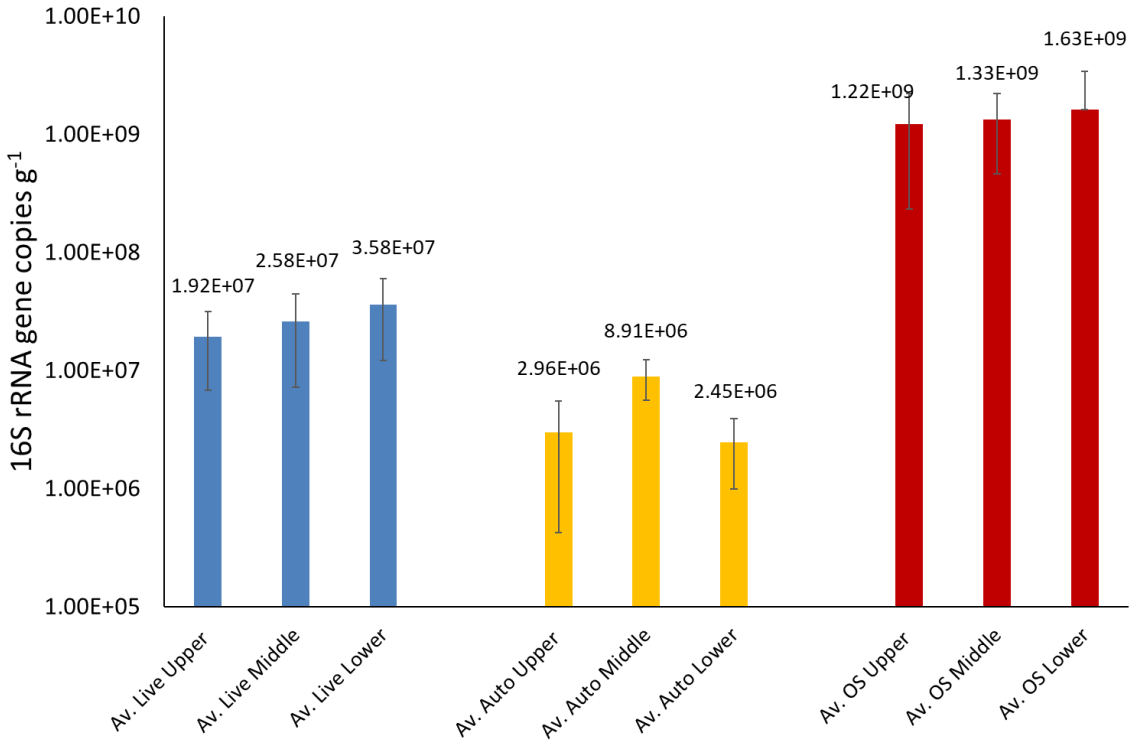

Figure 9.35 qPCR analysis of average archaeal 16S rRNA gene copies in post-experiment Parys Mt. 2 waste samples taken from various heights within columns

9.4.3.2. DGGE analysis and Sanger Sequencing

DGGE analysis of bacterial 16S rRNA genes was performed on all samples after an initial PCR amplification with the $357F_{gc}$- 518R primer pair. A DGGE gel was performed for each experimental column with a further gel utilising the "Middle 1 & 2" samples from each column to act as a comparison between columns and experimental variants.

Visual inspection of the DGGE profiles of the pre-experiment sample shows a low intensity profile with numerous diffuse bands and typically only 3-4 high intensity bands (Figure 9.36). A series of these bands were excised from the pre-experiment profiles. The bands excised and their identifiers are displayed in Appendix 4, while the results of sequencing and taxonomic identification for the excised pre-experiment sample bands, taken from the "Live" and "Organic Starved" columns are displayed in Table 9.2, with a graphical summary of taxa identified in the pre-experiment waste is shown in Figure 9.37. Of the bands sequenced there is no one taxa that is dominant. *Bryocella elongata*, a member of the phylum *Acidobacteria* identified in a methanotrophic culture, was the most abundant taxa identified with ~13% of bands matched to this taxa, though only had a shared identity of ~86% (Dedysh *et al.*, 2012). Approximately 26% of band sequences were matched closest with uncultured bacterium while ~17% were matched closest to uncultured cyanobacterium. Other identified cyanobacteria included *Croccosphaera* and *Leptonlyngbya*. Potential iron-reducing bacteria were identified in low abundance with ~4% of bands identified as *Desulfosporosinus* (87% sequence ident.) and ~8% of bacteria identified as *Alicyclobacillus* (86% sequence ident.) (Yahya *et al.*, 2008; Bertel *et al.*, 2012). Other taxa identified taxa included *Terriglobus* (95% sequence ident.)*, Planoglabratella* (99% sequence ident.) and *Leptolinea* (100% sequence ident.). The reliability of the identification of some of the taxa is subject to uncertainty due to the short length of the sequences available for identification (as low as 70bp). This is a result of poor quality reads, which is itself a result of inaccurate excision of diffuse bands. A phylogenetic tree of the 16S rRNA gene sequences obtained from pre-experiment Parys Mt. 2 waste is presented in Figure 9.38.

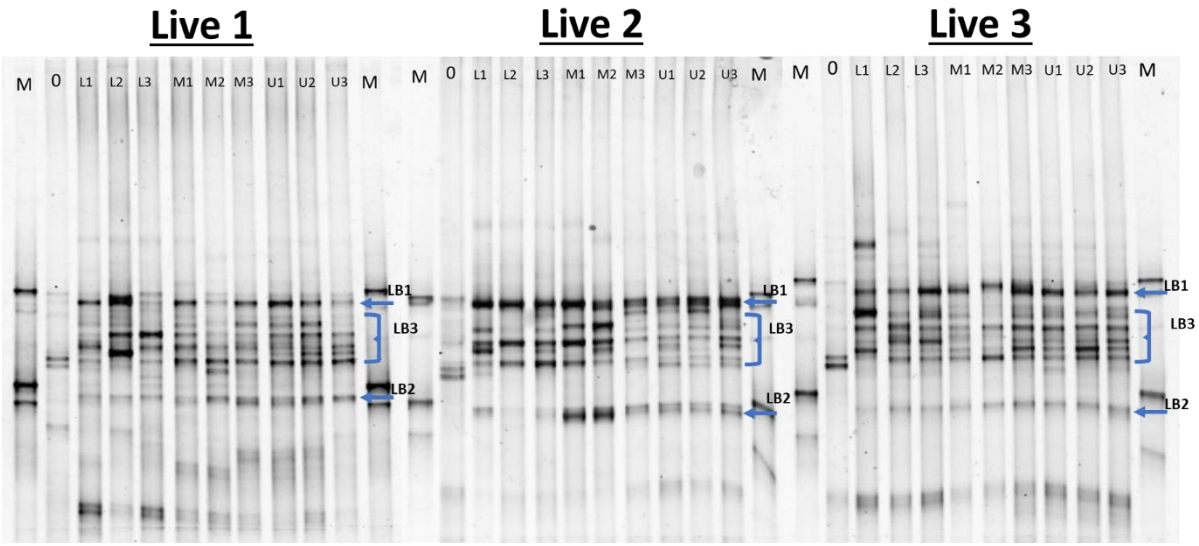

Figure 9.36 DGGE profiles for "Live" columns. M = Marker, 0 = Preliminary sample, L# =Lower column replicate sample, M# =Mid-column replicate sample, U# =Upper-column replicate sample. LB# arrows denote prominent bands consistent across gel profiles

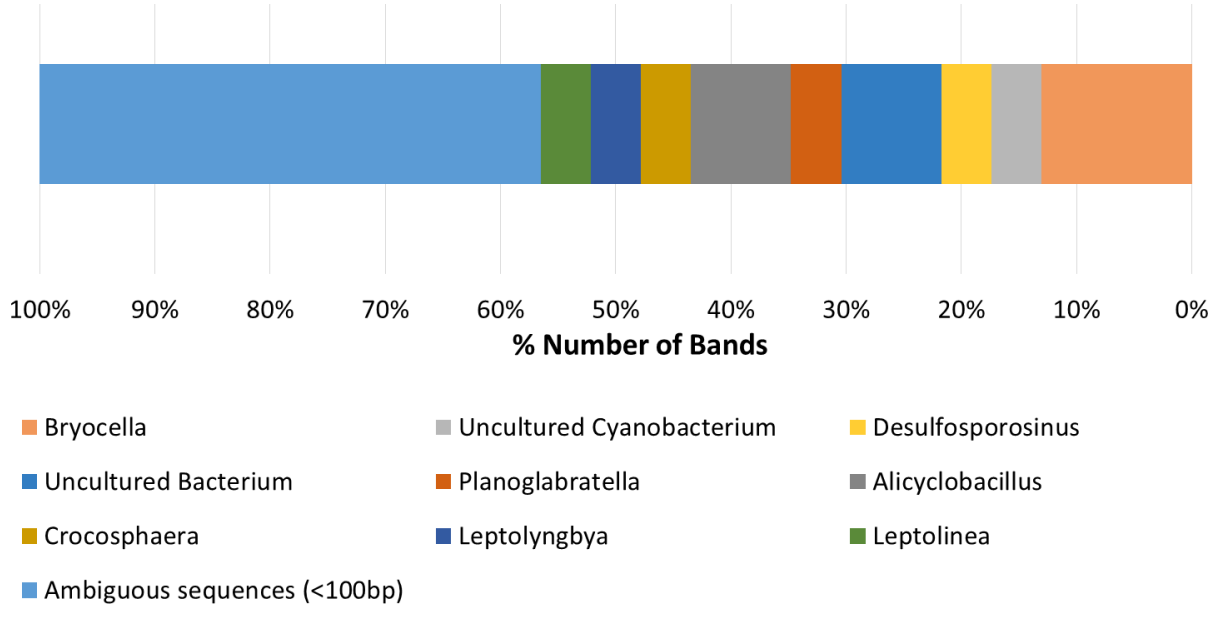

Figure 9.37 Graphical summary of closest 16S rRNA sequence matched to excised pre-experiment samples DGGE bands using BLASTN search tool

Table 9.2 Closest 16S rRNA sequence matched to excised pre-experiment samples DGGE bands using BLASTN search tool

Band Identifier	Closest Match	Accession Number	Sequence Identity	Alignment Length	Phylogenetic affiliation
L1	*Bryocella elongata strain SN10 16S* ribosomal RNA gene, partial sequence	NR_117052.1	87%	172	*Acidobacteriales*
L3	*Desulfosporosinus youngiae strain JW/YJL-B18* 16S ribosomal RNA gene, partial sequence	NR_115694.1	87%	190	*Clostridiales*
L17	Uncultured cyanobacterium clone Paddy_75_6569 16S ribosomal RNA gene, partial sequence	JF987271.1	97%	119	*Cyanobacteria*
OS1	Bryocella elongata strain SN10 16S ribosomal RNA gene, partial sequence	NR_117052.1	99%	161	Clostridiales
OS2	Uncultured bacterium clone FrsFi168 16S ribosomal RNA gene, partial sequence	JF747925.1	100%	122	Bacteria
OS3	Planoglabratella opercularis isolate GO863-27 small subunit ribosomal RNA gene, partial sequence; plastid	KP792485.1	99%	121	Foraminifera
OS5	Alicyclobacillus contaminans strain NBRC 103102 16S ribosomal RNA gene, partial sequence	NR_114203.1	87%	186	Bacillales
OS10	Crocosphaera watsonii strain WH 8501 16S ribosomal RNA gene, partial sequence	NR_115288.1	92%	162	Cyanobacteria
OS11	Uncultured bacterium clone 1200m_d2 16S ribosomal RNA gene, partial sequence	HM745456.1	81%	158	Bacteria
OS15	Alicyclobacillus contaminans strain NBRC 103102 16S ribosomal RNA gene, partial sequence	NR_114203.1	86%	189	Bacillales
OS24	Bryocella elongata strain SN10 16S ribosomal RNA gene, partial sequence	NR_117052.1	99%	161	*Acidobacteriales*
OS26	Leptolyngbya boryana strain PCC 6306 16S ribosomal RNA gene, partial sequence	NR_125501.1	95%	164	Cyanobacteria
OS27	Leptolinea tardivitalis strain YMTK-2 16S ribosomal RNA gene, partial sequence	NR_040971.1	100%	164	Anaerolineae

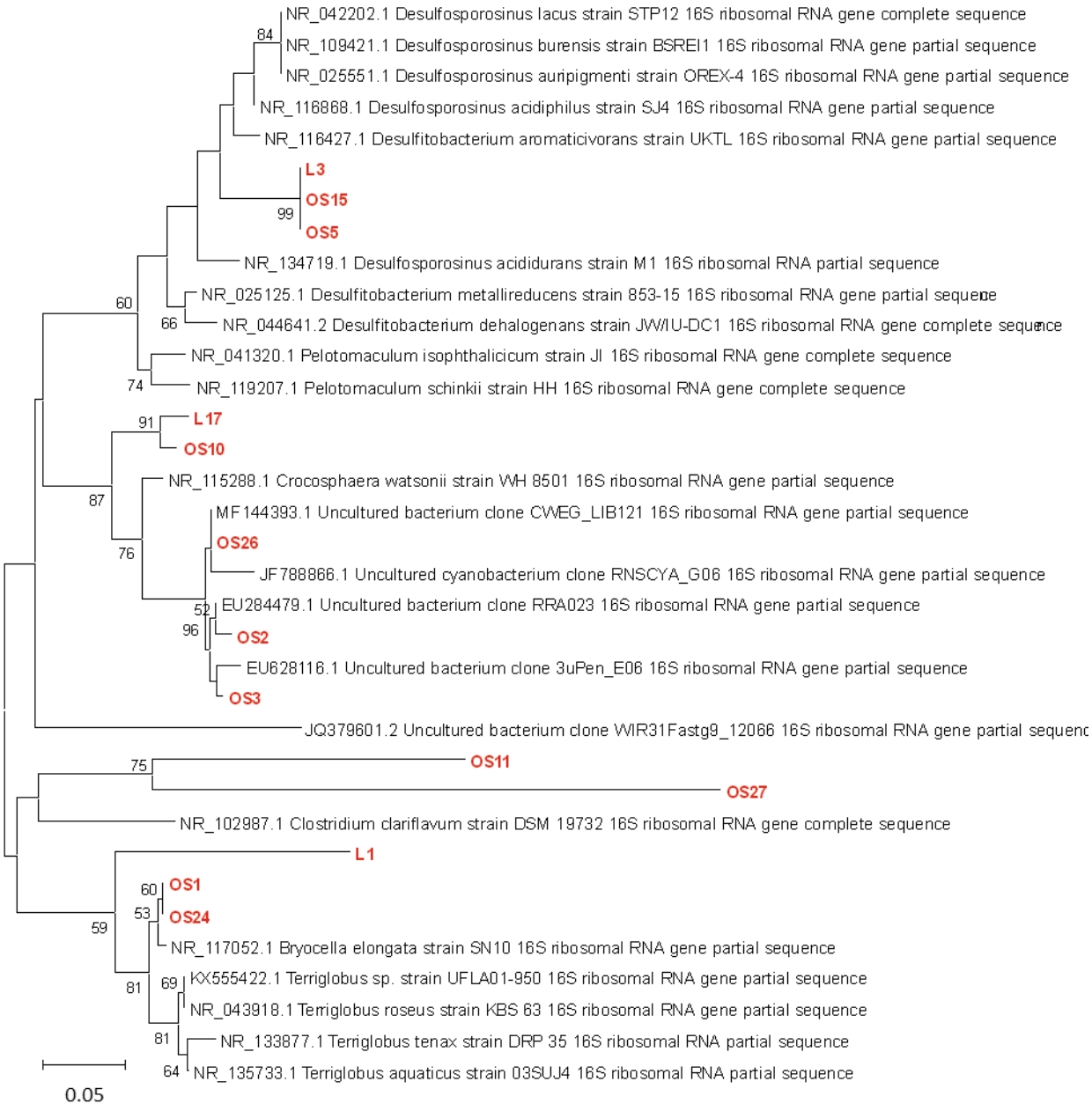

Figure 9.38 Phylogenetic tree showing relationship between 16S rRNA gene sequence clones DGGE bands retrieved from pre-experimental samples of Parys Mt. 2 waste and related reference sequences selected outgroups. Neighbour-joining tree constructed using the Jukes-Cantor substitution model. Bootstrap support values over 50% are shown (1000 replicates).

As can be seen in Figure 9.36 there has been significant change in the DGGE profile of the “Live” samples due to the introduction of glycerol and subsequent bioreduction. For example, the pre-experiment bacterial profiles comprise a small amount of low intensity bands, the post experimentation samples, by contrast, have an abundance of higher intensity, more readily discernible bands suggesting an amplification of a range of bacteria within the waste. While there is a degree of homogeneity in the band profiles of intra-column the post-experiment “Live” samples, there is variation in the profiles of inter-column samples. There is also heterogeneity in the relative strengths of similar bands across the samples. For example, prominent bands across all post-experiment samples are identified as “LB1” and “LB2” while a number of associated bands are denoted by “LB3” in Figure 9.36. Bands “LB1” and “LB2” are not identifiable within the pre-experiment sample, suggesting that these represent bacteria that have been stimulated into proliferation during experimentation. The same can be said of many of the bands within “LB3”. Within band “LB1” there is a disparity in the strength of the band across samples. It is much stronger within samples such as “L2”, “M1” and “U1” while it is much weaker in samples such as “L3”, “M2” and “U3”. There is no clear trend towards prevalence of the band at a specific height within the column. Band “LB2” has a similar heterogeneity in the strength of the bands though there is a slight increase in the strength of the bands in the upper and mid-column samples compared with the lower column samples.

Sample “L2” is visibly different to the majority of the other samples within “Live” column 1 with 3 particularly strong bands, 1 of which is not present at a similar strength within the other samples. The dendrogram, shown in Figure 9.39, produced by cluster analysis of the banding patterns demonstrates substantial difference in “L2” from the other post-experiment “Live” samples. Sample “L2” is located on a simplicifolious clade separate from the other post-experiment samples, highlighting the heterogeneity between “L2” and the other samples. This trend, of one substantially different sample from a column, is not seen in the other “Live” columns where more homogeneity between post-experiment samples is observed. One pattern that is consistent across all “Live” sample dendrograms is the substantial dissimilarity between the post-experiment “Live” samples and the pre-experiment samples.

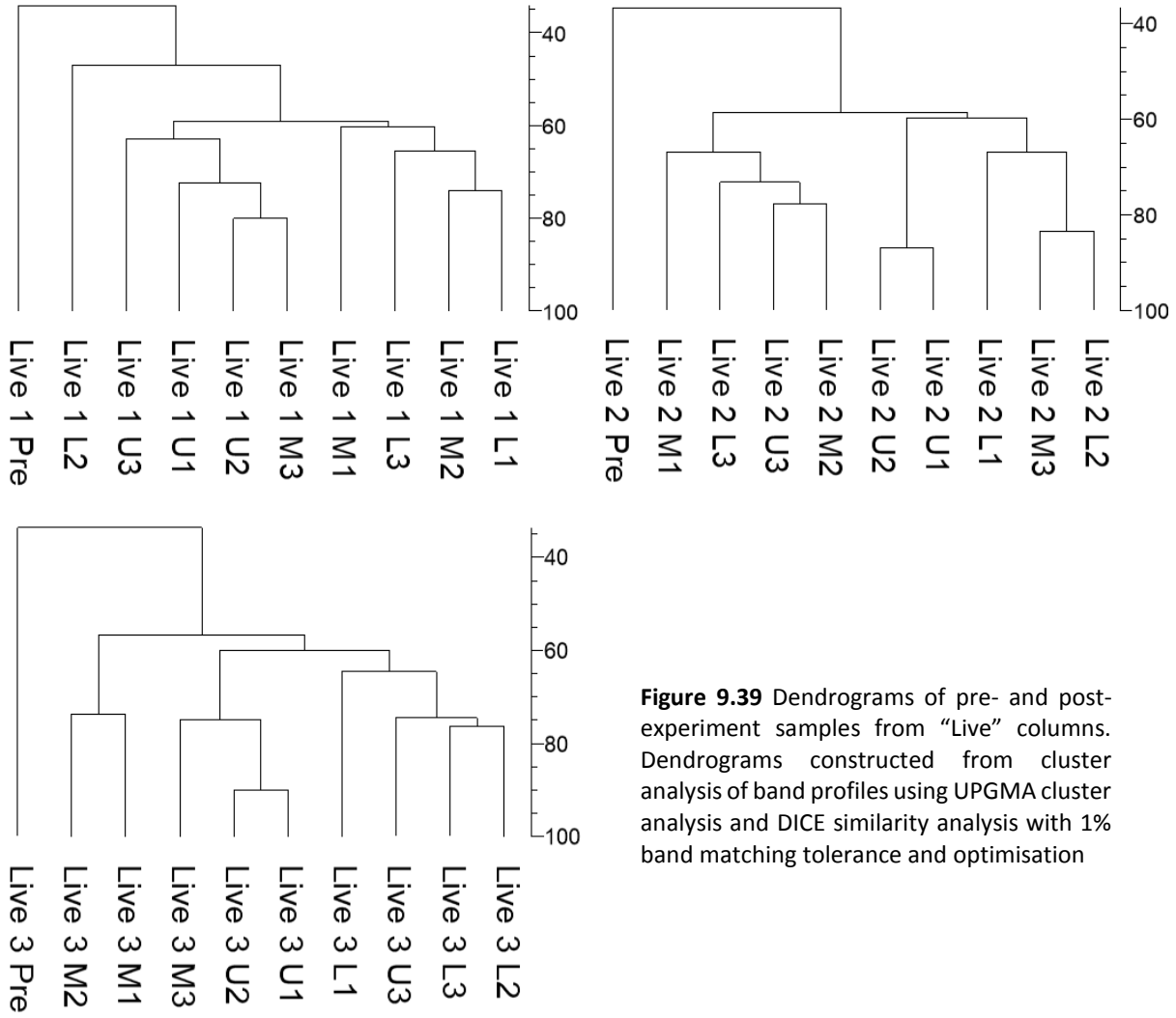

Figure 9.39 Dendrograms of pre- and post-experiment samples from "Live" columns. Dendrograms constructed from cluster analysis of band profiles using UPGMA cluster analysis and DICE similarity analysis with 1% band matching tolerance and optimisation

Excised "Live" bands and their identifiers are displayed in Appendix 4, while the results of sequencing and taxonomic identification are displayed in Table 9.3. The post-experiment samples appeared to have abundant *Desulfosporosinus spp.*, with ~60% of bands most closely matching with the genus (Figure 9.40). Various species of *Desulfosporosinus,* which have strains capable of both sulphate-reduction and iron-reduction in anaerobic conditions, were identified as the closest matches for excised bands including the species *D. lacus* (97-100% sequence ident.) (Ramamoorthy *et al.*, 2006), *D. burensis* (96-99% sequence ident.) (Mayeux *et al.*, 2013)*, D. orientis* (97% sequence ident.) (Pester *et al.*, 2012) *and D. meridei* (97% sequence ident.) (Robertson *et al.*, 2001). Though it should be noted that the relatively short read lengths prevents identification of microbes with a higher degree of certainty. Along with various series of bands within "LB3" group the "LB1" bands represent *Desulfosporosinus spp.* This trend

is continuous across all "Live" column. Other iron reducers were also identified including *Desulfitobacterium* (95% sequence ident.) and *Alicyclobacillus* (87% sequence ident.) (Yahya *et al.*, 2008; Kunapuli *et al.*, 2010; Burkhardt *et al.*, 2011). The bands denoted by "LB2" represent *Desulfitobacterium spp.* and one instance of *Anaerobacterium*.

Also identified were sequences related to the cellulose-degrading organisms *Anaerobacterium chartisolvens* (87% sequence ident.) and *Acetivibrio cellulolyticus* strain CD2 (95-100% sequence ident.). *An. chartisolvens* has been shown to be capable of fermenting carbohydrates to produce ethanol, lactate, succinate and acetate, though not able to utilise glycerol for growth (Horino *et al.*, 2014). *Acetivibrio cellulolyticus*, as a consortium of cellulose fermenters, has been observed to be capable of producing fermentation products which were then utilised as an organic carbon source for sulphate-reducing bacteria in acid mine drainage (Greben *et al.*, 2009). The presence of these cellulose fermenters suggests a more complex system wherein the degradation products from the oxidation of glycerol, or other organic compounds, are utilised within the system. This is similar to the observations of the microbial community within the previous experimentation with the Lindsay wastes. Other bacterial taxa identified, at low abundances, were *Pelotomaculum, Pseudorhodoplanes* and uncultured *Clostridium*. A phylogenetic tree displaying the relationships between the sample sequences is shown in Figure 9.41

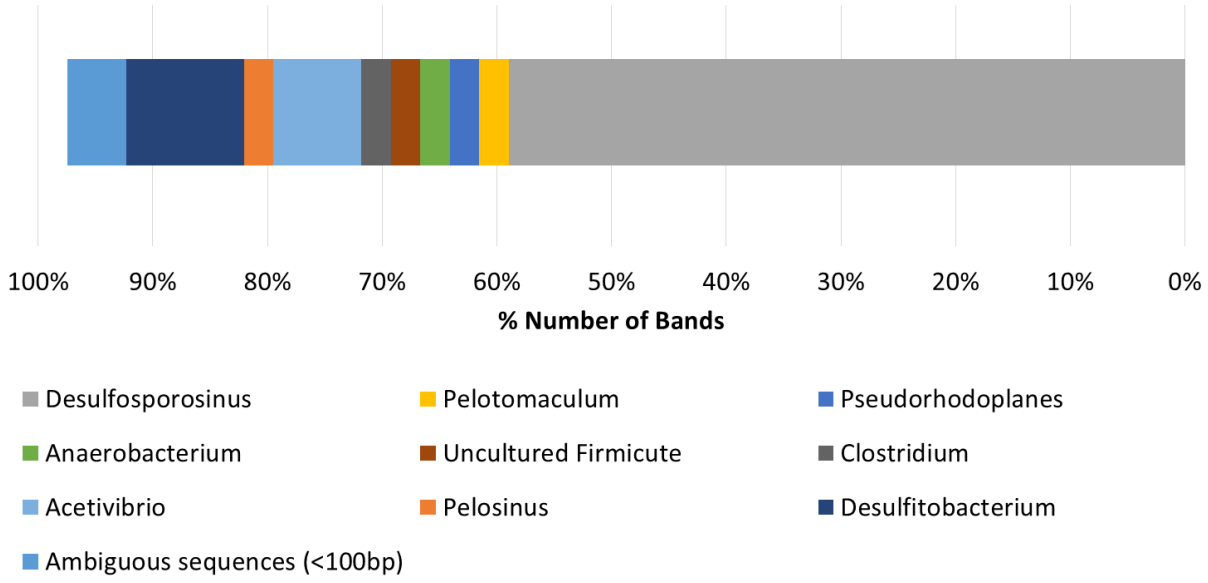

Figure 9.40 Graphical summary of closest 16S rRNA sequence matched to excised post-experiment "Live" samples DGGE bands using BLASTN search tool

Table 9.3 Closest 16S rRNA sequence matched to excised post-experiment "Live" samples DGGE bands using BLASTN search tool

Band Identifier	Closest Match	Accession Number	Sequence Identity	Alignment Length (bp)	Phylogenetic affiliation
L4	Desulfosporosinus lacus strain STP12 16S ribosomal RNA gene, complete sequence	NR_042202.1	100%	187	Clostridiales
L5	Pelotomaculum isophthalicicum strain JI 16S ribosomal RNA gene, complete sequence	NR_041320.1	98%	164	Clostridiales
L6	Desulfosporosinus lacus strain STP12 16S ribosomal RNA gene, complete sequence	NR_042202.1	100%	187	Clostridiales
L7	Desulfosporosinus lacus strain STP12 16S ribosomal RNA gene, complete sequence	NR_042202.1	99%	187	Clostridiales
L8	Desulfosporosinus lacus strain STP12 16S ribosomal RNA gene, complete sequence	NR_042202.1	98%	187	Clostridiales
L9	Desulfosporosinus lacus strain STP12 16S ribosomal RNA gene, complete sequence	NR_042202.1	99%	187	Clostridiales
L10	Pseudorhodoplanes sinuspersici strain RIPI 110 16S ribosomal RNA, partial sequence	NR_145909.1	97%	162	Alphaproteobacteria
L11	Anaerobacterium chartisolvens strain T-1-35 16S ribosomal RNA gene, partial sequence	NR_125464.1	87%	120	Clostridiales
L12	Desulfosporosinus lacus strain STP12 16S ribosomal RNA gene, complete sequence	NR_042202.1	99%	187	Clostridiales
L14	Uncultured Firmicutes bacterium 16S rRNA gene from clone QEDQ3CG01	CU923137.1	91%	163	Clostridiales
L16	Acetivibrio cellulolyticus strain CD2 16S ribosomal RNA gene, partial sequence	NR_025917.1	97%	162	Clostridiales
L20	Desulfosporosinus orientis strain DSM 765 16S ribosomal RNA gene, complete sequence	NR_074131.1	97%	187	Clostridiales
L21	Desulfosporosinus lacus strain STP12 16S ribosomal RNA gene, complete sequence	NR_042202.1	97%	187	Clostridiales
L22	Desulfosporosinus lacus strain STP12 16S ribosomal RNA gene, complete sequence	NR_042202.1	99%	187	Clostridiales
L23	Desulfosporosinus lacus strain STP12 16S ribosomal RNA gene, complete sequence	NR_042202.1	98%	187	Clostridiales
L24	Desulfosporosinus orientis strain DSM 765 16S ribosomal RNA gene, complete sequence	NR_074131.1	97%	187	Clostridiales
L25	Desulfosporosinus lacus strain STP12 16S ribosomal RNA gene, complete sequence	NR_042202.1	99%	187	Clostridiales
L26	Desulfitobacterium aromaticivorans strain UKTL 16S ribosomal RNA gene, partial sequence	NR_116427.1	95%	187	Clostridiales
L27	Pelosinus fermentans strain R7 16S ribosomal RNA gene, partial sequence	NR_109393.1	97%	187	Clostridiales
L28	Desulfosporosinus lacus strain STP12 16S ribosomal RNA gene, complete sequence	NR_042202.1	99%	187	Clostridiales
L29	Desulfosporosinus meridiei strain DSM 13257 16S ribosomal RNA gene, complete sequence	NR_074129.1	97%	187	Clostridiales
L30	Desulfosporosinus lacus strain STP12 16S ribosomal RNA gene, complete sequence	NR_042202.1	97%	187	Clostridiales
L31	Uncultured Desulfitobacterium sp. clone E41_bac 16S ribosomal RNA gene, partial sequence	EF464638.1	100%	110	Clostridiales
L34	Desulfosporosinus lacus strain STP12 16S ribosomal RNA gene, complete sequence	NR_042202.1	99%	187	Clostridiales

Table 9.3 Continued

L35	Desulfosporosinus lacus strain STP12 16S ribosomal RNA gene, complete sequence	NR_042202.1	99%	187	Clostridiales
L36	Desulfitobacterium aromaticivorans strain UKTL 16S ribosomal RNA gene, partial sequence	NR_116427.1	93%	111	Clostridiales
L37	Desulfosporosinus lacus strain STP12 16S ribosomal RNA gene, complete sequence	NR_042202.1	100%	187	Clostridiales
L38	[Clostridium] hungatei strain AD 16S ribosomal RNA gene, partial sequence	NR_114425.1	91%	120	Clostridiales
L39	Pelotomaculum isophthalicicum strain JI 16S ribosomal RNA gene, complete sequence	NR_041320.1	98%	164	Clostridiales
L40	Acetivibrio cellulolyticus strain CD2 16S ribosomal RNA gene, partial sequence	NR_025917.1	98%	162	Clostridiales
L41	Desulfosporosinus burensis strain BSREI1 16S ribosomal RNA gene, partial sequence	NR_109421.1	99%	187	Clostridiales
L42	Desulfosporosinus burensis strain BSREI1 16S ribosomal RNA gene, partial sequence	NR_109421.1	98%	187	Clostridiales
L43	Desulfitobacterium aromaticivorans strain UKTL 16S ribosomal RNA gene, partial sequence	NR_116427.1	95%	187	Clostridiales
L44	Desulfosporosinus lacus strain STP12 16S ribosomal RNA gene, complete sequence	NR_042202.1	99%	187	Clostridiales
L45	Desulfosporosinus lacus strain STP12 16S ribosomal RNA gene, complete sequence	NR_042202.1	100%	187	Clostridiales
L46	Desulfosporosinus lacus strain STP12 16S ribosomal RNA gene, complete sequence	NR_042202.1	100%	187	Clostridiales
L47	Acetivibrio cellulolyticus strain CD2 16S ribosomal RNA gene, partial sequence	NR_025917.1	95%	163	Clostridiales

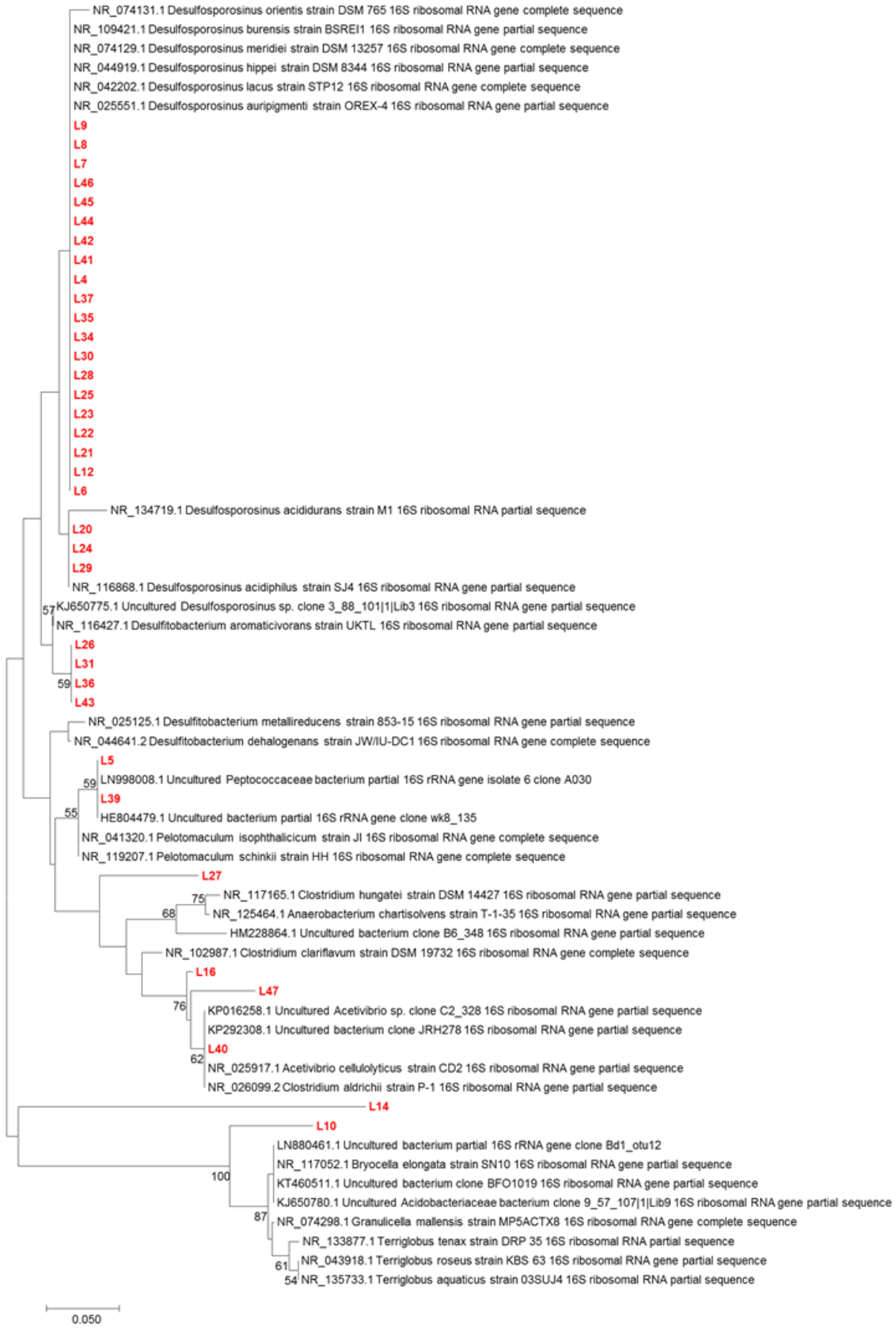

Figure 9.41 Phylogenetic tree showing relationship between 16S rRNA gene sequence DGGE bands retrieved from post-experiment "Live" samples of Parys Mt. 2 waste and related reference sequences. Neighbour-joining tree constructed using the Jukes-Cantor substitution model. Bootstrap support values over 50% are shown (1000 replicates).

While the “Live” samples have shown significant alteration in the DGGE profiles of the samples, much less alteration has occurred in the “Organic Starved” samples. While previously weak bands were amplified in the “Live” columns, the bands that have amplified within the “Organic Starved” wastes are all visible within the pre-experiment samples. Visually there is little distinction between either the pre- and post-experiment samples, replicate samples or those which represent different heights within the columns. This is also demonstrated by the dendrograms produced by cluster analysis of the DGGE profiles (Figure 9.42). “Organic Starved” column 3 is the exception to this with the dendrogram indicating that the samples from the upper section of the column, along with the sample “M3”, are substantially different to the other samples from the column.

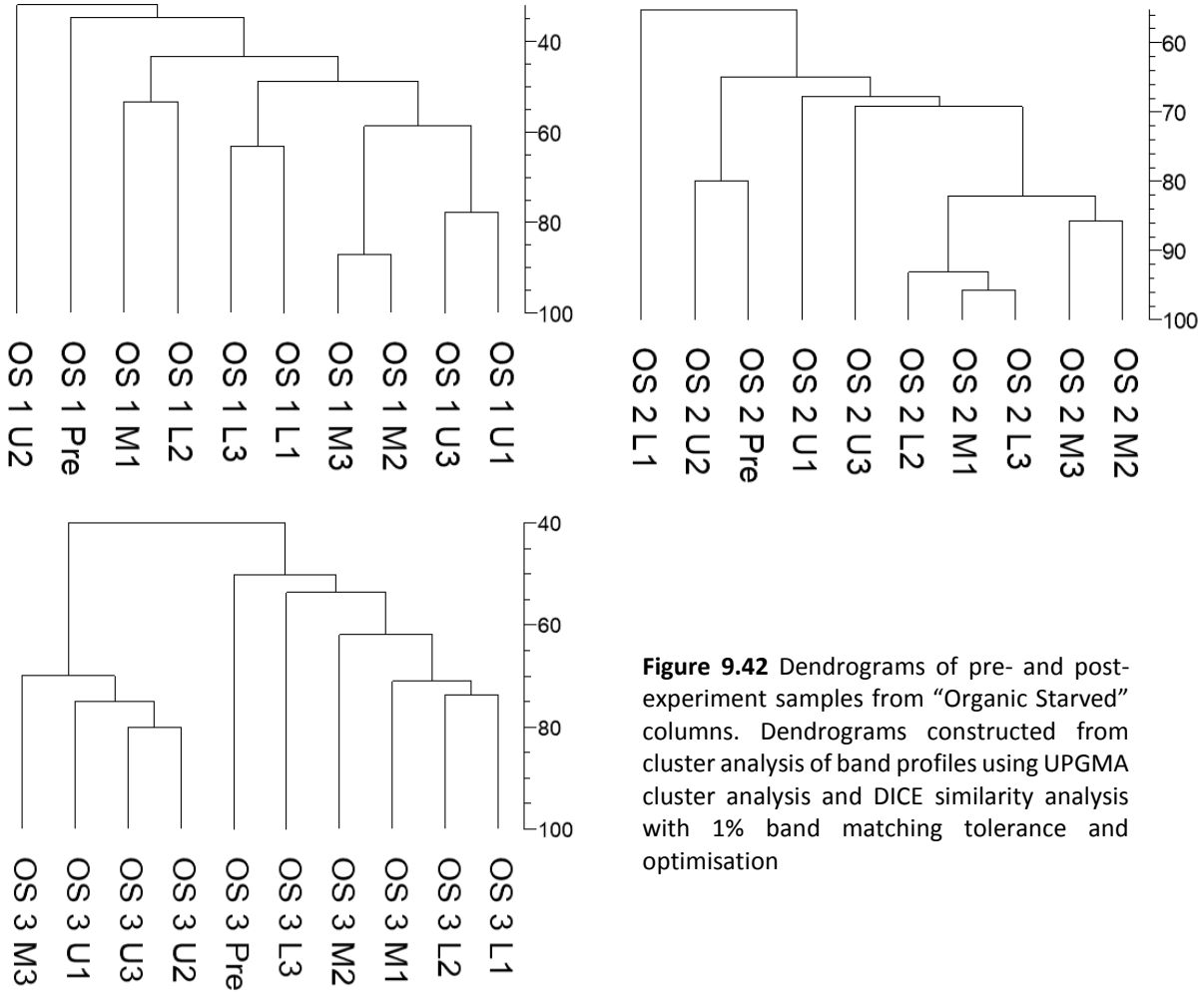

Figure 9.42 Dendrograms of pre- and post-experiment samples from “Organic Starved” columns. Dendrograms constructed from cluster analysis of band profiles using UPGMA cluster analysis and DICE similarity analysis with 1% band matching tolerance and optimisation

With a few exceptions, the bands in the “Organic Starved” profiles are generally less intense than in the “Live” equivalent samples (Figure 9.43). Within “Organic Starved” columns 1 and 2 the DGGE profiles are particularly low intensity suggesting that the bacteria within the waste have undergone negligible proliferation in the absence of an organic carbon source, in accordance with the results of the effluent analysis and qPCR results. “Organic Starved” column 3 again proves to be the exception with band intensities far more varied than the other columns. While the profile of the bands are similar to the other columns there are intense bands within samples “L1”, “M1”, “M2” and “U1”. With the exception of these more intense bands, very few of the bands were suitable for excision and sequencing due to being too small or diffuse to accurately excise. The excised bands and their identifiers are displayed in Appendix 4, while the results of sequencing and taxonomic identification for the excised “Organic Starved” sample band are displayed in Table 9.4.

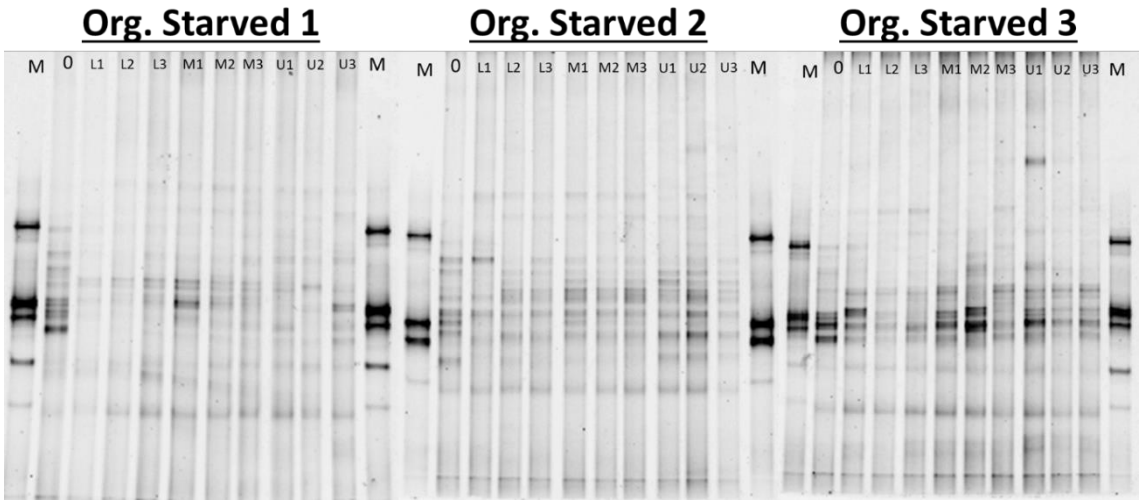

Figure 9.43 DGGE profiles for “Organic Starved” columns. M = Marker, 0 = Preliminary sample, L# =Lower column replicate sample, M# =Mid-column replicate sample, U# =Upper-column replicate sample.

Despite the dendrograms suggesting minimal differences between the pre-experiment and post-experiment, the results of sequencing the excised bands suggests that there has been alteration in the structure of the bacterial community (Figure 9.44). Of the taxa identified, sequences matching closest to *Bryocella elongata* were the most abundant with 30% of bands identified matching this species (93-99% sequence ident.). Its presence within the post-experiment “Organic Starved” samples suggests that the addition of glycerol in not necessary for the proliferation of *Bryocella elongata* as was

observed in the "Live" samples. This suggests that once anaerobic conditions are established the *Bryocella elongata* are utilising pre-existing organic carbon within the waste for growth. 5% of bands were identified as *Desulfosporosinus spp.* (84% sequence ident.) while a further 5% matched closest to an uncultured *Desulfosporosinus* (83% sequence ident.). This suggests there has been an increase in the abundance of *Desulfosporosinus* despite the lack of an external organic carbon source. The lack of clear indications of iron or sulphur-reduction in the "Organic Starved" effluent columns is indicative that despite, the presence of the iron/sulphur reducing *Desulfosporosinus*, they are not present at high enough abundance or active enough to stimulate significant iron-reduction. Other taxa that were matched closest with sequences taken from both the pre-experiment and post-experiment "Organic Starved" samples included *Leptolinea* (100% sequence ident.) and *Acetivibrio* (98% sequence ident.).

One genus which was identified in the post-experimental samples, despite not being identified within the pre-experiment samples, was *Nocardioides*. Though the only example of this genus that was identified was only matched with a sequence identity of 87% resulting in this identification lacking certainty. 40% of bands sequenced were matched closest with series of uncultured bacteria. This was due in part to low values of matched sequence identity, which itself is a result of difficulties in excising DGGE bands due to their diffuse nature and proximity of multiple bands. A phylogenetic tree displaying the relationships between the sample sequences is shown in Figure 9.45

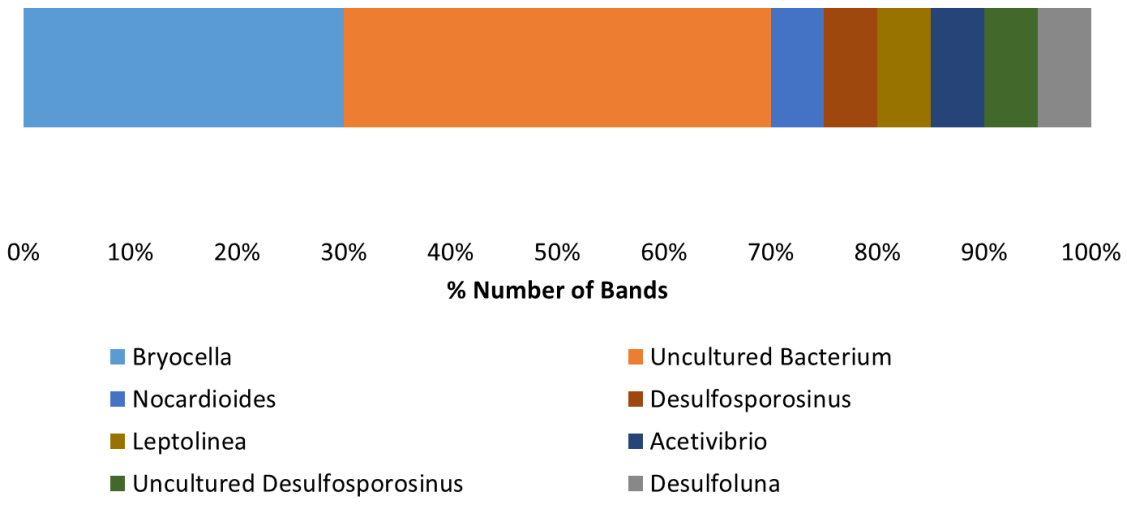

Figure 9.44 Graphical summary of closest 16S rRNA sequence matched to excised post-experiment "Organic Starved" samples DGGE bands using BLASTN search tool

Table 9.4 Closest 16S rRNA sequence matched to excised post-experiment "Organic Starved" samples DGGE bands using BLASTN search tool

Band Identifier	Closest Match	Accession Number	Sequence Identity	Alignment Length	Phylogenetic affiliation
OS6	Nocardioides daedukensis strain MDN22 16S ribosomal RNA gene, partial sequence	NR_104527.1	87%	164	Actinobacteria
OS7	Uncultured bacterium clone D6C_029 16S ribosomal RNA gene, partial sequence	EF444402.1	90%	121	Bacteria
OS8	Bryocella elongata strain SN10 16S ribosomal RNA gene, partial sequence	NR_117052.1	98%	162	Clostridiales
OS9	Bryocella elongata strain SN10 16S ribosomal RNA gene, partial sequence	NR_117052.1	99%	161	Clostridiales
OS16	Uncultured cyanobacterium clone ZJ0902B88 16S ribosomal RNA gene, partial sequence	KU173706.1	87%	141	Cyanobacteria
OS17	Bryocella elongata strain SN10 16S ribosomal RNA gene, partial sequence	NR_117052.1	98%	118	Clostridiales
OS18	Uncultured bacterium clone EV221H2111601SAH44 16S ribosomal RNA gene, partial sequence	DQ223210.1	91%	164	Bacteria
OS19	Bryocella elongata strain SN10 16S ribosomal RNA gene, partial sequence	NR_117052.1	98%	161	Clostridiales
OS20	Uncultured bacterium clone EV221H2111601SAH44 16S ribosomal RNA gene, partial sequence	DQ223210.1	96%	121	Bacteria
OS21	Uncultured bacterium clone CSBC4G12 16S ribosomal RNA gene, partial sequence	GU126997.1	95%	139	Bacteria
OS22	Bryocella elongata strain SN10 16S ribosomal RNA gene, partial sequence	NR_117052.1	93%	118	Clostridiales
OS23	Desulfosporosinus acidiphilus strain SJ4 16S ribosomal RNA gene, complete sequence	NR_074132.1	84%	110	Clostridiales
OS28	Acetivibrio cellulolyticus strain CD2 16S ribosomal RNA gene, partial sequence	NR_025917.1	98%	163	Clostridiales
OS29	Uncultured Desulfosporosinus sp. clone II_3b_4 16S ribosomal RNA gene, partial sequence	EU755180.1	83%	111	Clostridiales
OS30	Bryocella elongata strain SN10 16S ribosomal RNA gene, partial sequence	NR_117052.1	99%	161	Clostridiales
OS32	Uncultured bacterium clone PACOL4_13 16S ribosomal RNA gene, partial sequence	GQ257672.1	83%	164	Bacteria
OS33	Uncultured bacterium clone rPB38 16S ribosomal RNA gene, partial sequence	HQ330623.1	88%	162	Bacteria
OS34	Desulfoluna butyratoxydans strain MSL71 16S ribosomal RNA gene, partial sequence	NR_040975.1	87%	189	Bacteria
OS35	Leptolinea tardivitalis strain YMTK-2 16S ribosomal RNA gene, partial sequence	NR_040971.1	100%	161	Anaerolineae

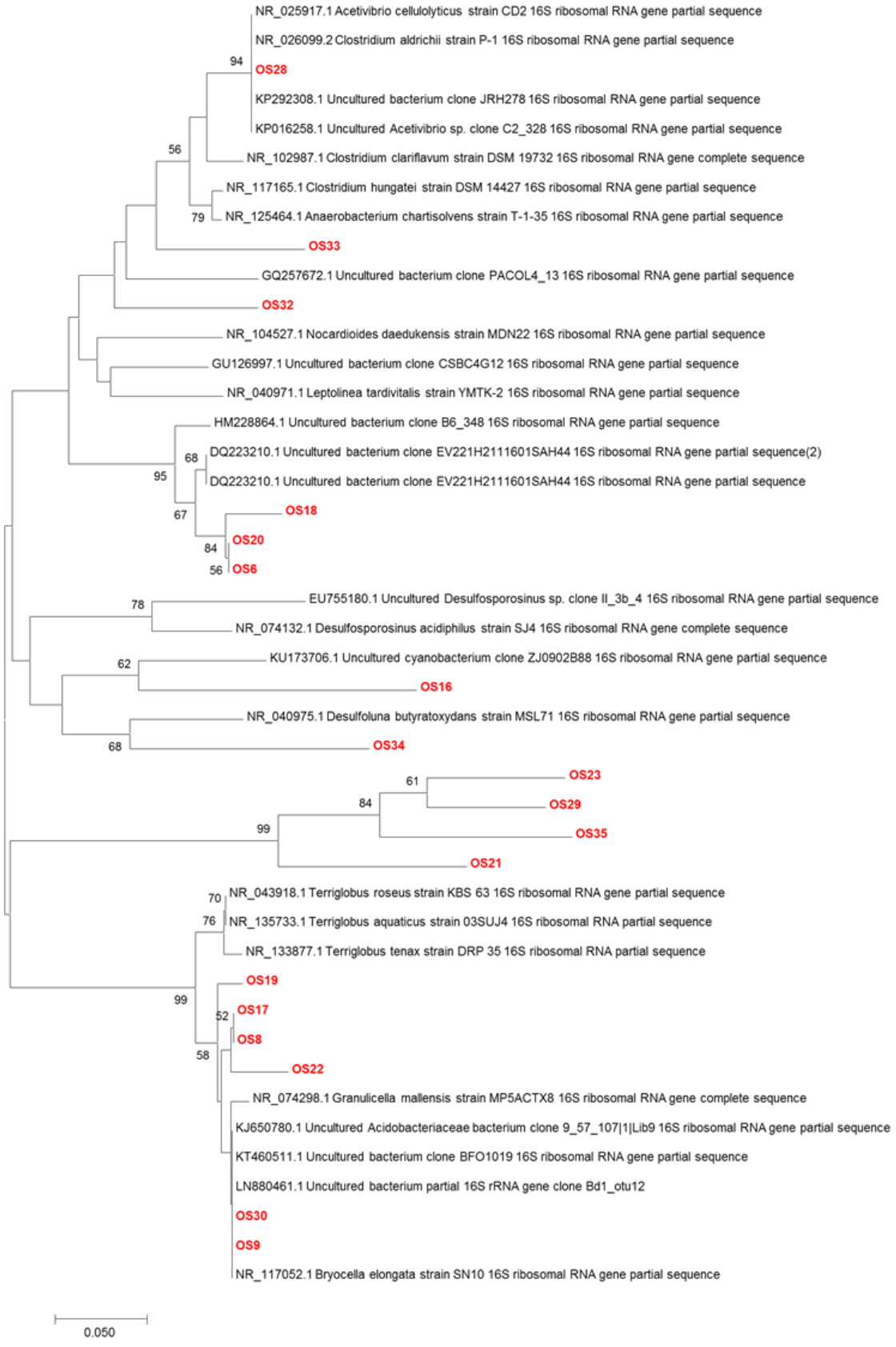

Figure 9.45 Phylogenetic tree showing relationship between 16S rRNA gene sequence DGGE bands retrieved from post-experiment "Organic Starved" samples of Parys Mt. 2 waste and related reference sequences. Neighbour-joining tree constructed using the Jukes-Cantor substitution model. Bootstrap support values over 50% are shown (1000 replicates)

The DGGE profile for the autoclaved pre-experiment samples are devoid of any bands. This confirms that the autoclaving process has been successful and despite the qPCR showing remnant gene copies after autoclaving these are no longer fully functional or able to be visualised by PCR-DGGE. Stimulation of remnant communities has clearly occurred however, as evidenced both by the analysis of the column effluents and the DGGE profiles (Figure 9.46). The profiles of the post-experiment "Autoclaved" samples are similar in pattern to the "Live" column profiles. Whilst there are, visually, a similar number of discrete bands to the "Live" samples, there are fewer high intensity bands.

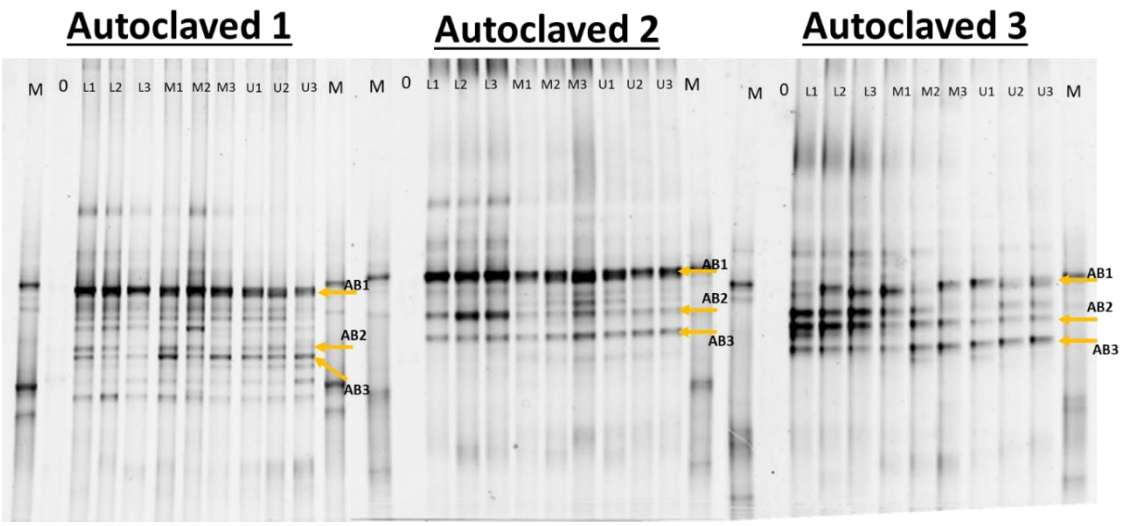

Figure 9.46 DGGE profiles for "Autoclaved" columns. M = Marker, 0 = Preliminary sample, L# =Lower column replicate sample, M# =Mid-column replicate sample, U# =Upper-column replicate sample. Arrows denote prominent bands consistent across gel profiles

The profiles of "Autoclaved" columns 1 and 2 samples, taken from all three positions within the columns, are relatively homogenous. Both columns are dominated by 3 brightly stained bands that are continuous throughout all samples. These are denoted "AB1", "AB2" and "AB3" in Figure 9.46, with the bands within "AB1" being the highest intensity bands observed. Bands "AB1" and "AB3" correlate with the positions of "LB1" and "LB2", respectively, from the "Live" columns, with the marker lanes acting as references. Bands "AB3" and "AB1", while still visible, are far less prominent in the "Autoclaved" column 3 profiles. The band denoted "AB2" is more prominent than seen in the other replicate columns. Within "Autoclaved" column 3 there is a clear

heterogeneity in the band intensities of samples at different heights in the column. The samples taken from the lower section of the column have produced profiles with a greater concentration of high intensity bands compared with the samples taken from the middle and upper sections of the column. This disparity is demonstrated by the dendrogram resulting from cluster analysis of the DGGE profiles (Figure 9.47). The dendrogram for the samples from "Autoclaved" column 3 show the lower samples located on claves separate from other samples. Despite not been initially clear from visual analysis the same relationship is seen in the dendrogram for the "Autoclaved" column 2 samples. This correlates with the results of qPCR analysis which identified higher concentrations of gene copies in the lower section of the columns and decreasing upwards. In all dendrograms the pre-experiment samples are located separately from the post-experiment samples highlighting the extensive alteration in the DGGE profiles.

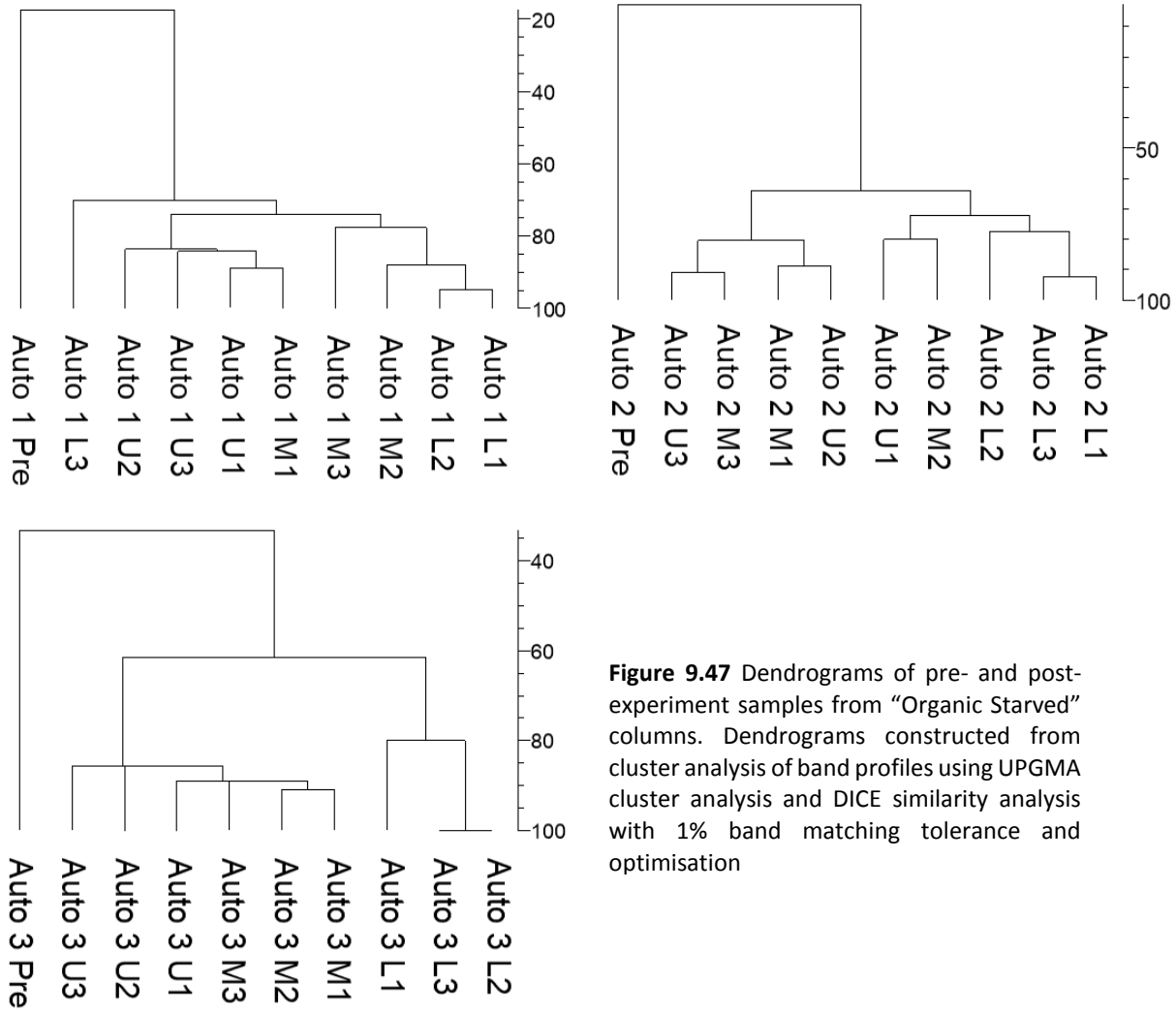

Figure 9.47 Dendrograms of pre- and post-experiment samples from "Organic Starved" columns. Dendrograms constructed from cluster analysis of band profiles using UPGMA cluster analysis and DICE similarity analysis with 1% band matching tolerance and optimisation

Bands were excised and sequenced to identify the phylotypes they represent. The excised bands and their identifiers are displayed in Appendix 4, while the results of sequencing and taxonomic identification for the excised "Autoclaved" sample band are displayed in Table 9.5. As can be seen in Figure 9.48, by far the most abundant taxa identified from the excised bands is the genus *Desulfosporosinus* with ~86% of excised bands matching closest with this genus (96-100% sequence ident.). This is similar to the observations of the microbial communities in the "Live" wastes where the genus *Desulfosporosinus* was also the most often identified taxa identified. All the bands taken from the "Autoclaved" columns 1 and 2 has sequences matching closest with *Desulfosporosinus spp.*, while the majority of bands taken from the "Autoclaved" column 1 were also attributable to this genus. The prominant bands denoted "AB1" and "AB2" both matched closest with *Desulfosporosinus spp.* All bands extracted from "AB2" band group matched closest with the 16S rRNA gene sequence for *Desulfosporosinus lacus* STP12, while the excised bands from the "AB1" group matched closest with a variety of *Desulfosporosinus* species (i.e. *D. acidiphilus, D. acididurans, D. otientis*). Members of the genus *Desulfosporosinus* are, in part, typified by their ability to form endospores when under stress. It is likely that this ability to sporulate is the mechanism by which they have seemingly survived autoclaving. The presence of spores, as opposed to surviving, functional bacteria, also correlates with the blank DGGE profiles of the autoclaved pre-experiment waste. This ability to survive autoclaving via sporulation has been observed in members of the *Desulfitomaculum* genus, a close relative of *Desulfosporosinus* (O'Sullivan *et al.*, 2015). As has been previously discussed, members of the genus *Desulfosporosinus* are capable of both sulphate and iron reduction under anaerobic conditions (Pester *et al.*, 2012), explaining the iron reduction indicated by the experimental column effluents.

In further similarity to the "Live" column samples sequences matching to both *Desulfitobacterium* (95% sequence ident.) (an iron/sulphate reducing genus) and *Acetivibrio* (93-98% sequence ident.) (a cellulose fermenting genus) were identified; though only in the bands excised from samples of "Autoclaved" column 1. Along with *Desulfosporosinus,* bands matching *Acetivibrio* sequences comprise the prominent band denoted "AB3". The only other taxon identified was one example of *Streptococcus rubneri* from sample "M2" in "Autoclaved" column 1. *Streptococcus rubneri* is typically

found in the human throat, suggesting that its presence in the analysis is a result of contamination of the DNA extract rather than a reflection of its presence in the waste (Huch *et al.*, 2013). Further suggestion that this is an anomaly resulting from contamination comes from the DGGE profile. The band identified to represent *Streptococcus rubneri* was a high intensity band that was not present in any other sample in any of the "Autoclaved" columns and has not been identified in the "Live" and "Organic Starved" columns either (Appendix 4). A phylogenetic tree displaying the relationships between the sample sequences is shown in Figure 9.49.

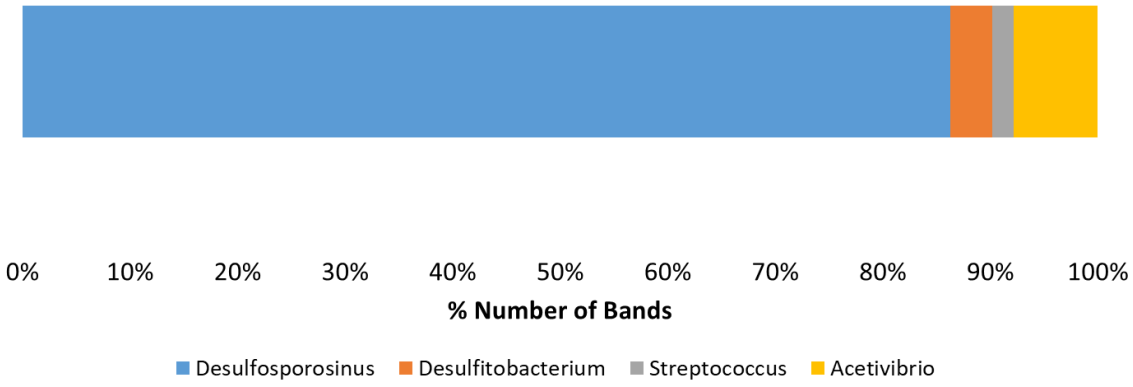

Figure 9.48 Graphical summary of closest 16S rRNA sequence matched to excised post-experiment "Autoclaved" samples DGGE bands using BLASTN search tool

Table 9.5 Closest 16S rRNA sequence matched to excised post-experiment "Autoclaved" samples DGGE bands using BLASTN search tool

Band Identifier	Closest Match	Accession Number	Sequence Identity	Alignment Length	Phylogenetic affiliation
A1	Desulfosporosinus acidiphilus strain SJ4 16S ribosomal RNA gene, partial sequence	NR_116868.1	97%	187	Clostridiales
A2	Desulfosporosinus lacus strain STP12 16S ribosomal RNA gene, complete sequence	NR_042202.1	98%	190	Clostridiales
A3	Desulfosporosinus acididurans strain M1 16S ribosomal RNA, partial sequence	NR_074132.1	97%	185	Clostridiales
A4	Desulfosporosinus lacus strain STP12 16S ribosomal RNA gene, complete sequence	NR_042202.1	99%	187	Clostridiales
A5	Desulfitobacterium aromaticivorans strain UKTL 16S ribosomal RNA gene, partial sequence	NR_116427.1	95%	187	Clostridiales
A6	Desulfosporosinus acidiphilus strain SJ4 16S ribosomal RNA gene, partial sequence	NR_116868.1	97%	187	Clostridiales
A7	Desulfosporosinus lacus strain STP12 16S ribosomal RNA gene, complete sequence	NR_042202.1	95%	183	Clostridiales
A8	Acetivibrio cellulolyticus strain CD2 16S ribosomal RNA gene, partial sequence	NR_025917.1	98%	162	Clostridiales
A9	Acetivibrio cellulolyticus strain CD2 16S ribosomal RNA gene, partial sequence	NR_025917.1	93%	113	Clostridiales
A10	Desulfosporosinus acididurans strain M1 16S ribosomal RNA, partial sequence	NR_134719.1	97%	187	Clostridiales
A11	Desulfosporosinus orientis strain DSM 765 16S ribosomal RNA gene, complete sequence	NR_074131.1	96%	187	Clostridiales
A12	Streptococcus rubneri strain LMG 27207 16S ribosomal RNA gene, partial sequence	NR_109720.1	98%	187	Lactobacillales
A13	Acetivibrio cellulolyticus strain CD2 16S ribosomal RNA gene, partial sequence	NR_025917.1	98%	118	Clostridiales
A14	Desulfosporosinus burensis strain BSREI1 16S ribosomal RNA gene, partial sequence	NR_109421.1	98%	187	Clostridiales
A15	Desulfitobacterium aromaticivorans strain UKTL 16S ribosomal RNA gene, partial sequence	NR_116427.1	97%	187	Clostridiales
A16	Acetivibrio cellulolyticus strain CD2 16S ribosomal RNA gene, partial sequence	NR_025917.1	99%	162	Clostridiales
A17	Desulfosporosinus auripigmenti strain OREX-4 16S ribosomal RNA gene, partial sequence	NR_025551.1	97%	162	Clostridiales
A18	Desulfosporosinus acidiphilus strain SJ4 16S ribosomal RNA gene, complete sequence	NR_074132.1	97%	187	Clostridiales
A19	Desulfosporosinus lacus strain STP12 16S ribosomal RNA gene, complete sequence	NR_042202.1	99%	187	Clostridiales
A20	Desulfosporosinus acidiphilus strain SJ4 16S ribosomal RNA gene, complete sequence	NR_074132.1	97%	187	Clostridiales
A21	Desulfosporosinus meridiei strain DSM 13257 16S ribosomal RNA gene, complete sequence	NR_074129.1	97%	187	Clostridiales
A22	Desulfosporosinus lacus strain STP12 16S ribosomal RNA gene, complete sequence	NR_042202.1	98%	187	Clostridiales
A23	Desulfosporosinus lacus strain STP12 16S ribosomal RNA gene, complete sequence	NR_042202.1	98%	187	Clostridiales
A24	Desulfosporosinus lacus strain STP12 16S ribosomal RNA gene, complete sequence	NR_042202.1	93%	158	Clostridiales

Table 9.5 Continued

A25	Desulfosporosinus lacus strain STP12 16S ribosomal RNA gene, complete sequence	NR_042202.1	98%	187	Clostridiales
A26	Desulfosporosinus lacus strain STP12 16S ribosomal RNA gene, complete sequence	NR_042202.1	100%	187	Clostridiales
A27	Desulfosporosinus lacus strain STP12 16S ribosomal RNA gene, complete sequence	NR_042202.1	99%	187	Clostridiales
A28	Desulfosporosinus lacus strain STP12 16S ribosomal RNA gene, complete sequence	NR_042202.1	100%	187	Clostridiales
A29	Desulfosporosinus lacus strain STP12 16S ribosomal RNA gene, complete sequence	NR_042202.1	98%	187	Clostridiales
A30	Desulfosporosinus lacus strain STP12 16S ribosomal RNA gene, complete sequence	NR_042202.1	98%	187	Clostridiales
A31	Desulfosporosinus lacus strain STP12 16S ribosomal RNA gene, complete sequence	NR_042202.1	99%	187	Clostridiales
A32	Desulfosporosinus lacus strain STP12 16S ribosomal RNA gene, complete sequence	NR_042202.1	99%	187	Clostridiales
A33	Desulfosporosinus lacus strain STP12 16S ribosomal RNA gene, complete sequence	NR_042202.1	98%	187	Clostridiales
A34	Desulfosporosinus orientis strain DSM 765 16S ribosomal RNA gene, complete sequence	NR_074131.1	97%	187	Clostridiales
A35	Desulfosporosinus lacus strain STP12 16S ribosomal RNA gene, complete sequence	NR_042202.1	98%	187	Clostridiales
A36	Desulfosporosinus lacus strain STP12 16S ribosomal RNA gene, complete sequence	NR_042202.1	99%	187	Clostridiales
A37	Desulfosporosinus lacus strain STP12 16S ribosomal RNA gene, complete sequence	NR_042202.1	98%	187	Clostridiales
A38	Desulfosporosinus lacus strain STP12 16S ribosomal RNA gene, complete sequence	NR_042202.1	99%	187	Clostridiales
A39	Desulfosporosinus lacus strain STP12 16S ribosomal RNA gene, complete sequence	NR_042202.1	99%	187	Clostridiales
A40	Desulfosporosinus lacus strain STP12 16S ribosomal RNA gene, complete sequence	NR_042202.1	98%	187	Clostridiales
A41	Desulfosporosinus lacus strain STP12 16S ribosomal RNA gene, complete sequence	NR_042202.1	98%	187	Clostridiales
A42	Desulfosporosinus orientis strain DSM 765 16S ribosomal RNA gene, complete sequence	NR_074131.1	97%	187	Clostridiales
A43	Desulfosporosinus lacus strain STP12 16S ribosomal RNA gene, complete sequence	NR_042202.1	99%	187	Clostridiales
A44	Desulfosporosinus lacus strain STP12 16S ribosomal RNA gene, complete sequence	NR_042202.1	98%	187	Clostridiales
A45	Desulfosporosinus lacus strain STP12 16S ribosomal RNA gene, complete sequence	NR_042202.1	100%	187	Clostridiales
A46	Desulfosporosinus lacus strain STP12 16S ribosomal RNA gene, complete sequence	NR_042202.1	99%	187	Clostridiales
A47	Desulfosporosinus lacus strain STP12 16S ribosomal RNA gene, complete sequence	NR_042202.1	97%	187	Clostridiales

Table 9.5 Continued

A48	Desulfosporosinus lacus strain STP12 16S ribosomal RNA gene, complete sequence	NR_042202.1	98%	187	Clostridiales
A49	Desulfosporosinus orientis strain DSM 765 16S ribosomal RNA gene, complete sequence	NR_074131.1	97%	187	Clostridiales
A50	Desulfosporosinus lacus strain STP12 16S ribosomal RNA gene, complete sequence	NR_042202.1	99%	187	Clostridiales
A51	Desulfosporosinus lacus strain STP12 16S ribosomal RNA gene, complete sequence	NR_042202.1	98%	187	Clostridiales

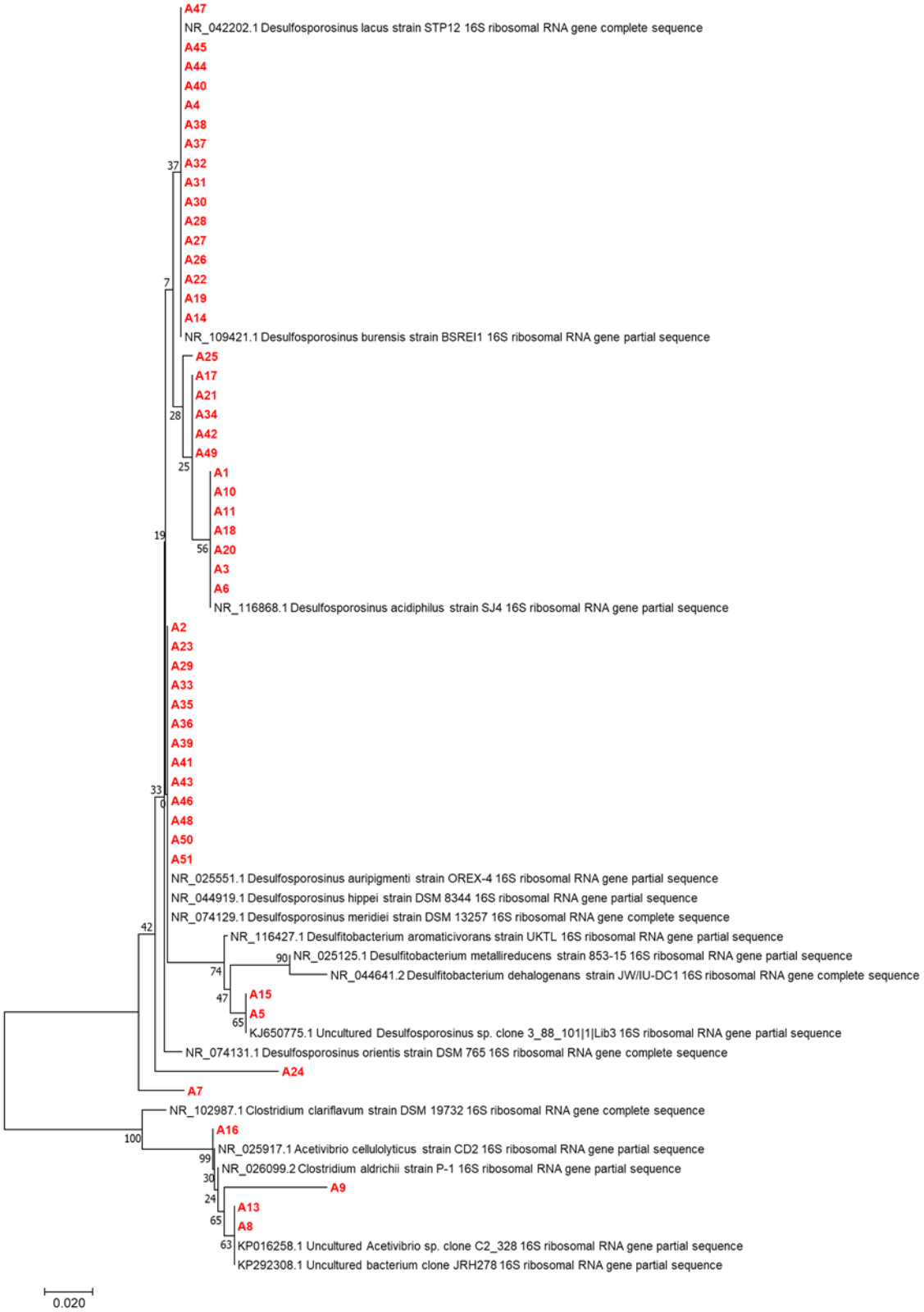

Figure 9.49 Phylogenetic tree showing relationship between 16S rRNA gene sequence clones retrieved from post-experiment "Autoclaved" samples of Parys Mt. 2 waste and related reference sequences. Neighbour-joining tree constructed using the Jukes-Cantor substitution model. Bootstrap support values over 50% are shown (1000 replicates)

Analysis of DGGE profiles has provided an indication of the relative diversity of microbial communities within the wastes and allowed visualisation of changes to said communities resulting from the introduction of glycerol as an organic electron donor. Sequencing of 16S rRNA gene sequences obtained from excised DGGE bands has also provided an indication of the constituents of the microbial communities. However, the limitations of these methods of analysis must be acknowledged. While excising bands for sequencing does provide genetic information it is heavily subjected to sampling bias as only the best defined, high intensity bands are generally suitable for excision and sequencing. The results are also limited by the quality of the excision, with poor excisions resulting in multiple gene sequences and poor-quality reads when sequencing. The use of only a single DNA extraction kit and analysis using only one primer pair also presents a source for potential bias as there may be bacteria under-represented in the analysis due to the inability of to either extract or amplify them with the chosen extraction/ amplification methodology.

Despite these limitations, the results of DGGE and sequencing has provided at least partial description of the microbial communities of the wastes. It has also described changes to these communities caused by autoclaving, addition (or starvation) of organic carbon or a combination of these factors. It also served reference from which to inform the choice of samples for more in-depth analysis and as a comparison for the subsequent results. For example, a reduced selection of samples from the “Autoclaved” samples were further analysed with the Illumina MiSeq methodology based on the suggested limited diversity of the communities in these samples. This selection comprised 9 samples, with a single sample covering the upper, middle and lower sections of each of the 3 “Autoclaved” experimental columns.

9.4.3.3. Taxonomic Identification by Illumina Sequencing of Bacterial and Archaeal 16S rRNA genes

Sequences generated by next generation Illumina sequencing were used to identify and characterize microbial communities within the Parys Mt. 2 wastes both pre- and post-experiment. Sequences were classified from phyla to genera level and quantified by relative abundance. The relative abundance of a given bacteria group was defined as the

number of sequences in a group divided by the total number of sequences within a sample.

A total of 14 different phyla were matched with >97% sequence identity to the OTUs identified in the pre-experiment Parys Mt. 2 waste, consisting of 12 bacterial phyla and 2 archaeal phyla (Figure 9.50). Of these, 8 of the bacterial and both archaeal phyla are present at ≥1% relative abundance. This suggests a substantially less diverse environment than the Lindsay waste studied previously which had sequences matching at >97% sequence identity with 40 different phyla. This is likely a result of the more challenging environment presented by the acidic, metalliferous Parys Mt. 2 waste as opposed to the circum neutral Lindsay waste which is devoid of any significant metal concentrations aside from iron. There is no single phylum that clearly dominates the sequences identified with *Planctomycetes* the most abundant with 23.9% of all sequences matching to >97% sequence identity within this phylum. The *Firmicute* phylum is the next most abundant (16.3%) followed by the *Proteobacteria* (14.1%). Both of these phyla are dominated by 2 classes with *Bacilli* (10.1%) and *Clostridia* (6.2%) representing the entirety of the *Firmicute* matched sequences, while *alphaproteobacteria* (4.9%) and gamma*Proteobactaria* (8.4%) represent the majority of the *Proteobacteria* matched sequences. The other bacterial phyla identified are; *Chloroflexi* (13.1%), *Cyanobacteria* (8.5%), *Acidobacteria* (4.2%), *Actinobacteria* (3.9%) *and Nitrospirae* (2.3%). The two archaeal phyla identified were *Euryachaeota* (7.6%) and *Thaumarchaeota* (5.3%).

In total 21 genera were observed, with >97% sequence identity matching to the identified OTUs, with abundances of ≥1%, 3 of which were archaeal genera (Figure 9.51). However, only 8 of these matched genera have been cultured and described at genera level with the remainder representing uncultured bacterium or archaeons of higher orders or classes. Uncultured bacterium within the *Planctomycetes* order *CPLa-3 termite group* were matched to >97% sequence identity to 18.5% of the sequences identified, while 12.9% of sequences matching to an uncultured bacterium within the *Cloroflexi* class *JG37-AG-4*. Of the 8 cultured genera identified the most abundant is *Acidibacillus* (10.0%) which represents the majority of the *Bacillus* class. Species within this genus are acidophiles with some, such as *Acidibacillus ferrooxidans* (Nancucheo et al., 2016) and *Acidibacilus Sulfooxidans* (Shiers *et al.*, 2016), capable of both iron-oxidation and

reduction. and have previously been identified in acidic metalliferous mine wastes (Shiers *et al.*, 2016). *Acidibacilus Sulfooxidans* has been utilised in metal recovery studies for the recovery of copper from mine tailings (Falagán *et al.*, 2017) and cobalt from limonitic ores (Smith *et al.*, 2017). The other genera matched to OTUs at >97% sequence identity are present at relatively low relative abundances; *Desulfosporosinus* (2.0%), *Clostridum sensu stricto 12* (1.7%), *Leptospirillum* (2.3%), *Acidiphilium* (1.9%), *Escherichia-Shigella* (1.7%), *Metallibacterium* (1.2%) and *Acidibacter* (1.0%). *Leptospirillum spp.* are known to oxidise iron (Sand et al., 1992; Ojumu et al., 2009) while species within the *Desulfosporosinus* (Spring & Rosenzweig, 2006), *Acidiphilium* (Johnson & Bridge, 2002), *Metallibacterium* (Ziegler et al., 2013) and *Acidibacter* (Falagán & Johnson, 2014) genus's are known to be capable of iron reduction. *Leptospirillum spp.* were previously identified, by Bryan *et al.* (2004), in surface spoil at Parys Mt.. *Acidiphilium* was observed, by Jenkins *et al.* (2000) in the AMD contaminated Afon Goch. Within these studies members of the *Acidithiobacillus*, *Thiobacillus* and *Ferromicrobium* were also identified in large quantities; but are absent from this investigations analysis. This suggests that the waste investigated in this study may have a microbial community distinct from that of the ore body and AMD. A total of 0.8% of sequences belonged to genera present at ≤1% abundance.

OTUs matching (with >97% sequence identity) 13 different phyla were identified in the post-experiment "Live" samples including 2 archaeal phyla (Figure 9.50). Of these 13 phyla a total of 6 bacterial and 1 archaeal phyla are present at ≥1% relative abundance. Of these phyla, all except the *Firmicute* phylum have shown a decrease in abundance relative to the pre-experiment equivalent. The relative abundance of *Planctomycetes* has decreased from 23.9% to 1.8%, *Proteobacteria* abundance decreased from 14.1% to 3.2% and *Chloroflexi* abundance decreased from 13.1% to 1.7%. The *Firmicute* phylum, by contrast, increased substantially from 16.3% to 86.8% resulting in *Firmicutes* dominating the sequences recovered from the waste microbial community in the post-experiment "Live" waste samples.

A total of 13 genera, with abundances of ≥1%, were matched, with >97% sequence identity, to sequences taken from the post-experiment "Live" samples (Figure 9.51). Of these 13 genera 5 were present at ≥1% in the pre-experiment samples while the other 8 have increased in abundance from <1% in the pre-experiment samples. Only one

archaeal genera, *Methanosaeta,* was identified at 1% abundance or greater. This correlates with the results of the qPCR which showed a decline in archaeal gene copies in the post experimentation samples. The most often matched genus was the *Firmicute Desulfosporosinus* which matched 39.4% of sequences recovered from the post-experimentation waste but matched only 2.0% of sequences in the pre-experiment equivalent. This correlates with the results of DGGE analysis/sequencing which also identified *Desulfosporosinus* as the dominant genus in the "Live" samples. Members of the genus *Desulfosporosinus* are typified by their ability to form endospores, motility provided by flagella and a strictly anaerobic metabolism, reflecting the anaerobic conditions established within the experimental columns (Spring & Rosenzweig, 2006). Several *Desulfosporosinus spp.* have been shown to be capable of coupling the oxidation of organic carbon to the reduction of sulphate, iron (Schippers *et al.*, 2010) or other metals such as arsenic (Ramamoorthy *et al.*, 2006; Vaxevanidou *et al.*, 2015) while being tolerant of elevated concentrations of heavy metals such as Cd, Co, Ni and Zn (Burkhardt *et al.*, 2011). Also present at 5.2% abundance (increased from 0.1%) is the closely related *Desulfitobacterium* genus. Members of this genus are known to reduce iron, arsenic, manganese, selenium and uranium (Villemur *et al.*, 2006) and be capable of the reductive dehalogenation of halogenated organic compounds (Kunapuli *et al.*, 2010).

The second most abundant genus identified in the post-experiment "Live" sample sequences was the *Firmicutes* genus *Thermincola* (20.8%) which was below detection limits in the pre-experiment sample returning an abundance of 0.0%. This taxon was not identified in the earlier PCR-DGGE analysis/sequencing. This may be due to sample bias where the relevant bands were not chosen for excision or a result of utilising different primer pairs for amplification. Members of the *Thermincola* genus are anaerobic, thermophilic, iron reducers but relatively few species have been cultured. Growth of *Thermincola spp.* have been observed at temperatures ranging from 37˚C to 70˚C and pH ranging from 5.9 to 9.5 (Sokolova *et al.*, 2005; Zavarzina *et al.*, 2007; Carlson *et al.*, 2012; Lusk *et al.*, 2015). These conditions are in contrast with those observed during the column experiments where the unregulated room temperature averaged at 20±1˚C and the pH only reached circum-neutral conditions in the later stages of experimentation. It is possible that the *Thermincola* present have increased in abundance in the later stages of experimentation as conditions became more favourable. Alternatively, given the

relatively low number of cultured species within the *Thermincola* genera, it is feasible that the abundance of this genera is a result of strains capable of growth at the lower end of mesophilic conditions and more acidic conditions. Other *Firmicute* matched OTUs that increased in relative abundance in abundance during experimentation included those matching *Hydrogenispora* (1.2%), *Ruminiclostridium* (1.1%), *Ruminiclostridium 6* (2.6%), uncultured *Peptococcaceae* (1.5%) and an uncultured *Ruminococcaceae* (2.6%). *Acidibacillus and Clostridium sensu stricto 12* have decreased in relative abundance from 10.0% and 1.7%, respectively, in the pre-experiment sample to 4.8% and 0.7%, respectively, in the post-experiment "Live" samples. The abundance of uncultured bacterium within the *CPLa-3 termite group* order decreased from 18.5% to 1.1% while the uncultured bacterium within the *JG37-AG-4* class also decreased from 12.9% to 1.6% as a result of experimentation. These declines explain the reduction in OTUS matching the *Chloroflexi* and *Planctomycetes* phyla respectively. A slight increase in genera present at ≤1% was observed, with 16.1% of sequences belonging to genera below this threshold up from 13.8% in the pre-experiment samples.

The dominance of OTUs matching *Desulfosporosinus, Thermincola* and other members of the *Firmicute* phyla as a result of experimentation is also evident from estimates for alpha diversity indices. Shannon's diversity index has sharply declined from 5.42 in the pre-experiment samples to 3.39 in the post-experiment "Live" samples. Simpson's diversity index showed a similar trend decreasing from 0.96 to 0.73. Despite the waste becoming less diverse there was in increase in species richness with the value of Chao1 index increasing from 269.76 to 331.18 (Table 9.6).

PCoA was used to visualise and compare the differences between the pre- and post-experiment "Live" samples. The first two coordination axis explain 73.57% of the variability in the microbial communities, while the third axis increases this to 83.71% of variability explained. The pre-experiment samples are not seen to cluster together tightly. While this may be an accurate representation of the pre-experiment waste it is possibly a feature caused by the limited number of samples tested or sampling bias. The post-experiment "Live" samples largely cluster together separately from the pre-experiment samples indicating the substantial differences between the pre- and post-experiment samples as suggested by the taxonomic identification an alpha diversity values (Figure 9.52). Within the post-experiment samples there are 3 distinct outliers.

These samples represent two samples from the middle portion of separate replicate columns (replicates 2 & 3) and a single sample from the upper portion of the waste within experimental column 2. The remainder of the samples can be seen to cluster together suggesting there is very little difference in the microbial communities spatially throughout the waste with the exception of the outliers previously mentioned (Figure 9.53).

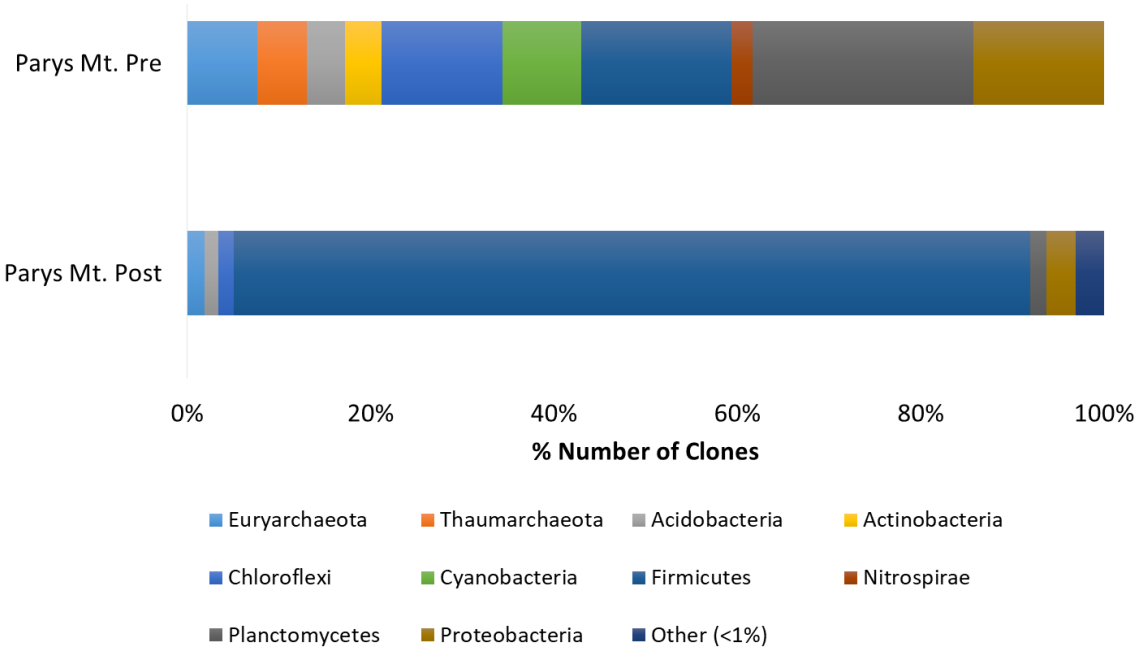

Figure 9.50 Taxonomic classification of 16S rRNA gene reads at phylum level in Parys Mt. 2 pre- and post-experiment "Live" samples

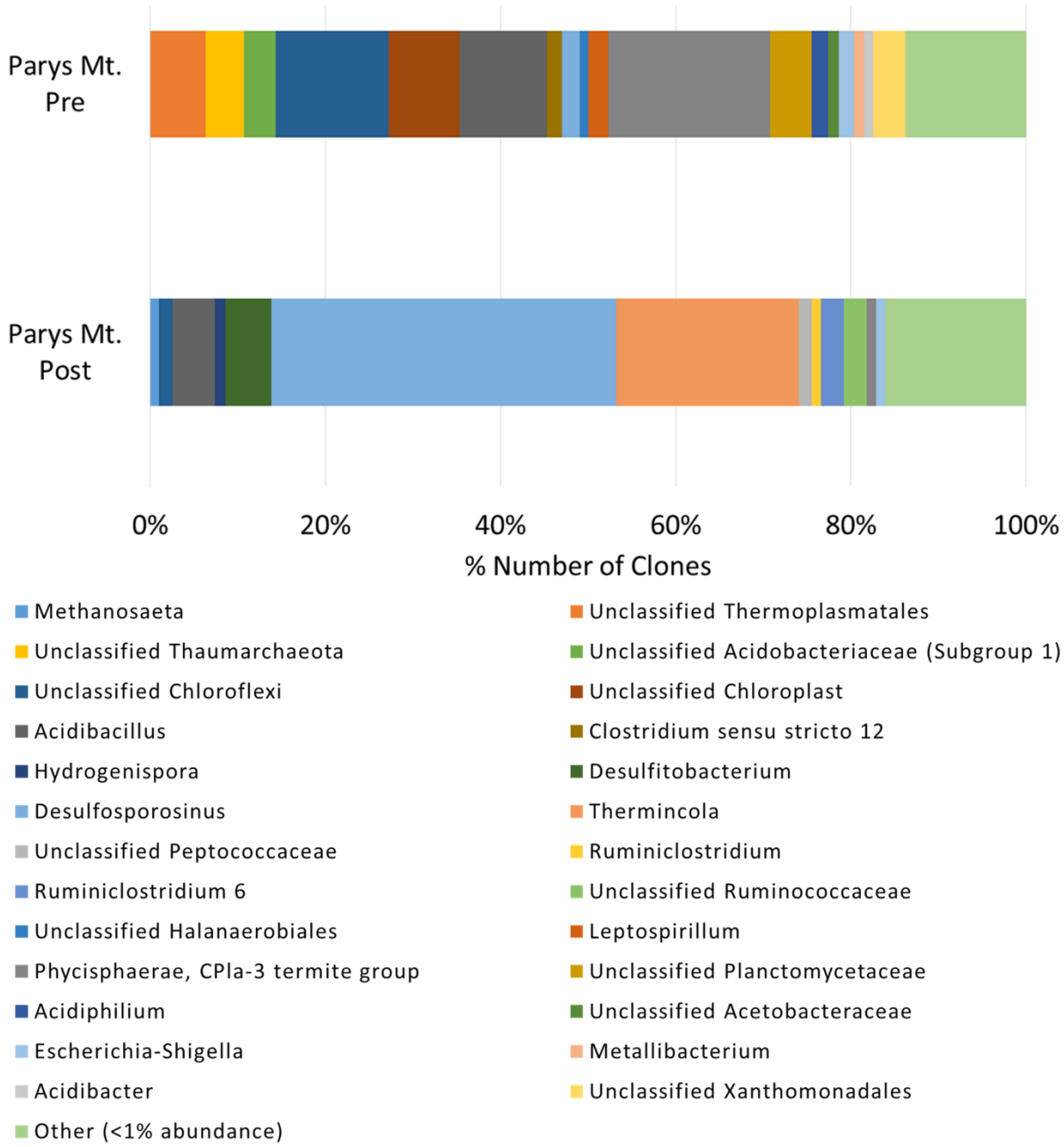

Figure 9.51 Taxonomic classification of 16S rRNA gene reads at genus level in Parys Mt. 2 pre- and post-experiment "Live" samples

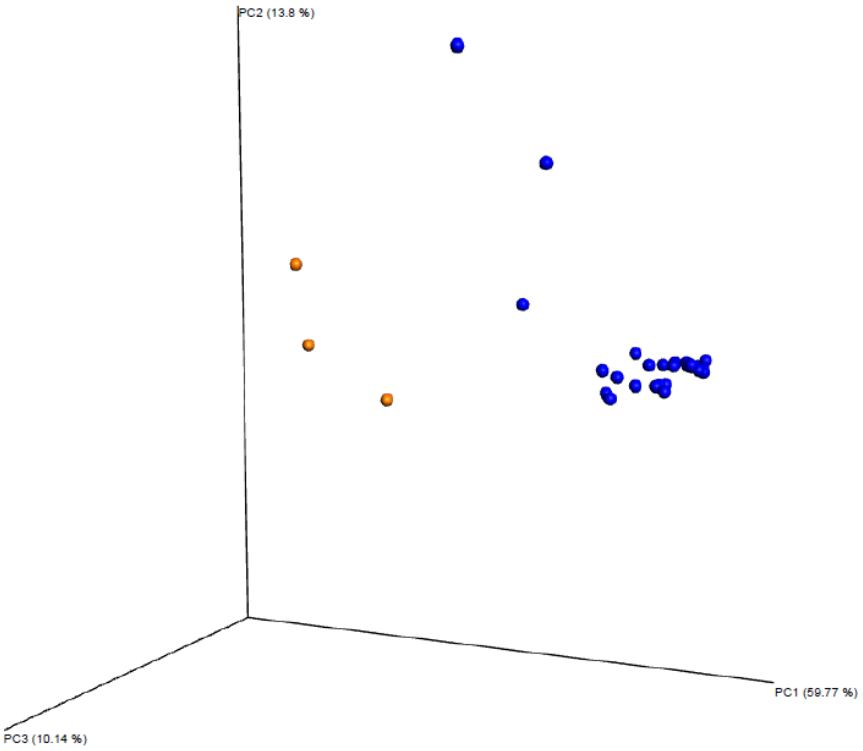

Figure 9.52 3D PCoA plot based on sequence data from Parys Mt.2 "Live" experimentation. Orange= Parys Mt. 2 waste pre-experiment, blue = Parys Mt. 2 "Live" post-experiment waste

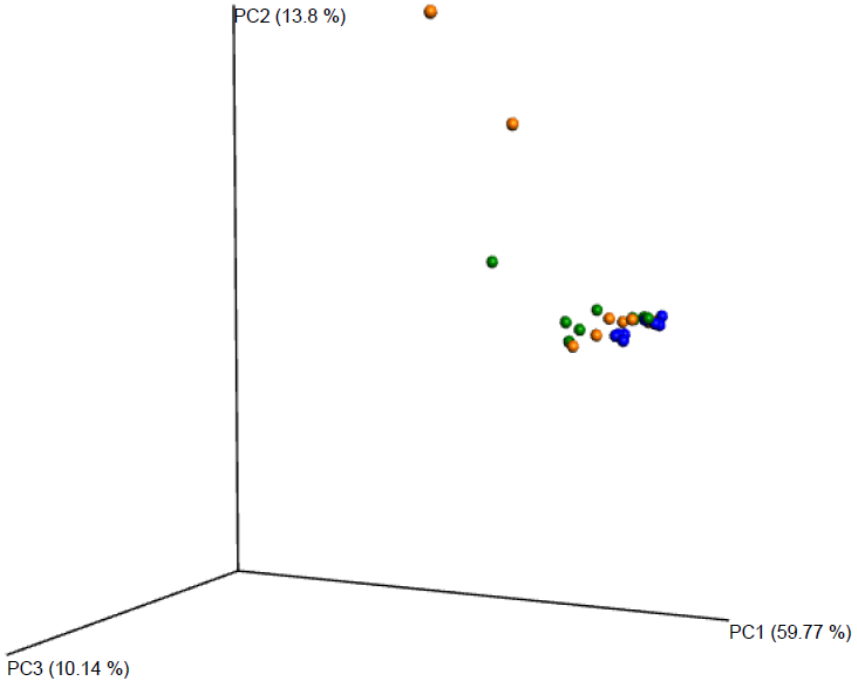

Figure 9.53 3D PCoA plot based on sequence data from Parys Mt.2 "Live" post-experiment samples at various height within columns. Green= Lower- column samples, Orange= Mid-column samples, Blue= Upper column samples

Table 9.6 Diversity indices for Parys Mt.2 "Live" pre- and post-experiment samples 16S rRNA sequences

Sample ID	No of QC Reads	Unique OTUs	Shannon's Diversity Index (*H'*)	Simpsons's Diversity Index (1-*D*)	Choa1	Goods Coverage (%)	S_{ace}
Pre 1	65058	271	5.57	0.960	306.05	0.9994	300.29
Pre 2	54939	294	5.36	0.948	378.18	0.9990	340.80
Pre 3	19384	171	5.32	0.957	206.06	0.9982	211.16
Live 1 L1	116490	299	3.84	0.817	376.54	0.9995	367.65
Live 1 L2	122693	259	1.93	0.411	322.03	0.9995	320.17
Live 1 L3	117297	299	3.10	0.675	362.00	0.9995	360.87
Live 1 M1	148094	357	4.26	0.880	539.40	0.9994	473.41
Live 1 M2	97389	287	4.26	0.879	332.12	0.9995	330.95
Live 1 M3	127874	278	3.67	0.776	360.88	0.9996	330.40
Live 1 U1	137200	342	3.87	0.807	411.00	0.9995	412.39
Live 1 U2	103710	387	4.66	0.898	472.80	0.9992	462.74
Live 1 U3	38601	229	4.67	0.904	268.38	0.9991	261.02
Live 2 M1	38109	125	2.31	0.585	173.00	0.9991	163.31
Live 2 M2	66698	350	4.31	0.842	418.90	0.9992	409.89
Live 2 M3	47348	140	3.21	0.779	167.00	0.9994	168.13
Live 2 L1	128310	156	1.08	0.250	225.46	0.9997	214.47
Live 2 L2	140636	182	2.06	0.563	210.33	0.9998	213.99
Live 2 L3	106465	173	1.92	0.461	228.50	0.9997	203.51
Live 2 U1	26249	158	4.27	0.865	193.00	0.9986	210.88
Live 2 U2	16109	96	3.11	0.712	109.60	0.9989	110.07
Live 2 U3	21953	126	2.84	0.655	153.27	0.9989	149.12
Live 3 L1	183834	282	2.37	0.643	347.56	0.9997	342.39
Live 3 L2	91051	278	3.27	0.767	345.03	0.9993	357.49
Live 3 L3	166757	267	3.06	0.738	328.22	0.9997	332.45
Live 3 M1	126300	247	3.14	0.688	325.00	0.9996	299.92
Live 3 M2	82237	453	5.67	0.927	564.00	0.9991	540.62
Live 3 M3	122240	259	3.34	0.736	344.00	0.9996	309.46
Live 3 U1	119492	248	3.44	0.782	309.88	0.9996	292.22
Live 3 U2	65187	207	3.61	0.808	256.50	0.9993	261.64
Live 3 U3	63299	232	4.31	0.868	257.59	0.9995	255.50

The microbial community composition and diversity within the post-experiment "Organic Starved" column samples show a more limited degree of alteration from the pre-experiment samples, compared with the "Live" equivalents. Additionally, what alteration is observed is distinctly different to that seen in the "Live" equivalent samples. (Figure 9.54). In total OTUs matching with >97% sequence identity to 18 distinct phyla, including 2 archaeal phyla, were identified in the post-experiment "Organic Starved" samples. 11 of these phyla, including both archaeal phyla, were identified at relative abundances of ≥1%. *Planctomycetes* has remained the most often matched phyla, increasing from a relative abundance of 23.9% to 42.8% during experimentation. Counteracting this increase are decreases in *Cyanobacteria* and *Firmicutes* from 8.5% and 16.3% to 0.8% and 7.1% respectively. The latter, in particular, highlights the difference between the "Organic Starved" and "Live" samples in which *Firmicutes* came to dominate the sequences obtained from the system. Changes in the other identified phyla were relatively minor. Sequences matching closest to the phylum *Euryarchaeota* increased slightly from 7.6% to 8.5%, though this was offset by a decrease in *Thaumarchaeota* matched sequences from 5.3% to 2.6%.

This increase in the relative abundance of the phylum *Planctomycetes* is manifested in an increase in OTUs matched closest to uncultured bacterium within the order *CPLa-3 termite group* which has increased from 18.5% to 40.7%. Aside from the sequences matched to the *CPLa-3 termite group* and the *JG37-AG-4* class, which remained relatively unchanged at 12.3% abundance, the other bacterial genera identified were present as relatively low abundances of 4.0% or less. 18.2% of sequences matched closest to genera at relative abundances of <1%. As would be expected given the lack of iron reduction suggested by the effluent analysis, there is a lack of OTUs matching (at >97% sequence identity) to iron-reducing genera at any significant relative abundances. In contrast to the "Live" post-experiment, in which they were the genera which matched most often to the identified sequences, only 0.2% of sequences belong to the genus *Desulfosporosinus* while *Thermincola* was not identified (Figure 9.55).

The increase in low abundance genera is also indicated by an increase in observed OTUs, to 286, in the post-experiment "Organic Starved" samples compared with 245 in the pre-experiment samples. This increase in OTUs is also displayed in the increase in species richness with Chao1 indices increasing from 269.76 to 331.64, commensurate with the

"Live" equivalent samples. Despite an increase in species richness and observed OTUs, diversity is seen to decrease with Shannon's index decreasing from 5.42 to 4.52 and Simpsons index decreasing from 0.96 to 0.87 (Table 9.7). This is a reflection of the increased abundance of sequences matched closest to the order *CPLa-3 termite group* which have increased in relative abundance but not to the same degree as the *Firmicute* genera were seen to increase in the equivalent "Live" sample. Despite these changes, PCoA shows a much closer association between the pre- and post-experiment "Organic Starved" samples than the "Live" equivalents (Figure 9.56). Again, there is no distinct difference between samples taken from different stratigraphic levels in the columns (Figure 9.57).

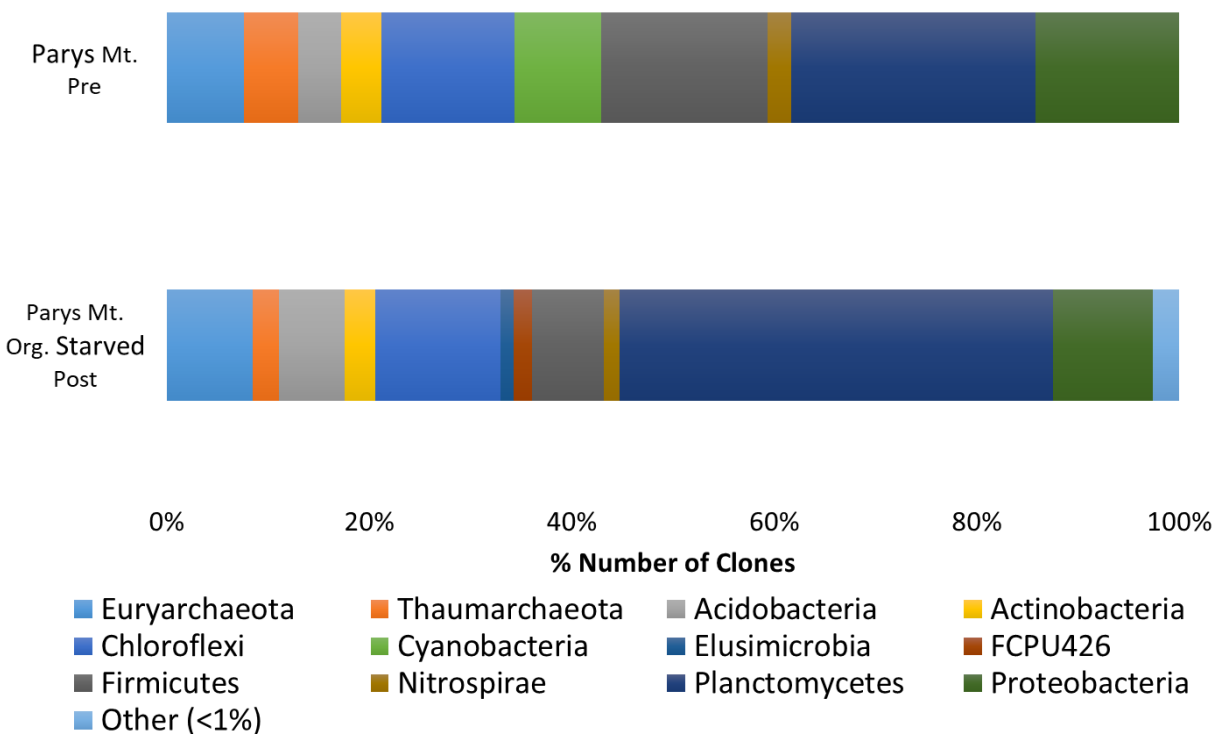

Figure 9.54 Taxonomic classification of 16S rRNA gene reads at phylum level in Parys Mt. 2 pre- and post-experiment "Organic Starved" samples

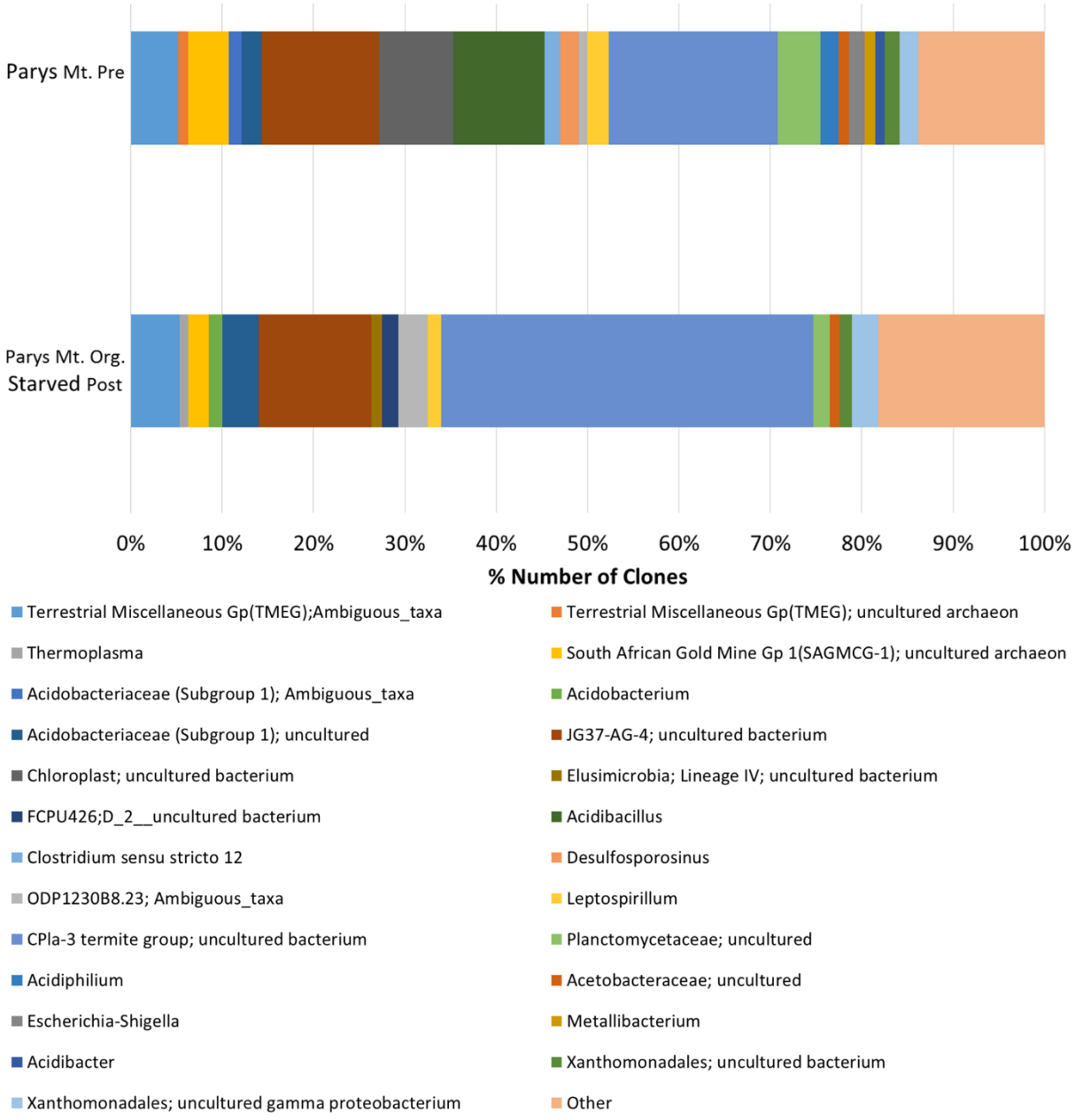

Figure 9.55 Taxonomic classification of 16S rRNA gene reads at genus level in Parys Mt. 2 pre- and post-experiment "Organic Starved" samples

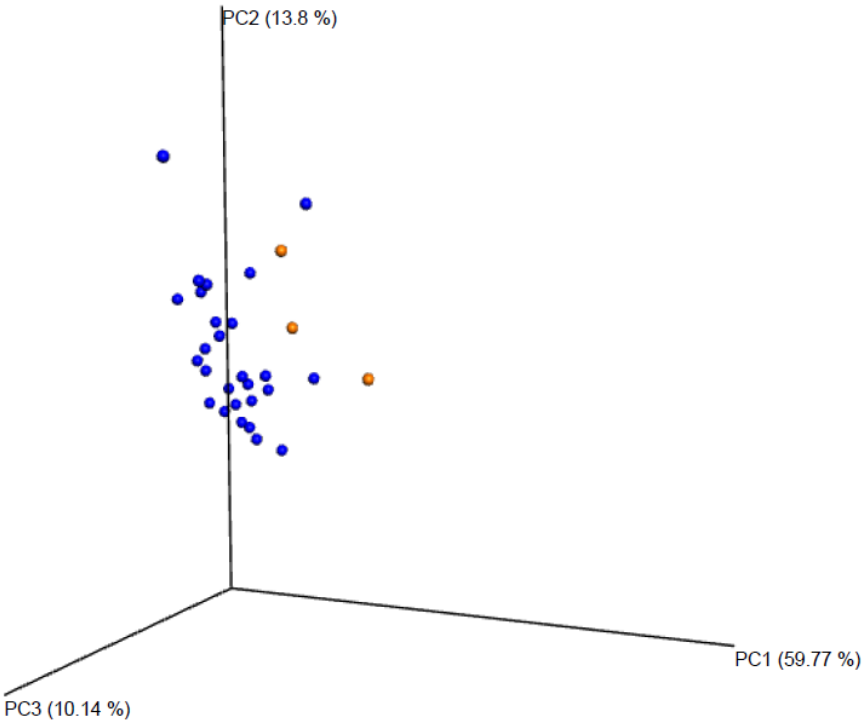

Figure 9.56 3D PCoA plot based on sequence data from Parys Mt.2 "Organic Starved" experimentation. Orange= Parys Mt. 2 waste pre-experiment, blue = Parys Mt. 2 "Organic Starved" post-experiment waste

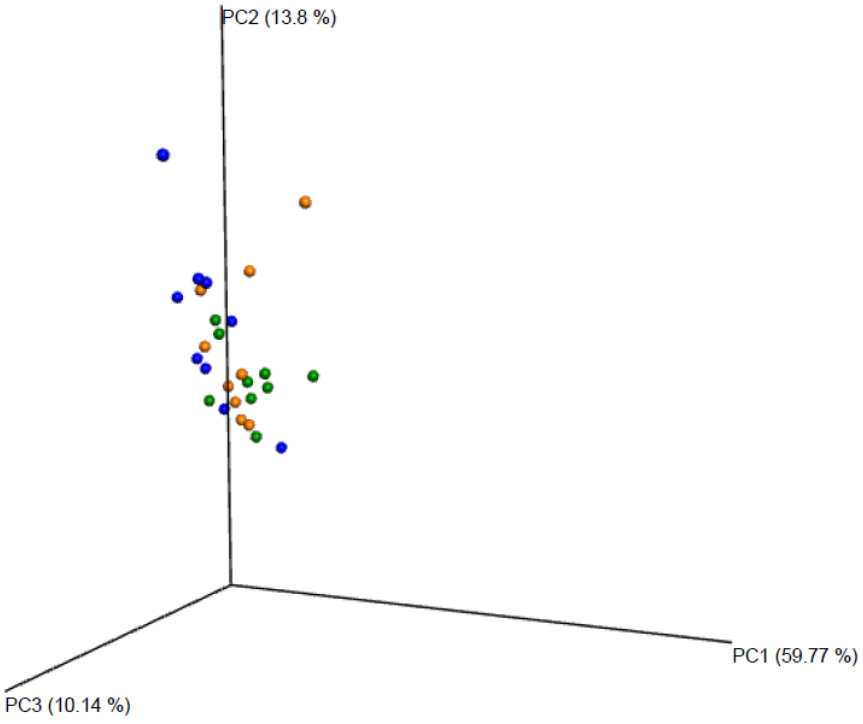

Figure 9.57 3D PCoA plot based on sequence data from Parys Mt.2 "Organic Starved" post-experiment samples at various height within columns. Green=Lowerof column samples, Orange= Mid-column samples, Blue=Upperof column samples

Table 9.7 Diversity indices for Parys Mt.2 "Organic Starved" pre- and post-experimentation samples 16S rRNA sequences

Sample ID	No of QC Reads	Unique OTUs	Shannon's Diversity Index (*H'*)	Simpsons's Diversity Index (1-*D*)	Choa1	Goods Coverage (%)	S_{ace}
Pre 1	65058	271	5.57	0.960	306.05	0.9994	300.29
Pre 2	54939	294	5.36	0.948	378.18	0.9990	340.80
Pre 3	19384	171	5.32	0.957	206.06	0.9982	211.16
OS 1 L1	114944	263	4.12	0.810	281.13	0.9997	282.56
OS 1 L2	84300	224	4.81	0.919	259.05	0.9996	261.02
OS 1 L3	85504	239	4.21	0.842	262.62	0.9996	266.26
OS 1 M1	121453	226	4.13	0.863	251.00	0.9998	241.34
OS 1 M2	93320	233	3.84	0.799	264.17	0.9996	256.64
OS 1 M3	96934	227	3.87	0.797	269.50	0.9996	259.48
OS 1 U1	97313	253	4.27	0.864	283.00	0.9996	282.61
OS 1 U2	65379	234	2.98	0.609	279.00	0.9993	275.69
OS 1 U3	108297	308	5.01	0.909	383.14	0.9995	367.92
OS 2 L1	92272	299	4.24	0.842	371.06	0.9995	336.43
OS 2 L2	88603	558	5.68	0.929	633.08	0.9991	630.85
OS 2 L3	120554	342	4.37	0.831	367.16	0.9997	370.49
OS 2 M1	114527	310	4.49	0.852	395.00	0.9996	355.31
OS 2 M2	115850	306	4.17	0.822	382.56	0.9995	353.72
OS 2 M3	118593	304	3.90	0.791	340.67	0.9996	336.70
OS 2 U1	129449	258	4.58	0.899	300.50	0.9997	292.33
OS 2 U2	84719	260	4.37	0.865	287.39	0.9996	289.32
OS 2 U3	96388	286	4.82	0.912	313.05	0.9996	311.42
OS 3 L1	138717	267	4.40	0.860	292.20	0.9998	284.90
OS 3 L2	2360	120	5.02	0.942	147.56	0.9864	150.98
OS 3 L3	129194	260	4.46	0.892	312.50	0.9997	288.87
OS 3 M1	104599	295	5.01	0.934	363.88	0.9994	356.69
OS 3 M2	67085	546	5.62	0.942	688.69	0.9984	671.54
OS 3 M3	94964	283	4.82	0.907	315.80	0.9996	318.67
OS 3 U1	100159	316	5.45	0.954	355.18	0.9996	341.11
OS 3 U2	88233	253	4.87	0.923	281.05	0.9996	279.25
OS 3 U3	76570	250	4.64	0.893	274.47	0.9996	273.96

The OTUs identified from sequences obtained from the autoclaved pre-experiment samples matched closest (>97% sequence identity) to 9 identifiable bacterial phyla. No archaeal phyla were identified in the pre-experiment sample sequences. Only 5 of the identified phyla were present at relative abundances of ≥1%. This is half the number observed in the non-autoclaved pre-experiment samples (Figure 9.58). This correlates with the results of the qPCR analysis which recorded a large decrease in the number of bacterial and archaeal gene copies per gram in the autoclaved pre-experiment waste compared with the non-autoclaved equivalents. The 5 matched phyla, present at ≥1% relative abundance, are *Actinobacteria* (1.4%), *Chloroflexi* (1.5%), *Planctomycetes* (1.3%), *Firmicutes* (12.0%) and the most abundant phylum *Proteobacteria* (82.9%). With the exception of the *Proteobacteria*, all of these phyla have undergone a decrease in relative abundance. This is most likely as a result of autoclaving as opposed to sampling bias in obtaining the sequences. The *Planctomycetes* and *Chloroflexi* have, in particular, been substantially reduced within the sequences obtained from the waste microbial community. The *Gammaproteobacteria* again the most often matched class within the phyla with 76.8% of sequences belonging to the class. The *alpha-* and *Betaproteobacteria* are present at 2.9% and 3.2% relative abundances while the *Deltaproteobacteria* are just above the limit of detection at 0.1%. The reduction in OTUs matching closest to the *Firmicutes* phyla has largely been within the *Bacilli* class which has seen its relative abundance more than halved from 10.1% to 5.0%, while the *Clostridia* has stayed relatively unchanged at 6.9% relative abundance.

At genera level the *Gammaproteobacteria* are largely represented by *Escherichia/Shigella*, which comprise 68.7% of identified sequences (Figure 9.59). The dominance of this genus is unexpected as it is only present in the non-autoclaved waste in low amounts. While there is evidence to suggest that *Escherichia/Shigella* species, such as *E. coli* are capable of surviving autoclaving (Markova *et al.*, 2010), it is far more likely a result of contamination of the extracted DNA sample during analysis given that 30.1% of sequences observed in the negative PCR control sample (a sample with no template DNA added) were identified as belonging to the genus *Escherichia/Shigella*. It has been shown that sequences of *E. coli* can be linked to contamination of *Taq* DNA polymerase and DNA extraction kits which may explain its presence within the negative (DNA template free) controls (Rochelle *et al.*, 1992). With the autoclaving process having

significantly reduced the microbial community within the wastes any contamination of the sample will have had a more significant impact and skewed the results, over representing the "contaminant bacteria" (i.e. *Escherichia/Shigella*). The *Firmicute* matched OTUs within the pre-experiment "Autoclaved" waste samples are represented by a more diverse set of genera including *Acidibacillus* (2.4%), *Bacillus* (1.5%), *Clostridium sensu stricto 12* (1.7%) and *Desulfosporosinus* (4.5%). Only 5% of sequences matched closest (with >97% sequence identity) to genera present at abundances of <1%.

As can be seen in the data presented in Table 9.6 and Table 9.8, autoclaving the Parys Mt. 2 waste has resulted in a substantial decrease in the Chao1 index estimate for species richness; from 296.76 to 46.32 in the non-autoclaved and autoclaved pre-experiment samples respectively. The number of observed OTUs decreased from 245 to 33, correlating with the observations made during taxonomic identification. Shannon and Simpson's indices have also decreased, as result of autoclaving the waste, from 5.42 and 0.96 respectively to 1.87 and 0.45 respectively describing the decreased diversity and dominance of *Escherichia/Shigella* in the sequences obtained from the "Autoclaved" pre-experiment waste samples.

The introduction of glycerol to the autoclaved waste has caused significant alteration to the microbial communities within the waste (Figure 9.58). While the changes to the waste have been considerable, with similarities in the changes observable in the "Autoclaved" wastes to the changes that were observed in the "Live" post-experiment waste. The most obvious similarity between the post-experiment "Live" and "Autoclaved" wastes is the dominance of OTUs matching closest (>97% sequence identity) to the *Firmicute* phylum, which has increased in relative abundance to 78.8% of all identified sequences, an increase of more than 6.5 times the original abundance (12.0%). This is the same trend that was observed in the "Live" samples where the *Firmicutes* proliferated to become the dominant phylum. The proliferation of *Firmicute* also correlates with the increase in bacterial gene copies suggested by the qPCR analysis. The increase in *Firmicute* matched OTUs has come at the expense of the *Proteobacteria* matched OTUs which have undergone a similarly dramatic decrease in relative abundance to 5.2%. Aside from these two phyla the only other bacterial phylum identified was *Synergistetes* which has increased from below the limit of detection to 3.7% relative abundance. Along with an increase in bacterial gene copies/gram, the

qPCR analysis also showed a slight increase in archaeal gene copies within the DNA recovered from the waste. This is expressed by an increase in the relative abundance of *Euryarchaeota*, the only archaeal phyla identified, to 8.9% from below the detection limit in the autoclaved pre-experiment samples. In total 3.4% of sequences identified matched closest (>97% sequence identity) to phyla that were present at <1%, suggesting a slight increase in community diversity (i.e. more distinct microbes present) from the pre-experiment sample in which all sequences were attributable to phyla with abundances ≥1%.

When the sequences are analysed at genera level this suggested slight increase in diversity is not initially clear (Figure 9.59). The number of OTUs matching with 97% sequence identity to genera present at relative abundances of ≥1%, has decreased from 12 pre-experiment to a total of 9 in the post-experiment "Autoclaved" wastes. Of the original 12, only 3 phyla remain above 1% relative abundance. These are *Acidibacillus*, which has remained unchanged at 2.4%, *Escherichia/Shigella*, which has decreased substantially to just 1.2% of total sequences and *Desulfosporosinus*, which has proliferated to an abundance of 62.1% from an initial 4.5%. This increase in *Desulfosporosinus* is similar what was observed in the equivalent "Live" samples, though no *Thermincola* matching OTU has been identified in the "Autoclaved" samples suggesting that the *Thermincola* has been killed by the autoclaving process. *Desulfosporosinus*, by contrast is seemingly able to survive autoclaving. This is likely a result of genus's ability to sporulate when under stress with the spores surviving autoclaving and subsequently proliferating during experimentation. Along with the dominant *Desulfosporosinus*; *Desulfitobacterium* (4.5%), *Alicyclobacillus* (6.1%) and *Acidibacillus* (2.4%) represent potential iron reducing genera identified in the post-experiment "Autoclaved" samples. Furthermore, the *Desulfosporosinus* (Spring & Rosenzweig, 2006) and *Desulfitobacterium* (Villemur et al., 2006) genera are known to be capable of reducing both ferric iron and sulphate, the latter forming hydrogen sulphide and resulting in indirect reduction of ferric iron (Santos Afonso & Stumm, 1992). These spore-forming, iron and sulphate reducing bacteria explain the observations of iron reduction in autoclaved waste and the anecdotal identification of hydrogen sulphide generation during experimentation.

The increase in archaea is represented by the increases in abundances of OTUs matching closest (with >97% sequence identity) to both *Methanosaeta* (7.0%) and *Methanosarcina* (1.3%). These genera were previously below the limit of detection. The proportion of sequences attributable to genera with <1% relative abundance has increased, from 5.0% in the "Autoclaved" pre-experiment samples, to 10.2% in the post-experiment samples; again, suggesting a slight increase in community richness. This is supported by the increase in observed OTUs, from 33 to 100, and the Chao1 index, from 46.32 to 158.04. Shannon's and Simpsons indices also show an increase in diversity increasing from 1.87 and 0.45 respectively to 2.22 and 0.53 respectively (Table 9.8). These values are not as high as those for the equivalent "Live" samples but again demonstrate that the addition of glycerol to the wastes, autoclaved or not, results in substantial changes to the structure of the microbial communities. PCoA analysis visually displays the change in the wastes with the post-experiment "Autoclaved" waste samples clustering separately from the pre-experiment "Autoclaved" samples (Figure 9.60). As with all other experiments there is no clear distinction between the samples taken from the "upper, middle and lower" sections of the waste, suggesting the microbial communities are generally homogeneous with regards to spatial distribution in the columns (Figure 9.61). The only potential exception to this comes from "Autoclaved" column 3. Both the mid and upper column samples are plotted separately as distinct outliers from the other samples suggesting some variation, though the majority of samples are seen to cluster tightly. A greater density of data is required to ascertain whether these outliers have any significance.

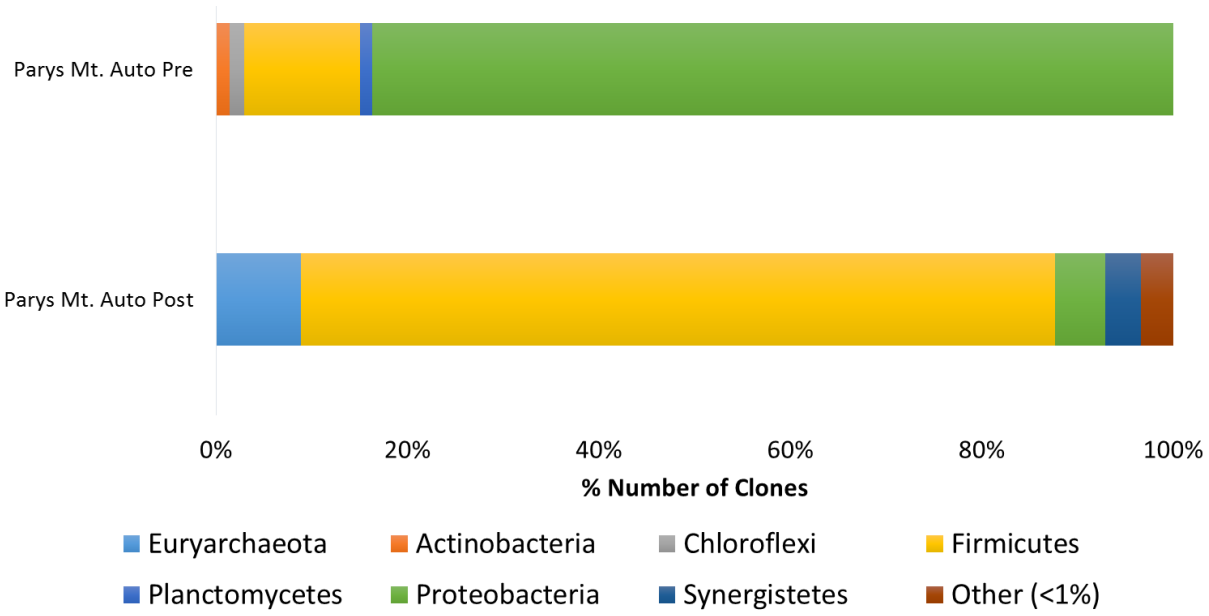

Figure 9.58 Taxonomic classification of 16S rRNA gene reads at phylum level in Parys Mt. 2 pre- and post-experiment "Autoclaved" samples

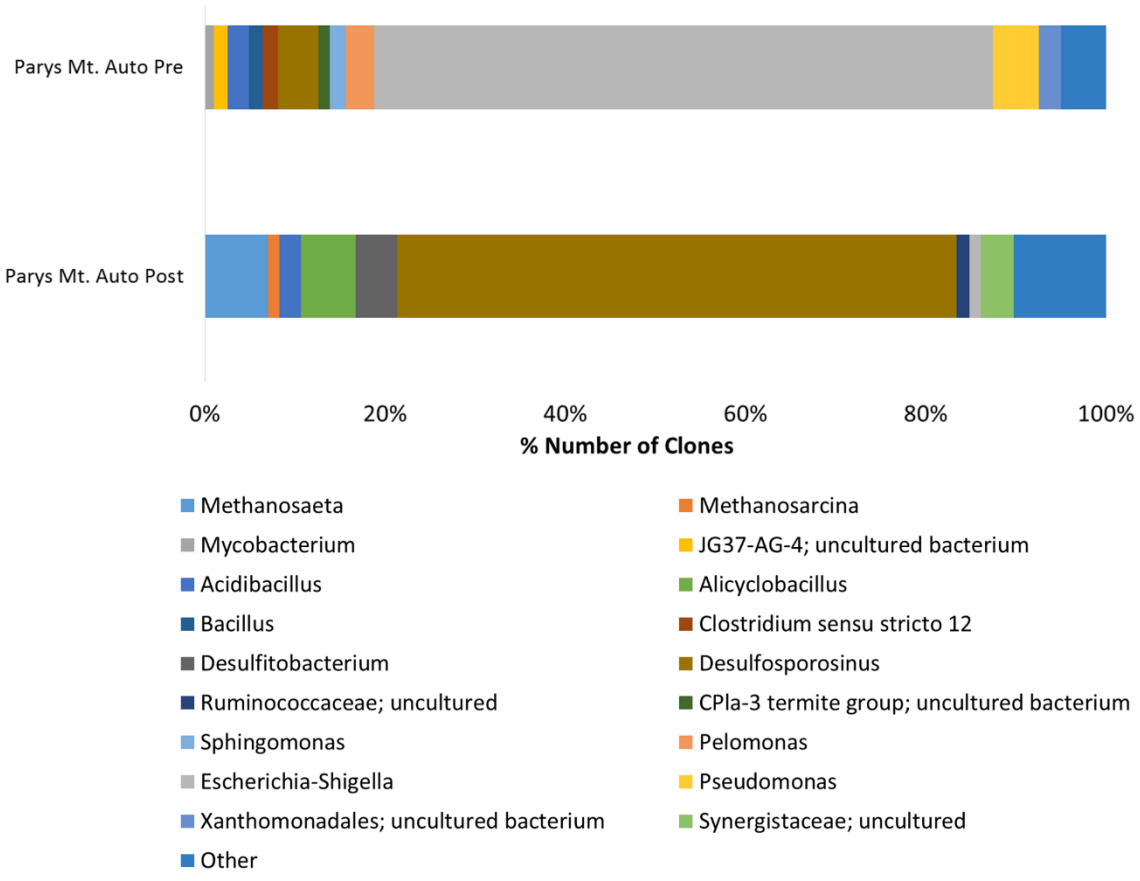

Figure 9.59 Taxonomic classification of 16S rRNA gene reads at genus level in Parys Mt. 2 pre- and post-experiment "Autoclaved" samples

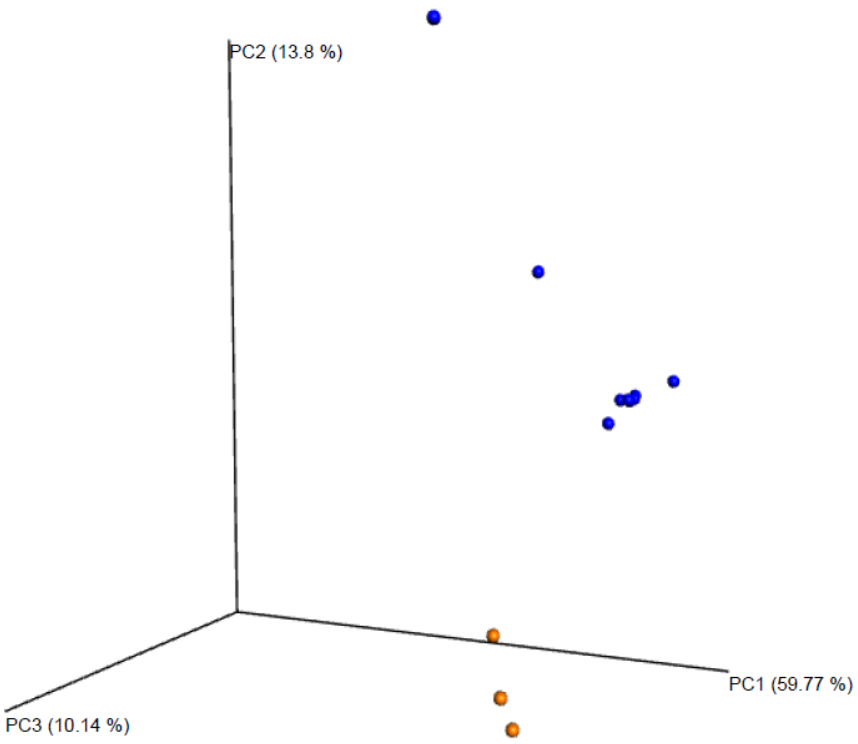

Figure 9.60 3D PCoA plot based on sequence data from Parys Mt.2 "Autoclaved" experimentation. Orange= Parys Mt. 2 waste "Autoclaved" pre-experiment, blue = Parys Mt. 2 "Autoclaved" post-experiment waste

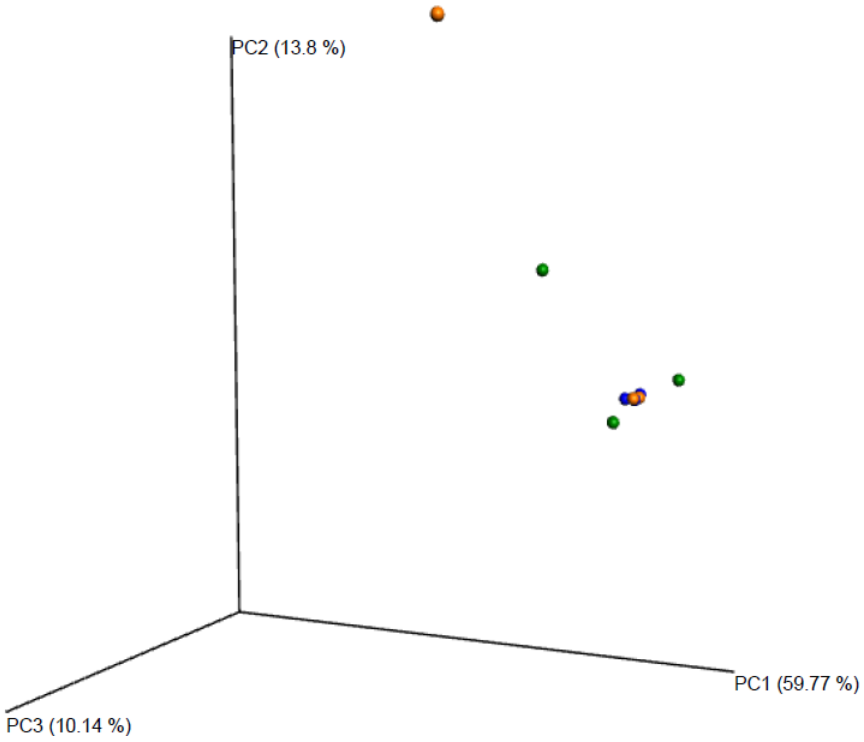

Figure 9.61 3D PCoA plot based on sequence data from Parys Mt.2 "Autoclaved" post-experiment samples at various height within columns. Green=Lower of column samples, Orange= Mid-column samples, Blue=Upper of column samples

Table 9.8 Diversity indices for Parys Mt.2 "Autoclaved" pre- and post-experimentation samples 16S rRNA sequences

Sample ID	No of QC Reads	Unique OTUs	Shannon's Diversity Index (*H'*)	Simpsons's Diversity Index (1-*D*)	Choa1	Goods Coverage (%)	S_{ace}
Auto Pre 1	1954	42	2.91	0.706	46.20	0.9964	46.01
Auto Pre 2	712	32	1.92	0.480	53.00	0.9789	61.54
Auto Pre 3	1361	26	0.79	0.174	39.75	0.9919	40.14
Auto 1 L2	23243	63	1.39	0.363	76.91	0.9992	80.36
Auto 1 M1	6372	52	2.87	0.756	80.50	0.997	84.74
Auto 1 U3	13422	71	3.36	0.854	88.10	0.9986	91.24
Auto 2 L3	104408	69	0.61	0.140	214.00	0.9997	122.19
Auto 2 M3	85817	49	1.14	0.330	56.50	0.9999	57.07
Auto 2 U1	11026	69	1.97	0.551	100.91	0.9976	106.16
Auto 3 L1	7529	49	0.68	0.162	166.00	0.9964	103.59
Auto 3 M3	72603	327	4.80	0.880	433.91	0.9993	385.44
Auto 3 U3	129029	150	3.17	0.747	205.50	0.9997	206.11

9.5. Conclusions and Key Points for Subsequent Work

As with the preliminary experimentation, the introduction of glycerol to the Parys Mt. 2 waste resulted in a sharp increase in total iron in effluents from the “Live” columns. An average peak total iron concentration of 1362.79 mg/l was observed. While the peak individual measurement was 1974.97 mg/l. These values represent increases of ~250% and >400% respectively from the peak iron concentration observed in the preliminary study; despite only doubling the concentration of glycerol. While the preliminary study represents only a single data point, these results suggest that the relationship between glycerol concentration and peak total iron concentrations is not linear. After an initial lag phase, both ferrous and total iron concentrations within the “Live” column effluents sharply increase, typical of microbial growth and previously observed in the preliminary experiment. However, unlike the preliminary experiment, no steady-state phase was observed. Instead, concentrations of both total and ferrous iron consistently decreased after peak iron was measured. Changes to the physicochemical parameters of the effluents also suggested microbially mediated reductive dissolution of iron. pH increased due to the production of alkalinity; rising from an initially acidic pH of 3.15 to a more circum-neutral state at pH 6.68 while redox potential was also seen to decrease. In total an average of 6.78% of iron was recovered from the “Live” columns, while averages of 3.07%, 0.34% and 0.14% of zinc, copper and lead, respectively, were recovered. Of the metals analysed only lead showed any correlation to iron concentrations within the effluents. The rapidly increasing pH has been identified as a limiting factor in the mobility and subsequent recovery of iron-associated metals. Sequential extraction of the wastes suggests that there has been an increase in the reactivity and leachability of some of these associated metals, particularly lead and copper. This is believed to be a result of the formation of metal hydroxides and the adsorption of aqueous phase metals to residual iron oxyhydroxide surfaces as increasing pH decreases metal mobility.

Furthermore, the pH is believed to be influencing the metabolic mechanisms of the indigenous microbial communities. In the early stages of experimentation evidence suggested direct microbial reduction of iron was occurring. However, during experimentation, as the pH increased sulphate-reduction became more energetically favourable seemingly limiting iron dissolution to indirect reduction by biogenic

hydrogen sulphide. Analysis of the microbial community structure supports this assertion as significant change has been observed with *Thermincola* and *Desulfosporosinus* dominating the post-experiment communities. While both are known to be capable of iron reduction, the latter is also capable of sulphate reduction suggesting a system that can react to, and tolerate, changing conditions within the experimental column.

qPCR analysis, DGGE and sequencing all suggest that autoclaving of the wastes has successfully reduced the size and diversity of the indigenous microbial communities Due to its ability to sporulate and survive autoclaving, *Desulfosporosinus* also dominates the post-experiment "Autoclaved" waste communities. This explains the higher than expected level of activity observed in the "Autoclaved" column effluents with iron and sulphur reduction again indicated within the "Autoclaved" columns. When this is considered in conjunction with the relative lack of activity in, or alteration of, the "Organic Starved" wastes, effluents or communities confirms that microbial iron-reduction, and indirect reduction due to sulphate reduction, is the mechanism for the observed mobilisation of iron and validates the findings of the preliminary study.

Further analysis of microbial community structures in the wastes has suggested that no consistent, discernible differences in the community structures at different heights within the columns exist. Despite this qPCR analysis has shown that the size of the bacterial communities decreases with greater height in the "Live" and "Autoclaved" column. This is likely in response to decreasing organic carbon concentrations higher in the column. While the "Live" community if dominated by *Thermincola* and *Desulfosporosinus* there is also evidence for a more complex system where the products of glycerol oxidation are further utilised in the wastes. For example, the fermenter *Anaerobacterium chartisolvens* was identified. This species is known to produce lactate, among other secondary products, from the fermentation of carbohydrates but is not capable of utilising glycerol, highlighting the complex organic carbon system in the waste. This is similar to observations of the communities in the Lindsay wastes and is a relatively unexpected consequence of utilising glycerol as the carbon source. This can be viewed as both a positive and negative for the experimental methodology. On the positive side, the wider consortium of bacteria utilising the glycerol is creating breakdown products which can be further utilised for iron reduction. On the negative

side, the presence of these bacteria, and their use of organic carbon, could be viewed as an inefficiency in the system where organic carbon is being oxidised with no resultant iron reduction. A summary of the biogeochemical processes occurring within the “Live” experimental columns is displayed in Figure 9.62.

While there are still a number of limitations and experimental parameters that require further research, the most significant of these is the issue of increasing pH. If further research could control the pH of the system, via a system such as acid dosing to offset alkalinity production, then a raft of issues experienced during this phase of experimentation can be addressed. Maintaining acidic pH would be beneficial for the indigenous acidophile communities, would keep iron-reduction as a more energetically favourable metabolic mechanism and retain a greater proportion of mobilised metals in solution to facilitate extraction.

To summarise:

- The introduction of glycerol has resulted in the stimulation of iron, and potentially sulphate, bioreduction in both the Live and Autoclaved columns. Doubling the glycerol concentration, relative to the preliminary experiment, has resulted in effluent iron concentrations increasing by >400% suggesting the relationship between glycerol concentration and effluent iron concentrations is not proportional.

- As in the preliminary experiment, XRD analysis has suggested that jarosite is the primary target for bioreduction within the waste.

- Recovery of metals of economic interest via the effluents has been limited largely as a result of increasing pH limiting their solubility. However, sequential extraction analysis indicates a substantial redistribution of these metals and a resulting increase in leachability.

- The increased pH may be impacting the balance between iron and sulphate reduction as higher pH makes reducing crystalline iron oxyhydroxides energetically unfavourable, in turn making sulphate reduction more favourable.

- The indigenous microbial community in the waste has undergone a substantial change becoming less diverse as a result of experimentation. Within Live column post-experiment waste communities the *Firmicute* iron-reducers *Thermincola* and *Desulfosporosinus* have proliferated significantly.

- *Desulfosporosinus* has shown to be capable of surviving a standard 121 ˚C autoclaving procedure and has proliferated within the Autoclaved post-experimentation samples.

The key knowledge gaps arising from this phase of experimentation are:

- Determining with greater certainty whether iron bioreduction transitions to sulphate bioreduction, and at what point during experimentation does the transition occur.

- To determine the fate of any solubilised metals. Establishing whether they are precipitating as metal hydroxides or co-precipitating with remnant or secondary iron oxyhydroxides.

- To determine whether leachability of metals has increased as a result of bioreduction, as suggested by sequential extraction analysis.

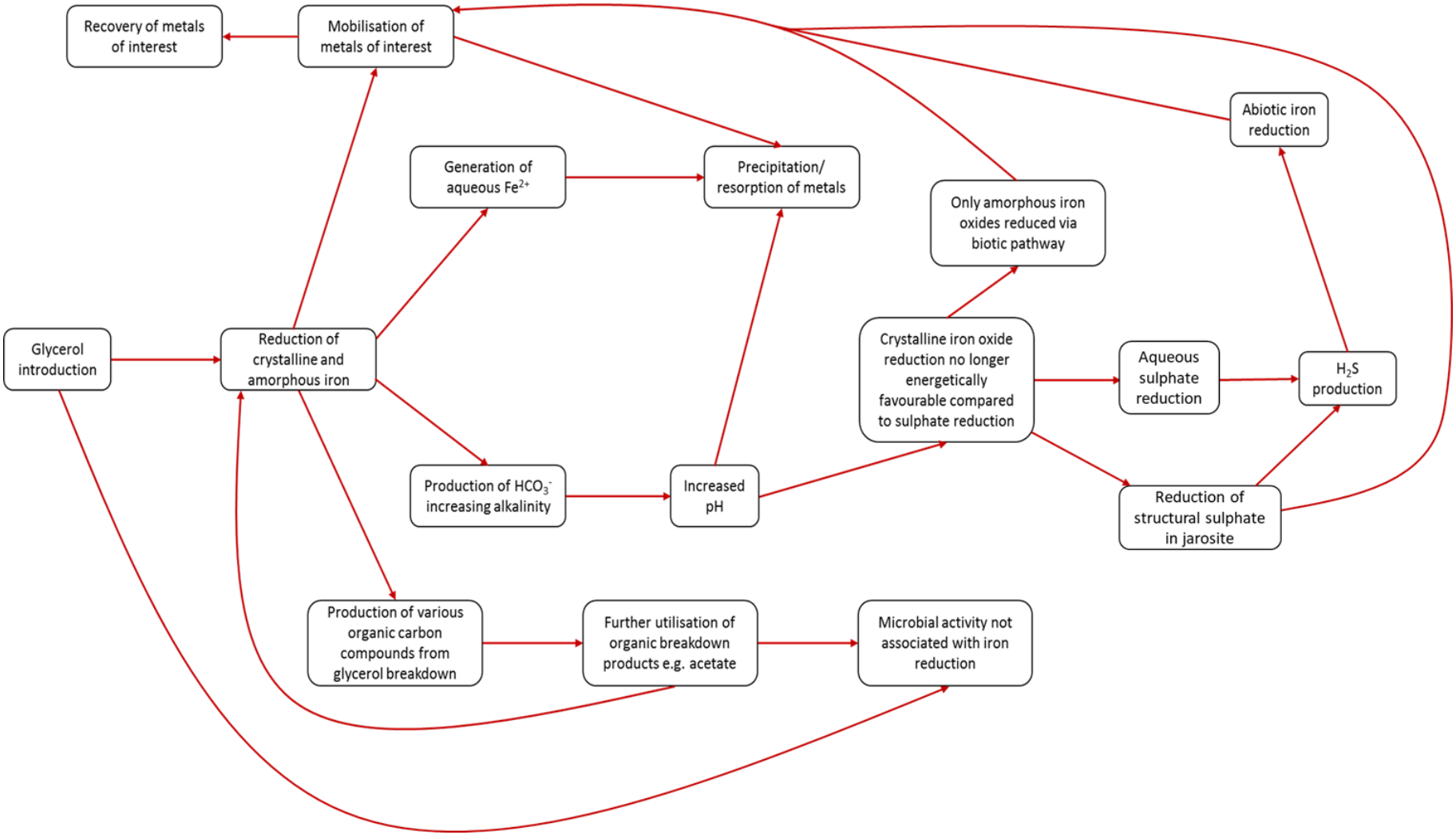

Figure 9.62 Conceptual model of biogeochemical processes occurring within the Parys Mt. 2 "Live" columns as a result of the introduction of glycerol

10. Leachability Analysis

10.1. Introduction

This chapter presents the experimental design and subsequent results of the post-bioreduction leaching of the Parys Mt. 2 wastes with a range of extractants. This chapter is split into the following sections:

Section 10.2: Objectives – Outlines the background to the experiment and the key objectives being investigated.

Section 10.3: Experimental Design, Materials and Methods – Describes in detail the specifics of the experimental design, the materials utilised and the analytical methods employed to measure experimental parameters.

Section 10.4: Results and Discussion – Presents, interprets and discusses the results and of leaching tests on post-column experimentation Parys Mt.2 wastes.

Section 10.5: Conclusions and Key Points for Subsequent Work.

10.2. Objectives

Column testing has demonstrated that the addition of glycerol to both the Lindsay and Parys Mt. wastes results in the microbially mediated reductive dissolution of iron. Within the Parys Mt. 2 waste this has been probably achieved through a combination of direct and indirect microbial reduction of iron by iron-reducers and sulphur-reducers respectively. Despite establishing iron-reduction within the wastes, and evidence of the coeval release of metals associated with iron oxyhydroxides, recovery of these metals from the column has been limited. The suspected reason for the low metal mobility has been due to an increase in pH towards circum-neutral conditions caused by bioreduction of iron. In this proposed model of the development of the biogeochemistry of the system the released metals are either sorbing to the surfaces of residual minerals or precipitating out of solution as secondary minerals e.g. metal hydroxides, green rusts. Sequential extraction analysis of the wastes suggests a redistribution of these metals

has occurred, with a greater proportion of the metals moving to more labile, readily leachable phases as a result of bioreduction. The primary focus of this stage of experimentation was to validate and further analyse the increase in leachability suggested by the previous sequential extraction results via a series of leaching tests on both pre-and post-experiment wastes utilising a range of acids and chelating agents.

A similar increase in leachability was described by Esther *et al.* (2015), who utilised bioreduction as a pre-treatment to enhance the recovery of nickel from chromite-overburden with a post-reduction acid leach. Using a 6M H_2SO_4 leach at 65˚C for 6h, a nickel recovery of 12% was achieved. An increase from 7.9% from waste not pre-treated by iron bio-reduction. When 2% glucose was introduced, as a reducing agent, to the leaching solution a maximum recovery of 52.9% was achieved (8.1% from non-treated waste). While implementing a similar physicochemical regime on the wastes whilst in-situ would be impractical, this stage of experimentation will also focus on establishing whether a similar system, though using more environmentally practicable conditions, represents a potentially effective recovery method for the metals held within the wastes. To summarise the objectives for this stage of experimentation were:

- To validate the results of sequential extractions and confirm there has been an increase in metal leachability caused by microbially mediated iron reduction.
- Establish whether initial autoclaving of the wastes has any impact on the leachability of metals within the wastes and whether the different microbial community structure that developed in “Autoclaved” wastes translates to differences in metal leachability
- Identify any correlations between leached metal concentrations to obtain greater understanding of metal/mineral associations in the waste both pre- and post-experiment.

10.3. Experimental Design, Materials and Methods

Further details of the materials, analysis techniques and procedures stated or outlined briefly in this section can be found in Section 5.

10.3.1. Materials

This stage of experimentation continued to focus on the Parys Mt. 2 waste used within the previous column experiments. Leachability analysis was performed on samples of Parys Mt. 2 wastes which had undergone a range of treatments covering pre-experiment waste, both unaltered and autoclaved, and samples from the post-experiment "Live", "Autoclaved" and "Organic Starved" columns. To assess the leachability of the metals within the waste, under conditions as analogous to the environment within the column as possible, the previously frozen (via freeze-drying) waste samples were thawed and homogenised within a glovebox under nitrogen, to prevent any mineral changes due to oxidation (Figure 10.1).

Figure 10.1 Thawing of post-experiment sludge under nitrogen within glovebox. Note sludge remains dark green-black rather than oxidising to rusty brown.

10.3.2. Experimental Design

Batch leaching tests were used to assess the efficacy of a range of leachants for the recovery of metals from both the bio-reduced waste and pre-experiment wastes. 2 grams of each wet sludge was used per test, with sub samples taken to measure solids content for subsequent dry mass calculations. Wet sludge was utilised to better represent the conditions within the experimental columns. The wastes were subjected to acid leaching using either hydrochloric acid (HCl), sulphuric acid (H_2SO_4) or citric acid ($C_6H_8O_7$) each at concentrations of 1 M, 0.5 M and 0.25 M and a 10:1 leaching ratio (cf. Esther *et al.* (2013)). Whilst citric acid is also considered a chelator, a further chelator leach was also assessed. Ethylene-diamine-tetraacetic acid (ETDA) was used as a chelating agent at concentrations of 10 mM (cf. Sun *et al.* (2001)), 5 mM and 2.5 mM. To ensure the dissolution of EDTA in solution the pH was raised to exactly 8.0 using sodium hydroxide. This also created the pH conditions at which metal ion/EDTA complexes are most stable in solution (Figure 10.2), though limits the leaching potential. Due to the non-selectivity of EDTA and the range of metals present in the waste, calculating a suitable metal- EDTA stoichiometry was prohibitively difficult. As a result, examples of EDTA concentrations from previously published studies were utilised.

Glycerol itself has been identified as a reducing agent in a variety of scenarios, including synthesis of nanoparticles (Díaz-Álvarez & Cadierno, 2013; Kou *et al.*, 2013; Kim *et al.*, 2014). To quantify the impact of glycerol on the leachability of metals, additional tests were performed on pre-experiment wastes where 10 mM of glycerol was added to the leachant. This allows for the differentiation between changes in leachability due to bioreduction and changes directly caused by the presence of glycerol. Using 10 mM of glycerol, represents the most extreme possible case of residual glycerol in the waste as previous work has established that glycerol was oxidised extensively in the columns and residual concentrations were likely low (Section 9.4.2).

All acid and chelator leach experiments were carried out in duplicate. All tests were constructed within a glovebox under N_2 and sealed so avoid contact with the atmosphere. Leaching was performed on an orbital shaker for 24hrs at a rate of 120rpm. The extracts were filtered through a 0.2 µm cellulose acetate filter and analysed by ICP-OES for iron, zinc, lead, aluminium, copper, arsenic and sulphur. As the metals of most

economic interest and abundance in the waste, analysis has focused on iron, zinc, copper and lead.

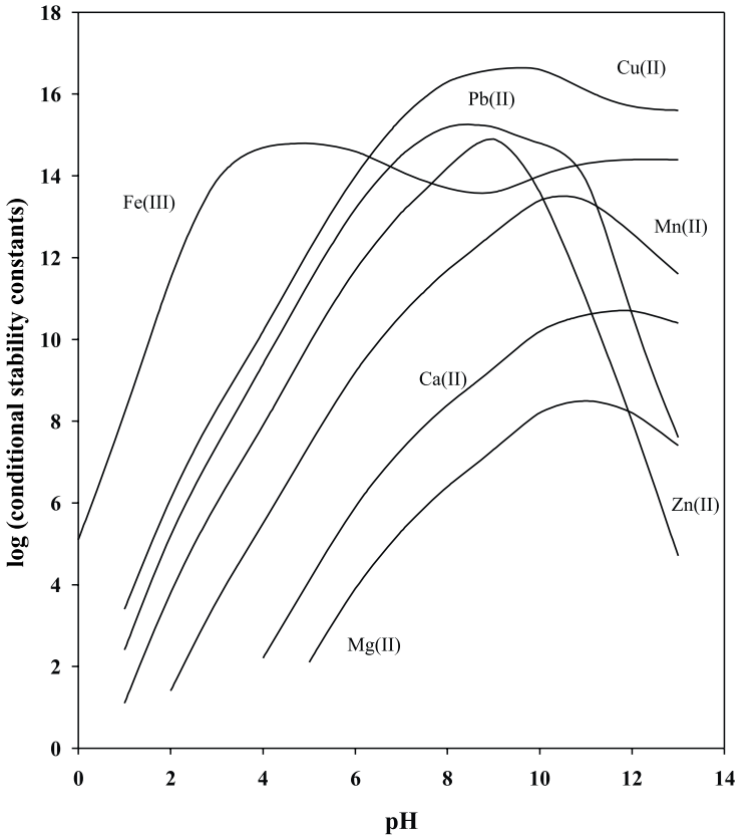

Figure 10.2 Effect of pH on conditional stability constants of metal-EDTA complexes at stoichiometry of 1:1 (Kim *et al.*, 2003)

10.4. Results and Discussion

10.4.1. Hydrochloric Acid Leaching

As shown in Figure 10.3, approximately 4.2% of iron within the pre-experiment waste is leachable with 1 M HCl. The use of 0.5 M and 0.25 M HCl leachants yielded ~1.8% and ~1.0% respectively. The decreasing leachability is to be expected given the decreasing concentration of the leachant. The introduction of glycerol to the waste and stimulation of bioreduction has resulted in an increase in the leachability of iron from the wastes. Approximately 5.7% of iron was leached from the post-experiment “Live” column wastes with a 1 M HCl leachant, representing a slight increase (1.5%) from the equivalent pre-experiment wastes. The increases in leachability of iron with the 0.5 M and 0.25 M HCl

leachants are more substantial increasing from the initial 1.8% and 1.0% respectively to ~4.6% for both concentrations. This represents increases of 2.8% and 3.6% of total iron leached respectively. The similarity of the measurements suggests that ~4% of iron in the post-experiment waste is present in a form highly susceptible to acid dissolution even with dilute acids (e.g. siderite). It should be noted, however, that the 0.5 M leaching results had a larger variability between replicates and so the correlation with the 0.25 M equivalent may not be a true reflection of the leachability of iron in the total waste mass.

The results of leaching the "Organic Starved" samples by contrast show, slight but consistent, decreases in leachability of iron in post-experiment samples. Approximately 2.8%, 1.2% and 0.6% of total iron was leached from post-experiment "Organic Starved" samples using 1 M, 0.5 M and 0.25 M HCl respectively. This represents a decrease of 1.4%, 0.6% and 0.4% total iron leached respectively. Given the lack of microbial stimulation in the "Organic Starved" columns, suggested by effluent analysis, sequential extraction and microbial community analysis, it seems most likely that this decrease in leachability is a result of an increase in the crystallinity of amorphous minerals resulting in more stable, less reactive minerals in the waste (Cornell & Schwertmann, 2003; Schroth & Parnell, 2005).

Autoclaving of the waste has resulted in a slight increase in the leachability of iron from the wastes. Approximately 4.7%, 2.1% and 1.2% of total iron leached with 1 M, 0.5 M and 0.25 M HCl leachants, increased from ~4.2%, 1.8% and 1.0% respectively. Despite these increases being relatively minor, they do suggest the possibility that the heat and/or pressure of autoclaving has increased the leachability of iron. Increased heat is known to increase the rate of amorphous mineral re-crystallisation, though this contradicts the observations of the "Organic Starved" column samples where this mechanism is considered responsible for the decrease in leachability. Thermal pre-treatment of ores and wastes is common practice to increase metal recovery yields, but these techniques regularly use temperatures in excess of 500˚C. Autoclaving, by comparison, only increases the temperature to 121˚C but may explain why only slight increases in leachability have been observed as a result of a very limited form of thermal pre-treatment. Martinez *et al.* (1999) observed that thermally induced transformation of ferrihydrite to goethite and haematite resulted in increased release of lead to

solution, though this was performed over a much longer period than the autoclaving process.

As with the "Live" column samples, there has generally been an increase in the leachability of iron in the post-experiment "Autoclaved" column samples. Approximately 4.4%, 3.5% and 2.9% of total iron was leached using 1 M, 0.5 M and 0.25 M HCl respectively. While the 0.5 M and 0.25 M leaches have yielded increased iron leachability, the 1 M HCl leach has shown a slight decrease, of 0.3%, in total iron leachability. The 0.5 M and 0.25 M leaches have shown increases of 1.4% and 1.7% in the leachability of iron, suggesting that there is an increase in readily leachable phases of iron within the waste as a result of bioreduction correlating with the results of the "Live" column leachability analysis. The minor difference between the leaching yields of the 0.25 M and 1 M HCl suggest that these readily leachable minerals are relatively minor in the waste and less reactive forms of iron still dominate the system.

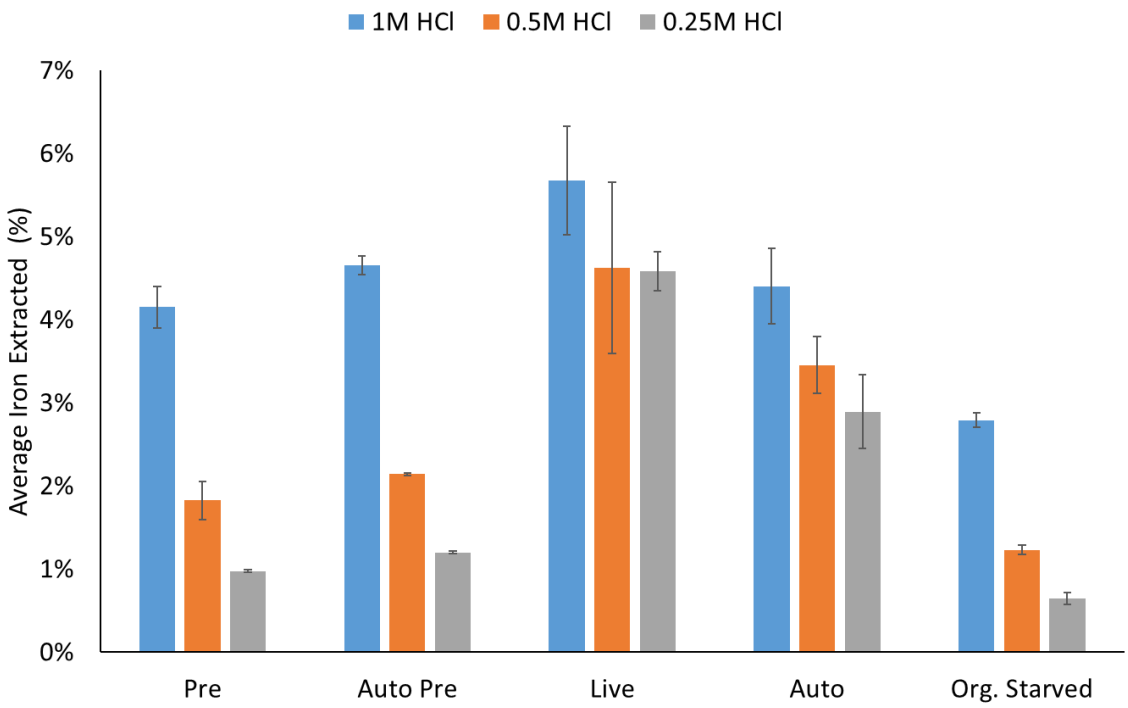

Figure 10.3 Leachability of iron from pre- and post-experiment wastes using HCl as a leachant

As can be seen in Figure 10.4, zinc leachability in the wastes show similar trends and responses to experimentation as iron; though changes in leachability have occurred to

a greater extent resulting in higher recovery yields. Approximately 1.5%, 0.9% and 0.7% of total zinc was recoverable from the pre-experiment wastes with 1 M, 0.5 M and 0.25 M HCl respectively. The introduction of glycerol and stimulation of bioreduction in the waste has had caused a change in the leachability of zinc. 1 M, 0.5 M and 0.25 M HCl leaches yielded ~7.1%, 6.4% and 5.9% recoveries of total zinc respectively. As with iron the greatest relative increase has been from the 0.25 M leach, with a near eight-fold increase in the recovery of zinc in the "Live" samples compared with the pre-experiment equivalent. The 1.2% difference in zinc recovery between the 1 M and 0.25 M leaches of post-experiment "Live" samples suggests that zinc has been partitioned into, or sorbed onto, a more reactive mineral phase, with increasing HCl concentrations yielding smaller increases in recovery as this secondary mineral phase(s) is readily dissolved by even dilute acid leaches whilst the remaining zinc minerals (or minerals to which zinc is associated) are clearly not readily soluble in 1 M HCl at room temperature.

The "Organic Starved" samples have also shown increases in zinc leachability. The 1 M and 0.5 M HCl leaches yielded total zinc recoveries of ~2.5% and 1.2% respectively, increased from 1.5% and 0.9% respectively in the pre-experiment equivalent. The 0.25 M leach showed negligible differences in zinc leachability between the pre- and post-experiment "Organic Starved" samples. The recrystallisation of amorphous iron bearing minerals again provides a potential explanation for the observed results of the "Organic Starved" samples. Whilst the increased crystallinity of iron produces a greater resistance to dissolution of the mineral itself, it also results in a substantial decrease in surface area. This reduction in surface area limits the availability of adsorption sites for the adsorption of associated metals (Cornell & Schwertmann, 2003)

Autoclaving of the waste has resulted in slight increases in the leachability of zinc. 1 M, 0.5 M and 0.25 M HCl leaches of pre-experiment autoclaved wastes yielded zinc recoveries of 2.0%, 1.1% and 0.8% respectively. These all represent minor increases in leachability but are consistent across all acid concentrations testes and with the results of the iron leachability analysis. Leachability of zinc in the post-experiment "Autoclaved" wastes has increased as a result of the stimulated bioreduction. Approximately 5.4%, 4.4% and 4.0% of total zinc was recovered using 1 M, 0.5 M and 0.25 M HCl respectively. All of these represent increases in zinc leachability compared to their pre-experiment equivalents but are lower than the recoveries from the "Live" columns. Following the

trends of other metals and column the greatest increase in recovery has been achieved by the weakest concentration of acid with an approximate five-fold increase in the leachability of zinc as a result of bioreduction using 0.25 M HCl as a leachant. This suggests the partitioning of zinc to more reactive, less stable mineral phases or to weak sorption sites on residual or secondary minerals.

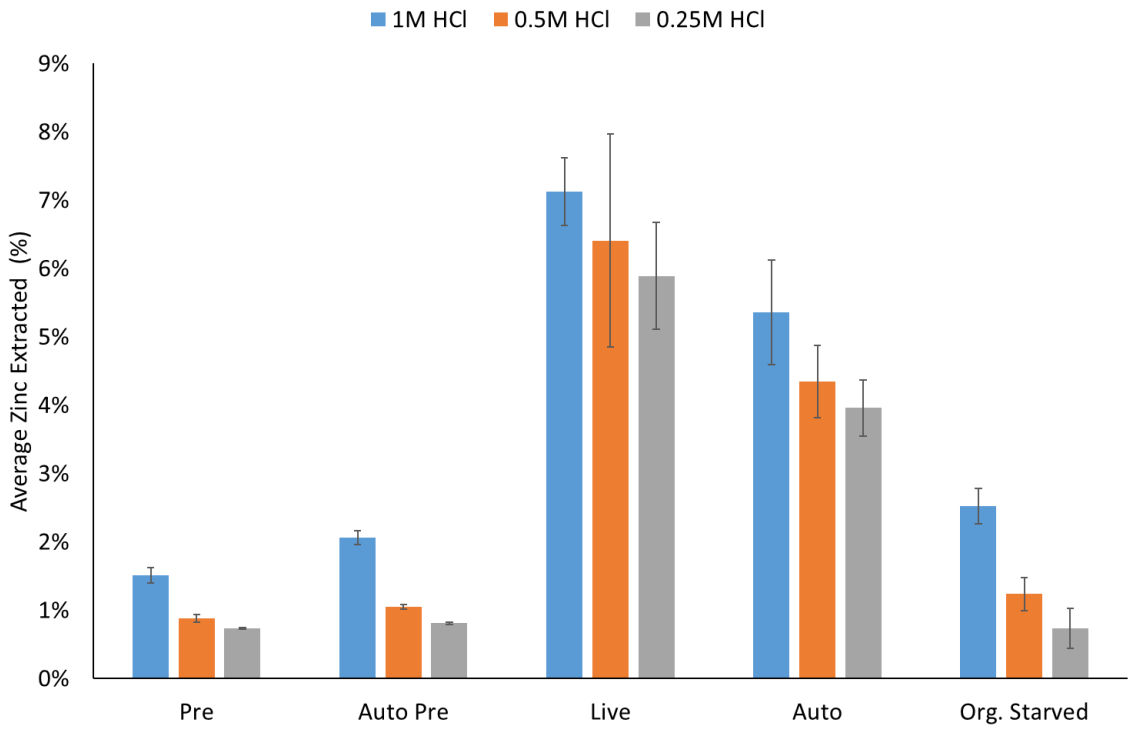

Figure 10.4 Leachability of zinc from pre- and post-experiment wastes using HCl as a leachant

The leachability of copper when using HCl as a leachant shows similar trends to that of zinc and iron but with higher recovery yields (Figure 10.5). Approximately 1.9%, 0.8% and 0.6% of total copper was recoverable from the pre-experiment wastes using 1 M, 0.5 M and 0.25 M HCl respectively. As with the other metals analysed, addition of glycerol has resulted in considerable increases in leachability of copper within the post-experiment "Live" column samples. Leaching with 1 M, 0.5 M and 0.25 M HCl resulted in the recovery of ~15.2%, 13.5% and 14.9%. The higher recovery of copper achieved with 0.25 M HCl compared with the 0.5 M equivalent is likely an anomaly caused by a high variation in readings caused by a sample with an anomalously high copper concentration. It is also notable that variability in the "Live" results is greater than those from any other experiment, with the pre-experiment samples having substantially lower

variability. Despite this variability in the "Live" leaching results, it is clear that there has been a substantial increase in the leachability of copper. The majority of the leachable copper is susceptible to dissolution by the most dilute leachants with only 1.7% difference in the lowest and highest copper recovery yields. Again, this suggests that copper has been redistributed from recalcitrant mineral phases to more reactive mineral phases. The greatest increase in leachability of copper was observed using the 0.25 M leachant where an increase of approximately 23.5 times was observed. This value may though be inflated by the uncertainty in the measurement. The 0.5 M leachant method yielded the second greatest increase of just over 16 times in the "Live" sample compared with the pre-experiment equivalent.

The "Organic Starved" column samples displayed much lower copper leachability than the "Live" samples, though as with other metals, still higher than the pre-experiment wastes. Leaching with 1 M, 0.5 M and 0.25 M HCl resulted in the recovery of 6.0%, 3.5% and 2.7% of copper respectively. Whilst being considerably lower than the results of the "Live" samples, these values represent leachability increases of 4.1%, 2.7% and 2.1% total copper respectively from the pre-experiment waste. As with other metals this is believed to be attributable to the transformation of amorphous iron oxyhydroxides to more crystalline forms and the resultant loss of sorption sites; as post-experiment analysis suggests there has been no significant change in physicochemical properties of the waste during experimentation. Alternately, this may be due to the presence of metallic copper in the waste as suggested during the characterisation of the waste.

Autoclaving of the pre-experiment waste has shown a minor increase in leachability of copper with 3.0%, 1.8% and 1.3% recovered using 1 M, 0.5 M and 0.25 M HCl respectively as leachants. As with the other metals analysed these represent minor increases when compared to those resulting from bioreduction but are consistent across metals analysed and leachant concentrations. Leachability of copper in the post-experiment "Autoclaved" wastes has increased as a result of glycerol addition and the resultant stimulated bioreduction. Approximately 14.3%, 13.1% and 12.0% of total copper was recovered using 1 M, 0.5 M and 0.25 M HCl respectively. These represent relatively similar values to those achieved using the "Live" waste with the 1 M and 0.5 M "Autoclaved" tests achieving yields only 0.9% and 0.4% lower than the "Live"

equivalents. The 0.25 M test has achieved an increase in copper leachability in excess of 9.5 times that of pre-experiment samples.

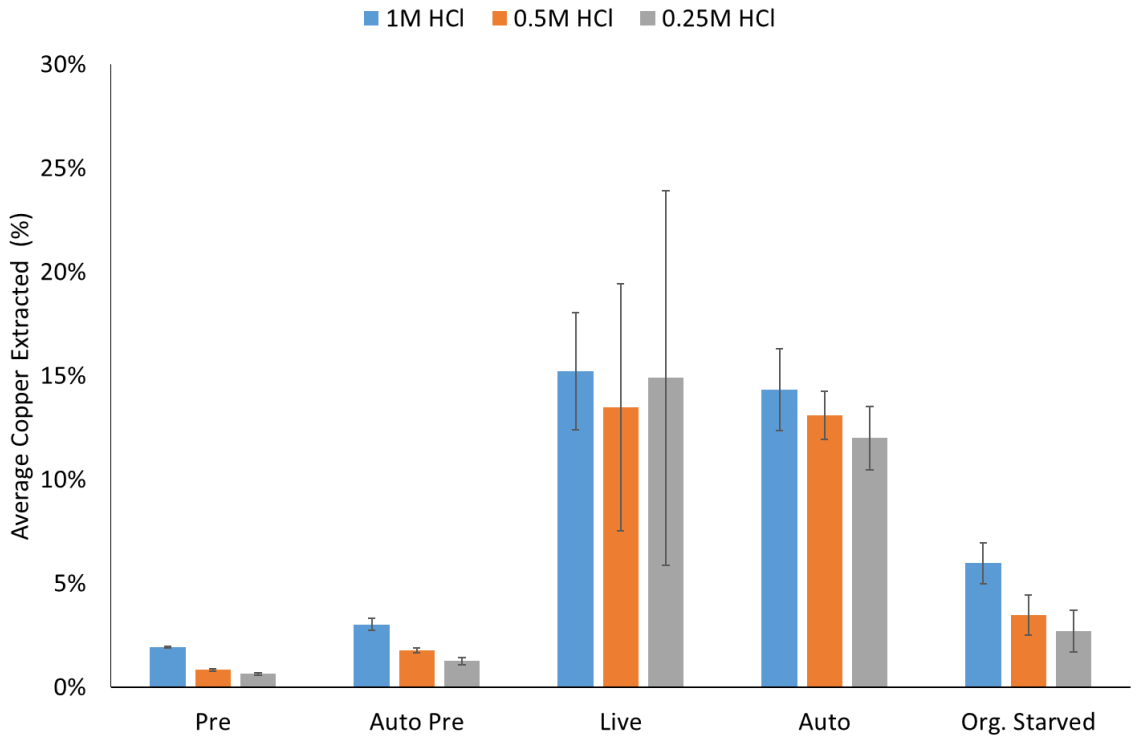

Figure 10.5 Leachability of copper from pre- and post-experiment wastes using HCl as a leachant

Of the metals analysed, lead had the highest rates of recovery from all experimental variants when HCl was used as the leachant. 9.3%, 4.0% and 2.0% of total lead was recovered from the pre-experiment samples with 1 M, 0.5 M and 0.25 M HCl respectively (Figure 10.6). Following the trend of other metals, the leachability of lead from the "Live" column samples has undergone a considerable increase as a result of bioreduction. Leaching of the "Live" column samples with 1 M, 0.5 M and 0.25 M HCl yielded recoveries of 29.9%, 30.9% and 34.8% lead respectively. Whilst this follows the trend of increased leachability in "Live" samples, these results are distinct due to the increasing recovery of total lead with decreasing acid concentration. Despite the uncertainty in the results there is still the suggestion of an increase in the abundance of very reactive lead being minerals, susceptible to dissolution by dilute acids. The 34.8% of total lead recovered with 0.25 M HCl represents an increase >17.6 times greater than that achieved from the pre-experiment equivalent. The 0.5 M HCl variant yielded an increase of more than 7.5 times that recovered from the pre-experiment sample.

The “Organic Starved” column samples displayed much lower lead leachability than the “Live” samples, though as with other metals, there is an increase in leachability compared with the pre-experiment wastes. Leaching of the “Organic Starved” samples with 1 M, 0.5 M and 0.25 M HCl recovered 12.9%, 6.2% and 3.7% respectively. This represents increases of 3.6%, 2.2% and 1.7% total lead respectively from the post-experiment “Organic Starved” wastes compared with the pre-experiment equivalent.

Autoclaving of the pre-experiment waste has shown a more substantial increase in leachability of lead than observed in the other metals. Approximately 15.5%, 9.0% and 5.1% of total lead was recovered from the pre-experiment autoclaved samples using 1 M, 0.5 M and 0.25 M HCl respectively as leachants. This represents an increase of 6.2%, 5.0% and 3.1% of total lead recovered, with 1 M, 0.5 M and 0.25 M HCl respectively, as a result of the autoclaving process. Glycerol addition and the resulting bioreduction appears to have resulted in an increase in lead leachability. Approximately 31.1%, 28.7% and 27.8% of total lead was recovered from the post-experiment “Autoclaved samples. These results are near comparable with the “Live” column equivalents, with differences in the lead recoveries achieved explainable through variability in the leachability data.

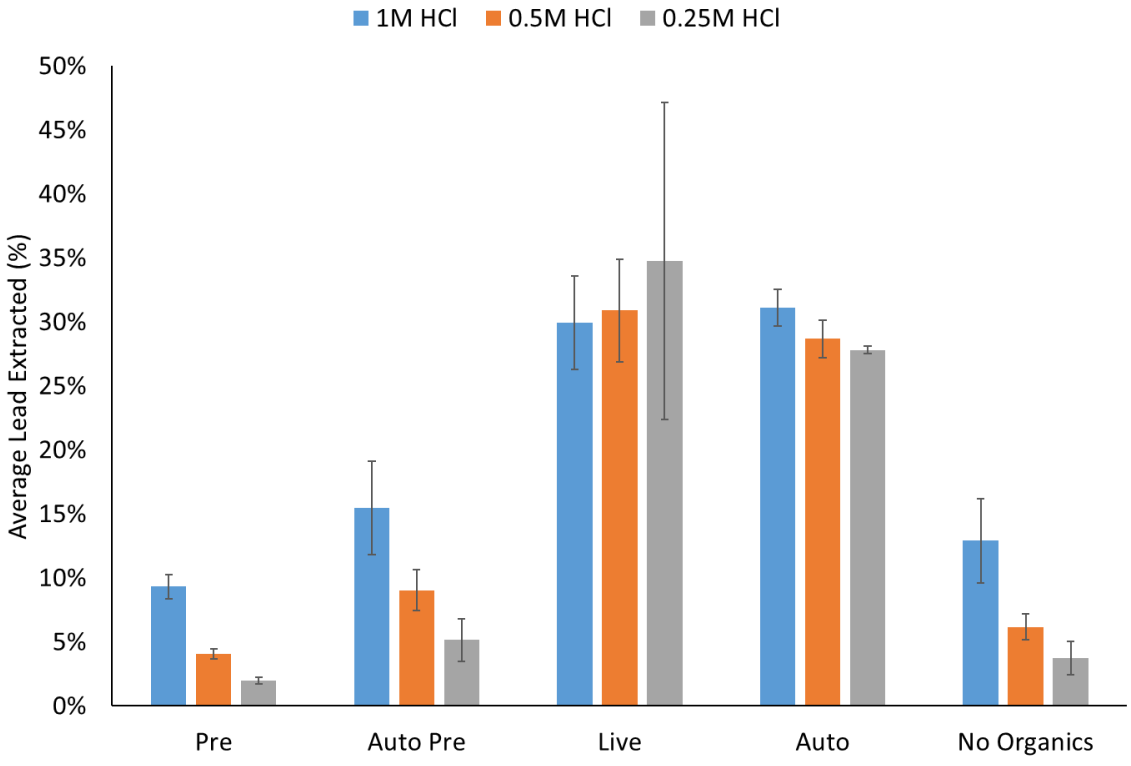

Figure 10.6 Leachability of lead from pre- and post-experiment wastes using HCl as a leachant

Table 10.1 Leachability of elements analysed, as a percentage of total in waste, from pre- and post-experiment waste by HCl

		Fe	Zn	Cu	Al	Pb	As	S
Pre	1 M	4.2%	1.5%	1.9%	0.3%	9.3%	0.8%	7.0%
	0.5 M	1.8%	0.9%	0.8%	0.2%	4.0%	0.3%	3.9%
	0.25 M	1.0%	0.7%	0.6%	0.1%	2.0%	0.2%	2.3%
Auto Pre	1 M	4.7%	2.1%	3.0%	0.3%	15.5%	2.2%	8.2%
	0.5 M	2.1%	1.0%	1.8%	0.2%	9.0%	0.6%	4.9%
	0.25 M	1.2%	0.8%	1.3%	0.1%	5.1%	0.3%	3.0%
Live 1	1 M	6.0%	6.9%	12.0%	1.9%	31.3%	0.7%	2.8%
	0.5 M	4.9%	6.2%	6.6%	1.6%	34.2%	0.3%	1.2%
	0.25 M	4.4%	5.7%	6.0%	1.3%	29.9%	0.1%	0.5%
Live 2	1 M	4.9%	6.8%	16.8%	1.1%	32.7%	1.4%	1.5%
	0.5 M	3.5%	4.9%	16.6%	0.8%	32.1%	0.9%	0.6%
	0.25 M	4.5%	5.2%	24.1%	0.6%	48.8%	0.3%	0.5%
Live 3	1 M	6.1%	7.7%	16.9%	2.4%	25.8%	0.5%	1.9%
	0.5 M	5.5%	8.1%	17.2%	2.2%	26.4%	0.2%	0.7%
	0.25 M	4.8%	6.7%	14.6%	1.9%	25.5%	0.1%	0.3%
Auto 1	1 M	4.0%	4.9%	15.5%	1.5%	32.5%	1.1%	3.3%
	0.5 M	3.3%	4.0%	13.5%	1.4%	27.8%	0.4%	1.2%
	0.25 M	2.6%	3.8%	12.6%	1.5%	28.1%	0.2%	0.5%
Auto 2	1 M	4.9%	6.2%	15.4%	2.0%	29.7%	0.6%	1.8%
	0.5 M	3.8%	5.0%	14.0%	1.6%	27.8%	0.2%	0.6%
	0.25 M	3.4%	4.4%	13.2%	1.4%	27.6%	0.2%	0.2%
Auto 3	1 M	4.3%	4.9%	12.0%	1.6%	31.1%	0.9%	3.2%
	0.5 M	3.2%	4.1%	11.8%	1.3%	30.4%	0.6%	1.5%
	0.25 M	2.6%	3.6%	10.3%	1.0%	27.7%	0.5%	0.4%
Org. Starved 1	1 M	2.9%	2.2%	4.9%	0.8%	15.8%	0.4%	7.0%
	0.5 M	1.2%	1.0%	2.4%	0.5%	6.5%	0.4%	3.2%
	0.25 M	0.6%	0.4%	1.6%	0.3%	2.6%	0.4%	1.3%
Org. Starved 2	1 M	2.7%	2.6%	6.3%	1.2%	9.4%	0.7%	5.9%
	0.5 M	1.2%	1.4%	3.8%	0.8%	5.0%	0.3%	2.4%
	0.25 M	0.7%	0.8%	3.1%	0.6%	3.5%	0.2%	1.0%
Org. Starved 3	1 M	2.8%	2.7%	6.7%	1.4%	13.5%	0.6%	6.3%
	0.5 M	1.3%	1.4%	4.3%	0.8%	6.9%	0.3%	2.5%
	0.25 M	0.7%	1.0%	3.5%	0.6%	5.2%	0.3%	1.2%

10.4.2. Sulphuric Acid Leaching

The results from analysis of iron leachability with H_2SO_4 bear considerable similarity to the results where HCl was used as the leachant. While the trends in the data are similar to that obtained from the HCl leaches, the H_2SO_4 leach data has yielded slightly higher recoveries of iron across all experimental variants (Figure 10.7). Approximately 5.0%, 3.4% and 2.0% of total iron was recovered from the pre-experiment wastes with 1 M, 0.5 M and 0.25 M H_2SO_4 as the leachant. As with HCl leaching, the addition of glycerol has resulted in an increase in the leachability of iron from the wastes with all concentrations of H_2SO_4 utilised. Leachability of iron from the Parys Mt. 2 waste has increased to 7.3%, 6.0% and 5.1% of total iron from the post-experiment "Live" waste samples using 1 M, 0.5 M and 0.25 M H_2SO_4 respectively. This represents an increase in iron recovery of 2.3%, 2.6% and 3.1% with 1 M, 0.5 M and 0.25 M H_2SO_4 respectively; with the 0.25 M variant representing an increase in total iron recovery of greater than 2.5 times that of the pre-experiment samples. Again, variability in the results of "Live" column samples is greater than that of the pre-experiment.

The results of leaching the "Organic Starved" samples again show a slight but consistent reduction in the leachability of iron in post-experiment samples, correlating with the HCl leach results. Approximately 3.7%, 2.5% and 1.5% of total iron was recovered from the post-experiment "Organic Starved" samples. This represents marginal reductions in iron leachabilities of 1.3%, 0.9% and 0.5% in the "Organic Starved" samples compared with the pre-experiment samples. This correlates with the results of the HCl leaches and supports the assertion that increased crystallisation of iron oxyhydroxides to less reactive minerals has reduced the leachability of iron in the waste.

Autoclaving of the waste has resulted in only marginal alteration in the leachability of iron from the waste with H_2SO_4. Iron leached with 1 M H_2SO_4 has increased slightly from 5.0% to 5.7%. Differences in the leachability of iron, in non-autoclaved and autoclaved preliminary wastes, with 0.5 M and 0.25 M H_2SO_4 are negligible and suggest that autoclaving has minimal impact on iron leachability. This contradicts what was observed in HCl leaches for iron and with the leachability data for other metals of interest. The introduction of glycerol to the wastes and subsequent iron bioreduction has resulted in an increase in iron leachability from the waste. Approximately 6.3%, 5.1% and 4.1% of

iron was recoverable from the post-experiment "Autoclaved" samples with 1 M, 0.5 M and 0.25 M H_2SO_4 respectively. This follows the recurring trend of leachability from post-experiment "Autoclaved" samples being lower than that from the "Live" samples and higher than that of the pre-experiment samples.

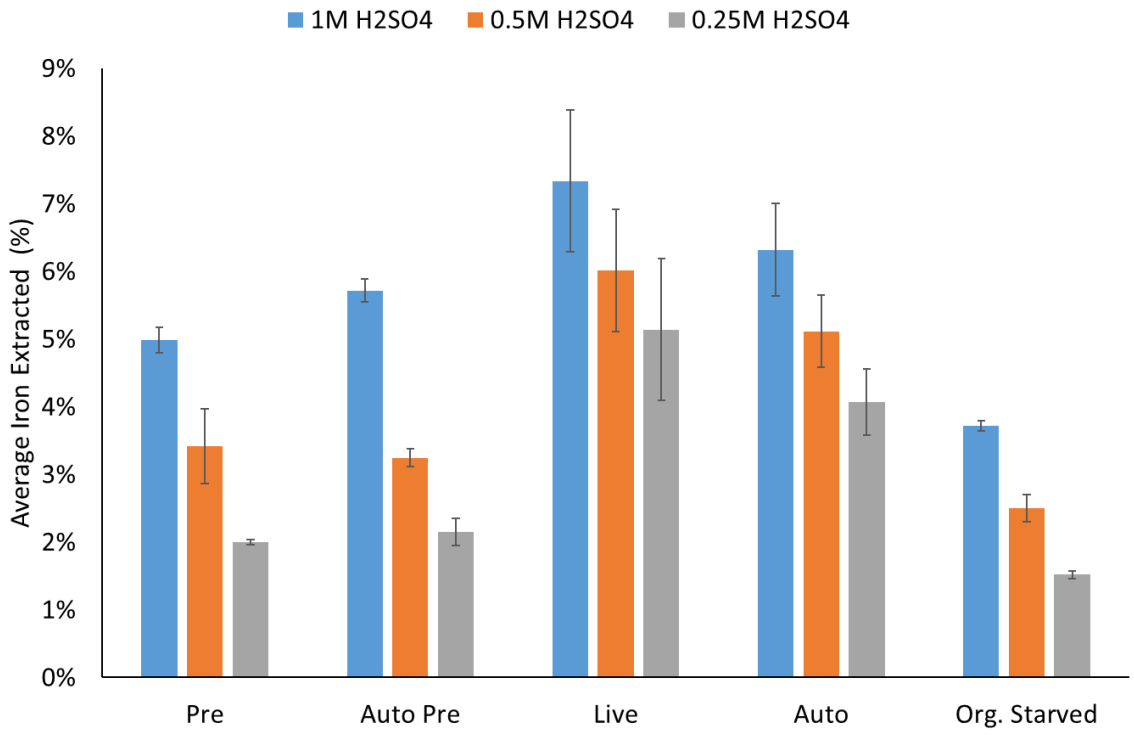

Figure 10.7 Leachability of iron from pre- and post-experiment wastes using H_2SO_4 as a leachant

The leachability of zinc with H_2SO_4 from the wastes show similar trends to that of iron, with a general trend of greater iron recovery compared with the HCl leaches. Approximately 1.5%, 1.1% and 1.0% of total zinc was recoverable from the pre-experiment wastes with 1 M, 0.5 M and 0.25 M H_2SO_4 respectively (Figure 10.8). Stimulation of bioreduction by the introduction of glycerol has resulted in the increased leachability of zinc in the "Live" column samples. Leaching with 1 M, 0.5 M and 0.25 M H_2SO_4 recovered 7.9%, 6.9% and 6.8% of total zinc respectively. These represent increases in iron recovery of 6.4%, 5.8% and 5.8% respectively, the latter two results being ~6.5 times greater than that of the pre-experiment sample. There is a much larger variability in the recovery of zinc in the "Live" samples compared with any other of the experimental variants with an average standard deviation of ~1.3% in the "Live" column

sample data. This variability may also explain the similarity between the 0.5 M and 0.25 M leaches.

Leachability of zinc has also increased slightly in the "Organic Starved" samples, as was observed with the HCl leaches. Approximately 2.7%, 1.9% and 1.5% of total zinc was recovered using 1 M, 0.5 M and 0.25 M H_2SO_4 respectively. This represents an increase in recovery compared with the pre-experiment sample but considerably less than that achieved from the "Live" samples. This correlates with the results of leaching zinc with HCl.

Autoclaving of the pre-experiment wastes again shows a marginal increase in zinc leachability. Approximately 1.8%, 1.4% and 1.1% of total zinc was recovered from the autoclaved pre-experiment waste using 1 M, 0.5 M and 0.25 M H_2SO_4 respectively. Leachability of zinc in the post-experiment "Autoclaved" wastes has increased further as a result of bioreduction. Approximately 6.4%, 5.6% and 4.9% of total zinc was recovered from the autoclaved pre-experiment waste using 1 M, 0.5 M and 0.25 M H_2SO_4 respectively. The largest increase in zinc leachability from post-experiment "Autoclaved" waste was observed from the 0.25 M leach with a recovery more than 4 times greater that of the pre-experiment equivalent. Variation in zinc recovery within the "Autoclaved" wastes samples is noticeably lower than that of the "Live" samples.

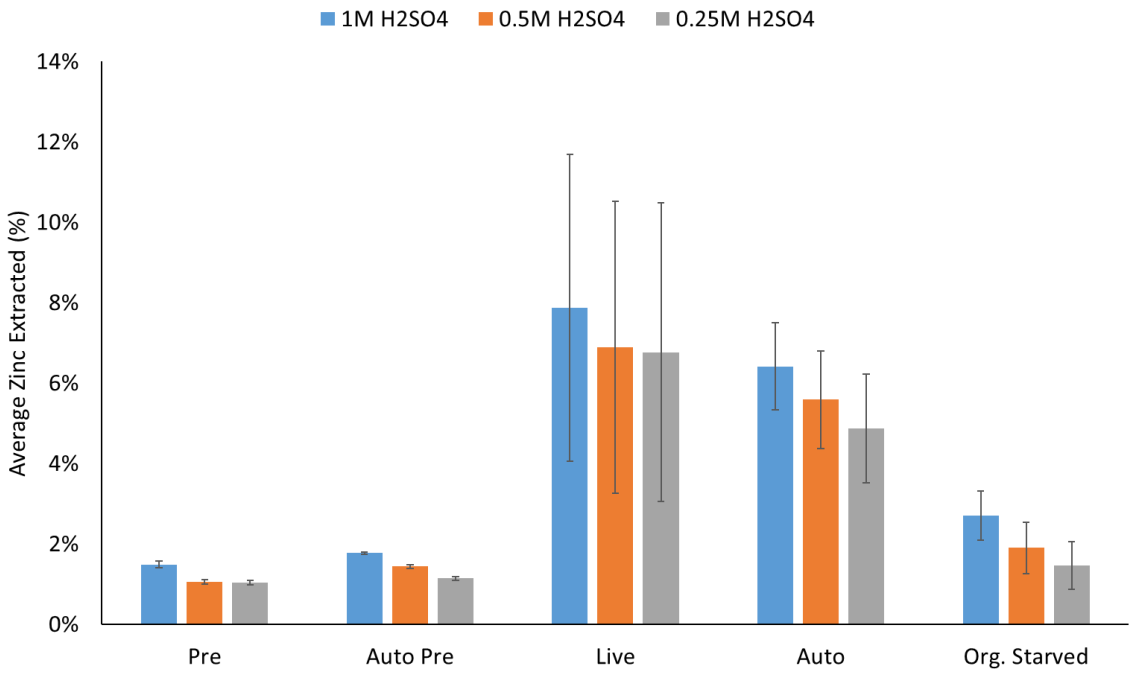

Figure 10.8 Leachability of zinc from pre- and post-experiment wastes using H_2SO_4 as a leachant

While the leachability of both iron and zinc with H_2SO_4 has increased relative to leaching with HCl, the leachabiltity of copper has generally decreased (Figure 10.9). Approximately 1.0%, 0.6% and 0.5% of total copper was recovered from the pre-experiment waste with 1 M, 0.5 M and 0.25 M H_2SO_4 respectively. Copper leachability in the "Live" column samples has increased to 9.1%, 9.0% and 9.1% with 1 M, 0.5 M and 0.25 M H_2SO_4 respectively. The latter of these results representing a recovery more than 16.5 times that of the pre-experiment equivilant. The similarity between the recoveries of copper across all concentrations of H_2SO_4, and the increase from the pre-experiment samples, is suggestive that copper has partitioned into more reactive, readily leachable mineral phases. This copper is leachable by even the most dilute acid utililized whilst increasing the concentration appears to have negligable impact on copper recovery suggesting the remainder of copper remains held within more recalcitrent mineral phases. As with other extractions from "Live" column samples there is a higher degree of variability in the leachability of copper from these samples than any other experimental variant.

Leachability of copper in the "Organic Starved" samples again shown a slight increase relative to the pre-experiment samples. Approximately 3.5%, 2.6% and 2.0% of total copper was recovered from the post-experiment "Organic Starved" waste samples with 1 M, 0.5 M and 0.25 M H_2SO_4 respectively. This represents increases of 2.5%, 2.0% and 1.5% total copper recovery, respectively, compared with the pre-experiment leaches.

Autoclaving of the pre-experiment waste has shown a minor increase in leachability of copper with 1.7%, 1.0% and 0.8% recovered from the autoclaved pre-experiment waste using 1 M, 0.5 M and 0.25 M H_2SO_4 respectively as leachants. Leachability of copper in the post-experiment "Autoclaved" wastes has increased as a result of glycerol addition and the resultant stimulated bioreduction. Approximately 10.1%, 9.4% and 8.8% of total copper was recovered using 1 M, 0.5 M and 0.25 M H_2SO_4 respectively. The 1 M and 0.5 M leaches of the "Autoclaved" column wastes achieved greater copper recovery than the equivalent leaches from the "Live" column. These results represent the only instances of metal recovery from the "Autoclaved" wastes exceeding that of the live wastes. Variability in copper recovery is noticeably less than that of the "Live" waste samples, though is higher than that of the pre-experiment samples.

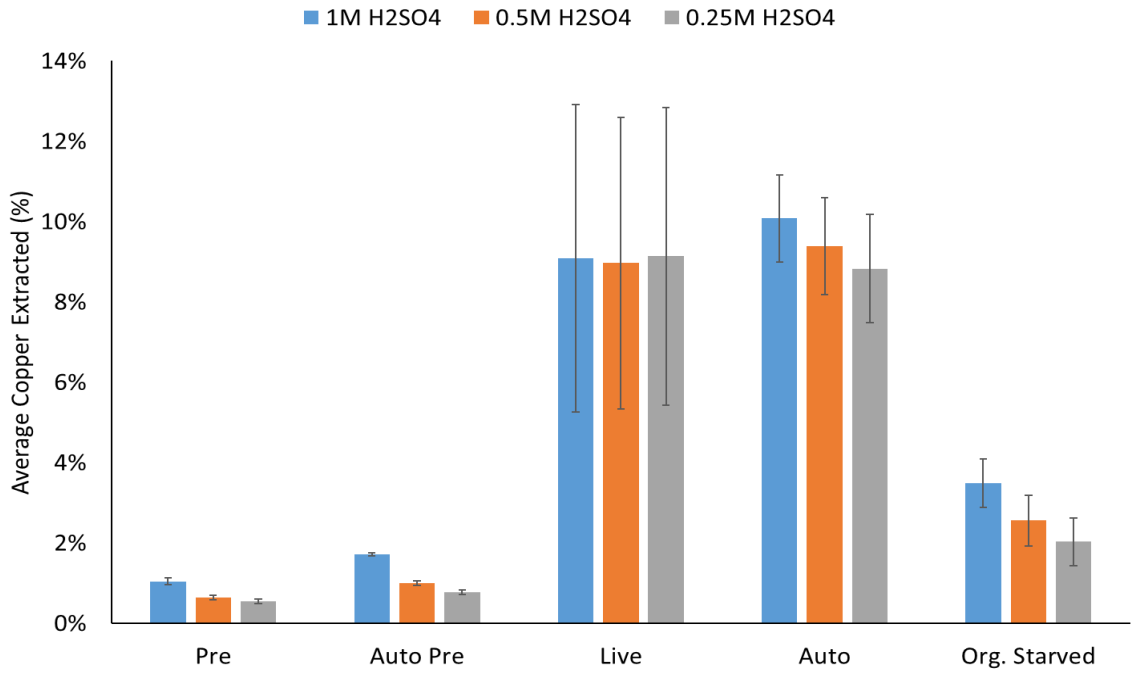

Figure 10.9 Leachability of copper from pre- and post-experiment wastes using H_2SO_4 as a leachant

Across all the experimental samples analysed, there are negligible differences between the recovery of lead with all concentrations of H_2SO_4 utilised. All samples generated recoveries of approximately 0.5% of total lead (Figure 10.10). This is due to the inability of cold dilute H_2SO_4 to solubilise lead, which itself is a result of the insolubility of lead sulphate formed when H_2SO_4 is introduced to the waste. (Thornton *et al.*, 2001).

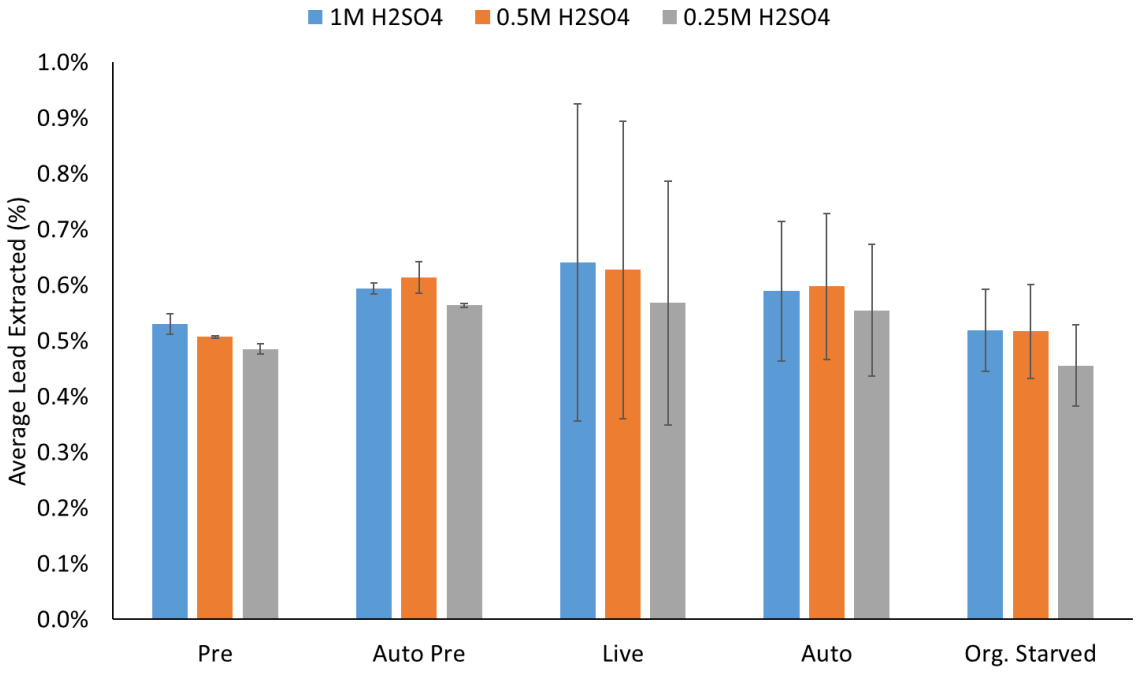

Figure 10.10 Leachability of lead from pre- and post-experiment wastes using H_2SO_4 as a leachant

Table 10.2 Leachability of elements analysed, as a percentage of total in waste, from pre- and post-experiment waste by H_2SO_4

		Fe	Zn	Cu	Al	Pb	As	S*
Pre	1 M	5.0%	1.5%	1.0%	0.3%	0.5%	3.4%	N/A
	0.5 M	3.4%	1.1%	0.6%	0.2%	0.5%	1.2%	N/A
	0.25 M	2.0%	1.0%	0.5%	0.2%	0.5%	0.6%	N/A
Auto Pre	1 M	5.7%	1.8%	1.7%	0.3%	0.6%	4.8%	N/A
	0.5 M	3.2%	1.4%	1.0%	0.2%	0.6%	1.6%	N/A
	0.25 M	2.1%	1.1%	0.8%	0.2%	0.6%	0.7%	N/A
Live 1	1 M	8.2%	8.1%	4.7%	2.4%	0.6%	12.2%	N/A
	0.5 M	6.6%	7.3%	4.8%	1.9%	0.6%	6.1%	N/A
	0.25 M	5.6%	7.6%	4.9%	1.7%	0.5%	3.0%	N/A
Live 2	1 M	6.2%	6.5%	11.4%	1.3%	0.9%	11.4%	N/A
	0.5 M	5.0%	5.5%	11.5%	1.1%	0.9%	8.1%	N/A
	0.25 M	3.9%	5.3%	11.9%	0.9%	0.8%	4.4%	N/A
Live 3	1 M	7.7%	9.0%	11.2%	2.4%	0.4%	5.8%	N/A
	0.5 M	6.5%	7.9%	10.6%	2.2%	0.4%	3.3%	N/A
	0.25 M	5.8%	7.5%	10.6%	2.1%	0.4%	2.0%	N/A
Auto 1	1 M	5.7%	6.1%	10.3%	2.6%	0.5%	6.9%	N/A
	0.5 M	4.6%	5.5%	10.1%	2.3%	0.6%	3.5%	N/A
	0.25 M	3.7%	5.1%	9.5%	2.0%	0.5%	2.0%	N/A
Auto 2	1 M	7.0%	7.1%	11.0%	2.3%	0.5%	6.5%	N/A
	0.5 M	5.7%	6.2%	10.1%	2.0%	0.5%	3.9%	N/A
	0.25 M	4.6%	5.7%	9.7%	1.7%	0.5%	2.4%	N/A
Auto 3	1 M	6.2%	5.9%	8.9%	2.0%	0.7%	8.5%	N/A
	0.5 M	5.0%	5.1%	8.0%	1.6%	0.7%	5.2%	N/A
	0.25 M	3.8%	3.9%	7.3%	1.4%	0.7%	3.2%	N/A
Org. Starved 1	1 M	3.8%	2.4%	2.8%	0.9%	0.5%	2.0%	N/A
	0.5 M	2.6%	1.8%	1.9%	0.7%	0.5%	1.1%	N/A
	0.25 M	1.6%	1.1%	1.3%	0.6%	0.5%	0.7%	N/A
Org. Starved 2	1 M	3.6%	2.7%	3.6%	1.4%	0.4%	2.4%	N/A
	0.5 M	2.3%	1.8%	2.6%	1.1%	0.4%	1.2%	N/A
	0.25 M	1.5%	1.5%	2.4%	0.8%	0.4%	0.6%	N/A
Org. Starved 3	1 M	3.7%	3.0%	4.0%	1.5%	0.6%	2.7%	N/A
	0.5 M	2.6%	2.1%	3.2%	1.2%	0.6%	1.4%	N/A
	0.25 M	1.5%	1.8%	2.3%	0.9%	0.5%	0.7%	N/A

*= Sulphur concentrations not applicable given sulphur in leachant

10.4.3. Citric Acid Leaching

Citric acid is a weaker acid than either HCl or H_2SO_4. However, this organic acid is also a known chelator of iron in aqueous solutions where as the other inorganic acids are not (Silva *et al.*, 2009). Despite this the leachability of iron from the wastes is generally lower than that achieved with the other two acids (Figure 10.11). Approximately 0.5%, 0.4% and 0.4% of total iron was recovered from the pre-experiment wastes with 1 M, 0.5 M and 0.25 M citric acid, respectively, as the leachant. These recovery rates are relatively small compared with the recoveries achieved with the other acids. This may result from citric acid being a relatively weak acid which is having limited impact on a waste that is already at pH≈3. The post-experiment "Live" samples yield higher recovery rates of iron. Approximately 3.7%, 3.7% and 3.0% of total iron was recovered, with 1 M, 0.5 M and 0.25 M citric acid respectively, from the "Live" column wastes. As with the pre-experiment waste, the results from the "Live" waste show only minor variation in recovery rates despite different leachant concentrations. The extraction with 0.5 M citric acid represents the greatest increase in copper recovery with a copper recovery of more than 8 times the pre-experiment sample.

As with other acid leaches then recovery of iron from the "Organic Starved" samples has marginally decreased relative to the pre-experiment samples. Approximately 0.4%, 0.3% and 0.3% of total iron was recovered from the "Organic Starved" wastes with 1 M, 0.5 M and 0.25 M citric acid respectively. Whilst these decreases in iron recovery are near negligible, they contribute to the continuing trend of reduced iron leachability within "Organic Starved" column wastes which has been attributed to an increased degree of crystallisation of iron oxyhydroxides.

Autoclaving of the pre-experiment waste has resulted in an increase in leachability with citric acid. Approximately 1.0%, 1.0% and 0.8% of total iron was recovered from the pre-experiment wastes with 1 M, 0.5 M and 0.25 M citric acid respectively. Iron leachability in the post-experiment "Autoclaved" wastes has increased with 2.5%, 2.6% and 2.7% of iron recovered with 1 M, 0.5 M and 0.25 M citric acid respectively. These results again show the trend of similar leachability of iron regardless of leachant concentration. The minor differences in the recoveries are readily explainable through variation within the data.

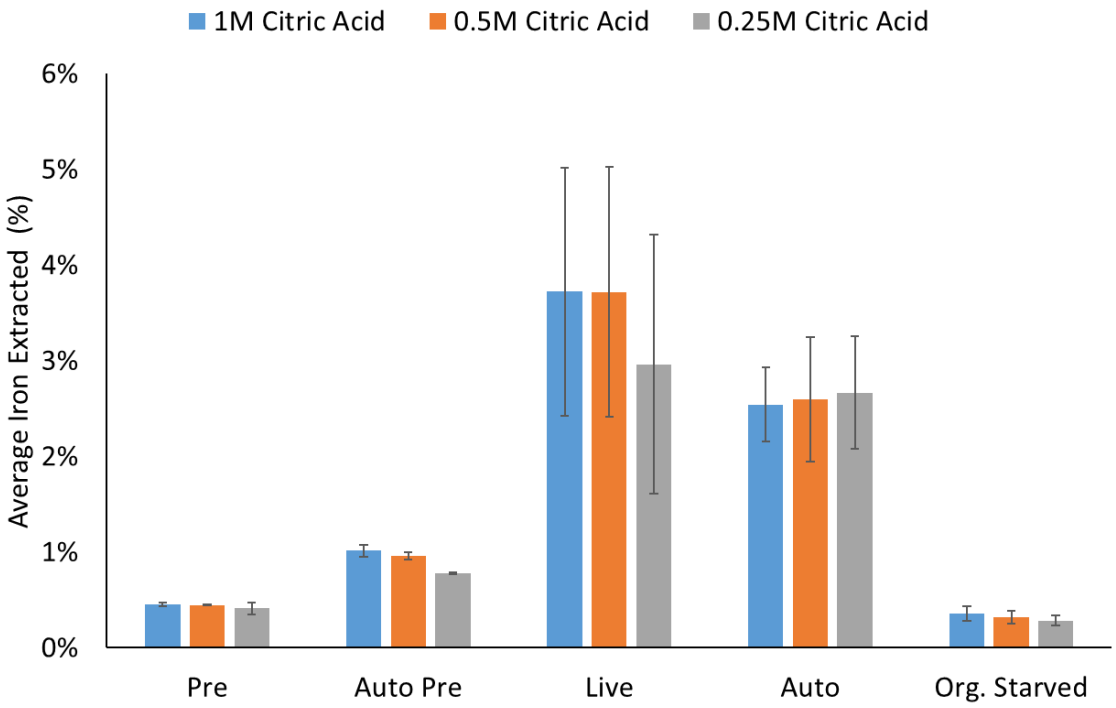

Figure 10.11 Leachability of iron from pre- and post-experiment wastes using citric acid as a leachant

The leachability of zinc from the pre-experiment wastes, using citric acid as a leachant, is lower than that observed with the inorganic acids (Figure 10.12). Approximately 0.6%, 0.6% and 0.5% of total zinc was recoverable from the pre-experiment wastes with 1 M, 0.5 M and 0.25 M citric acid respectively. These near negligible recovery rates show no correlation with increasing citric acid concentration, suggesting that the zinc is present within mineral phases resistant to dissolution by dilute citric acid at the pH of the experiment. As seen in the leaches with inorganic acids, stimulation of bioreduction by the introduction of glycerol has resulted in the increased leachability of zinc, by citric acid in the "Live" column samples. Leaching with 1 M, 0.5 M and 0.25 M citric acid yielded recoveries of 4.3%, 3.8% and 3.6% of total zinc respectively. Unlike the pre-experiment samples, there is a discernible difference in the rates of zinc recovery with increasing recovery correlating with increasing citric acid concentration. As with other experimental variants, zinc leachability from "Live" samples with citric acid is lower than that achieved with the inorganic acids.

Whereas the leachability of zinc from "Organic Starved" column samples has been seen to increase slightly with inorganic acid as a leachant, the same trend is not observed when citric acid has been utilised. Rather, leachability has remained relatively unchanged with 0.5%, 0.4% and 0.4% of total zinc was recoverable from the "Organic

Starved" samples with 1 M, 0.5 M and 0.25 M citric acid respectively. Variability in the results explains the observed minor decrease in leachability. This suggests there has been little alteration to the wastes and leachability of zinc, the opposite trend to what was observed with the inorganic acid leaches.

A further difference in the results of zinc leachability with citric acid (compared with inorganic acids) is seen in the results of leaching from the pre-experiment autoclaved wastes. Rather than the slight increase in leachability previously seen, there is no alteration in the leachability of zinc resulting from the autoclaving process. Approximately, 0.6%, 0.6% and 0.5% of total zinc was recovered from the autoclaved pre-experiment waste samples using 1 M, 0.5 M and 0.25 M citric acid respectively. The leachability of the post-experiment "Autoclaved" column samples has increased as a result of bioreduction, in agreement with what was observed in the other leaching experiments. Approximately, 2.9%, 2.6% and 2.5% of total zinc was recovered from the "Autoclaved" column waste samples using 1 M, 0.5 M and 0.25 M citric acid respectively. This correlates with the observations of experimentation with inorganic acids in that zinc leachability has increased, though not to the same extent as it has within the "Live" column samples.

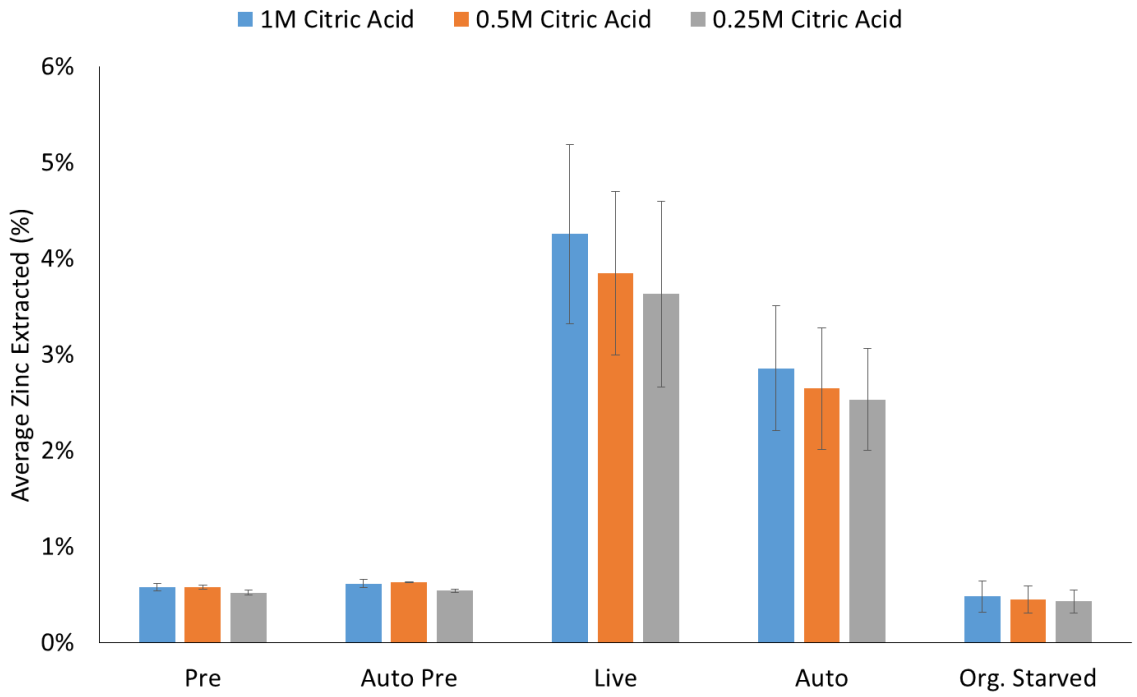

Figure 10.12 Leachability of zinc from pre- and post-experiment wastes using citric acid as a leachant

Following the trend observed in other metals, the leachability of copper with citric acid is lower than when inorganic acids were utilised (Figure 10.13). Approximately 0.3%, 0.3% and 0.4% of total copper was recovered from the pre-experiment waste with 1 M, 0.5 M and 0.25 M citric acid respectively. The similarity in results again demonstrates the ineffectiveness of citric acid as a leachant for the pre-experiment wastes as all three concentrations yielded similar and relatively minor recoveries of copper from the waste. Copper leachability in the "Live" column samples has increased to 3.4%, 2.5% and 1.7% with 1 M, 0.5 M and 0.25 M citric acid respectively. These extraction rates are far smaller than those achieved with inorganic acids though the recovery rate using 1 M citric acid does represent a recovery more than 12.5 times that of the pre-experiment equivilant. Variability in the results of from the "Live" columns are again large compared to the other experimental variants. In this instance it is do to leachability of copper from "Live" replicate column 2 far exceeding that of the other two replicate columns.

Leachability of copper from the post-experiment "Organic Starved" wastes has increased relative to the pre-experiment waste samples. Approximately 1.1% of copper was extracted with each of the concentrations of citric acid utilised. This similarity in leachability across concentrations matches the trend seen in the pre-experiment samples.

Autoclaving of the pre-experiment wastes has resulted in a slight increase in leachability of copper with citric acid. Leachability has increased to 0.6%, 0.6% and 0.5% with 1 M, 0.5 M and 0.25 M citric acid respectively. These increases are marginal and of no significant consequence with regards to extracting viable amounts of copper and, again, follow the trend of similar leachability rates despite increasing leachant concentration. Stimulation of bioreduction via the introduction of glycerol to the waste has caused an increase in the leachability of copper. Approximately 3.2%, 2.6% and 1.5% of total copper was recovered using 1 M, 0.5 M and 0.25 M citric acid respectively. These recovery rates are commensurate with the "Live" column results though variability in the data is much smaller than observed in the data from the "Live" columns.

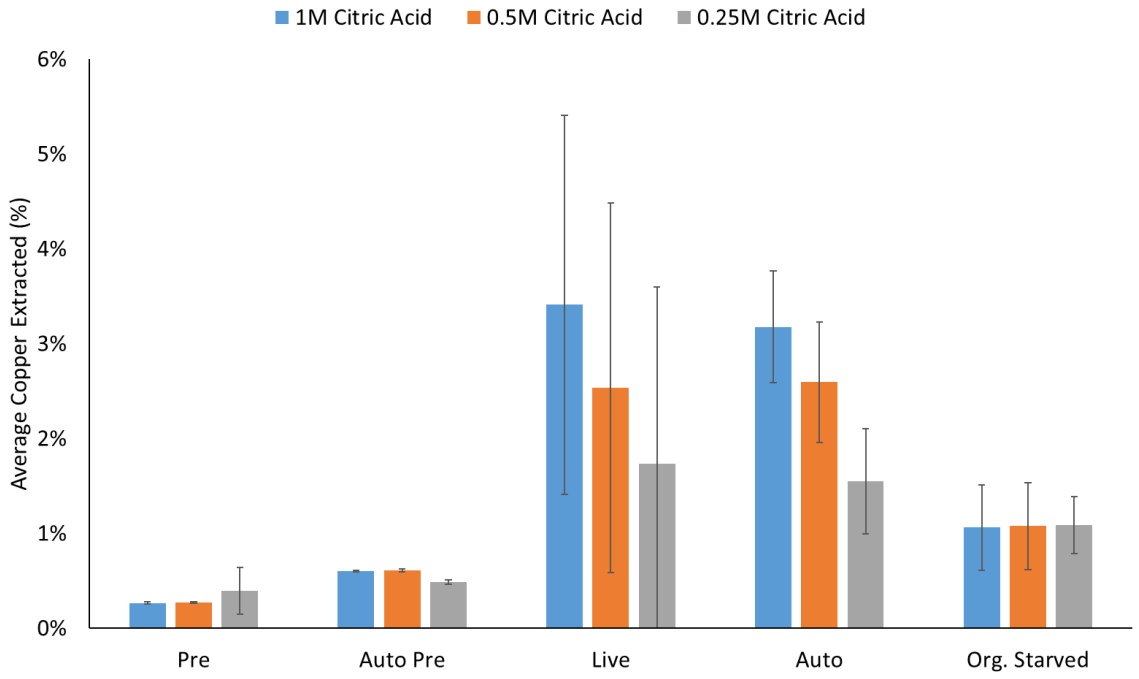

Figure 10.13 Leachability of copper from pre- and post-experiment wastes using citric acid as a leachant

As with the other metals analysed, leachability of lead within the pre-experiment samples is minimal (Figure 10.14). Leaching of the pre-experiment wastes with 1 M, 0.5 M and 0.25 M citric acid yielded lead recoveries of 0.6%, 0.4% and 0.4% respectively. Introduction of glycerol, and subsequent bioreduction, has caused the leachability of lead in the "Live" column wastes to increase substantially. Approximately, 15.5%, 14.1% and 9.1% of lead was recovered from the "Live" column samples using 1 M, 0.5 M and 0.25 M citric acid respectively. These recovery rates are similar to the recovery rates of lead from the pre-experiment autoclaved wastes with HCl used as a leachant, while less than half the rates from "Live" samples with HCl. This highlights the limitation of the weaker citric acid compared to a stronger inorganic acid such as HCl. Despite the lower leachability compared with the HCl leaches, the 0.5 M extraction represents an increase of more than 33.5 times that of the pre-experiment equivalent. This is the largest increase in leachability observed throughout experimentation. This also correlates with the sequential extraction data, observations of column effluents and the HCl leaches as lead has been the most mobile of the metals analysed, redistributing to more reactive phases.

The “Organic Starved” samples again show a minor, near insignificant increase in lead leachability relative to the pre-experiment samples. Leaching of the “Organic Starved” samples with 1 M, 0.5 M and 0.25 M citric acid recovered 1.0%, 0.8% and 0.7% respectively. This increase is much less than that observed in the HCl leaching.

Autoclaving of the pre-experiment waste has resulted in an increase in the leachability of lead by citric acid. This increase, whilst still relatively minor, is greater than that observed in the post-experiment “Organic Starved” samples. Approximately 1.8%, 1.4% and 0.9% of total lead was recovered from the pre-experiment autoclaved samples using 1 M, 0.5 M and 0.25 M citric acid respectively as leachants. Glycerol addition, and the resulting bioreduction, has resulted in an increase in lead leachability in the “Autoclaved” wastes. Approximately 11.6%, 11.2% and 8.9% of total lead was recovered from the post-experiment “Autoclaved” samples.

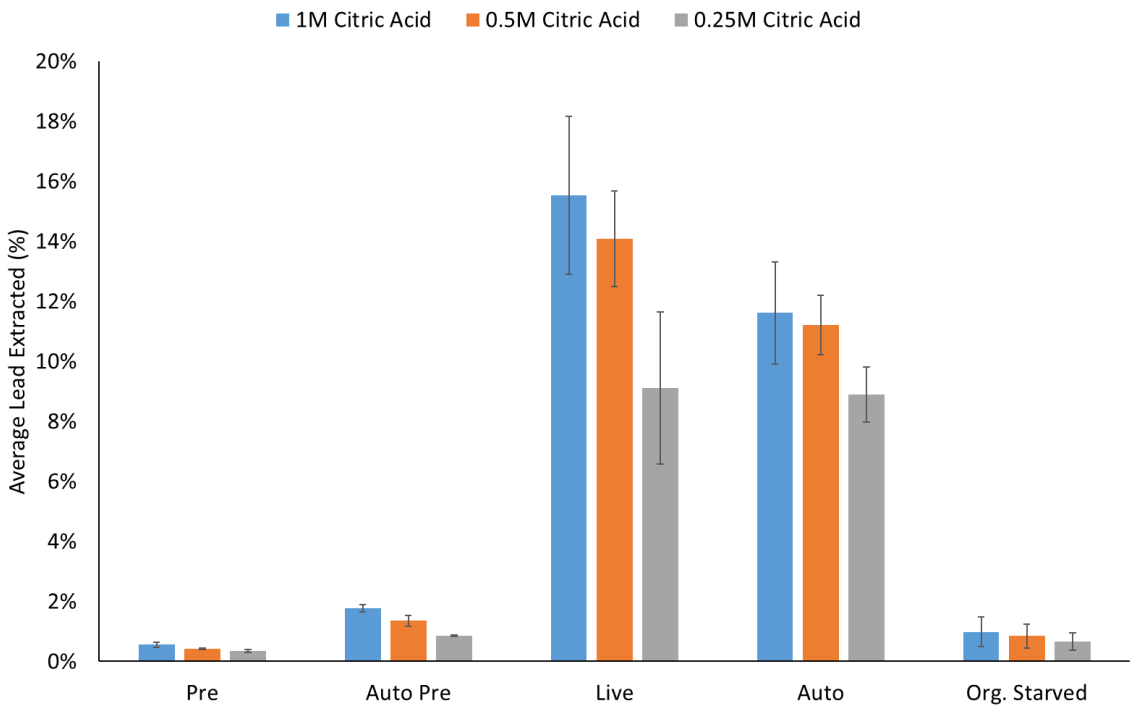

Figure 10.14 Leachability of lead from pre- and post-experiment wastes using citric acid as a leachant

Table 10.3 Leachability of elements analysed, as a percentage of total in waste, from pre- and post-experiment waste by citric acid

		Fe	Zn	Cu	Al	Pb	As	S
Pre	1 M	0.5%	0.6%	0.3%	0.1%	0.6%	1.0%	1.7%
	0.5 M	0.4%	0.6%	0.3%	0.1%	0.4%	0.7%	2.3%
	0.25 M	0.4%	0.5%	0.4%	0.1%	0.4%	0.5%	2.7%
Auto Pre	1 M	1.0%	0.6%	0.6%	0.1%	1.8%	1.6%	2.8%
	0.5 M	1.0%	0.6%	0.6%	0.1%	1.4%	1.0%	3.5%
	0.25 M	0.8%	0.5%	0.5%	0.1%	0.9%	0.6%	4.2%
Live 1	1 M	4.2%	4.4%	2.0%	1.0%	17.2%	1.0%	2.8%
	0.5 M	4.6%	4.5%	1.5%	1.1%	15.9%	0.7%	3.5%
	0.25 M	2.3%	3.6%	0.9%	1.0%	6.9%	0.3%	1.2%
Live 2	1 M	2.2%	3.3%	5.7%	0.4%	16.9%	3.6%	1.3%
	0.5 M	2.2%	2.9%	4.8%	0.4%	13.4%	2.1%	1.1%
	0.25 M	2.1%	2.7%	3.9%	0.4%	11.9%	1.6%	3.5%
Live 3	1 M	4.7%	5.1%	2.5%	1.3%	12.5%	1.0%	2.5%
	0.5 M	4.3%	4.1%	1.3%	1.3%	13.0%	0.7%	2.8%
	0.25 M	4.5%	4.6%	0.5%	1.3%	8.6%	0.5%	5.1%
Auto 1	1 M	2.5%	3.1%	3.9%	1.0%	13.5%	0.5%	2.8%
	0.5 M	2.4%	2.7%	3.3%	1.0%	11.9%	0.4%	3.2%
	0.25 M	2.5%	2.5%	2.0%	1.0%	8.8%	0.4%	5.3%
Auto 2	1 M	2.9%	3.4%	2.8%	0.8%	11.0%	0.7%	2.0%
	0.5 M	3.3%	3.3%	2.0%	1.0%	11.7%	0.8%	2.3%
	0.25 M	3.3%	3.1%	0.9%	0.9%	9.8%	0.6%	4.4%
Auto 3	1 M	2.2%	2.1%	2.9%	0.6%	10.3%	0.5%	3.0%
	0.5 M	2.1%	2.0%	2.5%	0.6%	10.1%	0.7%	3.1%
	0.25 M	2.2%	2.0%	1.7%	0.6%	8.0%	0.8%	5.9%
Org. Starved 1	1 M	0.3%	0.3%	0.5%	0.2%	0.5%	0.6%	1.6%
	0.5 M	0.3%	0.3%	0.6%	0.2%	0.6%	0.2%	2.0%
	0.25 M	0.2%	0.3%	0.7%	0.1%	0.4%	0.3%	2.8%
Org. Starved 2	1 M	0.4%	0.5%	1.3%	0.3%	0.9%	0.1%	1.8%
	0.5 M	0.3%	0.5%	1.2%	0.3%	0.7%	0.1%	1.3%
	0.25 M	0.3%	0.5%	1.3%	0.3%	0.6%	0.2%	2.0%
Org. Starved 3	1 M	0.4%	0.6%	1.4%	0.4%	1.5%	0.1%	1.4%
	0.5 M	0.4%	0.6%	1.5%	0.4%	1.3%	0.2%	1.6%
	0.25 M	0.3%	0.5%	1.3%	0.3%	1.0%	0.2%	2.3%

10.4.4. EDTA Leaching

Leaching of iron from the experimental wastes with the chelator, EDTA, has yielded results similar in pattern, but substantially lower in magnitude, to the acid leaching experiments (Figure 10.15). Approximately 0.4%, 0.2% and 0.2% of iron was recovered from the pre-experiment wastes with 10 mM, 5 mM and 2.5 mM EDTA respectively. This is substantially lower than the rates achieved with inorganic acid and roughly commensurate with the rate achieved with citric acid, another chelating agent. Leachability of iron increased in the post-experiment "Live" samples as a result of bioreduction. 1.4%, 1.0% and 0.9% of iron was recovered from the "Live" column wastes with 10 mM, 5 mM and 2.5 mM EDTA respectively. Whilst this does represent an increase in leachability of iron, it is also substantially lower than when acid was used as a leachant. In contrast to what was observed in the acid leaching experiments, the leachability of iron in the post-experiment "Organic Starved" wastes has marginally increased, though this increase is relatively insignificant. Iron leachability has increased to 0.5%, 0.5% and 0.4% with 10 mM, 5 mM and 2.5 mM EDTA.

Autoclaving of the pre-experiment waste has caused iron leachability to marginally increase to 0.6%, 0.6% and 0.4% with 10 mM, 5 mM and 2.5 mM EDTA respectively. This correlates with the observations of the acid leaching experiments. As with the "Live" column samples, bioreduction has increased the leachability of iron in the "Autoclaved" column samples. 1.1%, 0.9%, and 0.9% of total iron was recovered from the "Autoclaved" column samples by 10 mM, 5 mM and 2.5 mM EDTA respectively. Whilst this may be due to bioreduction increasing the proportion of iron within more readily leachable minerals, such as green rusts, the increasing pH induced by bioreduction may also be partly responsible. The EDTA solution is buffered to pH 8 to dissolve the EDTA and provide the ideal conditions for the stability of metal complexes (Figure 10.2). The pre-experiment wastes and "Organic Starved" wastes are acidic and will thereby neutralise the leachant limiting the effectiveness of the EDTA. The "Live" and "Autoclaved" column samples, by contrast, have become circum-neutral due to bioreduction meaning the neutralisation effect will be much less significant facilitating greater extraction of iron by the EDTA leachant.

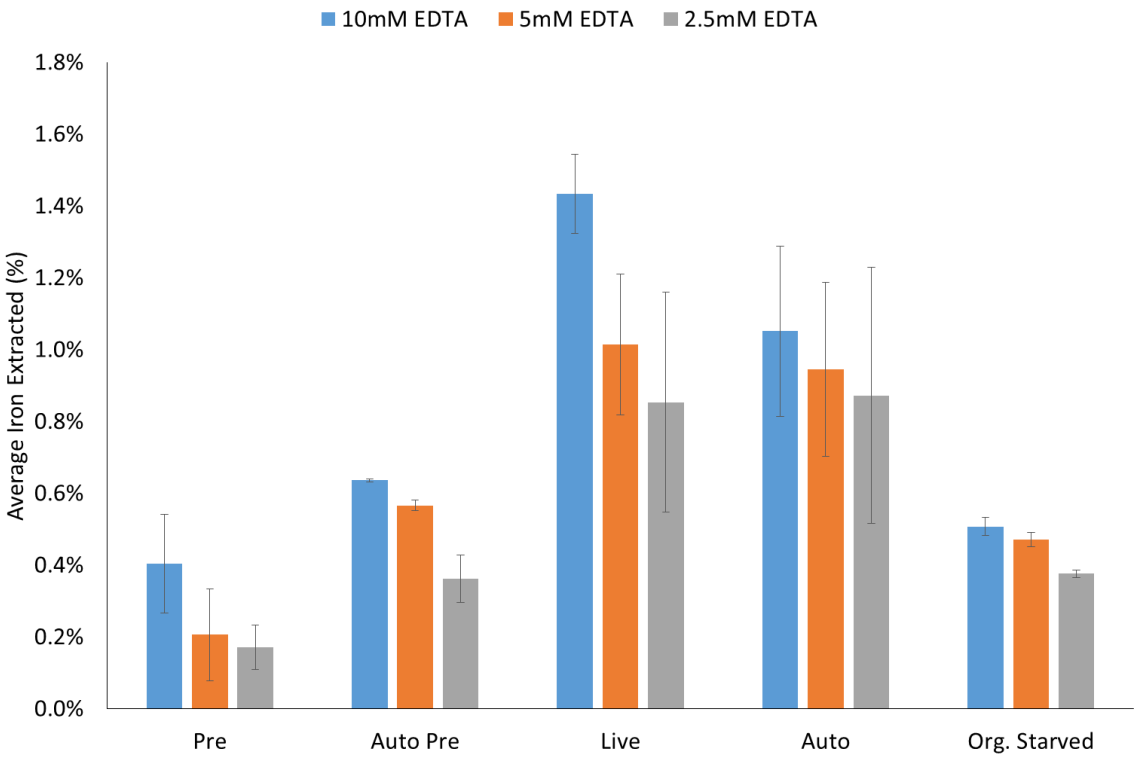

Figure 10.15 Leachability of iron from pre- and post-experiment wastes using EDTA as a leachant

As with iron, the leachability of zinc from pre-experiment wastes with EDTA closely correlate with the results of leaching with citric acid, another chelator (Figure 10.16). Approximately, 0.6%, 0.4% and 0.5% of total zinc was recovered from the pre-experiment wastes with 10 mM, 5 mM and 2.5 mM EDTA respectively. Zinc leachability has increased as a result of bioreduction with 3.9%, 2.4% and 2.3% of total zinc recovered from the "Live" column samples using with 10 mM, 5 mM and 2.5 mM EDTA respectively. It is notable that while the 10 mM leach has yielded a higher recovery of zinc the data also has much greater variability compared with either the other "Live" samples or other experimental variants. This high variation in this reading is due to a singular replicate returning a substantially higher zinc concentration (this was verified by repeating analysis). If this anomalous datum is excluded then the average zinc extracted by 10 mM EDTA from the "Live" columns is approximately 2.6%, similar to the results from the 5 mM and 2.5 mM EDTA leaches.

Zinc leachability has marginally increased in the "Organic Starved" column samples relative to the pre-experiment equivalents. 0.8%, 0.9% and 0.7% of total zinc was recovered from the post-experiment "Organic Starved" wastes with 10 mM, 5 mM and

2.5 mM EDTA respectively. As with the increases observed in these wastes from acid leaching, the increase in near insignificant but adds to the consistency of increased metal leachability in these columns.

Autoclaving appears to have had only a minimal impact of the leachability of zinc by EDTA. Leachability of zinc has increased to 0.7%, 0.6% and 0.6% with 10 mM, 5 mM and 2.5 mM EDTA respectively due to the autoclaving process. This increase is minor and likely insignificant with regards to extracting economic quantities of zinc from the waste. Bioreduction of the waste has increased the leachability of zinc slightly. Approximately, 1.8% of total zinc was extracted by all 3 concentrations of EDTA utilised. The similarity in the results despite varying leachant concentration bears similarity to the "Live" column samples (if the erroneous data is excluded). The relatively small increase in zinc leachability and the consistency in the data despite the increasing iron leachability at higher concentrations may suggest that the mobilised zinc within the bioreduced wastes has partitioned into non-iron bearing phases such as hydroxides, thereby limiting the leachability by EDTA compared with iron compounds. It is also possible that zinc is being outcompeted for EDTA binding sites by other ions in solution. Alternately, the increase in zinc leachability and consistency of the data may be due to the increased complex stability afforded by the circum-neutral wastes not buffering the pH 8 EDTA to the same extent as the non-bioreduced samples.

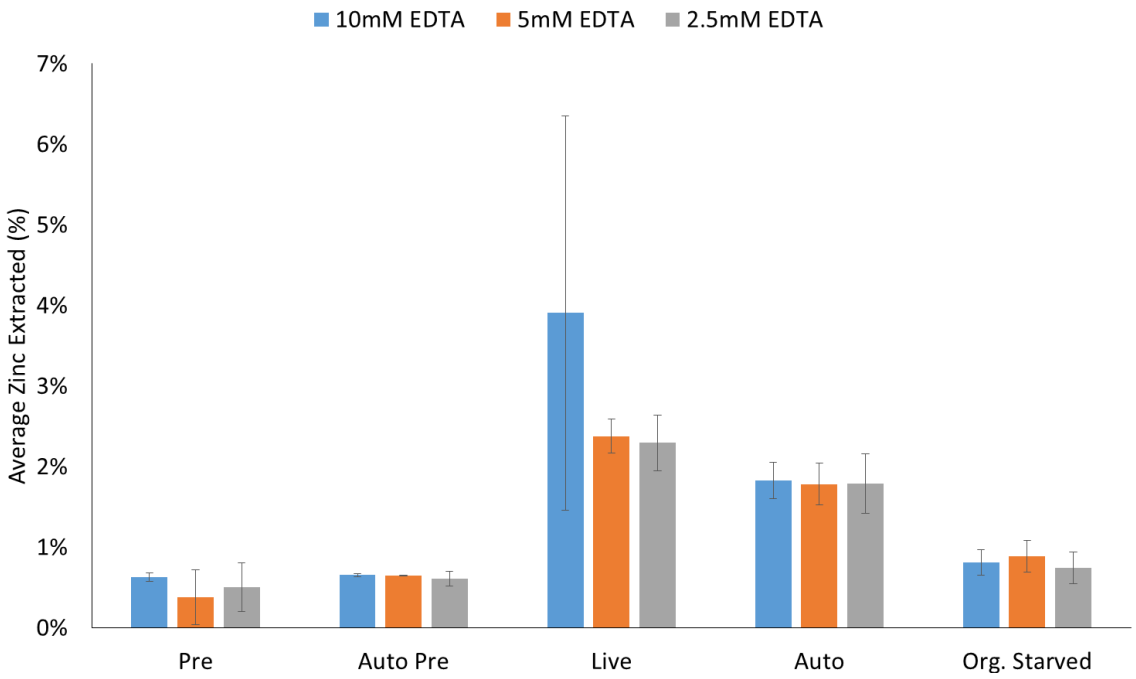

Figure 10.16 Leachability of zinc from pre- and post-experiment wastes using EDTA as a leachant

Leachability of copper from the pre-experiment waste with EDTA is similar to the leachability when citric acid is used as a leachant (Figure 10.17). Approximately, 0.4%, 0.5% and 0.5% of total copper was recovered from the pre-experiment wastes with 10 mM, 5 mM and 2.5 mM EDTA respectively. These low recovery rates also correlate with the low recoveries of iron and zinc from the pre-experiment wastes. Bioreduction in the waste has resulted in increased copper leachability in the post-experiment "Live" samples. Approximately, 6.2%, 4.9% and 4.1% of total zinc was recovered from the "Live" column samples with 10 mM, 5 mM and 2.5 mM EDTA respectively. These recovery rates of copper from the "Live" samples are higher than those achieved with citric acid as a leachant, a trend not observed with iron or zinc. Furthermore, despite uncertainty due to variation in the data, there appears to be a correlation between the amount of copper recovered and the concentration of EDTA as was observed for iron leachability but not zinc. The correlation in recovery trends between copper and iron could suggest that the recovered copper has been associated with iron within the waste as opposed to other mineral phases, such as copper hydroxides and carbonates.

Leachability of copper with EDTA has increased in the post-experiment "Organic Starved" samples relative to the pre-experiment equivalents. This is consistent with observations when acids were used as leachants. Recovery rates of 1.4%, 1.5% and 1.2% total copper were achieved using 10 mM, 5 mM and 2.5 mM EDTA respectively. These are only marginally higher than those obtained with citric acid leaching of the waste. As with citric acid leaching the leachability of copper from the "Organic Starved" wastes did not respond to increasing concentrations of leachant, contrasting the trend in the post-experiment wastes.

Autoclaving of the pre-experiment wastes has again proven to increase the leachability of copper by a very small amount. Recovery of copper from the autoclaved pre-experiment waste was 0.6%, 0.6% and 0.7% with 10 mM, 5 mM and 2.5 mM EDTA respectively, again showing minimal differences in leachability despite varying leachant concentrations. Leachability of copper by EDTA has increased in the post-experiment "Autoclaved" columns as a result of glycerol addition and subsequent iron reduction. Approximately, 5.2%, 4.9% and 4.1% of total copper was recovered from the post-experiment "Autoclaved" column samples with 10 mM, 5 mM and 2.5 mM EDTA respectively. Whilst the 10 mM leaching yielded less copper that the "Live" column

equivalent, the 5 mM and 2.5 mM leaches yielded similar copper leachabilities in the "Autoclaved" and "Live" columns. As with the "Live" samples, the leachability of copper shows a positive correlation with increasing leachant concentration. Variability was lower than observed in the "Live" samples.

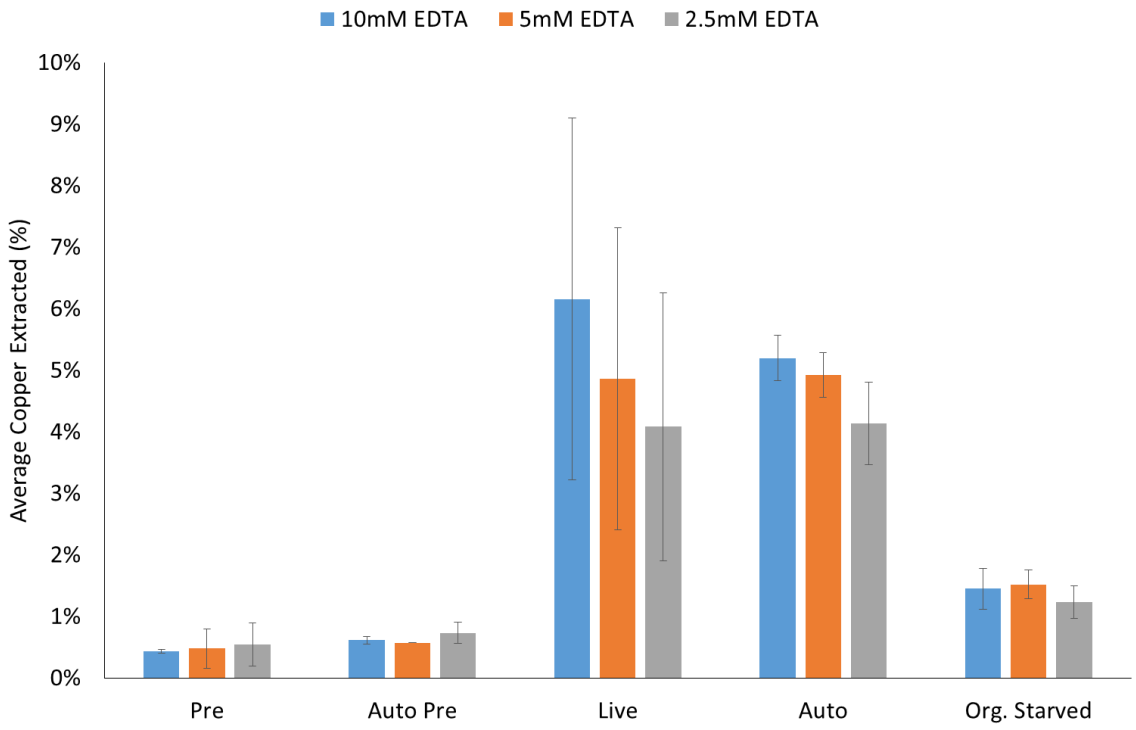

Figure 10.17 Leachability of copper from pre- and post-experiment wastes using EDTA as a leachant

Leaching of the pre-experiment wastes with EDTA has yielded the highest recovery of lead from all leaching experiments performed on the pre-experiment wastes (Figure 10.18). Approximately, 12.6%, 5.0% and 2.1% of total lead was leached from the pre-experiment wastes with 10 mM, 5 mM and 2.5 mM EDTA respectively. These are higher than the respective recoveries from the HCl, H_2SO_4 and citric acid equivalents. The 10 mM EDTA leachant recovery of lead from the pre-experiment waste is only slightly less than the recovery achieved by 1 M citric acid leaching of post-experiment "Live" waste samples.

Bioreduction of the waste, via the introduction of glycerol, has caused an increase in the leachability of lead by EDTA. Approximately, 18.9%, 24.9% and 20.7% of total lead was recovered from the "Live" column samples by 10 mM, 5 mM and 2.5 mM EDTA respectively. The results of the latter two concentrations has much larger variability than the 10mM leach data. No correlation between lead leachability and EDTA concentration

is observable, though the inability to identify any trend in the data may be a result of the variability in the data.

Lead in the post-experiment “Organic Starved” samples show reduced leachability by EDTA relative to the pre-experiment sample, suggesting there has been an alteration in the waste despite no significant bioreduction having occurred. This is the opposite of what was observed in the HCl and citric acid leaches. Approximately, 4.5%, 5.5% and 3.7% of total lead was recovered from the “Organic Starved” column samples by 10 mM, 5 mM and 2.5 mM EDTA respectively. The results do not show any correlation between lead leachability and leachant concentration further suggesting there has been some alteration of the waste despite no bioreduction having occurred.

Autoclaving of the pre-experiment waste has resulted in a reduction in lead leachability by both 10 mM and 5 mM EDTA. This contrasts with leachability, by EDTA, of the other metals analysed and the leachability of all metals with acids. Only the 2.5 mM EDTA leach from the autoclaved pre-experiment waste returned a higher lead recovery than the non-autoclaved equivalent. Approximately, 7.4%, 3.2% and 4.2% of total lead was recovered from the autoclaved pre-experiment column samples by 10 mM, 5 mM and 2.5 mM EDTA respectively. Despite the reduction in leachability, these still represent greater recoveries than were achieved from by acid leaching. Glycerol addition and bioreduction of the waste has increased the leachability of lead by EDTA in the post-experiment “Autoclaved” column wastes. Approximately, 17.3%, 17.6% and 14.2% of total lead was recovered from the autoclaved pre-experiment column samples by 10 mM, 5 mM and 2.5 mM EDTA respectively. As with other analyses, there is less variability in the leachability of lead from the “Autoclaved” columns than the “Live” column equivalents. The relative similarity in the leachability of lead across all concentrations of leachants tested contrasts to the positive correlation notable in the pre-experiment waste leaching tests. It may also suggest that, despite the variation in the “Live” column samples, there is no positive correlation in the “Live” samples either. The lack of response to increasing leachant concentrations and to the iron leaching rates is suggestive that a high proportion of lead is present in non-iron bearing phases such as lead hydroxides or carbonates.

The leachability of lead by EDTA has been much higher than other metals analysed throughout all variations of the experiment, with lead seemingly outcompeting the other metals for EDTA binding sites. This contradicts the observations of Sun *et al.* (2001) who found that zinc, copper and lead would be extracted from contaminated soils by EDTA at similar ratios in batch tests. Furthermore, in column leaching tests they identified that lead would be extracted at lower rates than copper or zinc.

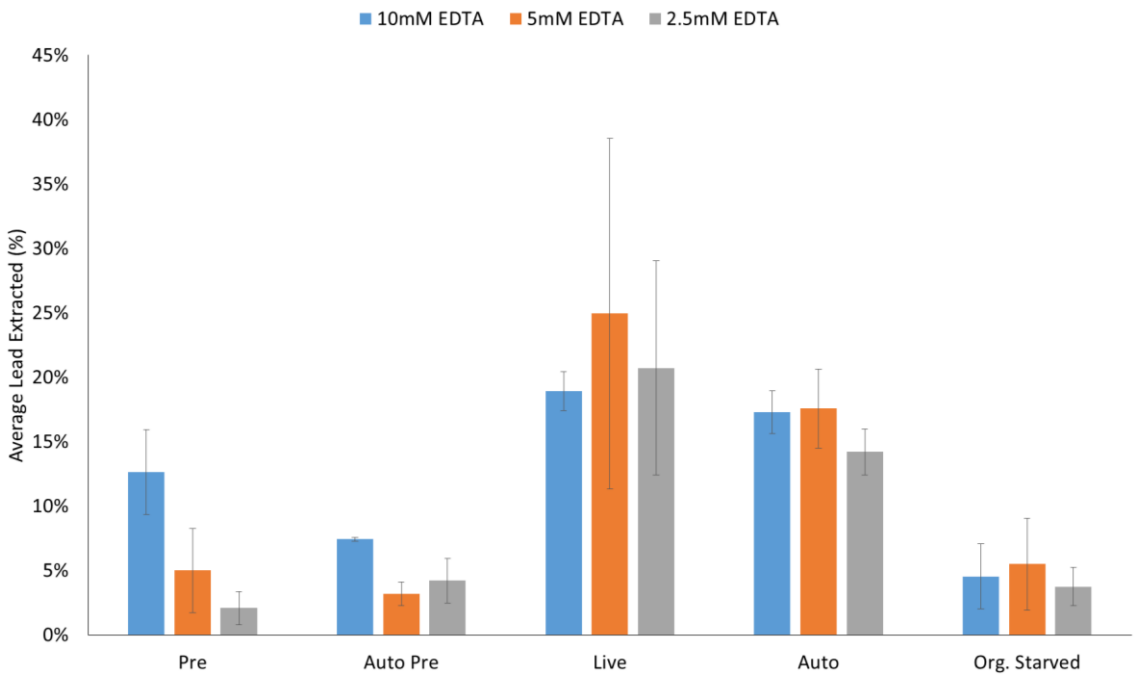

Figure 10.18 Leachability of lead from pre- and post-experiment wastes using EDTA as a leachant

Table 10.4 Leachability of elements analysed, as a percentage of total in waste, from pre- and post-experiment waste by EDTA

		Fe	Zn	Cu	Al	Pb	As	S
Pre	1 M	0.4%	0.6%	0.4%	0.1%	12.6%	1.0%	4.9%
	0.5 M	0.2%	0.4%	0.5%	0.0%	5.0%	0.9%	4.2%
	0.25 M	0.2%	0.5%	0.5%	0.0%	2.1%	1.1%	5.4%
Auto Pre	1 M	0.6%	0.7%	0.6%	0.1%	7.4%	1.8%	3.9%
	0.5 M	0.6%	0.6%	0.6%	0.0%	3.2%	1.6%	4.3%
	0.25 M	0.4%	0.6%	0.7%	0.0%	4.2%	2.0%	5.3%
Live 1	1 M	1.4%	2.3%	3.0%	0.8%	20.6%	5.0%	3.0%
	0.5 M	0.9%	2.1%	2.1%	0.7%	40.6%	4.8%	5.0%
	0.25 M	0.7%	2.0%	1.7%	0.6%	16.8%	6.5%	7.2%
Live 2	1 M	1.6%	6.7%	6.7%	1.8%	17.6%	4.9%	2.8%
	0.5 M	1.2%	2.5%	5.8%	1.9%	17.7%	5.8%	4.5%
	0.25 M	1.2%	2.7%	6.0%	2.0%	30.3%	7.7%	5.3%
Live 3	1 M	1.4%	2.7%	8.8%	0.5%	18.6%	4.1%	2.8%
	0.5 M	0.9%	2.5%	6.7%	0.5%	16.5%	4.7%	4.2%
	0.25 M	0.6%	2.2%	4.5%	0.4%	15.1%	5.5%	6.3%
Auto 1	1 M	0.8%	1.6%	5.2%	0.4%	15.6%	3.1%	2.8%
	0.5 M	0.7%	1.5%	4.5%	0.5%	14.7%	3.7%	3.4%
	0.25 M	0.6%	1.5%	3.5%	0.5%	12.2%	3.4%	3.4%
Auto 2	1 M	1.0%	1.8%	5.6%	1.1%	17.4%	3.9%	3.0%
	0.5 M	1.0%	1.9%	5.2%	1.3%	17.2%	4.7%	4.3%
	0.25 M	0.8%	1.7%	4.1%	1.3%	14.8%	4.0%	3.8%
Auto 3	1 M	1.3%	2.1%	4.8%	1.9%	18.9%	5.3%	3.5%
	0.5 M	1.2%	2.0%	5.0%	2.0%	20.8%	6.2%	5.3%
	0.25 M	1.3%	2.2%	4.8%	2.4%	15.6%	5.7%	5.5%
Org. Starved 1	1 M	0.5%	0.6%	1.1%	0.4%	2.7%	1.0%	4.1%
	0.5 M	0.5%	0.7%	1.3%	0.4%	3.3%	1.2%	4.7%
	0.25 M	0.4%	0.5%	0.9%	0.2%	3.3%	1.0%	4.1%
Org. Starved 2	1 M	0.5%	0.9%	1.8%	0.4%	7.4%	1.4%	3.1%
	0.5 M	0.5%	1.0%	1.6%	0.4%	3.6%	1.8%	3.5%
	0.25 M	0.4%	0.8%	1.4%	0.3%	2.5%	1.1%	3.2%
Org. Starved 3	1 M	0.5%	0.9%	1.5%	0.4%	3.4%	1.5%	3.5%
	0.5 M	0.5%	1.0%	1.7%	0.4%	9.6%	1.9%	3.5%
	0.25 M	0.4%	0.9%	1.4%	0.4%	5.4%	1.2%	3.3%

10.4.5. Impact of Glycerol on Leachability

Addition of glycerol to the waste has been proven to induce iron-bioreduction, and potentially sulphur-bioreduction, in the wastes. This bioreduction has also been proven to increase the leachability of elements of interest in the waste when inorganic acids, organic acids and chelating agents are used. As can be seen in Figure 10.19, the presence of glycerol during leaching on waste that has not undergone bioreduction has had a negligible impact on the leachability of metals from the wastes. The leachability of metals of interest from the pre-experiment wastes show no indication of consistent increase in leachability, relative to the glycerol free pre-experiment waste. This is true of all leachants utilized. Given the much higher concentration of glycerol used in these leaching tests, and the lack of substantial alteration to the results, it is unlikely that any residual glycerol in the post-experiment waste would cause any significant effect on metal leachability. From this result, it can be asserted that the observed increased in metal leachability in post-experiment bioreduced wastes is a consequence of the bioreduction, as opposed to an enhancement effect from residual glycerol.

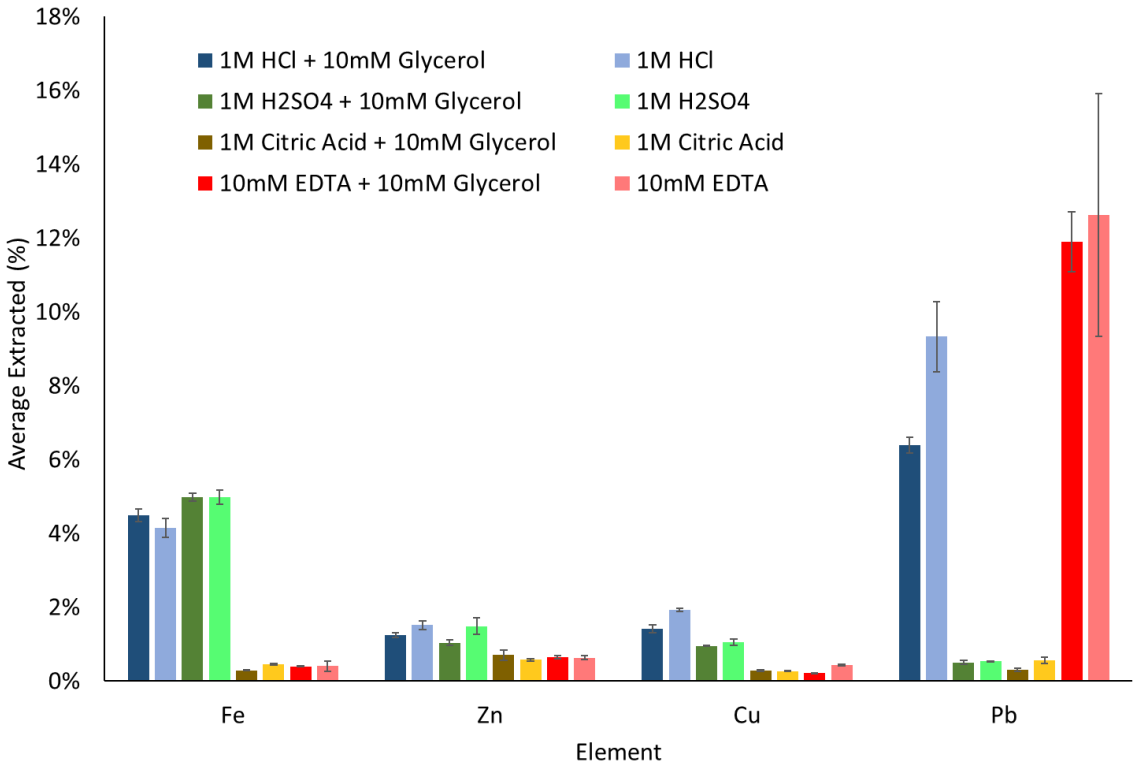

Figure 10.19 Leachability of iron, zinc, copper and lead from pre-experiment wastes with a variety of leachants and 10 mM of glycerol

10.4.6. Leachability Correlations

10.4.6.1. Pre-experiment

As shown in Figure 10.20a, when HCl was used as a leachant, there is a close association between iron and sulphur in both the autoclaved and non-autoclaved pre-experiment wastes. The correlation between these elements is demonstrated by an average R^2 value of 0.99. This correlates with the results of the XRD analysis which identified jarosite as the dominant iron bearing phases in the waste and has been previously identified in Parys Mt. wastes (Jenkins *et al.*, 2000). However, when citric acid is used as a leachant the same correlation is not observed. Instead citric acid shows limited increases in iron recovery with increasing sulphur leachability and an average R^2 value of 0.38, highlighting the lack of correlation. This is unexpected given citrate is known to complex iron. It also suggests that citric acid is not targeting jarosite within the waste unlike HCl.

Figure 10.20b displays a positive correlation between the mass of iron and lead extracted from pre-experimental wastes with an average R^2 value of 0.93. Furthermore Figure 10.21c demonstrates a positive correlation between lead and sulphur where HCl is used as the leachant. The strong correlations between iron and lead and sulphur and lead are suggestive that lead is associated with iron bearing minerals such as iron oxyhydroxides and iron oxyhydroxysulphates such as schwertmannite or jarosite, which was identified by XRD. While differentiating between the oxyhydroxide and oxyhydroxysulphate phases in not possible, (Webster *et al.*, 1998) noted that lead tended to adsorb onto 2-line ferrihydrite to a greater extent that to ferric oxyhydroxysulphates suggesting that the distribution of lead through the waste may be more complex than being described simply by association with jarosite. Figure 10.20c shows that, despite much lower leachability of zinc, there is a correlation between iron and zinc. At higher iron and zinc concentrations the correlation becomes weaker and more variable. When HCl is used as a leachant there is also a correlation between zinc and sulphur, though again citric acid leaching does not generate this correlation (Figure 10.21a). This suggests that zinc, as with lead, is associated with jarosite and iron oxyhydroxides in the pre-experiment wastes.

The relationship between copper and iron is more complex and variable dependent on the leachant utilised. Where H_2SO_4 was used as a leachant there is a clear correlation

between iron and copper, described by a R^2 values of 0.89 and 0.98 for non-autoclaved and autoclaved pre-experiment waste respectively. When HCl was used as the leachant a similarly strong correlation was observed (R^2= 0.97 for both non-autoclaved and autoclaved waste) but with a much shallower gradient representing a higher recovery of copper for a given iron recovery compared with H_2SO_4 leaching. Copper also shows a correlation to sulphur when HCl is used. Though due to the lack of H_2SO_4 leaching data for sulphur it is unknown whether the variation resulting from leachant type is present. The relationship between copper and sulphur, along with the more complex relationship with iron, suggests that a large proportion of the copper is associated with ferric oxyhydroxysulphates such as jarosite. Webster *et al.* (1998) observed that copper and zinc would preferentially sorb to ferric oxyhydroxysulphates rather than oxyhydroxides in natural AMD. This suggests that copper and zinc are likely primarily associated with jarosite in the waste and to a lesser extent the iron oxyhydroxide fractions in the waste. Citric acid fails to demonstrate any relationship between copper and sulphur in the pre-experiment waste (Figure 10.21b).

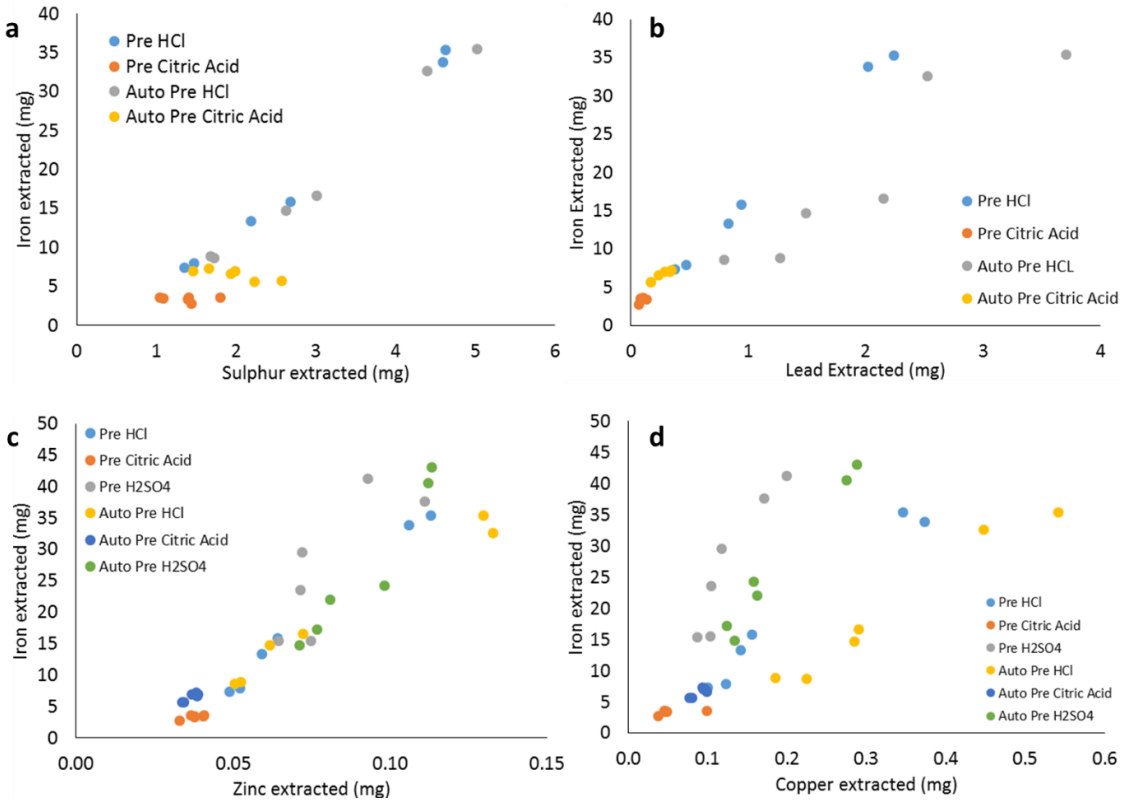

Figure 10.20 Relationship between iron and a) sulphur, b) lead, c) zinc and d) copper in leaching solutions from pre-experiment Parys Mt. 2 waste. Results of 1 M, 0.5 M and 0.25 M leaching with each extractant displayed.

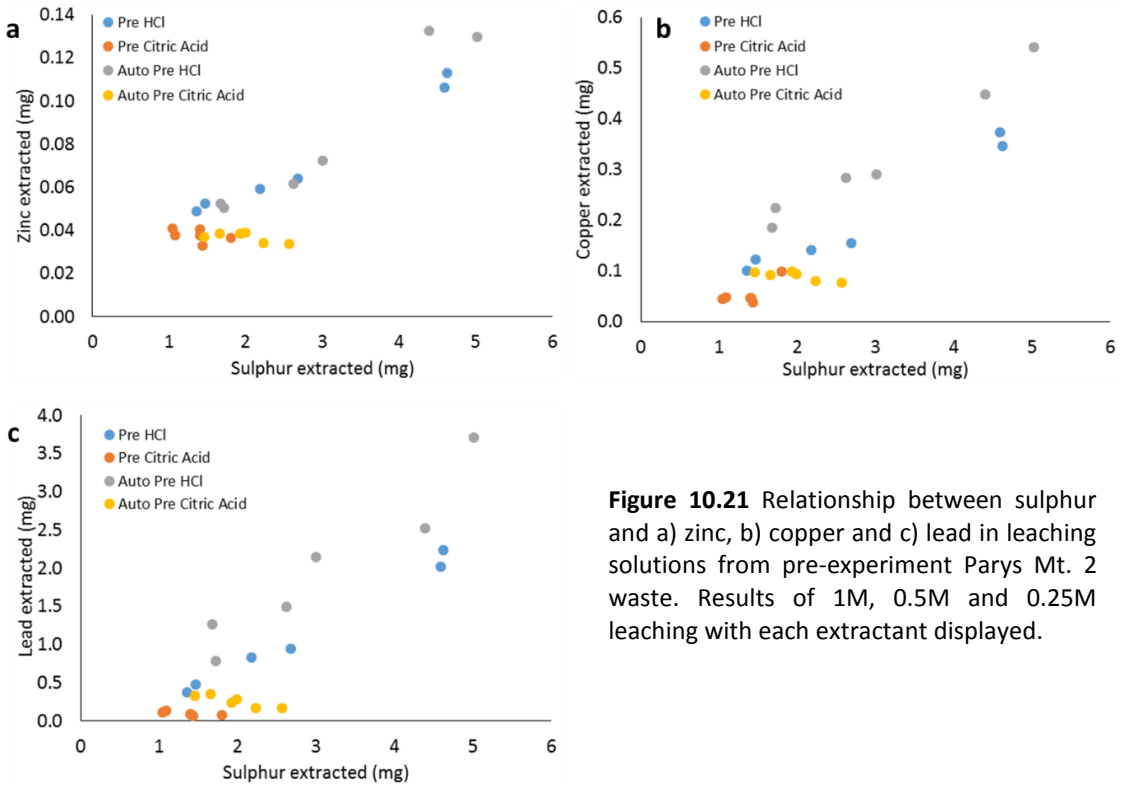

Figure 10.21 Relationship between sulphur and a) zinc, b) copper and c) lead in leaching solutions from pre-experiment Parys Mt. 2 waste. Results of 1M, 0.5M and 0.25M leaching with each extractant displayed.

10.4.6.2. Live Samples

While there were strong positive correlations between iron, sulphur and the metals of interest in the pre-experiment wastes, the same is not true of the post-experiment "Live" column samples (Figure 10.20 & Figure 10.21).

In the pre-experiment samples there was a positive correlation between iron and sulphur which was interpreted as suggesting the presence of jarosite, which supported mineral identification by XRD. In the post-experiment "Live" samples there is no clear correlation between iron and sulphur (Figure 10.22a). Most of the leachants from the "Live" column samples have extracted <1 Mg of sulphur, far less than in the pre-experiment samples but have extracted far more iron than the pre-experiment equivalents. The abundance of samples with high iron concentrations but near negligible sulphur is suggestive that non-sulphurous iron-bearing minerals, such as iron oxyhydroxides and non-sulphurous green rusts, have become more dominant in the waste. While there are some samples with higher sulphur content suggesting the survival of some sulphurous iron-bearing minerals, the lack of clear correlation between iron and sulphur agrees with the results of XRD analysis which suggested that jarosite

has been the primary target of bioreduction and has been depleted in the post-experiment “Live” waste. This lack of correlation also may also indicate the lack of acid soluble iron sulphides, formed due to sulphate-reduction, and sulphate green rusts. Alternatively, it may be a result of abundant non-sulphurous acid soluble iron bearing minerals. Despite the change in relationship between iron and sulphur, and inferred change in mineralogy, the leachability of iron in the waste has not increased substantially. This correlates with the observations of iron partitioning from previous sequential extraction work.

The initial correlation of lead with iron can still be discerned in the “Live” samples, despite greater quantities of both metals being extracted, albeit not as strongly as before with a reduced R^2 value of 0.54 describing the greater variation in the samples (Figure 10.22b). The correlation between lead and sulphur, however, has not been retained in the post-experiment “Live” wastes (Figure 10.23c). Leaching with HCl has extracted higher quantities of lead with relatively low sulphur. Citric acid leaching has not yielded the same extent of lead recovery but has extracted higher amounts of sulphur compared with the HCl leaches. The ratio of lead to sulphur has also increased in the waste with approximately 3mg of lead extracted for every 1 Mg of sulphur in the “Live” samples whilst this amount of sulphur related to <0.2mg lead extracted in the pre-experiment waste. This, in itself, does not suggest any relationship between lead and sulphur but does highlight the increase in lead leachability. The citric acid leach samples broadly cluster in two groups which may suggest a slight positive correlation and either remnant jarosite, lead sulphates unaffected by bioreduction (e.g. anglesite) or lead sulphides due to reaction with biogenic hydrogen sulphide. Despite this the lack of clear and consistent correlation between lead and sulphur and the apparent positive correlation of lead with iron is suggestive that as a result of bioreduction lead has redistributed from ferric oxyhydroxysulphates like jarosite to either iron oxyhydroxides, lead hydroxides or lead carbonates. The presence of the latter two cannot be determined from leaching data and were not identified by the XRD analysis. However, the sequential extraction analysis of “Live” column samples suggested an increase of lead within the “carbonate- associated” phase which would also likely remove hydroxides. These observations allow for the potential presence of all 3 mineral phases, but, given the lack of identification in XRD the abundance of lead hydroxides and

carbonates (if present) is minor compared to the iron oxyhydroxide goethite. This suggests that the majority of recoverable lead is associated more closely with iron oxyhydroxides such as goethite.

The positive correlation between iron and zinc in the pre-experiment wastes remains in the post-experiment "Live" samples (Figure 10.22c). The R^2 values describe a reduced correlation between the two metals decreasing from 0.88 to 0.63. Despite this there is a clear relationship between the two metals suggesting that zinc has remained associated with iron minerals throughout experimentation. As with lead, zinc shows no clear correlation with sulphur in the "Live" column samples contrasting the positive correlation shown by HCl leaching in the pre-experiment waste (Figure 10.23a). Again, mirroring the observations of lead/sulphur correlations, the majority of samples have recovered <1 Mg of sulphur but lead recovery ranges from ~0.08 to ~0.22mg. The correlation of zinc with iron, and lack of correlation with sulphur is, again, indicative of the removal of oxyhydroxysulphates like jarosite. It also suggests at the redistribution of zinc to either zinc hydroxides, carbonates, adsorption to residual iron oxyhydroxides or co-precipitation with secondary iron oxyhydroxides. The results of previous sequential extraction work suggests that zinc carbonates are not likely present, and given their similar reactivity, hydroxides are also unlikely to be dominant leaving adsorption and/or co-precipitation to iron oxyhydroxides the likely mechanism for the removal of zinc from solution and cause of the iron/zinc correlation. This redistribution effect has seemingly only affected a relatively minor proportion of the zinc with most of the zinc in the waste (>90%) remaining resistant to leaching with dilute acids.

The correlation of copper to iron was identifiable in the pre-experiment waste but is variable depending on the leachant utilised. In the post-experiment "Live" column samples the leachant-dependant variability is again evident (Figure 10.22d). Citric acid leaching has returned low copper contents and so obvious correlation with iron. H_2SO_4 and HCl, however, do show indications of a possible correlation. HCl leached samples generally recovered a greater mass of copper per mg of iron relative to H_2SO4. The R^2 values for H_2SO_4 and HCl leaches are inconclusive with regards to the potential of a correlation with values of 0.54 and 0.63 respectively. Unlike the pre-experiment wastes, the leaching of post-experiment "Live" column samples show no correlation between copper and sulphur (Figure 10.23b). Citric acid leaches having low copper recovery but

higher sulphur while HCl yielding better copper recovery but low sulphur. These trends suggest that, as with lead and zinc, the recoverable copper in the system has transitioned from jarosites and other ferric oxyhydroxysulphates to iron oxyhydroxides, copper hydroxides or copper carbonates. The hydroxides and carbonates have not been identified in the XRD and the “carbonate- associated” phase is relatively minor within the sequential extraction work previously performed. This leads to the conclusion that copper is likely more associated with iron oxyhydroxides than copper hydroxides or carbonates.

Given the inference that the metals of interest (Zn, Pb & Cu) have been solubilised from bio-reduced jarosite and redistributed to iron oxyhydroxides, coupled with the more substantial increase in leachability of these metals compared to iron, would suggest that most of the metals associated with iron had adsorbed as opposed to co-precipitated. This can be asserted as any co-precipitated or occluded metal within an iron oxyhydroxide would require the dissolution of said oxyhydroxide to become solubilised itself. Adsorbed metal cations by contrast would only require solubilisation from the surface of the oxyhydroxide explaining the sharp increase in leachability of the metals of interest. It should also be noted, however, that the limited increase in iron leachability is also likely a result of the wastes higher iron content.

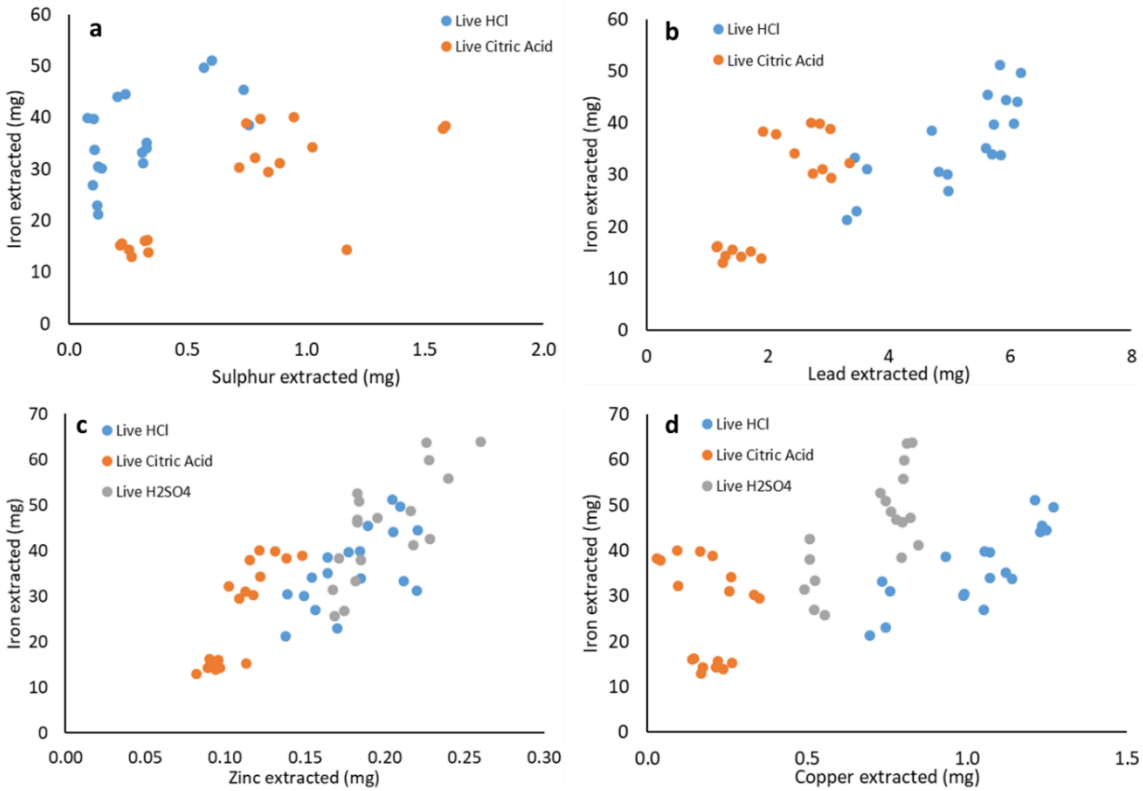

Figure 10.22 Relationship between iron and a) sulphur, b) lead, c) zinc and d) copper in leaching solutions from post-experiment "Live" column samples. Results of 1 M, 0.5 M and 0.25 M leaching with each extractant displayed.

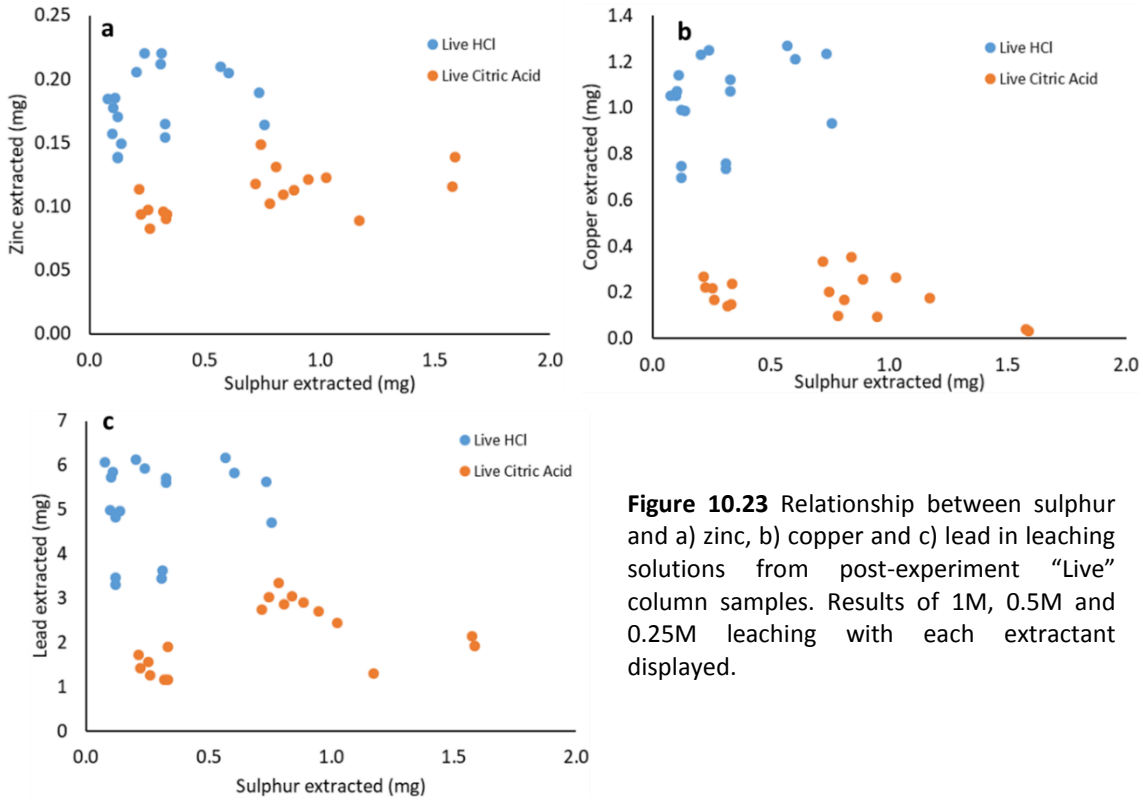

Figure 10.23 Relationship between sulphur and a) zinc, b) copper and c) lead in leaching solutions from post-experiment "Live" column samples. Results of 1M, 0.5M and 0.25M leaching with each extractant displayed.

10.4.6.3. Autoclaved Samples

The relationships between the elements analysed in the leachants from the post-experiment "Autoclaved" column wastes bear considerable similarities to those from the "Live" column wastes (Figure 10.24 & Figure 10.25).

As with the "Live" column samples, there is no clear correlation between iron and sulphur in the post-experiment "Autoclaved" column wastes (Figure 10.24a). The amount of sulphur extracted has reduced substantially relative to the pre-experiment wastes, though is slightly higher than in the "Live" samples. This potentially is a result of a lesser extent of bioreduction occurring in the "Autoclaved" columns compared with the "Live" columns. While sulphur recovery has decreased, iron recovery has increased compared with the pre-experiment waste. As with the "Live" samples, the HCl leaches have generally recovered more iron and less sulphur compared with the citric acid leaches. The lack of correlation between iron and sulphur, coupled with the reduced recovery of sulphur, suggests that the jarosite in the pre-experiment waste has been removed from the waste via bioreduction. This correlates with the results of both XRD analysis and the interpretation of the "Live" column extractions.

Lead and iron has retained the positive correlation observed in the pre-experiment sample (Figure 10.24b). The correlation between iron and zinc in the "Autoclaved" column samples bears substantial similarity to the "Live" column samples with a slightly higher R^2 value of 0.63 suggesting a slightly stronger correlation. HCl has recovered greater amounts of lead per mg of iron recovered than achieved by citric acid. This may imply that there are also lead-bearing, non-iron minerals such as lead hydroxides, that are resistant to dissolution by citric acid, in the waste. While the correlation with iron has survived experimentation, the correlation between lead and sulphur has been lost. The relationship between lead and sulphur, again, bear strong similarity to the "Live" column equivalents (Figure 10.25c). HCl has recovered more zinc than the citric acid and generally low to near negligible quantities of sulphur. This contrasts with the pre-experiment waste were a positive correlation between the two was observed. As with other metals in the "Live" wastes this likely represents a removal of metal-bearing jarosites in the waste with the lead then becoming associated with iron oxyhydroxides or other lead bearing minerals. Previous XRD analysis has shown the removal of jarosite

and the dominance of goethite in the post-experiment “Autoclaved” wastes, supporting the theory of redistribution of lead to iron oxyhydroxide minerals. Further evidence for this is the increase in lead within the “easily-reducible oxide” phases in the sequential extraction analysis. The sequential extraction also provides supporting evidence for the assertion that a proportion of the lead has precipitated as non-iron bearing minerals as the lead within “carbonate-associated phase has increased substantially suggesting the presence of lead carbonate, hydroxide or similarly reactive minerals.

Iron has also retained its correlation with zinc in the “Autoclaved” column waste samples despite higher recovery rates of zinc (Figure 10.24c). The strength of the correlation has reduced relative to the pre-experiment sample with an R^2 value of 0.71. This replicates the trend seen in the “Live” column leaching data. The correlation between zinc and sulphur observed in the pre-experiment waste is not observed in the “Autoclaved” wastes, again similar to what was seen in the “Live” column samples (Figure 10.25a). Again, HCl has recovered more zinc with less sulphur while the opposite is true of citric acid. The lack of correlation further suggests that jarosite has been preferentially reduced and the released zinc has become associated with iron oxyhydroxides. While this suggested change in mineralogy was also evident in the XRD analysis, it is not as clear in the results of sequential extraction analysis which showed minimal change in leachability and/or partitioning of zinc within the waste.

The relationship between iron and copper again shows a greater degree of variation depending on the leachant used (Figure 10.24d). Citric acid has yielded the lowest recoveries with all leaches clustering together showing no clear positive correlation. H_2SO_4 has achieved greater recoveries which plot into a marginally elongate cluster which has a slight suggestion of a positive correlation. HCl, meanwhile, has generally recovered a greater mass of copper. The HCl results also show a slight positive correlation between copper and iron suggesting a correlation between the two, despite this not being suggested in the data from the other leachants. This may suggest a range of copper-bearing minerals with copper only associated with less reactive ferric minerals which are seemingly only leachable by the stronger HCl and potentially H_2SO_4. As with the other metals of interest, the pre-experiment correlation between copper and sulphur has not translated to the post-experiment sample. As in the “Live” column wastes, higher copper recoveries with HCl are not typically associated with higher

sulphur. This again suggests the re-distribution of copper from the iron oxyhydroxysulphate jarosite to other residual or secondary minerals. The results of sequential extraction work suggest the majority of re-distributed copper has become associated with iron oxyhydroxides in the "easily-reducible oxide" phase, further supported by the presence of goethite in the post-experiment XRD. The remainder has become associated with carbonates or hydroxides as denoted by the increase in the "carbonate associated" phase.

The similarity in elemental relationships and trends in the "Live" and "Autoclaved" columns provides further evidence of the similar mechanisms and extent of bioreduction in the waste caused by the introduction of glycerol to the waste.

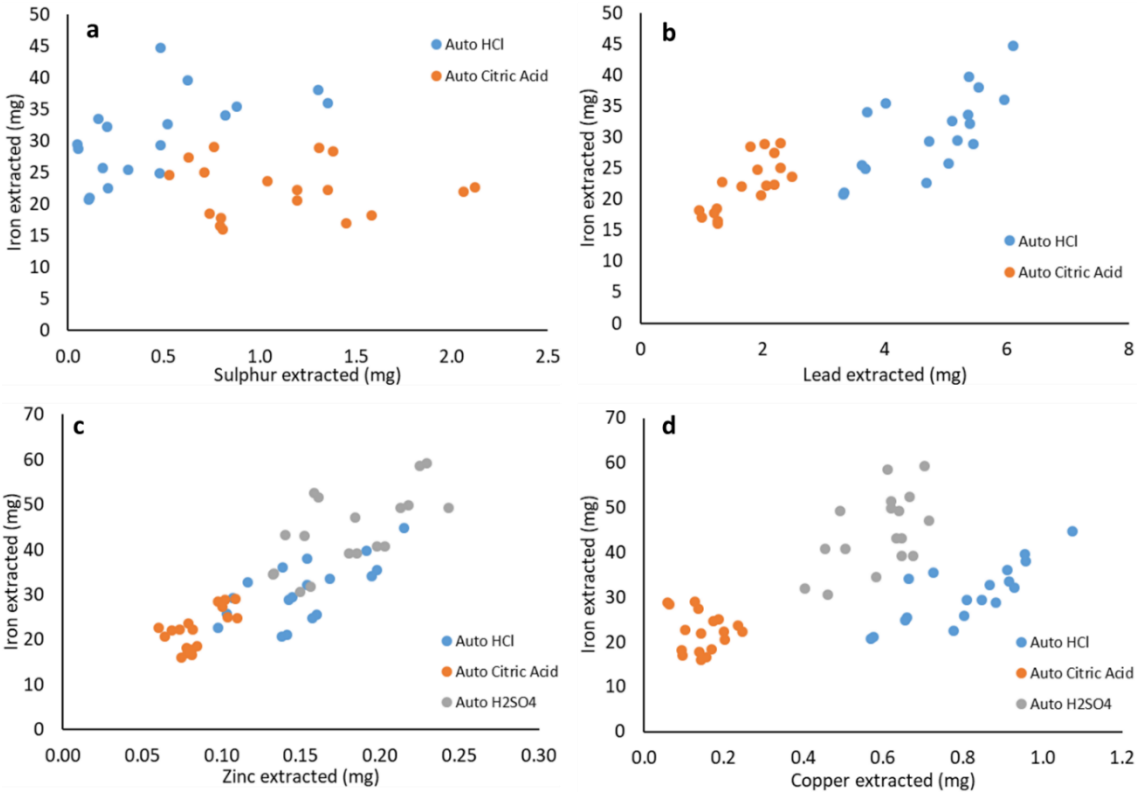

Figure 10.24 Relationship between iron and a) sulphur, b) lead, c) zinc and d) copper in leaching solutions from post-experiment "Autoclaved" column samples. Results of 1 M, 0.5 M and 0.25 M leaching with each extractant displayed.

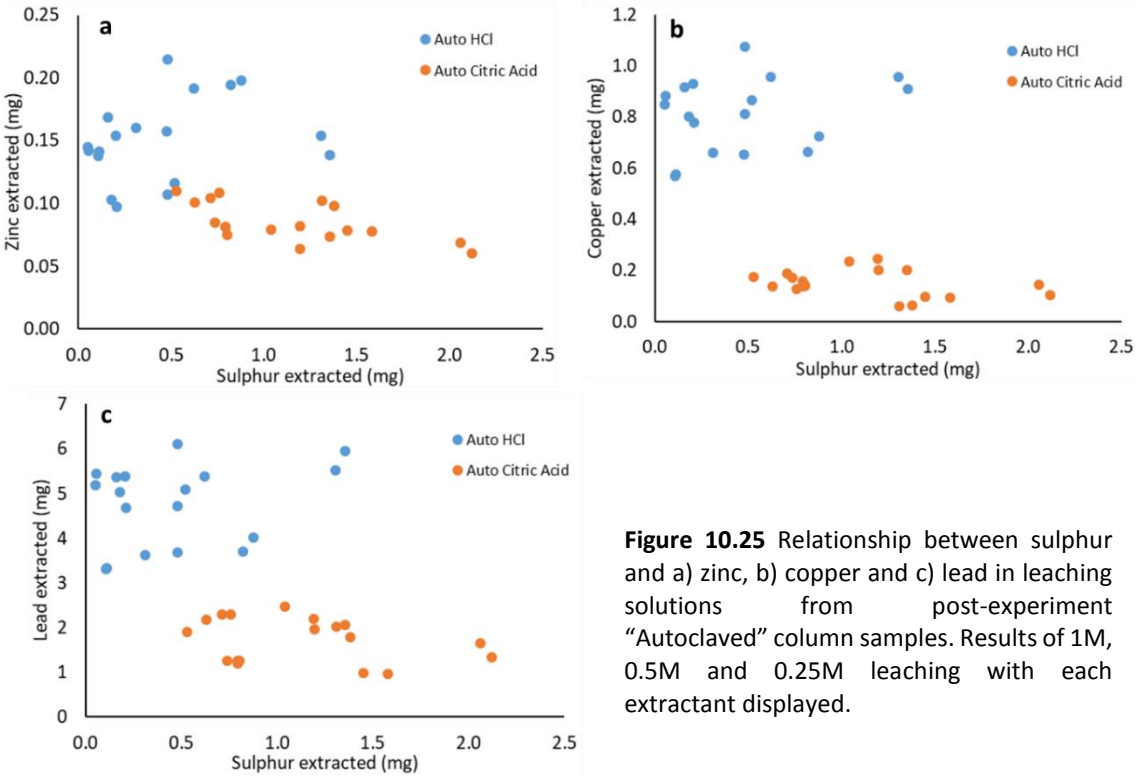

Figure 10.25 Relationship between sulphur and a) zinc, b) copper and c) lead in leaching solutions from post-experiment "Autoclaved" column samples. Results of 1M, 0.5M and 0.25M leaching with each extractant displayed.

10.4.6.4. Organic Starved Samples

Where the "Live" and "Autoclaved" column samples have exhibited considerable changes in elemental associations relative to the pre-experiment waste, the "Organic Starved" columns show little to no alteration (Figure 10.26 & Figure 10.27). This correlates with the observations of previous analysis which have shown negligible change in the physicochemical properties of the waste.

Aside from generally achieving lower recovery rates, there are only minor differences between the relationships of iron and other elements of interest in leachants from the pre-experiment and "Organic Starved" column wastes (Figure 10.26). Whilst positive correlations between metals and sulphur, similar to those seen in pre-experiment waste, are observable in the "Organic Starved" column leaches, the data plots are typically more diffuse (Figure 10.27). This indicates greater variation in the waste relative to the pre-experiment equivalent despite an apparent lack of activity in the columns. The increased variation of metals with relation to sulphur may be a result of the abiotic transformation of schwertmannite to jarosite or goethite, or jarosite to goethite, during experimentation leading metals to disassociate from the sulphurous

minerals (Vithana *et al.*, 2015). This may also explain the increased leachability of metals of interest other than iron. The correlation between copper and sulphur has shown the greatest increase in variability, whilst lead and zinc remain relatively unchanged. This observation agrees with the trace element retention scale suggested by Schroth & Parnell (2005) who observed that when schwertmannite transformed to goethite or jarosite metals are retained based on the following qualitative retention scale: Pb > Zn, Mn > As, Al, & Cu.

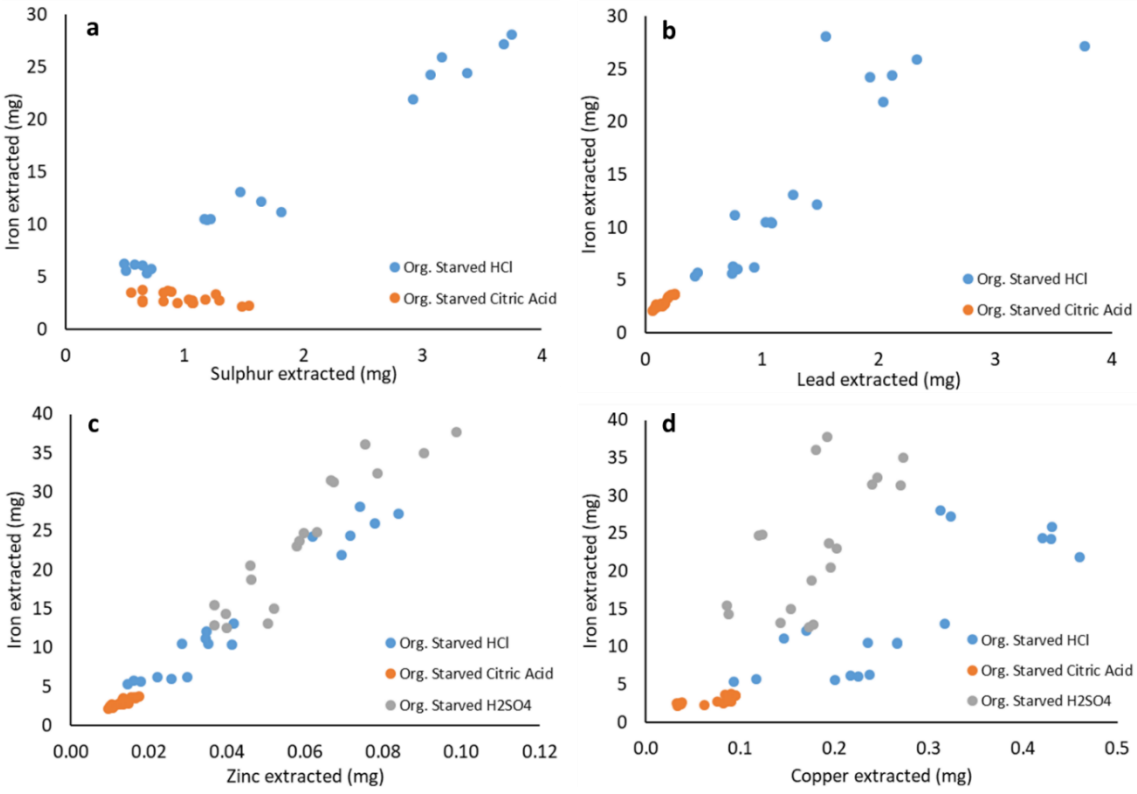

Figure 10.26 Relationship between iron and a) sulphur, b) lead, c) zinc and d) copper in leaching solutions from post-experiment "Organic Starved" column samples. Results of 1 M, 0.5 M and 0.25 M leaching with each extractant displayed.

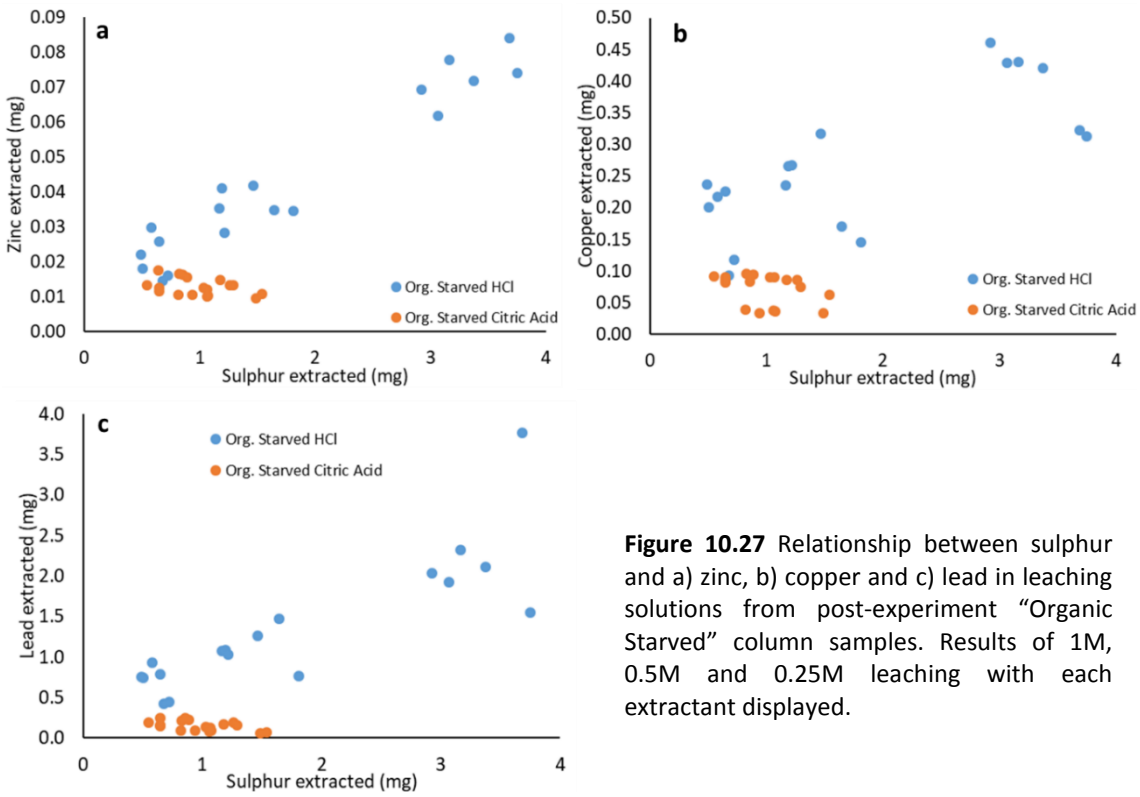

Figure 10.27 Relationship between sulphur and a) zinc, b) copper and c) lead in leaching solutions from post-experiment "Organic Starved" column samples. Results of 1M, 0.5M and 0.25M leaching with each extractant displayed.

10.5. Conclusions and Key Points for Subsequent Work

Leachability analysis of the pre- and post-experiment wastes has shown that leachability of metals of interest has increased as a result of the induced bio-reduction. Iron, zinc, copper and lead all saw increases in leachability with maximum recoveries of 7.3%, 7.9%, 15.2% and 34.8% respectively. They also saw maximum increases in recovery of approximately 8.5, 8.0, 23.5, and 33.5 times in post-experiment samples compared to the pre-experiment waste. The post-experiment "Autoclaved" columns showed increased leachability of metals relative to the pre-experiment waste though typically had lower metal leachability than the "Live" column samples. This correlates with the findings of effluent analysis and bioinformatics from the column studies which suggested bioreduction had occurred in the "Autoclaved" columns though to a lesser extent than in the "Live" columns. Metal leachability from the "Organic Starved" columns showed only minor differences from the pre-experiment waste confirming bioreduction as the mechanism for increased metal leachability. The impact of glycerol, as a direct reducing agent, on the leachability of metals has been shown to be minimal,

providing further confirmation that induced bioreduction is responsible for the increasing leachability of metals in the waste. The results of the leachability analysis have validated the findings of the sequential extraction analysis and added greater detail to the increased leachability phenomena.

Autoclaving of the pre-experiment waste resulted in slight increases in the leachability of metals within the waste. However, when compared to the increases induced by bioreduction of the waste the autoclaving effect can be considered negligible. “Autoclaved” columns generally saw smaller increases in metal leachability than the “Live” columns. This is a result of a more limited extent of bioreduction during column experimentation rather than changes in physicochemical parameters of the waste caused by autoclaving.

Within both the pre-experiment waste and “Organic Starved” column samples iron, copper, zinc and lead all tend to be associated with sulphur; while copper, zinc and lead also have an association with iron. This lead the author to conclude that jarosite was the primary metal being mineral dissolving in the dilute leachants used in this study. This correlates with the observations of XRD analysis which also identified jarosite as an important constituent mineral in the waste. Within the wastes that had experienced bioreduction the association of the metals of interest to iron remained but the association with sulphur has no longer observable. This has been interpreted as being the result of the preferential removal of jarosite in the waste by bioreduction; followed by the reabsorption or co-precipitation of copper, zinc and lead to remnant or secondary iron oxyhydroxides. Again, this supports the results of XRD analysis which showed the removal of jarosite from the waste during experimentation. The presence of non-ferric metal hydroxides or carbonates, suggested by the sequential extractions, could neither be confirmed nor refuted in from the data obtained.

Hydrochloric acid proved to be the most efficient leachant tested, largely giving the greatest recoveries of all elements analysed and across all concentrations tested. Whilst citric acid yielded the lowest metal recoveries of the acids tested it has the advantage that, as an organic acid, it is biodegradable which may allow for a wider range of applications in environments where inorganic acids, such as HCl, are not suitable.

With regards to the efficacy of a coupled bioreduction, dilute acid (or chelator) leaching methodology for the extraction of metals from in-situ wastes the results can be viewed as mixed. Whilst metal extractions are not as large as those seen in other bioreduction studies. This treatment led to a maximum eight-fold increase in zinc, twenty-two-fold increase in copper and thirty-three-fold leachability of lead, respectively, with only the addition of a non-specific, low cost organic substrate and dilute acids both of which could be applied in-situ. Whilst the scale of zinc recovery achieved may be too minor for industrial application in all but the largest waste deposits, the recovery of >15% total copper and ≈35% of total lead suggest substantial promise in the methodology as an easy and potentially significant low-cost technology.

To summarise:

- Leachability of metals has increased as a result of bioreduction
- The largest increase in leachability was a 33.5 times increase in lead leachability from the Live column waste utilising 0.25 M HCl as an extractant
- Leachability also increased in the post-experiment Autoclaved wastes though to a lesser extent. This is reflective of the lesser extent of bioreduction experienced by the Autoclaved columns
- No increase in leachability was observed in the Organic Starved samples, demonstrating that the increases in leachability were the result of bioreduction.
- Hydrochloric acid proved to be the most efficient extractant tested
- Correlations between iron, sulphur and other elements of interest indicate jarosite within the pre-experiment and Org. Starved samples though not within the Live and Autoclaved columns. This supports the assertion that jarosite has been the primary target for bioreduction.

11. Discussion of Potential Implementation and Efficacy of Work

11.1. Efficacy of Stimulating Indigenous Iron-Reducers for In-Situ Recovery of Metals from Waste

11.1.1. Efficacy of Process and Geochemical Constraints

The primary focus of this thesis was to ascertain the potential of stimulating indigenous iron reducing microbial communities, within in-situ oxidised mine and metallurgical wastes, for the recovery of metals of economic interest. Stimulation of indigenous iron reducing communities was not achieved in either wastes from alumina and steel production or waste from the active treatment of mine effluent. This effect was achieved in the "Lindsay" waste from passive coal mine drainage waste and two separate acid mine drainage wastes taken from "Parys Mountain" in N. Wales. With regards to recovery of metals of economic interest, there is less to be gained from the Lindsay waste, compared with the Parys Mt. waste, as it is comprised almost entirely of iron oxyhydroxides and contains little of any other metal of economic interest.

The efficacy of in-situ bioreduction/ metal recovery from the Parys Mt. wastes is a more complex matter. Experimentation has proven that the introduction of glycerol to this waste, under anaerobic conditions, will stimulate indigenous iron reducing communities to reduce ferric iron minerals. There has been an observed coeval release of ferrous iron and lead from the waste as a result of the stimulated iron reduction clearly demonstrating the potential for the technique in mobilising metals for recovery whilst the waste is in-situ. However, this trend was not observed for any of the other metals investigated. This was a result of what is, perhaps, the greatest constraint faced by this study in the form of rapid, biogenically mediated increase in the pH of the system causing severe limitations on both the iron reduction and metal recovery.

The rapid change in the system from acidic conditions to near-neutral has been shown to result in the dominance or sulphate reduction in the latter stages of experimentation at the expense of iron-reduction; as the reduction of iron is no longer energetically favourable for the microbes present. This presents a potential issue for in-situ application as a dominance of sulphate reduction within an in-situ waste would result in the generation of large quantities of hydrogen sulphide gas. As well as producing a foul

odour, hydrogen sulphide is poisonous and as such would represent a new hazard to the health of both the environment. This factor may be mitigates against by the abundance of reactive Fe present which would serve to react with, and remove the hydrogen sulphide. Whilst there is a chance that sulphate reduction may be targeting iron sulphates (e.g. jarosite) and thereby releasing metals of interest, there is also the issue of the formation of sulphides to consider. Sulphate reduction is known to result in the formation of iron sulphides that sequester the metals of interest from the aqueous phase thereby lowering the amount available for recovery, increasing inefficiency.

Furthermore, the increasing pH has also had a detrimental effect on both the structure of the microbial communities and the recovery of those metals mobilised by the iron reduction. At the circum-neutral state there is also an increased rate of loss of aqueous metals. Where they were once soluble in the acidic conditions, mobilised metals of interest are either not entering the aqueous phase or potentially precipitating out of solution. This precipitation may have been in the form of metal hydroxides or as part of secondary iron oxyhydroxides and carbonates and potentially sulphides as suggested by sequential extraction data (though not observed in XRD). Alternatively, they may be being sorbed to the surfaces of remnant iron oxyhydroxides. In any of these cases, the metals of interest are lost from the extractant solution and therefore lost to any potential recovery technique, limiting the potential of the system for metal recovery.

If this system were to be implemented on the waste whilst in-situ then the limitation of increased pH may potentially be easily circumvented by utilising the acid mine drainage which is produced on site. Utilising the drainage from the mine site would bring a number of advantages. Firstly, it would naturally keep the pH low allowing more efficient recovery of metals and proliferation of the indigenous microbial communities. The consistently low pH may then prevent the switch to sulphate reduction, thereby eliminating the issues arising from hydrogen sulphide production. Additionally, as this effluent is itself a waste product there would likely be far less additional costs the would be incurred by the use of an externally sourced extractant (both in production and transport); and would result in a reduction in the amount of AMD produced at Parys Mt. entering local watercourses and ultimately the Irish Sea as is currently the case.

Work utilising Parys Mt. AMD as an extractant was considered during this thesis; however, due to the high metal content of the AMD it would make it highly problematic to determine what quantity if any of the metals within the solid waste were being recovered as a result of the stimulated bioreduction. This does though present a fascinating future phase of this research.

If the pH issue was not addressed and the system was implemented at field scale under its current methodology there would be a potential issue with the stability of secondary minerals in the remnant waste. Analysis of the pre- and post-experiment wastes has suggested that a number of meta-stable minerals such as green rusts and acid volatile sulphides have been formed, along with crystalline goethite at the expense of jarosite and more amorphous iron oxyhydroxides such as ferrihydrite. These minerals are highly susceptible to changes in environmental conditions and have been seen to rapidly decompose when exposed to the atmosphere. Whilst recovery of metals of interest has not been as great as hypothesised, a substantial redistribution of these metals to these less stable phases and other secondary minerals has been observed. Therefore, if the remnant waste was subjected to a sudden change in physicochemical conditions, for example a sudden flood of AMD or acidic surface runoff from the mine, there may result a release of metals to the environment. While exploiting this increased leachability for metal recovery in a controlled method has been investigated, if it were to occur without control it has the potential to cause further environmental harm. This is yet another reason why the issue of increasing pH would need to be resolved before any attempt at field scale implementation could take place.

11.1.2. Potential Issues relating to Physical Application at Field Scale

Aside from issues relating to the geochemistry of the system there are issues relating to the physical implementation of an in-situ bioreduction recovery system. Primary amongst these issues is the need for an anaerobic environment for ferric iron reduction to occur. As the primary case study within this thesis, potential issues relating to implementation at field scale will be focused on the Parys Mt. site. The waste at Parys Mt. is exposed to the atmosphere, meaning that at least a minor change in the structure of the waste deposits are necessary for the system to be successfully implemented. This

could either consist of installing a capping system to prevent oxygen contacting the waste or creating ponds of waste held under water with a thin oxygenated layer at the waste surface. This would have to be constructed so that the oxidised layer reflects an acceptable loss of efficiency when compared with to the majority of the waste being held in anaerobic conditions.

If the latter of these two systems was implemented, due care would have to be given to the organic carbon delivery system. The organic carbon could not be introduced from the top of the waste as there would likely be unacceptable losses of organic carbon to aerobic, non-iron reducing processes. Therefor the organic carbon would have to be introduced from within or below the waste to prevent its loss to unwanted biological processes. Analysis of the size of the microbial communities has shown a decline in the average size of bacterial communities with greater distance from the organic carbon source. This was observed within a relatively small column experiment, and it stands to reason that in a field scale test this effect would be further amplified. To circumvent this a grid system of pipes would be required to supply organic carbon throughout the waste to prevent areas of the waste being starved of organic carbon. An example of a similar technique from which inspiration could be taken is the acid feeding system used in low grade heap leaching systems. This would also ensure that the entirety of the waste has access to either glycerol or a greater range of the secondary organic breakdown products rather than the latter simple organic carbon bi-products such as CO_2. This would facilitate the proliferation of *Desulfosporosinus* and *Thermincola* and subsequent iron bioreduction throughout the waste rather than in localised areas.

Finally, and perhaps most importantly, there would need to be an effective containment system to prevent the escape to the environment of the metalliferous effluents created in the process. At Parys Mt. a practical solution is already present in the form of pre-existing settling ponds and precipitation ponds previously used for copper recovery. Whilst these ponds are now in poor condition, they do at least provide a framework around which repairs and further construction can be based. The only potential limitation to this work is the protections currently afforded to the precipitations ponds as examples of unique local heritage and the SSSI designation of large parts of Parys Mt itself. In other sites where these ponds are not already present, the construction of these ponds, or similar containment system, would likely be required and the waste

transferred into these constructed ponds before any recover could take place. This may be problematic for existing waste as it requires the transport, however briefly, of the waste into the constructed tanks. For future waste streams, this would not be an issue as the waste could be directly deposited in a prepared tank/pond.

Many of these physical implementation obstacles are not unique to the Parys Mt. case study and would need to be overcome wherever a bioreductive dissolution extraction mechanism is implemented.

The final stage of the recovery process, which has not been the focus of this study, is consideration for the removal and recovery of solubilised metals from the leach liquor. Given that this thesis has not presented a method refined enough for industrial application, and each site will result in liquors with varying characteristics, it is difficult to suggest an applicable treatment for the leaching liquors. That being noted there are a number of options already widely employed for the recovery of metals from both process wasters and wastewaters. These include solvent extraction (Esther *et al.*, 2015; Hiskey & Copp, 2018), electrowinning (Esther *et al.*, 2015; Liu *et al.*, 2016; Gwak *et al.*, 2018), selective precipitation (Oh *et al.*, 2016; Ryan *et al.*, 2017; Zhou *et al.*, 2018) and ion exchange resins (Dabrowski *et al.*, 2004). It is likely that all of these methods would recover metals of interest from post bioreduction leaching liquors, though the relative efficacy of each for recovery cannot be stated with certainty. However, the use of ion exchange resins carries the advantage of being able to recover very low concentrations from solution (Karrs *et al.*, 1986); this is a substantial advantage for treating the more dilute column experiment effluents. Along with their high metal removal efficiency, ion exchange resins have the advantages of a high treatment capacity, rapid exchange kinetics and the potential to be tailored to preferentially recover specific metals (Dabrowski *et al.*, 2004; Fu & Wang, 2011).

11.1.3. Issues with Efficiency of Indigenous Microbial Communities

Aside from the tendency of the microbes to transition from iron-reduction to sulphate-reduction there are other factors, both positive and negative, to be considered when utilising indigenous microbial communities. Primary amongst these is the issue of

efficiency of the system with regards to organic carbon use. In a system with a greater degree of controls, specifically cultured iron-reducers and the ideal organic carbon source it can be guaranteed that no other non-iron reducing microbes are sequestering organic carbon. With the indigenous microbial communities used in this study being far more diverse there is a risk of a substantial proportion of the organic carbon provided being used for microbial processes other than iron reduction.

In the Parys Mt. wastes the greatest loss of organic carbon is as a result of the sulphate reduction in the latter stages of experimentation. It was not established whether the Desulfosporosinus spp. are reducing aqueous sulphate or structural sulphate in the form of jarosite. Whilst the latter would still be advantageous as the iron sulphate jarosite would be reduced this is not as efficient as direct iron reduction and as such can be considered a loss of organic carbon. Beyond this potentially large sink of organic carbon, the Parys Mt. system appears to experience only a slight loss of organic carbon to non-iron reducing processes; with the iron reducers Desulfosporosinus and Thermincola dominating. However, this is a qualitative assessment of the efficiency of organic carbon use and the process would benefit from a quantitative assessment.

The counter argument to the previous point, is that the mixed community may also be viewed as advantageous. With a greater variety of iron reducers there is the potential for the repeated, and complete, utilisation of organic carbon in the form of organic breakdown products. Furthermore, there is the potential for the conversion of organic carbon sources not suitable for use by the iron reducers present into a form that the iron reducers can use. An example of this was observed in the Lindsay waste testing, where the acetogen Acetobacterium was observed as the 2nd most abundant genus and was interpreted to be producing acetate which was in turn used by the iron reducing Anearomyxobacter spp. Such a system where waste organic carbon is recycled for reuse by iron-reducers would not be observed in a system where a single, inoculated iron reducer is used.

The final potential limitation of the use of indigenous microbial communities is the risk of heterogeneity in the waste. All of the studies performed in this thesis have utilised homogenised waste to provide increased consistency. However, this is not a true reflection of the condition of the waste whilst in-situ. As well as chemical heterogeneity,

there is potential for heterogeneity in the distribution of the indigenous microbial communities and the iron reducers within it. This heterogeneity is an issue not faced by the ex-situ processes, studies of which currently dominate the literature.

11.2. Efficacy of Stimulating Indigenous Iron-Reducers for Ex-Situ Recovery of Metals from Waste

While this thesis has primarily focused on the investigation of a in-situ method of metal recovery, there have been indications in the results of potential for use as an ex-situ process. The tests that have provided the greatest inspiration for the processes' potential ex-situ application are the "Autoclaved" Parys Mt. tests. Despite autoclaving of the waste, to sterilise it, significant proliferation of Desulfosporosinus spp. was observed due to their ability to sporulate and survive the autoclaving process. Whilst the results of the "Autoclaved" columns were generally slightly poorer than those of the equivalent "Live" tests there is enough evidence to suggest it may have some degree potential for metal recovery from waste due to the similarities in microbial communities between the "Live" and "Autoclaved" samples. Utilising the indigenous microbial communities of the Parys Mt. waste in an ex-situ recovery technique bring with it a number of advantages over an in-situ methodology, though equally there are potential drawbacks.

The dominance of the sporulating Desulfosprosinus spp. in the bioreduced Parys Mt. waste lends itself to potentially effective utilisation in an ex-situ setting. The capability of the Desulfosprosinus spp. to survive autoclaving via sporulation suggests that they would be capable of surviving the process of extraction and transporting the waste, thereby removing the requirement to inoculate the waste with expensive cultured microbes.

12. Conclusions and Recommendations for Future Work

12.1. Conclusions

Based on the research carried out in this study, the following conclusions based of the original aims of the study can be drawn:

- ***To identify a range of wastes, with significant concentrations of metals of economic interest, which may be targets for bio-reductive dissolution of iron for resource recovery.***

A number of iron dominated oxidised wastes from various mining and metallurgical scenarios were identified that may represent suitable candidates for metal recovery via iron reduction. Wastes from former metal mines, Wheal Jane and Parys Mountain were tested along with Red Mud from an alumina production operation. All of these were found to contain an abundance of iron oxyhydroxides and contained significant quantities of metals of economic interest associated with these oxyhydroxides. Work was also performed on a waste from the passive treatment of coal mine drainage (Lindsay) which despite being dominated by iron oxyhydroxides contained very little other metal of economic interest.

- ***Establish whether microbial communities, indigenous to these wastes, can be stimulated whilst in-situ by the application of an organic carbon source to the wastes.***

Of the wastes tested, only the Lindsay passive mine drainage sludge and the acidic Parys Mt. waste samples responded to the addition of an organic carbon source. In these two wastes the introduction of glycerol lead to a visible change in colour and changes to the physicochemical properties (e.g. ORP decrease) of the extractants suggesting increased microbial activity. Additionally, in both cases ferrous and total iron concentrations in the effluents were observed to increase suggesting the stimulation and activity of iron reducing communities.

Analysis of the microbial community sizes via qPCR confirmed that the introduction of glycerol resulted in the proliferation of microbial communities in both the Lindsay and

Parys Mt. wastes. In both cases the majority of the increases was largely due to an increase in bacterial gene copies as opposed to archaeal gene copies. Analysis also showed that there was a decrease in community size with greater distance from the source of organic carbon at the base of the column.

- ***Determine whether any metals will be released from iron oxyhydroxides, as a result of iron reduction. And whether they will remain in solution and are thereby extractable via the aqueous phase***

A coeval release of iron and lead from the Parys Mt. waste to the effluent, after the onset of microbial iron reduction, was observed. However, no similar trend was identified for the other metals of interest. The determining factor as to whether solubilised metals were retained in solution appeared to be the pH of the system. Initially, whilst the pH was low, lead was recovered at greater concentrations. As the pH of the system increased to a circum-neutral state, as a result of the microbial activity, the concentration of lead (and other metals) in the effluent declined. This is likely due to the lower solubility of these metals at circum-neutral conditions resulting in their loss to the solid phase rather than maintenance in solution.

- ***Record any changes in the chemical properties of the waste, beyond metal concentration/ mobility, resultant from the stimulation of indigenous microbial communities.***

In the Parys Mt. tests, when iron reduction occurred, pH was observed to increase to circum-neutral conditions, whilst the ORP decreased sharply. Both of these are characteristic observations of the initiation of microbial iron reduction. Whilst the ORP was observed to decline in the Lindsay tests, the pH did not increase as expected. Instead, a slight decrease in pH was observed.

Stimulated iron reduction in the Lindsay waste tests resulted in the alteration of the mineralogy of the waste. Before any experimentation the waste was dominated by two-line ferrihydrite which was transformed to goethite during experimentation. The Parys

Mt. waste also showed considerable alteration in mineralogy as a result of experimentation; with jarosite being preferentially reduced and removed from the waste. In both wastes there was substantial evidence for the presence of metastable green rusts after microbial iron reduction had occurred; with iron monosulphides potentially also present in the Parys Mt wastes.

- ***Determine the fate of metals not extractable via the aqueous phase. Establish whether these metals may be sequestered into secondary minerals and whether this facilitates alternative extraction methodologies.***

Those solubilised metals not retained in the effluent are believed to either sorb to residual iron oxyhydroxides, coprecipitate with secondary iron oxyhydroxides (e.g. green rusts) or to precipitate as metal hydroxides. Sequential extractions and leachability analysis have shown a substantial redistribution of metals, in particular lead and copper, from more recalcitrant mineral phases to more readily leachable phases. This has resulted in increases in copper and lead leachability of up to twenty-two times and thirty-three times, respectively, compared with the pre-bioreduction waste.

- ***Record any changes into the composition of indigenous microbial communities as a result of bioreduction***

Stimulation of iron bioreduction in both the Lindsay and Parys Mt. wastes has resulted in drastic alteration to the structure of the indigenous microbial communities. The Lindsay waste communities transitioned from being dominated by iron oxidisers such as *Gallionella* to a system with an abundance of iron reducers such as *Geobacter* and *Anearomyxobacter*. Also present in abundance was the acetogen *Acetobacterium*. The presence of this genus is suggestive of complex community structure where the breakdown products of glycerol oxidation are converted to acetate, which is then utilised further by the iron reducers.

The Parys Mt. waste transitioned from having a diverse community, containing iron oxidisers, iron reducers, cyanobacteria and phototrophs, to a far less diverse community dominated by iron reducers. The most abundant iron reducers identified were

Desulfosporosinus and *Thermincola*. The former of these is also capable of reducing sulphate; suggesting that as pH conditions tended towards neutral the community shifted towards sulphate reduction as iron-reduction became energetically unfavourable. This resulted in the system becoming self-rate limiting with regards to iron reduction.

In both wastes the "Autoclaved" experimental variants showed stimulation of iron reducing communities. These residual communities were comprised of bacterial species of iron reducers known to be capable of sporulation (e.g. *Desulphosporosinus, Thermincola* and *Pelosinus*) demonstrating the robust nature of the microbial communities and presenting the possibility of utilising the communities in an ex-situ technique.

12.2. Thesis Limitations and Potential Error

As with any study there are a number of sources of potential error within this thesis which have led to limitations to the efficacy of the study. Some of these limitations, such as the heterogeneity in the distribution of microbial communities, have already been discussed. Within this section other limitations and sources of error within this study are discussed.

12.2.1. Column Studies

The most significant source of error from the column testing is the lack of data acquisition from directly within the columns. By obtaining data from the column effluents it was possible to infer the physicochemical conditions within the columns. However, this method does not account for any changes to the effluent occurring within the collection vessel before aliquots were taken for sampling. Data was collected at a minimum of once every 24h. This provides ample time for the properties of the effluent to undergo changes e.g. alteration of ORP or oxidation and precipitation of iron oxyhydroxides, resulting in the data obtained not being a true representation of conditions within the columns. There is also an assumption that the effluent is representative of the conditions throughout the column. However, this is predicated on the assumption that the extractant is in contact with all the waste for the same length of time with equal flow rates throughout. This is highly unlikely though. A more likely scenario is that there are a series of preferential flow paths throughout the column resulting in areas of the waste receiving a much-reduced flow of extractant and therefor organic carbon to facilitate bioreduction. This may then result in differing conditions throughout the column with the single measurement of the effluent representing an average of the conditions and not the true complexity of conditions spatially within the column.

The precipitation of iron oxyhydroxides in the effluent collection vessel has also resulted in inaccuracy in the measurement of metal release from the columns. Whilst later recovery of the precipitated solids allowed for more accurate estimation of total metals removed the timing of the precipitated metal release in not known. This is potentially of

greater significant in the latter stages of experimentation where the pH had increased to circum-neutral conditions. Whilst this means released metals are less likely to remain in solution to vacate the column, those metals that do make it to the effluent collection vessel are more likely to be precipitated out of solution and thereby be underrepresented in the effluent analysis. While these metals were recovered by a later acid wash, the time at which they were released from the columns is not known.

The estimation of extractant residence time within the columns made within this study are inherently flawed. To produce such an estimate a value for the permeability of the waste is required. As work was performed on a variety of wastes, which all had differing physical properties, a typical value of permeability for natural soils was used to calculate an estimate of residence time. The use of an estimate, regardless of the logic behind it, introduces a potentially large source of error. To then use this value in a calculation results in compound error and a substantial lack of confidence in the resultant data.

12.2.2. Microbial Analysis

Due to the design of the columns, and the limited number of columns that could be run at one time, samples for microbial analysis could only be acquired at the end of experimentation. This resulted in a lack of clarity with regards to the timing of changes and development of the microbial communities. Given the substantial changes in physicochemical conditions it is possible that microbes other than those dominant at the end of experimentation experienced a period of proliferation and decline not expressed by the end-point data.

When extracting the DNA from the waste samples only a single brand of DNA extraction kit was used ("Fast DNA® SPIN Kit for Soil"). If this kit was incapable of successfully extracting certain sequences of DNA then these would remain unrepresented in the analysis. Without validating the results by extracting DNA with another kit there remains a degree of uncertainty whether the results of genome sequencing are representative of the microbial communities within the waste. Extraction of the DNA also produced further issues due to some samples being visibly impure with an abundance of PCR inhibitors causing issues with later amplification. To remedy this

situation diluting of the DNA up to 200 times was required to successfully amplify all samples. This in turn introduced a greater risk of contamination of the samples.

First generation sequencing generated a number of poor quality reads due in part to the issues listed above in conjunction with human error in excising the DGGE bands for sequencing. Furthermore, the selection of samples for analysis represented only a portion of the true microbial community. For example, *Thermincola* was not identified by the first generation sequencing. This omission is potentially due to sample selection or, alternately, due to the primer pair selection. It is possible that the primers used in this phase of analysis were unsuitable for targeting the region of DNA that distinguishes *Thermincola* from similar species resulting in it being missed in analysis. Whilst this situation, along with the small sample size of first generation sequencing, was rectified by performing next generation sequencing with a separate primer set; additional experimentation with yet more primer sets would provide further certainty that microbial species have gone unidentified.

12.3. Recommendations for Future Studies

A number of limitations to the studies conducted in this thesis have been identified and further study may enhance the accuracy of the results and the effectiveness of the system for potential future implementation. Areas which would likely benefit from further investigation include:

- The limitations of inferring physicochemical conditions within experimental columns have been outlined. A repetition of the column experiments with a system in place for the automatic recording of a range of physicochemical parameters throughout experimentation. This would not only facilitate measurements from within the column but also allow for the comparison of conditions within different areas/heights of the column.

- Develop a system for future studies for sub samples of waste to be obtained from the columns during experimentation. This would help in gaining an understanding of the development of the indigenous microbial communities throughout experimentation as opposed to having end-point only data for comparison.

- Further investigation of a greater number of iron-rich oxidised wastes to assess the potential of the developed system to a wider range of sites and processes. For example, there is significant interest in laterite wastes, jarosite sludge resulting from zinc production and pickling liquor sludge from the steel production which would all present potentially productive avenues for future study.

- Investigate the possibility of seeding wastes which yielded no microbial activity with wastes that did. For example, introducing a small quantity of Lindsay waste, and the microbial communities within it, to Wheal Jane waste in an effort to establish iron reducing communities without the cost of inoculating specific cultures.

- Repetition of leachability tests with varying leaching periods would allow for the determination of the most efficient leaching period to yield the highest recoveries for the shortest time leached.

13. References

Akai, J. et al. 2004. Mineralogical and geomicrobiological investigations on groundwater arsenic enrichment in Bangladesh. *Applied Geochemistry* 19(2), pp. 215-230.

Alloway, B. 1995. *Heavy Metals in Soils*. Glasgow: Blackie Academic and Professional.

Allwood, J. 2014. Squaring the circular economy: The role of recycling within a hierarchy of material management strategies. In: Worrell, E. and Reuter, M.A. eds. *Handbook of recycling*. Waltham, MA, USA: Elsevier.

Alpers, C. N. and Blowes, D. W. 1994. *Environmental Geochemistry of Sulphide Oxidation*. Washington D.C.: American Chemical Society.

Altschul, S. et al. 1990. Basic local alignment search tool. *Journal of Molecular Biology* 215, pp. 403-410.

Amaral, F. A. D. et al. 2014. Metals recovery from galvanic sludge by sulfate roasting and thiosulfate leaching. *Minerals Engineering* 60, pp. 1-7.

Amirbahman, A. et al. 2013. Kinetics of homogeneous and surface-catalyzed mercury(II) reduction by iron(II). *Environ Sci Technol* 47(13), pp. 7204-7213.

Anderson, P. and Malotky, D. 1979. The Adsorption of Protolyzable Anions on Hydrous Oxides at Isoelectric pH. *Journal of Colloid & Interface Science* 72, pp. 413-427.

Anderson, R. T. and Lovley, D. R. 2010. Naphthalene and Benzene Degradation under Fe(III)-Reducing Conditions in Petroleum-Contaminated Aquifers. *Bioremediation Journal* 3(2), pp. 121-135.

Anglesey Mining Plc. 2016. [Online]. Available at: http://angleseymining.co.uk/ParysHeritage/LeafletAHT98/history.htm [Accessed: 14/9/16].

Anthony, J. et al. 2017. Handbook of Mineralogy (Online Database). Chantilly, VA, USA: Mineralogical Society of America.

Antony, H. et al. 2008. Carbonate and sulphate green rusts—Mechanisms of oxidation and reduction. *Electrochimica Acta* 53(24), pp. 7146-7156.

Appelo, C. and Postma, D. 2005. *Geochemistry, Groundwater and Pollution*. 2 ed. Amsterdam, Netherlands: A.A. Balkema Publishers, p. 649.

Appelo, C. and Vet, W. 2003. Modeling in situ iron removal from groundwater with trace elements such as As. In: Welch, A. and Stollenwerk, K. eds. *Arsenic in Groundwater*. Springer US, pp. 381-402.

Bacon, J. R. and Davidson, C. M. 2008. Is there a future for sequential chemical extraction? *Analyst* 133(1), pp. 25-46.

Bailong, L. et al. 2013. Recovery of Gold and Iron from the Cyanide Tailings by Magnetic Roasting. *Rare Metal Materials and Engineering* 42(9), pp. 1805-1809.

Balch, W. et al. 1977. *Acetobacterium*, a New Genus of Hydrogen-Oxidizing, Carbon Dioxide-Reducing, Anaerobic Bacteria *International Journal of Systematic Bacteriology* 27, pp. 355-361.

Barbirato, F. et al. 1998. 1,3-propanediol production by fermentation: An interesting way to valorize glycerin from the ester and ethanol industries. *Industrial Crops and Products* 7, pp. 281-289.

Barnatt, J. and Penny, R. 2004. The lead legacy. In: English Heritage, P.D.N.P.A., Natural England ed. *The prospects for the Peak Distric's lead mining heritage*.

Barnes, A. 2008. *The rates and mechanisms of Fe(II) oxidation in a passive vertical flow reactor for the treatment of ferruginous mine water.* Cardiff University.

Barringer, J. L. et al. 2006. Mercury in ground water, septage, leach-field effluent, and soils in residential areas, New Jersey coastal plain. *Sci Total Environ* 361, pp. 144-162.

Batty, J. D. and Rorke, G. V. 2006. Development and commercial demonstration of the BioCOP™ thermophile process. *Hydrometallurgy* 83(1-4), pp. 83-89.

Bearcock, J. M. et al. 2006. Fe(II)/Fe(III) 'green rust' developed within ochreous coal mine drainage sediment in South Wales, UK. *Mineralogical Magazine* 70(6), pp. 731-741.

Benner, S. et al. 2002. Reductive Dissolution and Biomineralization of Iron Hydroxide under Dynamic Flow Conditions. *Environ. Sci. Technol.* 36, pp. 1705-1711.

Bertel, D. et al. 2012. Iron transformations induced by an acid-tolerant Desulfosporosinus species. *Appl Environ Microbiol* 78(1), pp. 81-88.

Bertolino, S. M. et al. 2014. Comparing lactate and glycerol as a single-electron donor for sulfate reduction in fluidized bed reactors. *Biodegradation* 25(5), pp. 719-733.

Bethke, C. M. et al. 2008. Origin of microbiological zoning in groundwater flows. *Geology* 36(9), p. 739.

BGS. 2004. Commodity Profile Zinc. [Online]. Available at: https://www.bgs.ac.uk/mineralsUK/statistics/mineralProfiles.html.

BGS. 2009. *Commodity Profile: Cobalt* [Online]. British Geological Society. Available at:

https://www.bgs.ac.uk/mineralsUK/statistics/mineralProfiles.html [Accessed.

BGS and DPHE. 2001. *Arsenic contamination of groundwater in Bangladesh*. British Geological Survey.

Bhowmick, S. et al. 2013. Arsenic mobilization in the aquifers of three physiographic settings of West Bengal, India: understanding geogenic and anthropogenic influences. *J Hazard Mater* 262, pp. 915-923.

Bigham, J. and Nordstrom, D. 2000. Iron and aluminum hydroxysulfates from acid sulfate waters. *Reviews in Mineralogy and Geochemistry* 40, p. 351.

Bigham, J. et al. 1996. Schwertmannite and the chemical modeling of iron in acid sulfate waters *Geochimica et Cosmochimica Acta* 60, pp. 2111-2121.

Bingjie, O. et al. 2014. Reduction of jarosite by Shewanella oneidensis MR-1 and secondary mineralization. *Geochimica et Cosmochimica Acta* 124, pp. 54-71.

Binnemans, K. et al. 2013. Recovery of Rare Earths from Industrial Waste Residues: A Concise Review. In: Malfliet, A. et al. eds. *Third International Slag Valorisation Symosium: The Transition to Sustainable Materials Management.* Leuven, Belgium. pp. 191-205.

Bjelkevik, A. and Knutsson, S. eds. 2005. *Swedish Tailings – Comparison of mechanical properties between tailings and natural geological materials*. Securing the Future, International Conference on Mining and the Environment Metals and Energy Recovery. Skellefteå, Sweden, June 27- July 1, 2005.

Borra, C. R. et al. 2015. Leaching of rare earths from bauxite residue (red mud). *Minerals Engineering* 76, pp. 20-27.

Brady, K. et al. 1986. Influence of sulfate on fe-oxide formation: Comparisons with a stream receiving acid mine drainage *Clays and Clay Minerals* 34, pp. 266-274.

Breitenstein, A. et al. 2002. Reclassification of Clostridium hydroxybenzoicum as Sedimentibacter hydroxybenzoicus gen. nov., comb. nov., and description of Sedimentibacter saalensis sp. nov. *International Journal of Systematic and Evolutionary Microbiology* 52(3), pp. 801-807.

Bridge, T. and Johnson, D. 2000. Reductive Dissolution of Ferric Iron Minerals by Acidiphilium SJH. *Geomicrobiology Journal* 17(3), pp. 193-206.

Bridge, T. and Johnson, D. B. 1998. Reduction of Soluble Iron and Reductive Dissolution of Ferric Iron-Containing Minerals by Moderately Thermophilic Iron-Oxidising Bacteria. *Applied and Environmental Microbiology* 64, pp. 2181-2186.

Brierley, C. L. 2008. How will bioming be applied in future. *Transactions of Nonferrous Metals Society of China* 18, pp. 1302-1310.

Brierley, C. L. and Brierley, J. A. 1999. Bioheap Processes: Operational Requirements and Techniques. In: W., J.G. ed. *Copper Leaching, Solvent Extraction and Electrowinning Technologies.* Littleton, Colorado: Society of Mining Engineers, pp. 17-27.

Britt, A. et al. 2017. Australia's Identified Mineral Resources 2017. In: Australia, G. ed. Canberra: Geoscience Australia.

Brown Jr., G. et al. 2008. Geochemistry of Mineral Surfaces and Factors Affecting their Chemical Reactivity. In: Nilsson, A. et al. eds. *Chemical Bonding at Surfaces and Interfaces*. Elsebier, p. 520.

Brown, S. D. et al. 2012. Draft genome sequences for two metal-reducing Pelosinus fermentans strains isolated from a Cr(VI)-contaminated site and for type strain R7. *J Bacteriol* 194(18), pp. 5147-5148.

Bryan, C. et al. 2004. Microbial Populations in Surface Spoil at the Abandoned Mynydd Parys Copper Mines. In: *International Mine Water Association Symposium 2004: Process, Policy and Progress.* Newcastle, UK. IMWA,

Burkhardt, E. M. et al. 2011. Heavy metal tolerance of Fe(III)-reducing microbial communities in contaminated creek bank soils. *Appl Environ Microbiol* 77(9), pp. 3132-3136.

Calvo, G. et al. 2016. Decreasing Ore Grades in Global Metallic Mining: A Theoretical Issue or a Global Reality? *Resources* 5(4), p. 36.

Canfield, D. E. et al. 2005. *Aquatic Geomicrobiology*. San Diego, Ca: Elsevier, p. 645.

Caporaso, J. et al. 2010. QIIME allows analysis of high-throughput community sequencing data. *Nature Methods* 7, pp. 335-336.

Carlson, H. et al. 2012. Surface multiheme c-type cytochromes from Thermincola potens and implications for respiratory metal reduction by Gram-positive bacteria. *Proceedings of the National Academy of Sciences of the United States of America* 109, pp. 1702-1707.

Castro, L. et al. 2013. Effectiveness of anaerobic iron bio-reduction of jarosite and the influence of humic substances. *Hydrometallurgy* 131-132, pp. 29-33.

Chapelle, F. H. et al. 2009. Distinguishing iron-reducing from sulfate-reducing conditions. *Ground Water* 47(2), pp. 300-305.

Charlet, L. et al. 2002. Natural attenuation of TCE, As, Hg linked to the heterogeneous oxidation of Fe(II): and AFM study. *Chemical Geology* 190, pp. 303-319.

Charlet, L. and Manceau, A. 1991. X-Ray Absorption Spectroscopic Study of the Sorption of Cr(III) at the Oxide-Water Interface. *Journal of Colloid & Interface Science* 148, pp. 443-458.

Chaudhuri, S. K. et al. 2001. Biogenic magnetite formation through anaerobic biooxidation of Fe(II). *Appl Environ Microbiol* 67(6), pp. 2844-2848.

Chen, T. et al. 2014. Pollution control and metal resource recovery for acid mine drainage. *Hydrometallurgy* 147-148, pp. 112-119.

Chou, Y. H. et al. 2015. Recovery of Cu(II) by chemical reduction using sodium dithionite. *Chemosphere* 141, pp. 183-188.

Ciani, A. et al. 2005. Light penetration in soil and particulate minerals. *European Journal of Soil Science* 56(5), pp. 561-574.

Ciriminna, R. et al. 2014. Understanding the glycerol market. *European Journal of Lipid Science and Technology* 116(10), pp. 1432-1439.

CL:AIRE. 2004. *Mine Water Treatment at Wheal Jane Tin Mine, Cornwall*. Ambleside, Cumbria: CL:AIRE.

Coal Authority. 2015. *Force Crag mine water treatment scheme* [Online]. Coal Authority. Available at: https://www2.groundstability.com/force-crag-mine-water-treatment-scheme/ [Accessed: 14/3/2016].

Cooper, D. C. et al. 2000. Zinc Immobilization and Magnetite Formation via Ferric Oxide Reduction by *Shewanella putrifaciens* 200. *Enviromental Science & Technology* 34, pp. 100-106.

Cornell, R. et al. 1987. Effect of silicate species on the transformation of ferrihydrite into goethite and hematite in alkaline media. *Clays and Clay Minerals* 35(21-28).

Cornell, R. and Schneider, W. 1989. Formation of goethite from ferrihydrite at physiological ph under the influence of cysteine *Polyhedron* 8, pp. 149-155.

Cornell, R. and Schwertmann, U. 2003. *The Iron Oxides: Structure, Properties, Reactions, Occurences and Uses*. 2nd ed. Wiley-VCH, p. 664.

Coto, O. et al. 2008. Cobalt and nickel recoveries from laterite tailings by organic and inorganic bio-acids. *Hydrometallurgy* 94(1-4), pp. 18-22.

Coughlin, B. R. and Stone, A. T. 1995. Nonreversible adsorption of divalent metal ions (Mnll, Coll, Nill, Cull and Pbll) onto goethite: Effects of acidification, Fell addition and picolinic acid addition. *Environmental Science & Technology* 29, pp. 2445-2455.

Coulton, R. et al. 2003. Wheal Jane mine water active treatment plant - design, construction and operation. *Land Contamination & Reclamation* 11(2), pp. 245-252.

Coupland, K. et al. eds. 2004. *Biogeochemistry of a subterranean acidic mine water body at an abandoned copper mine*. International Mine Water Association Symposium: Mine Water 2004 - Process, Policy and Progress. Newcastle upon Tyne, UK.

Crane, R. A. et al. 2017. Physicochemical composition of wastes and co-located environmental designations at legacy mine sites in the south west of England and Wales: Implications for their resource potential. *Resources, Conservation and Recycling* 123, pp. 117-134.

Crosby, S. 1983. Surface Areas and Porosities of Fe(III)- and Fe(II)-Derived Oxyhydroxides. *Enviromental Science & Technology* 17, pp. 709-713.

Cummings, D. et al. 1999. Arsenic Mobilization by the Dissimilatory Fe(III)-Reducing Bacterium Shewanella alga BrY. *Environ. Sci. Technol.* 33, pp. 723-729.

Dabrowski, A. et al. 2004. Selective removal of the heavy metal ions from waters and industrial wastewaters by ion-exchange method. *Chemosphere* 56(2), pp. 91-106.

Dang, Z. et al. 2002. Mobility of heavy metals associated with the natural weathering of coal mine spoils. *Environmental Pollution* 118, pp. 419-426.

Das, D. et al. 1996. Arsenic in groundwater in six districts of West Bengal, India. *Environmental Geochemistry and Health* 18, pp. 5-15.

Das, G. K. et al. 1997. Characterisation and acid pressure leaching of various nickel-bearing chromite overburden samples. *Hydrometallurgy* 44, pp. 97-111.

Das, S. et al. 2011. Transformation of Two-Line Ferrihydrite to Goethite and Hematite as a Function of pH and Temperature. *Environ. Sci. Technol.* 45, pp. 268-275.

Dash, D. C. 2011. *Analytical Chemistry*. New Dehli: PHI Learning, p. 581.

Davydov, A. et al. 1998. Mechanism of H_2S Oxidation by Ferric Oxide and Hydroxide Surfaces. *J. Phys. Chem. B.*, pp. 4745-4752.

De Leon, K. B. et al. 2015. Complete Genome Sequence of Pelosinus fermentans JBW45, a Member of a Remarkably Competitive Group of Negativicutes in the Firmicutes Phylum. *Genome Announc* 3(5).

Dedysh, S. N. et al. 2012. Bryocella elongata gen. nov., sp. nov., a member of subdivision 1 of the Acidobacteria isolated from a methanotrophic enrichment culture, and emended description of Edaphobacter aggregans Koch et al. 2008. *Int J Syst Evol Microbiol* 62(Pt 3), pp. 654-664.

DEFRA and Stewart, R. 2015. *Force Crag mine water treatment scheme opens in Cumbria* [Online]. DEFRA. Available at: https://www.gov.uk/government/news/force-crag-mine-water-treatment-scheme-opens-in-cumbria [Accessed: 14/3/16].

DeLong, E. 1992. Archaea in coastal marine environments *Proc. Natl. Acad. Sci. USA* 89, pp. 5685-5689.

Dempsey, B. et al. 2002. Heterogeneous Oxidation of Ferrous Iron for Treatment of Mine Drainage. In: *2002 National Meeting of the American Society of Mining and Reclaimation.* ASMR, pp. 487-495.

Dempsey, B. A. and Jeon, B. H. 2001. Characteristics of sludge produced from passive treatment of mine drainage. *Geochemistry: Exploration, Environment, Analysis* 1(1), pp. 89-94.

Díaz-Álvarez, A. and Cadierno, V. 2013. Glycerol: A promising Green Solvent and Reducing Agent for Metal-Catalyzed Transfer Hydrogenation Reactions and Nanoparticles Formation. *Applied Sciences* 3(1), pp. 55-69.

Dietz, J. and Dempsey, B. 2001. Treatment of Mine Drainage Using Recirculated Iron Oxides in a Complete Mix Reactor. In: *National Association of Abandoned Mine Lands Annual Conference.* Athens, Ohio.

Dousma, J. and DeBruyn, P. 1976. Hydrolysis-Precipitation Studies of Iron Solutions. I. Model for Hydrolysis and Precipitation from Fe(III) Nitrate Solutions. *Journal of Colloid and Interface Science* 56, pp. 527-539.

Dowling, C. B. et al. 2002. Geochemical study of arsenic release mechanisms in the Bengal Basin groundwater. *Water Resources Research* 38, pp. 1-20.

Dzombek, D. and Morel, F. 1986. Sorption of Cadmium on Hydrous Ferric Oxide at High Sorbate/Sorbent Ratios: Equilibrium, Kinetics and Modelling. *Journal of Colloid & Interface Science* 112, pp. 588-598.

Dzombek, D. and Morel, F. 1990. *Surface Complexation Modeling: Hydrous Ferric Oxide*. Wiley Interscience, p. 393.

EC, E. C. 2017. Communication from the commission to the european parliament, the council, the european economic and social committee and

the committee of the regions on the 2017 list of critical raw materials for the eu. Brussels: European Commission.

Edgar, R. 2010. Search and clustering orders ofmagnitude faster than BLAST. *Bioinformatics* 26, pp. 2460-2461.

Ehrenreich, A. and Widdel, F. 1994. Anaerobic Oxidation of Ferrous Iron by Purple Bacteria, a New Type of Phototrophic Metabolism. *Applied and Environmental Microbiology* 60, pp. 4517-4526.

Eickhoff, M. et al. 2014. Nickel partitioning in biogenic and abiogenic ferrihydrite: The influence of silica and implications for ancient environments. *Geochimica et Cosmochimica Acta* 140, pp. 65-79.

Emerson, D. et al. 2010. Iron-oxidizing bacteria: an environmental and genomic perspective. *Annu Rev Microbiol* 64, pp. 561-583.

EMF, E. M. F. 2014. *Towards the circular economy—Vol 3: Accelerating the scale-up across global supply chains.* Cowes, Isle of Wight, UK: Ellen MacArthur Foundation.

Esther, J. et al. 2013. Effect of dissimilatory Fe(III) reducers on bio-reduction and nickel-cobalt recovery from Sukinda chromite-overburden. *Bioresour Technol* 146, pp. 762-766.

Esther, J. et al. 2015. Enhanced recovery of nickel from chromite overburden (COB) using dissimilatory Fe (III) reducers: A novel Bio-Reduction Acid Leaching (BRAL) approach. *Hydrometallurgy* 155, pp. 110-117.

Etique, M. et al. 2016. Magnetite as a precursor for green rust through the hydrogenotrophic activity of the iron-reducing bacteria Shewanella putrefaciens. *Geobiology* 14(3), pp. 237-254.

Falagán, C. et al. 2017. New approaches for extracting and recovering metals from mine tailings. *Minerals Engineering* 106, pp. 71-78.

Falagán, C. and Johnson, D. B. 2014. Acidibacter ferrireducens gen. nov., sp. nov.: an acidophilic ferric iron-reducing gammaproteobacterium. *Extremophiles* 18(6), pp. 1067-1073.

Farahmand, F. et al. 2009. Brine leaching of lead-bearing zinc plant residues: Process optimization using orthogonal array design methodology. *Hydrometallurgy* 95(3-4), pp. 316-324.

Farley, K. et al. 1985. A Surface Precipitation Model for the Sorption of Cations on Metal Oxides. *Journal of Colloid & Interface Science* 106, pp. 226-242.

Fedje, K. K. et al. 2012. Initial studies of the recovery of Cu from MSWI fly ash leachates using solvent extraction. *Waste Managment & Research* 30, pp. 1072-1080.

Fredrickson, J. et al. 1998. Biogenic iron mineralization accompanying the dissimilatory reduction of hydrous ferric oxide by a groundwater bacterium. *Geochimica et Cosmochimica Acta* 62, pp. 3239-3257.

Fu, F. and Wang, Q. 2011. Removal of heavy metal ions from wastewaters: a review. *J Environ Manage* 92(3), pp. 407-418.

Fuge, R. et al. 1991. Acid Mine Drainage in Wales and Influence of Ochre Precipitation on Water Chemistry. In: Alpers, C.N. and Blowes, D. eds. *Environmental Geochemistry of Sulfide Oxidation*. Vol. 550. American Chemical Society.

Fulford, G. D. et al. 1991. Recovery of rare earth elements from Bayer process red mud. In: Patent, U. ed. United States of America.

Fuller, S. et al. 2015. Population Changes in a Community of Alkaliphilic Iron-Reducing Bacteria Due to Changes in the Electron Acceptor: Implications for Bioremediation at Alkaline Cr(VI)-Contaminated Sites. *Water Air and Soil Pollution* 226.

Fuller, S. et al. 2014. Extracellular Electron Transport-Mediated Fe(III) Reduction by a Community of Alkaliphilic Bacteria That Use Flavins as Electron Shuttles. *Applied and Environmental Microbiology* 80, pp. 128-137.

Gelencser, A. et al. 2011. The red mud accident in Ajka (Hungary): characterization and potential health effects of fugitive dust. *Environ Sci Technol* 45(4), pp. 1608-1615.

Genin, J.-M. et al. 1998. Thermodynamic Equilibria in Aqueous Suspensions of Synthetic and Natural Fe(II)-Fe(III) Green Rusts: Occurences of the Mineral in Hydromorphic Soils. *Environ. Sci. Technol.* 32, pp. 1058-1068.

GFMS Ltd. 2018. *World Silver Survey 2018*. London, UK: The Silver Institute.

Gihring, T. M. et al. 2011. A limited microbial consortium is responsible for extended bioreduction of uranium in a contaminated aquifer. *Appl Environ Microbiol* 77(17), pp. 5955-5965.

Glasauer, S. et al. 2003. Controls on Fe reduction and mineral formation by a subsurface bacterium. *Geochimica et Cosmochimica Acta* 67(7), pp. 1277-1288.

Gotoh, S. and Patrick, W. 1974. Transfromation of iron in a waterlogged soil as affected by redox potential and pH. *Proceedings of the Soil Science Society of America* 38, p. 66.

Graedel, T. E. and Nassar, N. T. 2013. The criticality of metals: A perspective for geologists. *Geological Society Special Publications* 393, pp. 291-302.

Gräfe, M. and Klauber, C. 2011. Bauxite residue issues: IV. Old obstacles and new pathways for in situ residue bioremediation. *Hydrometallurgy* 108(1-2), pp. 46-59.

Gräfe, M. et al. 2011. Bauxite residue issues: III. Alkalinity and associated chemistry. *Hydrometallurgy* 108(1-2), pp. 60-79.

Gramp, J. P. et al. 2009. Biogenic Synthesis and Reduction of Fe(III)-hydroxysulfates. *Geomicrobiology Journal* 26(4), pp. 275-280.

Greben, H. et al. 2009. Cellulose fermentation products as an energy source for biological sulphate reduction of acid mine drainage type wastewaters In: Division for Natural Resources and the Environment CSIR, P. ed. Pretoria: Water Research Commission p. 120.

Grobkopf, R. et al. 1998. Diversity and Structure of the Methanogenic Community in Anoxic Rice Paddy Soil Microcosms as Examined by Cultivation and Direct 16S rRNA Gene Sequence Retrieval. *Applied and Environmental Microbiology* 64, pp. 960-969.

Gupta, D. C. 1999. Environmental aspects of selected trace elements associated with coal and natural water of Pench Valley coalfield of India and their impact of human health. *International Journal of Coal Geology* 40, pp. 133-149.

Gwak, G. et al. 2018. New industrial application of forward osmosis (FO): Precious metal recovery from printed circuit board (PCB) plant wastewater. *Journal of Membrane Science* 552, pp. 234-242.

Gwynedd Archaeological Trust. 1995. *Mynydd Parys Dyffryn Coch Precipitation Pits Survey and Recording*.

Haas, W. et al. 2015. How Circular is the Global Economy?: An Assessment of Material Flows, Waste Production, and Recycling in the European Union and the World in 2005. *Journal of Industrial Ecology* 19(5), pp. 765-777.

Hall, G. H. and Puhlmann, T. 2005. Spatial distribution of iron oxidation in the aerobic cells of the Wheal Jane Pilot Passive Treatment Plant. *Sci Total Environ* 338(1-2), pp. 73-80.

Hallberg, K. and Johnson, D. B. 2001. Biodiversity of acidophilic prokaryotes. *Advances in Applied Microbiology* 49, pp. 37-84.

Hallberg, K. B. et al. 2011. Reductive dissolution of ferric iron minerals: A new approach for bio-processing nickel laterites. *Minerals Engineering* 24(7), pp. 620-624.

Hammarstrom, J. M. et al. 2005. Secondary sulfate minerals associated with acid drainage in the eastern US: recycling of metals and acidity in surficial environments. *Chemical Geology* 215(1-4), pp. 407-431.

Hanahan, C. 2004. Dissolution of hydroxide minerals in the 1 M sodium acetate, ph 5, extracting solution in sequential extraction schemes. *Environmental Geology* 45(6), pp. 864-868.

Hansel, C. M. et al. 2003. Secondary mineralization pathways induced by dissimilatory iron reduction of ferrihydrite under advective flow. *Geochimica et Cosmochimica Acta* 67(16), pp. 2977-2992.

Harris-Hellal, J. et al. 2010. Mercury mobilization by chemical and microbial iron oxide reduction in soils of French Guyana. *Biogeochemistry* 103(1-3), pp. 223-234.

Harvey, C. F. et al. 2002. Arsenic Mobility and Groundwater Extraction in Banglasdesh. *Science* 298, pp. 1602-1606.

Harvey, D. 2000. *Modern Analytical Chemistry*. McGraw-Hill, p. 798.

Haschke, M. et al. 2016. In-Situ Recovery of Critical Technology Elements. *Procedia Engineering* 138, pp. 248-257.

He, Q. and Sanford, R. A. 2003. Characterization of Fe(III) Reduction by Chlororespiring Anaeromxyobacter dehalogenans. *Applied and Environmental Microbiology* 69(5), pp. 2712-2718.

Heal, K. V. et al. 2004. Removing phosphorus from sewage effluent and agricultural runoff using recovered ochre. In: Valsami-Jones, E. ed.

Phosphorus in environmental technology: Principles and application. IWE Publishing, pp. 320-324.

Hedrich, S. et al. 2011. The iron-oxidizing proteobacteria. *Microbiology* 157(Pt 6), pp. 1551-1564.

Heijman, C. G. et al. 1993. Abiotic Reduction of 4-Chloronitrobenzene to 4-Chloroaniline in a Dissimilatory Iron-Reducing Enrichment Culture. *Applied and Environmental Microbiology* 59, pp. 4350-4353.

Hellal, J. et al. 2015. Mercury mobilization and speciation linked to bacterial iron oxide and sulfate reduction: A column study to mimic reactive transfer in an anoxic aquifer. *J Contam Hydrol* 180, pp. 56-68.

Hernandez, C. M. et al. 2007. Recovery of metals from Cuban nickel tailings by leaching with organic acids followed by precipitation and magnetic separation. *J Hazard Mater* 139(1), pp. 25-30.

Hicks, D. et al. 2010. F_1F_0-ATP synthases of alkaliphilic bacteria: lessons from their adaptations. *Biochimica et Biophysica Acta* 1797, pp. 1362-1377.

Hiskey, J. B. and Copp, R. G. 2018. Solvent extraction of yttrium and rare earth elements from copper pregnant leach solutions using Primene JM-T. *Minerals Engineering* 125, pp. 265-270.

Hofstetter, T. B. et al. 1999. Complete Reduction of TNT and Other (Poly)nitroaromatic Compounds under Iron-Reducing Subsurface Conditions. *Environ. Sci. Technol.* 33, pp. 1479-1487.

Hori, T. et al. 2010. Identification of iron-reducing microorganisms in anoxic rice paddy soil by 13C-acetate probing. *ISME J* 4(2), pp. 267-278.

Horino, H. et al. 2014. Description of Anaerobacterium chartisolvens gen. nov., sp. nov., an obligately anaerobic bacterium from Clostridium rRNA cluster III isolated from soil of a Japanese rice field, and reclassification of Bacteroides cellulosolvens Murray et al. 1984 as Pseudobacteroides

cellulosolvens gen. nov., comb. nov. *Int J Syst Evol Microbiol* 64(Pt 4), pp. 1296-1303.

Howard, A. J. et al. 2015. Preserving the Legacy of Historic Metal-Mining Industries in Light of the Water Framework Directive and Future Environmental Change in Mainland Britain: Challenges for the Heritage Community. *The Historic Environment: Policy & Practice* 6(1), pp. 3-15.

Howell, J. et al. 1998. Effects of microbial iron oxide reduction on pH and alkalinity in anaerobic bicarbonate-buffered media: implications for metal mobility *Mineralogical Magazine* 62A, pp. 657-658.

Hu, C. et al. 2014. Effects of microbial iron reduction and oxidation on the immobilization and mobilization of copper in synthesized Fe(III) minerals and Fe-rich soils. *J Microbiol Biotechnol* 24(4), pp. 534-544.

Huch, M. et al. 2013. Streptococcus rubneri sp. nov., isolated from the human throat. *Int J Syst Evol Microbiol* 63(Pt 11), pp. 4026-4032.

Hudson-Edwards, K. A. et al. 2008. *Assessment of Metal Mining-Contaminated River Sediments in England and Wales*. Bristol: Envrionment Agency.

Huyen, P. T. et al. 2016. Electrochemical copper recovery from galvanic sludge. *Hydrometallurgy* 164, pp. 295-303.

Iluka Resources. 2009. Mineral Sands Technical Information. [Online]. Available at: http://www.iluka.com/docs/default-source/industry-company-information/iluka-mineral-sands-technical-information-brochure-2009.pdf?sfvrsn=2.

Infomine. 2018. *Infomine Commodity and Metal Prices* [Online]. Available at: http://www.infomine.com/investment/metal-prices/ [Accessed: 11/09/2018].

Innovate UK. 2017. *Collaborations for a Circular Economy* [Online]. Available at: https://connect.innovateuk.org/web/collaborations-circular-economy [Accessed: 1/8/2018].

Invarson, K. and Hallberg, K. 1976. Formation of mackinawite by the microbial reduction of jarosite and its application to tidal sediments. *Geoderma* 16, pp. 1-7.

Invarson, K. et al. 1976. The pyritization of basic ferric sulfates in acid sulfate soils: A microbiological interpretation. *Canadian Journal of Soil Science* 56, pp. 393-406.

Ionescu, D. et al. 2015. Biotic and abiotic oxidation and reduction of iron at circumneutral pH are inseparable processes under natural conditions. *Geomicrobiology Journal* 32(3-4), pp. 221-230.

Irving, H. and Williams, R. 1953. The Stability of Transition-metal Complexes. *Journal of the Chemical Society*, pp. 3192-3210.

Islam, F. et al. 2004. Role of metal-reducing bacteria in arsenic release from Bengal delta sediments. *Nature* 430, pp. 68-71.

Ixer, R. A. and Budd, P. 1998. THE Mineralogy of Bronze Age Copper Ores from the British Isles: Implications for the Composition of Early Metalwork. *Oxford Journal of Archaeology* 17, pp. 15-41.

Jambor, J. and Dutrizac, J. 1998. Occurence and Constitution of Natural and Synthetic Ferrihydrite, a Widespread Iron Oxyhydroxide. *Chem. Rev.* 98, pp. 2549-2585.

Jenkins, D. et al. 2000. Mynydd Parys Cu-Pb-Zn Mines: mineralogy, microbiology and acid mine drainage. In: Cotter-Howells, J.D. et al. eds. *Environmental Mineralogy: Microbial Interactions, Antropogenic Influences, Contaminated Land and Waste Management*. London: Mineralogical Society, pp. 161-179.

Jiang, G.-m. et al. 2017. Recovery of valuable metals from zinc leaching residue by sulfate roasting and water leaching. *Transactions of Nonferrous Metals Society of China* 27(5), pp. 1180-1187.

Johannesson, K. H. and Neumann, K. 2013. Geochemical cycling of mercury in a deep, confined aquifer: Insights from biogeochemical reactive transport modeling. *Geochimica et Cosmochimica Acta* 106, pp. 25-43.

Johansson, N. et al. 2013. An integrated review of concepts and initiatives for mining the technosphere: towards a new taxonomy. *Journal of Cleaner Production* 55, pp. 35-44.

Johnson, D. et al. 2013. A New Direction for Biomining: Extraction of Metals by Reductive Dissolution of Oxidized Ores. *Minerals* 3(1), pp. 49-58.

Johnson, D. et al. 2008. *Abandoned Mines and the Water Environment*. Bristol: Environment Agency.

Johnson, D. B. 2012. Reductive dissolution of minerals and selective recovery of metals using acidophilic iron- and sulfate-reducing acidophiles. *Hydrometallurgy* 127-128, pp. 172-177.

Johnson, D. B. 2014. Biomining-biotechnologies for extracting and recovering metals from ores and waste materials. *Curr Opin Biotechnol* 30, pp. 24-31.

Johnson, D. B. and Bridge, T. 2002. Reduction of ferric iron by acidophilic heterotrophic bacteria: evidence for constitutive and inducible enzyme systems in *Acidiphilium spp. Journal of Applied Microbiology* 93, pp. 315-321.

Johnson, D. B. and Hallberg, K. B. 2003. The microbiology of acidic mine waters. *Research in Microbiology* 154(7), pp. 466-473.

Johnson, J. et al. 2007. Dining at the Periodic Table: Metals Concentrations as They Relate to Recycling. *Environ. Sci. Technol.* 41, pp. 1759-1765.

Jones, E. J. P. et al. 2006. Role of microbial iron reduction in the dissolution of iron hydroxysulfate minerals. *Journal of Geophysical Research* 111(G1).

Joseph, T. et al. 2015. Human health risk assessment from arsenic exposures in Bangladesh. *Sci Total Environ* 527-528, pp. 552-560.

Ju, S. et al. 2011. Clean hydrometallurgical route to recover zinc, silver, lead, copper, cadmium and iron from hazardous jarosite residues produced during zinc hydrometallurgy. *J Hazard Mater* 192(2), pp. 554-558.

Kappler, A. and Straub, K. 2005. Geomicrobiological Cycling of Iron. *Reviews in Mineralogy and Geochemistry* 59, pp. 85-108.

Karim, Z. 1984. Characteristics of ferrihydrite formed by oxidation of $FeCl_2$ solutions containing different amounts of silica. *Clays and Clay Minerals* 32, pp. 181-184.

Karrs, S. et al. 1986. Ion Exchange for Metal Recovery: A Discussion of Trade-off. *Plating and Surface Finishing* 73, pp. 60-66.

Karthikeyan, K. and Elliott, H. 1999. Role of surface precipitation in copper sorption by the hydrous oxides of iron and aluminium. *Journal of Colloid & Interface Science* 220, pp. 88-95.

Keith, C. and Vaughan, D. J. 2000. Mechanisms and rates of sulphide oxidation in relation to the problems of acid rock (mine) drainage. In: Cotter-Howells, J.D. et al. eds. *Environmental Mineralogy: Microbial Interactions, Anthropogenic Influences, Contaminated Land and Waste Management*. Mineralogical Society.

Kerin, E. J. et al. 2006. Mercury methylation by dissimilatory iron-reducing bacteria. *Appl Environ Microbiol* 72(12), pp. 7919-7921.

Kim, C. et al. 2003. Factors affecting EDTA extraction of lead from lead-contaminated soils. *Chemosphere* 51(9), pp. 845-853.

Kim, M. et al. 2014. Hydrothermal synthesis of metal nanoparticles using glycerol as a reducing agent. *The Journal of Supercritical Fluids* 90, pp. 53-59.

Kirby, C. S. and Elder Brady, J. A. 1998. Field Determination of Fe^{2+} Oxidation Rates in Acid Mine Drainage using a Continuously-Stirred Tank Reactor. *Applied Geochemistry* 13, pp. 509-520.

Klauber, C. et al. 2011. Bauxite residue issues: II. options for residue utilization. *Hydrometallurgy* 108(1-2), pp. 11-32.

Kocar, B. D. et al. 2008. Integrated biogeochemical and hydrologic processes driving arsenic release from shallow sediments to groundwaters of the Mekong delta. *Applied Geochemistry* 23(11), pp. 3059-3071.

Kock, D. and Schippers, A. 2006. Geomicrobiological investigation of two different mine waste tailings generating acid mine drainage. *Hydrometallurgy* 83(1-4), pp. 167-175.

Kock, D. and Schippers, A. 2008. Quantitative microbial community analysis of three different sulfidic mine tailing dumps generating acid mine drainage. *Appl Environ Microbiol* 74(16), pp. 5211-5219.

Kohl, A. and Nielsen, R. 1997. *Gas Purification*. 5th ed. Houston, Texes: Gulf Publishing, p. 900.

Koretsky, C. et al. 2003. Seasonal oscillation of microbial iron and sulfate reduction in saltmarsh sediments (Sapelo Island, GA, USA). *Biogeochemistry* 64, pp. 179-203.

Kossoff, D. et al. 2014. Mine tailings dams: Characteristics, failure, environmental impacts, and remediation. *Applied Geochemistry* 51, pp. 229-245.

Kostka, J. and Nealson, K. 1995. Dissolution and reduction of magnetite by bacteria. *Environ. Sci. Technol.* 29, pp. 2535-2540.

Kou, J. et al. 2013. Green Synthesis of Noble Nanometals (Au, Pt, Pd) Using Glycerol under Microwave Irradiation Conditions. *ACS Sustainable Chemistry & Engineering* 1(7), pp. 810-816.

Kozich, J. et al. 2013. Development of a Dual-Index Sequencing Strategy and Curation Pipeline for Analyzing Amplicon Sequence Data on the MiSeq Illumina Sequencing Platform. *Applied and Environmental Microbiology* 79, pp. 5112-5120.

Krishnamurti, K. and Kate, S. 1951. Changes in Electrical Conductivity during Bacterial Growth. *Nature* 168, p. 170.

Krumholz, L. R. et al. 1996. A Freshwater Anaerobe Coupling Acetate Oxidation to Tetrachloroethylene Dehalogenation. *Applied and Environmental Microbiology* 62, pp. 4108-4113.

Kumar, S. et al. 2016. MEGA7: Molecular Evolutionary Genetics Analysis Version 7.0 for Bigger Datasets. *Molecular Biology and Evolution* 33, pp. 1870-1874.

Kunapuli, U. et al. 2010. Desulfitobacterium aromaticivorans sp. nov. and Geobacter toluenoxydans sp. nov., iron-reducing bacteria capable of anaerobic degradation of monoaromatic hydrocarbons. *Int J Syst Evol Microbiol* 60(Pt 3), pp. 686-695.

Lacal, J. et al. 2003. Study of fractionation and potential mobility of metal in sludge from pyrite mining and affected river sediments: changes in mobility over time and use of artificial ageing as a tool in environmental impact assessment. *Environmental Pollution* 124(2), pp. 291-305.

Lamborg, C. H. et al. 2013. Mercury Speciation and Mobilization in a Wastewater-Contaminated Groundwater Plume. *Environmental Science & Technology* 47(23), pp. 13239-13249.

Langmuir, D. 1997. *Aqueous Environmental Chemistry*. Prentice Hall, p. 600.

Lèbre, É. et al. 2017. The Role of the Mining Industry in a Circular Economy: A Framework for Resource Management at the Mine Site Level. *Journal of Industrial Ecology* 21(3), pp. 662-672.

Lee, J.-U. et al. 2009. Enhancement of arsenic mobility by indigenous bacteria from mine tailings as response to organic supply. *Environment International* 35(3), pp. 496-501.

Lemos, F. A. et al. 2006. Copper electrowinning from gold plant waste streams. *Minerals Engineering* 19(5), pp. 388-398.

Lewis, D. 1997. Factors influencing the stability and properties of green rusts. *Advances in Geoecology* 30, pp. 345-347.

Li, F. B. et al. 2010. Enhanced reductive dechlorination of DDT in an anaerobic system of dissimilatory iron-reducing bacteria and iron oxide. *Environ Pollut* 158(5), pp. 1733-1740.

Li, X. et al. 2009a. Interactively interfacial reaction of iron-reducing bacterium and goethite for reductive dechlorination of chlorinated organic compounds. *Science Bulletin* 54(16), pp. 2800-2804.

Li, X. M. et al. 2009b. Fe(III) oxide reduction and carbon tetrachloride dechlorination by a newly isolated Klebsiella pneumoniae strain L17. *J Appl Microbiol* 106(1), pp. 130-139.

Li, Y.-L. et al. 2006. Reduction of Iron Oxides Enhanced by a Sulfate-Reducing Bacterium and Biogenic H2S. *Geomicrobiology Journal* 23(2), pp. 103-117.

Liang, Y. J. et al. 2012. Hydrothermal sulfidation and floatation treatment of heavy-metal-containing sludge for recovery and stabilization. *J Hazard Mater* 217-218, pp. 307-314.

Lide, D. 2004. *CRC Handbook of Chemistry and Physics*. 85 ed. CRC Press.

Liger, E. et al. 1999. Surface catalysis of uranium(VI) reduction by iron(II). *Geochimica et Cosmochimica Acta* 63, pp. 2939-2955.

Liu, B. et al. 2016. The electrowinning of vanadium oxide from alkaline solution. *Hydrometallurgy* 165, pp. 244-250.

Liu, H. et al. 2007. Fe(II)-induced transformation from ferrihydrite to lepidocrocite and goethite. *Journal of Solid State Chemistry* 180(7), pp. 2121-2128.

Liu, Y. and Naidu, R. 2014. Hidden values in bauxite residue (red mud): recovery of metals. *Waste Manag* 34(12), pp. 2662-2673.

Liu, Z. and Li, H. 2015. Metallurgical process for valuable elements recovery from red mud—A review. *Hydrometallurgy* 155, pp. 29-43.

Llewellyn, D. H. et al. 2017. Transforming landscapes and identities in the south Wales valleys. *Landscape Research*, pp. 1-18.

Lonergan, D. et al. 1996. Phylogenetic Analysis of Dissimilatory Fe(III)-Reducing Bacteria. *Journal of Bacteriology* 178, pp. 2402-2408.

Lottermoser, B. G. 2007. *Mine Wastes: Characterisation, Treatment, Environmental Impacts*. 2nd ed. Berlin: Springer.

Lovley, D. 1991. Dissimilatory Fe(III) and Mn(IV) Reduction. *Microbiological Reviews* 55, pp. 259-287.

Lovley, D. 1993. Dissimilatory Metal Reduction. *Annu. Rev. Microbiol* 47, pp. 263-290.

Lovley, D. 1995. Bioremediation of Organic and Metal Contaminants with Dissimilatory Metal Reduction. *Journal of Industrial Microbiology* 14, pp. 85-93.

Lovley, D. 1997. Potential for anaerobic bioremediation of BTEX in petroleum contaminated aquifers. *Journal of Industrial Microbiology & Biotechnology* 18, pp. 75-81.

Lovley, D. 2013. Dissimilatory Fe(III)- and Mn(IV)-Reducing Prokaryotes. pp. 287-308.

Lovley, D. and Lonergan, D. 1990. Anaerobic Oxidation of Toluene, Phenol, and p-Cresol by the Disssimilatory Iron-Reducing Organism, GS-15. *Applied and Environmental Microbiology* 56, pp. 1858-1864.

Lovley, D. and Phillips, E. 1987. Competetive Mechanisms for Inhibition of Sulfate Reduction and Methane Production in Zone of Ferric Iron Reduction in Sediments. *Applied and Environmental Microbiology* 53, pp. 2636-2641.

Lovley, D. et al. 1992. Acetate oxidation by dissimilatory Fe(III) reducers. *Applied and Environmental Microbiology* 58, pp. 3205-3208.

Loyaux-Lawniczak, S. et al. 2000. Trapping of Cr by Formation of Ferrihydrite during the Reduction of Chromate Ions by Fe(II)−Fe(III) Hydroxysalt Green Rusts. *Environmental Science & Technology* 34, pp. 438-443.

Lusk, B. G. et al. 2015. Draft Genome Sequence of the Gram-Positive Thermophilic Iron Reducer Thermincola ferriacetica Strain Z-0001T. *Genome Announc* 3(5).

Lv, C. C. et al. 2015. Comprehensive recovery of metals from cyanidation tailing. *Minerals Engineering* 70, pp. 141-147.

Ma, Q. et al. 2015. Identification of the microbial community composition and structure of coal-mine wastewater treatment plants. *Microbiol Res* 175, pp. 1-5.

Madigan, M. et al. 2015. *Brock Biology of Microorganisms*. Harrow: Pearson Education Ltd, p. 1030.

Malvern Instruments Ltd. 2007. *Sample Dispersion and Refractive Index Guide*. Malvern, Worcestershire: Malvern Instruments Ltd.

Markova, N. et al. 2010. Survival of *Escherichia coli* under lethal heat stress by L-form conversion. *International Journal of Biological Sciences* 6, pp. 303-315.

Martinez, C. et al. 1999. Thermally Induced Release of Adsorbed Pb upon Aging Ferrihydrite and Soil Oxides. *Environ. Sci. Technol.* 33, pp. 2016-2020.

Matisoff, M. et al. 1982. The Nature and Source of Arsenic in Northeastern Ohio Ground Water. *Ground Water* 20, pp. 446-456.

Mayeux, B. et al. 2013. Desulfosporosinus burensis sp. nov., a spore-forming, mesophilic, sulfate-reducing bacterium isolated from a deep clay environment. *Int J Syst Evol Microbiol* 63(Pt 2), pp. 593-598.

McArthur, J. M. et al. 2001. Arsenic in groundwater: Testing pollution mechanisms for sedimentary aquifers in Bangladesh. *Water Resources Research* 37, pp. 109-117.

McGill, I. et al. 1976. Crystal structure of green rust formed by corrosion of cast iron. *Nature* 259, pp. 200-201.

Melton, E. D. et al. 2014. The interplay of microbially mediated and abiotic reactions in the biogeochemical Fe cycle. *Nat Rev Microbiol* 12(12), pp. 797-808.

Min, X. et al. 2012. Metal Recovery from Sludge through the Combination of Hydrothermal Sulfidation and Flotation. *Procedia Environmental Sciences* 16, pp. 401-408.

Mohamed, S. et al. 2016. Process development for elemental recovery from PGM tailings by thermochemical treatment: Preliminary major element extraction studies using ammonium sulphate as extracting agent. *Waste Manag* 50, pp. 334-345.

Montero S, I. C. et al. 2005. Characterization of waste rock associated with acid drainage at the Penn Mine, California, by ground-based visible to short-wave infrared reflectance spectroscopy assisted by digital mapping. *Chemical Geology* 215(1-4), pp. 453-472.

Moore, J. N. et al. 1988. Partitioning of Arsenic and Metals in Reducing Sulfidic Sediments. *Environ. Sci. Technol.* 22, pp. 432-437.

Morgan, R. 2015. *Deputy Regional Manager, Veolia.*

Morin, D. H. R. and D'Huges, P. 2007. Bioleaching of a Cobalt-Containing Pyrite in Stirred Reactors: a Case Study from Laboratory Scale to Industrial Application. In: Rawlings, D.E. and Johnson, D.B. eds. *Biomining*. Heidelberg, Germany: Springer-Verlag, pp. 35-56.

Morse, J. et al. 1987. The Chemistry of the Hydrogen Sulfide and Iron Sulfide Systems in Natural Waters. *Earth-Science Reviews* 24, pp. 1-42.

Mudd, G. and Weng, Z. 2012. Base Metals. In: Letcher, T.M. and Scott, J.L. eds. *Material for a Sustainable Future*. London, UK: Royal Society of Chemistry.

Mulchandani, A. and Westerhoff, P. 2016. Recovery opportunities for metals and energy from sewage sludges. *Bioresour Technol* 215, pp. 215-226.

Murphy, P. and Frick, L. 2006. Titanium. In: Kogel, J.E. et al. eds. *Industrial minerals and rocks*. 7th ed. Littleton, Colorado: Society for Mining, Metallurgy and Exploration Inc, pp. 987-1003.

Murthy, C. P. 2008. *University Chemistry*. New Age International Limited Publishers.

Muyzer, G. et al. 1993. Profiling of Complex Microbial Populations by Denaturing Gradient Gel Electrophoresis Analysis of Polymerase Chain Reaction-Amplified Genes Coding for 16S rRNA. *Applied and Environmental Microbiology* 59, pp. 695-700.

Muyzer, G. et al. 1995. Denaturing gradient gel electrophoresis of PCR-amplified 16S rDNA. A new molecular approach to analyze the genetic diversity of mixed microbial communities. In: Akkermans, A. et al. eds. *Molecular microbial ecology manual*. Dordrecht, Netherlands: Kluwer Academic Publishers.

Nancucheo, I. et al. 2014. Extraction of copper from an oxidized (lateritic) ore using bacterially catalysed reductive dissolution. *Appl Microbiol Biotechnol* 98(14), pp. 6297-6305.

Nancucheo, I. et al. 2016. Draft Genome Sequence of a Novel Acidophilic Iron-Oxidizing Firmicutes Species, "Acidibacillus ferrooxidans" (SLC66T). *Genome Announc* 4(3).

Neal, C. et al. 2005. The water quality of the River Carnon, west Cornwall, November 1992 to March 1994: the impacts of Wheal Jane discharges. *Science of The Total Environment* 338(1-2), pp. 23-39.

Nickson, R. T. et al. 1998. Arsenic poisoning of Bangladesh groundwater. *Nature* 395, p. 338.

Nickson, R. T. et al. 2000. Mechanism of arsenic release to groundwater, Bangladesh and West Bengal. *Applied Geochemistry* 15, pp. 403-413.

Nioke, T. et al. 1983. Oxidation of ferrous iron by acidophilic iron-oxidising bacteria froma stream receiving acid mine drainage. *Water Research* 17, pp. 21-27.

Nordstrom, D. 1985. The rate of ferrous iron oxidation in a stream receiving acid mine effluent. *U.S. Geological Survey Water-Supply Paper 2270*, pp. 133-199.

Nordstrom, D. et al. 2000. Negative pH and Extremely Acidic Mine Waters from Iron Mountain California. *Enviromental Science & Technology* 34, pp. 254-258.

Nordstrom, D. K. 2011. Hydrogeochemical processes governing the origin, transport and fate of major and trace elements from mine wastes and mineralized rock to surface waters. *Applied Geochemistry* 26(11), pp. 1777-1791.

O'Loughlin, E. J. et al. 2007. Green Rust Formation from the Bioreduction of γ –FeOOH (Lepidocrocite): Comparison of SeveralShewanellaSpecies. *Geomicrobiology Journal* 24(3-4), pp. 211-230.

O'Sullivan, L. A. et al. 2015. Survival of Desulfotomaculum spores from estuarine sediments after serial autoclaving and high-temperature exposure. *ISME J* 9(4), pp. 922-933.

O'Sullivan, L. A. et al. 2008. Modified linker-PCR primers facilitate complete sequencing of DGGE DNA fragments. *J Microbiol Methods* 75(3), pp. 579-581.

Ochsenkuhn-Petropulu, M. et al. 1996. Recovery of Lanthanides and Yttrium from Red Mud by Selective Leaching. *Analytica Chimica Acta*, pp. 249-254.

Ochsenkuhn, K. M. et al. 2002. Pilot-Plant Investigation of the Leaching Process for the Recovery of Scandium from Red Mud. *Industrial & Engineering Chemistry* 41, pp. 5794-5801.

Oh, C. et al. 2016. Field application of selective precipitation for recovering Cu and Zn in drainage discharged from an operating mine. *Sci Total Environ* 557-558, pp. 212-220.

Ojumu, T. V. et al. 2009. The kinetics of ferrous-iron oxidation by Leptospirillum ferriphilum in continuous culture: The effect of temperature. *Biochemical Engineering Journal* 46(2), pp. 161-168.

Oleoline. 2017. *Glycerine Market Report*. Hong Kong: Oleoline inc.

Ona-Nguema, G. et al. 2002. Iron(II,III) Hydroxycarbonate Green Rust Formation and Stabilization from Lepidocrocite Bioreduction. *Environmental Science & Technology* 36, pp. 16-20.

Pagliaro, M. and Rossi, M. 2008. *The Future of Glycerol: New Usages for a Versatile Raw Material*. Cambridge, UK: RSC Publishing, p. 128.

Panda, S. et al. 2015. Sequential bioreduction–bioleaching and bioreduction–chemical leaching hybrid tests for enhanced copper recovery from a concentrator ball mill reject sample. *Hydrometallurgy* 157, pp. 171-177.

Parat, C. et al. 2003. Comparison of three sequential extraction procedures used to study trace metal distribution in an acidic sandy soil. *Analytical and Bioanalytical Chemistry* 376(2), pp. 243-247.

Park, B. and Dempsey, B. 2004. Mechanisms of Heterogeneous Fe(II) Oxidation in Acid Mine Drainage. In: *2004 National Meeting of the American Society of Mining and Reclamation* ASMR, pp. 1408-1423.

Park, S. Y. and Liang, Y. 2016. Biogenic methane production from coal: A review on recent research and development on microbially enhanced coalbed methane (MECBM). *Fuel* 166, pp. 258-267.

Parkes, R. J. et al. 1995. A combined ecological and physiological approach to studying sulphate reduction within deep marine sediment layers. *Journal of Microbial Methods* 23, pp. 235-249.

Pearce, N. J. G. 1994. Development and Conservation at Parys Mountain, Anglesey, Wales.*Geological and Landscape Conservation*. London: British Geological Society.

Peltier, E. et al. 2005. Metal Speciation in Anoxic Sediments: When Sulfides Can Be Construed as Oxides. *Environ. Sci. Technol.* 39, pp. 311-316.

Peng, N. et al. 2012. Recovery of iron from zinc calcines by reduction roasting and magnetic separation. *Minerals Engineering* 35, pp. 57-60.

Pester, M. et al. 2012. Complete genome sequences of Desulfosporosinus orientis DSM765T, Desulfosporosinus youngiae DSM17734T, Desulfosporosinus meridiei DSM13257T, and Desulfosporosinus acidiphilus DSM22704T. *J Bacteriol* 194(22), pp. 6300-6301.

Pleysier, R. et al. eds. 2009. *Characterisation of Ranger Mine water treatment sludge*. International Mine Water Conference. Pretoria, South Africa.

Polizzotto, M. L. et al. 2008. Near-surface wetland sediments as a source of arsenic release to ground water in Asia. *Nature* 454(7203), pp. 505-508.

Ponnamperuma, F. 1972. The chemistry of submerged soils. *Advanced Agronomy* 24, pp. 29-96.

Postma, D. 1985. Concentrations of Mn and separation from Fe in sediments-1. Kinetics and stoichiometry of the reaction between birnessite and dissolved Fe(II) at 10C. *Geochimica et Cosmochimica Acta* 49, pp. 1023-1033.

Postma, D. and Jacobson, R. 1996. Redox zonation: Equilibrium constraints on the Fe(III)/SO^{4-}reduction interface *Geochimica et Cosmochimica Acta* 60, pp. 3169-3175.

Poulton, S. W. and Canfield, D. E. 2005. Development of a sequential extraction procedure for iron: implications for iron partitioning in continentally derived particulates. *Chemical Geology* 214, pp. 209-221.

Power, G. et al. 2011. Bauxite residue issues: I. Current management, disposal and storage practices. *Hydrometallurgy* 108(1-2), pp. 33-45.

Qatibi, A. et al. 1998. Anaerobic Degradation of Glycerol by Desulfovibrio fructosovorans and D. carbinolicus and Evidence for Glycerol-Dependent Utilization of 1,2-Propanediol. *Current Microbiology* 36(283-290).

Qu, Y. et al. 2015. Leaching of valuable metals from red mud via batch and continuous processes by using fungi. *Minerals Engineering* 81, pp. 1-4.

Qu, Y. and Lian, B. 2013. Bioleaching of rare earth and radioactive elements from red mud using Penicillium tricolor RM-10. *Bioresour Technol* 136, pp. 16-23.

Qu, Y. et al. 2013. Bioleaching of heavy metals from red mud using Aspergillus niger. *Hydrometallurgy* 136, pp. 71-77.

Quicksall, A. N. et al. 2008. Linking organic matter deposition and iron mineral transformations to groundwater arsenic levels in the Mekong delta, Cambodia. *Applied Geochemistry* 23(11), pp. 3088-3098.

Ramamoorthy, S. et al. 2006. Desulfosporosinus lacus sp. nov., a sulfate-reducing bacterium isolated from pristine freshwater lake sediments. *Int J Syst Evol Microbiol* 56(Pt 12), pp. 2729-2736.

Rashid, G. M. et al. 2017. Delignification and Enhanced Gas Release from Soil Containing Lignocellulose by Treatment with Bacterial Lignin Degraders. *J Appl Microbiol*.

Rawlings, D. E. and Johnson, D. B. 2007. The microbiology of biomining: development and optimization of mineral-oxidizing microbial consortia. *Microbiology* 153(Pt 2), pp. 315-324.

Reichle, R. et al. 1975. Zinc Hydroxide: Solubility Product and Hydroxy-complex Stability Constants from 12.5–75 °C. *Canadian Journal of Chemistry* 53, pp. 3841-3845.

Renforth, P. et al. 2012. Contaminant mobility and carbon sequestration downstream of the Ajka (Hungary) red mud spill: The effects of gypsum dosing. *Sci Total Environ* 421-422, pp. 253-259.

Ribet, I. et al. 1995. The potential for metal release by reductive dissolution of weathered mine tailings. *Journal of Contaminant Hydrology* 17, pp. 239-273.

Rickard, D. and Morse, J. W. 2005. Acid volatile sulfide (AVS). *Marine Chemistry* 97(3-4), pp. 141-197.

Rimstidt, J. D. et al. 1994. Rates of Reaction of Galena, Sphalerite, Chalcopyrite and Arsenopyrite with Fe(III) in Acidic Conditions. In: Alpers, C.N. and Blowes, D.W. eds. *Envrionmental Geochemistry of Sulphide Oxidation*. Washington D.C.: American Chemical Society.

Rios, C. A. et al. 2008. Removal of heavy metals from acid mine drainage (AMD) using coal fly ash, natural clinker and synthetic zeolites. *J Hazard Mater* 156(1-3), pp. 23-35.

Robertson, W. et al. 2001. *Desulfosporosinus meridiei* sp. nov., a sporeforming sulfate-reducing bacterium isolated from gasolene-contaminated groundwater. *International Journal of Systematic and Evolutionary Microbiology* 51, pp. 133-140.

Rochelle, P. et al. 1992. DNase I treatment of Taq DNA polymerase for complete PCR decontamination. *BioTechniques* 13, p. 520.

Roden, E. and Urrutia, M. 1999. Ferrous Iron Removal Promotes Microbial Reduction of Crystalline Iron(III) Oxides. *Enviromental Science & Technology* 33, pp. 1847-1853.

Roden, E. et al. 2000. Bacterial reductive dissolution of crystalline Fe(III) oxide in continuous-flow column reactors. *Applied Environmental Microbiology* 66, pp. 1062-1065.

Rodwell, J. S. et al. 2017. The habitats directive in the UK: some wider questions raised by the definition, notification and monitoring of grassland habitats. *Fitosciologia* 44, pp. 37-47.

Ross, S. et al. 2007. UK Soil and Herbage Pollutant Survey. UKSHS Report No. 7: Environmental concentrations of heavy metals in UK soil and herbage. Bristol: Environment Agency. p. 123.

Rossini, G. and Bernardes, A. M. 2006. Galvanic sludge metals recovery by pyrometallurgical and hydrometallurgical treatment. *J Hazard Mater* 131(1-3), pp. 210-216.

Rowe, K. 2011. *Contaminated Land Remedial Works at Henwaith Settlement Ponds, Parys Mountain, Amlwch, Anglesey*. SKM Enviros.

Rusin, P. et al. 1992. Bioprocessing of refractory oxide ores by bioreduction: extraction of silver, molybdenum and copper. *Minerals Engineering* 5, pp. 10-12.

Ryan, M. J. et al. 2017. A study of selective precipitation techniques used to recover refined iron oxide pigments for the production of paint from a synthetic acid mine drainage solution. *Applied Geochemistry* 79, pp. 27-35.

Samal, S. et al. 2013. Proposal for resources, utilization and processes of red mud in India — A review. *International Journal of Mineral Processing* 118, pp. 43-55.

Sand, W. et al. 1992. Evaluation of *Leptospirillum ferrooxidans* for Leaching. *Applied and Environmental Microbiology* 58, pp. 85-92.

Santos Afonso, M. and Stumm, W. 1992. Reductive Dissolution of Iron(III) (Hydr)oxides by Hydrogen Sulfide. *Langmuir* 8, pp. 1671-1675.

Sapsford, D. et al. 2016. In Situ Resource Recovery from Waste Repositories: Exploring the Potential for Mobilization and Capture of Metals from Anthropogenic Ores. *Journal of Sustainable Metallurgy* 3(2), pp. 375-392.

Sarsby, R. 2013. *Environmental Geotechnics*. Westminster: ICE Publishing, p. 519.

Scheffer, F. and Schachtschabel, P. 1989. *Lehrbuch der Bodenkunde (Textbook of soil science)* [Online]. Stuttgart: Enke Verlag. Available at: http://soils.ifas.ufl.edu/faculty/grunwald/teaching/eSoilScience/oxides.shtml [Accessed: 03/03/2015].

Scheinost, A. et al. 2001. Kinetic Controls on Cu and Pb Sorption by Ferrihydrite. *Enviromental Science & Technology* 35, pp. 1090-1096.

Schippers, A. et al. 2010. The biogeochemistry and microbiology of sulfidic mine waste and bioleaching dumps and heaps, and novel Fe(II)-oxidizing bacteria. *Hydrometallurgy* 104(3-4), pp. 342-350.

Schmitz, R. et al. 2006. The anaerobic way of life. In: Dworkin, M. et al. eds. *The Prokaryotes: A Handbook on the Biology of Bacteria*. 3 ed., Vol. 2. New York: Springer.

Schroth, A. W. and Parnell, R. A. 2005. Trace metal retention through the schwertmannite to goethite transformation as observed in a field setting, Alta Mine, MT. *Applied Geochemistry* 20(5), pp. 907-917.

Schulze, D. G. and Schwertmann, U. 1987. The influence of aluminium on iron oxides: XIII. Properties of goethites synthesised in 0.3M KOH at 25°C. *Clay Minerals* 22, pp. 83-92.

Schwarz-Schampera, U. and Herzig, P. M. 2002. *Indium: Geology, Mineralogy and Economics*. Berlin: Springer-Verlag.

Schwertmann, U. 1991. Solubility and dissolution of iron oxides. *Plant and Soil* 130, pp. 1-25.

Schwertmann, U. and Cornell, R. 2000. *Iron Oxides in the Laboratory: Preparartion and Characterization*. 2nd ed. Wiley-VCH.

Schwertmann, U. and Fischer, W. 1973. Natural "amorphous" ferric hydroxide. *Geoderma* 10, pp. 237-247.

Schwertmann, U. et al. 1999. From Fe(III) ions to ferrihydrite and then to hematite. *Journal of Colloid & Interface Science* 209, pp. 215-223.

Shaw, R. A. et al. 2013. Resource Recovery from Mine Waste. In: Hester, R. and Harrison, R.M. eds. *Waste as a Resource*. Royal Society of Chemistry, pp. 44-65.

Shelobolina, E. S. et al. 2003. Use of Ferric and Ferrous Iron Containing Minerals for Respiration by Desulfitobacterium frappieri. *Geomicrobiology Journal* 20(2), pp. 143-156.

Sherwood, T. K. 1959. Mass Transfer Between Phases.*Phi Lamda Upsilon*. University Park, PA, USA: Pennsylvania State University.

Shiers, D. W. et al. 2016. Life in heaps: a review of microbial responses to variable acidity in sulfide mineral bioleaching heaps for metal extraction. *Res Microbiol* 167(7), pp. 576-586.

Shin, H. Y. et al. 2007. Regeneration of iron for trichloroethylene reduction by Shewanella alga BrY. *Chemosphere* 68(6), pp. 1129-1134.

Silva, A. M. et al. 2009. Iron(III) citrate speciation in aqueous solution. *Dalton Trans* (40), pp. 8616-8625.

Singer, P. and Stumm, W. 1970. Acidic mine drainage: the rate-determining step. *Science* 167, pp. 1121-1123.

Smeaton, C. M. et al. 2012. Simultaneous release of Fe and As during the reductive dissolution of Pb-As jarosite by Shewanella putrefaciens CN32. *Environ Sci Technol* 46(23), pp. 12823-12831.

Smedley, P. and Kinniburgh, D. 2002. A review of the source, behaviour and distrobution of arsenic in natural waters. *Applied Geochemistry* 17, pp. 517-568.

Smirnov, D. and Molchanova, T. 1997. The investigation of sulphuric acid sorption recovery of scandium and uranium from the red mud of alumina production. *Hydrometallurgy* 45, pp. 249-259.

Smith, S. L. et al. 2017. Reductive bioprocessing of cobalt-bearing limonitic laterites. *Minerals Engineering* 106, pp. 86-90.

Snars, K. and Gilkes, R. J. 2009. Evaluation of bauxite residues (red muds) of different origins for environmental applications. *Applied Clay Science* 46(1), pp. 13-20.

Sokolova, T. G. et al. 2005. Thermincola carboxydiphila gen. nov., sp. nov., a novel anaerobic, carboxydotrophic, hydrogenogenic bacterium from a hot spring of the Lake Baikal area. *Int J Syst Evol Microbiol* 55(Pt 5), pp. 2069-2073.

Soto, P. E. et al. 2013. Parameters influencing the microbial oxidation activity in the industrial bioleaching heap at Escondida mine, Chile. *Hydrometallurgy* 133(0), pp. 51-57.

Spring, S. and Rosenzweig, F. 2006. The genera *Desulfitobacterium* and *Desulfosporosinus*: Taxonomy. In: Dworkin, M. et al. eds. *The Prokaryotes*. Vol. 4: Bacteria: Firmicutes, Cyanobacteria. New York: Springer, pp. 771-786.

Straub, K. et al. 2001. Iron metabolism in anoxic environments at near neutral pH. *FEMS Microbiol Ecol* 34, pp. 181-186.

Straub, K. et al. 1996. Anaerobic, Nitrate-Dependent Microbial Oxidation of Ferrous Iron. *Applied and Environmental Microbiology* 62, pp. 1458-1460.

Strawn, D. et al. 1998. Kinetics and Mechanisms of Pb(II) Sorption and Desorption at the Aluminium Oxide - Water Interface. *Enviromental Science & Technology* 32, pp. 2596-2601.

Stumm, W. 1992. *Chemistry of the Solid-Water Interface: Processes at the Mineral-Water and Particle-Water Interface in Natural Systems*. John Wiley & Sons, p. 428.

Stumm, W. and Lee, F. 1961. Oxygenation of Ferrous Iron. *Industrial & Engineering Chemistry* 53(2), pp. 143-146.

Stumm, W. and Morgan, J. 1996. *Aquatic Chemistry: Chemical Equilibria and Rates in Natural Waters*. 3rd ed. Wiley Interscience, p. 1022.

Sumoondur, A. et al. 2008. Green rust as a precursor for magnetite: an <I>in situ</I> synchrotron based study. *Mineralogical Magazine* 72(1), pp. 201-204.

Sun, B. et al. 2001. Leaching of heavy metals from contaminated soils using EDTA. *Environmental Pollution* 113, pp. 111-120.

Sung, W. and Morgan, J. 1980. Kinetics and Product of Ferrous Iron Oxygenation in Aqueous Systems. *Environmental Science & Technology* 14(5), pp. 561-568.

Thamdrup, B. 2000. Bacterial Manganese and Iron Reduction in Aquatic Sediments. *Advances in Microbial Ecology* 16, pp. 41-84.

Thompson, J. et al. 2003. Multiple Sequence Alignment Using ClustalW and ClustalX. In: Baxevanis, A. et al. eds. *Current Protocols in Bioinformatics*

Thornton, I. et al. 2001. *Lead: The Facts*. London: IC Consultants.

Treude, N. et al. 2003. Strain FAc12, a dissimilatory iron-reducing member of the Anaeromyxobacter subgroup of Myxococcales. *FEMS Microbiology Ecology* 44(2), pp. 261-269.

Trivedi, P. and Axe, L. 2001. Predicting Divalent Metal Sorption to Hydrous Al, Fe, and Mn Oxides. *Enviromental Science & Technology* 35, pp. 1779-1784.

Tüfekci, N. and Sarikaya, H. Z. 1996. Catalytic effects of high Fe(III) concentrations on Fe(II) oxidation. *Water Science and Technology* 34(7–8), pp. 389-396.

Tüfekci, N. and Sarikaya, H. Z. 1998. Influence of ageing on the catalytic activity of ferric sludge for oxidation of Fe(II). *Water Science and Technology* 38(6 pt 5), pp. 129-137.

Tüfekci, N. et al. 2000. An experimental study on iron removal with ferric sludge recycling. *Water Science and Technology*. pp. 393-397.

U.S. Geological Survey. 2018. Mineral Commodity Summaries 2018. In: Survey, U.S.G. ed. U.S. Geological Survey. p. 200.

Vachon, P. et al. 1994. Chemical and Biological Leaching of Aluminium from Red Mud. *Enviromental Science & Technology* 28, pp. 26-30.

Valero, A. et al. 2011. Trends of exergy costs and ore grade in global mining.*Sustainable development in the minerals industry*. Aachen.

van Beinum, W. et al. 2005. Sorption kinetics of strontium in porous hydrous ferric oxide aggregates I. The Donnan diffusion model. *J Colloid Interface Sci* 283(1), pp. 18-28.

van Der Woude, J. H. A. and De Bruyn, P. L. 1983. Formation of colloidal dispersions from supersaturated iron(III) nitrate solutions. I. Precipitation of amorphous iron hydroxide. *Colloids and Surfaces* 8(1), pp. 55-78.

Van Gerven, T. et al. 2005. Carbonation of MSWI-bottom ash to decrease heavy metal leaching, in view of recycling. *Waste Manag* 25(3), pp. 291-300.

Vargas, M. et al. 1998. Microbial evidence for Fe(III) reduction on early Earth. *Letters to nature* 395, pp. 65-67.

Vaxevanidou, K. et al. 2015. Role of indigenous arsenate and iron(III) respiring microorganisms in controlling the mobilization of arsenic in a contaminated soil sample. *Bull Environ Contam Toxicol* 94(3), pp. 282-288.

Veolia. 2016. *Wheal Jane Teseimonial: Outsourcing operations at Wheal Jane Minewater Treatment Plant* [Online]. Marlow International, Parkway, Marlow, Buckinghamshire, SL71YL: Veolia Water Industrial Outsourcing Limited. Available at: http://www.veoliawatertechnologies.co.uk/vwst-uk/ressources/documents/1/31314,Wheal-Jane-Testimonial.pdf [Accessed: 6/4/16].

Vetriani, C. et al. 1999. Population structure and phylogenetic characterization of marine benthic archaea in deep-sea sediments. *Applied Environmental Microbiology* 65, pp. 4375-4384.

Villemur, R. et al. 2006. The Desulfitobacterium genus. *FEMS Microbiol Rev* 30(5), pp. 706-733.

Vincent, K. and Passant, N. 2006. Assessment of Heavy Metal Concentrations in the United Kingdom DEFRA.

Vithana, C. L. et al. 2015. Stability of schwertmannite and jarosite in an acidic landscape: Prolonged field incubation. *Geoderma* 239-240, pp. 47-57.

Walker, J. 1987. Was the Archaean biosphere upside down? *Letters to nature* 329(710-712).

Wang, W. et al. 2013. Recovery of scandium from synthetic red mud leach solutions by solvent extraction with D2EHPA. *Separation and Purification Technology* 108, pp. 96-102.

Weber, K. A. et al. 2006. Microorganisms pumping iron: anaerobic microbial iron oxidation and reduction. *Nat Rev Microbiol* 4(10), pp. 752-764.

Webster, G. et al. 2003. Assessment of bacterial community structure in the deep sub-seafloor biosphere by 16S rDNA-based techniques: a cautionary tale. *Journal of Microbiological Methods* 55(1), pp. 155-164.

Webster, G. et al. 2015. Archaeal community diversity and abundance changes along a natural salinity gradient in estuarine sediments. *FEMS Microbiol Ecol* 91(2), pp. 1-18.

Webster, J. et al. 1998. Trace Metal Adsorption onto an Acid Mine Drainage Iron(III) Oxyhydroxysulfate. *Environmental Science & Technology* 32, pp. 1361-1368.

Wei, M. et al. 2014. Microbial diversity and biogenic methane potential of a thermogenic-gas coal mine. *International Journal of Coal Geology* 134-135, pp. 96-107.

Welsh Assembly Government. 2002. Metal Mine Strategy for Wales. In: Wales, E.A. ed. Environment Agency Wales. p. 139.

Whitehead, P. G. et al. 2005. Chemical behaviour of the Wheal Jane bioremediation system. *Sci Total Environ* 338(1-2), pp. 41-51.

Whitehead, P. G. and Prior, H. 2005. Bioremediation of acid mine drainage: an introduction to the Wheal Jane wetlands project. *Sci Total Environ* 338(1-2), pp. 15-21.

Wiatrowski, H. A. et al. 2006. Novel Reduction of Mercury(II) by Mercury-Sensitive Dissimilatory Metal Reducing Bacteria. *Environ. Sci. Technol.* 40, pp. 6690-6696.

Williamson, M. A. et al. 1992. The kinetics of iron oxidation in acid mine drainage. In: *Programs and Abstracts, V. M. Goldschmidt Conference.*

Williamson, M. A. and Rimstidt, J. D. 1994. The Kinetics and Electrochemical Rate-Determining Step of Aqueous Pyrite Oxidation *Geochimica et Cosmochimica Acta* 58, pp. 5443-5454.

Woodruff, L. G. et al. 2017. *Titanium*. U.S. Geological Survey.

Xu, Y. et al. 2014. Enhanced abiotic and biotic contributions to dechlorination of pentachlorophenol during Fe(III) reduction by an iron-reducing bacterium Clostridium beijerinckii Z. *Sci Total Environ* 473-474, pp. 215-223.

Xue, A. et al. 2010. The technological study and leaching kinetics of scandium from red mud. *Nonferrous Metals Extractive Metallurgy* 2, pp. 51-53.

Yadav, I. C. et al. 2015. Reductive dissolution of iron-oxyhydroxides directs groundwater arsenic mobilization in the upstream of Ganges River basin, Nepal. *Journal of Geochemical Exploration* 148, pp. 150-160.

Yahya, A. et al. 2008. Iron and carbon metabolism by a mineral-oxidizing Alicyclobacillus-like bacterium. *Arch Microbiol* 189(4), pp. 305-312.

Yang, X. et al. 2015. Recovery of zinc from cyanide tailings by flotation. *Minerals Engineering* 84, pp. 100-105.

Ye, Q. et al. 2004. Alkaline Anaerobic Respiration: Isolation and Characterization of a Novel Alkaliphilic and Metal-Reducing Bacterium. *Applied and Environmental Microbiology* 70, pp. 5595-5602.

Yutin, N. and Galperin, M. Y. 2013. A genomic update on clostridial phylogeny: Gram-negative spore formers and other misplaced clostridia. *Environ Microbiol* 15(10), pp. 2631-2641.

Zabcic, N. et al. 2014. Using airborne hyperspectral data to characterize the surface pH and mineralogy of pyrite mine tailings. *International Journal of Applied Earth Observation and Geoinformation* 32, pp. 152-162.

Zachara, J. et al. 1998. Bacterial reduction of crystalline Fe^{3+} oxides in single phase suspensions and subsurface materials. *American Mineralogist* 83, pp. 1426-1443.

Zachara, J. et al. 2001. Solubilization of Fe(III) oxide-bound trace metals by a dissimilatory Fe(III) reducing bacterium. *Geochimica et Cosmochimica Acta* 65, pp. 75-93.

Zachara, J. et al. eds. 1996. *Surface chemical metering of bacterial iron oxide reduction and effects of reduction on Fe(III)-oxide reactive surface chemistry.* The 1996 International Symposium on Subsurface Microbiology.

Zachara, J. M. et al. 2002. Biomineralization of Poorly Crystalline Fe(III) Oxides by Dissimilatory Metal Reducing Bacteria (DMRB). *Geomicrobiology Journal* 19(2), pp. 179-207.

Zavarzina, D. G. et al. 2007. Thermincola ferriacetica sp. nov., a new anaerobic, thermophilic, facultatively chemolithoautotrophic bacterium capable of dissimilatory Fe(III) reduction. *Extremophiles* 11(1), pp. 1-7.

Zhang, J. et al. 2015a. Characterizing microbial communities dedicated for conversion of coal to methane in situ and ex situ. *International Journal of Coal Geology* 146, pp. 145-154.

Zhang, J. et al. 2015b. Mechanism of vanadium slag roasting with calcium oxide. *International Journal of Mineral Processing* 138, pp. 20-29.

Zhang, Y. et al. 1992. Adsorption of protons, Fe(II) and Al(III) on lepidocrocite. *Colloids and Surfaces* 63, pp. 259-268.

Zhang, Y. et al. 2012. Recovery of iron from cyanide tailings with reduction roasting-water leaching followed by magnetic separation. *J Hazard Mater* 213-214, pp. 167-174.

Zhou, K. et al. 2018. Selective precipitation of Cu in manganese-copper chloride leaching liquor. *Hydrometallurgy* 175, pp. 319-325.

Zhu, C. 2002. Estimation of surface precipitation constants for sorption of divalent metals onto hydrous ferric oxide and calcite. *Chemical Geology* 188, pp. 23-32.

Ziegler, S. et al. 2013. Metallibacterium scheffleri gen. nov., sp. nov., an alkalinizing gammaproteobacterium isolated from an acidic biofilm. *Int J Syst Evol Microbiol* 63(Pt 4), pp. 1499-1504.